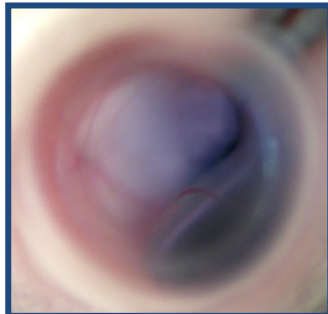# DEVELOPMENT OF A NON-VIRAL GENE THERAPY STRATEGY FOR CHOROIDEREMIA

ELHAM OSTAD-SAFFARI

A THESIS SUBMITTED FOR THE DEGREE OF DOCTOR OF PHILOSOPHY FROM IMPERIAL COLLEGE LONDON

2013

DECLARATION

I, Elham Ostad-Saffari, hereby declare that this thesis submitted for the degree of Doctor in Philosophy is my own work and was carried out by myself unless otherwise stated.

Elham Ostad-Saffari

ABSTRACT

_____

Non-viral plasmids harbouring scaffold matrix attachment regions (S/MARs) provide stable and functional episomal maintenance, resistance to epigenetic silencing and have been shown to be capable of sustained expression in murine tissues. S/MARs are an attractive alternative to conventional viral gene delivery vectors due to their low toxicity and reduced immunogenicity. This thesis documents the development of this novel non-viral episomal plasmid DNA (pDNA) expression system for persistently expressing vectors for Choroideremia (CHM) gene therapy. To this end, our goal was to analyse the ability of S/MAR plasmids to generate efficient and stable transgene expression in the mouse retina following subretinal injections. We generated and analysed a series of S/MAR constructs expressing either *REP1* cDNA or the reporter enhanced green fluorescent protein (*EGFP*) or Luciferase (*Luc*) genes driven by the elongation factor-1 short (EFS) or cytomegalovirus (CMV) early enhancer/chicken beta actin (CAG) promoter.

We demonstrate using the AtT20 cell line, the principle that S/MAR containing plasmids can provide long-term episomal *EGFP* and *REP1* transgene expression *in vitro.* Furthermore, long-term *REP1* expression was also analysed in CHM fibroblasts, where we showed in preliminary experiments that DNA constructs expressing *REP1* were able to rescue CHM derived cells by rescue of their Rab27a prenylation defect and provide long-term expression of *hREP1* after transfection of human and mouse CHM fibroblasts.

We also developed an optimised method for delivering S/MAR containing plasmids in the eye via subretinal injections of complexed pDNAs, and provide evidence for the utility and versatility of S/MAR plasmids in ocular tissue. We show for the first time the longitudinal transgene expression of *Luc* in the retina as measured using bioluminescent imaging. Long-term maintenance and expression of *EGFP* and *REP1* transgenes were also observed by PCR and Western blot analysis. Further analysis provided evidence for the long term episomal maintenance of these vectors in the eye as shown by Southern analysis. We provide evidence for the superiority of an S/MAR containing plasmid in providing long-term expression in the eye. All control pDNA constructs were shown to be incapable of sustaining significant transgene expression beyond one-month following pDNA delivery. We further demonstrate the lack of toxicity within the eye and show that fundus examinations as well as detailed histological examinations of retinal sections do not elicit an inflammatory response to our plasmids once subretinally injected in the eye.

Finally, we explored the therapeutic potential of the REP1-S/MAR episome, by subretinally injecting mouse models of CHM. Further repeat experiments in CHM mouse models would add confidence to the overall experiments; however initial findings were encouraging where a partial correction of the REP1 protein and functional rescue in the eye was shown.

To,

_____

Both sets of parents, my brothers and last but not least my husband. The love I have for each and every one of you is beyond that which words can explain. I would never have been able to achieve this goal had it not been for you all. For being there every step of the way. For loving me unconditionally. For the unlimited support and encouragement. For listening to the same problems over and over again. For being my pillars of strength. For accepting me. And for the millions of things I take for granted. I dedicate this thesis to you.

توانا بود هرکه دانا بود   زدانش دل پیر برنا بود

"Those who possess knowledge possess infinite abilities.

Through knowledge, even the spirit of the aged can yet again become jovial."

A quotation from the Shahnameh of Ferdowsi (Persian poet)

ACKNOWLEDGMENTS

_____

I would like to thank my supervisor Miguel Seabra for giving me the opportunity to do this PhD. Thank you for having the belief in me and my project. Thank you to Tanya Tolmachova for your guidance and help daily. Thank you for the mouse models without which this whole project may never have been possible. I would also like to thank my other mentor Richard Harbottle. Your tireless dedication to this project and expertise in the all things non-viral provided me with a great opportunity and standing through my whole project. You are not only me mentor but also my friend. Your door was always open and for that i am eternally grateful. I am particularly thankful to Dhani for her amazing knowledge in all things brown and furry. You were my right hand man in a lot of the animal experiments. Thank you from the bottom of my heart. We've shared some of the most amazing highs and some equally amazing lows over the years. I will cherish our friendship and our times at imperial for many years to come. I would also like to pass on my gratitudes to Orestis and Suet for showing me the ropes in the early days, as well as always being there for advice and help. A heart felt thank you to Mariya for joining my project and giving it the wings it needed. Thank you for your amazing technical abilities in all things small and round! Without your assistance, this work would never have been as successful as it has been. I would also like to thank Bronwen, Suzy and Simon for their technical abilities and advice throughout the years. Thank you to Oleg who helped me with my plasmids and cloning in my darkest hours. Finally I would like to thank Pam Renwick who initiated all of this many years ago at Guys Hospital. You had faith in me even early on in my naive scientific career and gave me the encouragement to keep going to achieve my goals.

Thank you to each and every one of you. Without you all none of these successes would have been possible.

CONTENTS

_____

LIST OF TABLES

_____

LIST OF FIGURES

_____

LIST OF ABBREVIATIONS

_____

AAT	alpha-1 antitrypsin
AAV	Adeno-associated virus
AdV	Adenoviral virus
AMD	age-related macular degeneration
apoE	apoliprotein E
BCA	bicinchonic acid
Bcl-2	B cell lymphoma 2
BLI	bioluminescent imaging
BP	base pair
BPV	bovine-papilloma virus
BSA	bovine serum albumin
CAG	CMV early enhancer/ chicken β-actin promoter
CAT	chloramphenicol acetyltransferase
cDNA	(First-strand) complementary DNA
CFH	complement factor H
CFTR	cystic fibrosis transmembrane conductance regulator
CHM	choroideremia
CMV	Cytomegalovirus
CNV	choroidal neovascularisation
DAPI	4',6-diamidino-2-phenylindole
DMEM	Dulbecco's Modified Eagle's Medium
Dpf	days post-fertilisation
dsOligo	double stranded oligonucleotide
EBV	Epstein-Barr Virus
E. coli	Escherichia coli

EDTA	ethylenediaminetetraacetic acid
EFS	elongation factor 1 short promoter (intronless version)
EF1α	elongation factor 1-α promoter
EGFP	enhanced green fluorescent protein
ELISA	enzyme-linked immunosorbent assay
ELOVL4	elongation of very long chain fatty acids-like 4
ERG	electroretinography
FACS	fluorescence activated cell sorting
FTase	farnesyl transferase
GAGs	glycosaminoglycans
GAPs	GTPase activating proteins
GCS	ganglion cell layer
GDFs	GDI-displacement factors
GEFs	guanine nucleotide exchange factors
GGTase I	geranylgeranyl transferase type I
GTA	gene transfer agent
HACs	human artificial chromosomes
HCE	human corneal epithelial
H&E	haematoxylin and eosin
hREP1	human Rep1 protein
HRP	horseradish peroxidase
INL	inner nuclear layer
IPL	inner plexiform layer
IRES	internal ribosome entry site
IS	inner segments
KB	kilo bases
KO	knock-out
LCA	Leber congential amaurosis

LCR	locus control regions
LDLR	low density lipoprotein receptor
Lenti	Lentivirus
LPS	lipopolysaccharides
MACs	mammalian artificial chromosomes
MSC	multiple cloning site
N/P	nitrogen/phosphate
NPC	nuclear pore complex
NR	neural retina
OCT	optimal cutting temperature compound/medium
ONL	outer nuclear layer
OPL	outer plexiform layer
Ori	origin of replication
OS	outer segments
pA	polyadenylation
PBS	phosphate buffered saline
PCR	polymerase chain reaction
pDNA	plasmid DNA
PECS	pigment epithelium/choroid/sclera
PEDF	pigment epithelium-derived factor
PEG	polyethylene glycol
PEI	polyethylenimine
PFA	paraformaldehyde
PI	post injection
PLA	polylactide
PLGA	polylactide co-glycolide
PLL	poly (l-lysine)
PLRs	pupillary light responses

PMN	polymorphonuclear leukocytes
PNS	post nuclear supernatant
PVDF	polyvinylidene difluoride membrane
RabGDI	rab GDP-dissociation inhibitor
RabGGTase	rab geranylgeranyl transferase
REP	rab escort proteins
ROSs	rod outer segments
RP	retinitis pigmentosa
RPE	retinal pigment epithelium
RT	room temperature
rt-PCR	reverse transcription polymerase chain reaction
SAF-A	scaffold attachment factor A
SDS-PAGE	sodium dodecyl sulphate-polyacrylamide electrophoresis gel
s.e.m.	standard error of the means
shRNA	short hairpin RNA
SLO	scanning laser ophthalmoscopy
S/MAR	scaffold matrix attachment region
STGD	Stargardt-disease
SV40	simian virus 40
TGN	trans-Golgi network
TLR9	toll-like receptor 9
TM	tamoxifen
UbC	ubiquitin C
UCOE	ubiquitous chromatin opening elements
USH2	Usher Syndrome Type 2
VEGF	vascular endothelial growth factor
WT	wild-type
X-SCID	X-linked severe combined immunodeficiency

1   INTRODUCTION

_____

1.1 Gene Therapy - designing the ideal vector

Following the sequencing of the human genome and the concomitant understanding of genotype-phenotype relationships, increasing attention has been made to apply this knowledge to treating inherited diseases. As a first step numerous disease causing genes have been identified and studied. However the real therapeutic breakthroughs will depend on the development of gene therapy (for these specific diseases). Gene therapy can be defined as the treatment of a disease by the transfer and modification of genetic material within the cells of a patient, to correct or compensate for an abnormal or absent gene, by adding a functional copy of the gene to the appropriate cells. Ultimately, the goal of gene therapy is to correct gene functions, and result in the permanent correction of the genetic disorder, as well as to restore normal protein production back to physiologically regulated levels. If correction or compensation can be achieved through gene delivery, it is conceivable that monogenic disorders could be prevented and/or treated.

An ideal gene delivery vehicle must be able to mediate long-term transgene expression as well as fulfil three key criteria: (i) protecting the transgene against degradation by nucleases in the nuclear matrix, (ii) delivery of the transgene across the plasma membrane and into the nucleus of target cells; within the nucleus it must be able to replicate and subsequently it must be passed on through cell divisions and finally, (iii) all these criteria must be met with no detrimental effect. To this end, the required transgene can be delivered to patients through the use of viral or non-viral vector gene delivery vehicles.

The first clinical trial of gene therapy for the treatment of infants with X-linked severe combined immunodeficiency (X-SCID) was initiated in 1990 (Blaese, Culver et al. 1995). However, it was not until April 2000 that Cavazzana-Calvo *et al.* actually reported the first clinical success with gene therapy. In their report they showed that interleukin 2 receptor γ chain (IL2RG) transgene was able to successfully restore the humoral activity in 21 young patients (Cavazzana-Calvo, Hacein-Bey et al. 2000). Despite the initial optimism surrounding

this trial, these observations were overshadowed with considerable adverse events seen in 5 treated children. In these cases, following the treatment, patients began to develop leukaemia which was later shown to be caused by the retrovirus integrating near the LMO2 proto-oncogene promoter. This study was an unfortunate and grim reminder that insertional mutagenesis and its oncogenic consequences are a significant hindrance in the viral gene therapy approaches (Pike-Overzet, van der Burg et al. 2007). In another study, in 1999, an 18 year old patient was treated with an adenovirus for a urea cycle metabolic disease called ornithine transcarbamylase deficiency (OTCD). Following treatment the virus induced a severe inflammatory response in the patient which ultimately led to death (Raper, Chirmule et al 2003).

Viral vectors are unquestionably able to mediate high and efficient gene transfer. Furthermore they also provide the possibility of long-term gene expression and satisfying 2 out of the 3 criteria of an ideal gene delivery vehicle. Despite these efficiencies, they are also coupled with safety concerns; particularly as viruses are inherently immunogenic and carry significant risks associated with insertional mutagenesis, which were uncovered in the gene therapy trials. While this still remains to be the case, at present due to their far superior efficiencies *in vivo* compared to non-viral vectors, in the field of gene therapy they are still the preferred vectors for gene delivery in clinical trials (Figure 1). Indeed there are currently over 1714 clinical trials which have been completed, are still running or have been approved, in more than 30 different countries, including at least one trial in every continent. These trials are in areas ranging from cancer, cardiovascular and ocular diseases; not surprisingly the majority of these cases apply to vectors of viral origin.
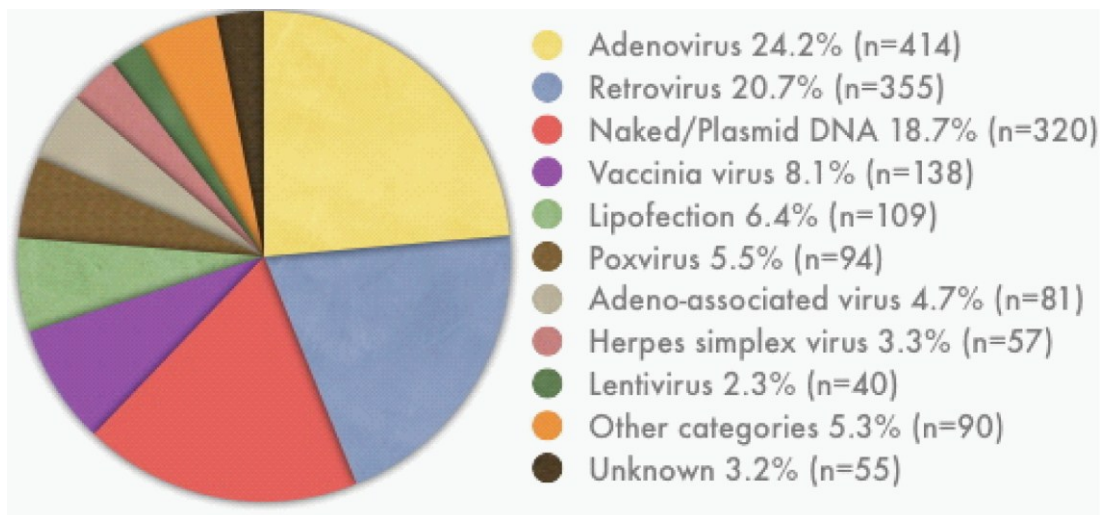
Figure 1: Current vectors used in gene therapy trials

The majority of trials in 2011 involve the use of viral vectors due to their unquestionable high transfection efficiencies, however shortly following viral vectors is naked/pDNA signifying the emerging interest in alternative therapies (www.wiley.co.uk/genmed/clinical).

In contrast to viruses, non-viral vectors have some key advantages, including safety as well as being relatively easy and cheap to produce. Despite this, the majority of non-viral vectors are still considerably less efficient than viral vectors, especially for *in vivo* gene delivery. Due to these constraints currently their successful applications in clinical trials have been limited to approximately 25% of the total clinical trials to date (Figure 1). Improvements in vector development, basic science of these vectors as well as gene transfer strategies may ultimately improve the preparation, delivery and expression of the current non-viral gene delivery vectors. Cumulatively this will lead to more efficient treatment of genetic disorders and much wider clinical applications.

1.2 Overview of viral vectors

Viruses provide a highly efficient vehicle for transferring genes to target cells or tissues where they mediate substantial expression *in vitro, ex vivo* as well as *in vivo.* They have evolved to develop highly efficient ways to enter target cells and facilitate their own expression. The viruses which have attracted the most attention of gene therapists are DNA-

based adenoviruses (AdV) and adeno-associated (AAV) vectors, as well as the RNA-based retrovirus and lentiviruses.
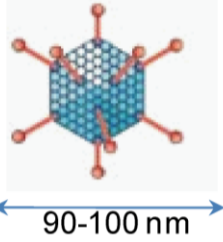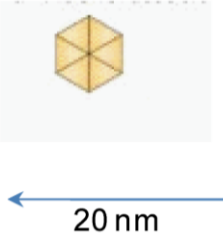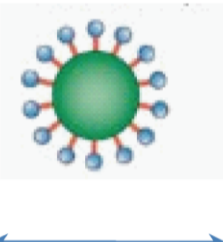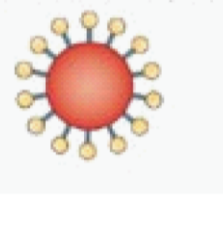
In spite of their high infection efficiency and successes, a number of worrying complications in early clinical trials resulting in oncogenesis or mortalities for OTCD (Raper, Chirmule et al 2003) and X-linked SCID (Kohn, Sadelain et al 2003; Hacein-Bey-Abina, von Kalle et al. 2003a) have been reported. These cases highlight the immunogenicity and cytotoxicity of viral vectors as gene transfer agents. Indeed the deaths of the X-SCID patients showed that following viral vector administration, insertional mutagenesis can occur. This is because the virus is able to integrate into the chromosomes of the patient receiving the gene therapy, leading to a disruption of tumour suppressor genes or the activation of oncogenes, which ultimately cause malignant transformation of cells. In contrast, the death of the OTCD patient was caused by an acute systemic inflammatory response to an adenovirus (AdV).

Worryingly, numerous reports have also shown problems with persistence of viral vectors in the brain following ocular viral delivery (Provost, Le Meur et al. 2005; Stieger, Colle et al. 2008). Furthermore, viral vectors can be hindered by the limited size of the expression cassette, difficulties in large scale production as well as safety issues resulting from repeat infections such as host immunity (Raper, Chirmule et al 2003; Thomas, Ehrhardt et al. 2003; Halbert, Miller et al. 2006; Baum, Kustikova et al. 2006). The advantages and disadvantages of the various types of viral vectors for gene therapy purposes are seen in Table 1.

Table 1: Typical viral vectors used in gene therapy as well as their advantages and disadvantages (O'Connor and Crystal 2006)

Virus	Advantages	Disadvantages
Adenovirus (AdV) 90-100 nm	- High titres achieved easily - Efficient and high infection of most tissues - Capable of infecting dividing and non-dividing cells - Large cloning capacity (~ 36 kb)	-Capsid induces a potent inflammatory response -Transient expression observed
Adeno-associated virus (AAV) 20 nm	-Non-inflammatory - Rare integration into host cells -Capable of infecting dividing and non-dividing cells -Strong transgene expression	-Limited cloning capacity (~ 4.5 kb maximum)
Retro/Lenti virus 80-100 nm	-Capable of infecting dividing and non-dividing cells -Lentivirus efficiently infects most tissues	-Retrovirus only transduced dividing cells -Integration may lead to oncogenesis -Difficult to obtain high titres -Limited cloning capacity (~ 8 kb maximum)
Herpes virus	- High titres achieved easily -Maintained episomally but latent injection can last a lifetime - Large cloning capacity (20-30 kb)	-Inflammatory -Potential to generate HSV infection in humans

1.3   Overview of non-viral vectors

The current gene delivery systems in use today are unquestionably gene therapy vectors based on modified viruses. However, recently crucial limitations including risks of insertional mutagenesis and adverse immune effects have been brought to light (Hacein-Bey-Abina, von Kalle et al. 2003a; Hacein-Bey-Abina, Von Kalle et al. 2003b; Thomas, Ehrhardt et al. 2003). Due to a safety concern, non-viral vectors become an attractive alternative to viral gene delivery due to their ease of production in large scale at low costs as well as their low toxicity. Furthermore they provide greater versatility as any size of gene or regulatory sequence can be incorporated with relative ease.

While non-viral vectors provide good levels of transgene expression *in vitro,* their efficiencies are still inadequate for realistic *in vivo* gene therapy as *in vivo* they still present poor transfection efficiencies*.* Ideally once a vector has been delivered to target cells it should also be maintained within the nucleus without disruption to the hosts' gene expression or signaling pathways. Furthermore, they must be sufficiently stable to permit the delivery to target tissues. Hence they must be protected from potential problems during this initial stage including sheer forces from the blood stream and enzymatic degradation of the vector or gene product (Kircheis, Wightman et al. 2001). Once inside the target cell, for efficient transfection the vector must resist cytoplasmic degradation from enzymes such as nucleases and must be able to pass through the double membrane structure of the nuclear envelope which encapsulates the nucleus (Lyman, Guan et al. 2002; Jans, Xiao et al. 2000; Zelphati, Uyechi et al. 1998).

In order to achieve some of these requirements and ultimately enhance non-viral gene expression, numerous methods to attempt to mimic the efficient gene delivery capacity of viruses have been utilised. Specifically these mechanisms include the nuclear maintenance and replication through: non-integrating episomes as well as artificial chromosomes.

1.3.1   Persistent non-integrating episomal vectors

Conventionally, genetic modification of cells has been done using potentially integrating viral vectors. An alternative is to utilise vectors which can replicate and segregate to

daughter cells (persist within the nucleus of cells) in an autonomous, extra-chromosomal and independent state. These vectors are particularly advantageous as they do not lead to cell transformation due to the inability of physical integration of these vectors into the host genome. Thus these vectors are devoid of problems associated with integration events, particularly, insertional mutagenesis, as seen with integrating viral vectors. If these vectors are based entirely on non-viral elements, they do not lead to immunological problems of the recipient organism or transformation of the cell caused by virally encoded proteins (Mazda, Satoh et al. 1997). Furthermore genes within such vectors cannot be interrupted or subjected to regulatory constraints which often occur from integration into cellular DNA. Additionally, episomal vectors persist in multiple copies in the nucleus, resulting in the high amplification of the gene of interest.

These key advantages have led to increase efforts in developing vectors capable of extra-chromosomal (episomal) replication that lack the ability of transgene integration events within the hosts' chromosome.

1.3.1.1 Episomal vectors based on replication deficient viruses

One such class of episomal vector systems include viruses such as simian virus 40 (SV40), Epstein-Barr Virus (EBV) and bovine-papilloma virus (BPV). These viruses normally replicate episomally within mammalian cells by using the cellular replication machinery. However viral proteins are also essential for the initial replication at the viral origin of replication (ori). Within the SV40 viral plasmids, the region of this virus or the viral protein required for its cellular replication is the large T-antigen (Tag) (Li, Zhao et al. 2003), and for the EBV virus, the EBV Nuclear Antigen-1 (EBNA1) (Wu, Ceccarelli et al. 2000) is required. Furthermore, these viral proteins are required for the segregation of viral episomes to progeny cells during cell division. This is through a poorly understood 'piggy-back' mechanism following the association with a mitotic chromosome, origin of replication complex (ORC)(White, Wade-Martins et al. 2001).

Importantly by including these viral ori sequences, episomal plasmids have been generated that can sustain expression of therapeutic transgenes. Studies have shown the development of an EBV-based episomal plasmid which contains the entire hypoxanthine phosphoribosyl

transferase (HPRT) locus. These studies also went onto show that this plasmid provided stable expression of HPRT at physiologically relevant levels for up to six months *in vitro* within HPRT-deficient human lung fibroblast cells (Wade-Martins, White et al. 2000). Despite these initial finding, the EBV-based episomes were gradually lost at a rate of 4% per cell division in the absence of antibiotic selection pressure. Furthermore the presence of a continuous selection pressure led to integration of the EBV plasmid into the host genome.

In another report, EBV vectors were shown to enhance B-cell (lymphoma) immortalization several 1000-fold (Humme, Reisbach et al. 2003). While this highlights their potential use as a model for immune therapy of cancer, this was seen alongside humoral and cellular immune responses (Taylor, Haigh et al. 2004). Similar cellular transformations were also seen when using the Tag gene from the SV40 plasmid. At physiological levels, the Tag gene is shown to disable the p53 tumour-suppressor and retinoblastoma pathways. As p53 is significantly important for cell cycle arrest and apoptosis, this alters the function of other key host cell proteins which in turn cause numerous transformations to occur (Ali, Kasper et al. 2004).

An alternative episomal viral vector system is based on replication deficient viruses or virus like particles (VLPs) such as AdVs and AAVs. These virus vectors are able to persist in the genome as a non-integrative state by utilising viral proteins. VLP based episomal systems are able to assemble as viral particles (virions) within producer systems unlike episomal systems based on EBV and SV40 replicons. Hence these VLP vectors are able to exhibit all viral functions; namely transduction of target cells and nuclear translocation of their genomes, however they importantly lack the ability to replicate and produce progeny. Despite this, reports have brought to light some considerable safety concerns. One such example is the induction of a host immune response following the leakage of viral products after the use of replication deficient AdVs. Furthermore low levels of integration and immunotoxicity, as well as high levels of multiplicities (which is a measure of the ratio of infectious virus particles to the number of target -host- cells) were observed against the viral capsid of AAV replication deficient viruses (Nakai, Montini et al. 2003).

1.3.2 Episomal vectors based entirely on chromosomal elements

1.3.2.1 Mammalian Artificial Chromosomes

Due to the safety concerns mentioned above for viral-based episomes, interest began on the development of episomal replicating vectors that were solely comprised of functional chromosomal elements – artificial chromosomes. These vectors have three main components: a centromere, two telomeres at both termini and several origins of replication. Artificial chromosomes have long been touted as an ideal vector for gene delivery; as such chromosomes would mimic the natural state of the DNA in the cell. This would mean essentially, unlimited amounts of DNA could be incorporated into such vectors. In the case of mammalian artificial chromosomes (MACs) such vectors could enable either whole genes or whole metabolic pathways with their entire natural genomic content containing all regulatory elements to be delivered. Furthermore these vectors would not integrate into the hosts' genome. Despite this, the first human artificial chromosomes (HACs) were commonly unstable and integration events caused disruption of the host genome (Harrington, Van Bokkelen et al. 1997). One exception was circular HACs which were shown to be mitotically stable in the absence of selection (Ebersole, Ross et al. 2000).

Human artificial chromosomes can be constructed either by the 'bottom-down' or 'bottom-up' approach. In the 'bottom-down' approach minichromosomes are created, whereby existing chromosomes are truncated to a minimal length using irradiation or telomere fragmentation (Farr, Stevanovic et al. 1992). While the 'bottom-up' approach involves the assembly of centromeric DNA (such as long synthetic arrays of α-satellite DNA which are present at the centromeres of all normal human chromosomes), telomeric DNA and genomic DNA sequences to be delivered (Farr, Stevanovic et al. 1992). However, artificial chromosomes to-date require specialized delivery techniques including delivery to mice using microcell medicated chromosome transfer as well as pronuclear injections (Basu and Willard 2005; Jackson, Juranek et al. 2006). Several studies have utilised HACs to provide long-term therapeutically relevant levels of gene expression. One such study includes a HAC containing the entire 250 kb genomic cystic fibrosis gene, cystic fibrosis transmembrane conductance regulator (*CFTR*), including regulatory sequences. This HAC was shown to stably express CFTR protein as well as providing persistent chloride secretory response *in vitro,* showing the potential application for treatment of the disease (Auriche, Carpani et

al. 2002). Despite this, the use of MACs is plagued with numerous ethical and safety issues. This is primarily because they require chromosomal elements which are removed from animal cells; thus must be stringently controlled.

1.3.2.2 Plasmid pEPI

As an alternative, a plasmid called pEPI was generated in 1999. This plasmid contains an SV40-ori sequence, however does require transforming viral proteins for episomal maintenance (Figure 2).
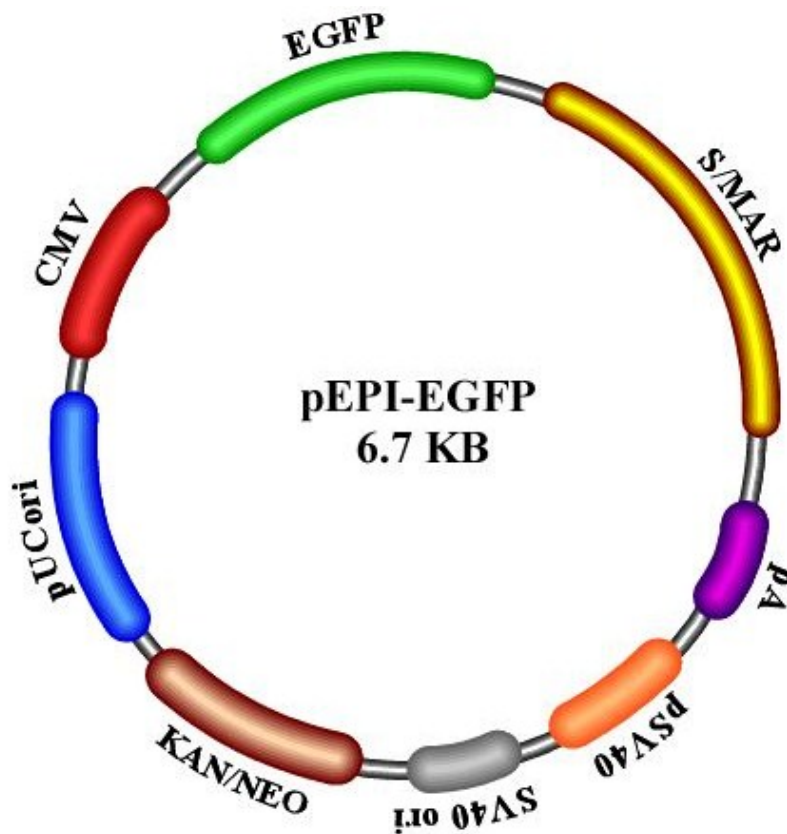
Figure 2: Schematic representation of pEPI-EGFP (or simplified pEPI)

Plasmid pEPI is shown, including all necessary elements for replication and maintenance.

Noteworthy is the study in haematopoietic stem cells, where this was the first application of S/MAR vectors in CD34^{+} stem cells (Papapetrou, Ziros et al. 2006). In this study, Papapetrou and colleagues showed that pEPI is maintained episomally for up to four weeks. However,

despite transgene silencing in the MEL cell line - as a result of histone deacetylation- pEPI continued to remain as an episome.

In another study, S/MAR vectors were shown to episomally modify pluripotent p19 embryonic cells (Sotirova, Calciano et al. 2006). Plasmid pEPI was modified slightly to express a short hairpin RNA (shRNA) against the endogenous proteins of β-tubulin III and cyclophilin A. Interestingly, when this vector was used together with a control non-S/MAR vector, it was shown that the S/MAR vectors were able to promote more efficient and sustained gene expression. In contrast the non-S/MAR vectors were not, while the episomal status of both vectors was also confirmed by Southern blot analysis. In an alternative study, S/MAR elements were included in a pDNA vector and were shown to restore functional levels of the human low density lipoprotein receptor (LDLR) in CHO ldlr$^{-/-}$ a7 cells. Importantly these were physiologically relevant levels and remained episomal for 11 weeks (Lufino, Manservigi et al. 2007).

Significantly, pEPI has also been used to create genetically modified pigs following sperm-mediated gene transfer of pEPI into oocytes. The vector was detected and retained as an episome in 12 out of 18 foetuses within different tissues analysed. Furthermore, strong reporter gene expression (of eGFP) was observed in 9 out of 12 episome-positive foetuses (Manzini, Vargiolu et al. 2006). While the foetuses were not brought to term due to legal reasons, this study highlights the ability of S/MAR plasmids in providing efficient and long-term expression *in vivo.*

Following this, pEPI vector was delivered to the mouse liver and lung. However in these studies, only transient expression was reported due to considerable silencing of the plasmid (Conese, Auriche et al. 2004; Argyros, Wong et al. 2008). To circumvent this problem Argyros *et al.* replaced the CMV promoter of pEPI with the liver-specific α1 antitrypsin promoter (AAT). This proved to be essential and led to the persistent transgene expression in the mouse liver for up to 6 months following a single vector administration (Argyros, Wong et al. 2008). Importantly, the removal of the S/MAR element from the vector resulted in silencing of pEPI within a week of administration. This was the first demonstration *in vivo* for persistent expression of S/MAR vectors with a tissue specific promoter. The authors showed that there appeared to be a synergistic relationship between the tissue-specific

promoter and pEPI. Furthermore they also showed that indeed this promoter was necessary for long-term transgene expression. Unfortunately the plasmid was not shown to be able to replicate *in vivo,* and following 70% partial hepatectomy, the CMV and AAT-based vectors failed to persist and expression was lost.

In contrast, Wong *et al.* reported in 2011 the first episomal replication of an S/MAR plasmid *in vivo* following an initial period of selection pressure which was required to reveal episomal maintenance (Wong, Argyros et al. 2011). The authors showed an *in vivo* liver selection strategy. Liver cells were transfected with an S/MAR plasmid bearing the B cell lymphoma 2 (*Bcl-2*) gene. These cells were shown to have a survival advantage over non-transfected cells after an initial selection pressure of the Fas anti-body Jo2. This is based on the induction of cell death by the Fas antigen, which induces apoptosis on engagement with its physiological ligand, FasL. Hence, *in vivo* this pathway can be activated following administration of an agonist Fas antibody, Jo2. Following hydrodynamic delivery to the livers of NOD/SCID mice and the twice weekly administration of Jo2, the authors showed that indeed the *Bcl-2* S/MAR plasmid was able to provide long-term luciferase reporter gene expression despite constant Jo2 challenges. Furthermore the plasmid was also able to replicate as an episomal entity. While this approach is not clinically relevant, it shows that S/MAR vectors are capable of preventing transgene silencing, are resistant to integration and are capable of conferring mitotic stability *in vivo* provided with a selective advantage.

1.3.2.3 Scaffold/Matrix Attachment Regions (S/MARs)

S/MARs are genomic DNA sequences which were first described by Cockerill *et al.* in 1986 while studying the organization of the nuclear matrix (Cockerill, Garrard et al. 1986). The organisation of the eukaryotic nucleus into chromosomal domains is thought to be mediated by the nuclear matrix or nuclear scaffold. It is composed of a highly proteinaceous intranuclear framework including branched core filaments. These filaments provide the supporting structure for the formation of DNA looped domains that participate in the numerous matrix-supported processes involving: DNA replication and transcription, RNA processing and transport, signal transduction and apoptosis. S/MARs are defined as the genomic DNA sequences which anchor the chromatin to the nuclear scaffold proteins (Heng,

Goetze et al. 2004; Mirkovitch, Mirault et al. 1984)(Figure 3). This binding then forms portioned looped domains that contribute structurally to the tight packaging of DNA in the nucleus - as described earlier - and functionally to the regulation of gene expression and replication of the genome. Hence S/MARs play a crucial role in chromatin structure, specifically in the organisation of eukaryotic genomes, particularly in maintaining the chromosome structure and function within the cell nucleus.

It has been estimated that the human genome contains thousands of S/MAR elements. However some of the most commonly used S/MAR sequences have been: the Eμ SMAR in the immunoglobulin heavy chain enhancer locus (Wiersma, Ronai et al. 1999), the apoBMAR from the human apolipoprotein B locus (Attal, Cajero-Juarez et al. 1995), the Ch-LysSMAR from the chicken-lysozome locus (Makarova, Gorneva et al. 1996) and the huIFNβSMAR from the human β-interferon locus (Piechaczek, Fetzer et al. 1999). Despite being evolutionary conserved, S/MARs appear to show little sequence or organisation conservation; rather they contain several recognisable motifs within and between species (Girod, Nguyen et al. 2007). S/MARs have a range of between 300-5000 bp and are known for their high AT content, which is usually higher than 65% (Mirkovitch, Mirault et al. 1984; Bode, Benham et al. 2000). It is this high AT content which is believed to at least partially aid the unwinding and destabilization of the DNA double helix (Bode, Kohwi et al. 1992; Bode, Winkelmann et al. 2006) and the formation of secondary DNA loop structures (von Kries, Buhrmester et al. 1991). Thus, the affinity of an S/MAR to the nuclear matrix appears to be affected by the location and organisation of the AT-rich regions. However, being an AT-rich region alone does not make a DNA fragment an S/MAR (Benham, Kohwi-Shigematsu et al. 1997). Indeed large S/MARs (of several kb) are found at borders of chromatin domains, while shorter S/MARs which have very similar physicochemical properties occur in close association with certain enhancers or introns. Therefore S/MARs are found either in non-transcribed regions or within transcription units, but rarely in coding regions (Bode, Benham et al. 2000). This observation implies that each gene has its own S/MAR – the so called 'one gene-one S/MAR' hypothesis (Frisch, Frech et al. 2002). These unique properties differentiate S/MARs from standard promoters, enhancers and coding sequences.
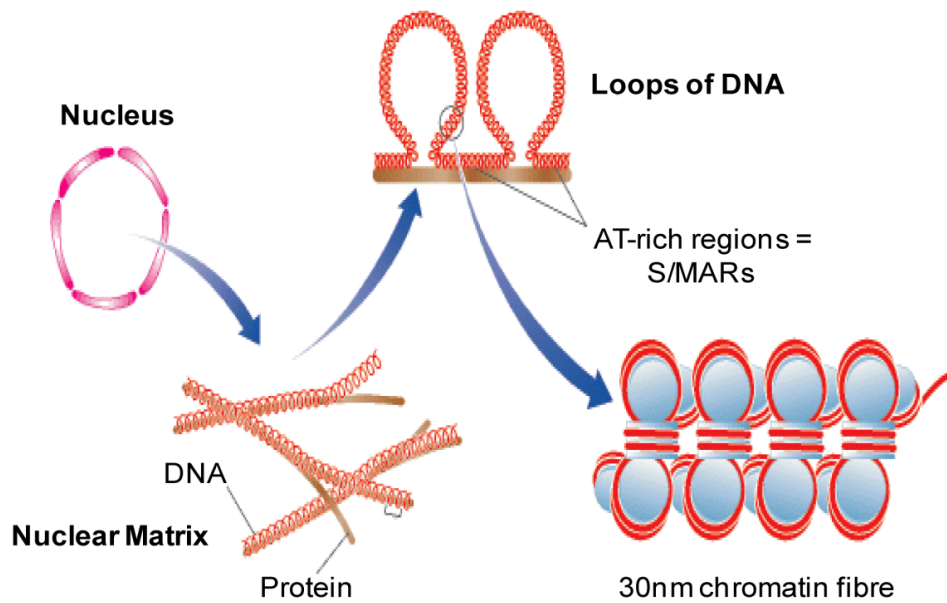
Figure 3: The nuclear matrix – organisation of S/MARs

DNA in eukaryotic genomes is organised in a complex structure within the nucleus. DNA in the nucleus interacts with histones and chromatin proteins to form a 30 nm fibre. The DNA is then condensed further and organised into chromatin loops. The formation of these chromatin loops is aided by the interaction of AT rich regions of the genome – S/MARs – with the nuclear matrix.
(Image modified from: www.ghastlyfop.com/blog/2005_09_01_archive.html)

1.3.2.4 S/MARs function as insulators

As described earlier, the interaction of S/MARs with the nuclear matrix/scaffold is crucial for the organisation of chromatin loops, which define the boundaries of independent chromatin domains (Heng, Goetze et al. 2004). These boundary domains are commonly located near genes, thereby insulating their coding regions from stimulatory or recessive effects from their surroundings as well as to provide local assess of transcription factors to enhancers and promoters (Goetze, Gluch et al. 2003; Jenuwein, Forrester et al. 1997). Indeed the 'one gene-one S/MAR' hypothesis mentioned previously predicts that each active gene has its own S/MAR element (Bonifer, Vidal et al. 1990). Therefore S/MARs could effectively insulate transgenes from integration into the host chromosome by creating independent domains.

Many genes are known to be shielded by so-called 'insulator' elements. Furthermore S/MARs have been commonly found in regions flanking genes, as well as colocalising with regions where such insulators are found. One such insulator is *gypsy,* which is a

retrotransposon in *Drosophila melanogaster,* suggesting that S/MARs indeed have an insulator function (Nabirochkin, Ossokina et al. 1998). In *Drosophila,* the nuclear matrix protein Su (Hw) binds to *gypsy,* creating a chromatin loop, however certain mutations in this protein disrupt the loop formation, rendering the *gypsy* insulator non-functional. This result suggests that the tethering of S/MARs to the nuclear matrix topologically constrains the DNA into looped structures, in turn protecting the DNA from regulatory elements outside the loop.

Similarly, in vertebrates, CTCF, which is a ubiquitous nuclear matrix protein, binds to insulators and has also been shown to interact with S/MARs (Yusufzai, Felsenfeld et al. 2004). While the mechanism whereby CTCF acts as an insulator remains largely unknown, it has been suggested that the binding of CTCF to S/MARs may block the interactions between promoters and unrelated enhancers. Furthermore this binding also creates loop structures which delimit different chromosome domains. Additionally as described previously, pEPI plasmid is able to mediate persistent transgene expression in a range of cells, however only transient expression is seen when transgenes lacking S/MARs were used. This indicates that in the pEPI plasmid, S/MARs are able to shield the transgene from the effects of the neighbouring host chromatin, hence enabling persistent and stable expression *in vitro* (Halweg, Thompson et al. 1999; Girod, Nguyen et al. 2007).

Taken together, these examples support the view that S/MARs provide a crucial function as insulators in gene regulation. Following the attachment of S/MARs to the nuclear matrix (in the case of pEPI via interactions with the scaffold attachment factor A (SAF-A) protein), this interaction forms a complex higher-order nucleoprotein structure. This in turn insulates chromatin domains while also controlling gene expression by forming bridges between components of the transcriptional machinery and the regulatory elements (Ottaviani, Leveret al. 2008), as shown in Figure 4.
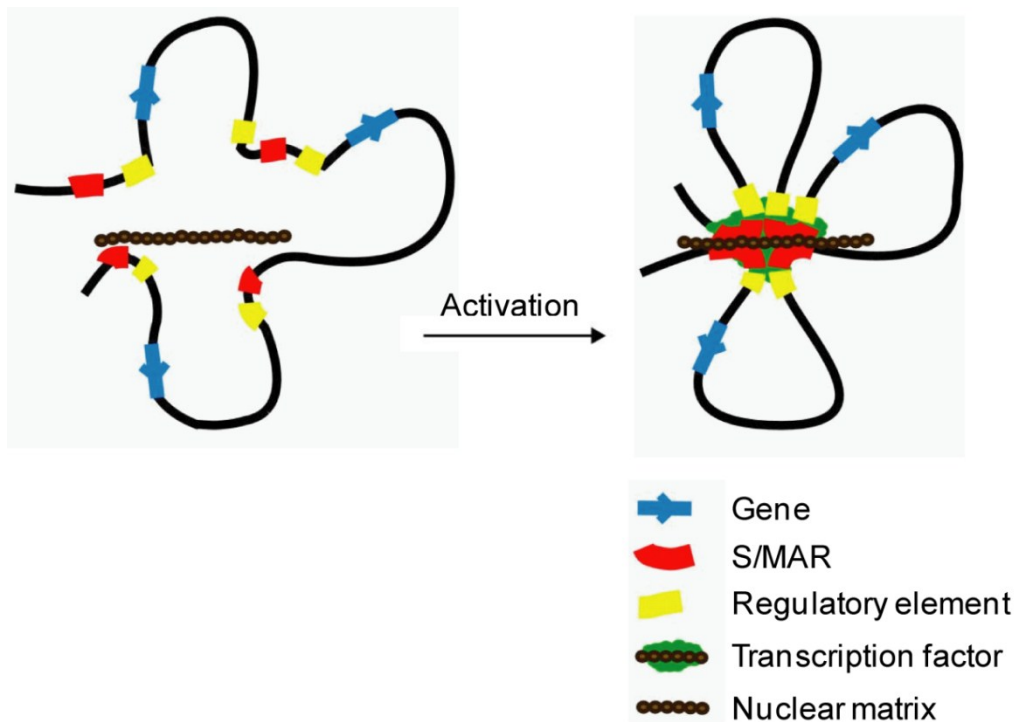
Figure 4: Schematic model depicting the function of S/MARs as insulators in gene regulation

Activation of transcription is accompanied by the binding of the S/MARs to the nuclear matrix. This results in the formation of anchored chromatin loops which importantly are insulated from the stimulatory or repressive effects of flanking chromatin. The transcription machinery is assembled at the site of the S/MAR, which aids in bringing together the gene coding sequences and regulatory elements to allow the coordinated regulation of specific genes (Figure adapted from (Ottaviani, Lever et al. 2008)).

1.3.2.5 S/MARs augment transcription

Interestingly, S/MARs may also act *in cis* to increase the transcription rates, even in the absence of an enhancer. Despite this, the precise mechanism of how S/MARs are able to switch on gene expression still remains largely unclear. Suggestions have indicated that the single chromatin loop which forms following the attachment of an S/MAR to chromatin is in fact not immobile. Therefore perhaps the changing of attachment points of the loops to different regions of the nuclear matrix many subsequently allow S/MARs to switch on gene expression (Kalos, Fournier et al. 2006). This implies that S/MARs are able to mediate successful transgene expression following its ability to change the structure of the chromatin in order to increase the likelihood of establishing an active locus (Ottaviani, Lever et al. 2008).

Interestingly, the binding of S/MARs to transcription factors may also influence transgene regulation. This is because following binding, this many allow the direct interaction of S/MAR elements with the components of the transcription machinery. Indeed S/MARs are also able to bind to nuclear matrix proteins such as the special AT-rich sequence-binding protein 1 - SATB1 (Galande, Purbey et al. 2007), SAF-B (Nayler, Stratling et al. 1998), topoisomerase II, histone H1 as well as acidic ribosomal protein PO, ARBP (Dickinson, Joh et al. 1992). Such binding allows the association of S/MARs with RNA polymerase; thus this increases the accessibility of an S/MAR containing plasmid to the transcription machinery of a cell and in turn influences gene expression. Interestingly, this is further confirmed following the fluorescence *in situ* hybridisation (FISH) analysis of the pEPI plasmid. These studies revealed areas of active sites which were present on the periphery of chromosome; implying that the chromatin is able to remain open for easy access to the transcription machinery.

The actual replication of pEPI is dependent on the active transcription of a gene which is located upstream of the S/MAR, with transcription continuing past the gene of interest and extending part of the way into the S/MAR (Stehle, Scinteie et al. 2003). This has been demonstrated by the loss of episomal replication following the removal of the promoter – cytomegalovirus (CMV) – which drives transcription or the insertion of sequences which result in the termination of transcription ahead of the S/MAR element (Stehle, Scinteie et al. 2003; Jenke, Stehle et al. 2004). This observation corroborates with the suggestions made previously, that transcription into the AT-rich S/MAR opens the surrounding chromatin structure of the plasmid, thus allowing access to the replication machinery (Schaarschmidt, Baltin et al. 2004; Stehle, Scinteie et al. 2003; Jenke, Stehle et al. 2004).

1.3.2.6 Mitotic stability

Plasmids harbouring S/MAR moieties are also believed to be mitotically stable, and several suggestions have been made to explain the molecular mechanism. Stehle *et al.* have shown that once the pEPI plasmid is established as an episome *in vitro,* it is then able to be maintained efficiently in active chromatin and importantly associate with early replicating chromosome sequences (Jenke, Scinteie et al. 2004). Noteworthy is the fact that vectors

without S/MAR or vectors in which the transcription was terminated before the S/MAR resulted in integration and loss of transgene expression – due to the silencing by promoter methylation (Jenke, Scinteie et al. 2004).

Interestingly, pEPI has also been shown to interact with mitotic chromosomes (Baiker, Maercker et al. 2000). This is thought to be mediated through the binding of the S/MAR element within this plasmid with the scaffold attachment factor A (SAF-A) protein (Jenke, Fetzer et al. 2002; Mearini, Nielsenet al. 2004), which is a principle component of cellular chromatin and chromosomes (Kipp, Gohring et al. 2000). This interaction most likely brings pEPI into contact with the host replication machinery, which is located on the nuclear matrix, hence facilitating pEPI replication once per cell cycle.

In another study, Jenke *et al.* showed that the pEPI plasmid is segregated to daughter cells. They showed that the S/MAR element within this plasmid is able to bind to a range of nuclear matrix proteins as mentioned previously. In particular, the S/MAR element was found to preferentially associate with the SAF-A protein (Jenke, Fetzer et al. 2002; Mearini, Nielsen et al. 2004). This suggests that during mitosis, pEPI is able to interact with mitotic chromosomes, following the interaction between the S/MAR element and SAF-A, this then allows the co-segregation of pEPI with the chromosomes during mitotic division (Jenke, Fetzer et al. 2002; Mearini, Nielsen et al. 2004). Therefore the S/MAR moiety of the pEPI plasmid performs a similar function to virally encoded proteins such as Tag and EBNA-1 of SV40 and EBV respectively (White, Wade-Martins et al. 2001, Wade-Martins, White et al. 2000) by allowing replication to occur through chromosome associations. Thus this association leads to helix destabilisation forming an open chromatin domain which mediates the assembly of the replication machinery and subsequent co-segregation of pEPI with chromosomes during mitosis (White, Wade-Martins et al. 2001; Baiker, Maercker et al. 2000).

While S/MARs have been shown to modulate transcription levels, other elements also have this same ability including: insulators, locus control regions (LCR) and ubiquitous chromatin opening elements (UCOE). Insulators are sequences of DNA which protect the integration of a transgene into the host genome, a phenomenon known as position effect variegation. They function by partitioning the genome into discrete functional domains which allows

independent regulation to occur preventing the overlap of promoter or enhancer signals at different loci (Kellum andSchedl 1992). Indeed, in studies involving adenoviral (Steinwaerder and Lieber 2000) and AAV vectors (Fitzsimons, Mckenzie et al. 2001), the presence of an insulator on the chicken β-locus in these vectors was shown is shield transgenes from the effects of flanking viral sequences. Similarly in pDNA vectors, increased reporter gene expression has been shown (Johansen, Tornoe et al. 2003).

Alternatively LCRs are long range transcriptional enhancers which provide strong chromatin opening abilities. While the majority of LCRs are tissue specific, some ubiquitous chromatin opening elements - UCOEs - have been identified in regions surrounding promoters of certain housekeeping genes (Antoniou, Harland et al. 2003). In an example Miao *et al* showed that the enhancement of human factor VIII and IX transgenes in liver tissues was achieved following the inclusion of a hepatocyte specific LCR derived from the apolipoprotein E (apoE) locus in pDNA (Miao, Ye et al. 2003).

It is important to remember that these elements provide a singular function - modulating transcription - however S/MARs have been shown to be extremely versatile and have the ability to provide numerous functions. Indeed similar to insulators, upon inclusion in a plasmid, S/MARs are able to shield a plasmid from the recessive or stimulatory effects within their surroundings. The important difference between insulators and S/MARs are that within a chromosome insulators mark the boundaries of active domains, in contrast, S/MARs are the boundaries by which chromatin is physically constrained into loops. Furthermore, it is this linkage with the nuclear matrix which provides S/MAR containing plasmids mitotic stability as well as segregation into daughter cells. Additionally, like LCRs and UCOEs, S/MARs are able to mediate domain opening. This in turn brings the transgene into close contact with promoters and other transcription factors, increasing the chances of possible interactions and hence potentially facilitating with transcription.

1.4   Non-viral gene delivery techniques

DNA does not require a vehicle to enter a cell. In fact most cells are able to take up DNA on their own, albeit at a very low efficiency. Systemic delivery of naked DNA is highly inefficient due to the rapid degradation by nucleases and clearance by the monocular phagocyte

system (Mahato, Takakura et al. 1997). Furthermore the phosphate group on the deoxyribose rings of DNA confer a negative charge to DNA molecules, which results in a low electrostatic interaction with anionic lipids in the cell membrane. Indeed direct injections of DNA into tissue may significantly increase the concentration of the vector in proximity to the target cell. For example with pulmonary administration for lung gene transfer, hepatic vein injections for liver gene transfer or subretinal and intravitreal injections for ocular gene transfer. Noteworthy is that this is not always possible due to the access of some tissues. Despite this, low levels of injected DNA may be taken up by target cells (Wolff, Williams et al. 1991). Therefore the main aim of non-viral gene delivery is to improve the efficiency of DNA uptake and prevent degradation outside the cell.

Commonly this is achieved by coating naked plasmid DNA (pDNA) with a positively charged lipid (cationic lipid) or cationic polymer, forming a gene transfer agent (GTA). These cationic lipids/polymers surround DNA such that the positive charge of the lipid/polymer is attracted to the negatively charged DNA, forming a complex called a lipoplex/polyplex. Within these complexes, the hydrophobic ends of lipids remain free and interact with the cell membrane facilitating entry into the cytoplasm of cells. Once within the cell, the entry of the DNA into the nucleus and subsequent expression of transgenes is not well understood.

In an alternative method, DNA can be administered directly to the required cells or tissues via physical methods such as ultrasound and electroporation. Furthermore, for specific routes for specialised tissues such as the eye more specialised routes may be required (as described in section 1.7.1).

1.4.1   Gene transfer by chemical carriers

1.4.1.1 Cationic Liposomes

The use of cationic lipids for gene delivery was first reported by Felgner *et al.* in 1987. Felgner and colleagues described a chemical carrier which was effective at binding and delivering DNA to cultured cells following a cationic liposome formulation, called Lipofectin (DOTM/DOPE)(Felgner, Gadek et al. 1987). This was quickly followed in 1989 by the first reports of *in vivo* transgene administration. In these studies gene expression of chloramphenicol acetyltransferase (CAT) in the lungs and liver of mice was reported for up

to 7 days following intravenous and/or intratracheal administrations of plasmid DNA complexed with Lipofectin (Brigham, Meyrick et al. 1989). Typically cationic lipids are comprised of a cationic head group, a hydrophobic lipid anchor and a linker bond between the two domains (Mintzer and Simanek 2009). A lipid anchor is normally comprised of a fatty acid chain or cholesterol ring group and determines the physical properties of a lipid bilayer such as membrane rigidity. The linker bond determines a cationic lipids stability and biodegradability. Finally the cationic head group is crucial for the transfection activity and toxicity following formulations. Since the initial studies involving Lipofectin, numerous other cationic lipids have been developed, differing mainly in the charge of their cationic head group as well as the detailed structure of their hydrophobic portion. Some of the most commonly used liposome formulations include: DOGS, DOTAP, DOTMA, CDAN and DOSPA.

The phosphate backbone of all nucleic acids has a single negative charge on it per base. In general, the formation of lipoplexes relays on the ionic interaction between the negatively charged phosphate backbone of the nucleic acid and that of the positive charge on the amino groups of lipids. Hence lipoplexes form instantly when cationic lipids are combined with DNA, through the electrostatic association of the polycationic liposome and polyanionic DNA. In general, when a low cationic liposome-to-DNA mole ratio is used, where the positive/negative charge ratio is less than 1, this results in small (< 40 nm) liposome/DNA complexes, which coexist as free or loosely bound DNA. In contrast, when a liposome-to-DNA mole ratio in excess of the neutral charge ratio is used, large (> 100 nm) complexes are formed. These complexes appear to encapsulate DNA within multilamellar lipid structures (Wasan, Reimer et al. 1996), where the DNA is sandwiched between the cationic lipid (Radler, Koltover et al. 1997). In these conditions, the large liposome/DNA complexes (lipoplexes) are most likely in dynamic equilibrium with smaller clusters, thinly lipid-coated DNA strands and free DNA. Therefore one can say that optimal gene delivery is achieved when the lipoplexes are at their most heterogeneous; for *in vivo* studies this appears to be when the positive/negative charge ratio is in excess of 1 (or neutral charge), while in some circumstances this may be higher (Miller 1998).

Following successful formation of a lipoplexes, this is then delivered to a cell surface and the 'lipofection' process occurs. During this process the complex fuses with the cell membrane and becomes internalised (by endocytosis) to form an endosome (Monkkonen and Urtti

1998). During the process of maturation, the endosomal walls begin to rupture allowing the DNA to be released into the cytoplasm. From here the DNA can then move towards the nucleus, cross the nuclear membrane and potentially result in gene expression. Alternatively limited expression may be observed because the DNA may not reach the nucleus due to it being degraded within the cytoplasm by lysosomes. A simplified version of this process is shown in Figure 5.
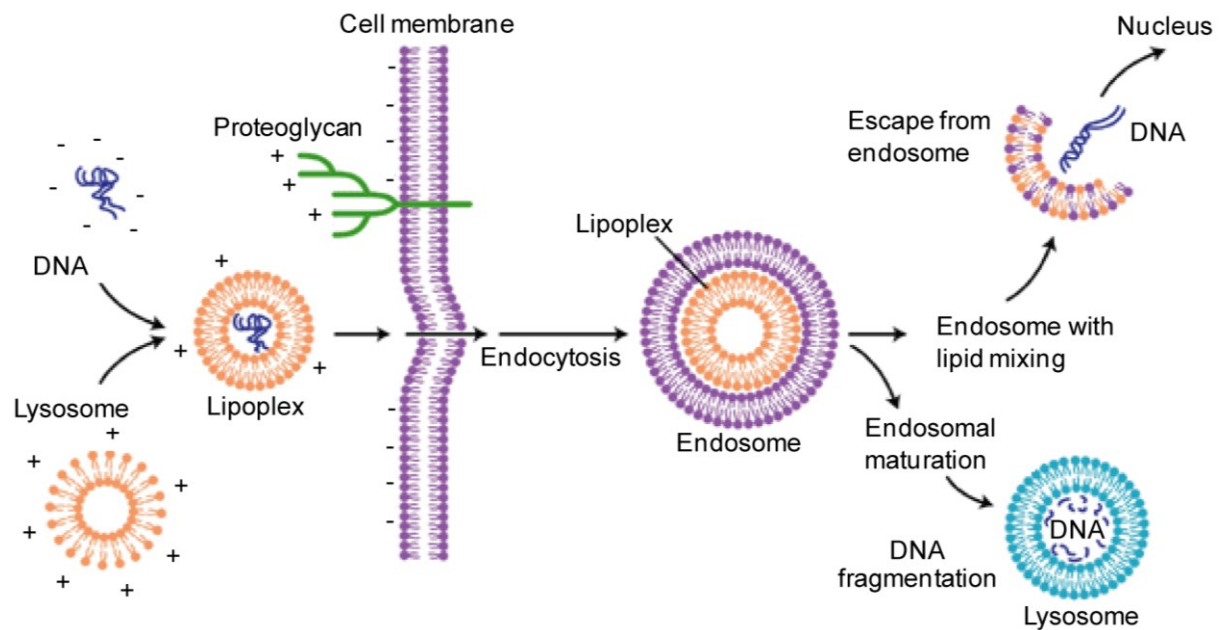
Figure 5: Liposome mediated transfection of DNA to form a lipoplex and the internalisation at the cell surface by endocytosis

Initially the liposome is complexed with DNA to form a liposome/DNA complex otherwise known as a lipoplex. This lipoplex is then added to cells in culture where it attaches to the cell membrane and becomes internalised by endocytosis. At this stage the DNA can be released and subsequently reaches the nucleus to allow successful gene expression, or it may become degraded by lysosomes within the cytoplasm (Parker, Newmanet al. 2003).

While lipoplexes show good levels of transgene expression *in vitro,* this is often not the case when applied to *in vivo* studies, where transgene levels are often very low or transient. Factors which may hinder the utility of liposomes *in vivo* could be the lack of stability and survival in the blood stream, as well as the size of the complex and electric charge (Smyth Templeton 2001). Furthermore serum proteins such as albumin which are negatively charged can also bind to the lipoplexes, causing a loss of cationic charge on the lipoplexes and in turn interfering with liposome-cell membrane associations. This can cause aggregates

to form which can lead to rapid clearance of these complexes by phagocytic cells. Ultimately these complexes disintegrate and the DNA becomes degraded preventing them from reaching the intended target cells.

Interestingly, modification of lipid and polymer complexes with hydrophilic polymers such as polyethylene glycol (PEG) can stabilise polyplexes against such inactivation. It is believed that PEG being hydrophilic is unable to interact with either DNA or cationic lipids. Therefore it provides longer circulation times of liposomes in blood circulation by minimising the binding of blood components and lipoplexes. However, this modification (PEGylation) has also been shown to cause an (dose-dependent) inhibition of transfection activity; in turn reducing the internalisation of untargeted polyplexes (Mishra, Webster et al. 2004). Furthermore PEGylated lipids are unable to efficiently condense DNA causing low stability of complexes in solution. Lipoplexes also appear to induce immune responses – albeit at a lesser extent than viral vectors – through the toll-like receptor 9 (TLR9) pathway which causes an increase of proinflammatory cytokines (Hemmi, Takeuchi et al. 2000; Ito, Kawakami et al. 2009). This has been shown to lead to vector-associated toxicity as well as the elimination of transfected cells and gene expression (Niidome and Huang 2002).

Due to these limitations *in vivo*, cationic lipids such as LipofectAMINE and LipofectAMINE 2000 (DOSPA/DOPE) are more readily only used for *in vitro* studies where they show good transfection efficiencies in many cell lines.

1.4.1.2 Cationic polymers (Polyplexes)

Cationic polymers constitute another category of DNA carriers that have been widely used for gene delivery. Cationic polymers - also known as polyplexes - are able to complex DNA in a similar way utilised by cationic liposomes mentioned previously, however they are able to condense DNA much more efficiently compared to lipid polymers. Many different types of polymers have been utilised for gene delivery including poly (L-lysine) (PLL) and polyethylenimine (PEI).

Poly-(L-lysine) (PLL) was one of the first class of cationic polymers used for gene transfer *in vivo* (Wu, Wilson et al. 1989). It is typically a polypeptide, composed of approximately 25-

30 amino acid lysine molecules, which possess a biodegradable nature making it highly desirable for *in vivo* studies. Despite this, PLL polyplexes rapidly bind plasma proteins and are cleared from the circulation in a similar way to liposomes (Ward, Read et al. 2001). Furthermore, PPL polyplexes alone have poor transfection abilities, and require the addition of chloroquine. Chloroquine is a lysosomotropic agent which reduces the lysosomal degradation of these lipoplexes; however, this still only results in moderate levels transfection. This is accepted to be the result of poor escape from the endocytic pathway. In general only PLL polymers with high molecular weights (> 3000 Da) are able to effectively condense DNA to form stable complexes (Kwoh, Coffin et al. 1999). Despite the effective condensing ability of high molecular weight PPL polyplexes, these compounds also exhibited relatively high cytotoxicity (Choi, Liu et al. 1998). Furthermore the heterogeneity in the chain length of commercially available PPL also results in inaccurate formulations. While the early studies on PPL were promising, their relatively low efficiency and high toxicity render them unfavourable for *in vivo* applications.

Contrary to PPL, polyethylenimine (PEI) is perhaps the most prominent example of a cationic polymer capable of efficient gene-delivery *in vivo.* Jean Paul Behr's group first introduced PEI in 1995 as an efficient and economical synthetic polymeric gene transfer agent (Boussif, Lezoualc'h et al. 1995). Importantly unlike PPL, PEI is able to mediate efficient levels of gene delivery in the absence of an exogenous endosomolytic agent. PEI exists as both a branched and linear structure differing in their structure and molecular weight (Figure 6). Several linear PEI transfection agents have been made commercially available, including ExGen500 and jetPEI, which are both linear derivatives of PEI (Ferrari, Moro et al. 1997). Linear PEI has been shown to mediate successful gene delivery *in vivo* into a wide variety of tissues, including the liver (Argyros, Wong et al. 2008; Wong, Argyros et al. 2011), lung (Wiseman, Goddard et al. 2003; Dif, Djediat et al. 2006), brain (Goula, Remy et al. 1998; Hassani, Franois et al. 2007), bladder (Ohana, Schachter et al. 2005) as well as the retina (Liao and Yau 2007). Furthermore the first used of jetPEI in a clinical trial included its use for complex formation with plasmid DNA (pDNA) and the successful transfection of tumour tissues (Ohana, Gofrit et al. 2004).
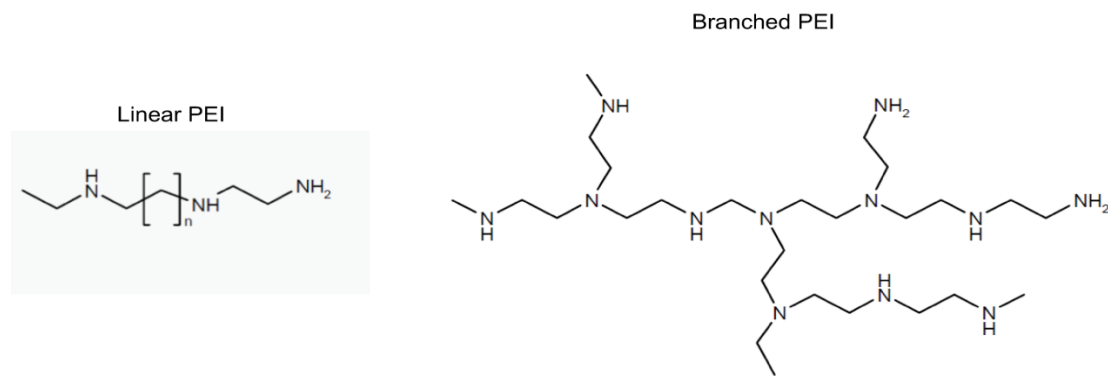
Figure 6: Structures of PEI

Cationic polymers can have a linear form such as Poly-(L-lysine) or a branched form such as PEI (Lavigne and Gorecki 2006).

Chemically, PEI is one of the most densely charged polymers; one third of the atoms are nitrogen and one sixth of the nitrogen atoms carry a positive charge at physiological pH. For PEI-mediated transfection, numerous factors determine the physical properties of PEI/DNA complexes (polyplexes) and their transfection activity. These can include: DNA-to-PEI ratios (the ratio between the amine groups from the PEI backbone (+) and the phosphate groups (-) of the nucleic acids – N/P ratio). Furthermore the molecular weight and configuration of PEI, the concentration of DNA as well as the polymer and the ionic strength of the solvent for preparation can also affect the properties of PEI/DNA polyplexes. Both linear PEI (L-PEI) and branched PEI (B-PEI) have excellent transfection efficiencies *in vitro*. However L-PEI is reportedly less toxic than its branched counterpart following systemic administration. This coincides with the fact that LPEI/DNA complexes are less condensed and are able to dissociate more efficiently than BPEI/DNA complexes. Studies have also revealed that LPEI/DNA complexes enter the nucleus more readily than branched complexes (Wightman, Kircheis et al. 2001).

Cellular trafficking usually directs the endocytosis of particles into lysosomes for degradation. Endosomes mature from an 'early' to 'late' stage when the pH drops from ~6 to ~5 via the active import of H^+ ions, and subsequently the endosomes fuse with lysosomes for degradation (Luzio, Mullocket al. 2001). Thus, the accumulation of polyplexes in endosomes would eventually lead to their degradation by the lysosomal enzymes and subsequently strongly limit gene transfer. Therefore gene transfer agents which possess

endosomolytic components should ensure early escape of polyplexes from lysosomes, resulting in enhanced transfection efficiency. Indeed, it has been proposed that the high gene transfer efficiency of PEI and its derivatives is due, at least in part, to their capacity to efficiently escape from the intracellular endocytic pathway through the 'proton-sponge' mechanism (Boussif, Lezoualc'h et al. 1995; Behr 1997) (Figure 7).
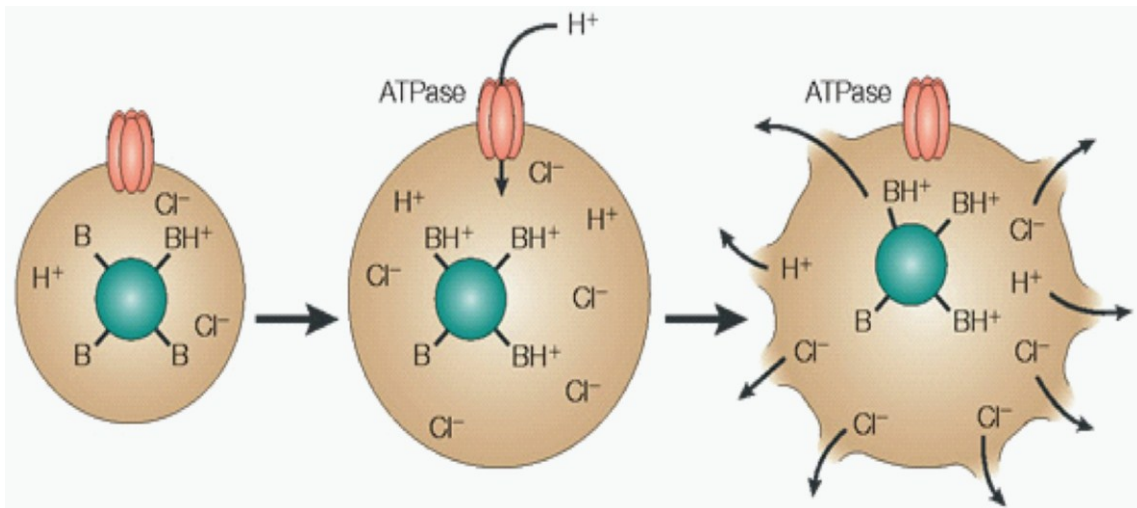
Figure 7: Schematic of the proton-sponge mechanism

Following the efficient condensation of DNA with PEI, PEI/DNA complexes interact with the cell membranes allowing the binding of complexes to anionic proteoglycans present at the cell surface, which facilitate entry into cells via endocytosis (*left* image). Within the cytoplasm, endosomes begin to mature following the activity of ATPase enzymes which actively transport protons (H^+ ions) from the cytosol into the endosomes causing a gradual decrease in the pH of the endosomes. As PEI contains 1 in 3 nitrogen atoms which are unprotonated/cationic, PEI lends itself to protonation during endocytic trafficking (*middle* image). The accumulation of protons in the endosomes must be balanced by an influx of counter ions (Cl^- ions). This increased ion concentration ultimately causes osmotic swelling and rupture of the endosomes membrane, which releases the polyplex into the cytosol (*right* image). Hence PEI is able to destabilise the endosomes by the 'proton-sponge' effect resulting in the escape of the polyplex from the endosomes (Pack, Hoffman et al. 2005).

At neutral or physiological pH, PEI is only partially protonated, with approximately one in three nitrogen atoms within the PEI remaining unprotonated/cationic. Hence due to this PEI lends itself to protonation. Therefore, within the endosome PEI acts as a 'proton-sponge' whereby continuous protonation of the remaining nitrogen atoms causes an influx of protons/chloride ions into the endocytic vesicles. This ultimately causes osmotic swelling and rupture of vesicles and the release of polyplexes into the cytoplasm (Boussif, Lezoualc'h

et al. 1995; Behr 1997). Complexes are then translocated into the nucleus followed by separation of DNA from the delivery vehicle PEI. The released DNA is then able to undergo transcription and translation; giving rise to protein production and gene expression (Thomas and Klibanov 2003). The presence of nitrogen atoms which are protonatable at low pH is a prerequisite for this 'proton-sponge' effect; indeed PLL, which possesses only primary amino groups and hence is incapable of further protonation, is a much less efficient gene transfer agent than PEI. Therefore PEI represents a versatile and promising approach to deliver naked DNA *in vitro* as well as *in vivo*.

1.4.1.3 Nanoparticles

A newer type of lipid based gene carrier is a solid-lipid nanoparticle and compared to traditional liposomes, these particles are reportedly easier to make as well as having a diameter of approximately 200 nm in diameter (Bondi, Azzolina et al. 2007). Nanoparticles can take many forms, and generally smaller particles (<25 nm) are considered to be more efficient at passing through the pores in the nuclear membrane, thus overcoming one of the significant barriers for successful transfection (Liu, Zhang et al. 2001). Gene delivery nanoparticles usually consist of a peptide of polymer base that condenses or encapsulates DNA. Some of the most commonly used nanoparticles include polylactide (PLA) - and polylactide co-glycolide (PLGA) - based particles and particles condensed with cationic polypeptides such as Poly-(L-lysine) (PLL).

The formation of polypeptide-based nanoparticles relies on the principle of DNA condensation. This principle relays on the idea that cells expand a significant amount of energy to keep DNA condensed enough to fit inside the nucleus, however importantly under specific conditions DNA is able to be condensed or compacted easier (Bloomfield 1997). Infact, a requirement for this to occur is the inclusion of a multivalent cation condensing agent, particularly because of the highly negative charge of the DNA backbone. These agents can vary from organic polyamines to inorganic polycations to polypeptides such as PLL. Ultimately, such condensing agents neutralize the negative charge on the DNA phosphate molecules, thus making the interactions between DNA and solvent less

favourable. This also enhances the attractive molecular forces and finally causes localised DNA bending which can encourage condensation to occur more readily (Bloomfield 1997).

The first case of utilising DNA compaction to generate gene therapy vectors was shown in 1979 by Wilson *et al.*, where they characterised a compact DNA particle of approximately 50 nm (Wilson and Bloomfield 1979). PLL has been used for nanoparticle compaction, however early studies involving compaction used high salt concentrations (~ 1M). This resulted in large variations in sizes of the condensed particles formed (ranging from 15-100 nm) (Perales, Ferkol et al. 1994; Perales, Grossmann et al. 1997).

In order to overcome the limitations of these high-salt particles, DNA was added in aliquots to a solution of lysine peptides, which were also sometimes coupled to PEG (Liu, Li et al. 2003). Following the addition of PEGylated PLL, these particles were observed to be of a neutral charge, homogenous in size and shape and consisted of only compact DNA. Importantly these DNA nanoparticles were observed to show limited aggregates hence were stable in physiological salt concentrations. The process of PEGylation involves the addition of repeat PEG molecules to proteins or polymers which ultimately increase the hydrophilicity and electrostatic binding properties as mentioned previously, as well as protecting compounds from degradation by cellular enzymes, thus increasing complex stability.

Current techniques in the PEGylation of PLL for the generation of nanoparticles involve mixing a purified 30-mer of PLL terminating with a single cysteine (CK30) and a methoxy-PEG10K-maleimide to create a covalently modified PEGylated CK30 peptide (CK30-PEG) (Liu, et Li al. 2003). These nanoparticles were shown to efficiently deliver genes to dividing as well as post-mitotic cells and have a plasmid capacity of at least 20 kb which is considerably more than that of viruses (~8 kb for Lenti and ~4.5 kb for AAV viruses)(Fink, Klepcyk et al. 2006; Liu, Li et al. 2003). Initial studies involved both CK30 and CK30-PEG nanoparticles carrying the luciferase gene under the control of the CMV promoter which were administered intranasally or intratracheally into the murine lung. Interestingly, when the CK30 compacted nanoparticles were delivered to the murine lung, no gene expression was observed in the airway tissue. However when CK30-PEG was used for compaction, efficient luciferase activity was observed in the airway. These results highlighted the importance of

PEGylation to improve transfection efficiency in vivo (Ziady, Gedeon et al. 2003). Furthermore these nanoparticles have also been used in clinical trials to deliver the cystic fibrosis transmembrane regulator (*CFTR*) gene to cystic fibrosis (CF) patients (Konstan, Davis et al. 2004) and are also being developed for the treatment of genetic brain diseases (Yurek, Flectcher et al. 2009).

Recently the same CK30-PEG nanoparticles were also shown to efficiently condense a CMV-EGFP containing plasmid vector (pZEOGFP5.1) for successful delivery to the eye (Farjo, Skaggs et al. 2006). Interestingly, the nanoparticles were able target most tissues within the eye by varying the site of injection (these will be described further in section 1.7.1). Following intravitreal injections, high levels of gene expression were observed in the lens of mice, while only moderate expression were found in the retina and little to no expression in the pigment epithelium/choroid/sclera (PECS). In contrast, after subretinal injection, expression in the retina and PECS was substantially higher than the lens. Furthermore gene expression was also observed in the outer nuclear layer (ONL) of photoreceptor cells, optic nerve head as well as in the extra-ocular muscle. Subsequently, nanoparticles were also used for the treatment of an inherited retinal degeneration - retinitis pigmentosa (rd - which is characterised as a progressive degeneration of the photoreceptor cells within the retina). Mice with rds were subretinally injected with nanoparticles containing the normal murine RDS cDNA driven by 1 of 3 promoters. Excitingly Cai *et al.* showed that following the subretinal delivery of these nanoparticles to the diseased mouse eye, nearly all photoreceptors were able to be transfected, resulting in a partial functional rescue of the retinitis pigmentosa disease phenotype (Cai, Nash et al. 2009).

These results highlight the utility of nanoparticles for *in vivo* studies, and current successes of nanoparticles for therapeutic gene therapy make this approach particular attractive for future clinical applications.

1.4.2   Barriers for non-viral delivery

For the non-targeted gene delivery of non-viral vectors using cationic liposomes or polyplexes, one of the first obstacles for efficient gene delivery is the extracellular membrane. Naked DNA is readily degraded by nucleases while transfection with cationic

lipids and polymers are often also hindered by hydrophobic negatively charged proteins such as albumin. The coating of the surface of liposomes with polyethylene glycol (PEG) has been shown to extend the circulation lifetime of vectors, due to the hydrophilic nature of PEG and its high ability to compact such polymers. However as mentioned before, PEGylated lipids are less efficient at condensing DNA, hindering ionic strength interactions and in turn reduce the internalisation of complexes into target cells (Mishra, Webster et al. 2004).

Non-viral gene delivery vehicles next face another barrier, the cell plasma membrane. The plasma membrane is composed of impermeable phospholipid glycoproteins that are crucial for the integrity of the cell as well as its contents. Apart from reducing in size, binding of cationic liposomes or polyplexes to DNA also imparts excessive positive charge. The positively charged polyplexes electrostatically interact with the cell membrane. This process is then followed by endocytosis, whereby localised regions of the plasma membrane invaginate and pinch off to form an endocytic vesicle. This can be a non-targeted charge-mediated step, or alternatively, depending on the size of complexes and the nature of the target cells, phagocytosis or receptor mediated endocytosis may be operational instead. Once in the cytoplasm, normal cellular trafficking usually directs endocytosed particles to lysosomes for degradation. Hence gene delivery agents must incorporate a mechanism of endosomal escape. Indeed, as mentioned previously, chloroquine is used alongside lipoplexes due to its ability to reduced lysosomal degradation, while PEI-based polyplexes are able to destabilise endosomal membranes and escape the endocytic pathway through the 'proton-sponge' mechanism.

Following endosomal escape, lipoplexes/polyplexes are then placed in the cytoplasm where they meet the next barrier. The cytoplasm is composed of a complex network of microfilament and microtubule systems as well as a variety of subcellular organelles. Within the cytoplasm the mobility of pDNA is severely impeded due to molecular crowding, immobile cytoplasmic obstacles as well as the association of pDNA with cytosolic DNA binding proteins. Indeed the lateral diffusion of macromolecules with comparable sizes to expression cassettes suggests that the mobility of pDNA is severely impeded in the cytoplasm, due to its large size (Dowty, Williams et al. 1995).

The nuclear envelope is the final and perhaps most challenging obstacle along the delivery pathway of pDNA. The trafficking and control of proteins and ribonucleoproteins to and from the nucleus is controlled by the nuclear pore complex (NPC), which forms an aqueous channel through the nuclear envelope. The size of the NPC channel is 25-30 nm and allows the passive diffusion of molecules below 40 kDa. In contrast molecules larger than 60 kDa usually contain a specific targeting signal (the nuclear localization sequence (NLS)) or associate with other polypeptides to pass through the NPC. Due to the size of pDNA, accumulating evidence suggests that pDNA is able to pass through the NPC via a mechanism reminiscent of the active transport of molecules larger than 60 kDa. Furthermore, the incorporation of a NLS to a vector may aid nuclear entry of pDNA into the nucleus by active transport (Lechardeur, Verkman et al. 2005; Clever, Yamada et al. 1991).

Once within the nucleus, the vector must provide sustainable transgene expression which will be discussed in section 1.5.

1.4.3 Gene transfer by physical methods

As an alternative to chemical gene delivery described in the earlier section, a physical approach can also be utilised. In such instances naked DNA (such as pDNA) can be delivered directly into the cytoplasm and thus bypassing the endosome and lysosomal degradation. The most common physical methods available include: direct injection, electroporation, sonication and gene gun.

1.4.3.1 Direct injection

The simple injection of pDNA directly into tissue without additional help from either chemical agent or physical force is the simplest approach one could use for gene transfer *in vivo.* This was discovered by chance by Wolff *et al.* in 1990, where they injected mouse skeletal muscle as a negative control for a gene delivery experiment with naked RNA and pDNA. To their surprise they observed expression for up to 2 months following injection (Wolff, Malone et al. 1990; Wolff, Williams et al. 1991). Since those initial studies, gene transfer with naked pDNA has been applied to the liver through direct intraportal injections

(Hickman, Malone et al. 1994; Budker, Zhang et al. 1996), to the skin through cutaneous injections (Choate and Khavari 1997) and to the lungs through airway instillations (Meyer, Thompson et al. 1995). Despite the broad applications of naked pDNA-mediated gene transfer, delivery by this method is highly inefficient and only 1% of injected DNA is taken up. Furthermore gene transfer is almost always limited to cells adjacent to the site of injection (Wolff, Williams et al. 1991).

1.4.3.2 Gene gun

Particle bombardment through a gene gun is an ideal method for gene transfer to skin, as well as tissues such as skeletal muscle that can be surgically exposed within a confined area. Naked DNA is deposited on the surface of gold particles, which are then accelerated by pressurised gas and expelled allowing direct penetration of cell membranes. However, the momentum only allows a short depth of the gold particle penetration, indeed in skeletal tissue this is less than 0.5 mm (Zelenin, Kolesnikov et al. 1997). Improvements to this approach include the chemical modification of the surface of gold particles to allow higher capacity and better consistency for DNA coating. Alternatively the fine tuning of the expelled force from the gene gun to control the final DNA distribution can also be utilised (O'Brien and Lummis 2002).

1.4.3.3 Ultrasound mediated permeabilisation

Another method for plasma membrane permeabilisation involves the application of focused ultrasound pulses at a specific site at which gene transfer is required. Ultrasound mediated permeabilisation was found to enhance reporter gene expression over that of naked DNA by up to 10-20 fold (Gao, Kim et al. 2007).The technique works on the principle that a medium such as naked DNA exposed to ultrasound experiences periodic pressure oscillations at the frequency and amplitude determined by an ultrasound source (Mitragotri 2005). However besides pressure oscillations, the most significant secondary effect of ultrasound application, namely cavitation (formation of gas bubbles in liquid due to ultrasonic pressure waves), can also induce fluid velocities, sheer forces and shock waves in surrounding tissues (Pecha and Gompf 2000). All of these effects cause a transient compromise of cell

membrane or tissue integrity, thereby achieving an enhanced uptake of applied naked DNA (Mitragotri 2005). Thus cavitation is believed to cause cell membrane permeabilisation, where application of ultrasound have been shown to enhance the transport and gene expression of naked DNA to cells (Fechheimer, Boylan et al. 1987; Liu, Lewis et al. 1998), as well as the skin (Mitragotri 2005), skeletal muscle (Taniyama, Tachibana et al. 2002a) and carotid artery (Taniyama, Tachibana et al. 2002b).

The transfection efficiency of this system is determined by several factors, including the frequency and output strength of the ultrasound applied, the duration of the treatment and the amount of pDNA used. To further enhance gene delivery, contrast agents such as air-filled microbubbles can be used, generating local shockwaves that transiently permeate surrounding cell membranes. Indeed studies have shown *in vitro* the combination of ultrasound exposure and microbubble-mediated gene delivery of DNA polyplexes can lead to a 300-fold increase in gene expression compared to that of naked DNA alone (Lawrie, Brisken et al. 2000).

Interestingly, focused ultrasound has also been shown to induce reversible and non-destructive disruptions of the blood-brain barrier which may facilitate drug delivery to the brain (Mesiwala and Mourad 2002). Moreover, ultrasound has also been utilised to enhance solute transport into the eye, where drug delivery was improved to the cornea with minimal changes to the corneal epithelium (Zderic, Clark et al. 2004), as well as ocular drug delivery for glaucoma (Zderic, Vaezy et al. 2002). While most studies utilising this technique have involved *in vitro* as well as *ex vivo* transfection, uses of ultrasound delivery *in vivo* are also slowly becoming more prevalent. The ability to precisely focus the required ultrasound beams within any tissue as well as the safety and possibility of repeat administrations makes this technique particularly promising for future clinical applications.

1.4.3.4 Electroporation

An alternative physical method for gene transfer includes electroporation which involved gene transfer based on the application of controlled electrical pulses. The principle being that the application of the electric field alters the structure of cell membranes such that transient pores are created through which large molecules like DNA - which normally cannot

permeate the membrane - can enter the cytoplasm (Andre and Mir 2004). Initially this technique was used *in vivo* in superficial tissues such as the skin and muscle, where long term episomal expression of pDNA expressing a dystrophin gene was observed in a mdx mouse model of Duchenne muscular dystrophy (Wolff, Williams et al. 1991; Wells 2004). Other examples include the pDNA administration through the portal vein followed by localised electroporation of rat liver. The results of this were widespread transfection of hepatocytes in the treated lobe but not in the surrounding lobes (Sakai, Nishikawa et al. 2005).

This raised the possibility that applied electroporation to selected areas can achieve localized gene transfer to specialised tissues and cells. Indeed electroporation has been successfully used in the eye, initially applied to the most accessible structure, the cornea (Oshima, Sakamoto et al. 1998, Oshima, Sakamoto et al. 2002). However it has also been used to deliver genes to the retinal ganglion cells in the adult rat retina following an intravitreous injection of pDNA (Dezawa, Takano et al. 2002; Mo, Yokoyama et al. 2002). Excitingly, subretinal injections of pDNA condensed with lipoplexes as well as naked pDNA alone following electroporation resulted in efficient transfection of the retinal pigment epithelial (RPE) cells in adult mice (Kachi, Oshima et al. 2005; Johnson, Berglin et al. 2008). Similarly, electroporation coupled with subretinal injections in adult mice have also facilitated the efficient gene transfer of non-viral nanoparticles into the RPE cells of the retina.

The utility of this technique is dependent on the accessibility of the target tissue to the DNA injection as well as the placement of the electrode. Thus, the protocol and highly skilled technique requires considerable adaptation for targeting different tissues, accounting for the differences in tissue densities and extracellular matrix compositions (Trezise 2002). Furthermore, substantial tissue damage and inflammation can occur if incorrect electric fields are applied. Considering these limitations, this approach is limited to broad clinical applications.

For delivery in specialised organs, such as the eye, specific routes of injection may be utilized. This would allow the delivery of pDNA and transfection of different tissues within

the eye by varying the site of injection. This will be described in more detail in section 1.7.

1.5   Regulation of transgene expression

In gene therapy, the amount of therapeutic correction one sees is dictated by the success of gene transfer one can achieve. Therefore following the successful delivery of genetic material to the target cells of interest, successful protein expression is required for a therapeutic benefit. This can be done by increasing the amount of protein produced by cells, or by increasing the number of transfected cells. As non-viral vectors may have limited transfection efficiencies, the need to have an optimal expression cassette which yields maximum therapeutic protein levels is essential. Currently, gene therapy vectors have common expression cassettes under the control of a promoter. The simplest approach would be to change the expression of a transgene cassette with the addition of an S/MAR moiety as well as a promoter to drive the strongest expression specific to target cells.

1.5.1   Choice of promoter

The promoter is a stretch of DNA which contains specific DNA sequences recognised by proteins as transcription factors. Arguably it is the key regulatory element which determines the strength of transgene expression from a pDNA vector. Transcription factors are able to bind to promoter sequences and in turn recruit RNA polymerase, the enzyme which is required for the synthesis of RNA from the coding region of a gene. Eukaryotic promoters are often diverse however typically they lie upstream of genes and have regulatory elements which can be as much as several kilobases away from the transcriptional start site. Promoters can be ubiquitously active or have specific tissue restricted activity, depending on the expression profile of the transcription factors which bind to them and are crucial for their activity.

1.5.1.1 The CMV promoter

One of the most commonly used promoters for gene therapy includes the promoter from the immediate early gene of the human cytomegalovirus (CMV). Its popularity rose from the extremely strong expression it confers in most cell types tested *in vitro* (Boshart, Weber et al. 1985). Since the CMV promoter was considered as one of the strongest promoters *in vitro,* it has also been utilised for many studies *in vivo* to show strong expression of reporter and therapeutic genes. However one of the drawbacks in using promoters of viral origin - including the CMV promoter as well as others such as the simian virus 40 early promoter (SV40) - is that eukaryotic organisms have evolved strategies in defence of viral pathogens. Indeed they are efficiently able to detect and subsequently stop the transcription of the viral genes. Thus strong expression *in vivo* is only short-term, where peak transgene expression typically is either 1 or 2 days following vector delivery. Importantly however within weeks of transfection, transgene expression is barely detectable or above background activity in many animal studies. This silencing of the CMV promoter has been attributable to the elimination of transduced cells extracellularly by the immune system through cytokine inhibition (Zhang, Ni et al. 1995) as well as the activation of repressor proteins that can cause methylation (Zhang, Ni et al. 1995; Sinclair, Baillie et al. 1992).

Alternatively a wide variety of ubiquitously expressed eukaryotic promoters have also been described which unlike viral promoters do not invoke such defensive responses from transduced cells or the host immune system. While most eukaryotic promoters are typically not as strong as their viral counterparts, they have the advantage of providing more sustainable transgene expression.

1.5.1.2 The CAG promoter

The CMV early enhancer/ chicken β-actin promoter (CAG or CBA) is 1.7 kb and is composed of: a CMV enhancer and a chicken β-actin promoter fused to 90 nucleotides of exon one of the chicken β-actin gene, 917 nucleotides of a hybrid chicken β-actin/ rabbit β-globin intron and 55 nucleotides of rabbit β-globin exon. This promoter is ubiquitously expressed and was first used to facilitate high levels of AAV-mediated gene expression in the brain

(Kaemmerer, Reddy et al. 2000). Furthermore this promoter has also been successfully used for retinal transduction, where successful long-term expression in the mouse RPE and photoreceptor cells have been observed following the subretinal injection of an Ad virus (Cashman, McCullough et al. 2007). Following this, similar successes were also observed using AAV-vector mediated gene replacement (by the CAG promoter) of the RPE65 gene in a canine model of childhood blindness, Leber congenital amaurosis (LCA). This study showed long-term restoration of photoreceptor cell function in the treated dogs (Acland, Aguirre et al. 2005). Following these significant results with the CAG promoter and lack of toxicity or immune response *in vivo*, this paved the way for three clinical trials for *RPE65* gene-replacement in patients with LCA (Cideciyan, Aleman et al. 2008; Hauswirth, Aleman et al. 2008; Maguire, Simonelli et al. 2008). These studies validate the clinical significance and importance of this promoter in the use of non-viral vectors for ocular gene therapy.

1.5.1.3 The EFS and EF1α promoter

Most eukaryotic cells express the polypeptide chain elongation factor-1α (EF1-α) which is responsible for the enzymatic deliver of GTP-dependent binding of aminoacyl-tRNA to ribosomes. Hence the gene has a house keeping function in all cells and is expressed in high level. Most importantly, due to its indispensible housekeeping function in all cells, EF1-α promoter expression is consistent and relatively insulated from changes in cell physiology and is cell type independent (Kim, Uetsuki et al. 1990; Wakabayashi-Ito and Nagata 1994; Goldman, Cutrone et al. 1996). An intronless version of this promoter also exists and is called the elongation factor 1 short (EFS), corresponding to the nucleotides 378-610 of the EF1-α gene. Expression from the EF1-α promoter has been shown to result in 10-fold lower expression compare to the CMV promoter following instillation to the lungs. However perhaps more importantly, transgene expression conferred by the CMV promoter was rapidly lost, while that of the EF1-α promoter was still detectable at 4 weeks post administration (Gill, Smyth et al. 2001). Furthermore the intronless version of this promoter, EFS has been shown to ubiquitously express transgenes broadly throughout the entire retina. This includes EFS facilitating GFP transgene expression in RPE cells, inner nuclear

layer (INL) cells of the photoreceptors as well as glial cells of the retina (Kostic, Chiodini et al. 2003).

1.5.1.4 The Ubiquitin C promoter

The ubiquitin C (UbC) promoter drives the expression of three known human ubiquitin genes, UbA-C. Ubiquitin is abundantly expressed in all eukaryotic cells and is responsible for marking proteins for destruction by attaching covalently to abnormal, misfolded or short-lived proteins. Importantly, in transgenic mice, the UbC promoter has been shown to facilitate strong ubiquitous expression (Schorpp, Jager et al. 1996). Furthermore, when contained in a pDNA, UbC is able to mediate high-levels of reporter gene expression for up to two months following delivery to the lungs. However expression was seen to gradually decline and by 6 months following administration expression was lost (Gill, Smyth et al. 2001).

1.6   The eye as a target organ
1.6.1   The retina

The retina is the most metabolically active tissue within the body and is the primary light sensing organ in vertebrates. In humans it is approximately 0.5 mm thick and lines the interior surface at the back of the eye. The light is it initially focused through the lens and then detected by the retina, where it is converted into signals that reach the brain through the optic nerve. The eye contains three chambers of fluid: the anterior, posterior and vitreous chambers. A radial section of a portion of the retina reveals that the ganglion cells are found on the inner most layer closest to the lens and the front of the eye. The ganglion cells function as the output neurons of the retina, forming long axons that extend into the brain together allowing the transmission of visual information from the retina to the brain. Collectively the axons of the ganglion cells make up the optic nerve. The other layer is the neural sensory retina which is composed of the photoreceptor cells, of which there are two types: rods and cones. These are the crucial photosensory cells which detect a photon of light and subsequently create the electrical signal that is crucial for vision. Photoreceptors lie against a monolayer of specialised epithelial cells called the retinal pigment epithelium

(RPE). RPE cells are the highly pigmented cells that firmly attach to the underlying choroid. The choroid contains the blood vessels that supply the retina with nutrients and oxygen as well as removing its waste products.

Between the photoreceptors and the ganglion cells there are many interneurons found within this region of the retina. All vertebrate retinas are composed of three further layers of nerve cell bodies and two of synapses. The three nerve layers are: (i) the outer nuclear layer (ONL) comprising of the rod and cone photoreceptors, (ii) the inner nuclear layer (INL) contains cell bodies of the bipolar cells, horizontal and Amacrine cells and (iii) the ganglion cell layer which contains cell bodies of ganglion cells and displaced Amacrine cells. The horizontal cells relay messages back and forth between the photoreceptor cells, the bipolar cells and each other. While the Amacrine cells are interconnected with the bipolar cells, the ganglion cells as well as each other. Both these types of interneuron cells play a major role in the processing of visual information at the level of the retina before it is passed to the brain for interpretation. The retina also has two layers of neuronal interconnections dividing these nerve cell layers: the outer plexiform layer (OPL) and the inner plexiform layer (IPL).

At the center of the retina is a region of approximately 5mm in diameter called the macula. Near the center of this is the fovea, a small region which contains the highest concentration of cone cells in the eye and is responsible for central and high acuity vision. This is evident by the fact that loss of peripheral vision may go unnoticed for some time, however damage to the macular causes loss of central vision which is usually immediately obvious. The progressive deterioration and loss of the macula is the primary consequence of age-related macular degeneration. The summary of the anatomy of the eye and the retinal architecture are shown in Figure 8.
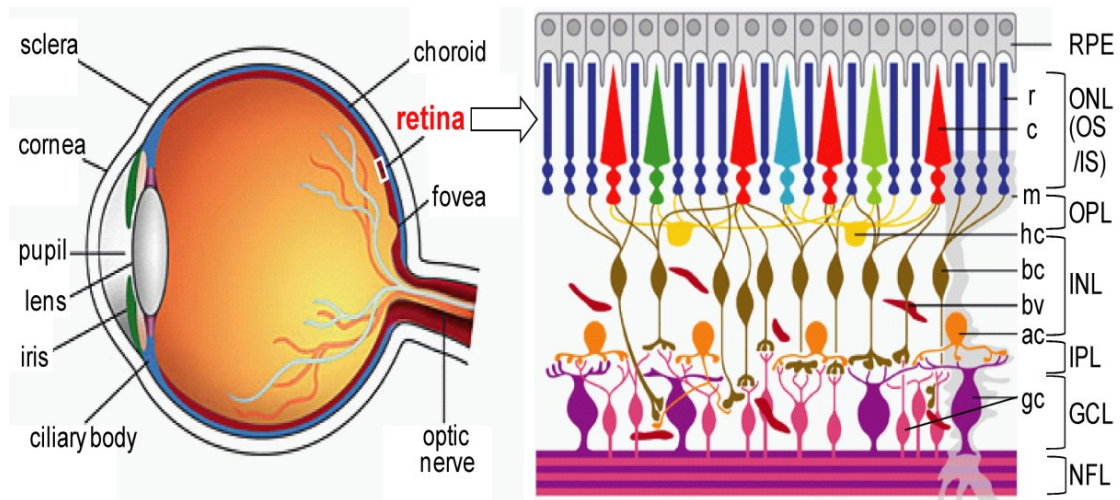
Figure 8: Anatomy of the eye and enlargement showing the organisation of the retinal architecture

The process of light detection and visual cycle occurs in the photoreceptors (constituting rod (r) and cone (c) cells) and retinal pigment epithelium (RPE) of the retina. Specifically, light is detected in the photoreceptor outer segments (OS). Photoreceptor outer and inner segments (IS) constitute the outer nuclear layer (ONL). Photoreceptor synapses with horizontal cells (hc) and bipolar cells (bc) constitute the outer plexiform layer (OPL). Horizontal, bipolar and Amacrine cells (ac) constitute the inner nuclear layer (INL). Bipolar and Amacrine cells synapse with ganglion cells (gc) of the ganglion cell layer (GCS) in the inner plexiform layer (IPL). Blood vessels (bv) as well as glial Müller cells (m) are seen throughout the neural retina. The nerve fiber layer (NFL) is formed by the expansion of the axons from ganglion cells which make up the the optic nerve (Figure adapted from (Kolb 2003)).

1.6.1.1 Retinal cycle

The human eye constantly metabolises vitamin A to function properly in a process known as the visual/retinal cycle. This process takes place in the photoreceptors and RPE of the retina and involves a series of enzymatic reactions. One particular enzyme, RPE65 which is the most abundant protein in the RPE, is crucial for the conversion of dietary vitamin A all-trans retinol into its derivative form 11-*cis*-retinol, which is taken up by the photoreceptor cells for processing of vision. In vertebrates, light detection is mediated by the photoreceptor cells, specifically within the rod and cone cells. Both cells consist of the two parts: the outer segments and inner segments. It is the outer segments which contain the machinery responsible for the biological conversion of a photon of light into an electrical signal (within the retina) – this process is referred to as visual phototransduction.

The sequence of events to generate signal to the brain for twilight (scotopic) and monochrome vision occurs in the rod cells, while for daylight (photopic) and colour vision this occurs in the cone cells (Shichida and Imai 1998). Both rod and cone cells consist of two parts, the outer segment (OS) and inner segment (IS). The OS contains the machinery responsible for this process, namely the light-absorbing pigment, opsin, which also contains the retinal chromophore 11-*cis*-retinal. Upon absorption of light by the pigment cells, the chromophore undergoes a photoisomerisation, or change in molecular arrangement, from 11-*cis*-retinal to all-*trans*-retinal. Following this isomerisation, this induces a conformational change in the photo-bleached opsin pigment which leads to the activation of an enzyme cascade to evoke a light response leading to vision (Lamb and Pugh 2006; Fu and Yau 2007). The product formed after light induction, *all-trans*-retinal, is then released from the opsin protein into the cytoplasm (Liu, Itagaki et al. 2000). Once in the cytoplasm, *all-trans*-retinal is reduced to *all-trans*-retinol (Vitamin A). This form of retinol then exits the photoreceptors, crosses the subretinal space bound to the interphotoreceptor retinoid binding protein (IRBP), and enters the RPE (Bunt-Milam and Saari 1983; Ala-Laurila, Crouch et al. 2006; Wu, Blakeley et al. 2007) .

In the RPE, *all-trans*-retinol is first esterified by lecithin-retinol acyltransferase (LRAT) (Saari and Bredberg 1989) and then simultaneous hydrolysis and isomerisation of all-*trans* esters yields 11-*cis*-retinol. This coupling of isomerisation and hydrolysis is facilitated by a single enzyme, the isomerohydrolase enzyme RPE65 (Redmond, Yu et al. 1998; Moiseyev, Chen et al. 2005). Indeed, RPE65 is essential for the regeneration of 11-*cis* retinoids, and there is no isomerohydrolase activity in its absence (Redmond, Poliakov et al. 2005). Finally, 11-*cis*-retinol from the isomerohydrolase reaction is oxidised to 11-*cis*-retinal (Simon, Hellman et al. 1995). The newly generated 11-*cis*-retinal is then transferred back to the outer segments where it can again be conjugated to an opsin protein; restore the light sensitivity of this protein and in turn regenerating the visual pigment to complete the cycle. It is this cycle of generation of 11-*cis*-retinal from all-*trans*-retinol and regeneration of all-*trans*-retinol from 11-*cis*-retinal which is known as the visual cycle (Figure 9A) and is essential for the continuous processing of vision.

Our current understanding of the visual cycle is largely based on studies from the rod photoreceptors (McBee, Palczewski et al. 2001). Cone photoreceptors are believed to rely

upon this same system; however they are also thought to have privilege to an alternative visual cycle pathway within the inner retina. Indeed there is growing evidence for a cone specific pathway involving the cone photoreceptors and the Müller glial cells of the inner retina (Znoiko, Crouch et al. 2002)(Figure 9B). Central to this theory is the ability of cone cells to regenerate 11-*cis* retinal from 11-*cis* retinol supplied to the inner segments (Jones, Crouch et al. 1989). In this proposed cone visual cycle, it has been suggested that that the all-*trans*-retinol generated in the photoreceptors is transported to the Müller cells and isomerized to 11-*cis* retinol by an unidentified isomerise. Following this, 11-*cis* retinol from the Müller cells then enters the inner segments of the cone photoreceptors and is oxidised to 11-*cis* retinal for visual pigment formation. Interestingly, the cone inner segments are in close proximity to the apical microvilli of Müller cells. These microvilli contain a retinoid binding protein which has a high affinity for 11-cis retinoids; cellular retinoid binding protein (CRALBP) (Bunt-Milam and Saari 1983). Furthermore, Müller cells have the ability to generate 11-*cis* retinol from *all-trans*-retinol (Das, Bhardwaj et al. 1992). Finally, IRBP which acts as a transporter in the visual cycle discussed earlier, appears to co-localise with the microvilli and is found in high concentrations around cone photoreceptors (Carter-Dawson and Burroughs 1992; Gonzalez-Fernandez, Baer et al. 2003). While the relationship between IRBP, Müller cells and cone inner segments in the cone-specific pathway still remains unproven, it may explain the ability of cone cells to function and efficiently regenerate visual pigment in conditions of constant light/daylight.
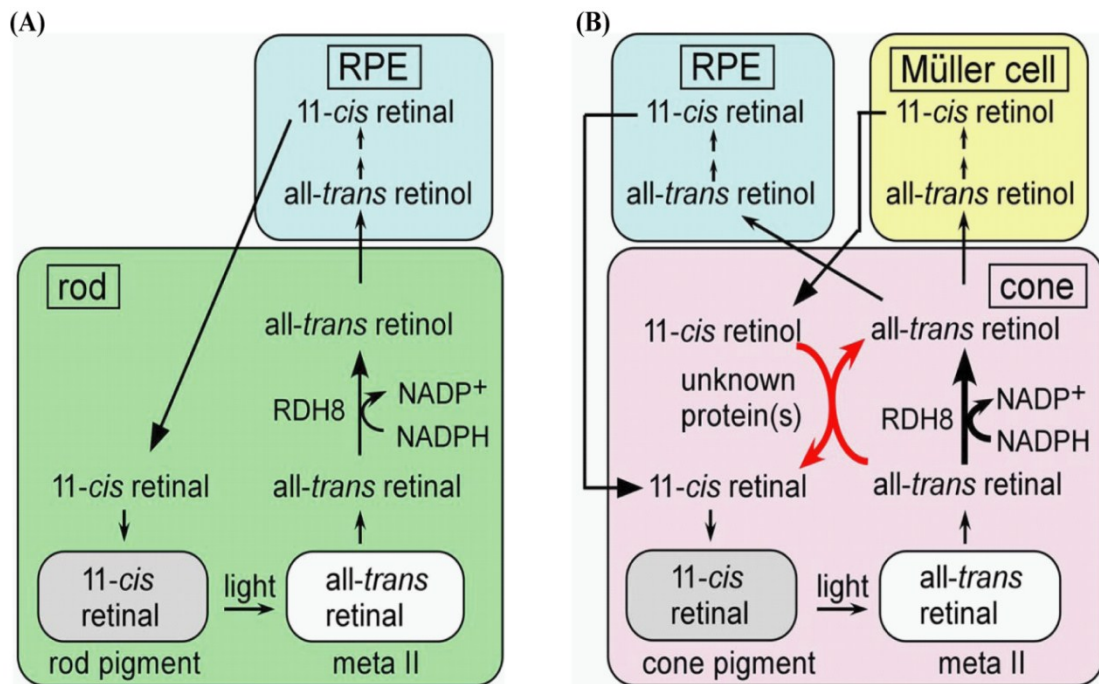
Figure 9: The rod and cone visual cycle

Shown is a scheme to show the current supported visual cycle of (A) rod and (B) cone photoreceptor cells. After absorption of light by the photoreceptor outer segments (OS), the visual pigment chromophore, 11-*cis* retinal, is isomerized to all-*trans* retinal. Following this all-*trans* retinal is detached from the opsin and reduced by the enzyme retinol dehydrogenase 8 (RDH8) to all-*trans* retinol. This reduced retinol is then transferred to the RPE where the all-*trans* from is isomerized into 11-*cis* form and is subsequently oxidised to 11-*cis* retinal. Following this 11-*cis* retinal is transferred back to the OS of rod cells to regenerate visual pigment. (B) A similar pathway of the visual cycle for cones is seen. However, in cones an additional pathway for the production of 11-*cis* retinal is present. In this alternative pathway, 11-*cis* retinol supplied from Müller cells is converted to 11-cis retinal (Miyazono, Shimauchi-Matsukawa et al. 2008).

1.6.1.2 The Photoreceptors

There are two types of photoreceptors, the rods and cones, each having a distinctive morphology, indeed the names of the respective cells come from their shapes (Figure 10). They are comprised of an outer segment, which contains membrane disks filled with photosensitive pigments called opsin proteins. The outer segment is connected through a cilium to the inner segment which contains mitochondria. Following this is the main cell body which contains all the organelles, and finally the synaptic endings where release of neurotransmitters occurs.
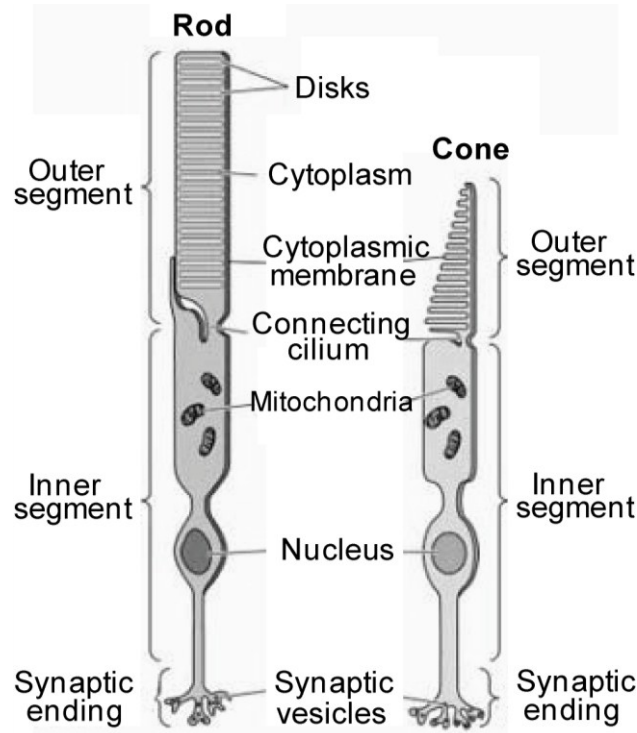
Figure 10: Generalised picture representing the structure of a vertebrate rod and cone photoreceptor

A schematic showing the structure of a vertebrate rod (*left*) and cone (*right*) photoreceptor. In rod photoreceptor cells opsins and photopigments are embedded in membranous disks of the outer segments. Distal tips of the outer segments are shed daily and phagocytosed by RPE cells before being recycled back to the photoreceptors. Cone photoreceptor cells have a similar cell body structure with the exception that outer segments appear shorter with a more conical morphology (Figure adapted from (Colella, Cotugno et al. 2009)).

Rod cells are concentrated at the outer edges of the retina and are used for peripheral vision. They are able to function under scotopic conditions (dim light) and are almost entirely responsible for night vision. This ability come from the fact that they are structurally narrower than cone cells as they have a higher area for visual pigment thus a substantial higher efficiency of light absorption in the retina. As vertebrates only possess light-sensitive pigment, rods have little if any role in colour vision.

Cone cells in contrast sense light under photopic (bright light) conditions. They are densely localised in the fovea, and gradually become sparser towards the periphery of the retina. While cone cells are less sensitive to light than rod cells (which detect low levels of light), they allow the perception of colour. In humans, there are three types of pigmented cells in

cone cells which provide basic colour vision. Each type of pigmented cell responds and has the greatest sensitivity to light from a different portion of the spectrum of visible light. These include sensitivities to short (S,~ 430nm, blue light), medium (M, ~ 530nm, green light) and long (L, ~ 560nm, red light) wavelengths of light (Terakita 2005). Hence colour vision is achieved with these cone-opsin based pigments with different colour sensitivities.

Visual transduction occurs in photoreceptor outer segments, with the photo-isomerisation of opsin bound 11-*cis* retinal (chromophore), as described earlier in section 1.6.1.1. The outer segments contain stacks of membranes/disks in which the opsin and chromophore complexes are embedded.

1.6.1.3 The Retinal Pigment Epithelium

The RPE is a pigmented layer that is found just after the neurosensory photoreceptor cells within the retina. It is an apically polarised monolayer which is essential for the function of photoreceptor cells and forms a part of the blood-brain barrier. The apical membranes of the RPE are lined with long microvilli which extend into the inter-photoreceptor space allowing the continual contact between the photoreceptor outer segments and the RPE. Indeed, each RPE cell is in contact with between fifty and one hundred photoreceptors, thus allowing the synergistic interaction of these tissues (Strauss 2005). Such integrations include the visual cycle, in which following light transduction retinal cycles between the photoreceptors (from all-*cis-* to all-*trans* retinal) and RPE (from all-*trans-* to all-*cis* retinal), a process essential for maintaining photoreceptor excitability. Another example is the phagocytosis of shed photoreceptor outer segments by RPE cells and the recycling of essential substances to be returned to the photoreceptors to rebuild light-sensitive outer segments from the base of the photoreceptors. As shown in Figure 11, the RPE performs multiple functions within the retina, many of which are also essential for the normal function of photoreceptor cells.
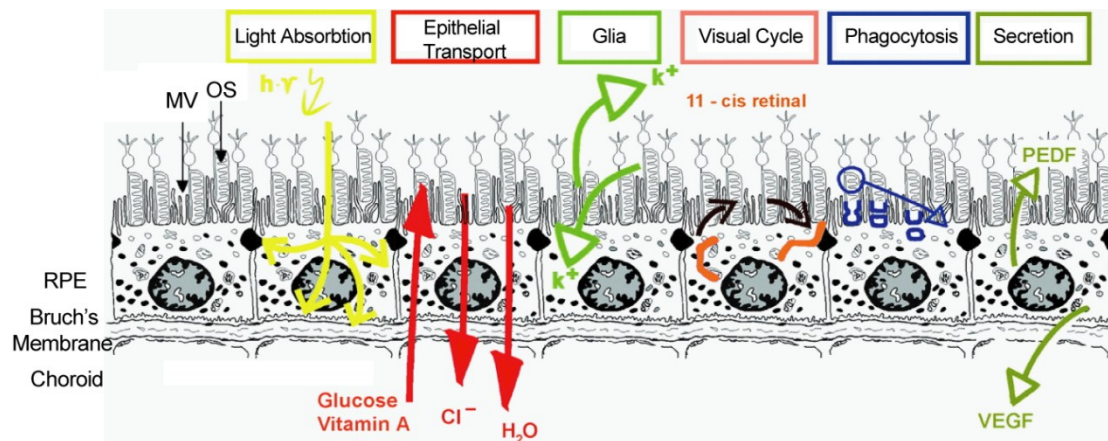
Figure 11: Functions of the Retinal Pigment Epithelium

The RPE performs numerous functions in supporting and maintaining the photoreceptor cells. Apical microvilli (MV) from the RPE extend into the photoreceptor outer segments (OS). The choroidal capillaries lie underneath the RPE and provide circulation for the retina. VEGF, vascular epithelium growth factor, PEDF, pigment epithelium derived growth factor (Figure adapted from (Strauss 2005)).

The RPE takes up nutrients such as oxygen, glucose, retinol (vitamin A) and fatty acids from the choroidal blood flow and delivers these to the photoreceptors. At the same time metabolic end products from the photoreceptors are removed from the inter-photoreceptor space for recycling via the RPE. The RPE is also able to secrete a variety of growth factors to help promote the survival, proliferation and differentiation of retinal cells.

With these complex different functions, the RPE is essential for visual function and a failure of any of these functions can lead to retinal degeneration, loss of visual function and blindness.

1.6.1.4 The Choroid

Encompassing the outer retina is a network of capillary vessels called the choriocapillaris, or better known as the choroid. The choroid receives the greatest blood flow (65-85%) (Henkind, Hansen et al. 1979) and is vital for the maintenance, supply of oxygen and nutrients to the outer retina particularly the RPE and photoreceptor cells. The remaining 20-30% of intra-ocular blood vessels support and nourish the inner retinal layers such as the neurons apical to the ONL. The choroid lies beneath the Bruch's membrane and the RPE,

and similar to the RPE, the choroid also contains pigmented cells to prevent damage from light to surrounding tissue.   A range of retinopathies have been well characterised in recent years, all of which arise due to problems and deterioration within any of the three key cell layers of the retina described above (choroid, photoreceptors and RPE). These diseases as well as the delivery routes used will be highlighted in more detail in the following sections.

1.7   Goals of Gene therapy – targeting eye disease

Gene therapy holds great promise for the treatment of eye diseases, and proof-of-principle as well as its efficacy have been provided by viral vectors and will be discussed in the following sections.

The eye is an excellent target for gene therapy due to its high accessibility and its unique compartmentalisation, allowing various routes of gene delivery to target different cell layers or cell types within the eye. Furthermore, the small tissue volume and size allow for low vector and/or gene doses in the eye. Unique to the eye is the presence of a blood-retina barrier which limits vector and/or gene leakage into the circulation and gives the eye a useful immune privileged status. This is highly advantageous as this significantly limits the immune response to vector components as well a transgenes. Furthermore many disease causing genes which lead to retinal degenerations have been identified. The availability of numerous animal models which have been created that showing considerable resemblance to the specific human pathologies is also an invaluable tool. This is particularly necessary for the validation and functional examinations in therapeutic gene therapy studies. Furthermore such models also enable clinical applications to be possible. The contralateral eye is also an invaluable control within ocular gene therapy, as this eye can either remain untreated or is treated with vehicle alone, while the other eye is subjected to the required treatment. Finally, the external layers of the retina (*in vivo*) can be easily monitored for function, morphology and retinal integrity using techniques such as scanning laser ophthalmoscopy (SLO) and electroretinography (ERG) as well more complex tests such as afferent pupillary light responses (PLRs).

1.7.1 Barriers for retinal gene delivery using non-viral vectors
1.7.1.1 Delivery routes for ocular gene therapy

Gene delivery to ocular tissues can commonly be performed through topical applications
(via eye drops) and injections including: intracameral injections, subconjunctival injections,
intravitreous injections as well as subretinal injections (Figure 12). Each technique allows
different regions of the eye to be transfected and these methods will be discussed in the
next section.
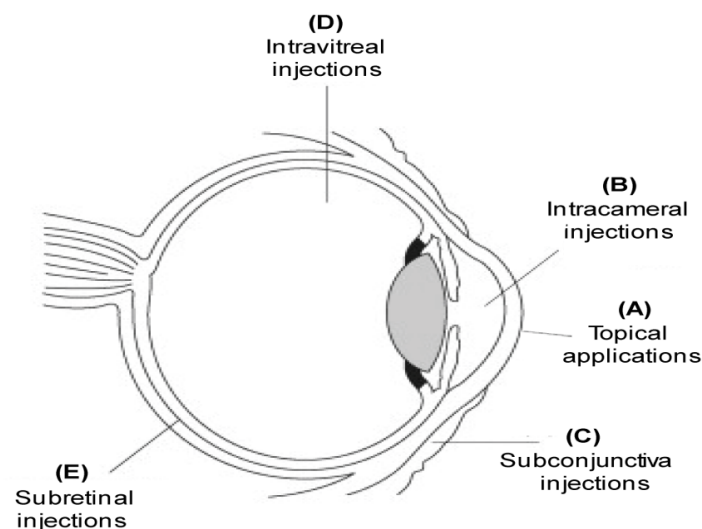
Figure 12: Delivery routes for ocular gene therapy

Gene delivery to the eye can be performed through several routes depending on the cell
to be targeted and the specific features of the vector used for gene delivery:
(A) Topical applications, (B) Intracameral injections, (C) Subconjunctival injections,
(D) Intravitreal injections and (E) Subretinal injections (Figure adapted from (Colella,
Cotugno et al. 2009)).

1.7.1.2 Topical applications and intracameral injections

Topical applications are the primary route of drug delivery to the anterior segment of the
eye. This route is relatively non-invasive, free from systemic side effects and easy to apply,
with either a punctal occlusion or gentle lid closure to minimise systemic drug absorption
(Figure 12A). A puncal occlusion is a procedure where some or all of the puncta in the eyes
are blocked. Puncta are small openings located on the nasal part of the inner eye lids,
through which tears drain. By blocking these openings, the surface of the eye becomes
more lubricated as the drainage of tears slows down.

To determine the most appropriate route of delivery in the eye, specifically to the retina and RPE, topical instillations as well as systemic administration are not a practical choice in gene delivery. The lack of extravasations into the eye after intravenous administration due to the presence of the tight blood-retina barrier (Duvvuri, Majumdar et al. 2003), means that systemic administration is not a practical choice in retinal gene delivery. Similarly, many features of the cornea, such as the topical ocular administration of small-molecular-weight compounds show limited diffusion across the large corneal surface to the retina (Tonjum 1974; Tonjum 1977; Maurice and Mishima 1984; Weinreb 2001). This is mainly due to the cornea being protected from environmental substances by rapidly secreted tears to flush its surface as well as the corneal epithelium being highly impermeable with tight junctions between cells (Maurice and Mishima 1984; Weinreb 2001; Rosenblatt and Azar 2004).

Despite this, previous reports show expression (of β-galactosidase (β-gal)) in various ocular tissues including anterior chamber, cornea, iris, choroid sclera, conjunctiva, RPE and the vitreous body after topical administration of (non-ionic PEO-PPO-PEO) polymer micelles (PM) with pDNA (pCMV-Lac Z pDNA) via eye drop delivery (Liaw, Chang et al. 2001). Expression was shown to be enhanced when pretreatment was carried out with cytochalasin B and ethylenediaminetetraacetic acid (EDTA), which are both known to open tight junctions of the corneal epithelium. This in turn enhances paracellular transport of formulated genes for further penetration of DNA to tissues other than the cornea (Madara, Barenberg et al. 1986). Furthermore, increases in intracellular calcium levels can also lead to increases in endocytosis which also help encourage complex uptake (Lam and Cullis 2000). While the mechanism of EDTA transport, whereby calcium can stimulate uptake of pDNA is not clear in the cornea, it appears that the internalisation and the transport mechanism of pDNA in the cornea may be influenced by endocytosis and enhanced (penetration) through the opening of tight junctions in the corneal epithelium.

As an alternative to topical instillations, direct injection into the anterior chamber of the retina - via an intracameral injection - can also be utilised to allow the transfection of anterior eye segment tissues (Figure 12B). This approach has been particularly useful for the delivery of secreted anti-inflammatory molecules to reduce inflammation after corneal transplantation. However, similar to the topical route, intracameral injections although effective for anterior segment disorders, this technique does not result in significant retinal

concentrations of most molecules (Maurice 2002).

1.7.1.3 Subconjunctival injections

Periocular routes of delivery are another method considered less invasive than direct injection into the retina and one such route includes the subconjunctival route. This route is performed by injecting vectors directly under the conjunctival membranes of the eye (Figure 12C). This route for delivery has been particularly useful for vector-mediated delivery of secreted antiangiogenic proteins that are able to enter the eye from the periocular space for treatment of neovascular diseases (Gehlbach, Demetriades et al. 2003). Periocular routes exploit the permeability of sclera for retinal drug delivery, as well as being particularly useful for the administration of sustained-release systems of potent drugs. While this route appears to be most suitable for the treatment of posterior segment ocular disorders, limited transfection of the retina has been observed; most likely due to the clearance of drugs via the choroidal circulation.

1.7.1.4 Intravitreous injections

Contrary to the methods described earlier, direct injection into the vitreal space / vitreous body is another route of delivery in the eye (Figure 12D). This route allows the transfection of the inner most cell layers of the retina. In particular this method has been useful for the treatment of inner retinal neovascularisation as well as glaucoma (Murata 2001; Gehlbach, Demetriades et al. 2003; Shahar 2006).

Importantly intravitreous injections are not suitable for delivery to photoreceptors in the outer retina because, injected vectors would need to diffuse through the vitreous – which functions as a molecular sieve restricting the diffusion of large molecules – as well as the neural retina before reaching the RPE (Maurice and Mishima 1984; Bishop 2000).The vitreous is made up of water (98%) and colloids (0.1%), with the rest of the solid material being ions and low-molecular-weight solutes (Pitkanen, Ruponen et al. 2003). The two major structural components of the vitreous are collagen (40-120 µg/ml) and hyaluronic acid (100-400 µg/ml) (Pitkanen, Ruponen et al. 2003). Hyaluronan is the most common

negatively charged glycosaminoglycan (GAG) in human vitreous and is known to interact with complexed polymeric and liposomal DNA (Ruponen, Ylä-Herttuala et al. 1999). Thus the vitreous is built up of a complex network of collagens, negatively charged GAGs and non-collagenous structural proteins. Within such a network, collagen fibrils are bridged by proteoglycan filaments which contain negatively charged GAGs (Bishop 2000). Furthermore the interfibrillar spaces of this network are also filled by a dense network of hyaluronan. This complex network within the vitreous has been shown to immobilize non-viral complexes, including nanoparticles composed of plasmid DNA and cationic lipids. Specifically, aggregations of lipoplexes within the vitreous have been shown to be caused by the binding of the negatively charged GAGs within the vitreous to the positively charged complexes (Pitkanen, Ruponen et al. 2003; Peeters, Sanders et al. 2005). Interestingly, this problem of aggregation can be overcome. Studies have shown that nanoparticles within the vitreous can be protected from aggregation by shielding their surface with polyethylene glycol (PEG); through a process named 'pegylation' (Pitkanen, Ruponen et al. 2003; Peeters, Sanders et al. 2005).

While pegylation can be used to avoid aggregation within the vitreous, vectors delivered to the vitreous must also be able to penetrate through the neural retina before reaching the RPE cells. However, the retina is also inefficiently permeable to non-pegylated liposomal (and polymeric) gene complexes (Pitkanen, Ruponen et al. 2003). Further to this, it has been shown that the strongest barrier in the neural retina is the inner limiting membrane (ILM) (Pitkanen, Ruponen et al. 2003). The ILM is the boundary region between the vitreous space in the posterior chamber and the retina. This ILM has been shown to restrict the penetration of polyethylenimine (PEI) polyplexes, (polyplexes, poly-L-lysine polyplexes and DOTAP liposomes) through the neural retina (Pitkanen, Ruponen et al. 2004).

1.7.1.5 Subretinal injections

Finally, subretinal injections deliver injected vectors between the distal tip of the outer segments of the photoreceptor, causing an initial subretinal bleb that usually is seen to regress quickly (Figure 12E and Figure 13). Hence this technique allows the targeting of the cells in the outer retina and the RPE cells.

Subretinal injections have been successfully used in many experimental models of ocular diseases including: Retinitis pigmentosa (RP)(Takahashi, Miyoshi et al. 1999; Chen, Moiseyev et al. 2006), Age Related Macular Degeneration (AMD)(Lai, Wu et al. 2001; Campochiaro, Nguyen et al. 2006) as well as diabetic retinopathy (Ideno J 2007). Furthermore, this technique has also been utilised in three recent ocular clinical trials for Leber congential amaurosis (LCA)(Bainbridge 2008; Bainbridge, Smith et al. 2008; Bainbridge and Ali 2008; Cideciyan, Aleman et al. 2008; Maguire, Simonelli et al. 2008).

Despite subretinal injections being very efficient, some major drawbacks include that it is relatively invasive but more importantly it is also a technically demanding procedure. However numerous approaches to the injection technique have been proposed including via a transcorneal/transvitreal route (Johnson, Berglin et al. 2008; Timmers, Zhang et al. 2001), transscleral route (Price, Turner et al. 1987) as well as transscleral-transchoroidal-Bruch's membrane route (Gekeler, Kobuch et al. 2004; Gerding 2007).
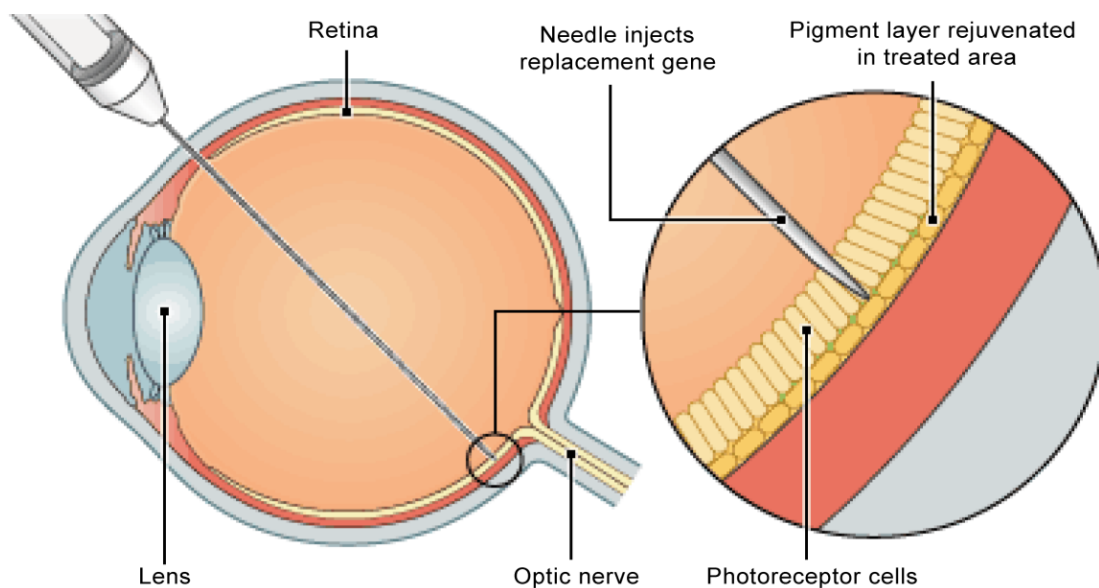
Figure 13: Schematic showing the subretinal injection procedure

A needle containing the required vector is inserted into the retina within the subretinal space – located between the plasma membrane of the photoreceptor and RPE cells of the retina. Upon injection of the vector into the subretinal space, a bleb occurs causing the two layers (photoreceptor and RPE cells) to become separated and the vector is able to spread along the retina. This usually regresses back quickly and the treated area including the pigmented RPE cells are able to rejuvenate within the treated area (Figure from Moorefield Eye Hospital).

1.7.2 Eye disorders
1.7.2.1 Macular Degeneration -Age related Macular Degeneration (AMD)

Macular degeneration is one of the most common causes of severe vision loss within the Western world, indiscriminately affecting the young and old. The most common subtype is age-related macular degeneration (AMD) affecting more than 8 million people worldwide, including 75% of age-related blindness in the Western world. It is a complex disorder in which depositions of material in and around the Bruch's membrane lead to dysfunction and death of the photoreceptors and RPE cells, as well as the eventual choroidal neovascularisation (CNV) which grows beneath the RPE and photoreceptors.

AMD occurs in two forms, dry and wet. In the dry form, patients often manifest deposits beneath the RPE, called drusen. Pigmentary changes are also seen in the retina, which indicates death of photoreceptors and RPE, for years before the onset of CNV. This stage of the disease is referred to as atrophic or non-neovascular AMD, often accompanied by mild visual dysfunction, particularly loss of photoreceptors in the central part of the eye.

In the wet form, visual prognosis becomes considerably worse by the conversion of the disease from non-neovascular to neovascular AMD. Initially, visual loss is caused by pockets of fluid seen beneath and within the retina, due to the leakage of the plasma membrane from abnormal growth of new choroidal blood vessels. During this stage of the disease, visual loss is reversible if the resorption of fluid occurs. Following this, choroidal blood vessels often haemorrhage which leads to blood entering the subretinal space (below the macula) resulting in loss of vision. However, again at this stage, vision can be improved with the resorption of the blood. The subsequent formation of new choroidal vessels, blood and plasma within the eye ultimately stimulates the migration and proliferation of RPE and glial cells, causing irreversible scaring that permanently destroys vision (de Jong 2006; Zarbin 2004).

To date, no effective treatments had been available for wet-AMD patients. However, recently a number of factors were shown to be responsible for the conversion from non-neovascular AMD to neovascular AMD. These include the vascular endothelial growth factor (VEGF) as well as the pigment epithelium-derived factor (PEDF)(Kwak, Okamoto et al. 2000). Studies have shown that neovascularisation results from unbalanced production of factors

such as VEGF or PEDF which result in the growth of abnormal blood vessels in the choroid and retina (Allocca, Tessitore et al. 2006). Studies in animal models showed that blocking VEGF or its signalling suppresses CNV (Kwak, Okamoto et al. 2000; Krzystolik, Afshari et al. 2002). This finding led to the prediction that VEGF antagonists could prevent the neovascularisation observed in AMD. This prediction was confirmed following two large scale clinical trials in which patients with neovascular AMD received repeat intravitreal injections of VEGF antagonists. In one trial this was pegaptanib, an aptamer which binds VEGF (Gragoudas, Adamis et al. 2004). In another trial, this was ranibizumab, which is a Fab fragment of an antibody that binds to all isoforms of VEGF-A. Results from the first trial showed the percentage of patients who experienced severe loss was reduced by 15% during the course of the 1 year trial. However results from the second trial were considerably better, where substantial improvement in patients' vision was increased from 4.6% to 34%.

PEDF is an anti-angiogenic molecule which is responsible for inducing and maintaining the avascularity of the cornea and vitreous compartments in physiological conditions (Allocca, Tessitore et al. 2006). PEDF gene transfer inhibits both retinal and choroidal neovascularisation. Intravitreal, subretinal and periocular administration of Adenoviral (Ad) or Adeno-associated (AAV) vectors encoding PEDF results in reduction of neovascularisation in various animal models (Gehlbach, Demetriades et al. 2003; Allocca, Tessitore et al. 2006). Following this, in a phase I clinical trial, patients with neovascular AMD received intravitreal injections of Ad-PEDF vectors (Campochiaro, Nguyen et al. 2006). Therapeutic efficacy was reported, where 94-71% of patients treated with the highest vector dose had a reduction in the size of CNV lesions within the retina (Campochiaro, Nguyen et al. 2006).

AMD is classed as a complex genetic trait, and suggestions have been made that an immunological contribution many lead to AMD pathogenesis. A common single nucleotide polymorphism in Complement Factor H (CFH), His402, has been associated with AMD. Homozygous individuals have been shown to be at a substantially higher risk of developing AMD compared to the homozygotes for the normal Tyr402 haplotype, while heterozygotes showed an intermediate risk (Edwards, Ritter et al. 2005; Klein, Zeiss et al. 2005). CFH has been shown to be a key component of the alterative complement pathway, where it is a negative regulator of the complement cascade. CFH binds activated Complement Factor 3 (known as C3b in its active state) and this promotes its digestion by Complement Factor I.

The mutation in CFH (His402) reduces the ability of CFH to recognise surface markers such as glycosaminoglycans. Hence this change reduces the ability of CFH to regulate complement in critical surfaces such as the specialised membrane at the back of the eye. Subsequently this leads to an increased inflammatory response within the macula. Interestingly, 20 out of the 84 *CFH* gene polymorphisms have been associated with an increased risk of developing AMD (Li, Atmaca-Sonmez et al. 2006); implying that *CFH* expression could determine AMD risk.

Another susceptibility locus has been mapped to chromosome 10q26; the causative variation has been shown to lie in a 'hypothetical gene' called *LOC387715* or in the promoter of the neighbouring gene *HTRA1* (Rivera, Fisher et al. 2005; Schmidt, Hauser et al. 2006).Two further complement regulatory proteins, complement factor B (CFB) and complement component protein C3 (C3) have also been shown to possess sequence variants which strongly associate with the occurrence of AMD (Maller, Fagerness et al. 2007; Yates, Sepp et al. 2007).

Indeed population attributable risks of AMD associated with variants in *CFH, CFB and LOC387715/HTRA1* have been shown to be at least 50% (Maller, George et al. 2006). These finding suggest that AMD is caused by aberrant complement activation, which causes a positive feedback loop of activated complement and pro-inflammatory peptides within the retina (Rattner and Nathans 2006).

1.7.2.2 Stargardt disease

Stargardt disease is the most common form of juvenile macular degeneration. It is inherited as an autosomal recessive trait, showing severe juvenile macular degeneration and has an incidence of 1 in 10,000. Disease progression usually starts between the ages of 6-12 years leading to rapid reduction in visual acuity. It is characterised by the appearance of lipofuscin-like protein deposits in the RPE underlying the macula, which cause atrophy of the macula and underlying RPE resulting in the loss of vision. The disease is caused by mutations in the ABCA4 gene at the locus 1p13-p21 (Arnell, Mantyjarvi et al. 1998). The ABC4A gene is expressed exclusively and at high levels in the retina. Specifically it is localised to the photoreceptor outer segments, where it translocates all-trans retinal

phosphatidylethanolamine from the outer segment disc lumen to the cytosol (Molday, Rabin et al. 2000). Failure of this process causes an accumulation of all-trans-retinal in the photoreceptor outer segments, which progressively causes the accumulation of a toxic compound called A2E which can induce apoptosis and dissolve cell membranes.

Stargardt disease also has a rare dominant form called Stargardt-disease 3 (STGD3) or Stargardt-like dominant macular dystrophy. This form of the disease is thought to be caused by mutations in the elongation of very long chain fatty acids-like 4 (ELOVL4) gene found on chromosome 6q14. The ELOVL4 gene is involved in the production of long-chain fatty acids, (via the fatty acid elongation pathway) which occurs exclusively in the photoreceptors (Edwards, Donoso et al. 2001). To date all types of mutations found in the ELOVL4 gene result in C-terminal truncated versions of the protein. As a result the protein cannot be retained in the endoplasmic reticulum of photoreceptor cells. Instead, the ELOVL4 protein forms clumps or aggregates adjacent to the nucleus (Grayson and Molday 2005). Since these aggregates cannot make long-chain fatty acids they may interfere with cell functions, ultimately leading to photoreceptor cell death. These findings suggest that aberrant subcellular localisation of wild-type ELOVL4 protein may contribute to STGD3 disease development.

1.7.2.3 LCA

One of the most clinically severe retinal degenerations is Leber congenital amaurosis (LCA). It is an early-onset inherited retinopathy as rods and cones are completely non-functional from birth and can be lost within the first few years of life (Cremers, van den Hurk et al. 2002; Ahmed and Loewenstein 2008). LCA is inherited in an autosomal recessive manner, where the incidence is 1:50 000-100 000, despite being a rare disorder it is the most common cause of infant blindness in schools for the blind. Patients possess a variety of eye-related abnormalities including roving eye movements where the eyes appear to slowly wander around not fixing or staying still on objects. Furthermore patients have deep-set eyes, fast to-and-fro movements of the eyes called Nystagmus and sensitivity to bright light.

To-date mutations in 14 genes are known to be associated with LCA and the mutations in these genes account for approximately 60% of all LCA cases (Koenekoop 2004). The 14 LCA genes identified encode retinal proteins which are necessary for normal vision. They play a variety of roles in the development and function of the retina. For example some of the genes associated with this disorder are necessary for normal photoreceptor development and vitamin A cycling, while others are involved in phototransduction, the process by which light enters the eye and is converted into electrical signals that are then transmitted to the brain (Koenekoop 2008). The genes have also been shown to participate in a wide variety of retinal pathways: retinoid metabolism (*RPE65*), phototransduction (*GUCY2D),* photoreceptor outer segment development (*CRX*). Mutations in the *CEP290*, *CRB1*, *GUCY2D* and *RPE65* genes are the most common causes of the disorder. Currently the most successful example of gene therapy for an ocular disease is gene therapy for LCA arising from mutations in the *RPE65* gene. These mutations account for 10% of all LCA cases and this will be the main mutation of focus for this section.

The first *RPE65* mutations were identified in humans with LCA by Marlhens *et al*. in 1997 (Marlhens, Bareil et al. 1997). The *RPE65* gene is expressed in the RPE -found in the smooth endoplasmic reticulum of the RPE cells - and encodes a 65-kDa protein that is a key component of the visual cycle. It is important for the regeneration of visual pigment after exposure to light as described previously in section 1.6.1.1. Specifically, *RPE65* encodes a protein requisite for the isomerohydrolase activity of the RPE; this activity produces 11-*cis*-retinal from all-*trans*-retinyl esters (Moiseyev, Chen et al. 2005). In RPE65 deficiency, photoreceptor cells do not regenerate their visual pigment and vision is not sustained (Perrault, Rozet et al. 1999; Moiseyev, Chen et al. 2005). Despite this, cone photoreceptors may have access to 11-*cis*-retinal chromophore through an alternative pathway which is independent of RPE-derived RPE65 (Znoiko, Crouch et al. 2002). Thus children with LCA often have cone mediated vision; however, progressive degeneration of the cone photoreceptors leads to the ultimate loss of this vision.

Dramatic restoration of vision with gene therapy was first reported in the Swedish Briard (*RPE65$^{-/-}$*) dog, a naturally occurring animal model with mutated *RPE65* (Acland, Aguirre *et al.* 2001). Visual impairment in the *RPE65$^{-/-}$* dogs is caused by a homozygous 4-bp deletion in the *RPE65.* This results in a frameshift mutation and formation of a premature stop codon

which truncates the protein in these dogs (Aguirre, Baldwin 1998). (Three) Homozygous $RPE65^{-/-}$ affected dogs each received a single subretinal injection of AAV virus serotype 2 (AAV2/2) carrying a chicken β-actin-promoter/CMV enhancer-driven wild-type canine $RPE65$ cDNA. At 4-months following injection, $RPE65^{-/-}$ dogs showed elevated ERG response/signal. This measures retinal function, specifically the activation of photoreceptors, primarily the rod cells. ERG analysis also measures the function of the inner retinal neuronal/bipolar cells, showing an improved retinal function. Furthermore qualitative visual assessment showed that under dim light dogs were able to constantly avoid objects directly in front of them and on the right (the side injected subretinally), while constantly failing to avoid objects on the left (injected intravitreally). In contrast, untreated affected dogs displayed no avoidance behaviour in any direction. This further showed that the $RPE65^{-/-}$ dogs had improved vision as determined by visual motility. Excitingly, over eight years after the AAV vector administration, the $RPE65^{-/-}$ dogs still maintained stable vision improvements (Narfstrom, Katz et al. 2003; Acland, Aguirre et al. 2005).

Studies involving AAV-vector mediated $RPE65$ gene therapy have also been described in murine models with $RPE65$ deficiency which has led to rescued morphological, biochemical and electrophysiological abnormalities (Dejneka, Surace et al. 2004; Pang, Chang et al. 2006).

1.7.2.3.1   Human Gene Therapy trials for LCA

Following the successful replacement of $RPE65$ in mice and canine models of LCA and the encouraging improvements in visual function, these results provided the impetus for three ongoing phase I clinical trials. These trials all used AAV2/2 vectors for gene-therapy in patients affected by LCA due to $RPE65$ mutations.

From the three studies, one has been conducted in London based at Moorfields Eye Hospital, led by Dr. Robin Ali as well as two others in the USA, conducted at the University of Pennsylvania, Philadelphia and the University of Florida, Gainesville, as well as another conducted at the Children's Hospital in Philadelphia.

In the first Philadelphia study, Maguire and colleagues used 1.5 x 10^{10} AAV particles containing recombinant AAV2.hRrpe65v2 – which is a replication deficient AAV – carrying the chicken-β-actin (CBA) promoter (Maguire, Simonelli et al. 2008). The 150 µl solution was injected into the subretinal space of three LCA patients aged between 19-26 years old. Two subjects carried the homozygous missense (p.Glu106Lys) and one a predicted null mutation (p.Arg234Ter) in the *RPE65* gene. No local - retinal and vitreous - or systemic adverse effects were observed. Following this lack of toxicity the Maguire group also performed functional analyses on their patients. They used pupillometry, which measures retinal sensitivity from the retina to the brainstream and nystagmus frequency which is an indirect measure of fixing ability. Additional measures included Early Treatment Diabetic Retinopathy Study - ETDRS - visual acuities, which are the gold standard of visual acuity measurements using chart and letter counts, as well as the ability to navigate an obstacle course before and after surgery. Measurements by electroretinography (ERG), which measures cone and rod photoreceptor responses in a-waves, as well as bipolar and Müller cell responses in b-waves, were not reported.

All three patients with LCA who received AAV2.hRrpe65v2 by subretinal injection showed evidence of improvement in retinal function. Improvements in ETDRS acuities where considerable, ranging from 3 to 4.5 lines. On average before surgery, patients had an 80° visual field width; however after surgery this was significantly increased to 200°. Obstacle course videos showed improvements in the confidence and time in all subjects. The frequency of nystagmus was improved as well as the significant improvements seen in the pupillometry studies which reflected enhanced sensitivity of the retina as well as better transmission to the brainstem.

In the London study, Bainbridge *et al.* used AAV 2/2.hRrpe65 carrying the human RPE65 promoter (Bainbridge, Smith et al. 2008). Three LCA patients were used in this study ranging from 17-23 years of age, with *RPE65* mutations, while *RPE65* null mutations were excluded. A volume of 1 x 10^{11} viral particles was injected via a single subretinal injection into the retinas of the patients. After injections, no evidence of disseminated virus or adverse ocular or systemic effect was observed. Furthermore, measurements included: ERG, ETDRS charts as well as mobility tests through an obstacle course.

Overall the visual acuities of the patients in the Bainbridge group were slightly better than those of the Maguire group. Indeed one patient's ETDRS acuities improved from 20/286 to 20/145 by 12 months. However, the investigators did not feel this improvement was significant as the control eye had also improved from 20/150 to 20/120. Bainbridge *et al.* suggested that due to the improvements in the frequency of nystagmus, this may have also improved the visual acuities in the control eye (Bainbridge, Smith et al. 2008). An alternative suggestion has been that the RPE65 protein was able to find its way to the control eye (Narfstrom, Katz et al. 2003). However this may be doubtful, as the other two patients showed no significant improvements in visual acuity, unlike the Maguire group. In another analysis, at 6 months following surgery, 1 of the 3 patients observed a highly significant 14 dB (25 fold) improvement in the sensitivity of the retina following microperimetry studies. Furthermore a significant enhancement of dark adapted perimetry was also observed in this patient, no improvement was seen in the control eye. Interestingly, this patient also showed significant improvements in mobility. This was assessed by the amount of time the patient took to go through an obstacle course before and after surgery, where the walking time through the course was reduced from 77 seconds to 14 seconds.

In the final study, Cideciyan and associates used a similar vector to the Maguire group, AAV2.*hRPE65* carrying the CBA promoter (Cideciyan, Aleman et al. 2008). Three patients were also included in this study, all with various *RPE65* mutations which were reported to have less than 3% isomerisation activity *in vitro* compared with wild-type. After injections, as with the other two trials, no signs of inflammation were observed. However, the investigators in this trial were considerably interested in not only showing retinal function and visual acuity, but specifically dissecting the precise location of correction and the cell types sub-serving any visual phenotype. They were eager to see whether a response was observed specifically within the rod or cone cells of injected subjects. Such an approach was not utilised in the previous two trials.

Retinal examinations to analyse the photoreceptor cell ONL thickness topography prior to treatment showed that all three patients had significantly reduced ONL thickness. However thickness remained significantly detectable to warrant treatment. Patients were aged between 21-24 years old and all had experienced severe visual disturbances since childhood. Patients received 1 single subretinal injection of 5.96×10^{10} viral particles in

150 µl solution, and their vision was analysed up to 90 days following surgery. In all three patients, the light sensitivity of the retina was measured before and after surgery. This showed that there was a statistically significant increase in the visual sensitivity localised to the areas that had received the vector at 30 days following treatment. However no further changes were seen between 30 and 90 days.

All patients were observed to have extended dark adaptation times. Normal human vision becomes more sensitive to light after an instantaneous decrease in ambient illumination – a process known as dark adaptation and this can take up to 1 hour in normal vision. However in the three patients this was considerably higher between 3-8 hours. The investigators suggested that this may be an indication that the kinetics of the reconstituted visual cycle in the study eyes may be abnormally slow. In order to define the kinetics of the dark adaptation, specifically to differentiate rod and cone kinetics, chromatic sensitivity was measured before and after desensitizing light flash. Both rod- and cone-photoreceptor-based vision was demonstrated in treated areas of all three patients, with an increase of 50 fold in cone cells, while for rod cells this increased by 63,000 fold. The group suggested that this considerable increase in rod sensitivity was likely to be driven by the increase in 11-*cis*-retinal chromophore from the wild-type protein that was introduced to the RPE by expression from the AAV vector. Importantly, the group argued that the magnitude of the increase observed as well as the lack of a visual function increase in the control sham injected eyes rules out these visual gains involving neurotrophic factors (Wen, Song et al. 1995) or secondary gains due to the actual subretinal injection procedure (Del Priore 2005) as suggested in previous studies.

The Cideciyan group also accessed what fraction of full vision potential was restored following the injection procedure. In order to achieve this, the group related the areas of light sensitivity to the level of remaining photoreceptors within the treated areas of the retina. They observed that the gene therapy could overcome nearly all the loss of sensitivity in the patients. However the group highlight that this resulted in a reconstituted visual cycle that was not completely normal. This is because despite cone-sensitivity recovery time being rapid, the kinetics of the newly treated rod cells in the patients required up to 8 hours or more for the attainment of full sensitivity.

Upon analysis of these three clinical trials for LCA, the differences in each trial included: the vector manufacturing procedures and the RPE65 expression cassette which contained either the CBA promoter (Cideciyan, Aleman et al. 2008; Hauswirth, Aleman et al. 2008; Maguire, Simonelli et al. 2008) or the RPE specific *RPE65* promoter (Bainbridge, Smith et al. 2008). Additionally the AAV vector injection volumes, as well as patients' baseline acuities (patients' visual function) were all different in each trial. Despite these differences, some important conclusions can also be made. No improvements were observed by ERG parameters in either the Maguire or Bainbridge lead trials (Bainbridge, Smith et al. 2008; Maguire, Simonelli et al. 2008). This may be due to the initially low ERG testing which is characteristic of LCA patients. Regardless of this, all the studies showed safety of the procedure and no reports of systemic toxicity or immune responses to the therapy were made. Furthermore each group showed significant efficacy of the various techniques adapted to measure visual function. These included the use of micro-perimetry to show visual field extension (Bainbridge, Smith et al. 2008) and navigation tests to indicate improvement of visual function (Bainbridge, Smith et al. 2008; Maguire, Simonelli et al. 2008).

Both the Maguire and Bainbridge groups (Bainbridge, Smith et al. 2008; Maguire, Simonelli et al. 2008) showed significant improvements in the papillary reflex and in turn enhanced sensitivity of the retina by pupillometry and microperimetry studies respectively. However Cideciyan and colleagues (Cideciyan, Aleman et al. 2008) took their analyses one step further and reported significant increases in visual sensitises, with evidence for both cone- and rod-based vision.

Overall these studies reflect some of the most profound advances in gene therapy to date, and highlight the possibilities for additional studies, including our disease of interest, Choroideremia, to take this route from bench to bedside.

1.7.3 Choroideremia (CHM)

Choroideremia (CHM) was originally described in 1872 in an Irish pig farmer who had emigrated to Canada. His family tree was analysed and it was found that all his children appeared unaffected and showed no signs of blindness, including all his sons and their descendants. However when the male descendants from his daughters lineage were analysed, they appeared to go blind over subsequent generations (McCulloch 1969). Following this, CHM was described as a progressive retinopathy that was exhibited as an X-linked recessive condition. Mutations in the R*ab Escort Protein 1 (REP1)* gene were found to underlie this condition (Seabra, Brown et al. 1992; Andres, Seabra et al. 1993; Seabra, Brown et al. 1993). However, to date, there is still no effective treatment for affected individuals although the first UK Phase 1 clinical tiral for choroidermia using AAV vectors has just started.

1.7.3.1 Clinical features of Choroideremia

Affected male patients begin to develop pathological changes gradually, often starting with night blindness and tunnel vision in their teens. Subsequently, visual loss progresses to the mid-periphery, with central vision preserved until complete loss of vision in the final stages of the disease 2-3 decades following onset.

Associated retina changes are evident as early as childhood, were CHM patients display spotted areas of depigmentation of the fundus, which reflect degeneration of the RPE. Furthermore, atrophy of choroidal vessels and sclera occurs around the optic disc in adolescence (Figure 14B). In the intermediate stages of the disease, the pattern of RPE and choroidal atrophy spreads even further within the retina. Furthermore, all sizes of choroidal vessels are affected, with the exception of those underlying the far periphery and macula; in turn the fundus appears off-white to yellow-white in colour (Figure 14C). Heterozygous female carriers usually retain normal/good visual function, but subtle changes in the fundus are evident, with patchy areas of depigmentation and chorioretinal degeneration due to random X-inactivation (Figure 14D)(MacDonald, Mah et al. 1998).
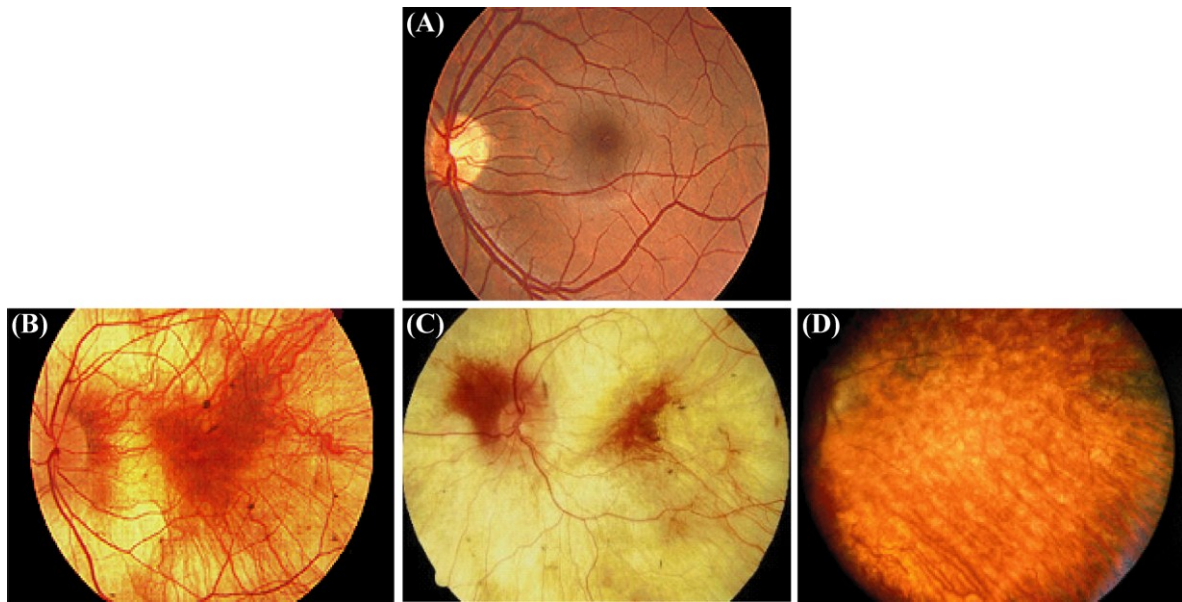
Figure 14: Fundus photographs of normal and choroideremia retinas

The fundus showing (A) normal human retina, (B) early and (C) late changes in the retinas of choroideremia patients (D) X-linked female choroideremia carrier retina. The fundus of choroideremia patients is off-white/yellow compared to a normal fundus. Choroideremia retinas show areas of depigmentation as well as islands of choroid, where widespread choroidal atrophy is prominent as opposed to an even distribution of the choroid. Asymptomatic carriers show more subtle fundus changes with patchy areas of depigmentation
(Images taken from http://webvision.med.utah.edu/ClinicalERG.html).

A study of CHM patients in 2006 measured the thickness of retinal laminae using *in vivo* high resolution optical imaging and describes the remodelling which occurs within the retina over several decades of the disease. This study suggests four stages of the CHM disease as shown in Figure 15 (Jacobson, Cideciyan et al. 2006). Young affected males (7-12 years of age) had small areas of photoreceptor abnormalities which co-localise with normal and abnormal RPE. Interestingly however, no abnormal RPE were seen in association with normal photoreceptors, thus photoreceptor loss was found to precede RPE depigmentation. In the peripheral rod-rich retina, normal thickness was maintained for approximately twenty years. After this time, a slow degeneration was seen which lead to a thinner, disorganised, bilaminar retina seen in 34 and 56 year old patients. The cone-rich fovea became thicken decades before cone dysfunction was apparent, measured by visual acuity. Patients from the age of 13 through to 40 displayed thickening of the fovea, followed by photoreceptor

degeneration, RPE depigmentation and finally loss of lamination. All these progressions result in a subnormal thinning of the retina from approximately the fifth decade of life.
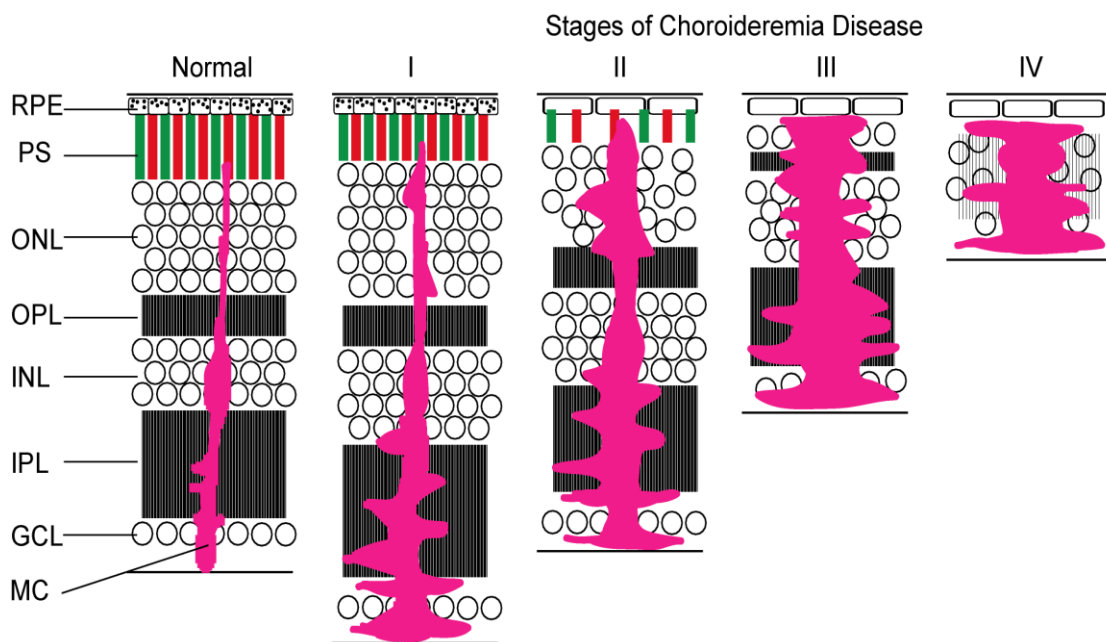
Figure 15: Schematic model of retinal remodelling in human choroideremia disease progression

The earliest detectable stage is the thickening of the retina, with otherwise normal lamination (Stage I). The next stages show clinical signs of disease progression characterised by loss of photoreceptor nuclei, inner and outer photoreceptor segment thinning and depigmentation of RPE cells (Stage II and III). The end stage of disease progression is further thinning of the retina, disorganisation of all retinal cell layers and loss of lamination (IV). Throughout the stages of disease, Müller cells filled in pink indicate progressive gliosis.
MC, Müller cells; RPE, retinal pigment epithelium; PS, photoreceptor outer and inner segments; ONL, outer nuclear layer; OPL, outer plexiform layer; INL, inner nuclear layer; IPL, inner plexiform layer; GCL, ganglion cell layer (Figure adapted from (Jacobson, Cideciyan et al. 2006)).

Jacobson *et al* speculated that the initial thickening of the retina seen in stage I of CHM disease progression was caused by Müller cell activation, hypertrophy or even proliferation in response to photoreceptor stress and damage (Jacobson, Cideciyan et al. 2006). This speculation was based on studies in aging rats with retinal degeneration, where Müller cells were found to be stimulated prior to photoreceptor loss (DiLoreto, Martzen et al. 1995). Furthermore glial cells are commonly activated after trauma or neuronal injury (Rattner and Nathans 2005).

There is considerable phenotypic variation seen between CHM members within the same family as well as members of different CHM families, specifically age of symptom onset as well as the subsequent rate of disease progression and severity (Jacobson, Cideciyan et al. 2006). In extreme cases, the earliest detectable retinal changes (stage I) have been seen in boys younger than four years of age, where they were reported to have developed night blindness. In comparison a 45 year old affected male had reported to have only slight visual changes and abnormalities (Ponjavic, Abrahamson et al. 1995; Mura, Sereda et al. 2007). In contrast, variation within female carriers is often the result of random X-inactivation.

A heterozygous female carrier was reported to have abnormal RPE depigmentation of irregular thickness as well as abrupt transitions between areas of normal and absent photoreceptors (Flannery, Bird et al. 1990). Photoreceptor loss was seen in areas of normal RPE, while abnormal RPE were also seen in association with areas of normal photoreceptors. Autofluorescent particles, presumably lipofuscin, were seen in pigmented RPE cells. In areas of complete atrophy, choroidal capillaries and photoreceptors were completely absent, while mild atrophy was coupled with reduced capillaries and abnormal photoreceptors. Areas of normal photoreceptors where always seen with normal choroid. Finally, deposits seen on the Bruch's membrane showed that the RPE had been functioning previously, but had stopped phagocytising outer photoreceptor segments. From these finding, the authors proposed that the CHM disease is primarily associated with RPE degeneration. However they also highlighted that they lacked to show evidence for the root and cause of the disease.

In another study of a female carrier, survival of photoreceptor cells neighbouring severely abnormal RPE cells was observed (Syed, Smith et al. 2001). Furthermore, minimal changes were seen in the choroid as well as normal pigmentation of RPE cells. However, lipofuscin accumulation was also seen in the RPE cells, and the preferential loss of rod photoreceptors was also observed. Interestingly, the end stage of the disease was characterised by the loss of all photoreceptor cells as well as pronounced damage of the choroidal capillaries. This suggested that the photoreceptor and RPE degenerations seen in association with CHM are independent. Furthermore, immunostaining of retinal sections showed REP1 staining in normal areas of rod inner segments and synapses, while an absence of staining was

observed in rod outer segments or cones. These authors suggested the rod cells are the primary site of disease in CHM, and importantly, that the disease is independent of the RPE.

While the pathogenesis and cellular origin of CHM remains complex and debatable, three areas of the retina have been implicated with the disease. These include the choroid, particularly in the late stages of the disease, as well as the RPE and photoreceptors. The latter two appear to be more associated with the early stages of CHM, where the degenerative process is believed to be cell autonomous - self directed- and develops independently in both these key affected layers (Syed, Smith et al. 2001; Tolmachova, Anders et al. 2006; Krock, Bilotta et al. 2007).

1.7.3.2 Genetic basis of choroideremia

The X-linked recessive pattern of inheritance was first noted by two independent authors in 1942. Estimates of incidence range from 1 in 50000 to 1 in 100000, classifying CHM as a rare disorder. CHM has been linked to the chromosome Xq21.2 (Cremers, van de Pol et al. 1990) and the causative gene responsible identified as the REP1 gene (Seabra, Brown et al. 1992; Andres, Seabra et al. 1993; Seabra, Brown et al. 1993). The REP1 gene spans 150 kb of chromosome Xq21.2, contains 15 exons and encodes a 653 amino acid protein (van Bokhoven, van den Hurk et al. 1994; van den Hurk, Hendriks et al. 1997). The gene is also flanked by genes associated with mental retardation and deafness type 3; hence these syndromes are also seen in CHM patients that have large deletions in this region.

Over 100 mutations have been detected in *REP1,* however these only represent 60% of familial cases and 30% of sporadic cases, showing the genetic heterogeneity of this disease (Preising and Ayuso 2004). Mutations in the *REP1* gene have been reported ranging in size from a few kilobases, removing of single exons, to those which encompass the entire *REP1* gene and most of the Xq21 band (van den Hurk, Schwartz et al. 1997; Fujiki, Hotta et al. 1999; McTaggart, Tran et al. 2002; van den Hurk, van de Pol et al. 2003). Furthermore translocations disrupting *REP1* have also been detected in female carriers, with autosomal breakpoints at 7p14 (X breakpoint in *REP1* exon 3 or 4; t(X;7)(q21;p14)), 13p12 (X breakpoint in *REP1* exon 12; t(X;13)(q21;p12)) and 4p16 (X breakpoint in *REP1* intron 8; 46,

X, t(X;4)(q21;p16))(Cremers, van de Pol et al. 1990; van Bokhoven, van den Hurk et al. 1994; Lorda-Sanchez, Ibanez et al. 2000; Garca-Hoyos, Sanz et al. 2005).

Furthermore a variety of nonsense, frameshift, missense and splice-site mutations have also been identified and until recently all mutations were thought to cause the protein to become truncated due to an early stop codon or absent (Seabra 1996; van den Hurk, van de Pol et al. 2003). However, recently new cases of missense mutations have also been observed in some CHM patients (Sergeev, Smaoui et al. 2009; Jung, Huh et al. 2011). Furthermore, Garcia *et al.* reported a novel mutation in three CHM families which did not result in a truncation or loss of REP1 protein. Instead this mutation caused the loss of various parts of the REP1 mRNA in-frame which all encoded conserved regions of the protein implicated in the interaction of Rab proteins (Garcia-Hoyos, Lorda-Sanchez et al. 2008).

No phenotypic correlations between the various types of mutations have been detected. Interestingly, recombinant REP1 lacking only the C-terminal end 49 amino acids results in defective *REP1* that is unable to interact with RabGGTase *in vitro.* This highlights the importance of full-length protein production to avoid loss of function (van den Hurk, Schwartz et al. 1997; Fujiki, Hotta et al. 1999; McTaggart, Tran et al. 2002; van den Hurk, van de Pol et al. 2003).

Furthermore, as over one third of all mutations have been identified as nonsense mutations (van den Hurk, Schwartz et al. 1997; Fujiki, Hotta et al. 1999; McTaggart, Tran et al. 2002; van den Hurk, van de Pol et al. 2003), this brings to light CHM as an excellent the disease candidate for (translational) gene therapy.

1.7.3.3 Functionality of Rab Escort Proteins

1.7.3.3.1 Rabs as cellular membrane organisers

The Rab proteins are the largest subfamily of small GTPases, with over 60 different members identified in mammals since their discovery in the 1980's. Rab proteins are key regulators of intracellular membrane trafficking and vesicular transport in both endocytic and secretory pathways. This includes the regulation of vesicular budding from donor

membranes, organelle transport along microtubules and actin filaments, vesicle tethering/docking to acceptor membranes and fusion of vesicles with the membrane of acceptor compartments in vesicular transport (Zerial and McBride 2001; Seabra, Mules et al. 2002; Barral and Seabra 2004; Seabra and Wasmeier 2004). Rabs are cytosolic proteins which localise to distinct intracellular membranes, in an organelle specific manner. Therefore they display localisation to particular sub-cellular membranes and this may determine a Rabs involvement in a specific transport step as well as contribute to defining organelle identity (Pfeffer 2001; Zerial and McBride 2001; Seabra, Mules et al. 2002; Barral and Seabra 2004; Seabra and Wasmeier 2004). Many Rabs are ubiquitously expressed; however others are highly tissue specific indicating specialised roles (Pfeffer 2005), this is illustrated in Figure 16. For example Rab 1 is involved in the regulation of transport between the endoplasmic reticulum (ER) and Golgi complex in cells, while Rab 5 is involved in the regulation of early endosome transport and motility from the plasma membrane to the ER. Cumulatively, both are ubiquitously expressed and common to stages of the exocytic and endocytic pathways respectively. In contrast Rab27a is involved in the capture and movement of melanosomes at the cell periphery and so is primarily found on melanosomes within highly pigmented cells called melanocytes.
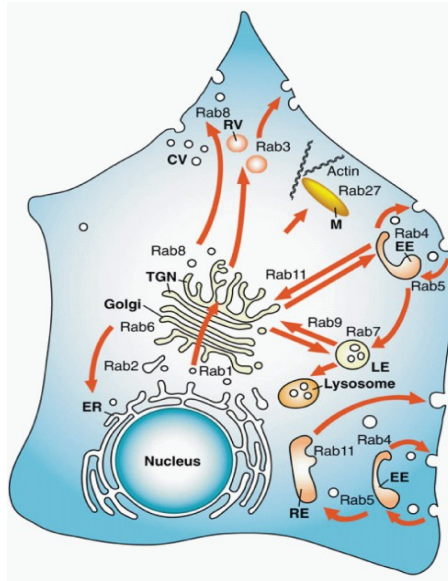
Figure 16: Intracellular vesicular transport and localisation of a selection of selected Rab proteins

In the endocytic pathway, phagocytosed material reaches early endosomes (EE). From here they can be recycled back to the surface of the plasma membrane either directly or via perinuclear recycling endosomes (RE), or transport to late endosomes (LE) and lysosomes. In the exocytic pathway, proteins are transported from the endoplasmic reticulum (ER) through the Golgi complex and to the plasma membrane/cell surface. In the *trans*-Golgi network (TGN), molecules enter either constitutive secretory vesicles (CV) or regulated secretory vesicles (RV). In specialise cell types, such as melanocytes, melanosomes (M) move to the cell periphery via actin and myosin interactions. Rab proteins regulate discrete steps in all these pathways (Stenmark and Olkkonen 2001).

The regulatory ability of Rab proteins is based on a conformational switch between 'inactive' GDP-bound and 'active' GTP-bound states (Takai, Sasaki et al. 2001). Furthermore, Rabs also cycle between membrane and cytosol. Hence, to be functionally active, a Rab protein must not only be GTP-bound but also membrane associated (Pfeffer 2001; Zerial and McBride 2001; Seabra, Mules et al. 2002; Barral and Seabra 2004; Seabra and Wasmeier 2004). When activated Rabs bind to a wide variety of Rab-specific effector proteins that mediate their downstream functions (Jordens, Marsman et al. 2005; Grosshans, Ortiz et al. 2006).

1.7.3.3.2   Lipid Modification of Rab Proteins – Prenylation

Rab proteins are intrinsically soluble proteins. In order to bind to intracellular membranes and in turn become functional, all Rab proteins must undergo post-translational lipid modification, termed prenylation. Prenylation involves formation of a covalent thioester bond between a farnesyl (15-carbon) or geranylgeranyl (20-carbon) lipid group and a C-terminal residue of newly synthesised Rab proteins. Prenylation is catalysed by one of three protein prenyltransferases: farnesyl transferase (FTase), geranylgeranyl transferase type I (GGTase I) or Rab geranylgeranyl transferase (RabGGTase)(Casey and Seabra 1996; Leung, Baron et al. 2007). Interestingly, RabGGTase, unlike the other prenyltransferases, cannot bind to its substrate protein directly, instead it requires association with Rab Escort Protein (Andres, Seabra et al. 1993; Shen and Seabra 1996). Rabs are either singly or predominately (87%) doubly prenylated, depending of the C-terminal cysteine motif they possess (Farnsworth, Seabra et al. 1994; Shen and Seabra 1996; Thoma, Iakovenko et al. 2001). The correct prenylation of Rab proteins is crucial for accurate membrane targeting and subsequently is essential for the correct function and membrane transport of Rabs (Calero, Chen et al. 2003; Gomes, Ali et al. 2003).

1.7.3.4 Rab Escort Proteins in disease – CHM

Rab escort proteins (REP) are accessory proteins involved in the prenylation of Rab proteins, described earlier. Two REP homologues are known to exist in mammals, REP1 and REP2.

REP1 was first purified as "component A" of RabGGTase, when RabGGTase was thought to be composed of two loosely associated components that were able to attach prenyl groups/lipids to Rab proteins (Seabra, Brown et al. 1992). The second component, "component B" was then presented as the catalytic subunit, but has now become known as RabGGTase (Seabra, Goldstein et al. 1992). Interestingly, lymphoblasts isolated from CHM patients showed a deficiency of component A (Seabra, Brown et al. 1993). Furthermore, the authors found that the deficiency was less pronounced when Rab1a was used as a substrate, resulting in 70-80% of normal prenylation levels in these cells. In contrast, when Rab3a was the substrate, only 20-25% normal levels were achieved. This lead to the

suggestion that there must be a second REP present and active in CHM cells, which is potentially acting as a compensatory protein, displaying some levels of substrate specificity.

Following on from this, during the stage of cloning the 5' end of REP1 cDNA, an autosomal homologue, named choroideremia-like (CHML), and later renamed Rab Escort Protein 2 (REP2), was found and was shown to functionally replace REP1 *in vitro* (Cremers, Armstrong et al. 1994). REP-2 is encoded by an intronless gene which spans 2.3 kb of chromosome 1p42 (Cremers, Molloy et al. 1992), where it is found in the *panopsin* gene (Halford, Freedman et al. 2001). This gene has been shown to be linked to Usher Syndrome Type 2 (USH2) which is an autosomal recessive disease leading to deafness and progressive visual loss (Cremers, van de Pol et al. 1990; van Bokhoven, van den Hurk et al. 1994; Lorda-Sanchez, Ibanez et al. 2000; Garca-Hoyos, Sanz et al. 2005). However no disease specific mutations were observed when USH2 patients were analysed for REP2 (Eudy, Weston et al. 1998).

The REP1 and REP2 proteins share 71% sequence identity (Cremers, Molloy et al. 1992). They are also both ubiquitously expressed, although some tissues express higher amounts than others. For example REP1 is highly expressed in tissues of the eye, brain and kidney (Desnoyers, Anant et al. 1996; Tolmachova, Anders et al. 2006). Interestingly, it has been suggested that in CHM, *REP1* deficiency can be overcome and compensated for by *REP2* activity. In turn *REP2* can partly substitute the prenylation of Rabs, in all tissues expect the eye, were this leads to the subsequent onset of retinal degeneration and ultimately blindness (Seabra 1996).

1.7.3.5 Rab Escort Protein function

The function of REP proteins can be divided into three key areas. Firstly they bind newly synthesised Rab proteins, secondly they present the Rabs to RabGGTase for prenylation and finally they deliver each Rab to its target membrane.

In the initial stages, REP forms a stable complex between itself and newly synthesised unprenylated Rabs (at a 1:1 ratio) (Anant, Desnoyers et al. 1998). REP then presents itself to RabGGTase for prenylation. RabGGTase itself does not bind to REP but only interacts with

REP to form a REP:RabGGTase complex (Andres, Seabra et al. 1993; Shen and Seabra 1996). Interestingly, the efficiency of Rab prenylation is not determined by the binding affinity of Rabs to REP, but rather seems to arise due to variations in the catalytic efficiency of the REP:RabGGTase complex. Both REP1 and REP2 show equivalent binding affinity (and activity) to Rab27a (Larijani, Hume et al. 2003). However REP1:Rab27a complex has a higher affinity for RabGGTase compared to REP2:Rab27a complex, resulting in twice as much prenylation of Rab27a (Rak, Pylypenko et al. 2004). This implies that substrate selectivity occurs during the formation of the RabGGTase:REP:Rab complex.

Once the REP:RabGGTase complex has been formed, RabGGTase then catalyses the prenylation reaction by the addition of prenyl lipid groups to the C-terminal cysteine residues of Rabs (Andres, Seabra et al. 1993). Following this, RabGGTase dissociates from the complex, leaving REP to escort the prenylated Rab to their target membrane (Alexandrov, Horiuchi et al. 1994). The actual mechanism of membrane delivery is still unclear. However factors thought to be involved include: RabGEFs (Rab guanine nucleotide exchange factors), specific targeting proteins or specialised GDI-displacement factors (GDFs). GDFs allow the Rab:REP complex to dissociate as well as facilitating in the insertion of the prenylated Rab to the membrane (Pfeffer 2001; Zerial and McBride 2001; Seabra, Mules et al. 2002; Barral and Seabra 2004; Seabra and Wasmeier 2004).These stages are summarised in Figure 17.
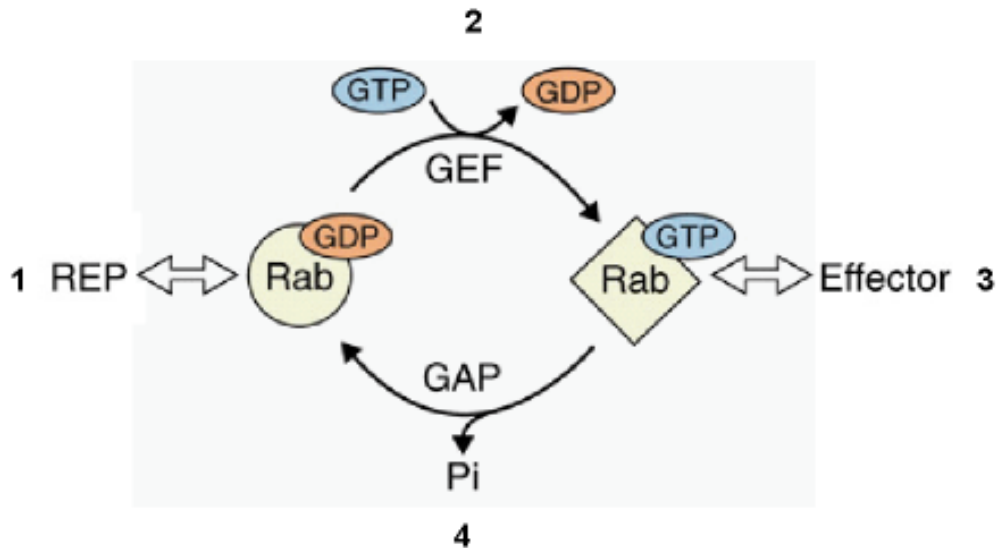
Figure 17: The role and function of REP in the Rab cycle

(1) Newly synthesised Rab proteins in the cytosol are inactive and become GDP-bound by association with Rab Escort Protein (REP) (2) REP then presents the Rab to RabGGTase which catalyses the prenylation reaction. After prenylation, REP remains bound to the prenylated Rab and escorts it to its target membrane. REP then dissociates from the Rab and assists with the prenylation of other newly synthesised Rabs, while the guanine nucleotide exchange factors (GEFs) replace GDP with GTP resulting in an activated Rab (3) This activated GTP-bound Rab protein is then able to become membrane associated, as well as able to recruit effectors (4) GTP hydrolysis is catalysed by GTPase activating proteins (GAPs) which remove Rabs from the membrane into the cytosol again (Figure adapted from (Stenmark and Olkkonen 2001)).

1.7.3.6 A subset of Rabs remain unprenylated in Choroideremia

In CHM, loss of REP1 activity gives rise to progressive retina degeneration, as demonstrated by the restoration of RabGGTase activity in CHM lymphoblasts following the addition of purified REP1 (Seabra, Brown et al. 1993). Indeed it has been suggested that the lack of a generalised phenotype and severity of the CHM disease limited to the eye alone in patients is due to REP2 which is able to partly compensate for this activity in all other tissue except the eye (Seabra 1996). In the eye, REP2 function is not able to fully compensate the lack of correct REP1 activity. This leads to a subset of Rab proteins, including Rab27a, to accumulate within the cytosol, as they are unable to be correctly prenylated and in turn also unable to function correctly (Seabra, Ho et al. 1995; Alory and Balch 2000; Tolmachova, Anders et al. 2006).

Indeed, Rab27a is highly expressed in the RPE cells and choriocapillaris, while no significant expression is observed in the photoreceptors. Despite being one of the Rabs that is affected in CHM, Rab27a is unlikely to be the only Rab responsible for the disease. In fact CHM patients do not develop symptoms of pigmentary dilution of the hair and skin - caused by the accumulation of pigmented melanosomes in melanocytes. Furthermore, CHM patients do not possess immune deficiencies - caused by uncontrolled T lymphocyte and macrophage activation - characteristic of Griscelli syndrome; a rare autosomal recessive disorder caused by mutations in the human *Rab27a* gene. Similarly, Griscelli syndrome patients do not develop retinal degeneration; however the early death of patients may prevent the manifestation of retina disease. Rab27a deficiency in *ashen* mice, results in ablation of melanosomes in the apical processes of RPE cells (Pereira-Leal, Hume et al. 2001), which has also been shown in a conditional knock-out mouse model of CHM (Tolmachova, Anders et al. 2006). However it should be mentioned that the *ashen* mouse does not show signs of retinal degeneration (Gibbs, Azarian et al*. 2004).

As mentioned previously, the severity of CHM is limited as a retina phenotype due to REP2 which is able to compensate for the lack of REP1 function. However, REP2 displays varying substrate specificity, indeed REP2 has been shown to prenylate Rab3a at only 25% of normal levels in CHM lymphoblasts (Seabra, Ho et al. 1995). Rab3a is a component of the neurological synaptic vesicles and regulates a late step in the synaptic vesicle fusion. However, the absence of a neurological phenotype in CHM is observed; implying that only 25% of normal Rab3a prenylation is sufficient for synaptic vesicle function.

Taken together, in CHM, the slow clinical development and combined genetic diagnosis makes CHM an attractive candidate for ocular gene therapy. As virtually no functional REP1 is produced, the presence of a low level of functional REP1 protein localised within the eye, could prove advantageous. This could potentially prenylate enough critical Rab proteins within the eye, resulting in the normal function and in turn potentially also preventing or arresting disease development and progression. While speculation and a full understanding of the molecular mechanisms underlying CHM still remain unclear, the potential of non-viral gene therapy for the CHM is an exciting route we hoped to explore during this study.

1.7.3.7 Animal models of choroideremia

The pathogenesis of CHM remains largely unclear. There are three affected areas (choroid, RPE and photoreceptors) within the retina which appear interdependent on one another causing progressive retinopathy. Certain questions still remain outstanding including where the primary site of degeneration is or where CHM originates in, which in turn leads to the demise of the other two layers. The RPE is the most likely candidate for the primary site of degeneration due to it close proximity and position between the other two degenerating layers (Krock, Bilotta et al. 2007). An alternative hypothesis could be that the degeneration of the RPE and photoreceptors within the retinas of CHM patients occur simultaneously; i.e. cell autonomously. In order to explore these ideas animal models of CHM were created and analysed. A summary of these studies and implications in understanding further the CHM disease pathogenesis and progression are discussed forthwith.

1.7.3.7.1 The Choroideremia Zebrafish

The CHM mutant zebrafish (CHM^{ru848}) was generated following random chemical mutagenesis with *N*-ethyl-*N*-nitrosourea (ENU) and was subsequently identified in a screen for balance and hearing defects (Starr, Kappler et al. 2004). Positional cloning revealed the CHM mutation in zebrafish was on a gene homologous to human REP1. This caused a nonsense mutation (C→T) and a premature stop codon, truncating the REP1 protein at amino acid position 33 of a 666 amino acid protein.

At 5 days post-fertilisation (dpf), mutants have defective swimming behaviour - moving in circles – showed absence of functional swim bladder (uninflated), reduced body length, curvature of the spin and increased pigmentation. Ocular features included noticeably smaller eyes and irregular eye pigmentation. Electron microscopic analysis showed that the retinal layers were disrupted in mutants (Starr, Kappler et al. 2004). The RPE were clearly disorganised, where some RPE were seen invading the ONL. Furthermore within the RPE layer, large vacuoles and undigested outer segments were observed. However, the *REP1* null mutation in zebrafish is embryonically lethal by 6 dpf. While the uninflated swim bladder seen in mutants prevents larvae from reaching the surface of the water to feed, lack of nutrition was not considered to be the cause of death. This was because wild-type larvae

are known to survive until 10 dpf without food (Starr, Kappler et al. 2004). As zebrafish do not possess a *choroideremia–like* gene (CHML/REP2), the CHM knock-out (KO) mutants manifest extremely severe systemic abnormalities that ultimately lead to lethality at 6 dpf (Starr, Kappler et al. 2004; Moosajee, Tulloch et al. 2009). Due to this extremely short survival rate, the use of the zebrafish KO model for CHM is limited.

1.7.3.7.2   The Choroideremia Mouse

Initial attempts to generate a *REP1* knock-out (KO) mouse surprisingly showed that null mutations were embryonically lethal in males and in heterozygous females when the mutation was transmitted through the female germline (van den Hurk, Hendriks et al. 1997). Death occurred *in utero* by E11.5 and it was suggested to be due to the lack of *REP1* in extra-embryonic tissues which was specifically seen to cause defects in trophoblast development and vascularisation of the yolk sac and placenta (Shi, van den Hurk et al. 2004). Lethality in the heterozygous female carriers was suggested to be due to the preferential inactivation of the paternal wild-type X chromosome in the extra-embryonic tissues, resulting in the expression of the mutant maternal allele (van den Hurk, Hendriks et al. 1997). Interestingly, histological analysis of carrier females (from chimeric males that had developed and transmitted the mutant *REP1* gene to female offspring) showed that these mice developed mild photoreceptor cell degeneration. While this model showed that murine *REP1* did indeed cause retinal changes, the mouse line was not possible to maintain as neither chimeric males nor carrier females could transmit the null alleles. Therefore further attempts to generate a mouse KO of *REP1* were warranted.

The process of generating mice with KO *CHM* alleles was described by Tolmachova *et al.* (Tolmachova, Anders et al. 2006) and is summarised in Figure 18.

The CHM mouse model was created using the *Cre/*loxP system of site specific recombination. For the initial stages, the targeting vector pTT55 (Figure 18B) which contains exons 3 and 4 of the murine *CHM* gene, as well as the *neomycin* and *spectinomycin* resistance cassette was generated. Two *loxP* sites were located either side of the resistance

cassette, positioned downstream from the 3' end of exon 4, while a third *loxP* site was inserted upstream from the 5' end of exon 4. Hence, two *loxP* sites where inserted either side of exon 4 in the murine *CHM* gene - as well as the resistance cassette. This allows for the conditional deletion of exon 4, which in turn causes a frameshift mutation leading to an early stop codon that results in the lack of a functional *CHM* gene in these mice. Targeting of ES cells with pTT55 and subsequent blastocyst injections resulted in the generation of *CHM*^*3lox* mice (Figure 18C).

These *CHM*^*3lox* mice were mated with the mouse line βMCM70, which expressed Cre protein as a fusion protein with 2 copies of the tamoxifen responsive (TM -responsive) estrogen receptor (MerCreMer) under the control of the ubiquitous CMV-enhanced chicken β-actin (CAG) promoter. When TM is bound to the MerCreMer receptor, this induces a nuclear translocation of the receptor which in turn catalyses the recombination event between the *loxP* sites. In this case, the recombination event between the two *loxP* sites both side of exon 4 and the subsequent KO of the *CHM* gene.

Male mice with an inducible *CHM* allele (*MerCreMer*^+ *CHM*^*3lox* males) were treated with TM which was administered to 6-8 week old mice by 5 intraperitoneal (i.p.) injections on 5 consecutive days (1 mg of TM per injection). This induced the recombination of the *CHM* floxed alleles and subsequent mutation in the germline in adulthood. When these mice were mated with WT females, the viable offspring carried the *CHM*^*WT* allele from the mother, and either the CHM^*3lox* or 1 of 3 possible deleted alleles, *CHM*^*Flox*, *CHM*^*null+Neo* or *CHM*^*null* from the father (corresponding to Figure 18D, E, F). In the case where *CHM*^*null+Neo* or *CHM*^*null* were transmitted, both are null alleles, while *CHM*^*Flox* is similar to wild-type, with the exception of two *loxP* sites on both side of exon 4.
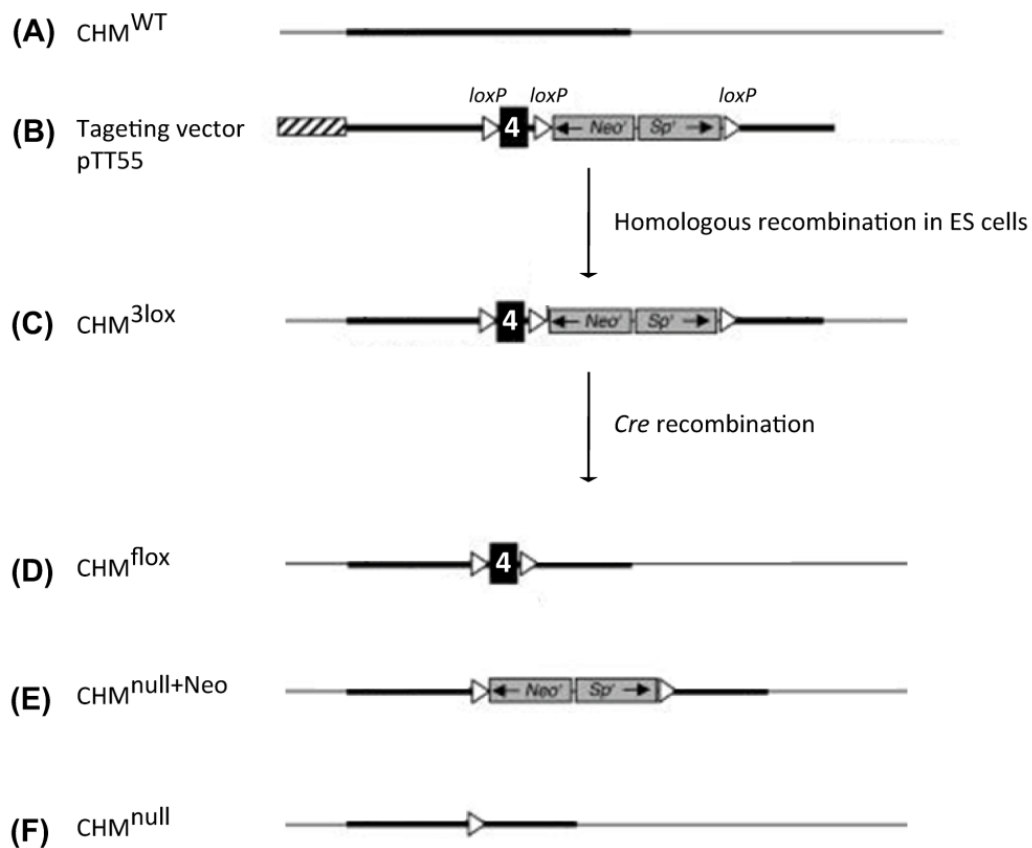
Figure 18: Summary of the generation of several CHM conditional and KO mice

Shown is the generation of mice carrying the conditional and KO *CHM* alleles. Several CHM mouse models were created using the *Cre/*loxP system of site specific recombination. (A) Initially the murine *CHM* gene was inserted into wild-type (WT) mice from (B) the targeting vector pTT55 which carries 3 *loxP* sites (indicated as white triangles), a *neomycin* and *spectinomycin* resistance cassette (indicated as grey box - Neo^r, Sp^r) and exons 3 and 4 of the murine *CHM* gene. The targeting vector was initially linearised and used for electroporation of GSI-1 embryonic stem (ES) cells *in vitro.* Followed this, isolated clones were then screening for correct integration of the vector using Southern blot analysis. Blastocyst injections of ES cells and subsequent homologous recombination in ES cells resulted in the transmission of the (C) *CHM^3lox* allele through the germ line. *Cre*-mediated recombination between the three *loxP* sites within the *CHM^3lox* allele resulted in three possible allele outcomes: (D) *CHM^Flox* (E) *CHM^null+Neo* (F)*CHM^null* (Figure adapted from (Tolmachova, Anders et al. 2006)).

This sophisticated approach ultimately produced heterozygous *CHM^null/WT* females that were viable carriers created to avoid the transmission of the *CHM*-null allele through the maternal germline. The *CHM^null/WT* females are mosaic for cells with normal REP1 function or no REP1 function. Hence approximately 50% of the cells are *CHM* KO cells. While this ratio may vary from one *CHM^null/WT* female mouse to another due to random X-inactivation, the analysis of

REP1 deficiency in these KO mice is highly valuable and can be used to understand and decipher the pathogenesis and disease progression of CHM further.

The first defects that were observed in the $CHM^{null/WT}$ females were RPE depigmentation by post-natal day (P) 7, as well as noticeable delays in the formation of photoreceptor outer segments and reduced thickness of the outer nuclear layer (ONL) by P17. By four months of age, retinal changes were more evident by areas of severe RPE depigmentation. This was accompanied by abnormal electroretinogram (ERG) readings. In these analyses white autofluorescent flecks were evident in some areas of intact retina. These most likely represent RPE depigmentation and lipid accumulation as a result of the photoreceptor outer segments not being digested normally by the RPE cells within the retina.

Histological analysis of older $CHM^{null/WT}$ mice (Figure 19) showed the late onset of photoreceptor degeneration. This was determined by counting the rows of nuclei in the ONL. It was observed that 2-month old female carriers showed a small reduction in ONL thickness from 10-12 to 8-10 nuclei. This was further reduced at 7 months where on average 7-8 nuclei were observed and by eight months only 5-6 nuclei were seen. Interestingly, the phenotype in the 8 month old carriers was variable between mildly affected areas and areas of severe degeneration where only 1-2 nuclei were seen. Furthermore mice also showed progressive degeneration of RPE cells resulting in patchy RPE depigmentation, RPE thinning and the occurrence of abnormal cells close to RPE cells. Indeed thinning of the RPE layer has also been characterised in human CHM patients (Syed, Smith et al. 2001).
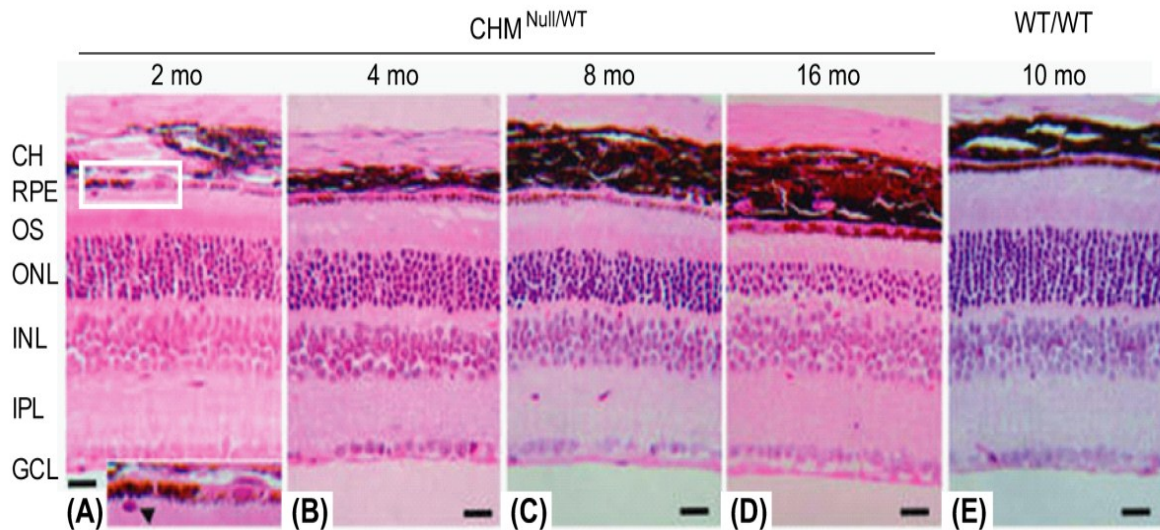
Figure 19: Histological analysis of eye sections from *CHM^null/WT* retinas at various time points

Shown are representative haematoxylin and eosin (H&E) stained retinal sections of *CHM^null/WT* mice at 2 (A), 4 (B), 8 (C) and 16 (D) months (mo), and *CHM^WT/WT* mice at 10 months (E). The retinas of *CHM^null/WT* mice shows the progressive photoreceptor degeneration with reduction of outer nuclear layer (ONL) thickness from 10-12 nuclei thick at 2 mo, to 5-6 nuclei at 8 mo and considerably less by 16 mo. This phenotype is also accompanied by RPE defects including patchy areas of RPE depigmentation as well as thinning. Furthermore occasionally abnormal cells were also seen in close proximity to the RPE cells (A, inset). CH, choroid; RPE, retinal pigment epithelium; OS, outer segments; ONL, outer nuclear layer; INL, inner nuclear layer; IPL, inner plexiform layer; GCL, ganglion cell layer (Figure adapted from (Tolmachova, Anders et al. 2006)).

Electron microscopy analysis of 9-month old *CHM^null/WT* mice (Figure 20) also showed considerable phenotypic variation. Some regions of the retina appeared normal, while others showed areas of depigmentation and the redistribution of pigment granules to the basal area of the RPE cells accompanied by normal rod outer segments (ROSs). Conversely, other areas of the retina showed severely depigmented RPE cells adjacent to shortened and structurally altered ROS. While in extreme cases severely degenerated photoreceptor cells were also seen.
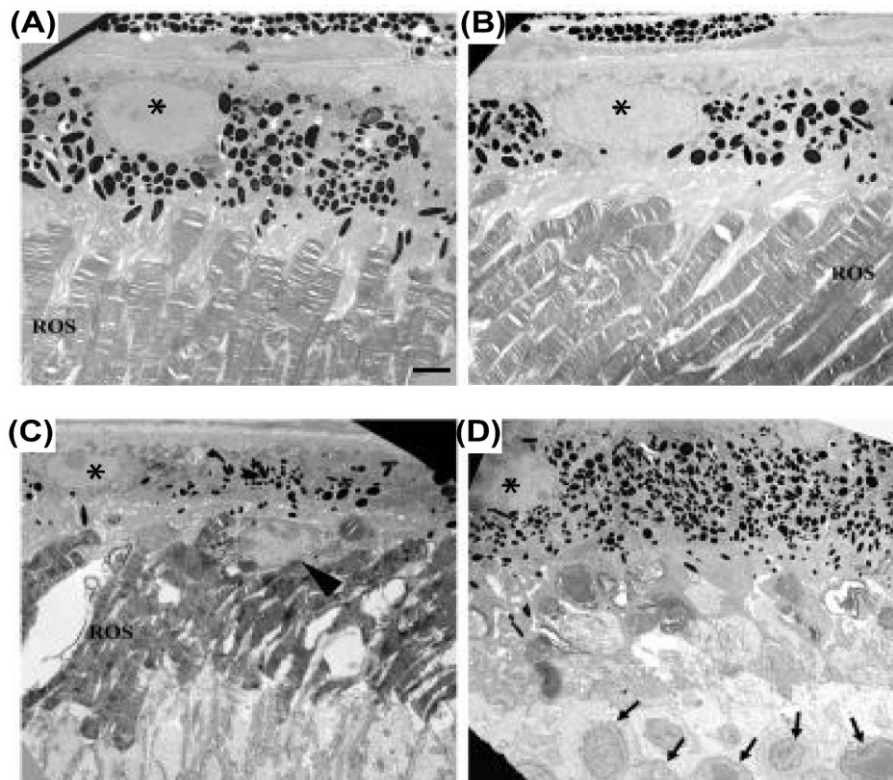
Figure 20: Electron microscopic analysis of a *CHM^null/WT* retina at 9 months old

Shown are representative electron micrographs of different regions from the same eye of a 9-month- old *CHM^null/WT* female mouse (A-D). (A) An area of the retina where the RPE and rod outer segments (ROSs) appear normal. (B) A region showing depigmented RPE cells with redistributed pigment granules in the basal area of the RPE cell, while ROSs are normal. (C) Another region of the retina shows severely depigmented RPE cells (highlighted by an asterisk) in close proximity to shortened and structurally altered ROSs. An abnormal cell close to the RPE is also seen (highlighted by an arrow head). (D) The final region highlights pigmented RPE cells which are adjacent to severely degenerated photoreceptors, where most of the ROSs have disappeared, resulting in photoreceptor nuclei (highlighted by an arrows) approaching the RPE cells (Figure adapted from (Tolmachova, Anders et al. 2006)).

Cumulatively, these data suggested that there was no direct correlation between depigmentation of the RPE and degeneration of the photoreceptors. Hence these two processes of degeneration in the photoreceptor and RPE cell layers may be independent. In order to investigate this further, a tissue-restricted *CHM* KO mouse was generated using the conditional alleles *CHM^3lox* and *CHM^Flox*. In the first model, *MerCreMer^+ CHM^3lox /Y* (and *CHM^3lox/3lox*) animals were induced with TM at 6-8 weeks of age as described earlier. These induced KO mice subsequently showed RPE degeneration which was also observed up to 14 months following induction with no effects on the photoreceptors.

An alternative model was also produced following the breeding of *CHM^Flox* mice with mice carrying a *six3-Cre* transgene (Furuta, Lagutin et al. 2000). Six3 is a transcription factor which is expressed in the neural retina during eye development (Bovolenta, Mallamaci et al. 1998; Hsieh, Zhang et al. 2002). Consistent with this, 2 months following TM induction these mice showed restricted KO in the neural retina, specifically prominent degeneration was observed in the photoreceptors where they showed shorter outer segments and a thinner ONL nuclei. Only mild RPE defects were observed including visible patchy RPE layer abnormalities. However these defects were attributed to the secondary changes observed due to the supportive role the RPE has towards the photoreceptors (Jaissle 2004).

Interestingly, *in vitro* prenylation reactions were performed on eye extracts from both tissue-restricted KO mouse models. The pattern of unprenylated Rabs in the eyes of the TM-induced *CHM^3lox/Y MerCreMer^+* mice were significantly different from that of the *CHM^Flox/Y six3-Cre^+* mice. This shows that in the RPE and neural retina, different subsets of Rabs are under-prenylated in the absence of *REP1* transgene. This implies both layers have intrinsic prenylation defects that ultimately lead to degeneration. Taken together, these results reflect independent degeneration of the photoreceptors and RPE cells in CHM.

To investigate the pathogenesis of the disease further, Tolmachova *et al.* recently showed the generation of three new *CHM* mouse models. These mice showed KO specifically seen in the photoreceptors, RPE cells or both layers and were called: *CHM^Flox, IRBP-Cre^+, CHM^Flox, Tyr-Cre^+* or *CHM^Flox, IRBP-Cre^+,Tyr-Cre^+* mice respectively (Tolmachova, Wavre-Shapton et al. 2010). Analysis of these mouse models was hoped to elucidate whether the *CHM* KO in one layer (either photoreceptors or RPE), could initiate or indeed affect the degeneration of the other layer. A summary of the histology analysis and main differences observed in these three *CHM* KO models is shown in Figure 21.

To achieve photoreceptor-specific *CHM* KO (*CHM^Flox, IRBP-Cre^+*), mice carrying the conditional allele *CHM^Flox* were crossed with the transgenic interphotoreceptor retinol binding protein (*IRBP-Cre*) mouse line. These mice express the *Cre*-transgene under the control of a tyrosinase promoter (as described previously in (Vooijs, te Riele et al. 2002). As described earlier, the *CHM^Flox* allele is a conditional allele that carries two *loxP* sites flanking exon 4 of the *CHM* gene. Thus recombination between these two sites leads to a frameshift

and early stop codon appearance (Tolmachova, Anders et al. 2006). Therefore *CHM^Flox*, *IRBP-Cre^+* mice have *CHM* KO specifically in the photoreceptors.

To create RPE specific *CHM KO* (*CHM^Flox*, *Tyr-Cre^+*), *CHM^Flox* mice were crossed with the transgenic *Tyr-Cre* mouse line (Tyr::CreB). These mice express the *Cre*-recombinase gene under the control of an artificial tyrosinase promoter (as described previously in (Delmas, Martinozzi et al. 2003)). This promoter is active in pigmented cells, including RPE and skin melanocytes. Therefore *CHM^Flox*, Tyr-Cre^+ mice have *CHM* KO specifically in the RPE cells. Finally to produce mice with *CHM* KO in both cell layers (*CHM^Flox*, *IRBP-Cre^+*, Tyr-Cre^+), the *CHM^Flox*, *Tyr-Cre^+* and the *CHM^Flox*, *IRBP-Cre^+* mice were mated together.

The histological analysis of *CHM^Flox*, *IRBP-Cre^+* mice showed slow progressive photoreceptor degeneration. Normal thickness in the ONL was observed at 6 months where approximately 8-10 nuclei were observed (Figure 21C & H). In contrast, by 12 months the ONL was reduced by as much as 30% showing only 7-8 rows of nuclei compared to control mice - *CHM^Flox* - which showed 10-12 nuclei at the same time point (Figure 21G & H). Conversely, the RPE cells retained a normal morphology with normal pigmentation and melanosome distribution.

Together, these date show that *CHM^Flox*, *IRBP-Cre^+* mice have late onset photoreceptor degeneration (due to the KO of functional REP1 in these cells), in the presence of normal RPE, implying that photoreceptors are an independent site of the CHM disease.

In contrast, *CHM^Flox*, Tyr-Cre^+ mice exhibited coat colour dilution. These mice were lighter (chocolate rather than black) coat colour compared to the *CHM^Flox* animals on the same C57BL/6 genetic background. This lightness is presumably is a result of the *CHM* deletion within the melanocytes, which in turn affects the biogenesis and transport of melanosomes within the skin cells - melanocytes - of these mice (Wasmeier, Hume et al. 2008).

Electron microscopy of these mice further confirmed the disruption of melanosomes distribution within the RPE. Areas of melanosomes remained in the main body of the cell and did not enter the apical processes as seen in wild-type mice. This phenotype is also observed in Rab27a mutant mice (Lopes, Ramalho et al. 2007); hence these changes may be caused by Rab27a dysfunction.

Histological analysis revealed normal photoreceptors and intact ONL, with no reduction in the number of cells. In contrast pigment/melanosome abnormalities were observed. Specifically, homogenous melanosomes distribution was not observed as seen in wild-type mice (Figure 21B & F). The analysis of this RPE specific KO model confirmed previous finding that the degeneration of the RPE and photoreceptors in CHM disease is caused by intrinsic events which occur within each layer. This is contrary to assumptions that the degeneration of one layer leads to secondary degeneration of the other layer. Thus both layers could be considered as the primarily sites in CHM.

In the final effort to understand whether one layer could influence the adjacent layer within the retina, *CHM* KO in all both photoreceptors and RPE cells was established and *CHM^Flox^, IRBP-Cre^+^*, Tyr-Cre^+^ mice were examined. Interestingly, histopathologic studies of 6-month-old mice showed normal morphology of RPE cells. In contrast photoreceptor degeneration was considerably enhanced. A dramatic decline in the number of ONL nuclei was observed compared to the control mice as well as the single-layered KO mice (Figure 21D & H). Despite this clear initial enhancement of photoreceptor degenerationat 6 months, the progression of degeneration remained steady and did not continuing to deteriorate at a rate higher than the single-layered KO mice. Indeed by 12 months, the level of photoreceptor degeneration in these mice was comparable to that of single-layered KO mice (Figure 21 H & I). This data suggests that the degeneration of the photoreceptors in this double KO *CHM* model is enhanced in the presence of normal RPE cells in younger mice. However this appears to level and in older mice this degeneration approaches that seen in the single layered KO mice.

Overall one can say that the combination of photoreceptor and RPE disease (observed in the double-layered KO mice) is not equal to the sum of the effects seen in each individual cell type (observed in the single-layered KO mice).

Interestingly, electroretinograms (ERGs) and scanning laser ophthalmoscopy (SLO) analysis were carried out on all three *CHM* mouse strains. Both analyses supported the histopathological findings seen in all three groups of mice. Noticeable abnormal autofluorescent mottling of the retina was seen in 8- and 14-month-old *CHM^Flox^,* Tyr-Cre^+^ and *CHM^Flox^* mice. Levels of autofluorescence were consistent and equally obvious at both

time points. This is consistent with pigment irregularities seen in these mice following electron microscopy analysis. The retinas of *CHM^Flox, IRBP-Cre^+*, mice showed normal autofluorescence levels at 8 months; while considerable multiple dot-shaped autofluorescence was observed in mice older mice presumably due to physiological aging of the RPE. Interestingly, in the double-layered KO mice, 8- and 14- month old mice presented abundant autofluorescence of both types (mottled and dot-like specks).

White autofluorescent mottled specks/flecks were observed which were dim in colour and irregular in appearance. These specks most probably represent areas of RPE depigmentation, while dot-like specks, which were round and regular in appearance, usually represent intraretinal changes. Analysis of the dot-like specs was carried out. This was done by staining of whole mounts for the ionized calcium adaptor molecule (Iba-1), which is a marker for cells of microglia origin. Following staining, significantly higher levels of Iba-1-positive structures where seen in the retinas of the double-layered KO, compared with both single-layered KO mice (Figure 21J). Microglia cells are scavenging cells presumably recruited to the retina to clear debris produced by dying photoreceptors. Indeed this is in agreement with the increase degeneration seen in these mice. Interestingly, this increased microglia phenotype is consistent with the retinal remodelling theory proposed previously to explain the various changes in the retinas of CHM patients (Jacobson, Cideciyan et al. 2006). In the early stages of CHM disease, retinal thickening is observed which has been shown to be one of the stages involved in retinal remodelling through Müller (microglia) cell hypertrophy.

If one takes the enhanced functional and photoreceptor defects seen in the younger double-layered KO mice, this implies that the presence of a diseased RPE considerably effects the rate of photoreceptor degeneration. Both these results highlight the significant interactions present between these adjacent cell layers and the influence that this has on the degeneration of the retina in CHM.

Interestingly, in older mice, the levels of photoreceptor degeneration appear to reach similar levels between the single layered photoreceptor *CHM* KO mice, and the double CHM KO mice. This suggests that the RPE disease does not negatively affect the ultimate fate of

the *CHM KO* photoreceptor survival. Taken further, the *CHM* RPE may be behaving similar to a prematurely aged RPE.

Other results also appear consistent with previous findings that both layers are the primary sites of CHM disease (Tolmachova, Anders et al. 2006). Indeed RPE abnormalities and normal photoreceptors were seen in the RPE-specific KO mice. Similarly, slow degeneration of the photoreceptors and normal RPE were seen in the photoreceptor-specific KO mice. Cumulatively the histological and functional studies show a complex relationship between the survival and function of photoreceptors, RPE status and aging.

Indeed the single-layered REP *CHM* KO mice show morphologically normal photoreceptor cells, however, upon functional ERG studies, the mice showed mild functional impairments of these photoreceptor cells. This supports the idea that CHM is a retinal disease that is initially manifested as sight impairment due to the functional defects within the cell layers affected in the disease. However this then leads to progressive cell death. This is potentially very important for future gene therapy of *CHM,* as functional deficit may potentially be overcome if the expression of *REP1* transgene is targeted to both RPE and photoreceptor cells.
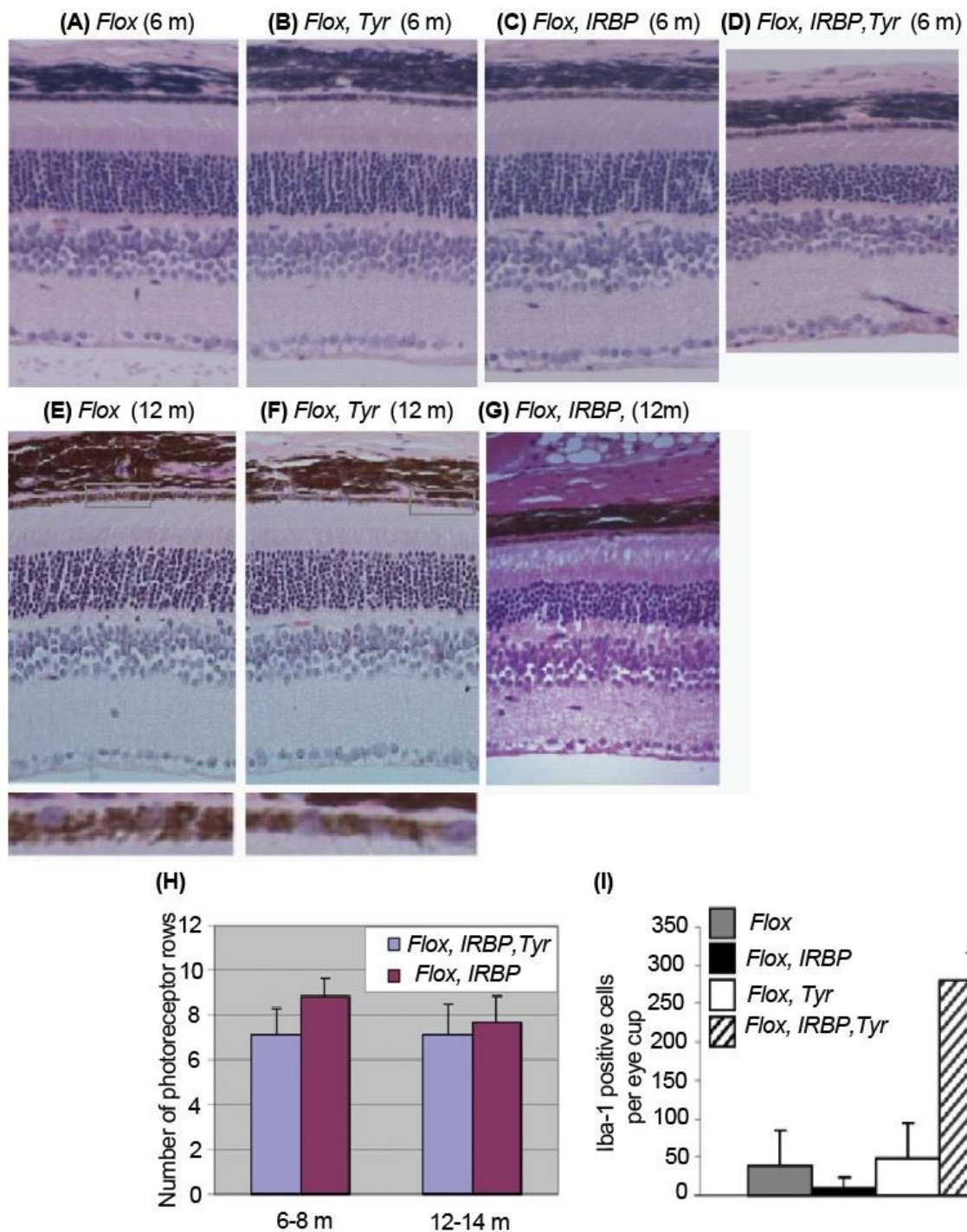
Figure 21: A summary of the main differences in the *CHM* KO mouse models

Histological analysis of sections of eyes from (A and E) *CHM^Flox* (Flox (control) mice, (B and F) *CHM^Flox,* Tyr-Cre+ (Flox, Tyr) mice, (C and G) *CHM^Flox, IRBP-Cre+* (Flox, IRBP) mice, (D) *CHM^Flox, IRBP-Cre+*, Tyr-Cre+ (Flox, IRBP, Tyr) mice at 6 and 12 months respectively.
(H) Morphometric analysis of the photoreceptor rows in the central retina in the Flox, IRBP (purple bars) and Flox, IRBP, Tyr (blue bars). (I) Quantitative data of the number of Iba1-positive cells per eye cup from 11-to 12-month-old Flox (gray bar), Flox, IRBP (closed bar), Flox, Tyr (open bar) and Flox, IRBP,Tyr (hatched bar) mice
(Figure adapted from (Tolmachova, Wavre-Shapton et al. 2010)).

1.8   Summary and Project Aims

Many efforts for ocular gene therapy are based on viral vectors, however currently there is neither a treatment nor cure for CHM patients. There are numerous reasons why CHM is a suitable candidate for local gene therapy:

(1) The complete human cDNA, which encodes the REP-1 gene has been identified and cloned.

(2) CHM patients have mutations in the REP-1 gene, which cause the loss of function of the REP-1 gene in majority of cases.

(3) A mouse model of CHM was recently created (Tolmachova, Anders et al. 2006; Tolmachova, Wavre-Shapton et al. 2010), which has all the characteristic hallmarks of CHM: progressive degeneration of photoreceptors, patchy depigmentation of the RPE and defects in Rab prenylation.

(4) CHM is particularly suitable for gene therapy due to the slow rate of degeneration, as well as the possibility of early diagnosis before the onset of detrimental changes occurs.

(5) The small size and the high degree of compartmentalisation of the eye allows accurate delivery of vector suspensions to necessary tissues. Specifically subretinal injections enable the delivery of vector suspensions into the potential space between the photoreceptors and the RPE (Bainbridge, Tan et al. 2006), key areas affected in CHM.

Our hypothesis is that S/MAR based vectors are suitable gene delivery plasmids for CHM, due to their non-viral nature and the fact that CHM is not a life threatening disease. Currently non-viral vectors face two main problems when compared to the efficient viral gene therapy alternatives. These include: delivery of the vector and the maintenance of the transgene. Hence we will endeavour to utilise techniques currently being used by our group for viral vector administration.

For efficient delivery of S/MAR vector chemical formulations combined with direct subretinal injections will be used, thus we will overcome these hurdles and establish a long-term transgene expression within the eye.

We aim to utilise S/MAR based vectors for the development of a persistently expressing vector for CHM. In particular the aims of this project are:

- Demonstrate the potential of S/MAR sequences to drive long-term transgene expression *in vitro* to verify and extend previous observations reported in the literature.
- Development of a novel non-viral S/MAR vector for the therapeutic purposes of CHM gene therapy, specifically the development of an S/MAR based vector containing REP1.
- Development of proof-of-principle experiments validating novel non-viral S/MAR vectors *in vitro,* including the introduction of the S/MAR vectors containing REP1 into CHM derived cells as well as the analysis of phenotypic correction/rescue.
- Development of S/MAR vectors for long-term gene delivery in the mouse retina, including delivery optimisation and plasmid safety validation *in vivo.*
- Delivery of novel S/MAR vectors in CHM mice, the analysis of long-term gene expression in the mouse retina of CHM disease as well as the analysis of phenotypic and functional rescue/correction.

2 MATERIALS &METHODS

_____

2.1 Materials

2.1.1 General Chemicals

Agarose electrophoresis grade	Invitrogen (UK)
Ampicillin	Sigma-Aldrich (USA)
Bovine Serum Albumin (BSA)	New England Biolabs
2'-desoxynucleotide 5'-triphosphate mix (dNTPs)	Invitrogen
EDTA (ethylenediaminetetraacetic acid)	BDH (UK)
Ethanol	BDH
Ethidium bromide	Sigma-Aldrich
Formaldehyde	BDH
Glucose	BDH
Glycerol	BDH
Isopropanol	Sigma-Aldrich
Kanamycin	Sigma-Aldrich
LB broth	Invitrogen
Luciferin	Gold Biotechnology (USA)
Molecular weight DNA markers	Invitrogen and Bioline (USA)
Paraformaldehyde Invitrogen	Sigma-Aldrich
Sodium dodecyl sulphate (SDS)	Sigma-Aldrich

2.1.2 Enzymes and molecular biology reagents

All restriction enzymes were from NEB Biolabs (New England Biolabs, Hitchin, UK) and were used with the appropriate buffer.

2.1.2.1 Enzymes for DNA manipulation

Klenow large DNA polymerase I	Invitrogen
T4 DNA ligase	Invitrogen

2.1.2.2 PCR reagents and DNA size markers

DNA Ladders (100 bp and 1 kb)	Invitrogen
dNTPs	Invitrogen
Taq DNA polymerase	Invitrogen

2.1.2.3 Buffers, Solutions and Media

DNA Loading Buffer 6x	5 Mm EDTA
	40% (v/v) Glycerol in ddH$_2$0
	0.25% (w/v) Bromophenol Blue
SSC 20 x	3M NaCl
	0.3M Sodium Citrate, pH 7.0
Luria Broth - LB medium (1x concentration)	12.5 g / 500 ml of LB + 500 ml sterile H$_2$0
LB + Agar (1x concentration)	12.5 g / 500 ml of LB 7.5 g / 500 ml of Agar + 500 ml sterile H$_2$0

2.1.3 Tissue culture reagents

Dulbecco's Modified Eagle medium (DMEM)	Invitrogen
RPMI 1640	Invitrogen
DMEM:F-12	Invitrogen
OPTIMEM serum-free medium	Invitrogen
1 x PBS	Invitrogen
Trypsin-EDTA solution	Invitrogen
Penicillin/streptomycin reagent	Invitrogen
Lipofectamine 2000 reagent	Invitrogen
Lipofectin	Invitrogen
Fetal Calf Serum (FCS)	Invitrogen
Geneticin (G418)	Invitrogen
Antibiotic-Antimycotic	Invitrogen
Dispase	Sigma-Aldrich

2.1.4 Antibiotics

Stocks solutions of antibiotics were prepared at working concentrations below and stored at -20°C.

Ampicillin (Amp)	100 mg/ml	Sigma-Aldrich
Kanamycin (Km)	50 mg/ml	Sigma-Aldrich

2.1.5 DNA extraction and purification kits

QIAGEN Endotoxin Free Plasmid kit	Qiagen Ltd (UK)
QIAquick PCR Purification Kit	Qiagen Ltd
QIAquick Gel Extraction Kit	Qiagen Ltd
Sigma GenElute Mammalian Genomic DNA	Sigma-Aldrich

2.1.6 Plasmids

Plasmids	Size (bp)	Original source (group)	Resistance
pEOS	5084	Personal Efforts	Kanamycin
pEFS-EGFP	6184	Personal Efforts	Kanamycin
pEFS-EGFP-Control	4184	Personal Efforts	Kanamycin
pEOS-CAG-S/MAR	6810	Personal Efforts	Kanamycin
pEOS-CAG-MCS-S/MAR	6838	Personal Efforts	Kanamycin
pCAG-EGFP	7691	Personal Efforts	Kanamycin
pCAG-EGFP-Control	5691	Personal Efforts	Kanamycin
pEOS-EFS-S/MAR	5384	Personal Efforts	Kanamycin
pEFS-REP1	7352	Personal Efforts	Kanamycin
pEFS-REP1-Control	5352	Personal Efforts	Kanamycin
pCAG-REP1	8830	Personal Efforts	Kanamycin
pCAG-REP1-Control	6830	Personal Efforts	Kanamycin
pEPI-MCS1	5366	Ms. Azadeh Cheraghchi Bashi (Masters Student – Imperial College London)	Kanamycin
pEPI-EGFP	6695	Prof. Hans Lipps, Witten, Germany	Kanamycin
pEPI-Luc	7611	Prof. Hans Lipps, Witten, Germany	Kanamycin
pUbqC-Luc	7619	Prof. Hans Lipps, Witten, Germany	Kanamycin
pWPT-GFP		Dr D. Trono, University of Geneva, Switzerland and/or Addgene	Ampicillin
pBC SK +	3400	Commercial - Stratagene	Chloramphenicol
pWPI-REP1	13101	Dr D. Trono, University of Geneva, Switzerland	Ampicillin

2.2 Methods

2.2.1 Growth and Maintenance of Cells

2.2.1.1 Mammalian cells

Mouse anterior pituitary cells (AtT20 cells) were maintained in a 3:1 ratio of Dulbecco's Modified Eagle's Medium (DMEM):F-12 (Invitrogen, UK), supplemented with 25 mM glucose, 15% fetal bovine serum (FBS), 100 U/ ml penicillin and streptomycin 100 U/mL penicillin. Mouse RPE cells were maintained in RPMI 1640 (Invitrogen), while Porcine RPE were maintained in DMEM supplemented with 10% FBS, 100 U/ ml penicillin and streptomycin 100 µg/mL. All cells were grown at 37°C in a humidified incubator with 10% CO_2. All cells were allowed to reach 80-90% confluency before being split by aspirating the growth medium, washing with phosphate buffered saline (PBS) to remove the remaining medium, adding Trypsin-EDTA and incubating at 37°C until all the cells had begun to detach. Media was then added to neutralise the trypsin solution. Cells were then pelleted by centrifugation at 1000 g for 5 mins. An aliquot of these cells were then seeded into a new flask.

2.2.1.2 Long-term storage in liquid nitrogen

For the long-term storage of all cells, confluent cells were trypsinised and centrifuged as above and resuspended in FCS containing 10% DMSO. They were then aliquoted into cryotubes and frozen slowly at -80°C for 24 h. After which the vials of cells were stored in liquid nitrogen until required. To bring cells up from the liquid nitrogen, the cells were thawed rapidly by placing then in a water bath at 37°C. Once thawed, this aliquot was diluted in fresh growth medium and cells were pelleted at 1000 g for 5 mins, before which they were resuspended in the required growth medium and seeded into a new tissue culture flask. The following day, the media was aspirated away and replaced with fresh medium to ensure the removal of any traces of remaining DMSO.

2.2.2 Primary fibroblasts

Human primary fibroblasts were maintained in DMEM supplemented with 25 mM glucose, 15% fetal bovine serum (FBS), 100 U/ ml penicillin and streptomycin 100 U/mL penicillin.

While mouse primary fibroblasts were maintained in DMEM supplemented with25 mM glucose, 15% heat inactivated FBS (65°C for 30 min), 500 U/ ml penicillin, 500 U/ml streptomycin and 25 µg/ ml amphotericin B (PSA).

2.2.2.1 Isolation of primary mouse fibroblasts

Mouse fibroblasts were isolated from 2-3 day old pups. Necks were dislocated following with the removal of the head, legs, arms and tail. Starting from the neck, a small incision was made and using blunt scissors the skin was peeled away from the body while trying to maintain the skin in one piece. Once removed, the skin was washed twice in 5% PBS/PSA, and the dermis (the side of the skin on the inside of the mouse) was cleaned to removal blood and fat from this layer. The entire dermis was then cut into small pieces (~1 cm^2) and epidermis side-up, was placed into 1-well of a 6-well plate. Following a brief period of attachment, 1 ml of medium containing 5% dispase/medium was gently added to the cells, to allow for the gentle dissociated of the epidemis and dermis layers. Tissues were then incubated at 37°C for 1-2 hours or overnight at 4°C. After this time, the dermis was removed with a scalpel while and the epidermis (dryer and whiter layer) was discarded. The dermis was then cut into very small pieces with scissors and a sterile scalpel and placed into a fresh 1-well of a 6-well plate, were they were then allowed to dry and attach for a brief period of no more than 10 mins. Following this fresh medium supplemented with PSA and heat inactivated FBS was added to the dermis and incubated for 2-3 days at 37°C in 10% CO$_2$. This allowed sufficient time for cells to growing underneath the pieces of attached demise. Following this period of incubation, the dermis was detached by the addition of growth medium and vortexed vigorously 10-20 times before being centrifuged at 0.8 g for 5 mins. Medium was aspirated off and the pelleted cells were placed in a new 10-cm dish for regrowth. This allowed the fibroblasts which had attached to the base of the dermis pieces to be removed and evenly spread in the 10-cm dish. The following day, the medium containing all the dermis and unattached cells were removed and replaced with fresh complete medium. Once the cells had reached 80-90% confluency in the first passage cells were detached with trypsin-EDTA as described earlier, counted using a haemocytometer where they were replated at a density no greater than 5 x 10^4 cells per flask. This ensured

that the cells in the first passage were allowed sufficient space to grow and establish. Densities larger or smaller considerably affected the subsequent growth of the cells.

2.2.2.2 *Isolation of primary RPE cells*

Retinal pigment epithelium (RPE) primary isolations were described previously (Lopes, Ramalho et al. 2007). Porcine RPE were harvested in a similar manner with the exception that cells were released from the posterior eyecups by treatment with 10x Trypsin (Invitrogen).

2.2.3 Preparation of Bacterial Plasmids
2.2.3.1 *Small scale plasmid preparation*

For small scale plasmid isolation the QIAGEN Miniprep Kit (Qiagen) was used. Bacterial cultures for plasmid preparation were grown from single colonies which were picked from a freshly streaked selective plate. A single colony was incubated in 5 ml LB broth containing the appropriate antibiotic and grown at 37°C in a shaking incubator (225 rpm) overnight. Bacteria were then pelleted by centrifugation at 4 000 rpm for 5 mins in a benchtop centrifuge. The pellet was then resuspended and lysed in the provided lysis buffer. The solution was neutralised and proteins were precipitated by added neutralisation buffer. Debris was spun out by centruifugation at 13 000 g for 15 mins. The resulting supernatant was then passed through a Spin Column Assembly to allow binding to the column matrix. Following two washes, the pDNA was eluted in 50 µl of elution buffer or sterile water.

2.2.3.2 *Large scale plasmid preparation*

For the large scale plasmid isolation the Endo-free Plasmid Maxiprep kit (Qiagen) was used according to the manufacturer's recommendations. Briefly, a 5 ml starter culture of *E. coli* strain containing the required plasmid of interest was used to inoculate 500 ml of fresh sterile LB broth in a 2 L flask containing the appropriate antibiotic. Bacterial cells were subsequently harvested by centrifugation for 15 mins at 6000 rpm using a Sorvall GSA-1500

rotor. The pellet was then resuspended in resuspension buffer, before being lysed at room temperature for 5 mins followed by neutralisation with neutralization buffer. Lysate was then passed over a column with an ion-exchange resin, which binds DNA at a pH of 7 and ionic strength of 750 mM NaCl. A medium salt wash was used to remove RNA, proteins and low molecular weight impurities. The DNA was eluted followed by precipitation with isopropanol and pelleted by centrifugation at 15 000 g for 30 minutes in a Sorvall SA-600 rotor. The pellet was subsequently washed with 70% ethanol before being resuspended in sterile water and stored at -20°C.

2.2.4 Preparation of genomic DNA

For the preparation of genomic DNA from cells and tissues, GenElute Mammalian Genomic DNA Miniprep kit (Sigma) was used according to the manufacturer's recommendations.

2.2.5 Determination of DNA purity and concentration

Ultraviolet absorbance spectrophotometry was used to determine the purity and concentration of DNA. The absorbance of nucleic acids at 260 nm was used to calculate the concentration of nucleic acid in the sample. The absorbance ratio of A_{260}/A_{280} provides an estimate for the purity of the nucleic acid. Acceptable levels of purity have ratios between 1.7-1.9. The optical density was measured using a Nanodrop ND1000 Spectrophotometer (Thermo Fisher Scientific, Wilmington, Delaware, USA).

2.2.6 Digestion with restriction enzymes

DNA was digested with restriction endonucleases according to the manufacturer's instructions. DNA samples were digested with appropriate enzyme in the compatible buffer supplied, with distilled water and bovine serum albumin (BSA) if required. For cloning purposes normally 2 μg of vector DNA and 3 μg of insert DNA were digested for 2 hours at 37˚C in a total volume of 20 μl or 30 μl respectively. The appropriate 10 x Buffer was added to the reaction volume (final concentration 1 x) with the remaining volume made up with

distilled water. For proceeding steps, all digested vector or insert DNA was heat inactivated by incubation at 65˚C for 20 minutes. Double digestions were either performed in one step if the enzymes performed optimally in the same buffers or in two steps with DNA precipitation between digests. The amount of DNA was reduced to 200 ng if the digestion was used as a general check for the correct insertion of a DNA fragment.

2.2.7 Digestion with DNA modifying enzymes
2.2.7.1 Klenow reaction

Prior to ligations, vector and insert DNAs with incompatible sticky ends were treated with Klenow fragment (Invitrogen) in order to blunt end the fragments. The Klenow fragment of *E. coli* DNA polymerase I is a large protein fragment that exhibits 3' to 5' exonuclease activity as well as 5' to 3' polymerase activity. Digestions with restriction enzymes in some circumstances leave 5' overhangs; therefore the subsequent digestion with Klenow enzymes is able to create blunt ends in these DNA fragments. For the enzyme to proceed with the filling-in reaction, the entire DNA from a digestion reaction was treated with 1-2 µl of Klenow enzyme (0.5U/µl) with the provided buffer and dNTPs (final concentration of 0.1 mM). The reaction was incubated at room temperature for 30 minutes after which the enzyme was heat inactivated at 65˚C for 20 minutes.

2.2.7.2 Ligation

In order to subclone insert DNA fragments into vectors - with either sticky or blunt ends – the T4 DNA ligase enzyme (Invitrogen) was used for ligations. Hence DNA fragments generated after restriction digestion or after blunt ending were ligated together in a total volume of 10 or 20 µl overnight at either 14˚C or room temperature for sticky or blunt end ligations respectively. Reactions consisted of 1-2 µl T4 ligase (1U/ µl) in the provided 10 x T4 ligase buffer. The ratio of vector to insert in the ligation reaction was 1:11 as the vector DNA was not dephosphorylated. The ligation mixture was subsequently digested with an appropriate enzyme which allowed the cleavage and subsequent inactivation of self-ligated

vector DNA as well as other unwanted plasmid or ligation species in the ligation mixture, as previously described in (Tolmachov 2009). When using this selection approach, the vector, the desired insert sequence as well as their junctions where checked to ensure they did not contain any internal sites for the restriction enzyme used to digest the ligation mixture. Hence this technique linearises unwanted circular products within the ligation reaction and renders them incapable of replicating in bacteria. DNA precipitation was performed on the DNA after the overnight ligation reaction and before the subsequent digestion of the ligation mixture. From this digested ligation reaction, 5 µl was transformed into competent JM109 cells. The quality, quantity and digestion of DNA was analysed after each digestion step by agarose gel electrophoresis on gels ranging from 0.8-1.2%.

2.2.8   Transformation of bacteria

For cloning steps JM109 competent cells were used (Promega). This *E. coli* based strain contains the recA mutation was prevents undesirable recombination events and leads to plasmid stability. For plasmid isolation 30-100 ng of DNA was transformed into ultracompetent *E. coli* DH5α or XL10-Gold cells (Invitrogen).

2.2.9   Polymerase Chain Reaction (PCR) amplification

Colonies that formed from the transformation of competent cells were amplified and screened by PCR analysis using a Robocycler thermal cycler (Stratagene) to check if the correct insert was present. The usual PCR reaction mixture contained a 12.5 µl reaction mix was prepared containing:

Component (concentration)	Volume (µl)	Final amount or concentration
10x Taq-Buffer (Invitrogen)	1.25	1 x
MgCl$_2$ (50mM)	0.375	1.5 x
DNTP mixture (1mM)	2.5	0.2 mM
Forward Primer (2.5mM)	2.5	0.5 mM
Reverse Primer (2.5mM)	2.5	0.5 mM
Sterile H$_2$O	3.25	
Taq DNA polymerase (5 U/ µl)	0.125	
	12.5	

The primers used were: For the PCR analysis of plasmid pEFS-EGFP,
Forward: F EGFP6 (5'- CGAGAAGCGCGATCACATGG -3') and
Reverse: R S/MAR (5'- GCAAAGCATGAGATGTGTGGGGAT -3').
This yielded a 450 bp fragment.

For PCR analysis of plasmid pCAG-EGFP,
Forward: F CAG F3 (5'- GCAACGTGCTGGTTGTTGTGC -3') and
Reverse: R EGFP R1 (5'- CATCTGCACCACCGGCAAG -3')
This yielded a 250 bp fragment.

For PCR analysis of plasmid pEFS-REP1,
Forward: F RH4 (5'- ATTCGTCAGACATCAGCAGG -3') and
Reverse: R S/MAR (5'- GCAAAGCATGAGATGTGTGGGGAT -3')
This yielded a 590 bp fragment.

For PCR analysis of plasmid pCAG-REP1,
Forward: F CAG F3 (5'- GCAACGTGCTGGTTGTTGTGC -3') and
Reverse: R REP1R2 (5'- TATGCCAGTCAGGATTTGCATGAA -3')
This yielded a 430 bp fragment.

For the annealing of MCS2,
Forward: MCS2 Forward/Upper2 (5'- TCGAAGGATCCTAGCACGCGTGTCGACA -3') and
Reverse: MCS2 Reverse/Lower2 (5'- TCGATGTCGACACGCGTGCTAGGATCCT -3')

The specific PCR reaction conditions used were:

Step	pEFS-EGFP & pCAG-EGFP	pEFS-REP1 & pCAG-REP1
(1) Activation	95°C – 3 min	95°C – 5 min
(2) Denaturation	95°C – 40 min	95°C – 40 min
(3) Annealing	**59**°C – 40 min	**57**°C – 40 min
(4) Elongation	72°C – 1 min	72°C – 1 min
(5) Prolonged elongation	72°C – 10 min	72°C – 10 min

Repeat of steps (2)-(4) for 32 cycles.

As a positive control, 1 µl of a 1 in 10 dilution of the ligation reaction was included. Amplified colonies were checked by running samples on 1.2% agarose gels. Colonies that tested positive after PCR amplification were isolated for small-scale plasmid preparation and subsequent restriction digestion (described above) to analyse the integrity of restriction sites within the newly formed plasmid.

2.2.10 Transfection and gene expression experiments
2.2.10.1   *Cells Transfections*

One day prior to transfection B16-F10 and AtT20 cells were seeded in either 10-cm dishes or 6-well plates at a concentration of 5 x 10^5 or of 2.5 x 10^5 per dish or plate for AtT20 and B16-F10 cells respectively, while fibroblasts were seeded in 12-well plates at a concentration of 5 x 10^4 cells per well. Transfections were carried out using Lipofectamine 2000 (Invitrogen), Calcium Phosphate (Promega) or *in vivo*-jet-Polyethylenimine (PEI) (Invivogen) following the manufacturer's instructions. The following ratios of DNA:transfection reagent were used: 0.4 µg DNA: 1 µl Lipofectamine 2000, 1 µg DNA: 3.1 µl Calcium Phosphate, 1 µg DNA: 2 µl jet-PEI.

The DNA used in transfections with Lipofectamine 2000 was diluted in OptiMEM (Invitrogen), while the DNA in calcium phosphate and PEI transfections was diluted in HBS and NaCl respectively. Complexes were allowed to form for 20-30 minutes at room temperature. During the incubation time cells were gently washed with PBS prior to the

addition of the transfection reagent/DNA complex. The cells were incubated with the complexes overnight, at which time the transfection mixture was removed and replaced with normal growth medium. Cells were incubated for 48 hours before they were analysed for transient transfections.

Primary fibroblasts were transfected with pCAG-REP1 plasmid by nucleofection using the AMAXA nucleofector apparatus and the fibroblast kit (Lonza, Cologne). Briefly, 5×10^5 cells were pelleted by centrifugation at 200 g for 5 mins and resuspended in 100 µl of transfection solution supplied with the kit. Plasmid DNA pCAG-REP1 (20 µg) was added to the cells and the suspension was added to cuvettes. Nucleofection was performed in the apparatus using the setting programmes P32, P24 and Q32 for human fibroblasts or programmes Q32, U23 and W32 for mouse fibroblasts. Following nucleofection, cells were taken out of the cuvettes and gently added to 2 ml of pre heated complete medium. Cells were incubated overnight prior to analysis.

Primary RPE cells were transfected using Lipofectin reagent (Invitrogen) according to manufacturer's recommendations. Briefly, the transfection medium containing 1 µg of plasmid DNA (pDNA) and 6 µl of Lipofectin reagent in serum free medium was incubated for 15 min at room temperature (RT) and then added to RPE cells overnight. Expression of EGFP was analysed 48 hours post transfection by immunofluorescence of transfected cells.

2.2.10.2   Drug-resistance selection

AtT20 cells were seeded in 6-well plates, stably transfected and re-plated into 2 x 10 cm dishes 18 hours after transfection. Stably transfected AtT20 cells were selected 24 hours after transfection by the addition of Geneticin (G-418) (Invivogen) in DMEM:F-12 medium (0.5 mg/ml). G418 selection lasted 2 weeks, with G418-supplemented media being changed every 3-4 days. After 2 weeks of selection, isolated cell colonies (containing the *neo* drug resistance gene) were picked and transferred into fresh 24 well plates for re-growth. After sufficient growth, half the cells were grown in medium with selection (G418 medium) while

the other half was maintained in normal medium. At different time intervals, GFP expression was analysed by FACS analysis.

2.2.11 Flow Cytometry

The long term transfection efficiency as well as EGFP expression of AtT20 stably transfected cells was determined by fluorescent activated cell sorter (FACS) analysis at different time intervals post transfection. Cells were washed twice with FACS buffer (PBS, 0.5% BSA, 0.01% sodium azide) containing TOPRO-3-iodide (Molecular Probes, Paisley, UK) to stain dead cells. Fluorescence was analysed using a FACSCalibur system (Becton Dickinson biosciences, San Jose, CA), equipped with a 488 nm argon ion laser. Results were analysed using CellQuest software (Becton Dickinson biosciences, San Jose, CA). For each sample, a minimum of 10,000 events were collected. The cells were visualised on an FSC (forward scattering) versus SSC (side scattering at 90%) display. The samples were analysed on the cytometer and plots of sidescatter (SSC) against EGFP fluorescence (FL1) were plotted. A threshold level of fluorescence was set such that 1% of untransfected cells fell about it. The percentage of cells fluorescing at a level above this threshold was taken as the percentage of cells transfected and this was shown graphically on the histograms obtained for each sample by M1.

2.2.12 Antibodies

The following antibodies were used at the dilutions indicated: anti-α-tubulin mouse monoclonal (Sigma), 1:5,000; anti-GFP rabbit polyclonal (Abcam, Cambridge, UK), 1:200 for immunofluorescence on frozen and whole mount sections; anti-GFP mouse polyclonal (Roche), 1:2,000 for immunoblotting and 1:200 for immunofluorescence; anti-RPE65 mouse monoclonal antibody (Abcam), 1:200 for immunofluorescence; anti-Rab27a mouse monoclonal (4B12) antibody, 1:10,000 for immunoblotting; anti-mouse 2F1 monoclonal (Sigma), 1: 500 for immunoblotting and 1:300 for immunofluorescence; anti-rabbit J905 monoclonal (Sigma), 1:500 for immunoblotting and 1:300 for immunofluorescence; anti-Rab11 mouse (Sigma), 1:1000 for immunoblotting. Secondary antibodies were conjugated to horseradish peroxidase (HRP) were purchased from DAKO (Glostrup, Denmark). Alexa-

488 and -568 conjugated secondary antibodies were purchased from Molecular Probes (Eugene, OR, USA). Anti-rabbit or anti-mouse HRP, 1:10,000 for immunoblotting (DAKO), anti-rabbit or anti-mouse Alexa 488 or 568 (Molecular Probes), 1:500 for immunofluorescence.

2.2.13 Immunofluorescence and confocal fluorescence microscopy

Cells used for immunofluorescence were grown on glass coverslips, and transfected with pDNA where indicated. Cells were washed with phosphate buffered saline (PBS), fixed with 4% (w/v) paraformaldehyde (PFA) in PBS for 30 min, rinsed twice with PBS, blocked and permeabilised with 0.05% (w/v) saponin, 0.5% (w/v) bovine serum albumin (BSA) in PBS (PBS/BSA) for 20 min. Permeabilised cells were incubated with the primary GFP antibody for 1 h at room temperature (RT), followed by four washes and incubation with species specific Alexa-conjugated secondary antibody for another hour at RT. All incubations and washing steps were carried out in PBS/BSA. The coverslips were mounted in immuneO mounting medium (MP biomedicals, Solon, Ohio) and visualised using a Zeiss inverted LSM-510 confocal microscope. Images were processed using Adobe Photoshop software. All images shown are single sections in the z-plane and representative of at least 80% of transfected cells.

2.2.14 Immunoblot Analysis

Protein extracts were either obtained from transfected cells or injected mouse retinas (isolated RPE and neural retinal cells obtained during the process of RPE isolation). Samples were lysed in protein lysis buffer (10 mM Tris-HCl (pH 7.5), 2% (w/v) Sodium Dodecyl Sulphate (SDS), 1 x protease inhibitor (Roche)) by sonication for 10 second with an amplitude of 5 μm (MSE Soniprep 150). The protein concentration was determined using a bicinchonic acid (BCA) protein assay kit (Pierce) for the colourimetric detection and quantification of total protein, following the manufacturer's protocol. Samples with 50 μg of total protein lysate were resolved by 12% SDS-polyacrylamide gel electrophoresis and transferred to a polyvinylidene difluoride (PVDF) membrane (Millipore). Membranes were blocked in 5% non-fat milk and 0.1% Tween-20 in PBS (PBS-T), incubated with the primary

antibody, washed three times, incubated with HRP conjugated species specific secondary antibody, and washed as above. All incubations and washing steps were carried out in PBS-T. Bound antibody was detected using the ECL Plus Western Blotting detection system (GE Healthcare).

2.2.15 Southern Analysis

Protocols for Southern blot analysis have been described previously (Argyros, Wong et al. 2008; Wong, Argyros et al. 2011). Briefly, for DNA analysis in vitro as well as in vivo, total eye DNA (from three to four injected retinas per condition) or cell DNA (from transfected cells) was extracted using a GenElute mammalian genomic DNA kit (Sigma-Aldrich). Isolated genomic DNA was quantified using a Nanodrop ND1-1000 spectrophotometer (Labtech International Ltd., Ringmer, UK). Genomic DNAs (30 μg retinal homogenates or 10 μg transfected cells) were digested with a single cutter to all plasmids *Stu*I restriction enzyme overnight, separated by agarose gel electrophoresis (30V, 30mA overnight) and transferred to Hybond-N+ nylon membranes (Amersham). Membranes were hybridized overnight with ^{32}P-labeled *Alw*NI fragment (Rad-Prime labelling kit, Invitrogen) (408-bp DNA fragment of a segment of the kanamycin region, which is common to all plasmids). Membranes were hybridised in Church buffer (0.25M sodium phosphate buffer (pH 7.2), 1mM EDTA, 1% BSA, 7% SDS) at 65°C. After 3 washes at 65°C with high stringency buffer (2x saline-sodium citrate (SSC)/0.5% SDS for 10 min, 1X SSC/0.5% SDS for 15 min, followed by 0.1x SSC/0.5% SDS 10 min), specific hybridization signals were detected by exposing the membranes to x-ray film with intensifying screens at -80°C.

2.2.16 Subcellular Fractionation

To perform in vitro prenylation on CHM transfected cells as well as CHM injected mouse retinas, subcellular fractionation was performed at different time intervals (either 6 months or 6 weeks) post transfection or subretinal injection respectively. This enables the separation of cellular membranes including membrane associated proteins from cytosolic components. Adherent cells were harvested either mechanically or using Trypsin-EDTA as

described previously and centrifuged at 1000 x g for 5 minutes at 4°C. The supernatant was aspirated and cells were washed with PBS and centrifuged once more. Cells were then resuspended in lysis buffer. RPE cells were isolated from CHM mice following subretinal injections as described previously. Samples were then resuspended in protein lysis buffer and lysed by sonication.

Lysates were centrifuged at 800 x g for 10 minutes at 4°C to remove large cell debris obtain the post nuclear supernatant (PNS). The PNS was then transferred to a Beckman Centrifuge Tube and subjected to ultracentrifugation at 100,000 x g for 1 hour at 4°C using a TLA45 Beckman rotor. The resulting supernatant (S100, abbreviated to 'S') which contained the cytosolic fraction was transferred to a fresh tube, while the pellet (P100, abbreviated to 'P') which contained the membrane fraction was resuspended in an equivalent volume of lysis buffer to the S100 fraction. The P100 was then sonicated for 10 seconds and protein concentration was determined using BCA as described previously. Both S and P fractions were then analysed by immunoblot/Western blot analysis as described previously (probed with anti-Rab27a (4B12) or anti-Rab11 antibodies).

2.2.17 RNA isolation and Reverse Transcription PCR (RT-PCR)

To determine the level EGFP or REP1 transcript, reverse transcription-polymerase chain reaction (RT-PCR) was performed. Total RNA was extracted from tissues (using three to four injected retinas per condition) or cells using TRIzol reagent (Invitrogen) according to manufacturer's recommendations. The concentration of RNA was determined using spectrophotometry. First-strand complementary DNAs (cDNAs) were generated from RNA using the Superscript III first strand synthesis system (Invitrogen) according to the manufacturer's recommendations. Following this, extracted RNA samples (250 ng for cells or 1.5 µg for tissue) were allowed to proceed at 20°C for 10min, 42°C for 30 min, heated at 99°C for 5 min, then incubated at 3°C for 5 min using the First-Strand cDNA synthesis kit (Invitrogen). Amplification of cDNAs was carried out by Polymerase Chain Reaction (PCR) using EGFP (as described previously (Chan,Chong et al. 2001)) or REP1 specific primers:

For GFP RT-PCR,

GFP-rtF Forward: (5´-ACGGCAAGCTGACCCTGAAG-3´) and

GFP-rtR Reverse: (5´- CAACCACTACCTGAGCACCC -3´)

This yielded a 495 bp fragment.

For REP1 RT-PCR,

REP-rtF forward primer (5'-GCTGTTCGGGTCATTGAGTTATGT -3') and

REP-rtR forward primer (5'-TCAGACATCAGCAGGAGCTGTTAT-3')

This yielded a 240 bp fragment.

Primers were designed manually and supplied through Invitrogen. PCR comprised of sterile water, -Mg 10x PCR buffer, 25 x MgCl2, 10 mM dNTP mix and primers. This reaction was done in a 45 µl reaction and 0.5 µl of Taq polymerase (Invitrogen) was added to the tubes. Samples were then inserted into Robocycler thermal cycler (Stratagene). The PCR programmes were as follows: initial denaturation at 94°C for 3 min, then 40 cycles of 40 sec melting at 94°C, 1 min annealing at 60°C, and 1 min extension at 72°C. After the last cycle, the polymerisation step was extended by 10 min at 72°C to ensure that all strands were completed.The rt-PCR products were confirmed by agarose gel and showed the specific band of predicted size. The primer set GFP-rtF and GFP-rtR yielded a 494-bp amplicon after amplification of GFP cDNA, while for REP1 the 240-bp amplicon was seen after amplification of REP1 cDNA. For negative controls, no RT products were used as templates in the PCR and were verified by the absence of gel-detected bands. Samples were run on 1.5% agarose gels and a gel imager was used to view amplified products from cDNA.

2.2.18 Animal work

One-month old C57BL/6 mice (wild-type) (25-30g) were bred and maintained on 12-h light/dark cycle at the Central Biomedical Services of Imperial College London. MF1 mice (3-4 month old) were purchased from Charles River Laboratories (UK). All CHM mouse lines were bred in house and generated as described previously (Tolmachova, Anders et al. 2006; Tolmachova, Wavre-Shapton et al. 2010). All animals were maintained in accordance

with the rules and regulations of the Home Office. Mice were killed by cervical dislocationand eyes immediately enucleated.

2.2.18.1   *Preparation of complexes (PEI:DNA)*

S/MAR pDNA was complexed with the 22 kDa cationic linear polymer polyethylenimine (PEI) (in vivo-JetPEI, Polyplus Transfection, UK) to form stable polyplexes according to the manufacturer's instructions. Briefly, for the subretinal injection of a mouse eye with a polyplex at an N/P 8 ratio, 30 µg of pDNA was diluted in 5% isotonic glucose solution to a final volume of 30 µl, 4.8 µl of in vivo-jetPEI was diluted in another aliquot of 5% isotonic glucose solution to a final volume of 30 µl. Diluted PEI was then added directly to diluted pDNA and vortexed briefly prior to injection of 1-2 µl of complexed DNA into the subretinal space.

2.2.18.2   *Gene transfer to ocular tissues in vivo*
2.2.18.2.1   **Topical administration**

Protocols for the topical administration of formulations have been described previously (Liaw, Chang et al. 2001; Tong, Chang et al 2007). Briefly, for the in vivo eye drop delivery studies, the eyes of MF1 mice were initially pre-treated with an enhancer for gene transfer, 5mM EDTA (10 µl per eye), which was applied as topical eye-drops to the cornea. Mice were held such that the eye was held open slightly for a few seconds while the eye drops were allowed to penetrate the cornea and be absorbed before the mouse was allowed to blink and move freely. This pretreatment occurred 10 minutes before pDNA was applied to the eye. The eye was delivered with 0.5 µg/µl of complexed pDNA with PEI (pCAG-Luc)(10 µl per mouse eye, three times per day for one day). Formulated pDNA was made fresh each time the topical administration was applied to the cornea. One eye would receive drops while the other contralateral eye was used as a control and either received plasmid alone or PEI formulated pDNA without enhancer pretreatment. To evaluate the gene transfer in vivo, mice were imaged for bioluminescence by the IVIS Imaging 50 Series (Xenogen) after 24 and 48 hours of the first topical administration.

2.2.18.2.2 Intravitreal injections

For all intravitreal and subretinal injections, fluid lines, surgical equipment and needles were sterilised by repeat rinsing with 70% ethanol and sterile water. Furthermore wild-type mice of MF1 strain (3-4 months old) were anesthetised by intraperitoneal injection of ketamine/xylazine (ketamine, 80 mg/kg; xylazine, 15 mg/kg, (Sigma-Aldrich). This was followed by topical anesthesia in the form of one proparicaine drop (proparacaine hydrochloride ophthalmic solution USP 0.5%, Akorn Inc., Buffalo Grove, IL). The pupil was then dilated with one drop of tropicamide (tropicamide ophthalmic solution 1%, Falcon Pharmaceuticals, Ft. Worth, TX) which usually took 90 s to fully dilate. If the pupil did not adequately dilate within this time, another drop of tropicamide was placed on the cornea. Following dilation, surgery was usually complete within 30-90 s.

Intravitreal injections were performed under a dissecting microscope with a 10 µl Hamilton syringe fitted with a 32 gauge, beveled-tip needle. The needle was inserted through the sclera, posterior to the ora serrata in the superotemporal quadrant. Solution was injected slowly (1-2 µl) into the vitreous chamber of the eye. The needle was held in place for 5 seconds to allow for the pressure to equilibrate within the vitreous, before which it was withdrawn and the injection was complete. Once the needle had been removed, triple antibiotic ophthalmic cream (Taro Pharmaceuticals, Inc., Hawthorne, NY), which contains bacitracin, neomycin sulfate, and polymyxin B was applied to the eye.

2.2.18.2.3 Subretinal injections

Injections in C57BL/6 mouse strain were initially performed by Dr Tanya Tolmachova, however some injections were also performed by Dr Mariya Moosajee. While all MF1 and CHM mouse injections were performed by Dr Mariya Moosajee.

Subretinal injections were performed using one of two dissecting microscope systems. The first was a Leica binocular microscope (Leica Microsystems, Bannockburn, IL) with a fiber-optic halogen illuminator & dual gooseneck light guide (Dolan-Jenner, Inc., Boxborough, MA). This system did not include avideo camera. The second system was an Olympus

binocular microscope (Hunt Optics; Pittsburgh, PA). This microscope system contained a video attachment module at the top and using a portable Panasonic video camera (Panasonic Electronic Devices, Knoxville, TN), recordings or still pictures of the surgical techniques were taken. The pictures and video were stored on a HD cardand transferred for analysis and editing using Apple Final Cut Pro editing software (version 6; Apple Computer).

A heating pad was used to maintain the mice at 37°C during the process of anaesthesia (T/Pump TP500; Gaymar, Orchard Park, NY). All surgical needles were supplied from Hamilton Life Science.

For the subretinal injections, a glass Hamilton syringe (10 or 50 µl syringe) was fitted with a blunt 27 gauge RN (removable) needle with the following details: 10/20 mm in length, PST3 (blunt –point style 3). Tubing (0.6mm) in the form of intramedic non-radiopaque polyethylene tubing (Becton Dickinson, Franklin Lakes, NJ) was attached to this 27 gauge needle (50-100 mm but normally no more than 100 mm in length). The remaining free end of the tubing was attached to a beveled 33 gauge RN (removable) needle - which was the actual needle used to inject the retina – with the following details: 10 mm in length, PST2 (point style 2), tapN (metal hub).

The attachment of the tubing meant that while one person was performing the injection procedure - insuring the needle was positioned correctly within the retina - another person was able to inject the required amount into the retina using the syringe without moving or disturbing the needle that was already in the correct position in the retina. Hence this meant that once the required pDNA was loaded into the syringe and the mice were adequately anesthetized, the actual injection procedure was relatively quick, whereby numerous mice could be injected within a short period of time without the need for reloading the syringe or additional complications associated with the needle being moved unnecessarily within the eye if the person injecting and positioning the needle within the retina were the same person.

2.2.19 In vivo luciferase measurements

To measure the luciferase expression in tissue, a luciferase assay was performed. Tissues

were removed before being lysed with 250 μl 1 x reporter lysis buffer (Promega). Samples were then homogenised manually. From this lysed material, 20 μl was removed and added to 50 μl of luciferase substrate-assay buffer in a glass tube which was inserted into a luminometer (Berthold Technologies Lumat LB 9507) and relative luciferase units (RLU) per second were recorded. Protein concentrations were also determined using BCA as described previously and luciferase expression was represented as μg/protein.

2.2.20 In Vivo Bioluminescence Imaging

At regular intervals after subretinal injections, mice were injected intraperitoneally with 300 μl of luciferin substrate, D-luciferin (Gold Biotechnology, Inc., St Louis, MO, USA) (15 mg ml^{-1} in PBS), anaesthetized with 2.5% isoflurane and then 10 minutes later, imaged for bioluminescence (transgene expression) using the IVIS Imaging 50 Series (Xenogen, Caliper Life Sciences Ltd., Runcorn, UK). Bioluminescent imaging (BLI) was performed in a light-tight chamber on a temperature-controlled, adjustable stage, while isoflurane was administered by means of gas manifold at a flow rate of 2%. Images were acquired at a medium binning level (8) and acquisition times were 30-60 seconds, depending on the intensity of the luminescence. The Xenogen system reports bioluminescence as photons s^{-1} cm^{-2} sr^{-1} in a 0.7-1 cm diameter region of interest encompassing the eye. Data were analysed using LivingImage 2.50 software (Xenogen). Background levels of bioluminescence were 2 x 10^4 photons/sec/cm^2/sr.

2.2.21 Whole mounting and staining

Mice were subretinally injected with EGFP plasmids and eyes were enucleated at relevant times post injection. The eyecup whole mount was prepared by piercing the cornea with a 27 gauge needle, before immersing in 4% PFA for 1 hour. Using iridectomy scissors, an incision was made around the ora serrata, and the eye was separated into anterior and posterior segment. The lens and cornea were carefully removed from the posterior segment of the eye, and the neural retina was peeled away to expose the RPE. Four radial cuts starting from the peripheral edge of the eye cup extending toward the optic nerve were made. If necessary, a razor blade was used to extend the initial cuts started with the

iridectomy scissors. The flattened eye cups were either analysed immediately for EGFP or immunohistochemistry was performed for EGFP expression. Samples were blocked for two hours (PBS, 5% non-specific goat serum (Invitrogen), 3% Triton X100), before being incubated with GFP antibody in blocking solution overnight at 4°C. After 2 washes in PBS at room temperature (RT), sections were incubated with fluorescent-conjugated secondary antibodies in blocking solution for two hours at RT and washed with PBS. Eyes were then mounted onto glass slides in aqueous mounting medium and covered with glass coverslips and viewed using fluorescence microscopy. Controls were made by omitting the primary antibody or by carrying out immunohistochemistry on uninjected whole mount eyes. No labelling was observed in either control sections.

2.2.22 Histological analysis and Immunohistochemistry

Mouse eyes for histological analysis were fixed in Karnovsky's Fixative (2% PFA, 2.5% glutaraldehyde, 0.1 M cacodylate buffer) for 1 hour. Samples were serially dehydrated in alcohol before they were embedded in paraffin wax. Sections were cut at 4 µm thickness and stained with haematoxylin and eosin (H&E). Sections were imaged with a camera (SIS ColorView IIIU; Olympus, Tokyo, Japan) mounted on a microscope (CKX41; Olympus).

For frozen section analysis mouse eyes were fixed in 4% PFA in PBS for 1 hour. After removal of the lens, eyes were cryoprotected using 10% sucrose in PBS for 30 min, and 20% sucrose in PBS over night at 4°C. Eyes were embedded in optimal cutting temperature compound (OCT) (Tissue Tek, Sakura Finetek, Thatcham, UK), frozen in Isopentane on dry ice and stored at -80°C until sectioning. Samples were serially sectioned at 10 µm thickness through the center of the eye and the optic nerve head in a superior-inferior plane. Sections were cut on a Leica CM1850 cryostat set to between 19-23°C (Leica Microsystems), and collected onto superfrost microscope slides (Fisher). Slides were stored at -80°C until staining. Frozen retinal sections were air dried for at least 30 min before rehydration with PBS. For EGFP immunohistochemistry, unspecific binding sites on the sections were blocked for one hour with PBS, 1% BSA (Sigma), 0.025% Sodium azide (Sigma), 10% non-specific goat serum (Invitrogen) including 0.2% Triton X100 for permeabilisation before being incubated with GFP antibody in blocking solution overnight at 4°C. After 2 washes in PBS at RT, sections

were incubated with species specific fluorescent-conjugated secondary antibodies for 40 min at RT, washed again in PBS and either counterstained with propidium iodide (P-4170, Sigma) (0.5% in water) or DAPI to visualise nuclei and mounted in aqueous mounting medium (ProLONG Gold antifade reagent; Invitrogen) and viewed using confocal fluorescence microscopy. Controls were made by omitting the primary antibody or by carrying out the immunostaining on uninjected control wild-type eyes. No labelling was observed in either control sections.

2.2.23 Apoptosis detection and analysis - TUNEL Assay

Protocols for TUNEL assay have been described previously (Moosajee, Tulloch et al. 2009). Briefly, retinal sections that had been processed and analysed for histological analysis were dewaxed by two washes in clearing agent Histoclear (National Diagnostics, Atlanta) followed by two washes in 100% ethanol and one wash in 70% ethanol before rinsing in deionized H_2O. After rehydration, retinal sections were digested with proteinase K (10 μg/ml) (Sigma) for 15 min, washed twice in H_2O, followed by 3% hydrogen peroxide incubation, to block the endogenous peroxide activity in the tissue, followed by two final washed with PBS. Levels of apoptotic cell death were measured using a detection kit: ApopTag Peroxide In Situ Apoptosis Detection Kit (Millipore, Billerica, MA) according to manufacturer's instructions. Retinal sections from various injection groups were compared to negative control wild-type uninjected eyes to determine the level of background apoptosis in the mouse retina, as well as positive control LPS dosed retinas.

2.2.24 Immunological analysis: Enzyme-Linked Immunosorbent Assay (ELISA)

Levels of TNF-α, MCP1 and IFN-γ cytokines were determined by using enzyme-linked immunosorbent assay (ELISA) kits according to manufacturer's instructions using a microplate reader at 450 nm (Molecular Devices, Sunnyvale, CA). Kits were purchased from ebioscience (San Diego, CA, USA). Briefly, for ELISA analysis of inflammatory cytokine levels in injected retinal homogenates at 1 and 7 days post injection, retinas were enucleated, the anterior part of the eye including the lens and cornea were removed, and eyes were homogenised on ice in lysis buffer (as described above) for one hour, centrifuged at

14,000 rpm/10,000 g for 15 min at 4°C. Protein concentrations from supernatants were quantified using the BCA Protein Assay Kit (Pierce), were 50 ng of supernatants were used for each sample. Standards were analysed in duplicates, while each sample was analysed in triplicates, and each time point as well as treatment was repeated in three to five independent experiments. Uninjected eyes or eyes injected subretinally with sterile glucose were used as negative controls in this study.

Inflammatory samples to be used as positive controls were described previously (Bonnet, Erbacher et al. 2008). Briefly, to induce a strong inflammatory response and to serve as a positive inflammatory eye sample, mice were dosed with a lethal dose of ketamine and xylazine, before subretinally injecting 2 µl of Escherichia coli (*E. coli*) Lipopolysaccharides (LPS) (Product # L 6143, Sigma/Aldrich), and collecting eyes between 5-15 min post subretinal injection.

2.2.25 Statistical analysis

Comparison of inflammatory cytokine levels from pDNA injected retinal homogenates and blood serum were analysed by one-way analysis of variance (ANOVA) to access statistical significance, with significance level p=0.05 and 0.01. Student t-test was also used where appropriate.

3   RESULTS

_____

Experimental outline and rational

We planned to exploit the S/MAR vector technology for the development of novel non-viral persistently expressing vectors for Choroideremia (CHM) gene therapy. To this end, we created a series of constructs comprising either the reporter gene EGFP or REP1, with various promoters, with and without an S/MAR element from the plasmid pEPI. Hence all constructs had identical plasmid backbones, with either the reporter gene EGFP or REP1 with or without the S/MAR element. We performed initial steps to validate the transient expression of both transgenes EGFP and REP1 *in vitro* in a wild-type mouse anterior pituitary (AtT20) cell line as well as a melanoma (B16-F10) cell line. The plasmid pEPI, which contains the S/MAR element, has been shown to provide long-term EGFP expression in a number of cell lines. These include the chinese hamster ovary (CHO-K1) cells (Piechaczek, Fetzer et al. 1999; Papapetrou, Zoumbos et al. 2005), human cervical cancer (HeLa) cells (Schaarschmidt, Baltin et al. 2004), mouse embryonic fibroblasts (NIH 3T3) (Broll, Oumard et al. 2010) as well as haematopoietic stem cells (including human haematopoietic progenitor K562 and CD34^{+} cell lines) (Papapetrou, Ziros et al. 2006). Interestingly, control plasmids lacking the S/MAR element were not able to sustain EGFP expression in the above mentioned cell lines. Hence we sought to demonstrate the principle that the S/MAR containing plasmids we constructed can provide long-term transgene expression *in vitro* as well as *in vivo.* We extend and demonstrate with the AtT20 cell line we routinely use in our laboratory, the principle that S/MAR containing plasmids can provide long-term EGFP and REP1 transgene expression *in vitro.* Furthermore, REP1 long-term expression was also analysed in mouse and human CHM primary fibroblasts. Proof-of-principle experiment in these CHM cells *in vitro* showed not only rescue of REP1 protein levels, but also functional rescue of the CHM phenotype. Following expression of constructs *in vitro,* we analysed the expression of constructs *in vivo.* We developed an optimised method for delivering S/MAR containing plasmids in the eye via subretinal injections of complexed pDNAs, and showed the utility of S/MAR plasmids in the eye. We provide evidence for the first time to show the longitudinal transgene expression of luciferase constructs (with the same plasmid backbones as pEPI and EGFP as well as REP1

constructs made) as measured using a bioluminescence bioimager. Long-term expression of EGFP and REP1 transgenes were also observed (by rt-PCR of mRNA levels, PCR of plasmid DNA levels and Western blot analysis of protein levels), as well as evidence for the long episomal maintenance of these vectors in the eye. We provide evidence for the superiority of an S/MAR containing plasmid in providing long-term expression in the eye. We further demonstrate the lack of toxicity within the eye and show that fundus examinations as well as detailed histological examinations of retinal sections do not elicit an inflammatory response to our plasmids once subretinally injected in the eye. The final part of this project, investigates the subretinal injection of CHM mice using an S/MAR based pDNA vector expressing the *REP1* transgene. We provide evidence for the persistence of transgene expression within the retinas of these mice. Following further molecular analysis, we also show for the first time the partial correction and rescue of the CHM phenotype in CHM$^{null/WT}$ mice using a plasmid vector.

3.1   Plasmid production and *in vitro* analysis of EGFP transgene

The first step towards designing a novel non-viral S/MAR plasmid was the development of the initial universal S/MAR cloning vector pEPI-MCS1. This was successfully created by Ms Azadeh Cheraghchi Bashi as part of her Masters Degree in the Molecular Medicine department. The resulting vector, pEPI-MCS1, has the same plasmid backbone as the original pioneering plasmid pEPI-EGFP with a few key exceptions. The pEPI-MCS1 vector lacked the CMV promoter and EGFP gene upstream of the S/MAR element, while it had the insertion of a unique multiple cloning site (MSC) instead. This modified version of the original plasmid allowed for easy insertion of various promoter and transgene sequences upstream of the S/MAR element and provided the preliminary vector to build upon for subsequent cloning strategies (Figure 22).
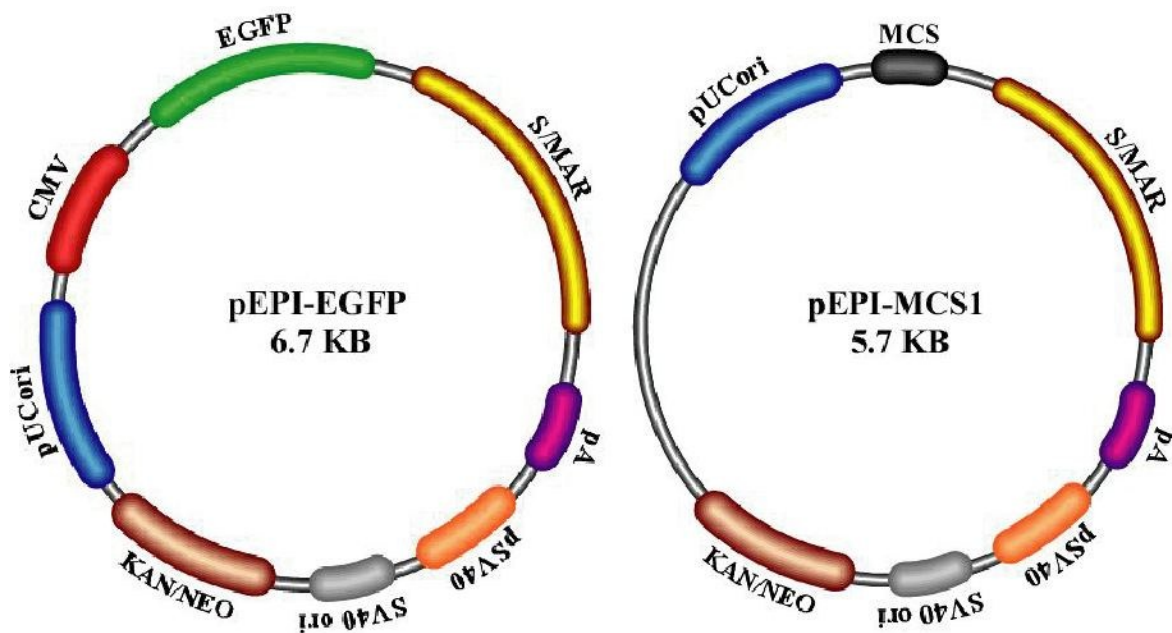
Figure 22: The original plasmid pEPI-EGFP and the modified pEPI-MCS1 plasmid used for subsequent cloning strategies

Both plasmids harbour a similar plasmid backbone including similar bacterial components and antibiotic selection elements. These include an SV40 ori (SV40 origin), required for replication in mammalian cells expressing the SV40 T-antigen, a kanamycin/neomycin (kan/neo)   resistance cassette consisting of an SV40 early promoter, the kan/neo resistance gene from *Tn5* (Aiuti, Slavin et al. 2002) and polyadenylation signals from the Herpes simplex virus thymidine kinase (*HSV TK)* gene which allows stable transfection of eukaryotic cells using G418 antibiotic. The bacterial promoter upstream of this cassette expresses kanamycin resistance in *E. coli.* Both plasmids also contain a pUC origin of replication for propagation in *E. coli* and an f1 origin for single-stranded DNA production. The pEPI-EGFP plasmid contains the human immediate early cytomegalovirus (CMV) promoter, driving transcription of the enhanced green fluorescent gene (*EGFP*)*,* followed by the SV40 polyadenylation tail (pA) downstream of the *EGFP* gene which directs the correct processing of the 3' end of the EGFP mRNA*.* In contrast the pEPI-MCS1 plasmid has had the insertion of a 30 base pair (bp) MCS consisting of unique restriction enzyme sites not found on the plasmid including *Not*I, *Eco*RV, *Hind*III and *Xho*I. The *EGFP* gene and MCS sequence (and so subsequent insertion of other genes of interest in the future) from the pEPI-EGFP and pEPI-

MCS1 plasmids respectively, are followed directly by the S/MAR sequence and the SV40 pA for mRNA stability. It has been proposed (Stehle, Scinteie et al. 2003) that S/MARs bind to components of the nuclear matrix and so plasmids carrying S/MAR elements are able to use cellular replication machinery for their replication. However the close association with nuclear matrix is not sufficient to initiate replication of the S/MAR plasmid. Episomal DNA replication and transcription upstream of the S/MAR is dependent on the active transcription of a gene upstream of the S/MAR, with transcription continuing past the gene of interest and extending into the S/MAR (Lipps, Jenke et al. 2003; Conese, Auriche et al. 2004). This in turn may lead to a conformational change of the vector (Mielke, Kohwi et al. 1990; Zhong,Gulottaet al. 1990) or to a modification of its chromatin structure (Turner 2002) making the plasmid vector more accessible for the replication enzymes.

Interestingly, within the 2000 bp S/MAR sequence, there appears to be a cryptic termination site at approximately position 1500 -1700 bp (Stehle, Scinteie et al. 2003). Furthermore, the orientation of the expression cassette is crucial for correct S/MAR function. This is because episomal replication was lost and random vector integration was observed when transcription was not able to pass through the S/MAR. This has been attributed to the removal of the promoter which drives transcription or the insertion of sequences that terminate transcription ahead of the S/MAR element (Lipps, Jenke et al. 2003; Conese, Auriche et al. 2004).

While the CMV promoter of the plasmid pEPI-EGFP provides high transgene levels *in vitro*, expression *in vivo* is often only transient and short lived as viral promoters such as CMV are often transcriptionally silenced due to methylation of the promoter (Brooks, Harkins et al. 2004; Jenke, Stehle et al. 2004; Kachi, Oshima et al. 2005; Kachi, Esumi et al. 2006). Hence to minimise the potential for loss of transgene expression *in vivo,* we developed other plasmids harbouring different promoters.While the use of the tissue specific promoters is an option when designing plasmid vectors, our ultimate goal was to create plasmid vectors that could transfect the cell layers in the eye most affected in our disease of interest, CHM. The two cell layers of most interest in the eye for CHM are the retinal pigment epithelium (RPE) and photoreceptor cells. The elongation factor-1 promoters (EF1-α and its intronless version EFS) and (CMV) early enhancer/chicken beta actin promoter (CAG) have been shown in the past to maintain efficient expression in the RPE and photoreceptor cells (Kostic, Chiodini et

139

al. 2003; Cashman, McCullough et al. 2007). Hence as CHM is a disease affecting more than one cell type, creating a plasmid vector that utilises a ubiquitously expressed promoter based on either the EFS or CAG promoter was deemed more advantageous compared to a vector that possessed a tissue specific promoter. Using this approach of a ubiquitous promoter we hoped to provide long-term transgene levels in both cell types in the eye.

Based on this information, our initial approach involved the creation of an S/MAR plasmid with the *EGFP* reporter gene based on the pEPI-MCS1 and pEPI-EGFP plasmids described above. We initially wanted to achieve this in a single cloning step; whereby the *EGFP* with the EF1-alpha promoter from the pWPT-GFP plasmid or the CAG promoter from the pCAGGs plasmid could be cloned into pEPI-MCS1. However due to the significant problems associated with the cloning, it was decided that the cloning process should be done in stages. Hence two cloning strategies were employed for the pEFS-EGFP and pCAG-EGFP vector series.

3.1.1   Modifying the pEPI-MCS1 vector – Plasmid pEOS

For the initial stage in creating the pEFS-EGFP vector, the universal pEPI-MCS1 vector was initially modified by excising a 282 bp fragment from the end of the S/MAR with *Mlu*I and *Eco*RI enzymes. The remaining 5084 bp fragment was blunt ended with Klenow and ligated overnight. The vector was not dephosphorylated because this was deemed to reduce the overall efficiency of cloning (Tolmachov 2009). As the ligation mixture still contained the excised fragment from the vector, the mixture was precipitated and digested with *Sal*I. This site was only found in the 282 bp insert sequence that we aimed to remove. The ligation mixture was then transformed into JM109 competent cells. Of the colonies that grew, 6 were grown as overnight cultures and the plasmid DNA was isolated and screened for the removal of *Mlu*I, *Sal*I and *Bam*HI restriction enzymes, as well as restoration of the *Eco*RI site. Correctly ligated plasmids would be undigested with *Mlu*I, *Sal*I and *Bam*HI, while digestion with *Eco*RI would be positive giving a linearised vector that would produce a single fragment at 5084 bp. All 6 colonies analysed gave the correct digestion patterns (Figure 23D). This modified vector was named pEOS plasmid.
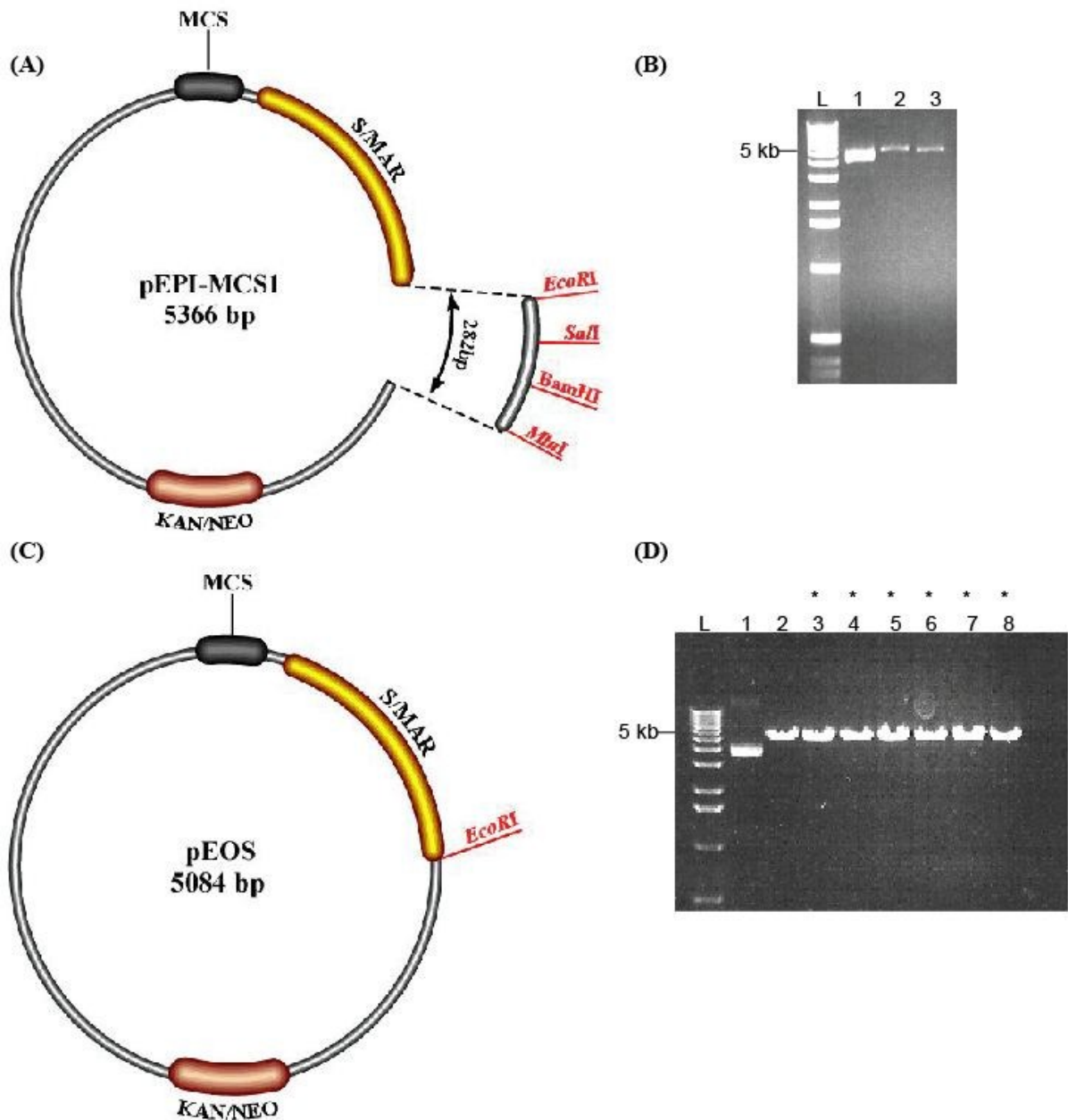
Figure 23: Generation of the modified pEOS plasmid

The cloning strategy for the generation of pEOS plasmid involved the removal of the 282 bp fragment from the pEPI-MCS1 vector is illustrated in (A) The correct fragment sizes of the digested pEPI-MCS1 vector before ligation are shown in (B), where lane 1: undigested pEPI-MCS1 vector, lanes 2 and 3: digested pEPI-MCS1 vector with *Mlu*I and *Eco*RI restriction enzymes respectively. Successful ligation would result in the pEOS plasmid as illustrated in (C). Finally (D) shows the restriction analysis of six clones picked after ligation (lanes 3-8) with all clones showing the restoration of the *Eco*RI site (*). Lane 1 and 2 represent undigested and *Eco*RI digested pEPI-MCS1 vector respectively. L: 1 Kb ladder (Invitrogen).

3.1.2 Production of an EGFP expressing plasmid driven by EFS – Plasmid pEFS-EGFP

The next step was the insertion of the EFS promoter and *EGFP* transgene upstream of the S/MAR element. The cloning strategy is illustrated in Figure 24. In preparation for the insertion of EFS-EGFP, both pEOS and pWPT-GFP plasmids were digested with *Xho*I. This excised the 1.1 kb insert fragment from the pWPT-GFP plasmid (Addgene) which was ligated with linearised vector overnight at a molar vector: insert ratio of 1:5. The ligation mixture was transformed into JM109 competent cells. Out of the colonies obtained overnight, 70 colonies were screened by PCR analysis using EGFP and S/MAR specific primers as described in the methods. Six clones showed a positive signal from the PCR analysis showing the presence of the insert as well as the correct orientation of the insert in the clones. All 6 clones were selected for plasmid isolation and analysed further for the correct insert sequence and orientation using *Eco*RI *and Mlu*I, *Eco*RI and *Bam*HI or *Hind*III restriction digestion analysis. Correctly ligated plasmids in the 5' to 3' orientation would produce three fragments when digested with *Hind*III, 5196 bp, 820 bp and 268 bp. Of the 6 clones, 5 gave the expected fragment patterns (Figure 24D). One colony was selected for isolation with a MaxiPrep kit, its quality and quantity was measured using a Nanodrop spectrophotometer. This vector was named pEFS-EGFP plasmid.
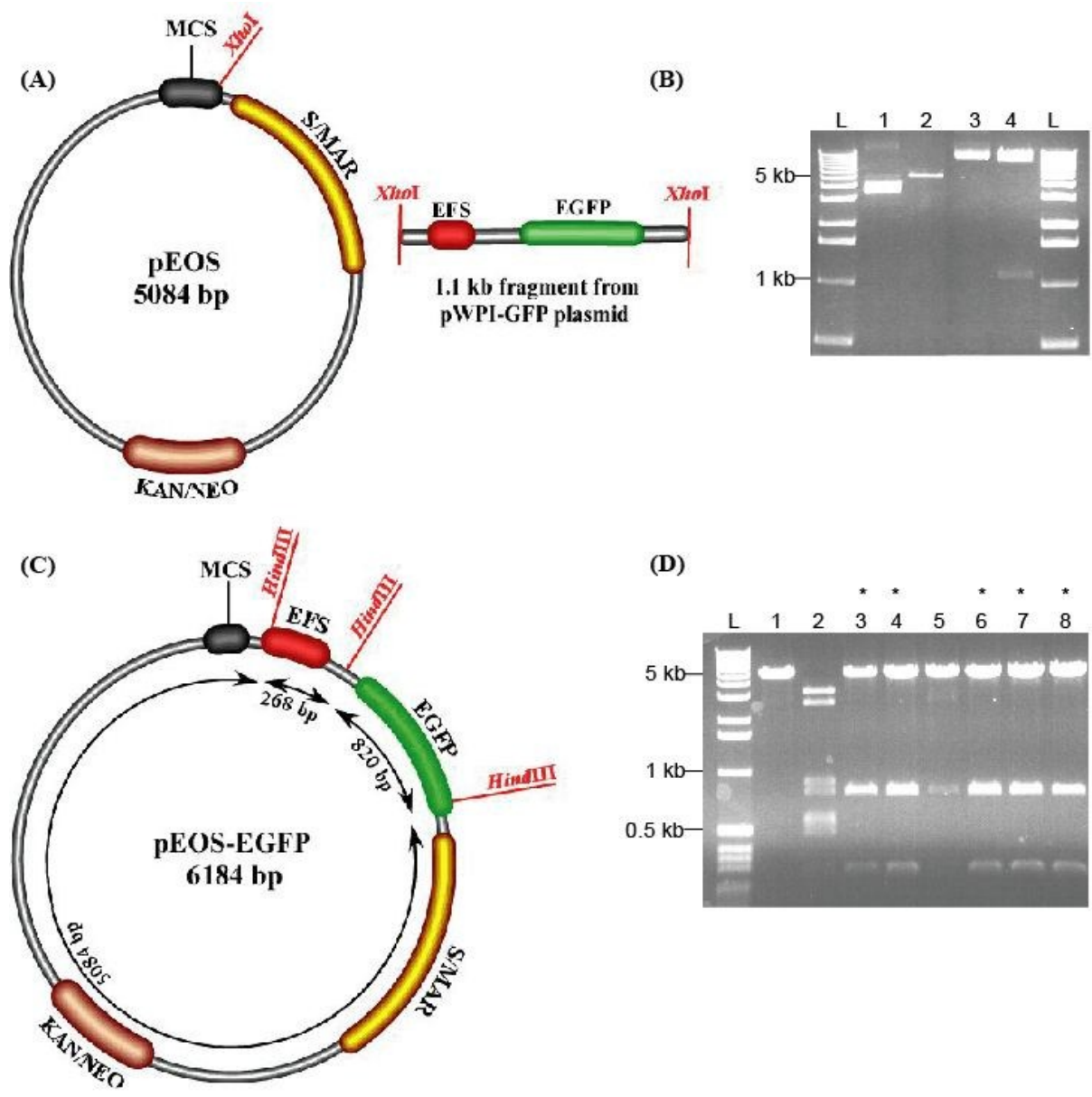
Figure 24: Generation of pEFS-EGFP plasmid

The cloning strategy for the generation of pEFS-EGFP plasmid involved inserting the 1.1 kb EFS-EGFP fragment into the pEOS plasmid is illustrated in (A). The correct fragment sizes of the digested pWPT-GFP vector and linearized pEOS vector before ligation are shown in (B), where lanes 1 and 3: undigested pEOS and pWPT-GFP vector respectively, lanes 2 and 4: digested pEOS and pWPT-GFP vector with *Xho*I restriction enzyme respectively. Successful ligation would result in the pEFS-EGFP plasmid as illustrated in (C). Finally (D) shows the restriction analysis of six clones picked after ligation (lanes 3-8) with clones 1, 2, 4, 5 and 6 showing the expected three bands (*), indicating colonies with the correct restriction pattern, consistent with the successful insertion of EGFP and development of pEFS-EGFP. Lane 5 represents the partial insertion of the insert with only the EGFP insertion. Lane 1 and 2 represent *Hind*III digested vector and insert pEOS and pWPT-GFP vectors respectively. L: 1 Kb ladder (Invitrogen).

3.1.3 Production of an EFS control counterpart - Plasmid pEFS-EGFP-Control

The final step in the pEFS-EGFP vector series involved the development of the control counterpart to the pEFS-EGFP plasmid. The cloning strategy is illustrated in Figure 25. In preparation for the removal of the 2 kb S/MAR element, pEFS-EGFP plasmid was digested with *Hpa*I and *Bgl*I. This excised the 2 kb S/MAR fragment from the pEFS-EGFP plasmid and the linearised vector was blunt ended with Klenow before being ligated overnight. The ligation mixture was transformed into JM109 competent cells. Out of the colonies obtained overnight, 8 were selected for plasmid isolation and analysis with *Stu*I restriction enzyme. Correctly ligated plasmids would give a linearised vector that would produce a fragment at 4184 bp. All 8 clones had the expected plasmid sizes (Figure 25D). One colony was selected for isolation with a MaxiPrep kit, its quality and quantity was measured using a Nanodrop spectrophotometer. As the newly constructed plasmid did not harbour an S/MAR element, the plasmid was named pEFS-EGFP-Control plasmid.

Figure 25: Generation of pEFS-EGFP-Control plasmid

The cloning strategy for the generation of pEFS-EGFP-Control plasmid involved removing the 2 kb S/MAR motif from the pEFS-EGFP plasmid is illustrated in (A). The correct fragment sizes of the digested pEFS-EGFP plasmid before ligation is shown in (B), where lane 1: undigested pEFS-EGFP and lane 2: digested pEFS-EGFP with *Hpa*I and *Bgl*I restriction enzymes. Successful ligation would result in the pEFS-EGFP-Control plasmid as illustrated in (C). Finally (D) shows the restriction analysis of 8 clones picked after ligation (lanes 2-10) where all clones showed the correct size of the plasmid (*), indicating the successful S/MAR excision and development of pEFS-EGFP-Control. Lane 1 represents undigested pEFS-EGFP plasmid. L: 1 Kb ladder (Invitrogen).

3.1.4 Production of Plasmid pEOS-CAG-S/MAR

The next stage involved the development of the pCAG-EGFP vector series. As an initial step in creating the pCAG-EGFP plasmid, the CAG promoter was inserted upstream of the S/MAR element. The cloning strategy is illustrated in Figure 26. The CAG promoter was excised from the pCAGGs plasmid by digestion with *Sal*I and *Xho*I*,* resulting in the removal of the 1.7 kb fragment corresponding to the CAG promoter*.* The vector pEOS was also linearised with *Xho*I*,* blunt ended with Klenow and ligated overnight with the CAG insert at a molar vector:insert ratio of 1:4. Usually a 1:10 ratio of vector:insert is used where the insert is added in excess to minimise the chance of the vector or insert re-ligating back on/with themselves (as neither were dephosphorylated). However, in this situation the pCAGGS plasmid contains the ampicillin resistant gene; hence re-ligated pCAGGs plasmid would not grow on kanamycin plates that were used during the cloning process. The ligation mixture was then transformed into JM109 competent cells. Out of the colonies obtained overnight, 70 colonies were screened by PCR analysis using CAG and EGFP specific primers as described in the methods. 7 clones showed a positive signal from the PCR analysis showing the presence of the insert as well as the correct orientation of the insert in the clones. All 7 clones were selected for plasmid isolation and analysed further for the correct insert sequence and orientation using *Xho*I and *Hind*III, *Xho*I and *Not*I or *Xho*I and *Eco*RI restriction digestion analysis. Correctly ligated plasmids in the 5' to 3' orientation would produce two fragments when digested with *Xho*I and *Hind*III, 5084 bp and 1700 bp. Of the 7 clones, 2 gave the expected fragment patterns (Figure 26D). This vector was named pEOS-CAG-S/MAR plasmid.
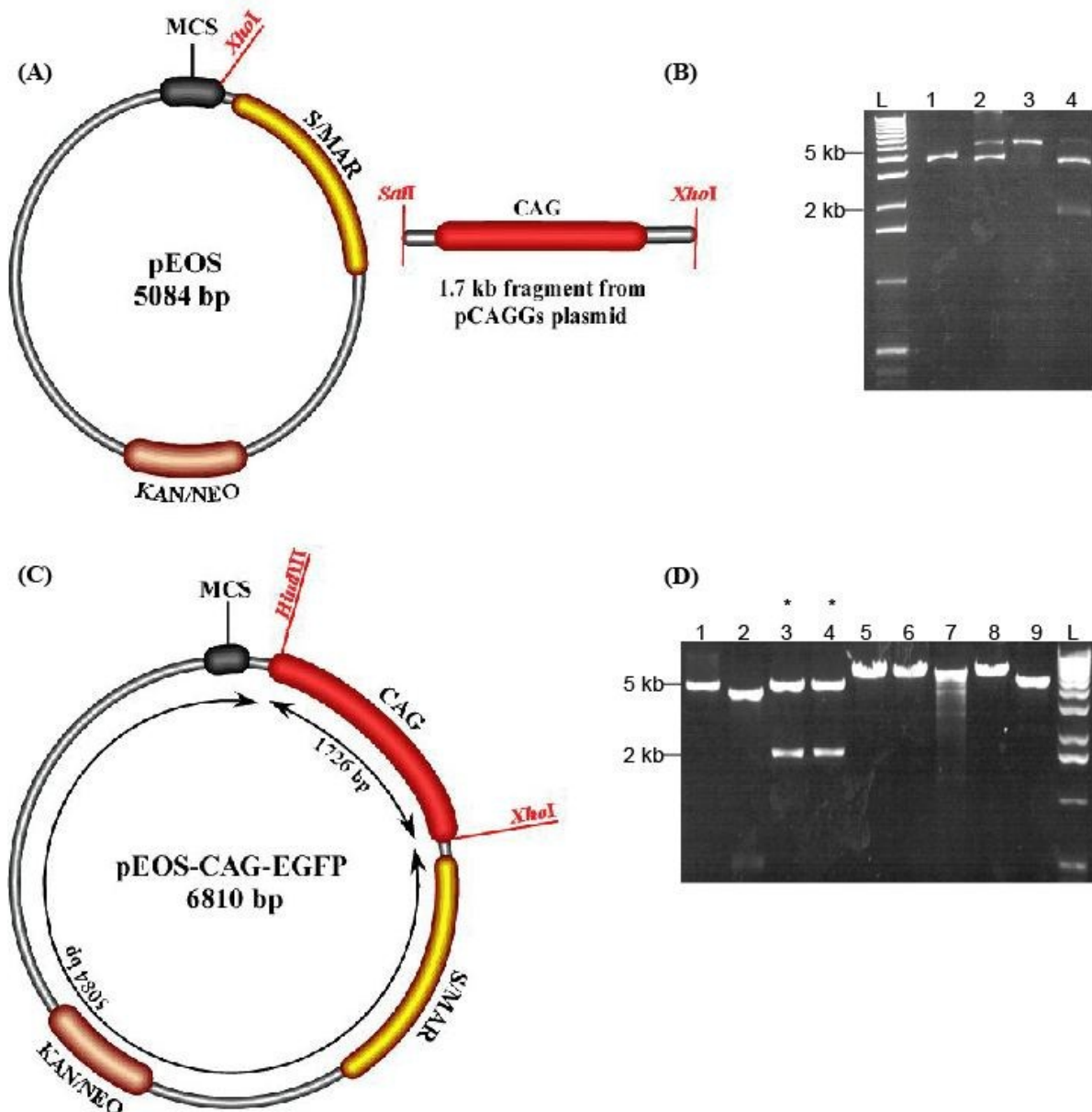
Figure 26: Generation of pEOS-CAG-S/MAR plasmid

The cloning strategy for the generation of pEOS-CAG-S/MAR plasmid involved the insertion of the 1.7 kb CAG fragment as illustrated in (A). The correct fragment sizes of the digested pCAGGs vector and linearized pEOS before ligation are shown in (B), where lanes 1 and 2: undigested pEOS and pCAGGs plasmids and lanes 3 and 4: digested pEOS and pCAGGs plasmids with *Xho*I and *Sal*I-*Xho*I restriction enzymes respectively. Successful ligation would result in the pEOS-CAG-S/MAR plasmid as illustrated in (C). Finally (D) shows the restriction analysis of 7 clones picked after ligation (lanes 3-9) with clones 1 and 2 showing the correct size of the plasmid (*), indicating the successful CAG promoter insertion and development of pEOS-CAG-S/MAR. Lanes 1 and 2 represent *Xho*I and *Hind*III digested pEOS and pCAGGs vectors respectively. L: 1 Kb ladder (Invitrogen).

3.1.5 Production of Plasmid pEOS-CAG-MCS-S/MAR

The next step was the insertion of a pair of complimentary oligonucleotides (MCS2 upper and MCS2 lower). These were designed so that after annealing they formed a multiple cloning site (MCS) double stranded oligonucleotide (dsOligo) containing the unique restriction sites recognised by *Bam*HI*, Mlu*I and *Sal*I restriction enzymes, downstream of the CAG promoter. The addition of this oligonucleotide would allow relatively easy insertion of other genes downstream of the CAG promoter. The cloning strategy is illustrated in Figure 27. The oligonucleotide primers were annealed at 94 °C as described in the methods and ligated overnight with pEOS-CAG-S/MAR vector linearised with *Xho*I restriction enzyme. The ligation mixture was then transformed into JM109 competent cells. Of the colonies that grew, 6 were grown as overnight cultures and their plasmids isolated and screened for the insertion of the MCS dsOligo in the 5' to 3' orientation, with the addition of *Bam*HI*, Mlu*I and *Sal*I restriction enzyme sites. Correctly ligated plasmids would produce a single linear fragment of approximately 6838 bp when digested with *Bam*HI enzyme alone, while digestion with *Eco*RI and *Bam*HI together would produce two fragments of 2000 bp and 4838 bp. Of the 6 clones, 1 gave the expected fragment patterns (Figure 27D). This modified vector was named pEOS-CAG-MCS-S/MAR plasmid.
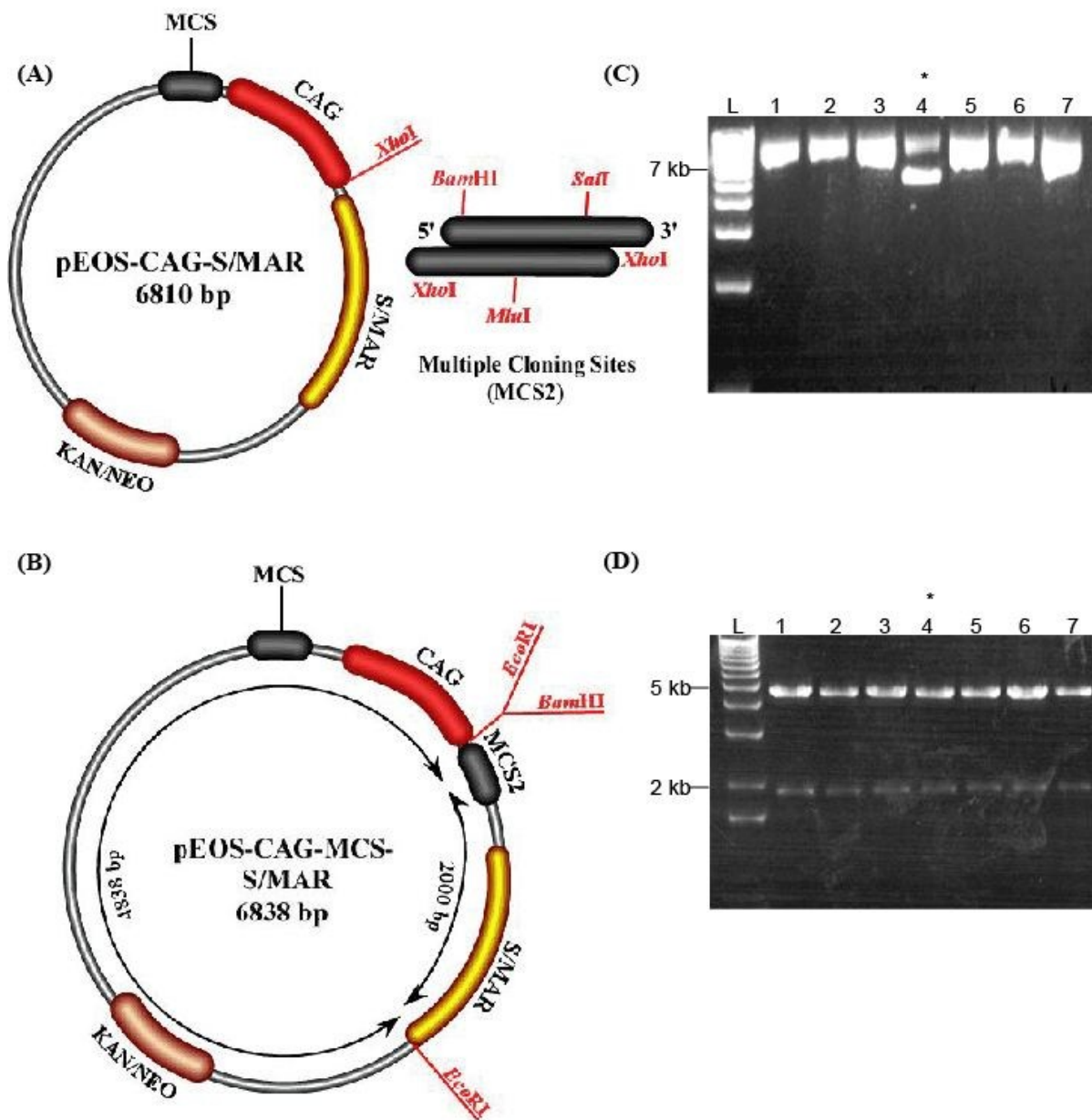
Figure 27: Generation of pEOS-CAG-MCS-S/MAR plasmid

The cloning strategy for the generation of pEOS-CAG-MCS-S/MAR plasmid involved the insertion of the multiple cloning site double stranded oligonucleotide (MCS dsOligo) as illustrated in (A). Successful ligation would result in the pEOS-CAG-MCS-S/MAR plasmid as illustrated in (B). The restriction analysis of 6 clones after ligation (lanes 2-7) is shown in (C and D) after *Bam*HI digestion alone as shown in (C) or *Bam*HI and *Eco*RI double digestion as shown in (D), with clone 3 showing the correct size of the plasmid after both digestions (*), indicating the successful insertion of the MCS and development of pEOS-CAG-MCS-S/MAR. Lanes 1 represents digested pEOS-CAG-S/MAR vector. L: 1 Kb ladder (Invitrogen).

3.1.6   Production of Plasmid pCAG-EGFP

The next step was the insertion of the *EGFP* transgene downstream of the CAG promoter
and MCS. The cloning strategy is illustrated in Figure 28. In preparation for the insertion of
EGFP, both pEOS-CAG-MCS-S/MAR and pEFS-EGFP plasmids were digested with *Mlu*I and
*Sal*I. This excised the 853 bp EGFP insert fragment from the pEFS-EGFP plasmid which was
ligated with digested pEOS-CAG-MCS-S/MAR vector overnight at a molar vector: insert ratio
of 1:10. The ligation mixture was transformed into JM109 competent cells. Out of the
colonies obtained overnight, 70 colonies were picked for PCR analysis using CAG and EGFP
specific primers as described in the methods. 3 clones showed a positive signal from the PCR
analysis showing the presence of the insert as well as the correct orientation of the insert.
All 3 clones were selected for plasmid isolation and analysis with *Afl*III restriction enzyme.
Correctly ligated plasmids in the 5' to 3' orientation would produce three fragments,
2015 bp, 2752 bp and 2924 bp. All three clones gave the expected fragment patterns
(Figure 28D). One colony was selected for isolation with a MaxiPrep kit, its quality and
quantity was measured using a Nanodrop spectrophotometer. This vector was named
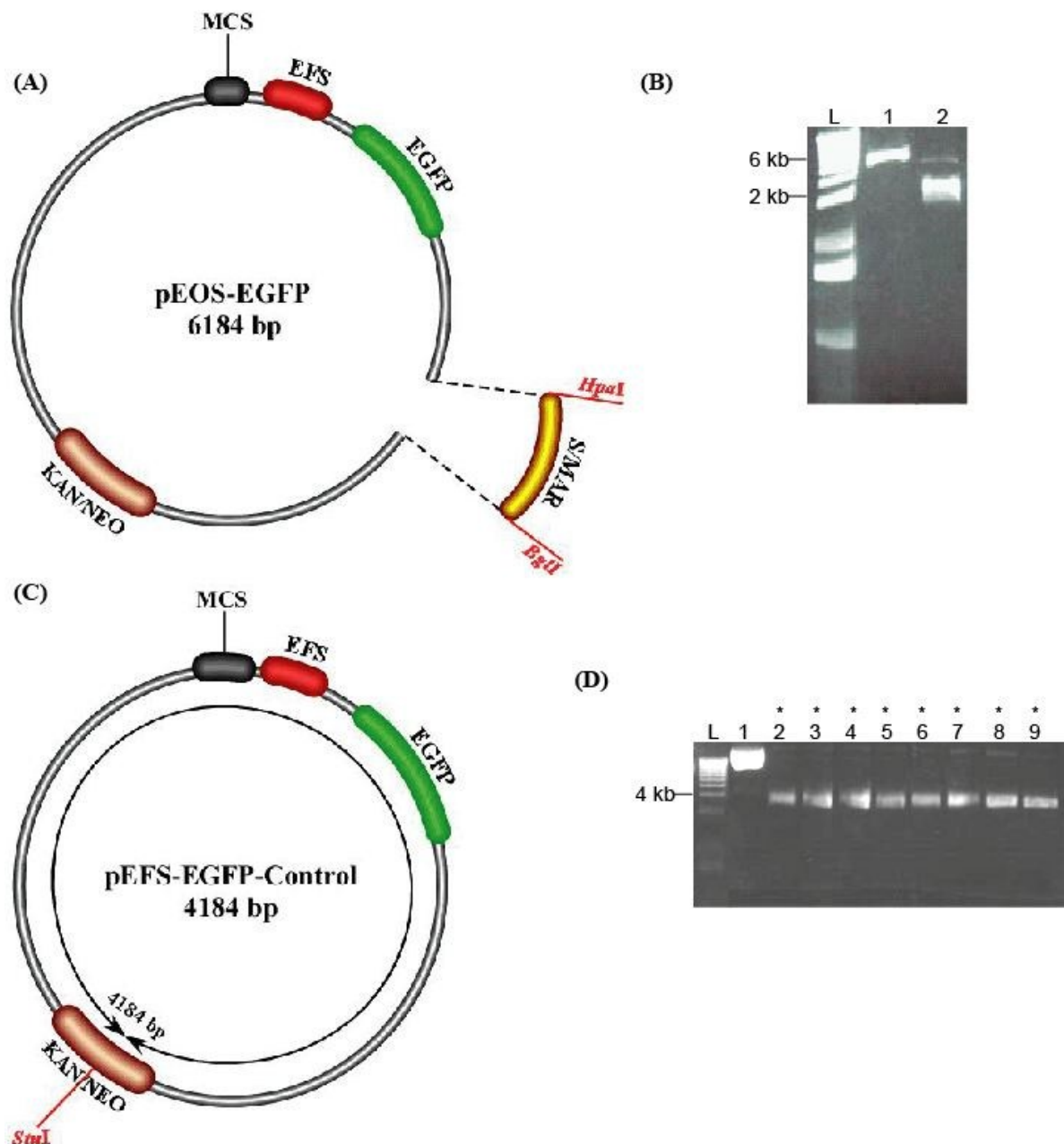pCAG-EGFP plasmid.
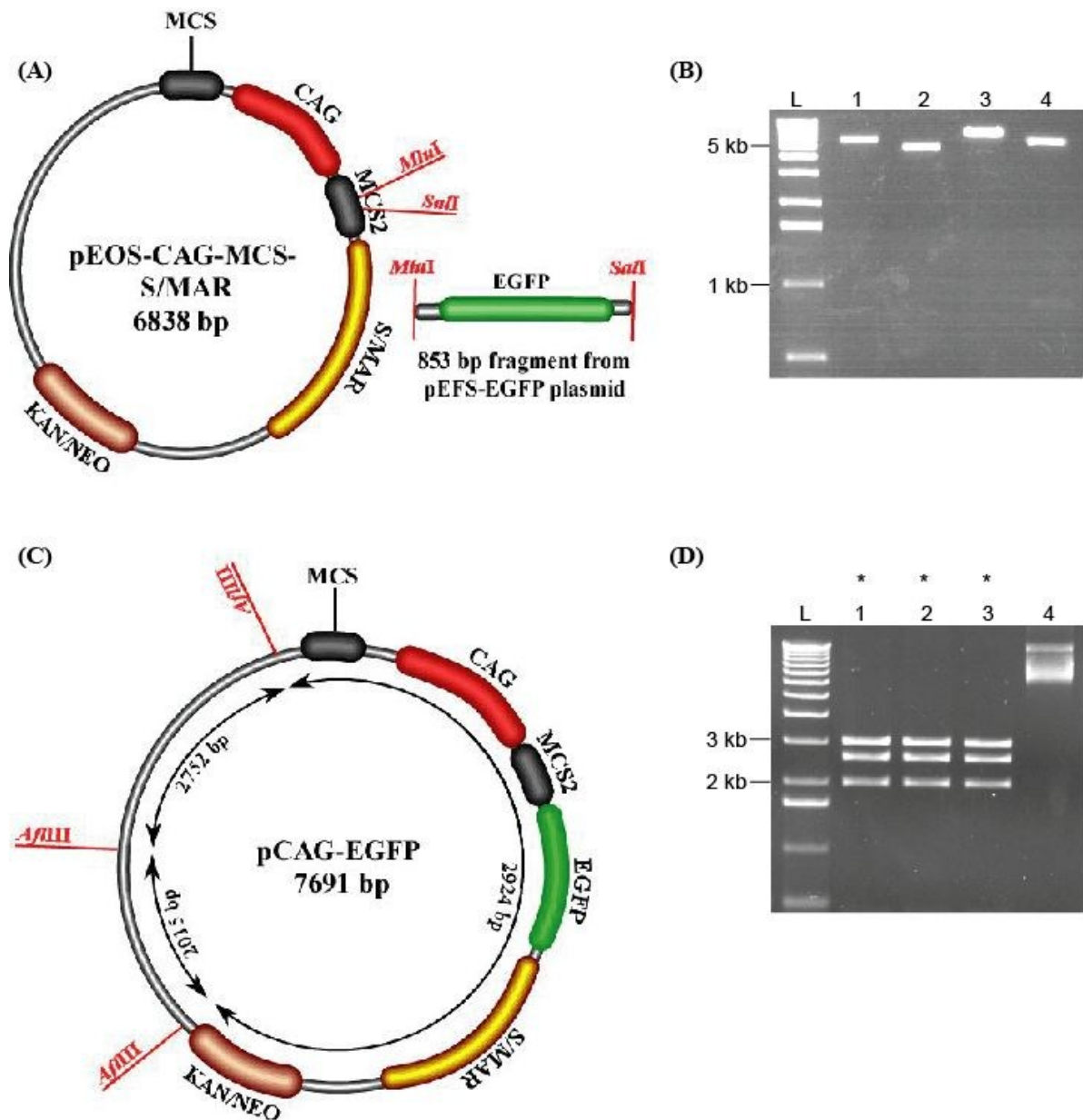
Figure 28: Generation of pCAG-EGFP plasmid

The cloning strategy for the generation of pCAG-EGFP plasmid involved the insertion of the *EGFP* transgene as illustrated in (A). The correct fragment sizes of the digested pEOS-CAG-MCS-S/MAR vector and pEFS-EGFP before ligation are shown in (B), where lanes 1 and 2: undigested pEOS-CAG-MCS-S/MAR and pEFS-EGFP plasmids and lanes 3 and 4: digested pEOS-CAG-MCS-S/MAR and pEFS-EGFP plasmids. The 853 bp fragment from pEFS-EGFP is faint but seen clearer on the digital image. Successful ligation would result in the pCAG-EGFP plasmid as illustrated in (C). Finally (D) shows the restriction analysis of 3 clones after ligation (lanes 2-4) with all clones showing the correct size of plasmid after digestion (*), indicating the successful *EGFP* transgene insertion and development of pCAG-EGFP. Lane 4 represent undigested pEOS-CAG-MCS-S/MAR vector. L: 1 Kb ladder (Invitrogen).

3.1.7   Production of a CAG control counterpart - Plasmid pCAG-EGFP-Control

The final step in the pCAG-EGFP vector series involved the development of the control counterpart to the pCAG-EGFP plasmid. The cloning strategy is illustrated in Figure 29. In preparation for the removal of the 2 kb S/MAR element, pCAG-EGFP plasmid was digested with *Nsi*I restriction enzyme. This excised the 2 kb S/MAR fragment from the pCAG-EGFP plasmid and the linearised vector was ligated overnight. The ligation mixture was transformed into JM109 competent cells. Out of the colonies obtained overnight, 8 were selected for plasmid isolation and analysis with *Stu*I restriction enzyme. Correctly ligated plasmids would produce a single fragment at 5691 bp. Of the 8 clones, 4 gave the expected plasmid sizes (Figure 29D). One colony was selected for isolation with a MaxiPrep kit, its quality and quantity was measured using a Nanodrop spectrophotometer. As this plasmid did not contain an S/MAR element, the plasmid was named pCAG-EGFP-Control plasmid.
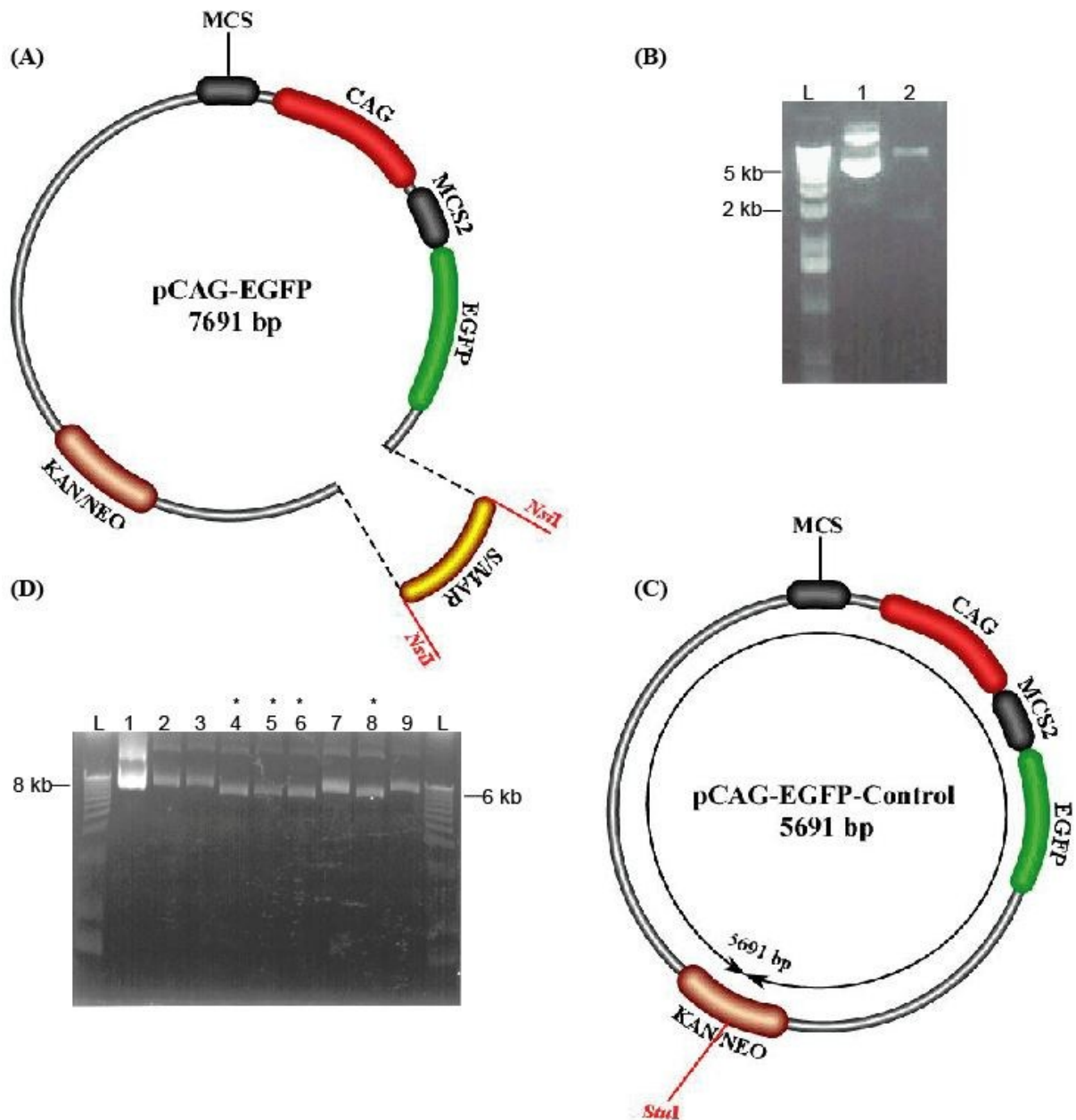
Figure 29: Generation of pCAG-EGFP-Control plasmid

The cloning strategy for the generation of pCAG-EGFP-Control plasmid involved the removal of the 2 kb S/MAR motif from the pCAG-EGFP plasmid as illustrated in (A). The correct fragment sizes of the digested pCAG-EGFP plasmid before ligation are shown in (B), where lanes 1 and 2: undigested and digested pEOS-CAG-MCS-S/MAR plasmids. The 2 kb fragment from pCAG-EGFP is faint but seen clearer on the digital image. Successful ligation would result in the pCAG-EGFP-Control plasmid as illustrated in (C). Finally (D) shows the restriction analysis of 8 clones picked after ligation (lanes 2-9) with clones 3, 4, 5 and 7 showing the correct size of plasmid after digestion (*), indicating the successful S/MAR excision and development of pCAG-EGFP-Control. Lanes 1 represents undigested pCAG-EGFP vector. L: 1 Kb ladder (Invitrogen).

3.1.8 Transient transfection of AtT20 and B16-F10 cells with pEGFP-S/MAR plasmids

To analyse our new sets of pDNA vectors, the pEFS-EGFP and pCAG-EGFP plasmids as well as their control counterparts without S/MARs were transfected into AtT20 and B16-F10 cells. This was done to ensure the integrity and to confirm expression of the EGFP transgene. Furthermore this also allowed one to check any differences in reporter gene expression resulting from the EFS and CAG promoters as well as the insertion of the S/MAR sequence. For transfections, large scale plasmid preparations were carried out using the Purelink HiPure Plasmid Maxiprep Kit (Invitrogen). DNA stock prepared using this kit has reduced levels of endotoxins, and should therefore cause less toxicity to cells following transfection.

Cells were seeded into 24-well plates at a density of 1×10^5 or 5×10^4 for AtT20 and B16-F10 cell respectively at least 24 hours prior to transfection. After overnight attachment cells were 60-70% confluent and were transfected with Lipofectamine 2000 (Invitrogen) transfection reagent. Briefly, 0.8 µg of each pDNA was complexed with Lipofectamine 2000 and added to each well, according to the manufacturer's recommendations. Complexed DNA/Lipofectamine 2000 was left on the cells overnight, and removed the following morning, cells were washed with PBS and fresh medium (3:1 ratio of DMEM:F-12 supplemented with 15% FCS and 100 U/ml penicillin and 100 µg/ml streptomycin (p/s) for AtT20 cells and DMEM supplemented with 15% FCS and p/s for B16-F10 cells) was added. At 48 hours following transfection, cells were checked under a fluorescent microscope for EGFP expression as well as quantification of expression using fluorescence activated cell sorting (FACS) analysis.

Strong levels of EGFP expression were observed in both cell lines at 48 hours post transfection from all constructs as shown in Figure 30 and Figure 31. Both pEFS-EGFP and its control were able to mediate moderate EGFP levels, with 38.2% ± 0.6 and 34.1% ± 0.27 of the total AtT20 cell population, and 27.8% ± 1.27 and 24.2% ± 0.83 of the total B16-F10 cell population respectively expressing EGFP. In comparison, pCAG-EGFP and its control were able to mediate significantly higher EGFP levels, with 62.7% ± 0.56 and 55.3% ± 0.52 of the total AtT20 cell population, and 44.8% ± 0.84 and 43.8% ± 1.32 of the total B16-F10 cell population respectively expressing EGFP. When comparing levels of EGFP expression from

pEFS-EGFP and pCAG-EGFP, a subtle difference was also evident by immunofluorescent analysis of cells. Levels of pEFS-EGFP appeared lower than pCAG-EGFP in both cell lines; indeed FACS analysis confirmed this too, as levels of pEFS-EGFP were approximately 1.6 fold/20% lower in both AtT20 and B16-F10 cells when compared to pCAG-EGFP. This reduction in EGFP expression is not surprising, as previous studies show that the CAG promoter yields higher transgene levels than most ubiquitous mammalian promoters. The differences in expression between pEFS-EGFP and its control, as well as pCAG-EGFP and its control are probably due to variation in transfection success.
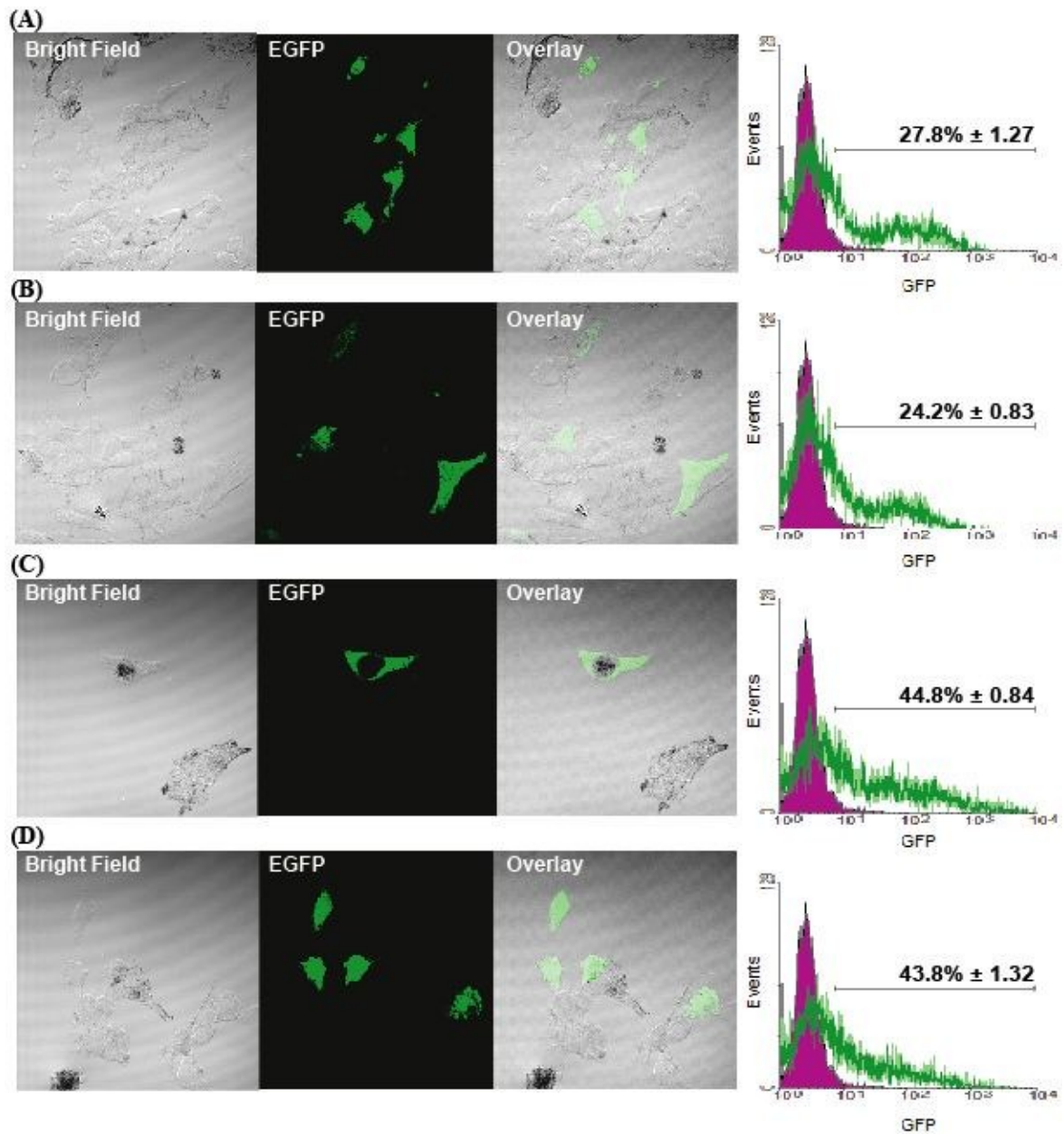
Figure 30: Transfection efficiency of B16-F10 cells 48 hours post transfection

The figure shows representative images of B16-F10 cells 48 hours post transfection with plasmids (A) pEFS-EGFP, (B) pEFS-EGFP-Control, (C) pCAG-EGFP or (D) pCAG-EGFP-Control. Bright field (*left panel*), fluorescent (*middle*) and their merge images (*right*), at 40x magnification are shown. At the same time, EGFP expression mediated by each construct was quantified using FACS analysis (*far right panel*). In all cases, histograms show measured events (*y axis*) against levels of EGFP fluorescence in the FL1-H channel (*x axis*). Untransfected B16-F10 cells appear as a purple graph on the left side of the histogram, while cells expressing EGFP appear green (as an overlay). Gated cells expressing EGFP are expressed as a percentage (%) of the total untransfected population – a threshold of 1% untransfected cells was always set - and appear above the bracketed histogram regions. Percentages are mean values from four independent experiments ± standard error of the means (s.e.m.). Images are representative of three independent experiments.
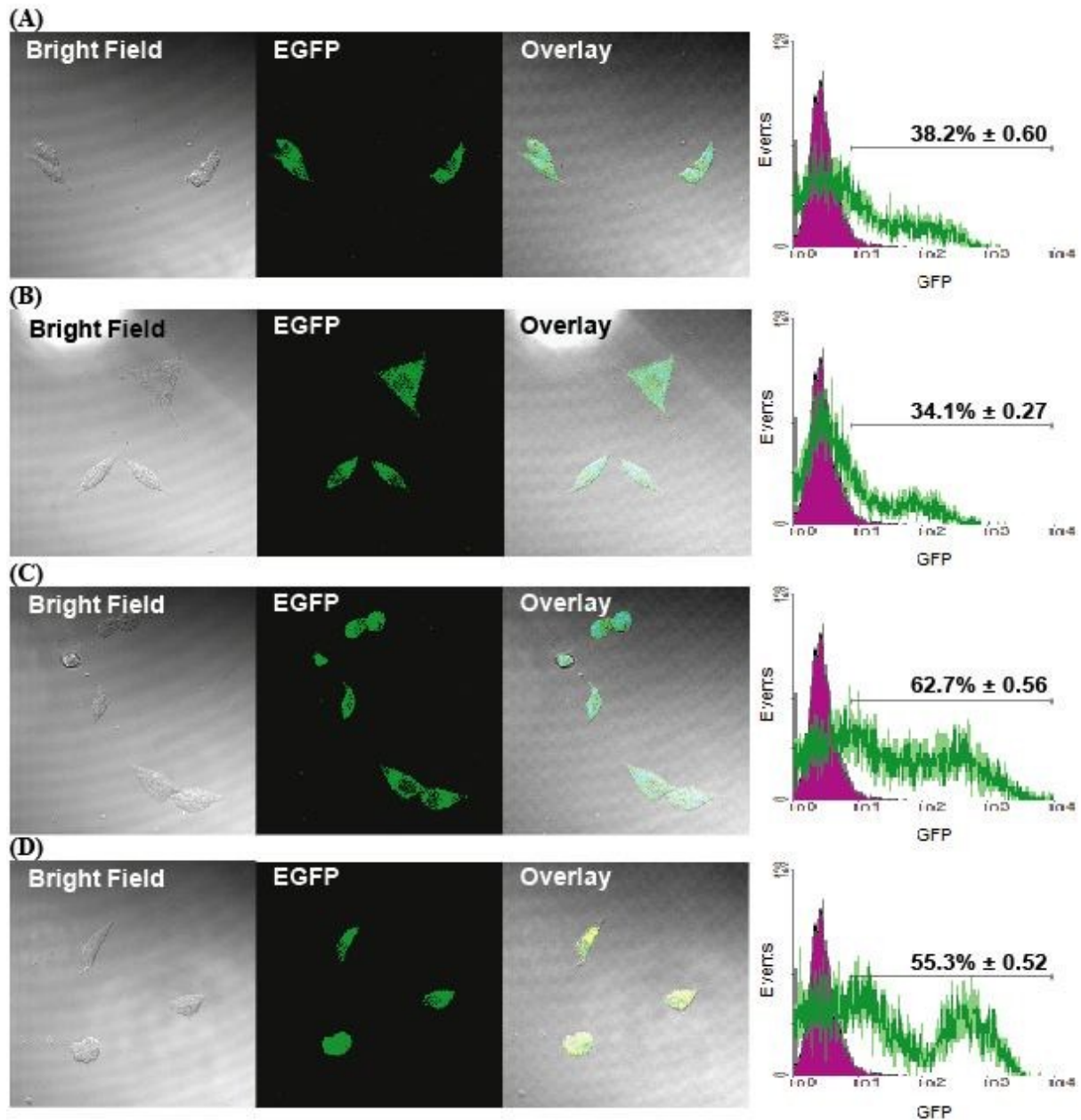
Figure 31: Transfection efficiency of AtT20 cells 48 hours post transfection

The figure shows representative images of AtT20 cells 48 hours post transfection with plasmids (A) pEFS-EGFP, (B) pEFS-EGFP-Control, (C) pCAG-EGFP or (D) pCAG-EGFP-Control. Bright field (*left panel*), fluorescent (*middle*) and their merge images (*right*), at 40x magnification are shown. At the same time, EGFP expression mediated by each construct was quantified using FACS analysis (*far right panel*). In all cases, histograms show measured events (*y axis*) against levels of EGFP fluorescence in the FL1-H channel (*x axis*). Untransfected AtT20 cells appear as a purple graph on the left side of the histogram, while cells expressing EGFP appear green (as an overlay). Gated cells expressing EGFP are expressed as a percentage (%) of the total untransfected population – a threshold of 1% untransfected cells was always set - and appear above the bracketed histogram regions. Percentages are mean values from four independent experiments ± standard error of the means (s.e.m.). Images are representative of three independent experiments.

157

Taken together, the fluorescence analysis of EGFP expression on fixed cells as well as the FACS analysis shows that AtT20 cells appear to provide higher levels of EGFP expression from all constructs compared to B16-F10 cells. Following on from this, both cell lines were also used to confirm EGFP protein expression from all constructs by Western blot analysis. Briefly, cells were seeded into 10 cm dishes 24 hours prior to Lipofectamine 2000 transfection, at a density of 5×10^5 cells per dish for AtT20 cells and 2.5×10^5 per dish for B16-F10 cells and 24 μg of each pDNA was complexed as described before. At 48 hours following transfection, total protein was isolated from AtT20 cells transfected with all four pDNAs (pEFS-EGFP, pCAG-EGFP as well as both control plasmids) and electrophoretically separated on a 12% Sodium Dodecyl Sulphate (SDS) - polyacrylamide gel before being transferred to a polyvinylidene difluoride (PVDF) membrane. Membranes were probed with an anti-mouse EGFP antibody and secondary horseradish peroxidase (HRP) – conjugated anti-mouse IgG (Dako) secondary antibody and visualised by ECL chemiluminescence. Cells transfected with pEPI-EGFP served as positive control for EGFP expression. Untransfected cells as well as cells transfected with empty vector, pEOS plasmid, were used as negative controls. Both pEFS-EGFP and pCAG-EGFP as well as the control plasmids showed expression of EGFP protein at the correct molecular weight expected for the EGFP protein (~ 50 kDa), as shown in Figure 32.
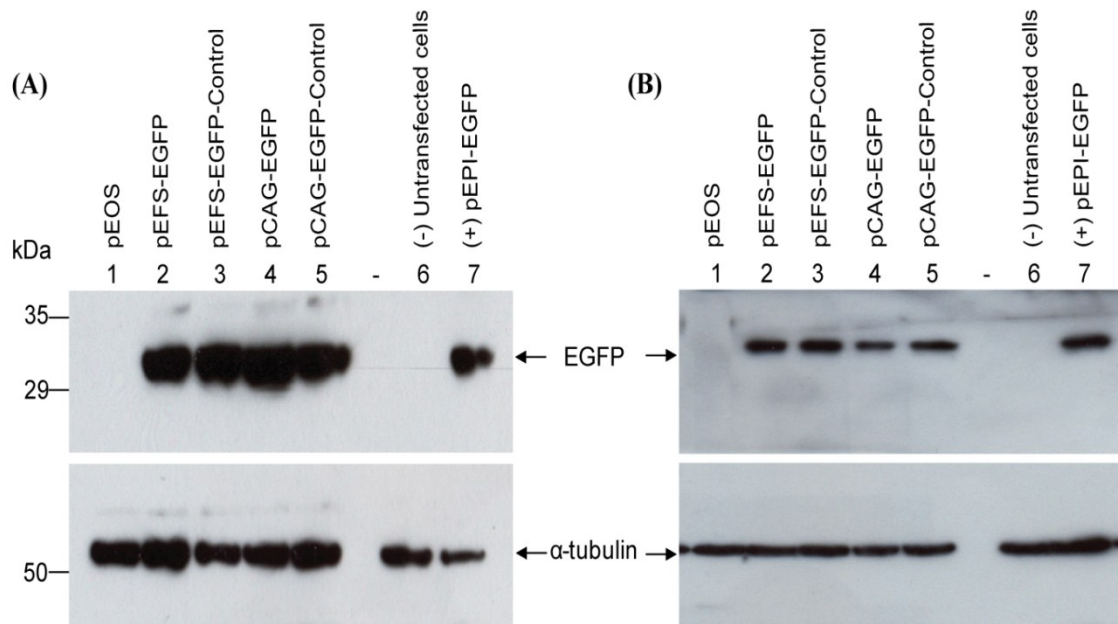
Figure 32: Western blot analysis of EGFP protein levels in AtT20 and B16-F10 cells 48 hours post transfection

The figure shows (A) AtT20 and (B) B16-F10 cells transfected with plasmids pEFS-EGFP, pEFS-EGFP-Control, pCAG-EGFP and pCAG-EGFP-Control (lanes 2, 3, 4 and 5 respectively). Expression of GFP was analysed by Western analysis of cell pellets (50 μg) 48 hours post-transfection using an anti-mouse EGFP antibody. Untransfected cells as well as cells transfected with (an empty expression cassette) the original pEOS vector served as negative controls (lane 1 and 6; (-)), while pEPI-EGFP served as a positive control (lane 7; (+)) and α-tubulin was used as a loading control. Results are representative of three independent experiments.

During the cloning process of the pCAG-EGFP plasmid, we were also able to get a pCAG-EGFP plasmid from Professor Hans Lipps, University of Witten, Germany who originally provided us with the pEPI-EGFP plasmid. This pCAG-EGFP plasmid was based on the pEPI-EGFP plasmid; therefore it had the CAG promoter inserted in place of the CMV promoter upstream of the S/MAR region. Interestingly, this plasmid did not have the removal of the 283 bp fragment at the end of the S/MAR sequence, described in the earlier section 3.1.1. Previously the 5'-end of the S/MAR sequence has been shown to be most important and crucial sequence for the correct function of S/MAR sequences (Stehle, Scinteie et al. 2003). Hence one would predict that the removal of the 283 bp fragment from the 3'-end should not affect the overall function of the EGFP transgene or corresponding pDNA vectors. To analyse this, both pCAG-EGFP plasmids (for this section plasmids will be referred to as pCAG-EGFP (EOS) (currently made) and pCAG-EGFP (HL) (from Professor

159

Lipps) respectively for ease of identification), were transfected into AtT20 cells and the transfection efficiency of both plasmids was compared by FACS analysis. As can be seen in Figure 33, both pCAG-EGFP plasmids were able to transfect AtT20 cells at a similar level 57.7% for pCAG-EGFP (HL) and 55.6% for pCAG-EGFP (EOS).

Considering this, one can confidently say that the removal of the 283 bp fragment from the original pEPI-MCS1 plasmid and the creation of the pEOS vector (see section 3.1.1 for details) did not affect the overall *EGFP* transgene expression levels. Indeed constructs made based on the pEOS vector (pEFS-EGFP and pCAG-EGFP as well as the corresponding control plasmids), were also able to produce EGFP protein of the correct size. Furthermore one can be confident that the EGFP-S/MAR constructs made as well as S/MAR constructs to be made in the future based on these plasmids are not hindered in any way and provide sufficient transgene expression levels as analysed by EGFP.
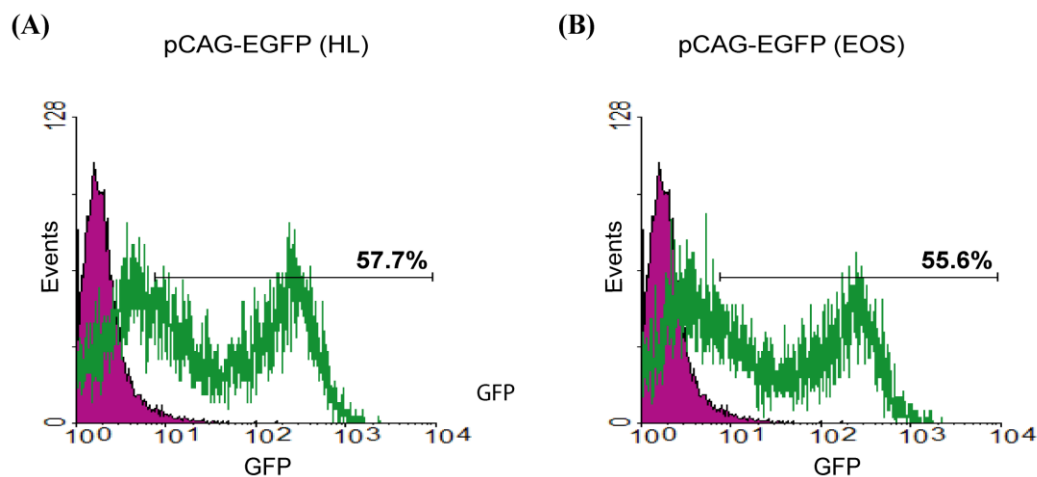
Figure 33: FACS analysis of EGFP expression levels 48 hours post transfection in AtT20 cells transfected with both pCAG-EGFP plasmid vectors (pCAG-EGFP (HL) and pCAG-EGFP (EOS))

ATt20 cells were transfected with either (A) pCAG-EGFP (HL) or (B) pCAG-EGFP (EOS) plasmids and EGFP expression of each construct was quantified using FACS analysis. Histograms show measured events (*y axis*) against levels of EGFP fluorescence in the FL1-H channel (*x axis*). Untransfected AtT20 cells appear as a purple graph on the left side of the histogram, while cells expressing EGFP appear green (as an overlay). Gated cells expressing EGFP are expressed as a percentage (%) of the total untransfected population – a threshold of 1% untransfected cells was always set - and appear above the bracketed histogram regions. Levels of EGFP expression for both pCAG-EGFP HL and EOS plasmid vectors were similar at 57.7% ± 0.89 and 55.6% ± 0.35 respectively. Percentages are mean values from five independent experiments ± standard error of the means (s.e.m.).

3.1.9   Transient EGFP transfection in RPE cells *in situ*

While AtT20 and B16-F10 transfections are important for confirming the expression of pEFS-EGFP and pCAG-EGFP plasmid constructs, it was also deemed advantageous to show the EGFP transgene expression in cells more relevant to the eye. As one of the target cells in this project is RPE cells, primary mouse and porcine RPE cells were selected for the subsequent transfections. These experiments would help investigate the behaviour of the new EGFP plasmids under conditions more closely resembling those found *in vivo.* Primary RPE cells were isolated from adult C57BL/6 mouse eyes (wild-type) as described previously (Lopes, Ramalho et al. 2007), as well as from porcine eyes. RPE cells were plated onto glass coverslips in 24-well plates where they were approximately 80-90% confluent after overnight attachment. Cells were subsequently transfected with 1 μg of pEFS-EGFP or pCAG-EGFP plasmid, and 6 μl of Lipofectin reagent (Invitrogen) as described previously (Faure, Hecquet et al. 1999). One day following transfection, cells were visualised for EGFP expression under a fluorescent microscope, as shown in Figure 34. The gene transfer of RPE cells *in situ* has been shown to be difficult to achieve, thus while transfection was achieved, the efficiency observed was low. Despite this were gene transfer was observed both constructs were able to mediate strong EGFP expression in primary RPE cells.
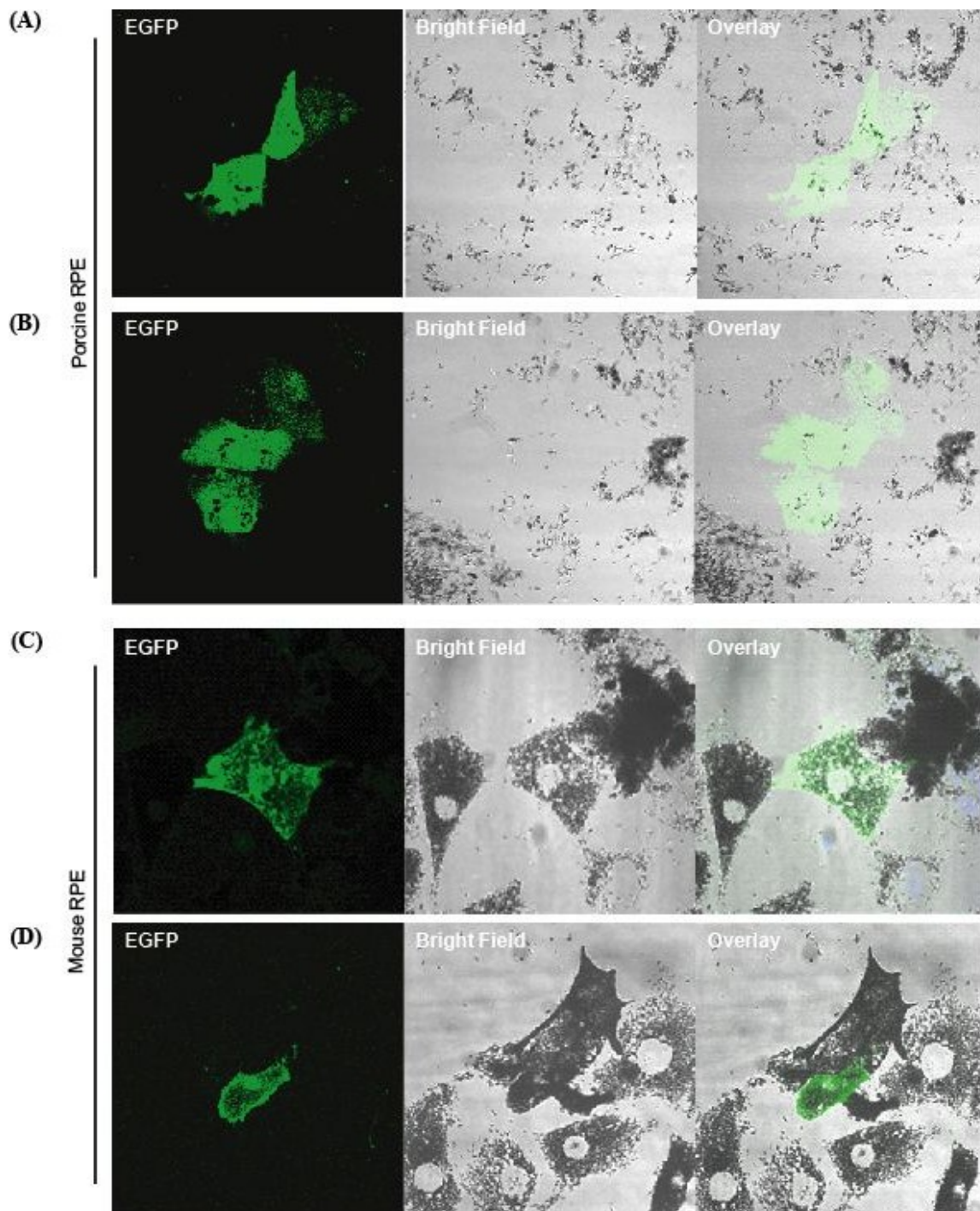
Figure 34: **Expression of pEFS-EGFP and pCAG-EGFP following transfection of primary RPE cells**

Primary RPE cells were isolated from mouse and porcine eyes, plated onto 24-well plates and transfected with 1 µg of plasmid pEFS-EGFP or pCAG-EGFP and 6 µl Lipofectin transfection reagent. Twenty fours hours post transfection cells were visualised for EGFP expression, and representative images are shown with plasmids pCAG-EGFP (A & C) and pEFS-EGFP (B & D). Fluorescent (*left panel*) bright field (*middle*) and their merge images (*right*), at 40x magnification are shown. Panels A & B represent porcine primary RPE cells, while panels C & D represent mouse primary RPE cells. Images are representative of two independent experiments.

3.1.10 Long-term EGFP expression in AtT20 cells

As AtT20 cells appear to provide higher levels of EGFP expression from all constructs (see Figure 30 - Figure 32), these transfected cells were also used for the long-term analysis of EGFP expression levels from all constructs. Primary RPE cells were not used for the long-term studies because although they closely resemble in vivo conditions, they are not an immortal cell line. Primary RPE cells only survive under optimal conditions for a short period of time. They have limited cell divisions once cells are split a few times in culture as well as reduced viability over time; hence their use in long-term analysis is unfortunately limited and inappropriate.

AtT20 cells were seeded into 6-well plates and transfected as described previously (see section 3.1.8), with plasmids pEFS-EGFP, pCAG-EGFP as well as the corresponding control plasmids. Plasmid pEPI-EGFP and its control were used as a positive and negative control in experiments. Forty eight hours post transfection, cells were transferred to a 10 cm dish and G418 antibiotic was applied at a concentration of 0.5 mg/ml for a period of two weeks, with medium being changed every 3 days. This allows for the selection of cells that express the *neo* gene present on all plasmids and so these plasmids would confer resistance to the G418 antibiotic applied and should survive the selection period. On the contrary non-transfected cells as well as cells that may have been transfected, but the plasmid has not been maintained during cell division will die away. Previous studies have shown that this two week period of selection is necessary for the selection of the pEPI plasmid in other eukaryotic cells (Baiker, Maercker et al. 2000; Jenke, Stehle et al. 2004) and is sufficient to eliminate all cells that do not express the *neo* gene.

At the end of the two week selection process, six well-formed, antibiotic-resistant AtT20 colonies expressing EGFP were isolated and split into medium with and without G418 antibiotic. Although the EGFP expression from some cells (such as CHO-K1 cells) has been shown to be stable even in the absence of a selection pressure (Piechaczek, Fetzer et al. 1999), this has yet to be shown in AtT20 cells. Therefore it was deemed necessary for our AtT20 cells to be cultured under the two different conditions, in medium with and without G418.

At regular time intervals, EGFP expression was quantified by FACS analysis, where a minimum of 10,000 cells/events were collected from each sample. The samples were analysed on the cytometer and histogram plots of measured events (y axis) against EGFP fluorescence (FL-1 – x axis) were plotted. A threshold level of fluorescence was set such that 1% of untransfected cells fell above it. The percentage of cells expressing EGFP at a level above this threshold was taken as the percentage of the total cells expressing EGFP, and this was shown graphically on histograms obtained for each sample by M1 or a bracketed region with the percentage indicated. Representative plots are shown in Figure 35- Figure 37. For each plasmid analysed (pEFS-EGFP, pCAG-EGFP and positive control pEPI-EGFP) 4 colonies were picked for long-term FACS analysis of EGFP expression as shown in Table 2. For illustrative purposes, a representative colony is used in the text and figures (expression of clone 3 from all plasmids over time).

Table 2: Percentage of EGFP expression in isolated AtT20 cell colonies transfected with pEFS-EGFP, pCAG-EGFP and pEPI-EGFP over time

AtT20 cells were transfected with plasmid pEFS-EGFP (top four columns), pCAG-EGFP (middle four columns) or pEPI-EGFP positive control (bottom four columns) and maintained in G418 medium for 2 weeks. Colonies were then picked and cultured for a period of 12 weeks either in the presence of a selection pressure (+G418), or no selection pressure (-G418). Each week cells were passaged and a representative portion of each colony was analysed by FACS analysis to determine the percentage of each individual colony expressing EGFP over time. Colony 3 (red font) from each plasmid group was selected as a representative colony for that plasmid over time. Numbers are given as percentages of EGFP expressing cells in the total cell population of each colony at time points 2, 4, 8 and 12 weeks post transfection.

Clone / Weeks PT	2 +G418	2 -G418	4 +G418	4 -G418	8 +G418	8 -G418	12 +G418	12 -G418
pEFS-EGFP 1	28.1	-	83.4	74.5	75.6	70.2	77.9	74.7
2	32.7	-	59.1	55.8	40.0	37.6	39.2	38.4
3	34.1	-	49.4	47.7	72.9	67.7	83.4	74.5
4	38.4	-	52.8	47.2	63.3	54.3	70.5	63.4
pCAG-EGFP 1	30.8	-	52.3	48.6	68.6	65.8	82.6	80.0
2	35.6	-	55.6	49.5	67.9	62.3	78.3	72.2
3	40.0	-	83.4	74.5	86.5	75.8	90.9	85.3
4	27.2	-	45.2	42.0	56.7	52.6	76.1	70.8
pEPI-EGFP 1	17.6	-	49.4	47.7	48.3	42.6	50.8	45.2
2	26.2	-	34.1	32.8	37.6	27.5	28.3	29.4
3	36.9	-	50.6	46.0	68.1	53.3	75.7	70.2
4	38.1	-	56.1	45.9	64.4	58.1	70.1	65.3

As can be seen for all plasmids analysed in Figure 35, 36 and 37, there is a steady and stable increase in the expression of EGFP in AtT20 cells up to 12 weeks following transfection. For colony 3 stable AtT20 cells transfected with pCAG-EGFP, there is a stable increase of EGFP expression in transfected cells. Levels of EGFP start at 40% at week two post transfection and reach 90.9% and 85.3% in cells maintained in G418 medium (+ G418) and normal medium (- G418) respectively, at 12 weeks post transfection. A similar level was also obtained for the colony 3 stable pEFS-EGFP transfected cells, with EGFP expression starting at 34.1% after two weeks of selection and increase to 83.4% and 74.5% in cells maintained with and without selection (+ and – G418) respectively, at 12 weeks post transfection. The positive control colony 3 for pEPI-EGFP also performed similarly, providing a stable increase in EGFP levels starting at 36.9% two weeks post transfection, and reaching 75.7% and 70.2% in G418 + and G418 – cells respectively at 12 weeks post transfection. Overall the highest level of EGFP expression were observed in cells transfected with pCAG-EGFP, then pEFS-EGFP and finally pEPI-EGFP stable AtT20 cells at 12 weeks post transfection. Importantly, EGFP expression was stable for all plasmids analysed irrespective of whether cells were maintained in selection or not. Levels of EGFP expression were similar in the other three pCAG-EGFP, pEFS-EGFP and pEPI-EGFP colonies analysed as seen in Table 2.

One might have expected to observe a more uniform population close to 100% of the population expressing EGFP after the initial two weeks of G418 selection was applied to transfected cells. However due to the limitations of the colony isolation method, whereby isolated clones may have been picked and included cells that may not have expressed EGFP, this would have meant that these cells would not have been killed off during the G418 selection process due to the presence of the *neo* gene in their nucleus, and so would have survived alongside EGFP expressing cells (throughout the entire experiment). Importantly, resistant colonies that grew from At20 cells transfected with control plasmids lacking the S/MAR element (pCAG-EGFP-Control, pEFS-EGFP-Control and pEPI-EGFP-Control) were also maintained in G418 or normal medium for up to 12 weeks post transfection. In all control plasmids, levels of EGFP expression were similar to background levels of untransfected AtT20 cells; reaching levels no higher than 3.1% (Figure 35B, Figure 36B and Figure 37B). This result verifies results seen by others in other cells (Piechaczek, Fetzer et al. 1999; Schaarschmidt, Baltin et al. 2004; Papapetrou, Zoumbos et al. 2005).
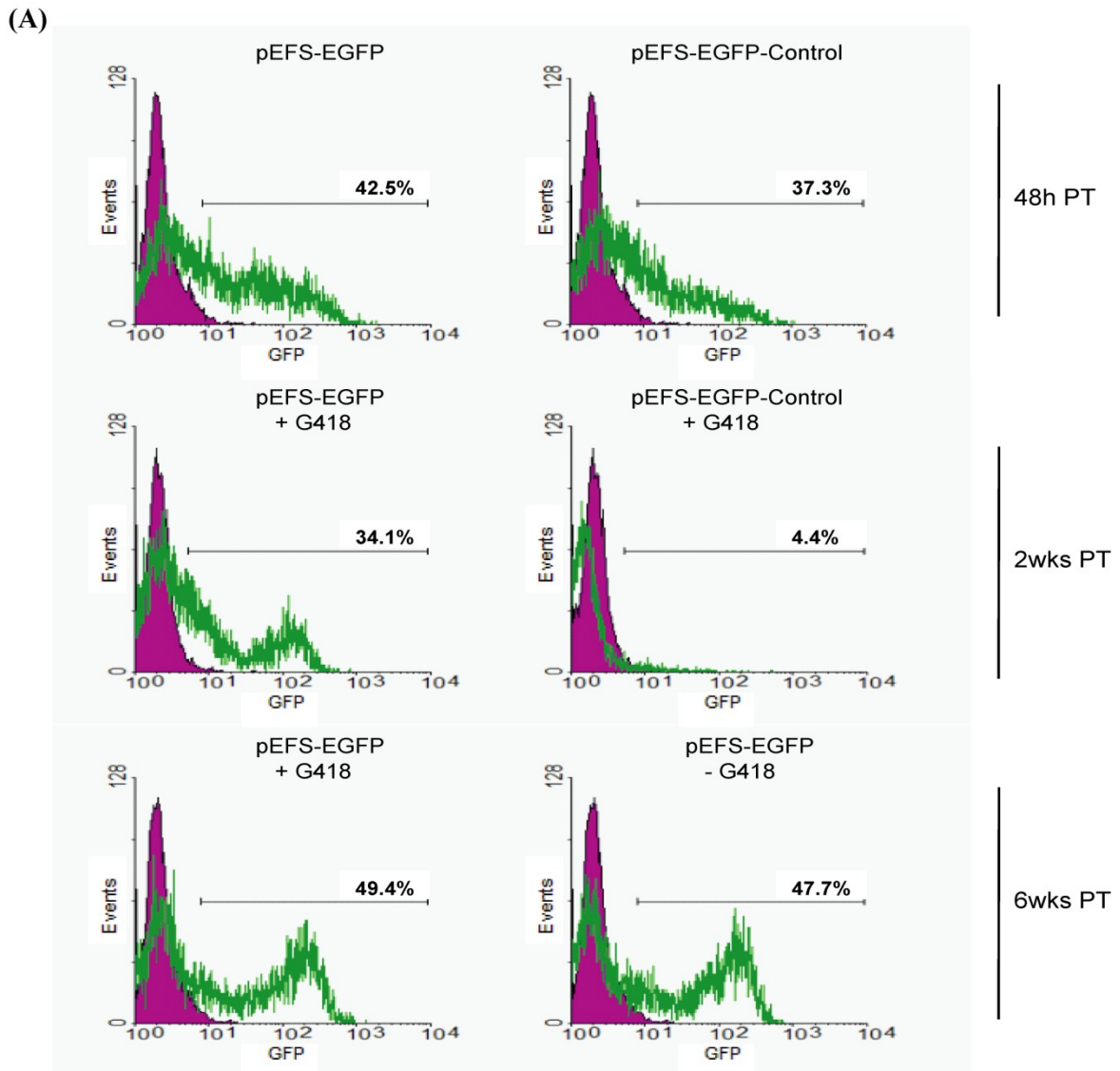
Figure 35: FACS analysis of EGFP expression levels over time in AtT20 cells transfected with pEFS-EGFP and pEFS-EGFP-Control plasmid vectors

(A) AtT20 cells were transfected with plasmids pEFS-EGFP or pEFS-EGFP-Control and analysed by FACS analysis 48 hours post transfection (PT) (*top panel*). EGFP expression levels from both plasmids showed good levels of transfection after 48h PT (42.5% and 37.3% of the total population respectively). Selection pressure with G418 antibiotic was applied to both cell populations for a period of 2 weeks at which point cells were analysed for EGFP expression at the end of the 2 week selection period (*middle*). Levels of EGFP expression were sustained in cells transfected with pEFS-EGFP (34.1% of the initial population) while EGFP expression was lost in pEFS-EGFP-Control transfected cells (4.4% of the initial population). Individual colonies that had formed from cells transfected with pEFS-EGFP were picked, where half were maintained under selection while the other half was maintained in normal medium (+G418 and –G418 respectively). Cells transfected with pEFS-EGFP and maintained for 6 weeks with and without G418 selection were analysed for EGFP expression by FACS analysis (*bottom*). Levels of EGFP expression were maintained for both cell populations with and without G418 selection (49.4% and 47.7% respectively).
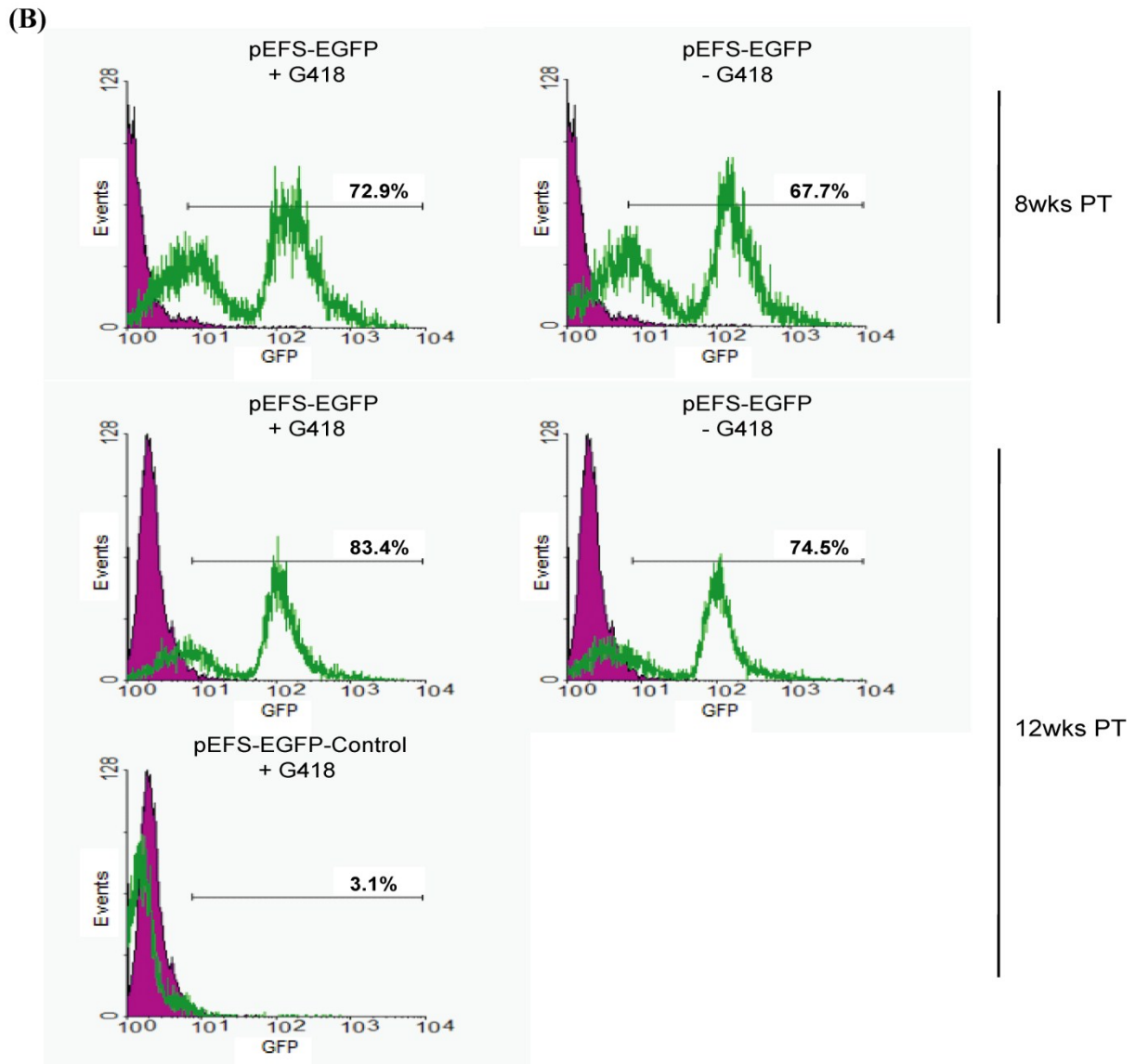
Figure 35: FACS analysis of EGFP expression levels over time in AtT20 cells transfected with pEFS-EGFP and pEFS-EGFP-Control plasmid vectors

(B) EGFP expression levels from pEFS-EGFP transfected cells at 8 weeks PT with and without selection pressure (*top panel*); levels of EGFP were maintained (72.9% and 67.7% respectively). Levels of EGFP expression were also measured at 12 weeks PT with and without selection pressure from pEFS-EGFP, as well as from cells transfected with pEFS-EGFP-Control maintained with G418 selection pressure (*bottom*). At 12 weeks PT, levels of EGFP expression in cells from pEFS-EGFP maintained with and without selection pressure were sustained (83.4% and 74.5% respectively), while EGFP expression from cells transfected with pEFS-EGFP-Control was lost (3.1%).

In all cases, histograms show measured events (*y axis*) against levels of EGFP fluorescence in the FL1-H channel (*x axis*). Untransfected AtT20 cells appear as a pink graph on the left side of the histogram, while cells expressing EGFP appear green (as an overlay). Gated cells expressing EGFP are expressed as a percentage (%) of the total untransfected population – a threshold of 1% untransfected cells was always set - and appear above the bracketed histogram regions.

Figure 36: FACS analysis of EGFP expression levels over time in AtT20 cells transfected with pCAG-EGFP and pCAG-EGFP-Control plasmid vectors

(A) AtT20 cells were transfected with plasmids pCAG-EGFP or pCAG-EGFP-Control and analysed by FACS analysis 48 hours post transfection (PT) (*top panel*). EGFP expression levels from both plasmids showed good levels of transfection after 48h PT (69.9% and 60.6% of the total population respectively). Selection pressure with G418 antibiotic was applied to both cell populations for a period of 2 weeks at which point cells were analysed for EGFP expression at the end of the 2 week selection period (*middle*). Levels of EGFP expression were sustained in cells transfected with pCAG-EGFP (40.0% of the initial population) while EGFP expression was lost in pCAG-EGFP-Control transfected cells (3.7% of the initial population). Individual colonies that had formed from cells transfected with pCAG-EGFP were picked, where half were maintained under selection while the other half was maintained in normal medium (+ G418 and – G418 respectively). Cells transfected with pCAG-EGFP and maintained for 6 weeks with and without G418 selection were analysed for EGFP expression by FACS analysis (*bottom*). Levels of EGFP expression were maintained for both cell populations with and without G418 selection (83.4% and 74.5% respectively).
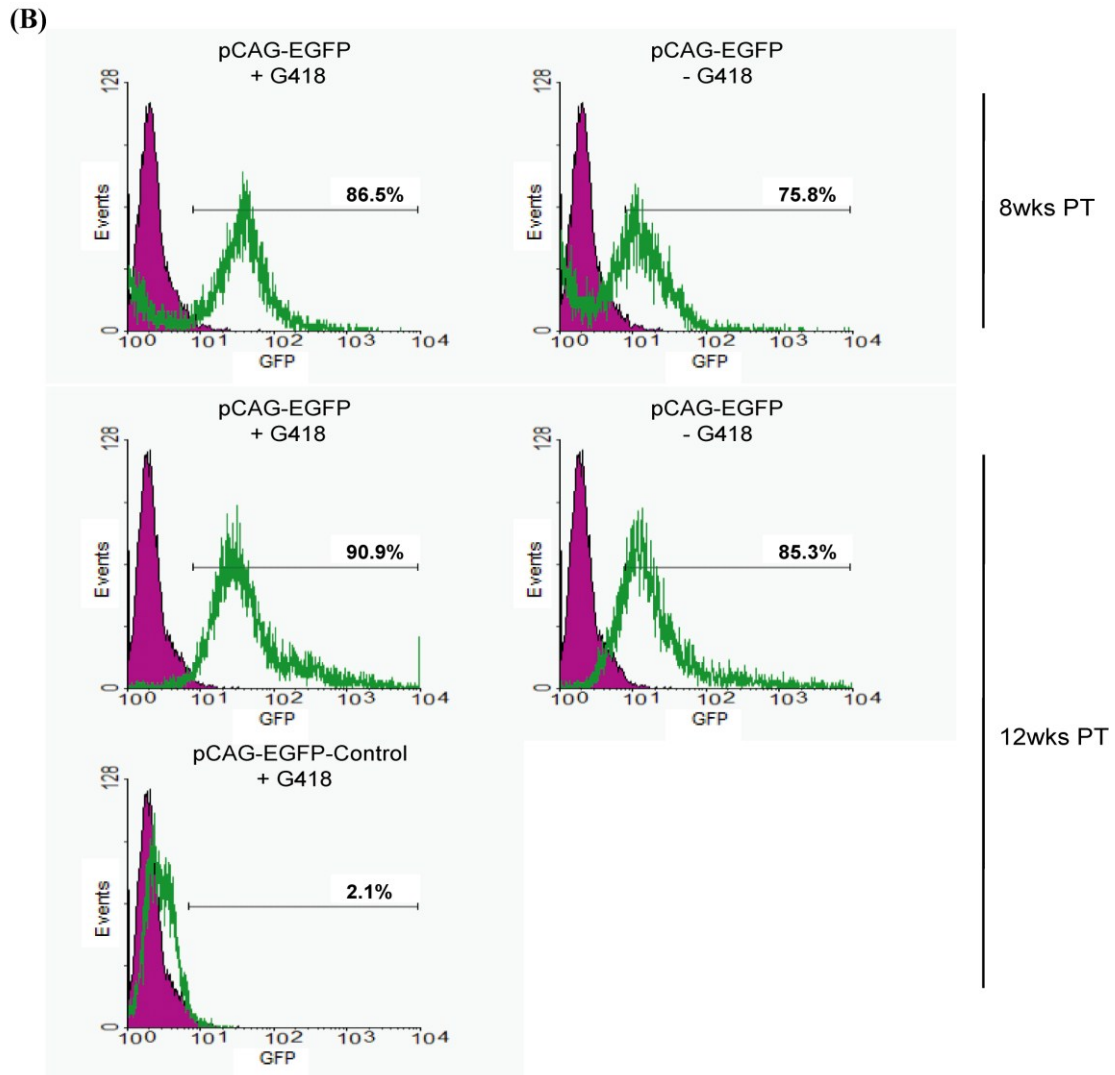
Figure 36:   FACS analysis of EGFP expression levels over time in AtT20 cells transfected with pCAG-EGFP and pCAG-EGFP-Control plasmid vectors

(B) EGFP expression levels from pCAG-EGFP transfected cells at 8 weeks PT with and without selection pressure (*top panel*); levels of EGFP were maintained (86.5% and 75.8% respectively). Levels of EGFP expression were also measured at 12 weeks PT with and without selection pressure from pCAG-EGFP, as well as from cells transfected with pCAG-EGFP-Control maintained with G418 selection pressure (*bottom*). At 12 weeks PT, levels of EGFP expression in cells from pCAG-EGFP maintained with and without selection pressure were sustained (90.9% and 85.3% respectively), while EGFP expression from cells transfected with pCAG-EGFP-Control was lost (2.1%).

In all cases, histograms show measured events (*y axis*) against levels of EGFP fluorescence in the FL1-H channel (*x axis*). Untransfected AtT20 cells appear as a pink graph on the left side of the histogram, while cells expressing EGFP appear green (as an overlay). Gated cells expressing EGFP are expressed as a percentage (%) of the total untransfected population – a threshold of 1% untransfected cells was always set - and appear above the bracketed histogram regions.

Figure 37: FACS analysis of EGFP expression levels over time in AtT20 cells transfected with (+ control) pEPI-EGFP and pEPI-EGFP-Control plasmid vectors

(A) AtT20 cells were transfected with plasmids pEPI-EGFP or pEPI-EGFP-Control and analysed by FACS analysis 48 hours post transfection (PT) (*top panel*). EGFP expression levels from both plasmids showed good levels of transfection after 48h PT (53.8% and 44.8% of the total population respectively). Selection pressure with G418 antibiotic was applied to both cell populations for a period of 2 weeks at which point cells were analysed for EGFP expression at the end of the 2 week selection period (*middle*). Levels of EGFP expression were sustained in cells transfected with pCAG-EGFP (36.9% of the initial population) while EGFP expression was lost in pEPI-EGFP-Control transfected cells (5.4% of the initial population). Individual colonies that had formed from cells transfected with pEPI-EGFP were picked, where half were maintained under selection while the other half was maintained in normal medium (+ G418 and –G418 respectively). Cells transfected with pEPI-EGFP and maintained for 6 weeks with and without G418 selection were analysed for EGFP expression by FACS analysis (*bottom*). Levels of EGFP expression were maintained for both cell populations with and without G418 selection (50.6% and 46.0% respectively).
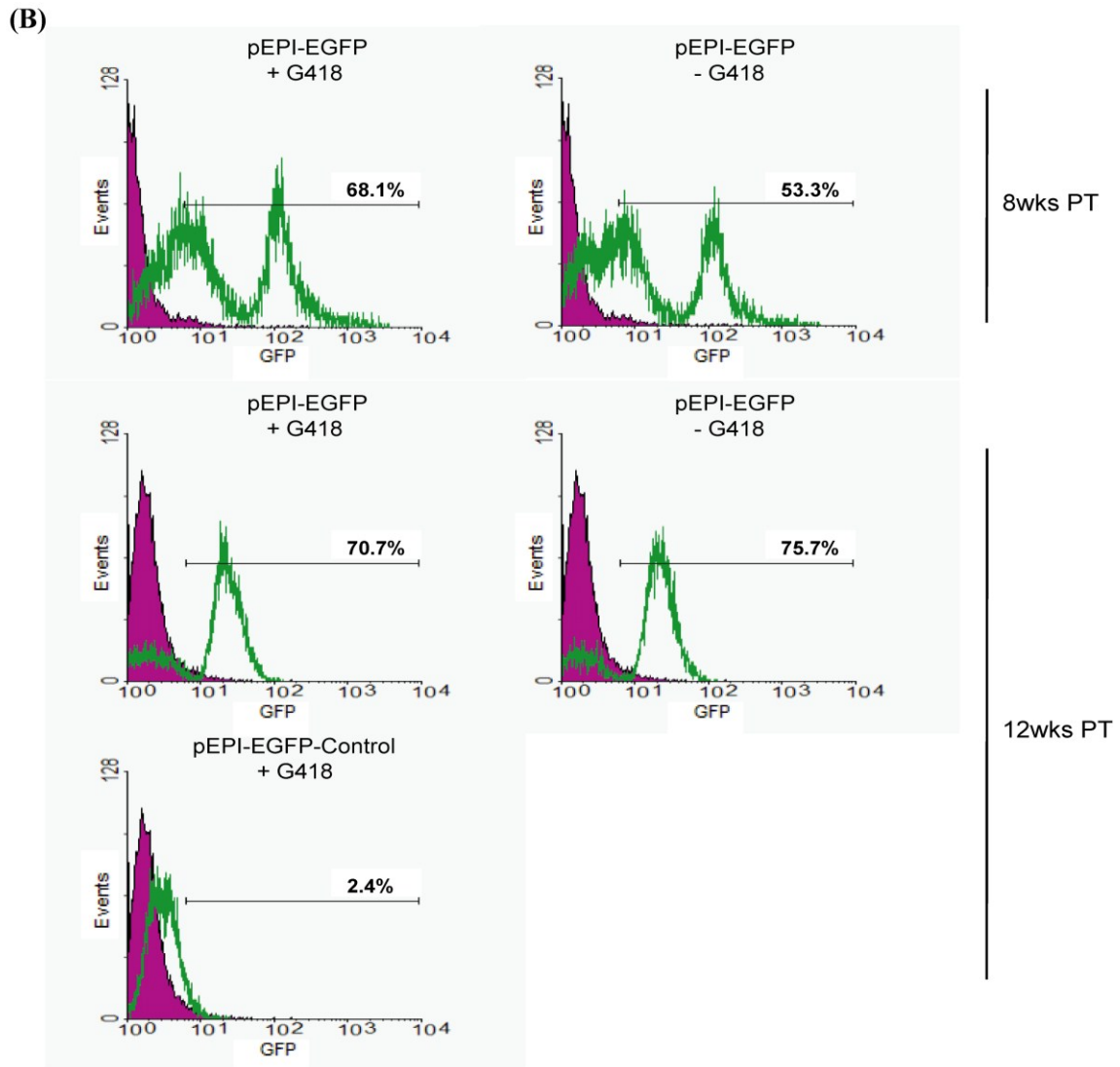
Figure 37: FACS analysis of EGFP expression levels over time in AtT20 cells transfected with (+ control) pEPI-EGFP and pEPI-EGFP-Control plasmid vectors

(B) EGFP expression levels from pEPI-EGFP transfected cells at 8 weeks PT with and without selection pressure (*top panel*); levels of EGFP were maintained (68.1% and 53.3% respectively). Levels of EGFP expression were also measured at 12 weeks PT with and without selection pressure from pEPI-EGFP, as well as from cells transfected with pEPI-EGFP-Control maintained with G418 selection pressure (*bottom*). At 12 weeks PT, levels of EGFP expression in cells from pEPI-EGFP maintained with and without selection pressure were sustained (70.7% and 75.7% respectively), while EGFP expression from cells transfected with pEPI-EGFP-Control was lost (2.4%).

In all cases, histograms show measured events (*y axis*) against levels of EGFP fluorescence in the FL1-H channel (*x axis*). Untransfected AtT20 cells appear as a pink graph on the left side of the histogram, while cells expressing EGFP appear green (as an overlay). Gated cells expressing EGFP are expressed as a percentage (%) of the total untransfected population – a threshold of 1% untransfected cells was always set - and appear above the bracketed histogram regions.

PCR analysis was also performed on total DNA isolated from short and long-term AtT20 cells transfected with both pDNA vector sets (pEFS-EGFP and pCAG-EGFP as well as the corresponding control plasmids) without G418 selection pressure (Figure 38). PCR analysis of both vectors revealed the presence of pDNA in AtT20 cells up to 12 weeks post transfection, consistent with the FACS data observed above for the vectors.

Results from the FACS and PCR analysis of pDNA was further verified by rt-PCR analysis of EGFP mRNA levels from short and long-term AtT20 cells transfected with each pDNA vector set (Figure 39). Long-term EGFP mRNA transcript was observed in AtT20 cells transfected with both vectors pEFS-EGFP and pCAG-EGFP. No bands were observed for the PCR analysis of RNA samples using the same primers to amplify pDNA in AtT20 cells (data not shown), verifying that the EGFP mRNA expression observed in Figure 389 is true and not a contamination of genomic DNA.
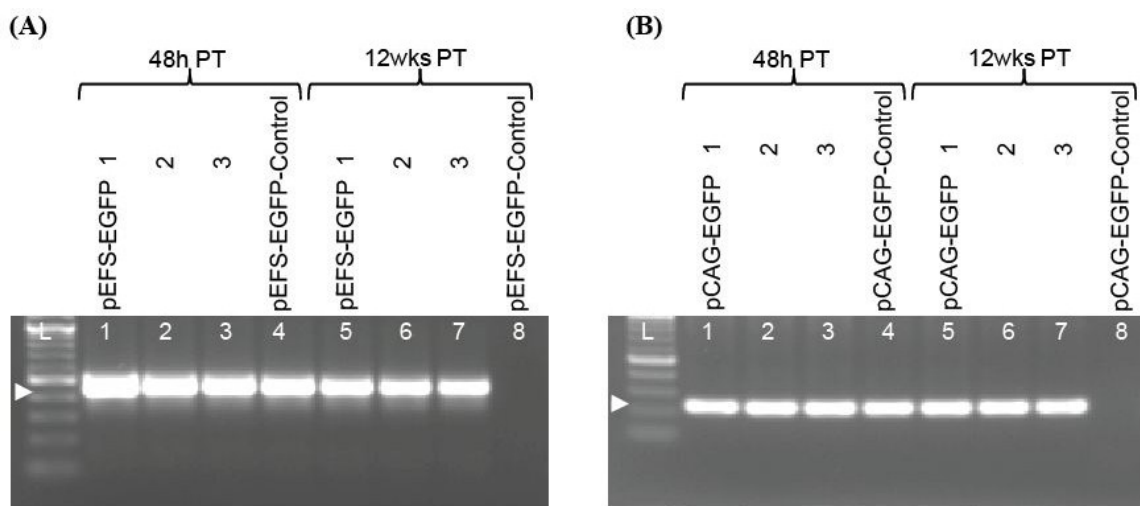
Figure 38:   PCR detection of pEFS-EGFP and pCAG-EGFP pDNA vectors in AtT20 cells extracted short term and long-term post transfection without G418 selection pressure

PCR analysis of (A) pEFS-EGFP and pEFS-EGFP-Control and (B) pCAG-EGFP and pCAG-EGFP-Control pDNA vectors at 48 hours (lanes 1-4) and 12 weeks (lanes 5-8) post transfection (PT) without G418 selection pressure. PCR samples were separated by agarose gel electrophoresis and a positive PCR band was observed using EFS-EGFP or CAG-EGFP specific primer sets yielding a product size of 450 bp or 250 bp respectively. The arrowhead indicates the size corresponding to pDNA 450 bp on (A) and 250 bp on (B). Results are representative of three independent experiments. L= 100 bp ladder (Invitrogen).
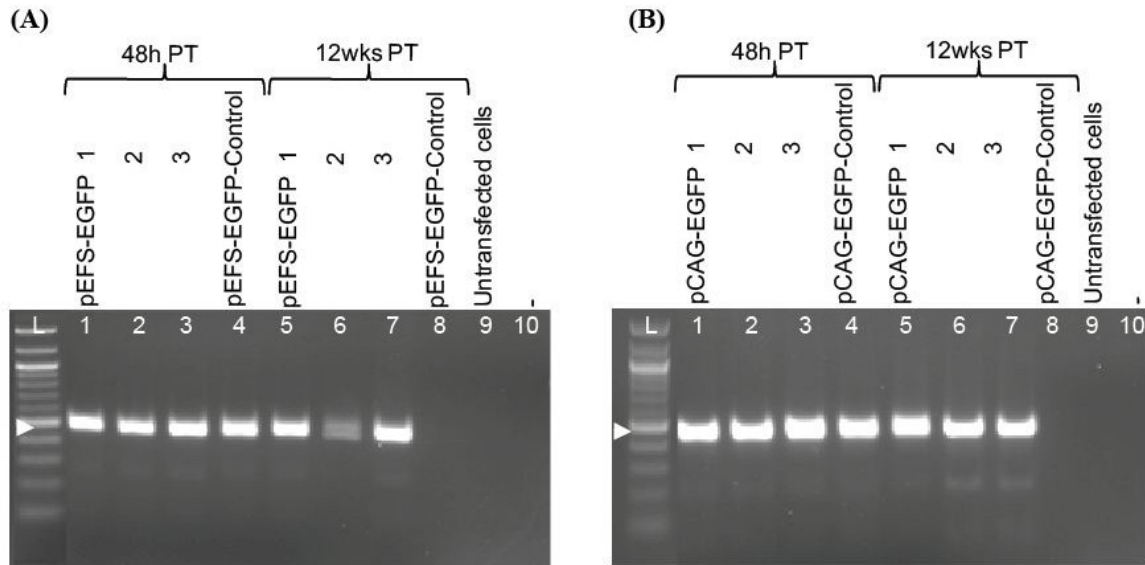
Figure 39: RT-PCR analysis of EGFP mRNA from AtT20 cells transfected with EGFP-S/MAR plasmids at 48 hours and 12 weeks post transfection without G418 selection pressure

Total RNA was extracted from AtT20 cells transfected with (A) pEFS-EGFP and pEFS-EGFP-Control and (B) pCAG-EGFP and pCAG-EGFP-Control pDNA vectors at 48 hours (lanes 1-4) and 12 weeks (lanes 5-8) post transfection, without G418 selection pressure. Total RNA was isolated and used to generate cDNA. PCR was performed with two EGFP specific primers to yield a product size of 494 bp, as indicated by the arrowhead on (A) and (B). Untransfected cells as well as no RNA product/water served as a negative control (lanes 9 and 10). Results are representative of three independent experiments. L= 100 bp ladder (Invitrogen).

3.1.11 Replication analysis of pEGFP-S/MAR vectors in AtT20 cells

To assess whether plasmids pEFS-EGFP and pCAG-EGFP were able to replicate in AtT20 cells, long-term transfected cells were analysed by *Dpn*I and *Mbo*I restriction digestion analysis. The *Dpn*I enzyme recognises bacterial DNA sequences, while *Mbo*I enzyme recognises mammalian DNA sequences. Total genomic DNA was extracted from cells and was digested with both enzymes independently followed by analysis by PCR for the presence or absence of a band using plasmid specific primers. Hence sequences of DNA that had not been cut by the restriction enzyme would also not be able to be PCR amplified and so no detectable PCR band would be observed. In contrast, samples that had been digested with either enzyme would cause the DNA to become linearised and so PCR analysis would yield a PCR band.

Figure 40 shows the representative PCR analysis of pEFS-EGFP, pCAG-EGFP and pEPI-EGFP plasmids following *Mbo*I and *Dpn*I digestion of AtT20 cells 12 weeks following transfection with and without G418 medium. The results show that all the plasmids analysed in the AtT20 cells were able to replicate during the 12 weeks post transfection. Therefore all plasmids were transform from pDNAs of bacterial origin - which they all would have been when pDNAs were originally amplified and purified - to pDNAs of mammalian origin after being cultured with the AtT20 cells at the end of the 12 week period. Noteworthy is the fact that the replication of the plasmids was unaffected regardless of whether the cells were maintained in G418 selection medium or normal medium. Hence both pEFS-EGFP and pCAG-EGFP pDNA vectors were able to replicate and mediate long expressing levels of the *EGFP* transgene in AtT20 cells.
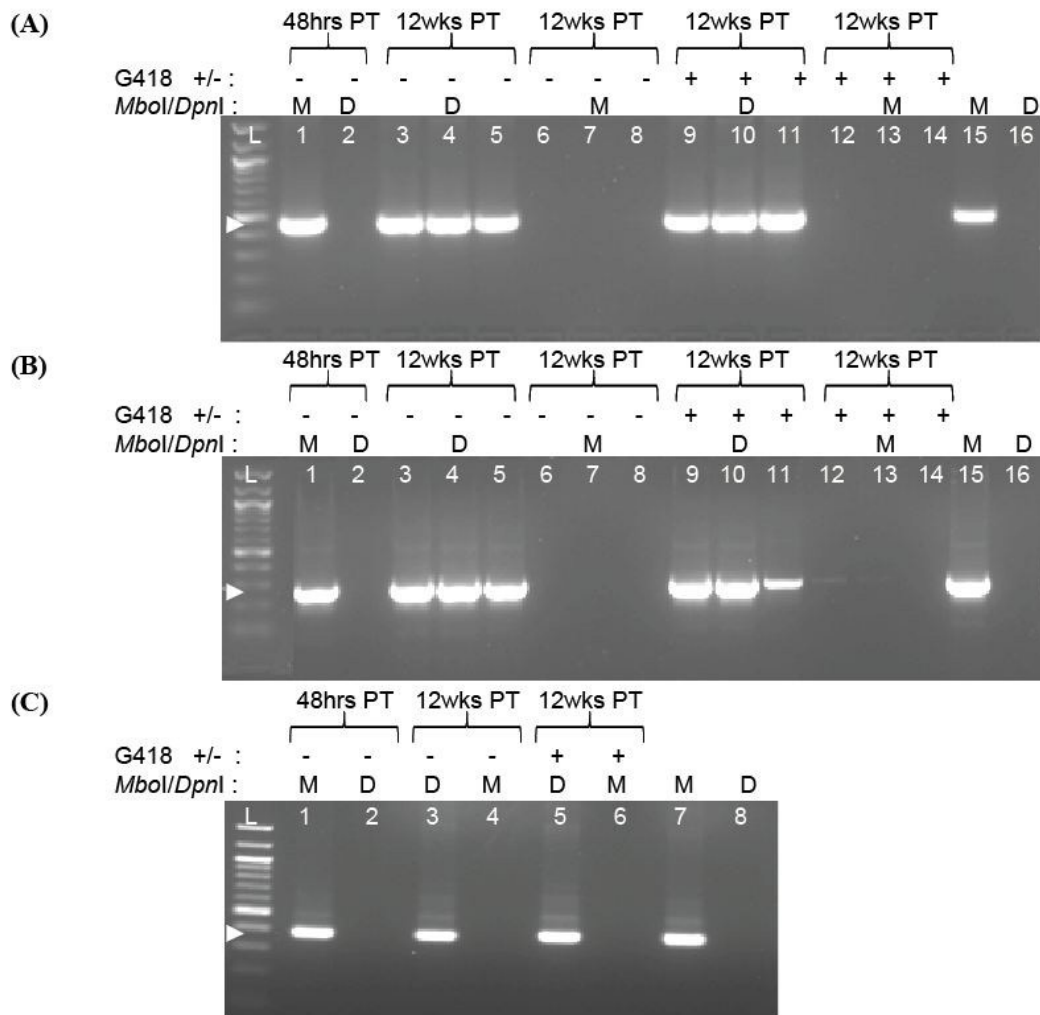
Figure 40: Long-term PCR analysis of *Mbo*I or *Dpn*I digested AtT20 cells transfected with EGFP-S/MAR plasmids 12 weeks post transfection with and without G418 selection pressure

Genomic DNA was extracted from AtT20 cells 48 hours (lanes 1 and 2) and 12 weeks (lanes 3-14) post transfection (PT) with (A) pEFS-EGFP (B) pCAG-EGFP and (C) pEPI-EGFP pDNA vectors. Long-term cells (at 12 wks PT) were maintained either with or without G418 selection pressure (+/-). Genomic DNA was digested with either *Mbo*I (lanes 1, 6-8, 12-14 in (A) and (B) or lanes 1, 4 and 6 in (C)) or *Dpn*I (lanes 2, 3-5, 9-11 in (A) and (B) or lanes 2, 3 and 5 in (C)) (M or D respectively) and assessed by PCR analysis using EFS-EGFP, CAG-EGFP or CMV-EGFP specific primer sets yielding a product size of 450 bp, 250 bp or 350bp for pEFS-EGFP, pCAG-EGFP or pEPI-EGFP plasmids respectively. PCR samples were separated by agarose gel electrophoresis and a positive PCR band was observed using the correct corresponding pDNA and primer set, yielding product sizes above. The arrowhead indicates the size 450 bp on (A), 250 bp on (B) and 350 bp on (C). For the PCR reaction, pDNA (25 ng) pEFS-EGFP, pCAG-EGFP or pEPI-EGFP (in the case of (A), (B) or (C) respectively) digested with *Mbo*I served as a positive control (lane 15 in (A) and (B) or lane 7 in (C)), while pDNA digested with *Dpn*I served as a negative control (lane 16 in (A) and (B) or lane 8 in (C)). Results are representative of four independent experiments. L= 100 bp ladder (Invitrogen).

176

3.1.12 Episomal maintenance of pEGFP-S/MAR vectors in AtT20 cells

To trace the presence and localisation of the EGFP pDNA vector series at the end of the experiment (12 weeks PT), plasmid rescue experiments were performed. As such *E.coli* bacterial cells were transformed with 1 μg of total DNA isolated from 1×10^6 cells at 12 weeks PT with either pEFS-EGFP, pCAG-EGFP or pEPI-EGFP plasmids. Kanamycin resistant bacterial colonies were obtained 24 hours after transformation at a rate of approximately 2-5 colonies per plate, irrespective of the plasmid DNA being analysed, which indicates a low copy number of all plasmids in AtT20 cells. This is in agreement with previous reports which indicate that S/MAR plasmids transfected in cells such as CHO-K1 or HeLa cells also have low plasmid copy numbers (Piechaczek, Fetzer et al. 1999; Schaarschmidt, Baltin et al. 2004). Plasmid DNA extracted from these clones were digested with various restriction enzymes and analyzed by gel electrophoresis.

Clones isolated from AtT20 cells transfected with pEFS-EGFP vector were analysed by digestion with *Xho*I and *BamHI* restriction enzyme. The digestion fragments from these clones where compared to the positive control of digested pEFS-EGFP plasmid, giving the fragments 5104 bp and 1080 bp when digested with *Xho*I and linearised plasmid of 6184 bp when digested with *BamHI*. Clones from the AtT20 pCAG-EGFP cells were analysed by *Nde*I and *Hind*III restriction analysis. The digestion fragments from these clones were also compared to the positive control of digested pCAG-EGFP plasmid, giving the fragments 3500 bp, 2410 bp and 1781 bp when digested with *Nde*I and giving the fragments 3142 bp and 4549 bp when digested with *Hind*III. Finally the colonies from the AtT20 pEPI-EGFP cells were digested with the *Afl*III and *Nde*I restriction enzymes. The digestion fragments from pDNA isolated from these clones were also compared to the positive control of digested pEPI-EGFP plasmid, giving the fragments 3700 bp and 3000 bp when digested with *Afl*III and 5100 bp and 1600 bp when digested with *Nde*I. The restriction digestion fragments observed from all three EGFP pDNA vectors (pEFS-EGFP, pCAG-EGFP and pEPI-EGFP) extracted from AtT20 cells is shown in Figure 43. The digested pDNA from 4 antibiotic resistant bacterial clones was identical to the restriction fragments observed in the corresponding original pDNA. This confirms the presence of an intact episomal pEFS-EGFP, pCAG-EGFP and pEPI-EGFP plasmid in the AtT20 cells.
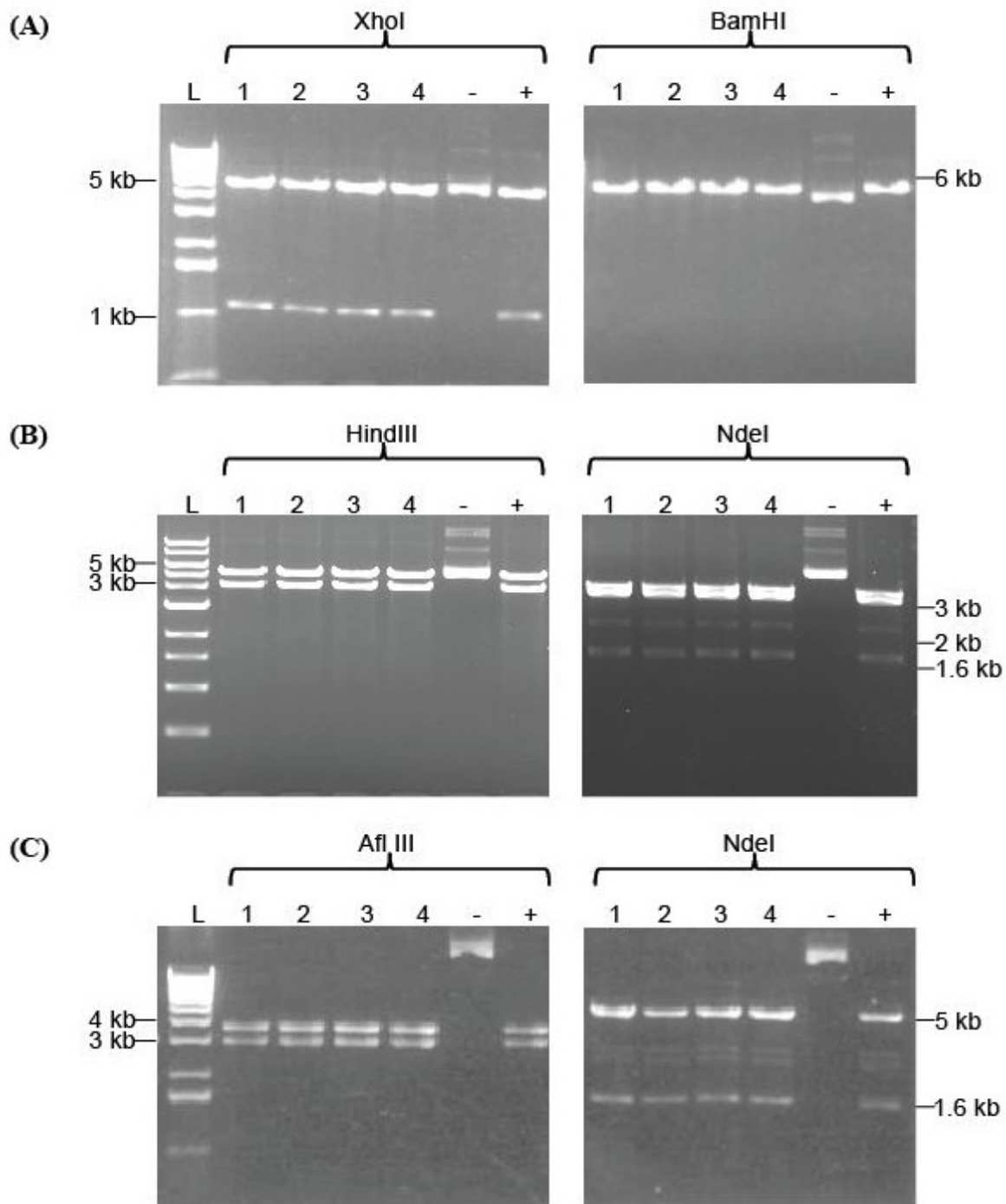
Figure 41: Plasmid rescue of pEFS-EGFP, pCAG-EGFP and pEPI-EGFP vectors isolated from AtT20 cells

Plasmid rescue analysis of pDNA isolated from 4 randomly chosen clones (lanes 1-4) after transformation of *E.coli* bacteria with 1 µg of total DNA isolated from AtT20 (A) pEFS-EGFP (B) pCAG-EGFP and (C) pEPI-EGFP stable cell lines, as described in the text. Undigested plasmid served as a negative control (lane 5; (-)), while all bands show identical sizes with the positive control of original pEFS-EGFP, pCAG-EGFP and pEPI-EGFP plasmids respectively (lane 6; (+)), demonstrating that pEFS-EGFP, pCAG-EGFP and pEPI-EGFP vectors are retained episomally in AtT20 cells. Results are representative of four independent experiments. L: 1 kb Ladder (Invitrogen).

The episomal state was further confirmed by Southern blot analysis. The highest expressing two clones from AtT20 pEFS-EGFP and pCAG-EGFP transfected cells and one clone from pEPI-EGFP at 12 weeks post transfection were isolated from 1×10^{6} cells for each clone as described in the methods, and subjected to Southern blot analysis. Total cellular DNA (10 µg) was isolated from each clone and digested with a single cutter to all plasmids *Stu*I restriction enzyme, which linearises all three plasmids pEFS-EGFP, pCAG-EGFP and pEPI-EGFP. Digested DNA was then analysed by Southern hybridisation with a ^{32}P-labelled *Alw*NI fragment - a 408 bp DNA fragment of a segment of the kanamycin region, which is common to all plasmids - as a probe. As shown in Figure 42 the hybridisation pattern clearly confirms the episomal state of all three plasmids, pEFS-EGFP, pCAG-EGFP pEPI-EGFP vectors. In all clones analysed, irrespective of whether the clones were maintained in G418 medium or not, a distinct band identical in size to the original pEFS-EGFP, pCAG-EGFP and pEPI-EGFP plasmids (+) is seen.
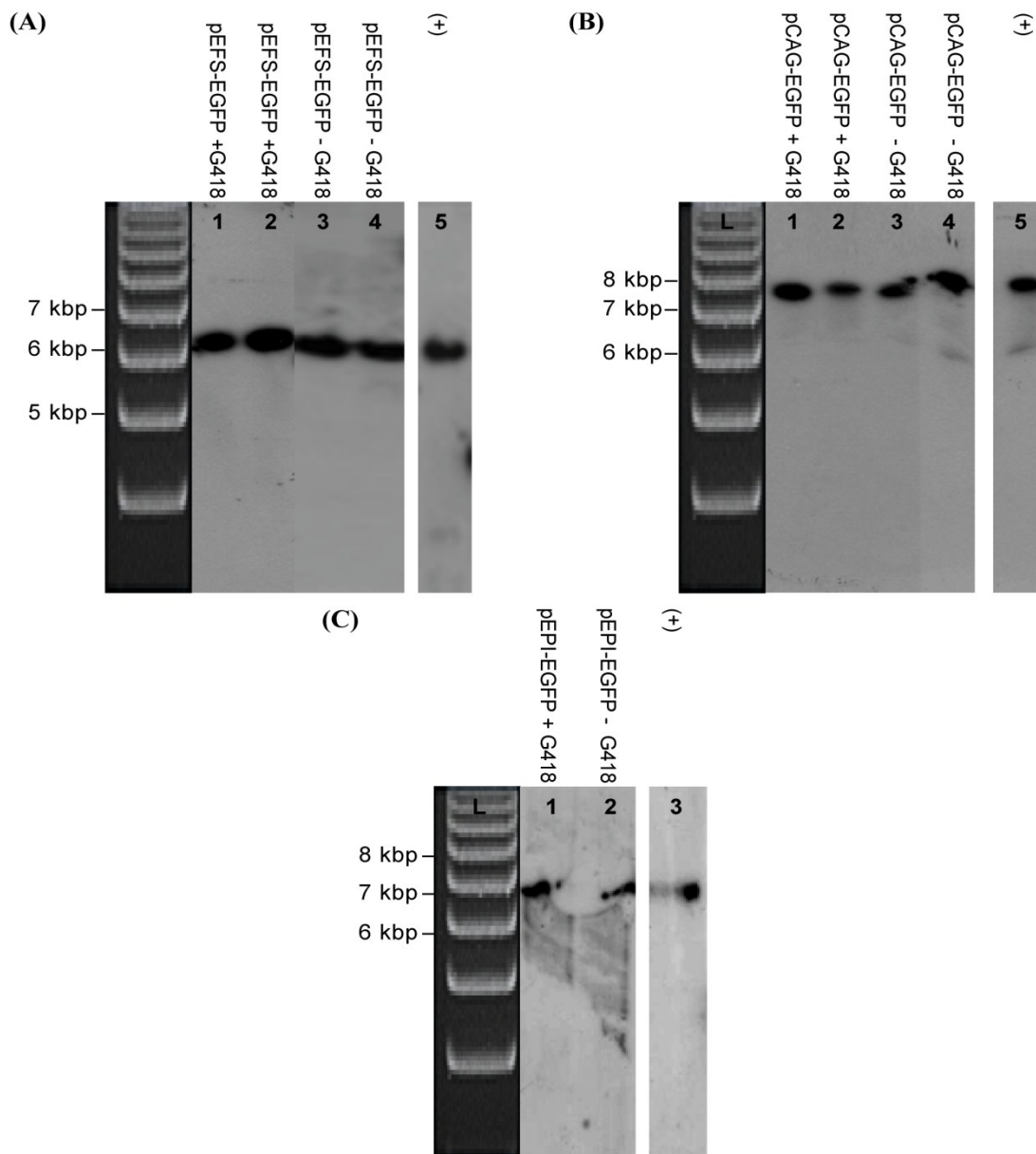
Figure 42: Southern blot analysis of the episomal status of pEFS-EGFP, pCAG-EGFP and pEPI-EGFP vectors isolated from AtT20 cells

Southern blots of total DNA isolated from two clones of AtT20 cells transfected with (A) pEFS-EGFP and (B) pCAG-EGFP and (C) pEPI-EGFP vectors and cultured for 12 weeks in medium with or without G418. DNA (10 µg) was separated on 0.8% agarose gels and hybridized with ^{32}P-labelled *Alw*NI probe. In (A) and (B) lanes 1-2, *Stu*I digested total DNA from AtT20 cells maintained in G418 medium, while lanes 3-4, the same clones digested with *Stu*I maintained in normal medium. In (C) lane 1, clone maintained in G418 medium, lane 2, the same clone maintained in normal medium. All clones produced a clear distinct band after *Stu*I digestion, identical to the band arising after digestion of 8 ng of corresponding positive control original pDNAs (pEFS-EGFP on (A); lane 5 (+), pCAG-EGFP on (B); lane 5 (+) or pEPI-EGFP on C; lane 3 (+)). Results are representative of three independent experiments. L: 1 Kb ladder (Invitrogen).

In conclusion, at the end of the *in vitro* analysis of pEFS-EGFP, pCAG-EGFP and pEPI-EGFP vectors, all vectors were able to maintain the active long-term expression of the *EGFP* transgene (and EGFP mRNA) located upstream of the S/MAR element in the absence of selection pressure in the AtT20 cell line, as demonstrated by FACS, PCR and rt-PCR analysis. Perhaps more importantly, all vectors were also able to be maintained as an active episome during the many cycles of replication and cell divisions, as shown by plasmid rescue and Southern blot analysis. These results are in agreement with previously published reports (Piechaczek, Fetzer et al. 1999; Schaarschmidt, Baltin et al. 2004; Papapetrou, Zoumbos et al. 2005).

3.2 Plasmid production and *in vitro* analysis of REP1 transgene

The ultimate goal of this project was the development of a unique non-viral plasmid vector suitable for the gene therapy of CHM. Similar to the cloning process of the *EGFP* transgene, our initial aims were to achieve this in a single cloning step; whereby the *REP-1* gene driven by the EF1-α promoter from the pWPI-REP-1 or the CAG promoter from the pCAGGs plasmid could be cloned into pEPI-MCS1. However, due to significant problems associated with the cloning, it was decided that the cloning process should be done in stages. Hence as with the *EGFP* transgene cloning process, two cloning strategies were employed for the pEFS-REP1 and pCAG-REP1 vector series.

3.2.1 Production of an expression plasmid with EFS alone – Plasmid pEOS-EFS-S/MAR

The initial cloning step involved the creation of a plasmid vector expressing only the EFS promoter. The cloning strategy is illustrated in Figure 43. Hence the 800 bp *EGFP* transgene from the pEFS-EGFP plasmid (see section 3.1.2 and Figure 24) was excised by *Mlu*I and *Sal*I restriction digestion. This was in preparation for cloning a plasmid with an EFS promoter and S/MAR sequence, to allow the insertion of REP1 cDNA downstream of the promoter. Digested vector was blunt ended and ligated overnight. The ligation mixture was transformed into JM109 competent cells. Out of the colonies obtained overnight, 3 were selected for plasmid isolation and screened for correct ligation in the 5' to 3' orientation, with the restoration of *Sal*I and *Mlu*I sites, as well as the analysis with *Xho*I restriction enzyme. Correctly ligated plasmids would produce two fragments of 268 bp and 5116 bp when digested with *Xho*I enzyme. Of the 3 clones, all clones gave the expected plasmid sizes (Figure 43D). This vector was named pEOS-EFS-S/MAR plasmid.
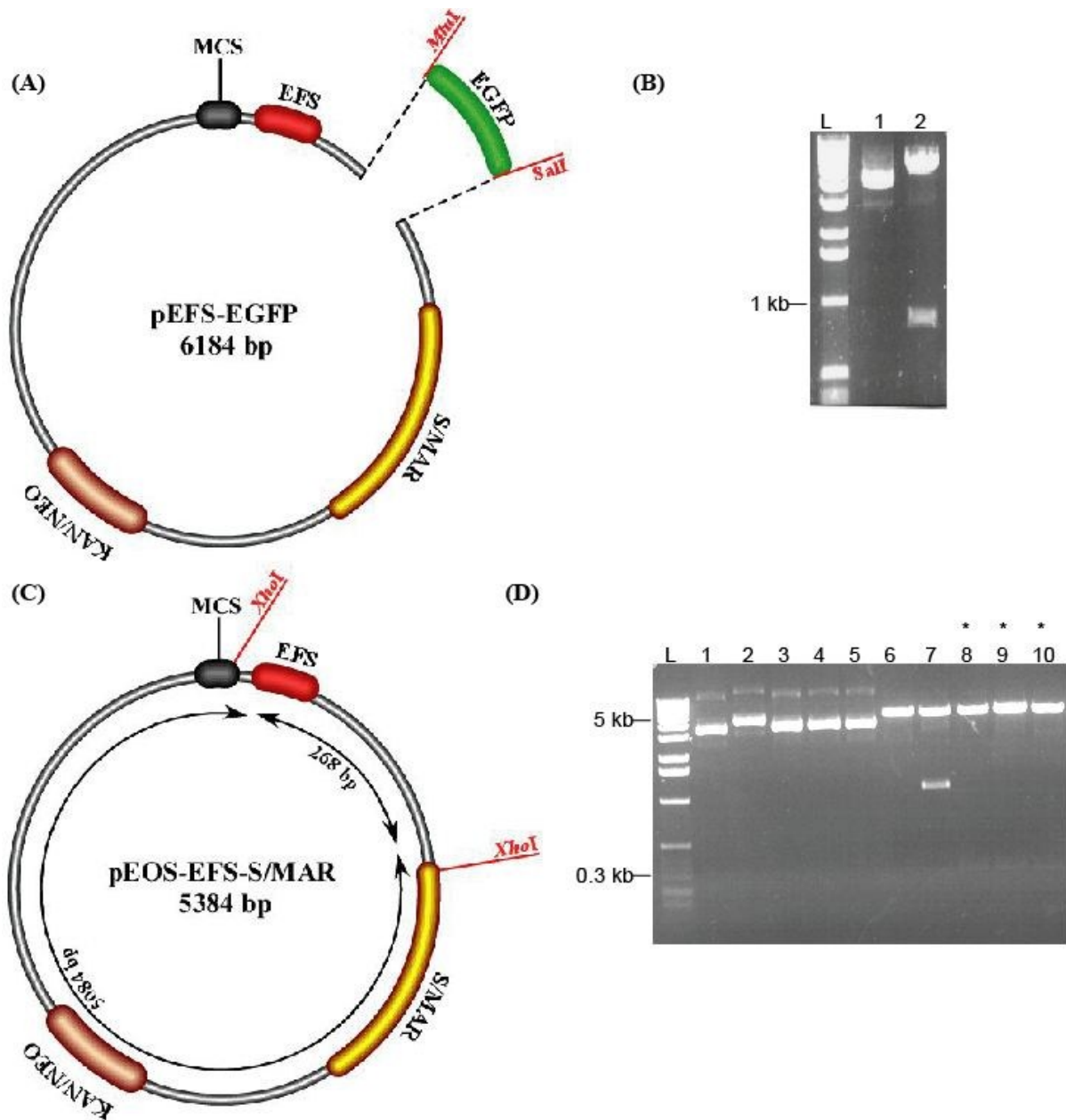
Figure 43: Generation of pEOS-EFS-S/MAR plasmid

The cloning strategy for the generation of pEOS-EFS-S/MAR plasmid involved the removal of the *EGFP* gene from the pEFS-EGFP plasmid as illustrated in (A). The correct fragment sizes of the digested pEFS-EGFP plasmid before ligation are shown in (B), where lanes 1 and 2: undigested and digested pEFS-EGFP vector respectively. Successful ligation would result in the pEOS-EFS-S/MAR plasmid as illustrated in (C). Finally (D) shows the restriction analysis of 3 clones picked after ligation and digested with *Xho*I (lanes 8-10) with all clones showing correct size of plasmid after digestion (*), indicating the successful removal of the *EGFP* transgene and development of pEOS-EFS-S/MAR. The 268 bp fragment from pEFS-EGFP-S/MAR is faint but seen clearer on the digital image. Lanes 1-5: undigested DNA, lane 6-10: *Xho*I digested DNA, lane 1 and 6: pEOS vector, lane 2 and 7: pEFS-EGFP-S/MAR, lane 3-5 & 8-10: colonies 1-3. L: 1 Kb ladder (Invitrogen).

3.2.2 Production of a REP-1 expressing plasmid driven by EFS – Plasmid pEFS-REP-1

The next step involved the insertion of REP1 cDNA into pEOS-EFS-S/MAR. The cloning strategy is illustrated in Figure 44. Initially both vector pEOS-EFS-S/MAR and insert pBC-REP1 (Stratagene) plasmids were digested with *Mlu*I and *Bam*HI. The excised 2 kb REP1 cDNA from pBC was ligated with digested vector overnight at a molar vector: insert ratio of 1:10. The ligation mixture was transformed into JM109 competent cells. Out of the colonies obtained overnight, 72 colonies were picked for PCR analysis using EFS and REP1 specific primers as described in the methods. Of the colonies picked for PCR analysis and that gave a positive signal on the PCR for the insertion and correct orientation of the insert, 5 clones were selected for plasmid isolation and analysis with *Xho*I and *Eco*RI restriction digestion analysis. Correctly ligated plasmids in the 5' to 3' orientation would produce 3 fragments 3600 bp, 2300 bp and 1600 bp. All 5 clones analysed gave the expected fragment patterns (Figure 44D). One colony was selected for isolation with a MaxiPrep kit, its quality and quantity was measured using a Nanodrop spectrophotometer. This vector was named pEFS-REP1 plasmid.
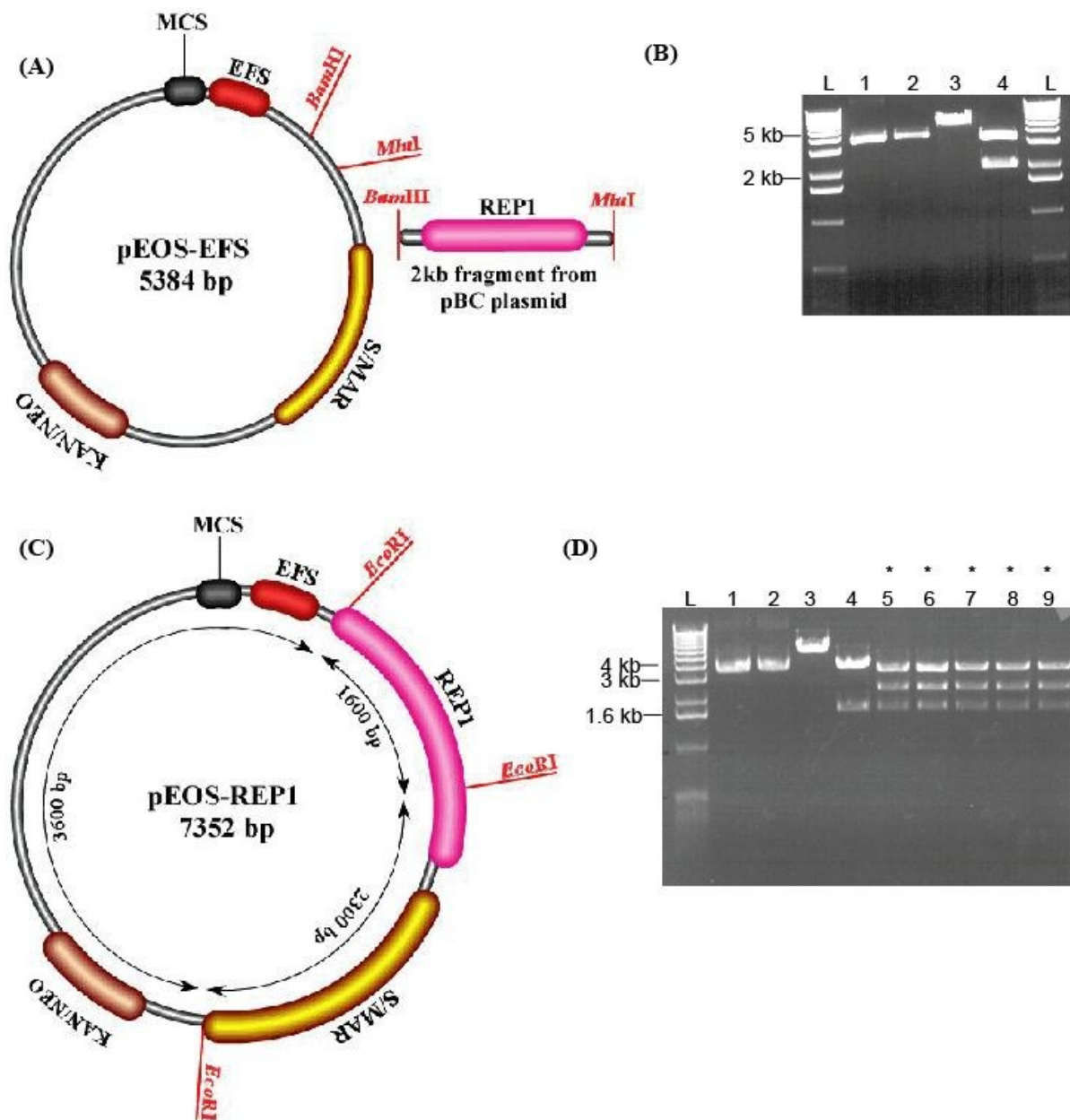
Figure 44: Generation of pEFS-REP1 plasmid

The cloning strategy for the generation of pEFS-REP1 plasmid involved the insertion of the REP1 cDNA from the pBC-REP1 plasmid is illustrated in (A). The correct fragment sizes of the digested pEOS-EFS-S/MAR and pBC-REP1 plasmids before ligation are shown in (B), where lanes 1 and 2: undigested pEOS-EFS-S/MAR and pBC-REP1 and lanes 3 and 4: digested pEOS-EFS-S/MAR and pBC-REP1 vectors respectively. Successful ligation would result in the pEFS-REP1 plasmid as illustrated in (C). Finally (D) shows the restriction analysis of 5 clones picked after ligation and digested with *Eco*RI (lanes 5-9) with all clones showing correct size of plasmid (*), indicating the successful insertion of the *REP1* transgene and development of pEFS-REP1. Lanes 1 and 2 show undigested pEOS-EFS-S/MAR and pBC-REP1 DNA, lane 3 and 4 show *Eco*RI digested pEOS-EFS-S/MAR and pBC-REP1, lane 5-9 show *Eco*RI digested colonies 1-5. L: 1 Kb ladder (Invitrogen).

3.2.3 Production of EFS control counterpart - Plasmid pEFS-REP1-Control

The final step in the pEFS-REP1 vector series involved the development of the control counterpart to the pEFS-REP1 plasmid. The cloning strategy is illustrated in Figure 45. In preparation for the removal of the 2 kb S/MAR element, pEFS-REP1 plasmid was digested with *Hpa*I and *Bgl*I. This excised the 2 kb S/MAR fragment from the pEFS-REP1 plasmid and the linearised vector was ligated overnight. The ligation mixture was transformed into JM109 competent cells. Out of the colonies obtained overnight, 4 clones were selected for plasmid isolation and analysis with *Stu*I restriction enzyme. Correctly ligated plasmids would give a linearised vector that would produce a fragment 5352 bp. All of the clones gave the expected plasmid sizes (Figure 45D). One colony was selected for isolation with a MaxiPrep kit, its quality and quantity was measured using a Nanodrop spectrophotometer. As the newly constructed plasmid did not harbour an S/MAR element, the plasmid was named pEFS-REP1-Control plasmid.
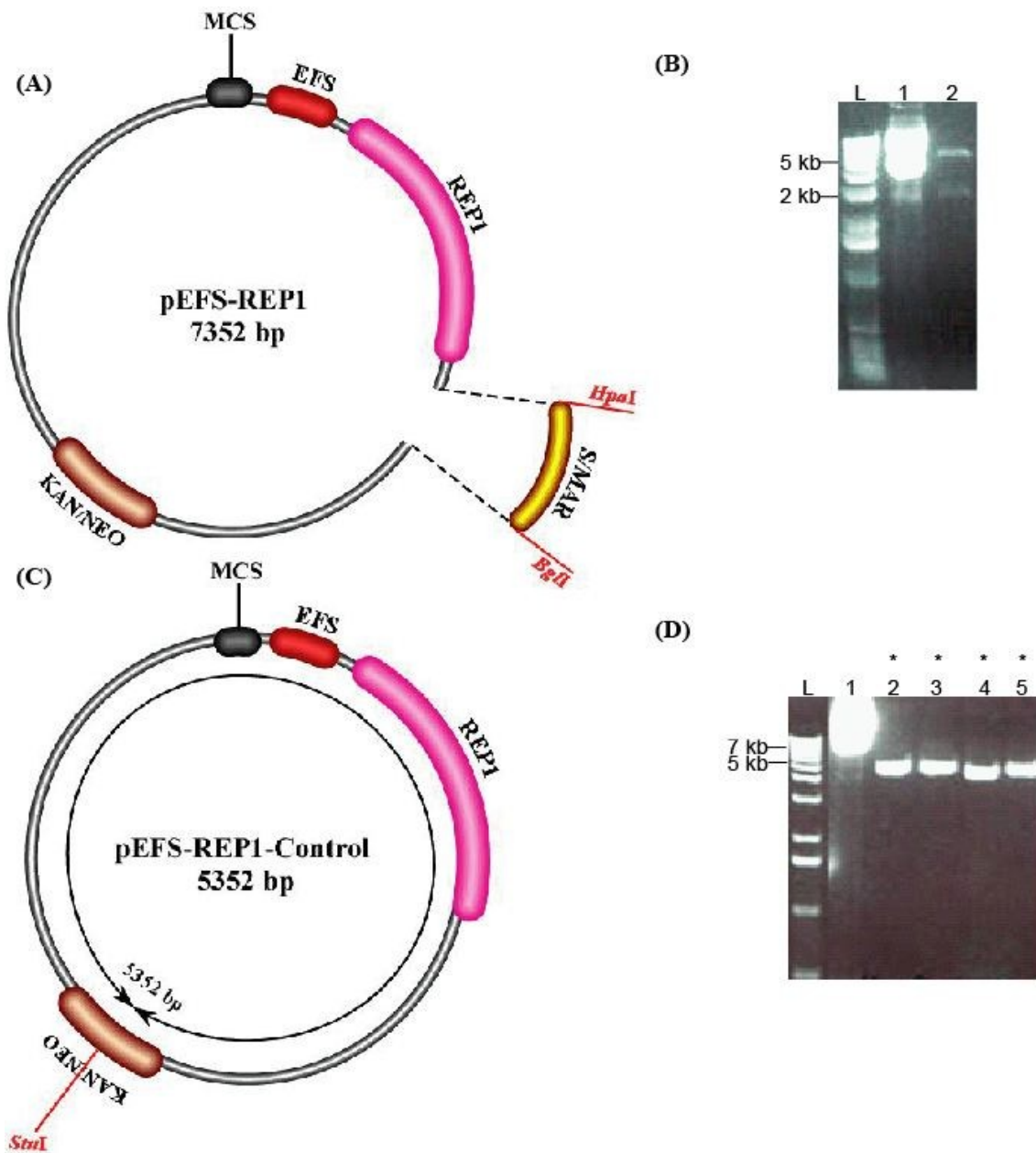
Figure 45: Generation of pEFS-REP1-Control plasmid

The cloning strategy for the generation of pEFS-REP1-Control plasmid involved the removal of the 2 kb S/MAR motif from the pEFS-REP1 plasmid as illustrated in (A). The correct fragment sizes of the digested pEFS-REP1 plasmid before ligation are shown in (B), where lanes 1 and 2: undigested and digested pEFS-REP1 vector respectively. The 2 kb fragment from pEFS-REP1 is faint but seen clearer on the digital image. Successful ligation would result in the pEFS-REP1-Control plasmid as illustrated in (C). Finally (D) shows the restriction analysis of 4 clones picked after ligation (lanes 2-5) with all clones showing correct size of plasmid (*), indicating the successful S/MAR excision and development of pEFS-REP1-Control. Lane 1 represents undigested pEFS-REP1 vector. L: 1 Kb ladder (Invitrogen).

3.2.4 Production of Plasmid pCAG-REP1

The next stage involved the development of the pCAG-REP1 vector series. The vector created previously pEOS-CAG-MCS-S/MAR plasmid (see section 3.1.5) was used to insert the REP1 cDNA from the pEFS-REP1 plasmid downstream of the CAG promoter. The cloning strategy is illustrated in Figure 46. Both pEOS-CAG-MCS-S/MAR and pEFS-REP1 plasmids were digested with *Bam*HI and *Mlu*I, resulting in the removal of the 2 kb REP1 cDNA fragment from the pEFS-REP1 plasmid. Digested vector and insert were ligated overnight at a molar vector: insert ratio of 1:10. The ligation mixture was then transformed into JM109 competent cells. Out of the colonies obtained overnight, 72 colonies were picked for PCR analysis using CAG and REP1 specific primers as described in the methods. Of the colonies picked for PCR analysis and that gave a positive signal on the PCR for the insertion and correct orientation of the insert, 5 clones were selected for plasmid isolation and analysis with *Xho*I and *Not*I, *Bam*HI and *Eco*RV or *Eco*RV (alone) restriction enzymes. Correctly ligated plasmids in the 5' to 3' orientation would produce 2 fragments at 2110 bp and 6720 bp when digested with *Eco*RV restriction enzyme. Of the 5 colonies analysed, 4 clones gave the expected fragment patterns (Figure 46D). One colony was selected for isolation with a MaxiPrep kit, its quality and quantity was measured using a Nanodrop spectrophotometer. This vector was named pCAG-REP1 plasmid.
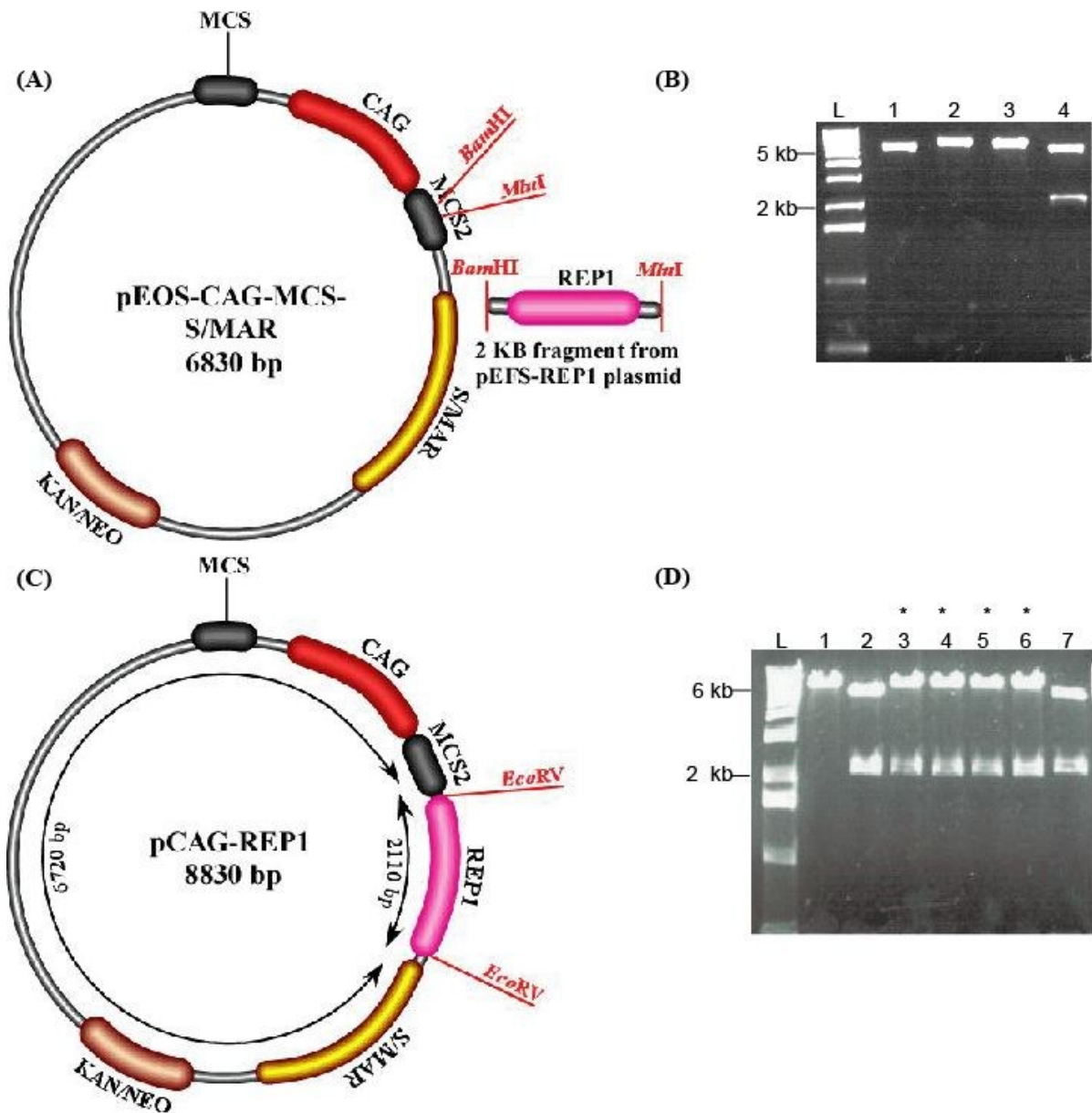
Figure 46: Generation of pCAG-REP1 plasmid

The cloning strategy for the generation of pCAG-REP1 plasmid involved the insertion of the 2 kb REP1 cDNA fragment as illustrated in (A). The correct fragment sizes of the digested pEFS-REP1 and pEOS-CAG-MCS-S/MAR vectors before ligation are shown in (B), where lanes 1 and 2: undigested pEOS-CAG-MCS-S/MAR and pEFS-REP1, while lanes 3 and 4: digested pEOS-CAG-MCS-S/MAR and pEFS-REP1 vector respectively. Successful ligation would result in the pCAG-REP1 plasmid as illustrated in (C). Finally (D) shows the restriction analysis of 5 clones picked after ligation (lanes 3-7) with clones 1-4 showing the correct size of plasmid (*), indicating the successful *REP1* transgene insertion and development of pCAG-REP1. Lanes 1 and 2 represent digested pEOS-CAG-MCS-S/MAR and pEFS-REP1 vectors respectively. L: 1 Kb ladder (Invitrogen).

3.2.5 Production of CAG control counterpart - Plasmid pCAG-REP1-Control

The final step in the pCAG-REP1 vector series involved the development of the control counterpart to the pCAG-REP1 plasmid. The cloning strategy is illustrated in Figure 47. In preparation for the removal of the 2 kb S/MAR element, pCAG-REP plasmid was digested with *Not*I and *Dra*III restriction enzymes. This excised the 2 kb S/MAR fragment from the pCAG-REP1 plasmid and the linearised vector was ligated overnight. The ligation mixture was transformed into JM109 competent cells. Out of the colonies obtained overnight, 8 were selected for plasmid isolation and analysis with *Stu*I restriction enzyme. Correctly ligated plasmids would give a linearised vector that would produce a fragment at 6830 bp. Of the 8 clones, 1 gave the expected plasmid sizes (Figure 47D). One colony was selected for isolation with a MaxiPrep kit, its quality and quantity was measured using a Nanodrop spectrophotometer. As the newly constructed plasmid did not harbour an S/MAR element, the vector was named pCAG-REP1-Control plasmid.
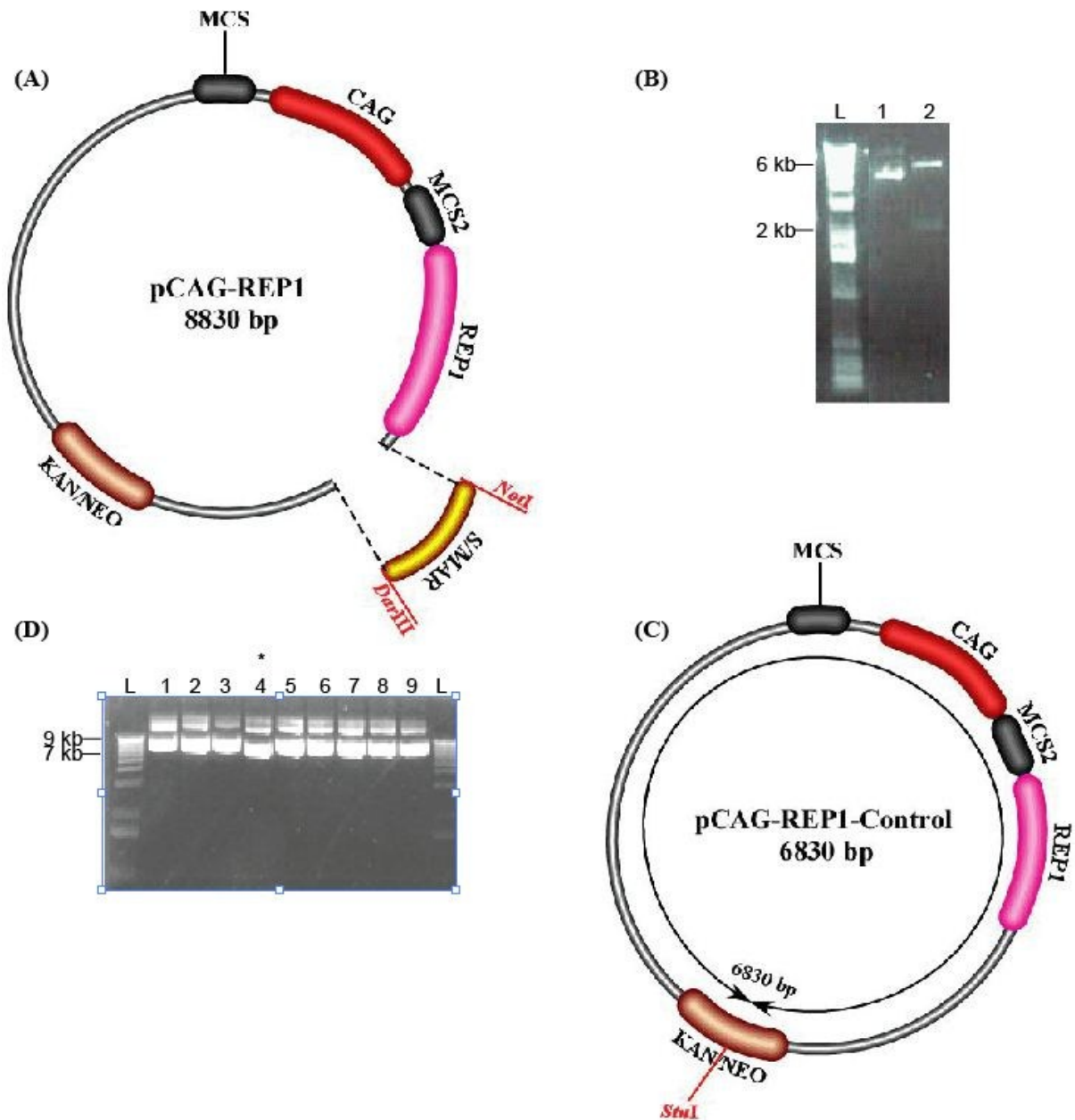
Figure 47: Generation of pCAG-REP1-Control plasmid

The cloning strategy for the generation of pCAG-REP1-Control plasmid involved the removal of the 2 kb S/MAR motif from the pCAG-REP1 plasmid as illustrated in (A). The correct fragment sizes of the digested pCAG-REP1 plasmid before ligation are shown in (B), where lanes 1 and 2: undigested and digested pCAG-REP1 vector respectively. The 2 kb fragment from pCAG-REP1 is faint but seen clearer on the digital image. Successful ligation would result in the pCAG-REP1-Control plasmid as illustrated in (C). Finally (D) shows the restriction analysis of 8 clones picked after ligation (lanes 2-9) with 1 clone showing the correct size of plasmid (*), indicating the successful S/MAR excision and development of pCAG-REP1-Control. Lanes 1 undigested pCAG-REP1 vector. L: 1 Kb ladder (Invitrogen).

3.2.6   Transient transfection of AtT20 cells with pREP1-S/MAR plasmids

To analyse the new REP1 vectors pEFS-REP1 and pCAG-REP1 as well as their control counterparts without S/MARs, plasmids were separately transfected with Lipofectamine 2000 into AtT20 cells (0.8 µg of each pDNA). This experiment aimed to confirm the expression of the *REP1* transgene, in a similar strategy used for the analysis of the *EGFP* transgene from the pEFS-EGFP and pCAG-EGFP as well as the control plasmids.

At 48 hours following transfection, cell pellets were collected for REP1 protein expression by Western blot analysis. Briefly, cells were lysed and protein lysates (50 µg) were separated on a 7% SDS-polyacrylamide gel and blots were probed with anti-mouse REP1 antibody 2F1 (Santa Cruz Technology, Santa Cruz, California) which recognises human Rep1 protein. Strong *REP1* expression levels were observed in AtT20 cells 48 hours post transfection from all constructs as shown in Figure 48.
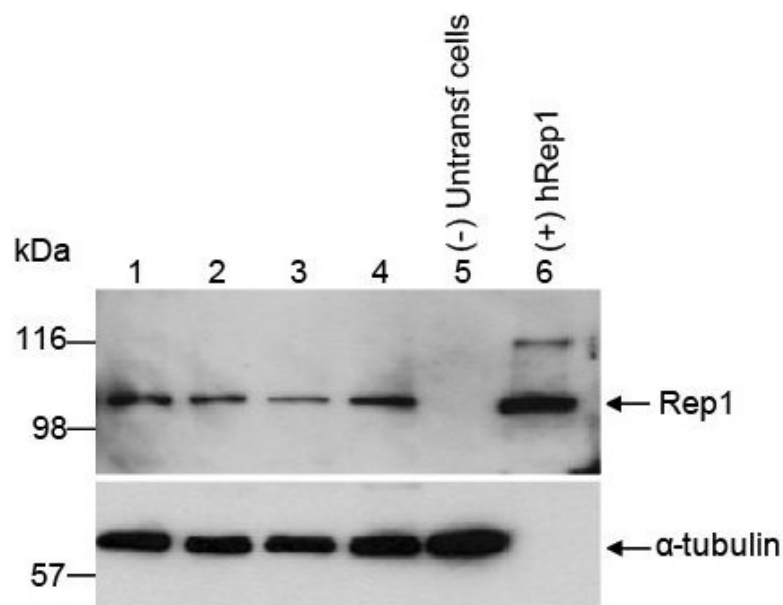
Figure 48:   Western blot analysis of REP1 protein expression levels in AtT20 cells 48 hours post transfection

The figure shows expression of REP1 protein levels by Western analysis of AtT20 cell pellets (50 µg) 48 hours post-transfection using anti-mouse REP1 antibody 2F1 which recognises human Rep1 protein. Cells were transfected with plasmids pEFS-REP1, pEFS-REP1-Control, pCAG-REP1 and pCAG-REP1-Control pDNA vectors (lanes 1-4 respectively), where all plasmids show expression of REP1 protein. Untransfected cells served as negative control (lane 5; (-)), human Rep1 protein (hREP1) served as a positive control (lane 6; (+)) and α-tubulin was used as a loading control. Results are representative of three independent experiments.

Expression of *REP1* transgene was further confirmed in these cells by immunofluorescence analysis of fixed AtT20 cells. Briefly, 48 hours following transfection, AtT20 cells were rinsed in phosphate buffered saline (PBS), fixed in 4% paraformaldehyde (PFA) before being incubated with the REP1 antibody 2F1. As shown in Figure 49, immunofluorescent analysis of transfected cells shows both pEFS-REP1 and pEFS-REP1-Control plasmids mediate moderate levels of REP1 protein, while pCAG-REP1 and pCAG-REP1-Control plasmids were able to mediate higher REP1 levels.
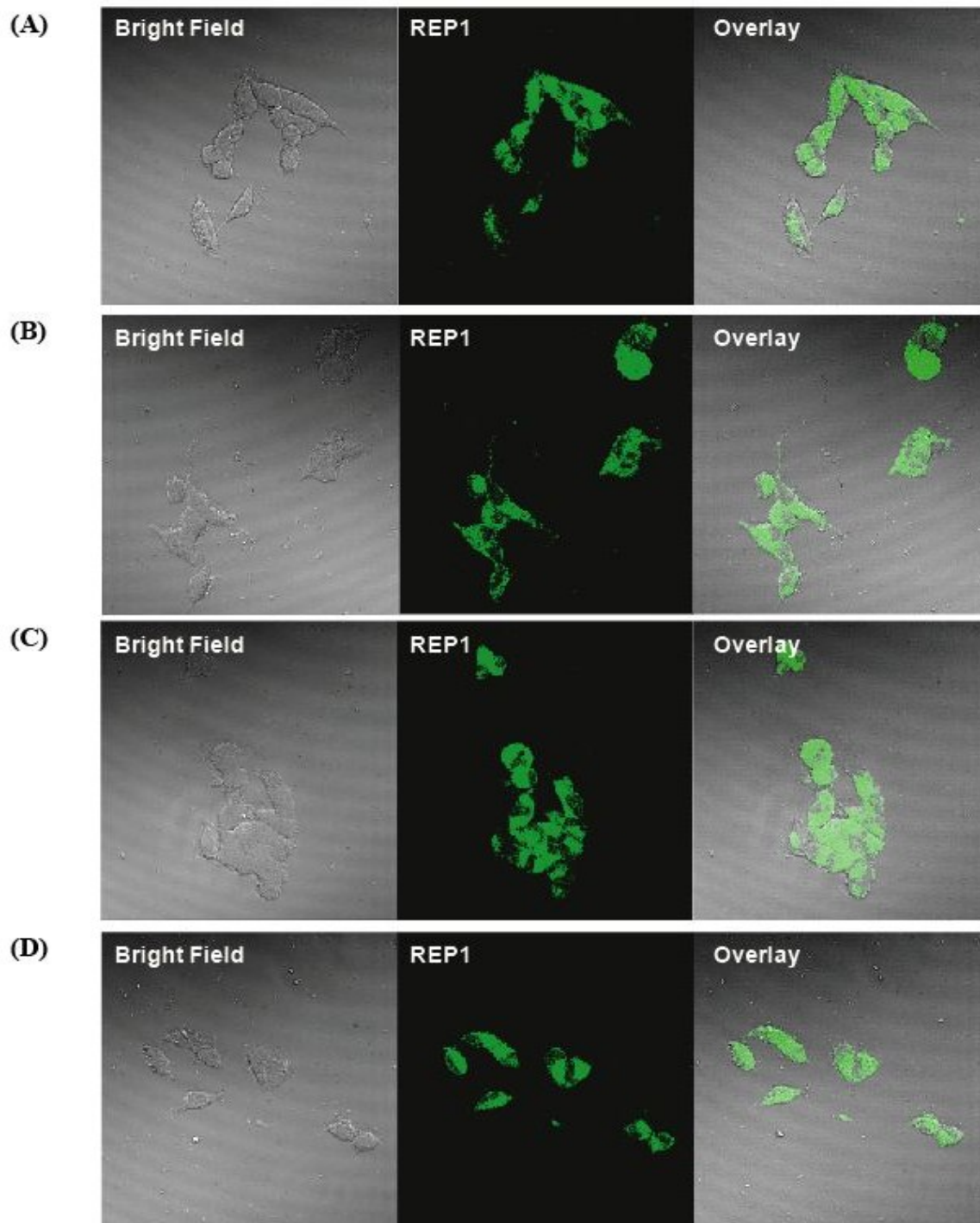
Figure 49: Expression of REP1 in AtT20 cells as analysed by immunofluorescence analysis of REP1 protein levels 48 hours post transfection

AtT20 cells were transfected with plasmids (A) pEFS-REP1, (B) pEFS-REP1-Control, (C) pCAG-REP1 or (D) pCAG-REP1-Control. Expression of REP1 was observed within the cells at 48 hours post transfection by incubating with mouse anti-2F1 antibody (which recognises human REP1 protein) followed by anti-mouse 488 conjugated secondary antibody. Representative images are shown with all four plasmids where bright field (*left panel*), fluorescent (*middle*) and their merge images (*right*), at 40x magnification are shown. Images are representative of three independent experiments.

3.2.7　Transient REP1 transfection in RPE cells *in situ*

To provide proof of principle testing of pEFS-REP1 and pCAG-REP1 plasmid constructs,
primary RPE cells were also isolated from mouse and porcine eyes, and transfected with
Lipofectin reagent (Invitrogen). This was done in order to assess the ability of REP1 plasmids
to express in cells more relevant to the eye (compared to AtT20 and B16-F10 cells) as well as
to transfect cells closely resembling those found *in vivo* in the eye. Briefly, RPE cells were
transfected with 1 μg of pEFS-REP1 or pCAG-REP1 plasmid complexed with 6 μl of Lipofectin
reagent in serum free medium overnight. One day post transfection, cells were rinsed with
PBS and fixed in 4% PFA before being incubated with a REP1 antibody (2F1) which
specifically recognizes human REP1 protein. Similar to the EGFP observations described in
the earlier section 3.1.9, the efficiency of gene transfer in RPE cells with both REP1 plasmids
was low. Despite this, were gene transfer was observed, both constructs were able to
provide strong levels of REP1 expression in isolated RPE cells. Representative
immunofluorescence pictures of pEFS-REP1 and pCAG-REP1 transduced RPE cells are shown
in Figure 50.
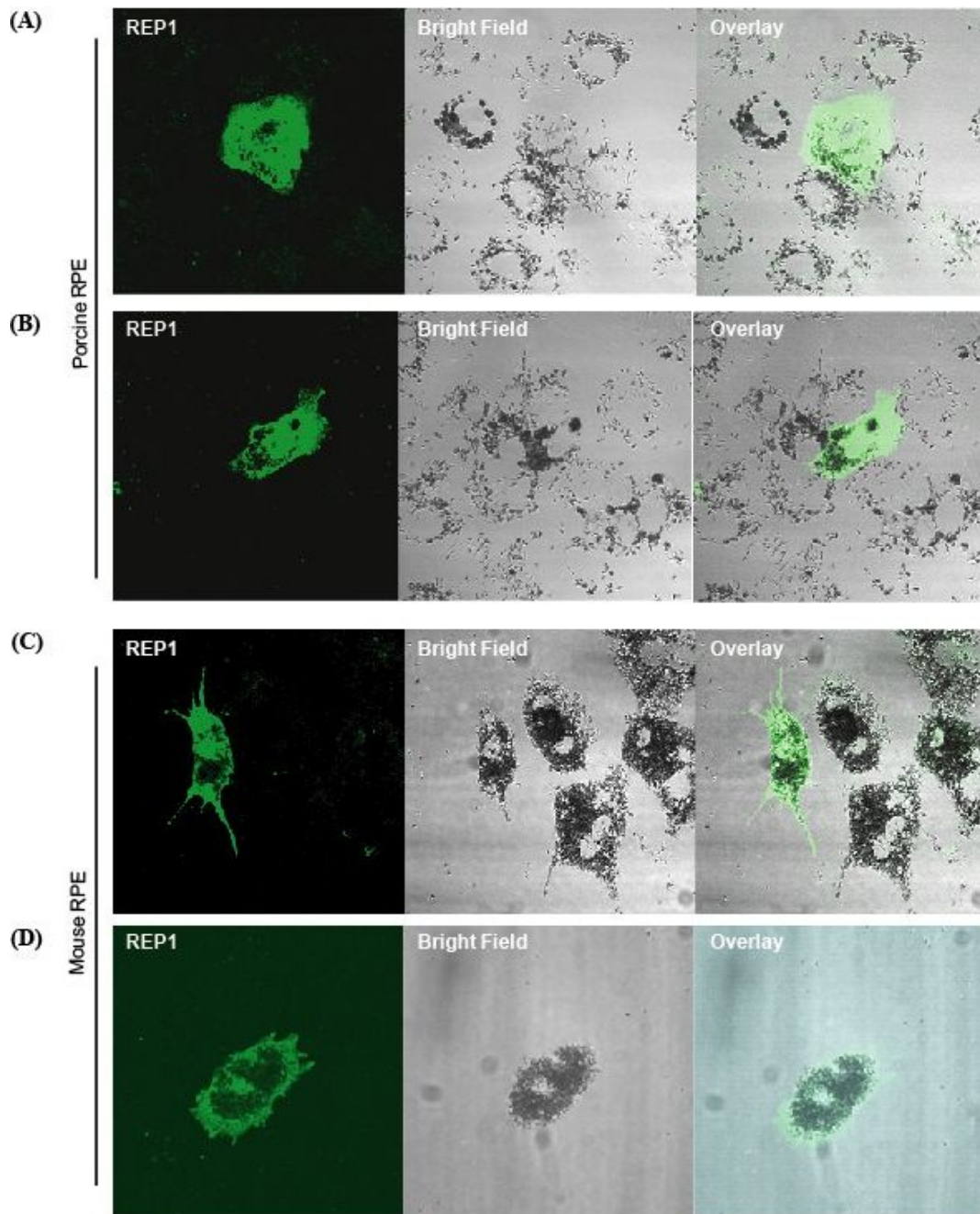
Figure 50: Expression of pEFS-REP1 and pCAG-REP1 following transfection of primary RPE cells – in situ

Primary RPE cells were isolated from mouse and porcine eyes, plated onto 24-well plates and transfected with 1 μg of plasmid pEFS-REP1 or pCAG-REP1 and 6 μl Lipofectin transfection reagent. Twenty four hours post transfection to detect REP1 expression, cells were incubated with mouse anti-2F1 antibody (which recognising human REP1 protein) followed by anti-mouse 488 conjugated secondary antibody. Representative images are shown with plasmids pCAG-REP1 (A & C) and pEFS-REP1 (B & D). Fluorescent (*left panel*), bright field (*middle*) and their merge images (*right*), at 40x magnification are shown. Panels A & B represent porcine primary RPE cells, while panels C & D represent mouse primary RPE cells. Images are representative of two independent experiments.

3.2.8 Long-term REP1 expression in AtT20 cells

AtT20 cells were also used for the long-term analysis of REP1 expression level from all constructs. Utilising a similar approach to that performed for the new EGFP pDNA vector series, AtT20 cells were transfected with plasmids pEFS-REP1, pCAG-REP1 or the corresponding control plasmids, G418 selection was applied 48 hours post transfection, and isolated clones were maintained in selection for up to 2 weeks, at which time cells were split into medium with or without G418. At regular time intervals, stable AtT20 cells transfected with either REP1 plasmids (pEFS-REP1, pCAG-REP1), were collected for Western blot analysis to observe the expression of REP1 protein in the isolated cells. Three colonies were picked for the stable and long-term REP1 expression analysis, where colonies were maintained in normal or G418 medium (Figure 51).

Similar to the EGFP pDNA vector series, both pEFS-REP1 and pCAG-REP1 plasmids were able to maintain stable REP1 protein expression in all colonies analysed. Noteworthy was the fact that by 12 weeks post transfection, the Western blot analysis of AtT20 cells transfected with control non-S/MAR plasmids (pEFS-REP1-Control and pCAG-REP1-Control) could not be performed because there were insufficient cells to collect for analysis. This was most likely due to the fact that cells transfected with either of the control plasmids did not survive the long selection process with the presence of G418 in the culture medium, showing that only transient antibiotic resistance was initially observed, however this was not maintained persistently.
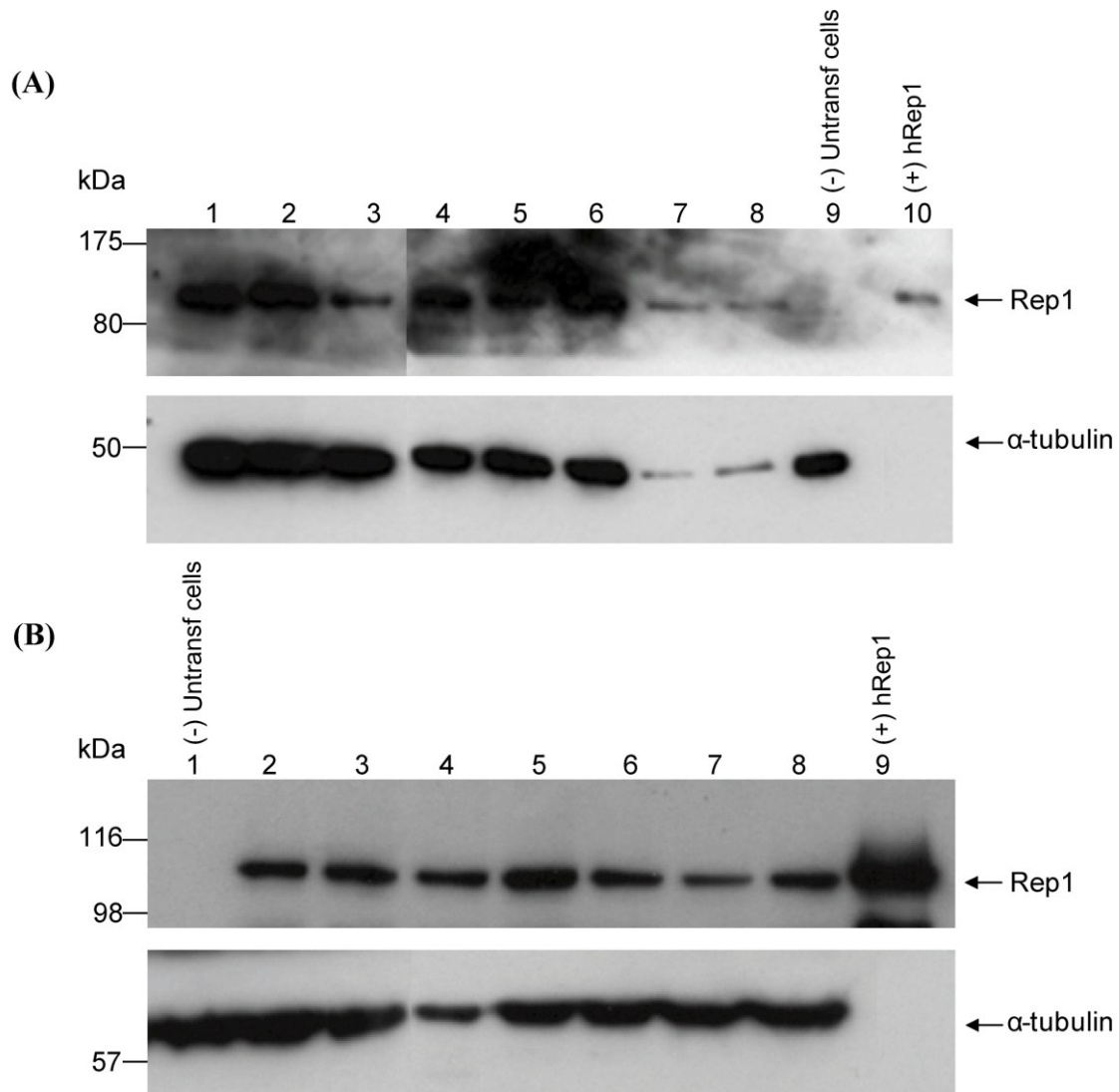
Figure 51: Western blot analysis of REP1 protein expression levels over time in three stable AtT20 cells transfected with pEFS-REP1 and pCAG-Rep1 plasmid vectors

AtT20 cells transfected with either (A) pEFS-REP1 or (B) pCAG-REP1 plasmids show good transfection efficiency 48 hours after transfection. G418 selection pressure was applied for a period of two weeks at which point three colonies (clones 1-3) for each plasmid were picked and split into medium with and without G418 antibiotic (+ G418 and – G418 respectively). Cells were analysed for REP1 expression at regular time intervals post transfection (PT) (50 µg).

On (A) lane 1: 48 hours transient transfection; lane 2 and 3: clone 1 at 12 weeks PT + and – G418 respectively; lane 4, 5 and 6: clone 2 at 4 weeks, and 12 weeks PT + and – G418 respectively; lane 7 and 8: clone 3 at 12 weeks PT + and – G418 respectively.

On (B) lanes 2, 3-4, 5-6 and 7-8: 48 hours transient transfection and clones 1-3 at 12 weeks PT + and – G418 respectively.

Untransfected cells served as a negative control (-), human Rep1 protein (hREP1) served as a positive control (+) and α-tubulin was used as a loading control. Control plasmids without the S/MAR were not able to survive the selection process. Results are representative of three independent experiments.

Total DNA was also isolated from AtT20 cells at 48 hours and 12 weeks post transfection with either pEFS-REP1 or pCAG-REP1 vectors without G418 selection pressure and analysed for the PCR detection of the appropriate vector (Figure 52). As seen with the EGFP pDNA vectors, PCR analysis revealed the persistence of pEFS-REP1 and pCAG-REP1 pDNA in transfected AtT20 cells for up to 12 weeks post transfection, confirming the similar long-term REP1 protein expression levels also observed in the stably transfected AtT20 cells.

To further verify the Western blot and PCR analysis results, REP1 RNA was also analysed in transient and long-term pEFS-REP1 or pCAG-REP1 transfected AtT20 cells by rt-PCR analysis (Figure 53). Indeed REP1 mRNA transcript was observed in AtT20 cells for up to 12 weeks post transfection, regardless of pDNA (pEFS-REP1 or pCAG-REP1 vectors). Noteworthy is the fact that pDNA levels as well as REP1 mRNA were observed in AtT20 cells maintained in normal medium lacking G418 selection (although an initial selection process of two weeks was required and standard practice).
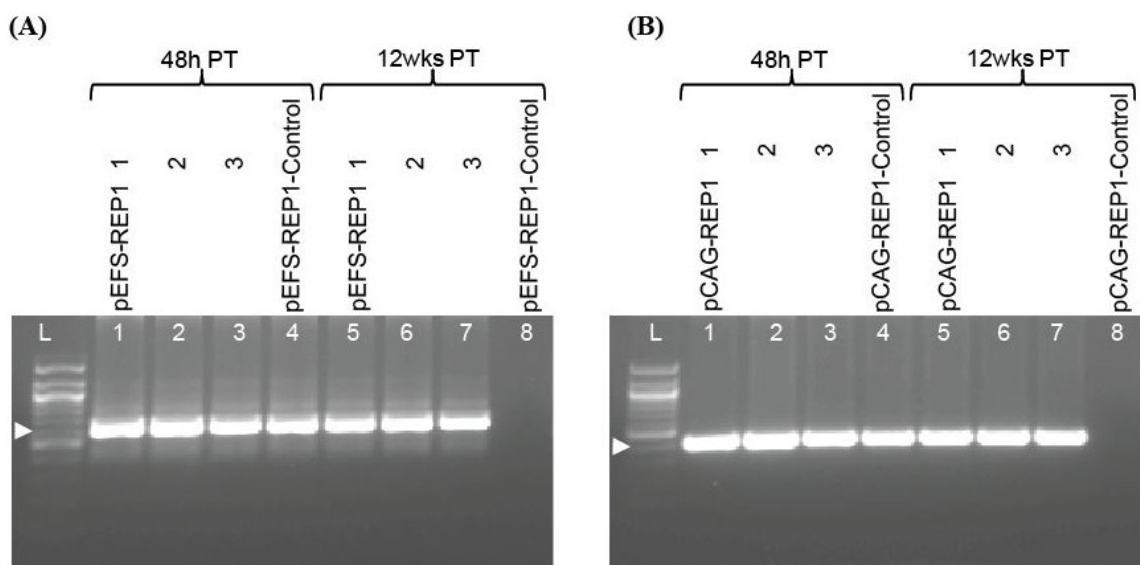
Figure 52: PCR detection of pDNA in AtT20 cells extracted short-term and long-term post transfection without G418 selection pressure

PCR analysis of (A) pEFS-REP1 and pEFS-REP1-Control and (B) pCAG-REP1 and pCAG-REP1-Control pDNA vectors at 48 hours (lanes 1-4) and 12 weeks (lanes 5-8) following transfection. PCR samples were separated by agarose gel electrophoresis and a positive PCR band was observed using EFS-REP1 or CAG-REP1 specific primer sets yielding product sizes 590 bp and 430 bp respectively. The arrowhead indicates the size corresponding to pDNA 590 bp on (A) or 430 bp on (B). Results are representative of three independent experiments. L= 100bp ladder (Invitrogen).
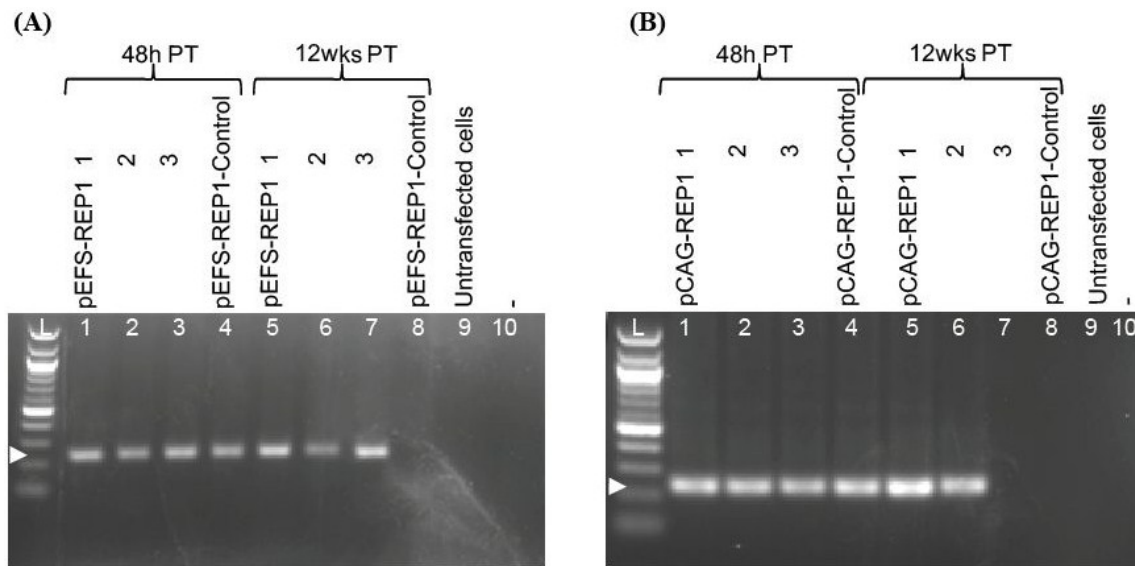
Figure 53: RT-PCR analysis of REP1 mRNA from AtT20 cells transfected with REP1-S/MAR plasmids at 48 hours and 12 weeks post transfection without G418 selection pressure

Total RNA was extracted from AtT20 cells transfected with (A) pEFS-REP1 and pEFS-REP1-Control and (B) pCAG-REP1 and pCAG-REP1-Control pDNA vectors at 48 hours (lanes 1-4) and 12 weeks (lanes 5-8) post transfection, without G418 selection pressure. Total RNA was isolated and used to generate cDNA. PCR was performed with two REP1 specific primers to yield a product size of 240 bp, as indicated by the arrowhead on (A) and (B). Untransfected cells as well as no RNA product/water served as a negative control (lanes 9 and 10). Results are representative of three independent experiments. L= 100bp ladder (Invitrogen).

3.2.9   Replication analysis of pREP1-S/MAR vectors in AtT20 cells

Experiments to confirm that the plasmids pEFS-REP1 and pCAG-REP1 were able to replicate in AtT20 cells, were similar to the experiments performed for the pEGFP-S/MAR vectors. Cellular pDNA was isolated from AtT20 cells at 12 weeks post transfection of both plasmids where cells were maintained either in G418 medium or normal medium without antibiotic. Plasmid DNAs were then digested with enzymes *DpnI* and *MboI* and analysed by PCR analysis for the presence or absence of a PCR band when amplified using plasmid specific primers. Figure 54 shows representative PCR results demonstrating that both REP1 plasmids pEFS-REP1 and pCAG-REP1 were able to replicate in AtT20 cells after 12 weeks post transfection, shifting from pDNA of bacterial origin to producing the restriction digestion pattern of pDNA of mammalian origin.
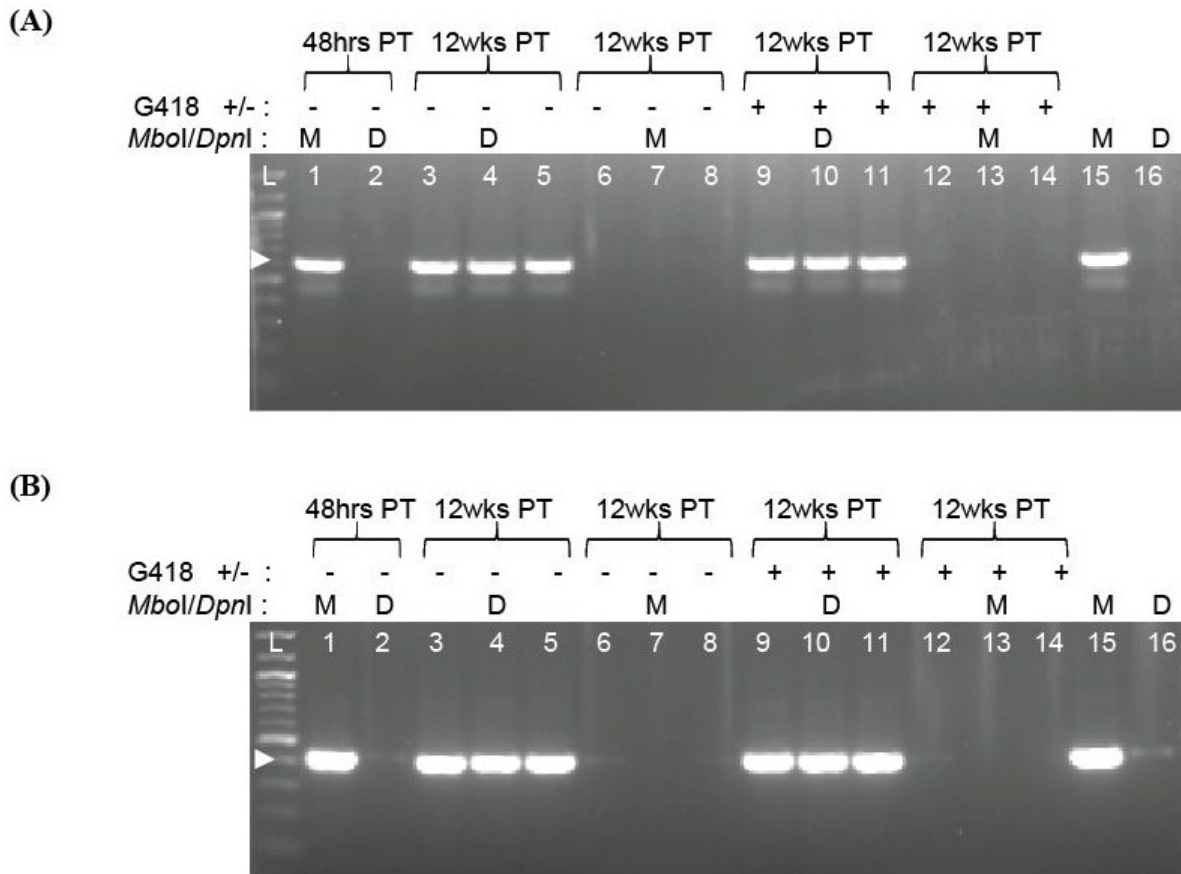
Figure 54: **Long-term PCR analysis of *Mbo*I and *Dpn*I digested AtT20 cells transfected with REP1-S/MAR plasmids at 12 weeks post transfection with and without G418 selection pressure**

Genomic DNA was extracted from AtT20 cells 48 hours (lanes 1 and 2) and 12 weeks (lanes 3-14) post transfection (PT) with (A) pEFS-REP1 and pEFS-EGFP-Control and (B) pCAG-REP1 and pCAG-EGFP-Control pDNA vectors. Long-term cells (at 12 wks PT) were maintained either with or without G418 selection pressure (+/-). Genomic DNA was digested with either *Mbo*I (lanes 1, 6-8, 12-14) or *Dpn*I (lanes 2, 3-5, 9-11) (M or D respectively) and assessed by PCR analysis using EFS-REP1 or CAG-REP1 specific primer sets yielding a product size of 650 bp and 430 bp for pEFS-REP1 or pCAG-REP1 plasmids respectively. PCR samples were separated by agarose gel electrophoresis and a positive PCR band was observed using the correct corresponding pDNA and primer set, yielding product sizes above. The arrowhead indicates the size 650 bp on (A) and 430 bp on (B). For the PCR reaction, pDNA (25 ng) pEFS-REP1 (in the case of (A)) or pCAG-REP1 (in the case of (B)) digested with *Mbo*I served as a positive control (lane 15), while pDNA digested with *Dpn*I served as a negative control (lane 16). Results are representative of four independent experiments. L= 100 bp ladder (Invitrogen).

3.2.10 Episomal maintenance of pREP1-S/MAR vectors in AtT20 cells

To trace pEFS-REP1 and pCAG-REP1 at 12 weeks post transfection, different AtT20 clones were selected and the total DNA was isolated from 1×10^6 cells for each clone as described in the methods. These were then subjected to Southern blot analysis to determine the episomal state of pEFS-REP1 and pCAG-REP1 AtT20 clones. To ensure that the selection pressure applied to AtT20 pEFS-REP1 and pCAG-REP1 clones had not forced the pDNAs to integrate into the genomic DNA, total cellular DNA was isolated from two of the strongest expressing clones that were either maintained in normal or G418 medium. As with the analysis of the EGFP pDNA vectors, DNAs were then digested with *Stu*I enzyme. Linearized pEFS-REP1 and pCAG-REP1 plasmids were subsequently hybridized with the ^{32}P-labeled *Alw*NI fragment that was used as a probe for the Southern blot. As shown in Figure 55, the hybridisation patterns clearly demonstrate the episomal nature of both pEFS-REP1 and pCAG-REP1 vectors. In all clones analysed, there was a distinct band identical in size to the original pEFS-REP1 and pCAG-REP1 plasmids (that were used as positive controls). Importantly, clones remained episomal regardless of whether they were maintained in G418 selective medium or not.
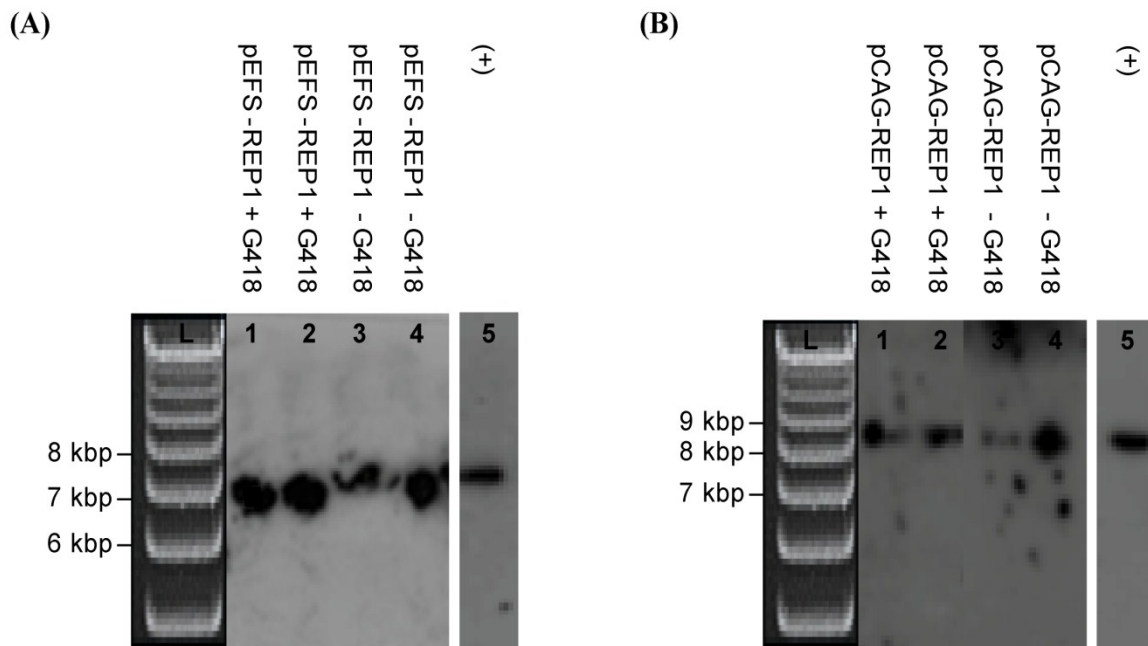
Figure 55: Southern blot analysis of the episomal status of pEFS-REP1 and pCAG-REP1 vectors isolated from AtT20 cells

Southern blots of total DNA isolated from two clones of AtT20 cells transfected with (A) pEFS-REP1 and (B) pCAG-REP1 vectors at 12 weeks post transfection, cultured either in normal or G418 selection medium. DNA (10 µg) was separated on 0.8% agarose gels and hybridized with ^{32}P-labelled *Alw*NI probe. Lanes 3-4, *Stu*I digested total DNA, from AtT20 cells maintained in G418 medium, while lanes 1-2, the same clones digested with *Stu*I maintained in normal medium. All clones produced a clear distinct band after *Stu*I digestion, identical to the band arising after digestion of 8 ng of corresponding positive control original pDNAs (pEFS-REP1 in (A) and pCAG-REP1 in (B); (+)). Results are representative of three independent experiments. L: 1 Kb ladder (Invitrogen).

The episomal state was further confirmed by plasmid rescue experiments similar to the experiments carried out for the EGFP pDNA vectors. *E.coli* bacterial cells were transformed with 1 µg of total DNA isolated from 1 x 10^6 cells at 12 weeks post transfection with either pEFS-REP1 or pCAG-REP1 plasmids. 24 hours after transformation, four colonies were isolation with a MiniPrep kit and plasmid DNA extracted from these clones was digested with various restriction enzymes and analysed by gel electrophoresis.

Clones that arose from AtT20 cells transfected with pEFS-REP1 vector were analysed by digestion with *Xho*I and *Eco*RI restriction enzymes, while pCAG-REP1 transfected AtT20 clones were digested with *Eco*RV and *Eco*RI restriction enzymes. The digestion patterns of all clones were compared to digested original plasmid DNA, pEFS-REP1 or pCAG-REP1 vectors.

Clones from the AtT20 pEFS-REP1 cells digested with *XhoI,* give the fragments 4902 bp, 1300 bp and 1150 bp, as well as the fragments 1651 bp, 2301 bp and 3400 bp when digested with *Eco*RI. While colonies from the AtT20 pCAG-REP1 cells digested with *Eco*RV gave the fragments 2110 bp and 6720 bp, as well as the fragments 4830 bp, 2300 bp and 1700 bp when digested with *Eco*RI. As can be seen from Figure 56 all digestion patterns of isolated colonies were identical to the corresponding original pDNA. This further validates the episomal status of pEFS-REP1 and pCAG-REP1 plasmids in AtT20 cells.
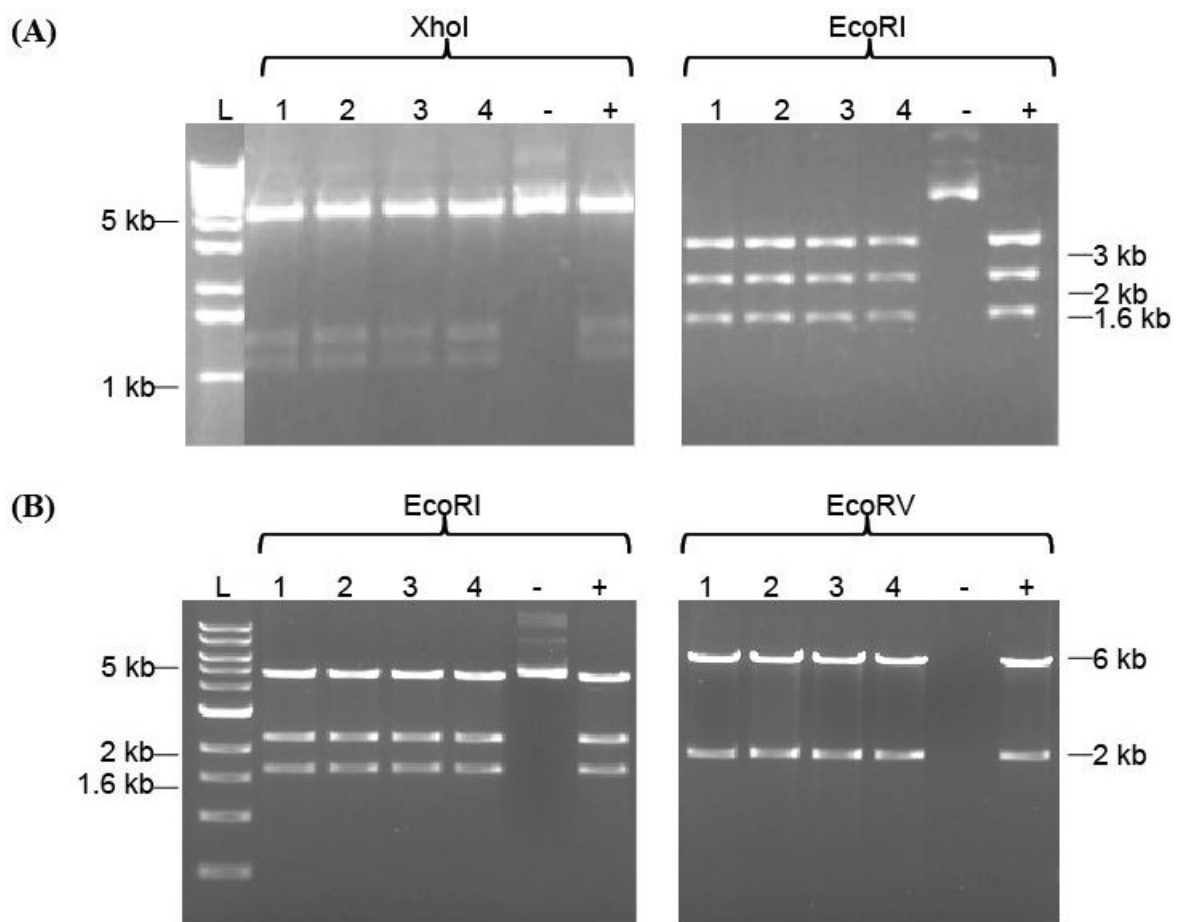
Figure 56: Plasmid rescue of pEFS-REP1 and pCAG-REP1 vectors isolated from AtT20 cells

Plasmid rescue analysis of pDNA isolated from 4 randomly chosen clones (lanes 1-4), after transformation of *E.coli* bacteria with 1 µg of total DNA isolated from AtT20 (A) pEFS-REP1 and (B) pCAG-REP1 stable cell lines, as described in the text. Undigested plasmid served as a negative control (lane 5 (-)), while all bands show identical sizes with the positive control of original pEFS-REP1 and pCAG-REP1 plasmid respectively (lane 6 (+)), demonstrating the episomal status of pEFS-REP1 and pCAG-REP1 vectors in AtT20 cells. Results are representative of four independent experiments. L: 1 kb Ladder (Invitrogen).

3.2.11 Functional studies in human and mouse fibroblasts (CHM4 and Chm^{Flox} cells)

Our previous experiments involved the transfection of wild-type cells *in vitro* and the examination of EGFP as well as REP1 transgene expression within these transfected cells. Since our research is mainly orientated around the eye disease CHM; we were also eager to carry out similar experiments with the pEFS-REP1 and pCAG-REP1 vectors in CHM knock-out (KO) cell lines to show functionality of the vectors in knockout cells. Previous *in vitro* experiments for CHM assessed the rescue and delivery of REP1 to defective lymphocytes and fibroblasts through protein and enzymatic activities (Seabra, Brown et al. 1993; Anand, Barral et al. 2003). Hence as a proof-of-principle for the development of a novel non-viral genetic modification of RPE cells, initial experiments were carried out *in vitro* as before using either lymphocyte or fibroblast cells from CHM patient or CHM mice. To this end, primary human fibroblasts isolated from CHM affected patients (CHM4 cells) were obtained from a collaborator Dr Ian Macdonald at the National Eye Institute (NIH). These CHM4 cells were entirely devoid of REP1 protein and were a full REP1 knockout cell line.

3.2.11.1 Isolation and KO of mouse fibroblasts

Primary mouse fibroblasts were also isolated from a mouse CHM cell line (Chm^{Flox}) as described in the methods. As CHM KO in mice is embryonically lethal, various CHM mouse models have been created to analyse the pathogenesis of the disease including mice with Chm^{Flox} alleles, expressing the Cre protein under the control of a tamoxifen (TM) inducible promoter (MerCreMer - MCM)(Tolmachova, Anders et al. 2006). This mouse model was created using the *Cre/*loxP system of site specific recombination, whereby two *loxP* sites were inserted either side of exon 4 in the murine *CHM* gene. This allows for the conditional deletion of exon 4 (upon TM treatment), which in turn causes a frameshift mutation and ultimately the appearance of an early stop codon in the *CHM* gene. Hence this mouse model was chosen as an ideal candidate to use for the isolation of primary fibroblasts and subsequent treatment with TM to induce a CHM null/KO cell line similar to the CHM KO human fibroblast cell line.

Briefly, CHM pups were culled 2-3 days after birth from a breeding cage of a heterozygous

Chm^{Flox}/Y MCM + male and Chm$^{Flox/Flox}$ female breeding pair. All pups from this breeding pair were screened by PCR analysis for the presence of the Cre transgene using the 4B primer pair as described in the methods (Figure 57Ai). This breeding scheme was required to produce offspring which were homozygous for the Chm^{Flox} allele and carried the Cre transgene under the control of the MCM promoter. Fibroblasts were derived directly from excised skin explants from the above breeding cage. As this procedure of dermal fibroblast isolation from the mouse skin requires isolation prior to the development of pigment and hair follicles around day 4 after birth, this meant that all isolations were initially done on each pup individually. However once the PCR analysis was performed the fibroblasts were grouped into Chm^{Flox} Cre^{+} or Chm^{Flox} Cre^{-} fibroblasts and will be referred to as Flox, Cre^{+} and Flox, Cre^{-} fibroblasts respectively from this stage onwards.

The knockout of exon 4 and subsequent creation of a Chm^{null} cell line was the next experiment that was needed once the primary fibroblasts had been isolated from the Chm^{Flox} mice. This was achieved by treating the isolated Flox, Cre^{+} cells with various concentrations of TM to induce the CHM KO genotype. Briefly, primary mouse fibroblasts were plated into 10 cm dishes at a density of $5x10^{4}$ cells along with varying concentrations of TM. Cells were cultured for 48 hours in the presence of TM which catalyses the recombination between the *loxP* sites and subsequent induction of the null genotype. As the cell doubling time was fast, cells were plated such that they were sparse enough to divide to prevent reintegration of the excised fragment. After 24 hours only a partial knockout was seen – data not shown. The KO event was analysed by PCR analysis using primers to identify the Chm^{WT}, Chm^{Flox} and Chm^{Null} alleles as shown in Figure 57Aii. The cells treated with 5-10 µM TM (dissolved in EtOH) showed the most effective conversion from flox to null genotype, while cells treated with 20 µM were not as viable due to the toxicity of the high TM concentration. Importantly, after the 48 hours of TM treatment, cells were maintained in normal fibroblast medium, and it was shown that the treatment of TM is also non-reversible or permanent as the null genotype was maintained in TM induced cells despite a number of cell divisions *in vitro* (Figure 57Bi). As a negative control Flox, Cre^{-} fibroblasts were also isolated and treated with TM, however as expected no change in the genotype of the cells was observed (Figure 57Aiii).
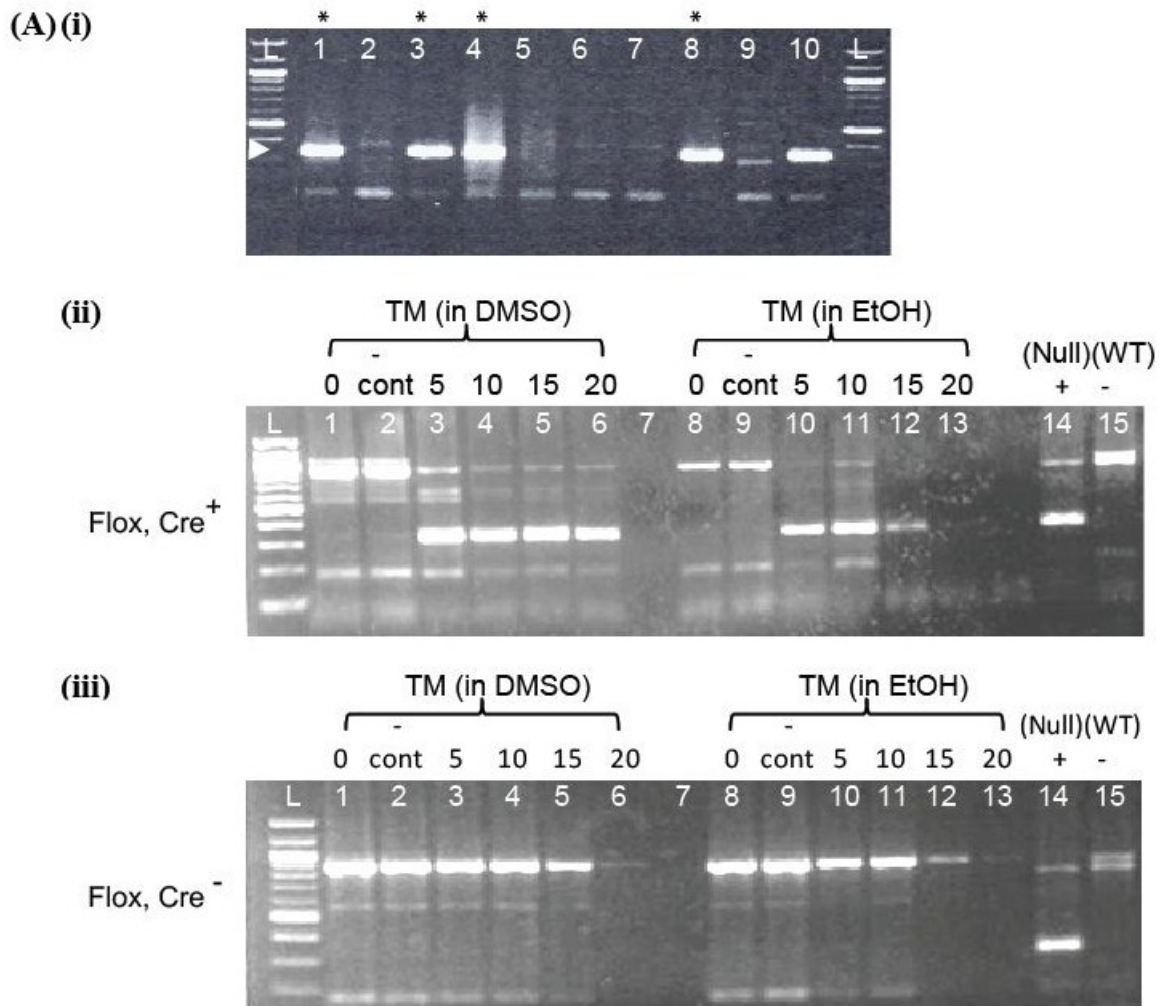
Figure 57: PCR analysis of the Chm^WT, Chm^Flox and Chm^Null alleles following tamoxifen induction of isolated primary fibroblasts (Generation of KO CHM fibroblasts)

(A) Primary fibroblasts were isolated from CHM pups and analysed by (i) PCR analysis using primers to specifically amplify the Cre gene, yielding a product size of 350 bp as indicated by the arrowhead on (i). Initially 8 CHM primary fibroblast cultures were established from 8 individual pups (lanes 1-8) with 4 pups showing the presence of the Cre gene (lanes 1, 3, 4, and 8 (*)). These fibroblasts were labelled Chm^Flox Cre+ (Flox, Cre+) and pooled, while the remaining fibroblasts which were absent for the Cre gene (lanes 2, 5, 6 and 7) were also pooled and labelled Chm^Flox Cre- (Flox, Cre-). Lane 9 and 10 served as a negative and positive control respectively for the PCR reaction. Subsequently isolated (ii) Flox, Cre+ and (iii) Flox, Cre- fibroblasts (at passage 3) were treated with 0-20 μM Tamoxifen (TM) dissolved in either DMSO (lanes 1-6) or EtOH (lanes 8-13) for 48 hours, and analysed for the conversion to the Chm^Null allele after *Cre*-recombination. Lanes 1 and 8 were untreated cells, while lanes 2 and 9 were DMSO and EtOH treated cells (without TM); which served as a control for the TM treatment and dosage. Lanes 14 and 15 served as positive and negative control for the PCR reaction. Lane 7 is empty. Results are representative of five independent experiments. L: 100bp ladder (Invitrogen).

(B) (i)
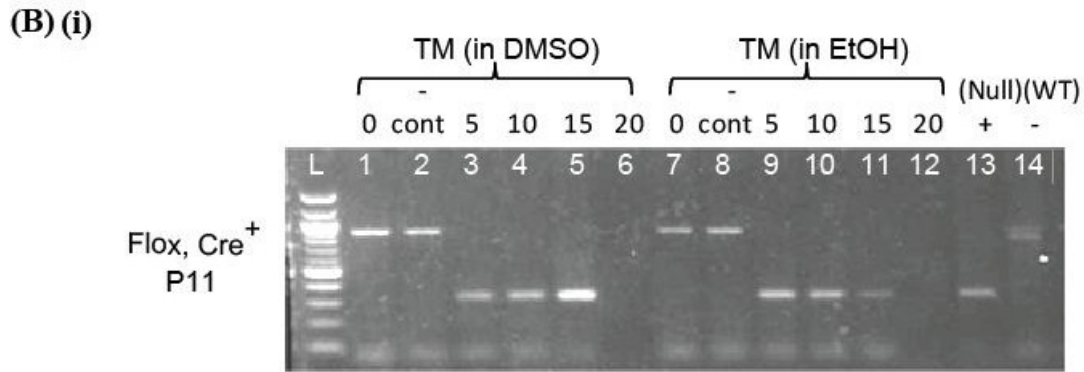
Figure 57: PCR analysis of the ChmWT, ChmFlox and ChmNull alleles following tamoxifen induction of isolated primary fibroblasts (Generation of KO CHM fibroblasts)

(B)(i) The same Chm^{Flox} Cre$^+$ (Flox, Cre$^+$) cells at passage 3 (from Figure 57Aii) were also maintained in normal medium (after the initial 48 hours of TM treatment) and analysed again at passage 11 for the permanent conversion to the Chm^{Null} allele. Results are representative of five independent experiments. L: 100bp ladder (Invitrogen).

The TM-treated Chm^{Flox} cells were also analysed by Western analysis at 48 hours after TM treatment to further validate the extent of the null genotype / KO of mouse REP1 protein levels in these cells. Briefly, total protein was isolated from TM treated mouse fibroblasts and analysed by Western blot using an anti-rabbit J905 antibody which recognises human and mouse REP1, and secondary conjugated anti-rabbit IgG.

Figure 58 validates the PCR analysis of TM treated Flox, Cre$^+$ cells, and shows that cells treated with either 5 or 10 μM TM (dissolved in EtOH) have the most effective knockdown of mouse REP1 protein levels. When the percentage of REP1 protein in the TM treated cells was compared to the untreated Flox, Cre$^+$ cells, approximately 37.9% and 25.2% (corresponding to 5 or 10 μM TM respectively regardless of whether TM was dissolved in EtOH or DMSO) of REP1 protein was still present in the Chm^{Flox} cells. Repeated treatments with TM reduce this percentage further to make even better substantial knockout cells (data not shown).

(A) Flox +

(B) Flox -
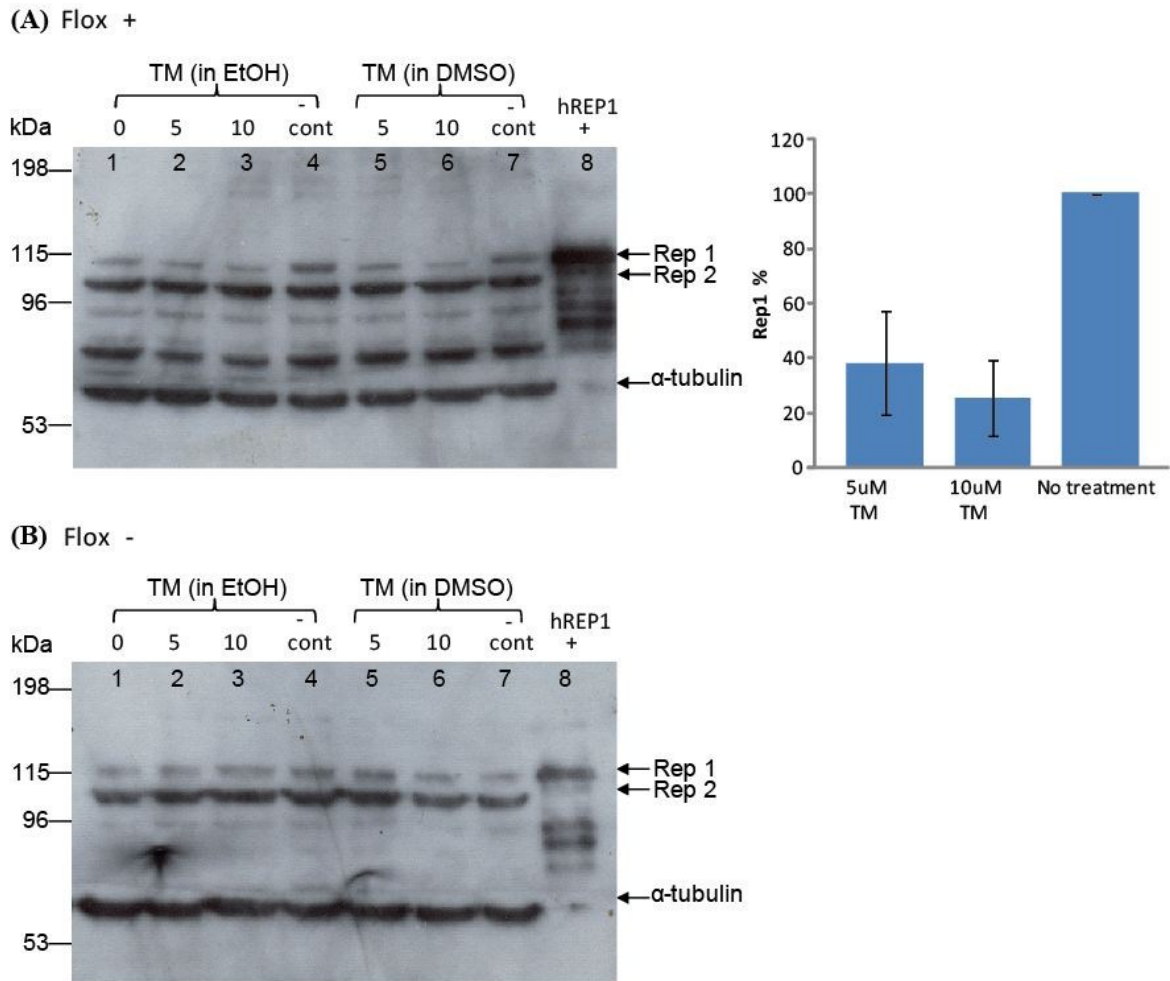
Figure 58: Western analysis of REP1 protein knockdown in Chm^{Flox} Cre⁺ and Chm^{Flox} Cre⁻ cells by tamoxifen treatment (Generation of KO CHM fibroblasts)

Primary fibroblasts (A) Chm^{Flox+} Cre$^+$ (Flox, Cre$^+$) or (B) Chm^{Flox-} Cre$^-$ (Flox, Cre$^-$) cells were treated with 0-10 µM Tamoxifen (TM) dissolved in either EtOH (lanes 2-4) or DMSO (lanes 5-7). The reduction of endogenous (mouse) REP1 protein levels were analysed by Western analysis of cell pellets (50 µg) 48 hours post-TM treatment, using anti-REP1 antibody J905, which recognises both human and mouse Rep1 as well as Rep2 protein. Levels of REP1 protein were quantified in the analysed cell pellets comparing untreated and TM-treated cells (*right graph*). Error bars represent the standard error of the means (s.e.m.). REP1 protein levels were approximately reduced to 37.9% ± 13.4 and 25.2% ± 9.7 when treated 5 and 10 µM TM respectively. Untreated cells (lane 1) as well as cells treated with DMSO or EtOH alone (lanes 4 and 7 respectively) served as negative controls as did the Flox, Cre$^-$ cells. Human Rep1 protein (50 ng) (lane 8) served as a positive control and α-tubulin was used as a loading control. Results are representative of three independent experiments.

3.2.11.2 *Transient transfection of human and mouse fibroblasts*

Once we had established an effective method of isolating and creating knockout mouse fibroblasts, we hoped to use the human and mouse KO cell lines in parallel experiments to show the functionality of the pCAG-REP1 vector in restoring the expression of REP1 protein levels in these cells. The pCAG-REP1 vector was chosen (rather than pEFS-REP1) as this plasmid has higher *REP1* transgene expression levels, as shown in Figure 49.

Initial experiments involved the transfection optimisation of CHM4 cells with pEPI-GFP vector. Previously published reports show efficient transfection of primary fibroblasts with the chemical transfection reagents including: Fugene, Lipofectamine, Lipofectamine 2000, Calcium Phosphate and linear polyethylenimine (PEI). Therefore based on this, human CHM4 cells were initially plated onto either 6 or 12-well plates and individually transfected with the transfection reagents mentioned above according to the manufacturers recommendations. The expression of EGFP was analysed in transfected cells after 48 hours by FACS analysis. Figure 59 shows that conventional transfection reagents such as Fugene, Lipofectamine 2000 and Calcium Phosphate did not efficiently transfect human CHM4 cells with only 7.2% ± 0.45, 5.8 % ± 0.26 and 8.4% ± 0.32 of cells showing EGFP expression levels respectively. The highest levels of EGFP expression were seen in cells transfected with the cationic polymer PEI; with 12.2% ± 0.29 of cells showing EGFP expression (Figure 59D).
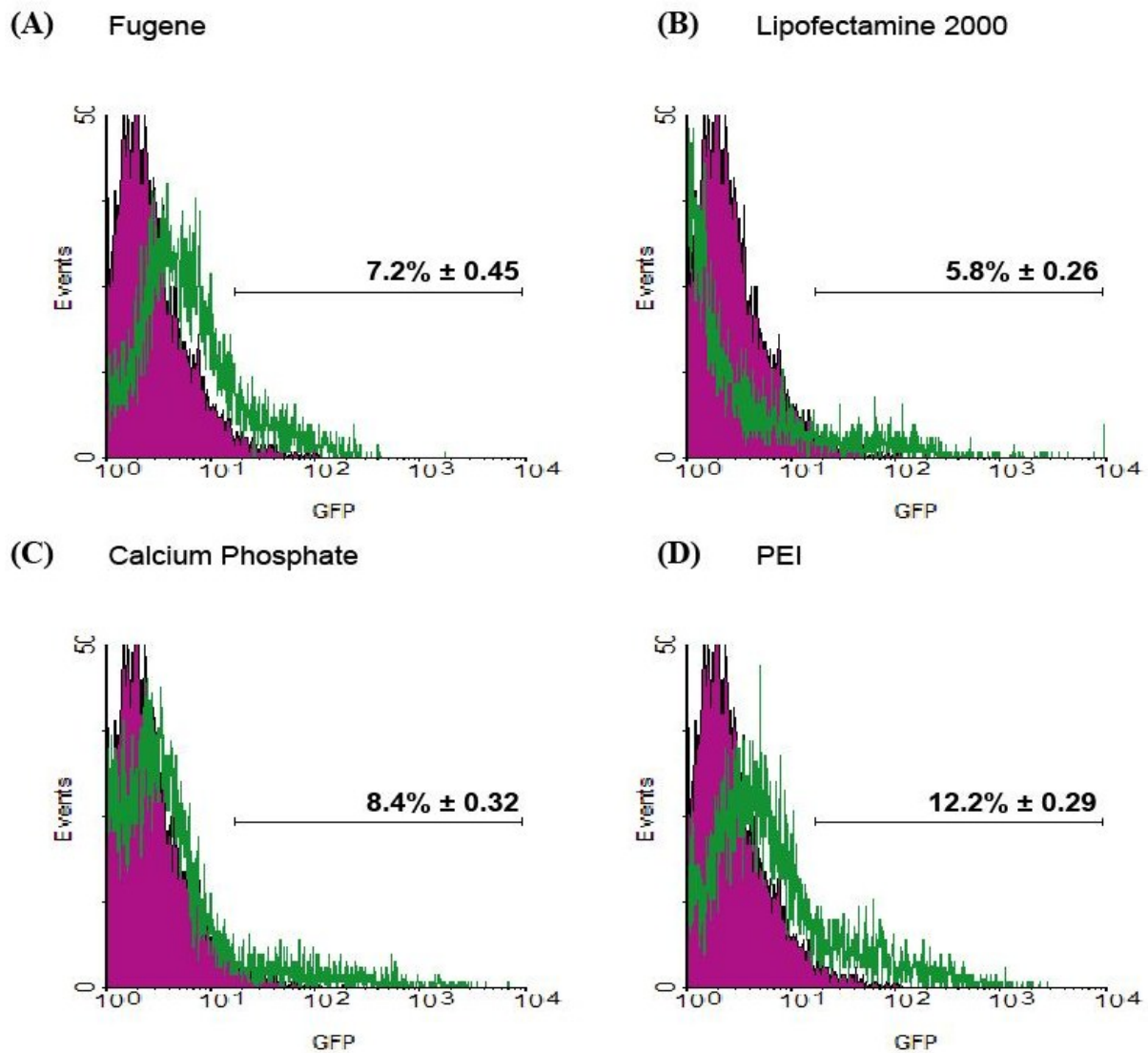
Figure 59: FACS analysis of EGFP expression in CHM4 human fibroblast cells 48 hours post transfection with pEPI-EGFP vector

CHM4 cells were transfected with pEPI-EGFP using the following transfection reagents: (A) Fugene, (B) Lipofectamine 2000, (C) Calcium Phoshate or (D) PEI and showed 7.2%, 5.8%, 8.4% and 12.2% EGFP expression levels respectively by FACS analysis after 48 hours. PEI transfection of CHM4 cells resulted in the highest EGFP expression levels. In all cases, histograms show measured events (*y axis*) against levels of EGFP fluorescence in the FL1-H channel (*x axis*). Untransfected CHM4 cells served as a negative control and appear as a pink graph on the left side of the histogram, while cells expressing EGFP appear green (as an overlay). Gated cells expressing EGFP are expressed as a percentage (%) of the total untransfected population – a threshold of 1% untransfected cells was always set - and appear above the bracketed histogram regions. AtT20 and/or B16-F10 cells were included as positive controls with all transfection reagents (data not shown). Percentages are mean values from four (or three for (B)) independent experiments ± standard error of the means (s.e.m.).

Similar disappointing and low levels of transfection were also observed in the mouse Flox, Cre^{+} cells (data not shown). As these low levels of transfection were deemed unacceptable, mechanical transfection in the form of AMAXA nucleofection was employed to efficiently transfect the mouse (Flox, Cre[+]) and human (CHM4) cells. AMAXA transfection is a non-viral approach to transfect difficult-to-transfect cell lines using a combination of specific electrical pulses as well as cell-type specific solutions to transfect DNA directly into the nucleus of cells. Furthermore AMAXA transfection does not require cell division for the transfer of DNA into the nucleus. This was deemed particularly important for CHM4 cells as they appeared to have a very slow doubling rate (personal observations). Hence perhaps this slow growth rate could account for the low transfection efficiency observed with the normal chemical/non-viral transfection methods employed above, which rely on cell division for the transfer of DNA into the nucleus.

AMAXA transfections were optimised using the basic fibroblast AMAXA kit. During the optimisation process a range of programmes were used as well as varying the concentration of pDNA and cell density. Optimisation was based on viability and transgene expression levels. In summary 5×10^5 cells were used per reaction, with 20 µg pCAG-REP1 vector, using programmes P32, P24 and Q32 for CHM4 KO cells and programmes Q32, U23 and W32 for of Flox, Cre^{+} KO cells. Only low passaged cells were transfected as this minimised cell death following AMAXA transfection. One day following transfection, cells were fixed and stained for REP1 expression by FACS analysis. Figure 60 shows representative expression observed at 24 hours for REP1 in CHM4 and Flox, Cre^{+} cells transfected with pCAG-REP1 vector.
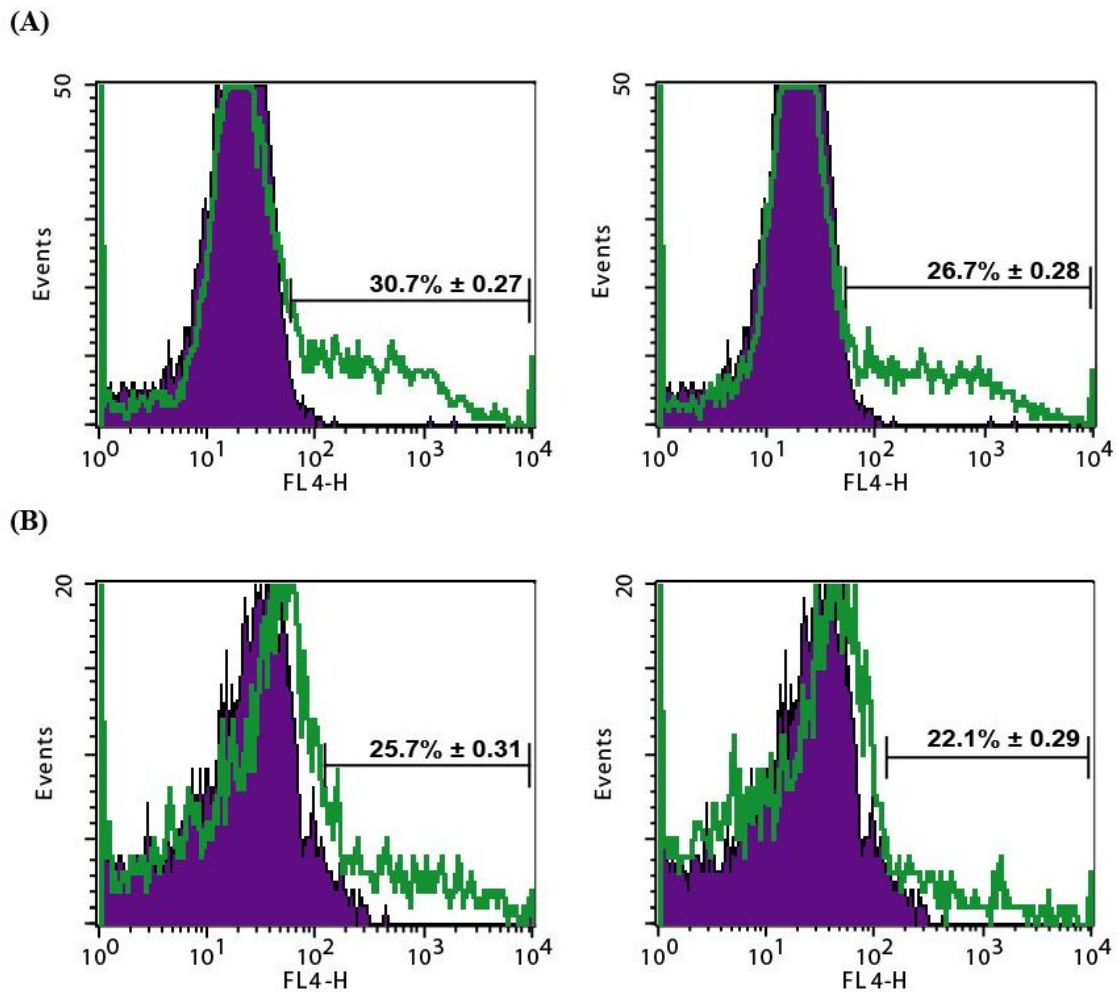
Figure 60: Efficient FACS analysis of REP1 expression in human and mouse CHM KO fibroblasts 24 hours post transfection with pCAG-REP1 vector

Both KO (A) Human CHM4 cells and (B) Mouse Flox, Cre+ (+TM) cells were transfected with 20 μg of pCAG-REP1 vector using AMAXA nucleofection. Cells were fixed and REP1 expression levels were analysed by FACS analysis after 24 hours using an anti-Rep1 antibody 2F1 which recognises human Rep1 protein. Levels of REP1 expression varied from 30.7 % (for programme P32 – *top left histogram*) and 26.7% (for programme P24- *top right histogram*) for human fibroblasts and 25.7% (for programme Q32 – *bottom left histogram*) and 22.1% (for programme U23 – *bottom left histogram*) for mouse fibroblasts depending on the transfection programme chosen. Programme P32 and Q32 resulted in the highest REP1 expression levels in human and mouse fibroblasts respectively.

In all cases, histograms show measured events (*y axis*) against levels of REP1 fluorescence in the FL4-H channel (*x axis*). Untransfected CHM4 (*top histograms*) or Flox + (*bottom histograms*) cells served as a negative control and appear as a purple graph on the left side of the histogram, while cells expressing REP1 appear green (as an overlay). Gated cells expressing REP1 are expressed as a percentage (%) of the total untransfected population – a threshold of 1% untransfected cells was always set - and appear above the bracketed histogram regions. Percentages are mean values from four independent experiments ± standard error of the means (s.e.m.). +TM= Treatment with tamoxifen (TM).

After 24 hours following AMAXA transfection with the pCAG-REP1 vector, cells were also fixed and REP1 expression was further confirmed by immunofluorescence of transfected cells using the REP1 antibody 2F1 which recognises only human REP1 protein. Untransfected Flox, Cre[+] fibroblasts were also stained with J905 antibody which recognises both human and mouse REP1 protein. This was carried out to show the extent of mouse REP1 which was still present in the cells despite TM treatment. Figure 61A and B show representative images of pCAG-REP1 transfected CHM4 cells and mouse TM-treated Flox, Cre[+] fibroblasts respectively. This shows that pCAG-REP1 was able to mediate strong levels of REP1 expression in both cell lines following transfections with two different AMAXA programmes (programmes P32 and P24 for human cells, or Q32 and U23 for mouse cells). Importantly, Flox, Cre[+] fibroblasts stained with J905 antibody showed limited staining (Figure 61B (iii)) confirming that the TM treatment and the subsequent KO event was successful and that limited mouse REP1 protein was still present in these cells.

(A) Human CHM4 cells
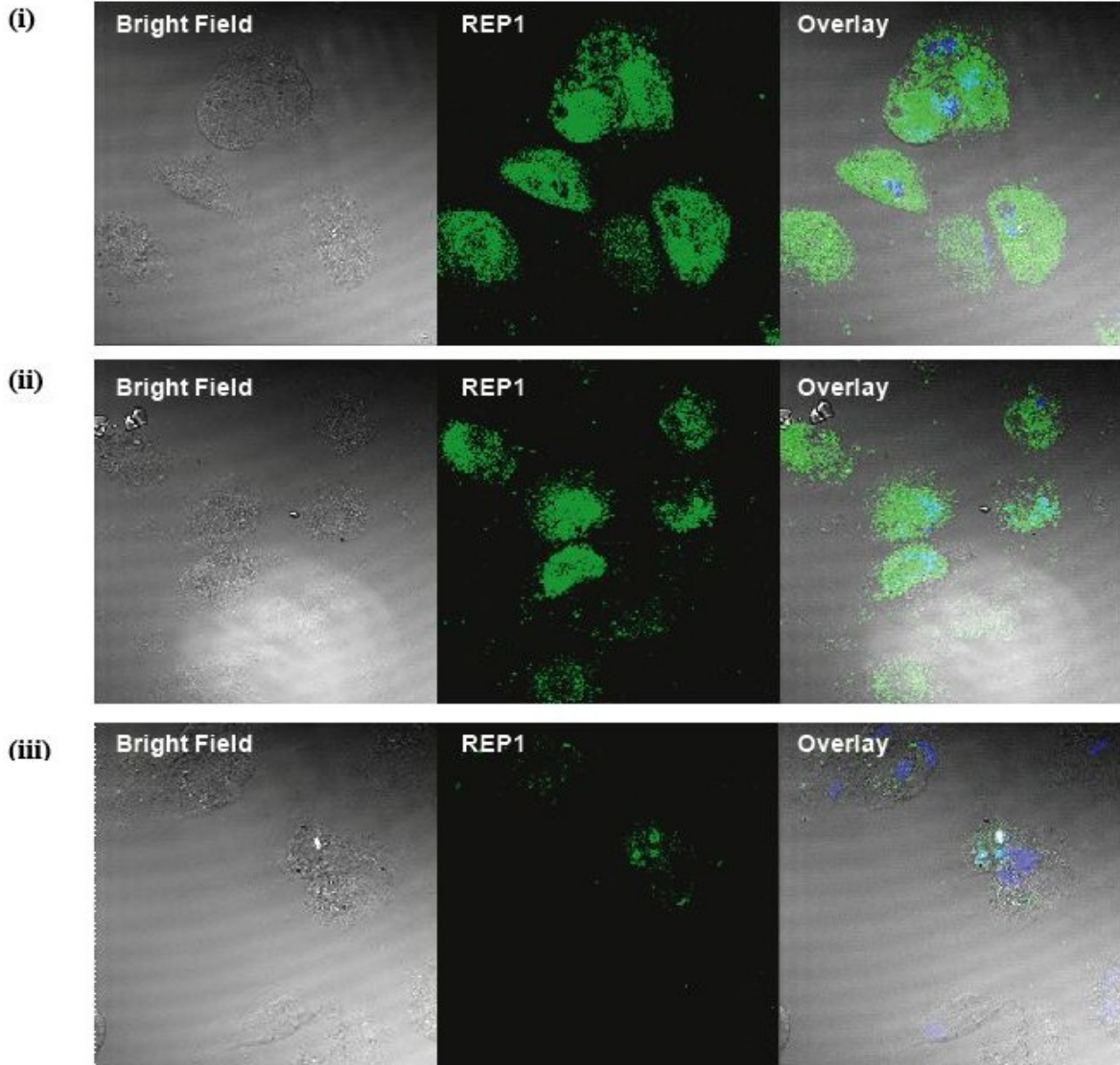
Figure 61: Expression from pCAG-REP1 following AMAXA transfection of human and mouse CHM KO cells

(A) Human CHM4 cells were AMAXA transfected with 20 µg of pCAG-REP1 vector. After 24 hours, cells were fixed and to detect REP1 expression, cells were incubated with mouse REP1 antibody (2F1) which recognises human REP1 protein only, followed by anti-mouse 488 conjugated secondary antibody. Dapi was also added to stain the nuclei blue for easier distinction of cells. Representative images are shown for AMAXA transfections with programmes (i) P32 and (ii) P24 as well as (iii) untransfected cells. Bright field (*left panel*), fluorescent (*middle*) and merge images with Dapi (*right*) at 40x magnification are shown. Images are representative of three independent experiments.

(B) Mouse Flox, Cre⁺ (+TM) cells
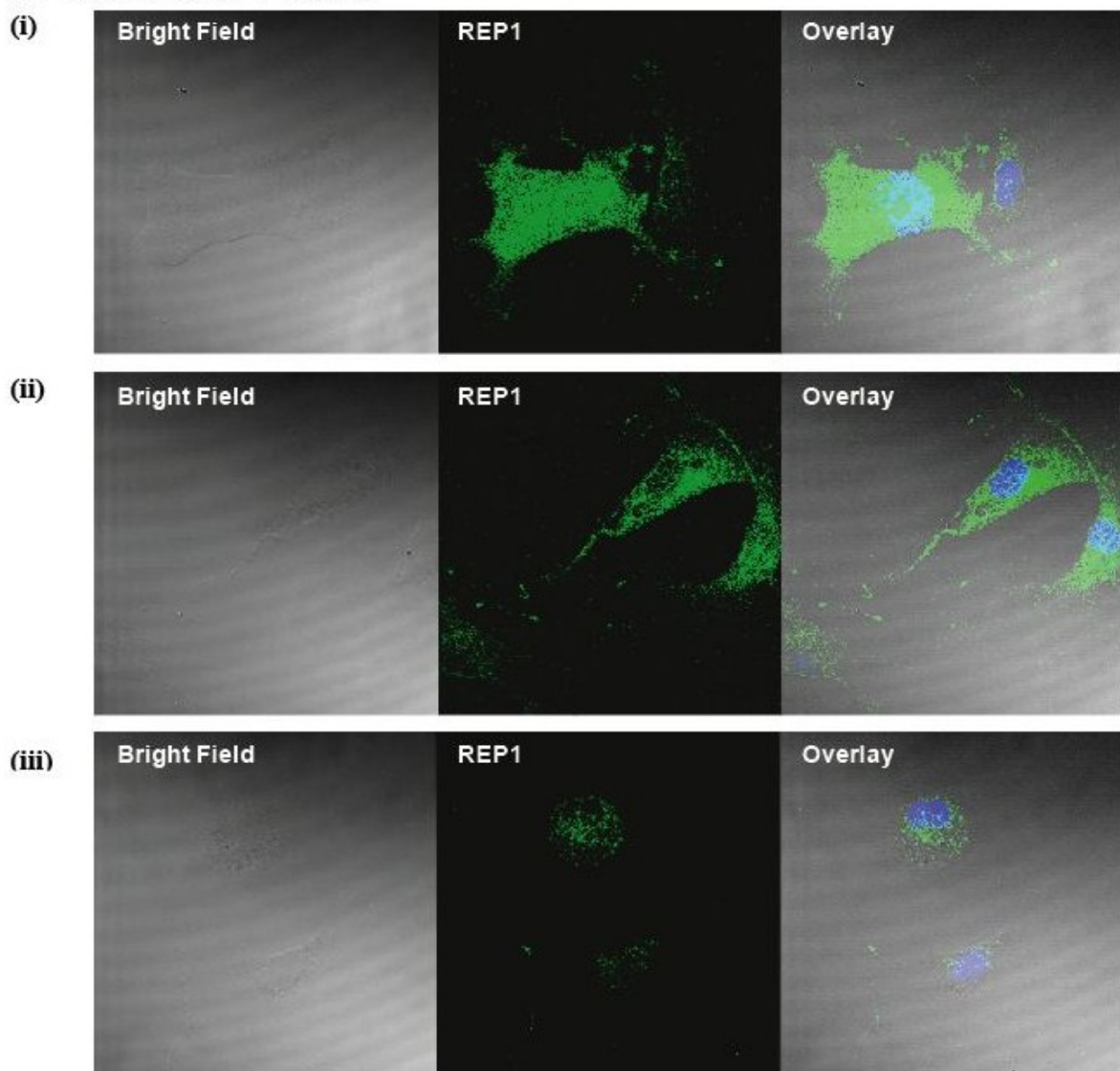
Figure 61:   Expression from pCAG-REP1 following AMAXA transfection of human and mouse CHM KO cells

(B) Mouse fibroblasts were isolated from Flox, Cre⁺ pups between 1-4 days after birth. Once confluent, cells were treated with 10 μM TM to induce the knock-down/KO of REP1 protein in the cells. Following successful knock-down/KO, mouse CHM KO cells were AMAXA transfected with 20 μg of pCAG-REP1 vector. After 24 hours, cells were fixed and to detect REP1 expression, cells were incubated with mouse REP1 antibody (2F1) which recognises human REP1 protein only or J905 antibody for untransfected cells, which recognises both mouse and human REP1 protein. This was followed by either anti-mouse or rabbit Alexa 488-conjugated secondary antibody. Dapi was also added to stain the nuclei blue for easier distinction of cells. Representative images are shown for AMAXA transfections with programmes (i) Q32 and (ii) U23 as well as (iii) untransfected TM+ cells. Bright field (*left panel*), fluorescent (*middle*) and merge images with Dapi (*right*) at 40x magnification are shown. Images are representative of three independent experiments. +TM= Treatment with tamoxifen (TM).

3.2.11.3   *Long-term expression of REP1 in human and mouse fibroblasts*

To investigate if the pCAG-REP1 vector could maintain extra-chromosomal stability similar to the results shown for the same plasmids (as well as the pEFS-EGFP and pCAG-EGFP vectors) in AtT20 cells, long-term analysis was also carried out in the mouse and human KO fibroblasts. Hence cells were AMAXA transfected with pCAG-REP1 vector and 48 hours following transfection cells were placed in G418 selective medium for 2 weeks. Antibiotic resistant clones were then isolated and cultured in normal medium for a further 4 weeks after which Western blot analysis was performed. This showed whether the expression of REP1 was sustained and as colonies were not maintained in G418 antibiotic medium, the expression of REP1 was also analysed for mitotic stability in the absence of selection pressure. No clear colonies grew following the transfected with pCAG-REP1-Control vector. Similar results were also seen with the long-term analysis of pCAG-REP1 and its control counterpart in AtT20 cells. Hence as before, control plasmids did not survive the prolonged selection procedure as these cells lacked the S/MAR element, and so were only transiently resistant to the G418 antibiotic and so were not able to be permanently established.

Western blot analysis was performed to confirm REP1 expression at 6 weeks post transfection. Briefly, total protein lysates were isolated from 2 colonies after transfection with pCAG-REP1 vector and analysed by Western blotting, probing with antibodies for REP1; 2F1 (for the human CHM4 cells) or J905 (for the mouse Flox cells). Figure 62 shows representative Western blots showing that REP1 protein expression was maintained for up to 6 weeks in both human and mouse KO cell lines. In a complimentary experiment, in parallel with Western analysis at 6 weeks post transfection, cells were also analysed by FACS analysis for REP1 expression. Indeed as shown by Figure 63, levels of REP1 protein are undiminished in both cell lines at 6 weeks post transfection.

(i)

24h PT 6wks PT (-) Untransf cells (+) hRep1

kDa

116 — ← Rep1

98 —

← α-tubulin

57 —

(ii)

Untransduced / WT cells

24h PT 6wks PT 24h PT 6wks PT (+) hRep1

← Rep1
← Rep2

← α-tubulin

Tamoxifen (10 μM)	-	+	+	+	+	+	+	+	+
Amaxa	-	+	-	+	-	-	+	-	+
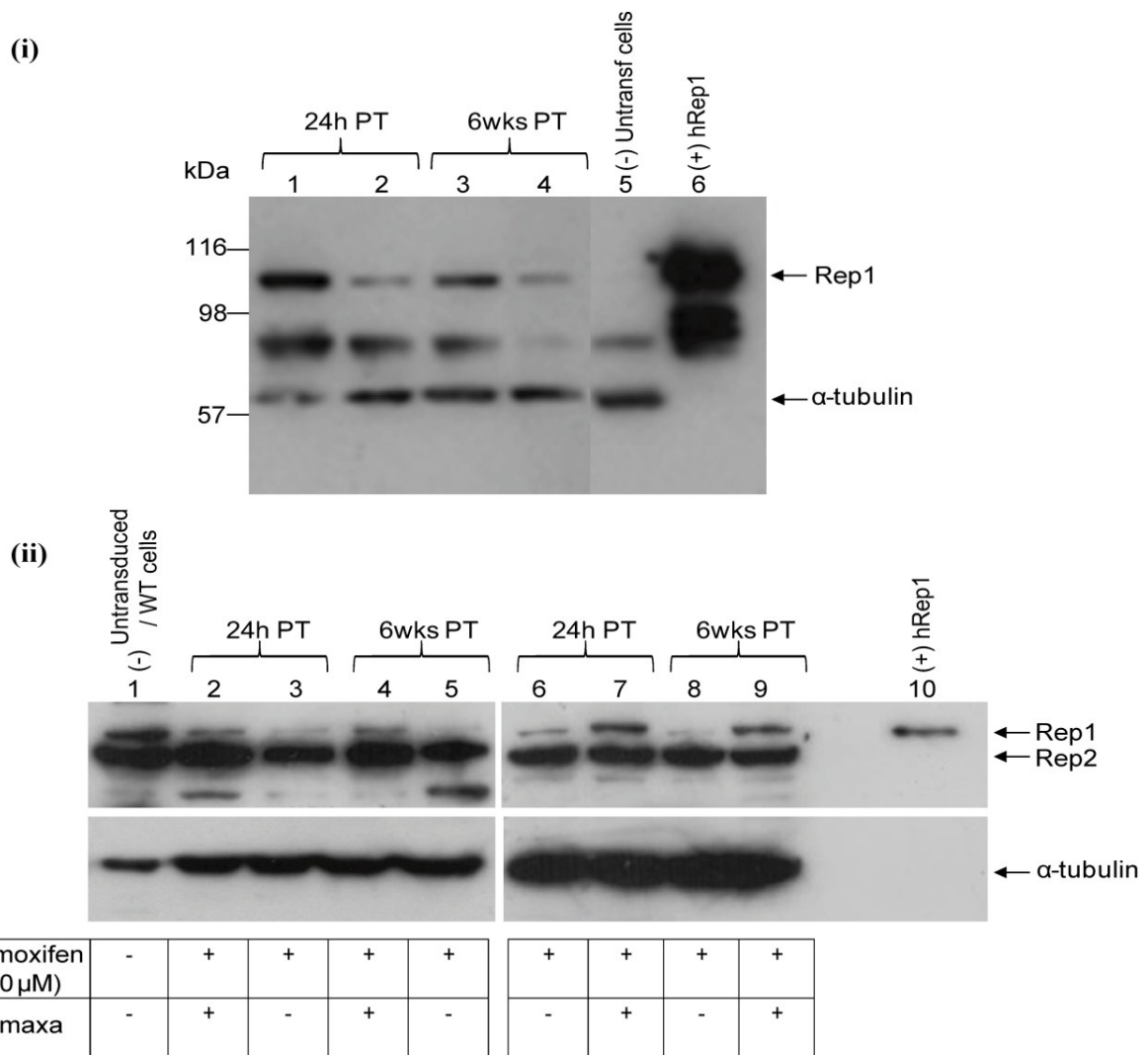
Figure 62: Western analysis of long-term pCAG-REP1 vector expression in CHM KO cells

Primary KO fibroblasts from (i) Human CHM4 cells and (B)(i) Mouse TM-treated Chm^{Flox+} Cre$^+$ cells (CHM KO) were AMAXA transfected with 20 μg of pCAG-REP1 vector. 48 hours following transfection, cells were maintained in G418 selection medium for 2 weeks, after which isolated clones were picked and grown for a following 4 weeks in normal medium without G418 antibiotic. Cell lysates (50 μg) were collected from two isolated clones each for human and mouse KO cells at 24 hours and 6 weeks after transfection. Lysates were then analysed by Western analysis for the expression of REP1 protein using anti-Rep1 antibody J905 for mouse cell lysates – as this antibody recognises both human and mouse Rep1 – or 2F1 antibody for human cell lysates – as this antibody specifically recognises only human REP1. Lanes 1 and 3 as well as lanes 2 and 4 on (i) represent clone 1 and 2 respectively. Lanes 1-5 as well as lanes 6-9 on (ii) represent clone 1 and 2 respectively. Untransfected fibroblasts served as a negative control in human KO cells (lane 5), while untransduced/WT cells not dosed with TM and cells treated with tamoxifen but not transfected with pCAG-REP1 served as negative controls in mouse KO cells (lanes 1, 3, 5, 6 and 8). Human Rep1 protein was used as a positive control and α-tubulin was used as a loading control. Results are representative of three independent experiments. +TM= Treatment with tamoxifen (TM).

(i)

(ii)
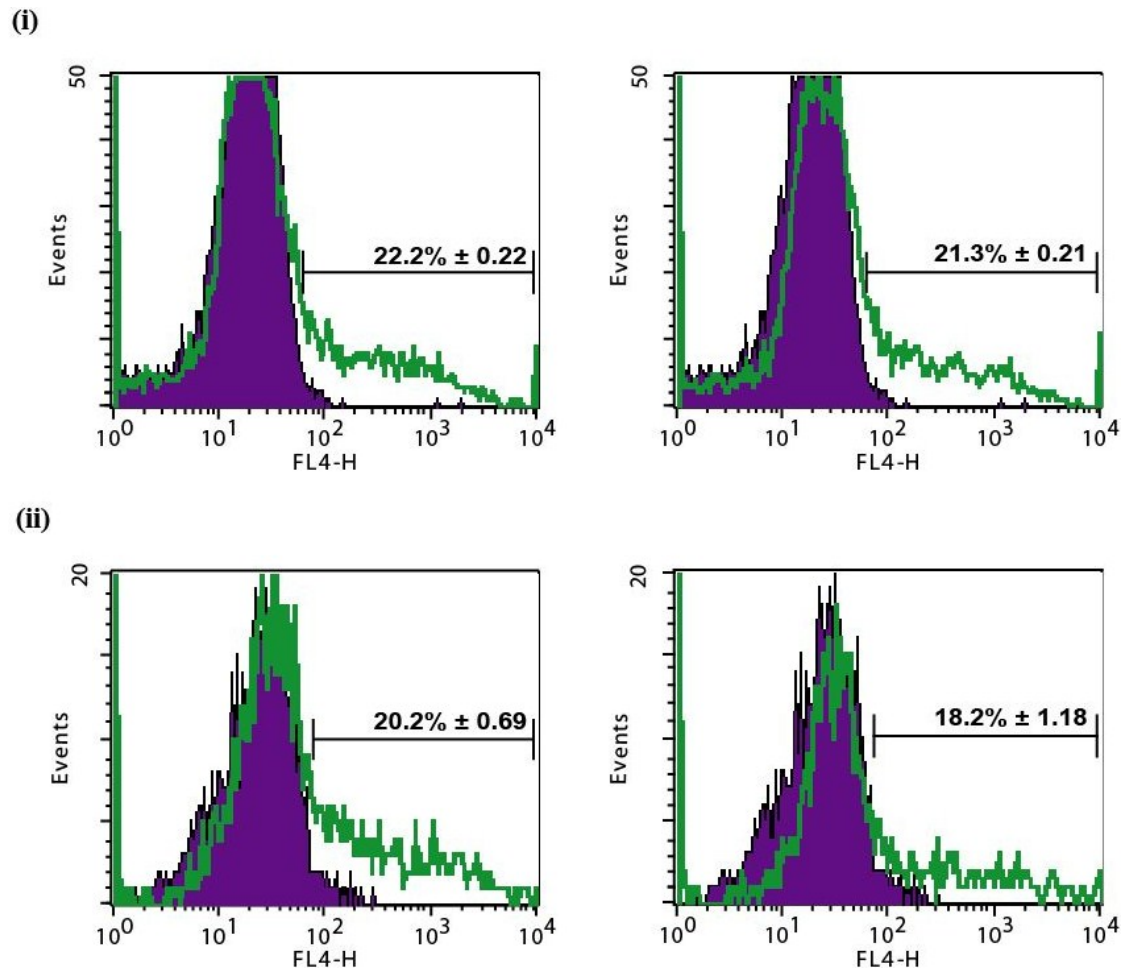
Figure 63: FACS analysis of long-term pCAG-REP1 vector expression in CHM KO cells

At 6 weeks post transfection (i) Human CHM4 cells and (ii) Mouse TM-treated Chm[Flox+] Cre^{+} cells (CHM KO) cells were also fixed and REP1 expression levels were analysed by FACS analysis using an anti-Rep1 antibody 2F1 which recognises human Rep1 protein. Levels of REP1 expression varied from 22.2% and 21.3% for human fibroblasts (corresponding to transfection with AMAXA programmes P32 and P24 - *top left and right histograms* respectively) and 20.2% and 18.2% for mouse fibroblasts (corresponding to transfection with AMAXA programmes Q32 and U23 - *bottom left and right histograms* respectively). This showed that levels of *REP1* were not diminished after 6 weeks *in vitro*.

In all cases, histograms show measured events (*y axis*) against levels of REP1 fluorescence in the FL4-H channel (*x axis*). Untransfected CHM4 (*top histograms*) or Flox + (*bottom histograms*) cells served as a negative control and appear as a purple graph on the left side of the histogram, while cells expressing REP1 appear green (as an overlay). Gated cells expressing REP1 are expressed as a percentage (%) of the total untransfected population – a threshold of 1% untransfected cells was always set - and appear above the bracketed histogram regions. Percentages are mean values from three independent experiments ± standard error of the means (s.e.m.). +TM= Treatment with tamoxifen (TM).

Total DNA was also isolated from CHM KO cells transfected with pCAG-REP1 vector. This was used to perform analysed by PCR analysis for the presence of pCAG-REP1 pDNA in transfected cells up to 6 weeks post transfection. Figure 64 shows the long-term presence of pCAG-REP1 pDNA in both mouse and human KO cell lines.

The persistence of REP1 transcript was also verified in transfected CHM KO cells by the isolation of RNA from cell pellets and subsequent rt-PCR analysis. Figure 65 shows that REP1 mRNA levels were maintained for up to 6 weeks in both cell lines.
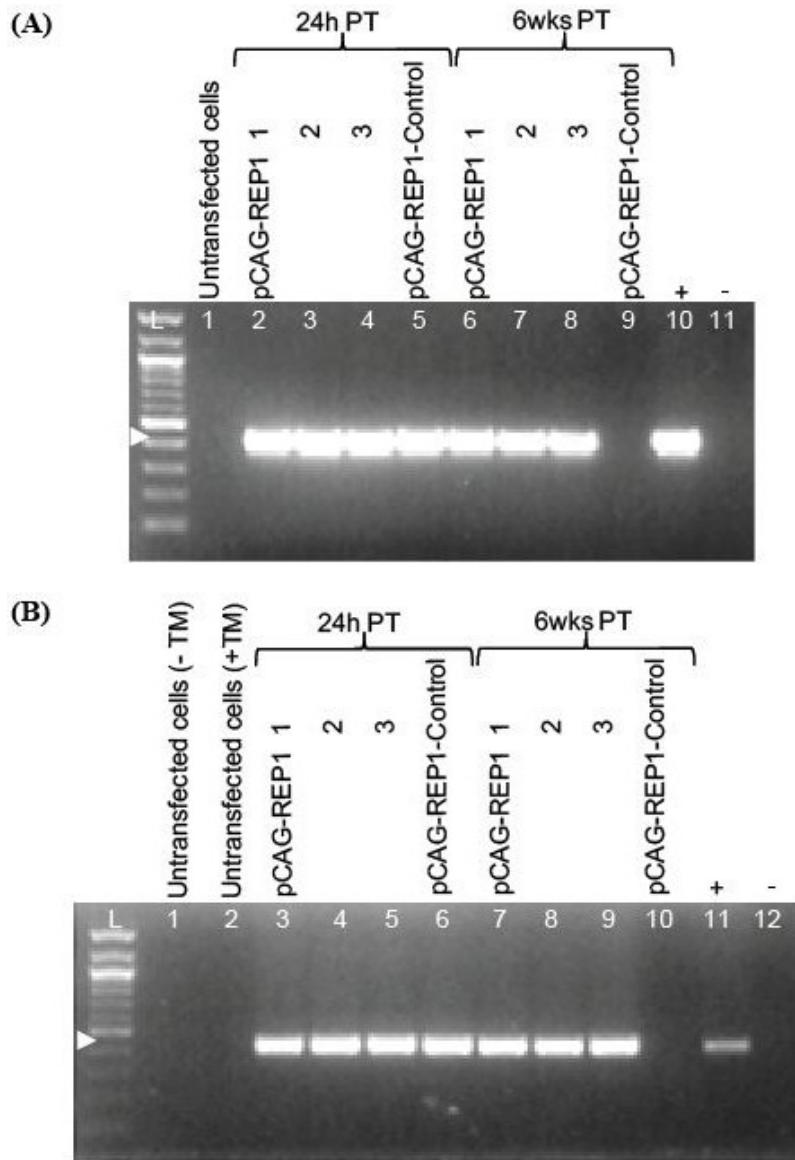
Figure 64: PCR detection over time of pCAG-REP1 pDNA in CHM KO cells after AMAXA transfection with pCAG-REP1 vector

PCR analysis of pCAG-REP1 in (A) Human (CHM4 cell line) and (B) Mouse (Chm^{Flox+} Cre$^+$ +TM) cells following AMAXA transfection with 20 µg of pCAG-REP1 vector at 24 hours and 6 weeks following transfection. AMAXA programmes P24, P32 and Q32 were used for human cells, while programmes Q32, U23 and W32 were used for mouse cells. Lanes 5 and 9 on (A) and lanes 6 and 10 on (B) represent cells transfected with pCAG-REP1-Control vector at 24 hours and 6 weeks following transfection respectively. PCR samples were separated by agarose gel electrophoresis and a positive PCR band was observed using CAG-REP1 specific primer set yielding a product size of 430 bp. The arrowhead indicates the size 430 bp on (A) and (B). Untransfected cells, untransfected and TM dosed as well as no PCR product/water served as a negative control (lane 1 in A and B, lanes 2 and 11 in B respectively), while pCAG-REP1 pDNA (25 ng) served as a positive control (lane 10 in A, lane 11 in B) for the PCR reaction. Results are representative of three independent experiments. +TM= Treatment with tamoxifen (TM), L= 100bp ladder (Invitrogen).
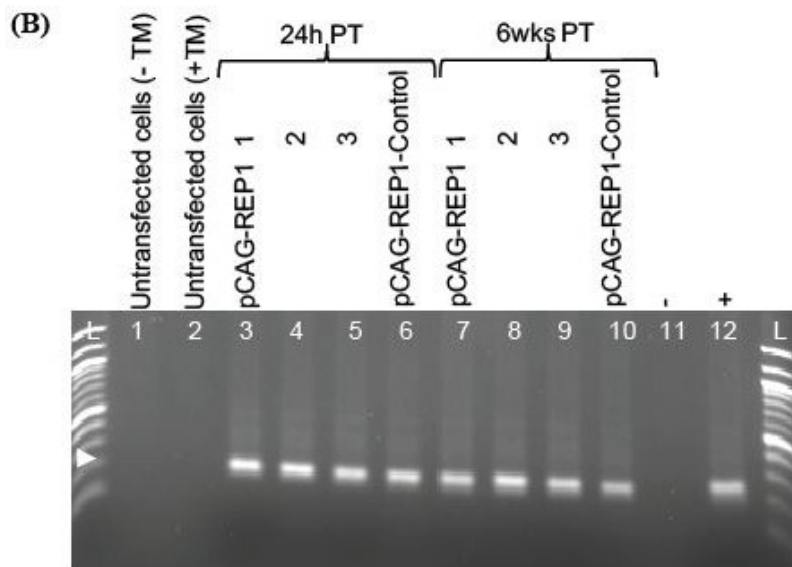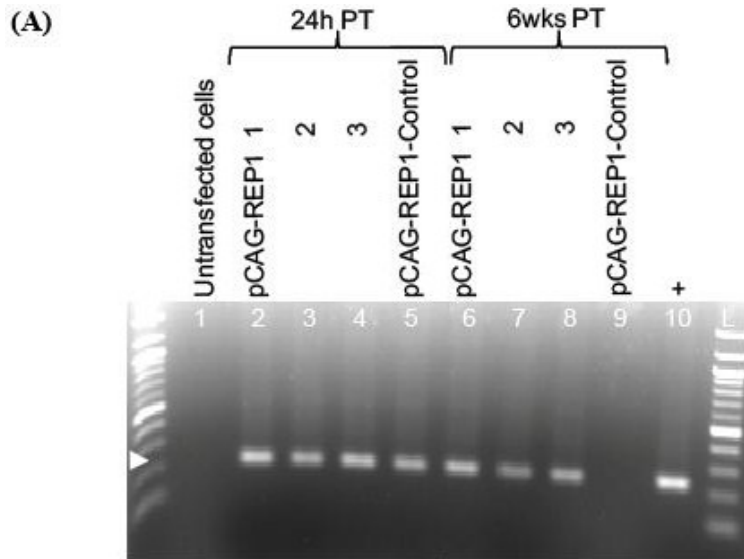
Figure 65: RT-PCR analysis over time of REP1 mRNA from CHM KO cells after AMAXA transfection with pCAG-REP1 vector

Total RNA was extracted from (A) Human (CHM4 cell line) and (B) Mouse (Chm^{Flox+} Cre$^+$ +TM) cells following AMAXA transfection (with three different programmes) with 20 µg of pCAG-REP1 vector at 24 hours and 6 weeks following transfection. AMAXA programmes P24, P32 and Q32 were used for human cells, while programmes Q32, U23 and W32 were used for mouse cells. Lanes 5 and 9 on (A) and lanes 6 and 10 on (B) represent cells transfected with pCAG-REP1-Control vector at 24 hours and 6 weeks following transfection respectively. Total RNA was isolated and used to generate cDNA. PCR was performed with human REP1 specific primers to yield a product size of 240 bp as indicated by the arrowhead on (A) and (B). RNA from untransfected cells, untransfected and TM dosed as well as no RNA product/ water served as a negative control (lane 1 in A and B, lanes 2 and 11 in B respectively), while RNA isolated from AtT20 cells transfected with pCAG-REP1 after 48 hours served as a positive control (lane 10 in A, lane 12 in B) for the rt-PCR reaction. Results are representative of three independent experiments. +TM= Treatment with tamoxifen (TM), L= 100bp ladder (Invitrogen).

3.2.11.4 *Episomal status of stable human and mouse cell lines*

To trace the presence of pCAG-REP1 at 6 weeks post transfection in both mouse and human CHM KO cells, plasmid rescue was performed whereby *E.coli* bacterial cells were transformed with 1 µg of total DNA isolated from 5×10^5 cells, at 6 weeks post-transfection. Cells showing the highest levels of pCAG-REP1 after transfection of mouse and human cells were picked; human cells transfected with P32 programme, and mouse cells transfected with Q32 programme. Kanamycin resistant colonies were obtained after 24 hours at a rate of 4-5 colonies per plate, which indicates a low plasmid copy number of pCAG-REP1 plasmid in both KO cell lines. Plasmid DNA was extracted from 6 antibiotic resistant clones and digested with *Eco*RV restriction enzyme and analysed by gel electrophoresis (Figure 66). All clones have the same bands as the original pCAG-REP1, confirming the presence of an intact episomal plasmid in both CHM KO cell lines.

In a complimentary approach, the episomal state of pCAG-REP1 was also analysed by Southern blot analysis. Total cellular DNA (10 µg) was isolated from the two long-term clones from both cell lines and digested with *Stu*I restriction enzyme - which linearises pCAG-REP1 plasmid - and hybridised with a ^{32}P-labelled *Alw*NI fragment as a probe. As shown in Figure 67 the hybridisation pattern clearly confirms the episomal state of pCAG-REP1 vector in the CHM KO cell lines. In all clones analysed, a distinct band identical in size to the original pCAG-REP1 plasmids (+) is seen.

(A)

(B)
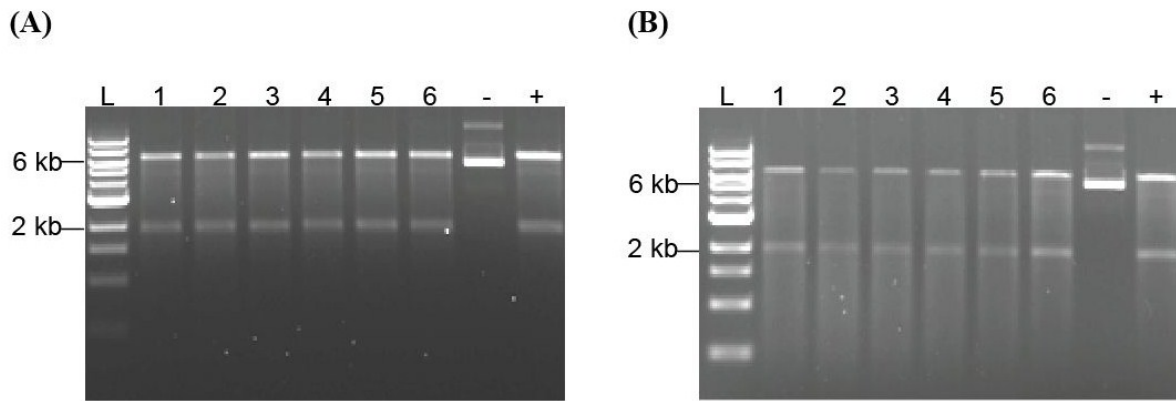
Figure 66: Plasmid rescue of pCAG-REP1 vector isolated from CHM KO cells

Plasmid rescue analysis of pDNA isolated from 6 randomly chosen clones (lanes 1-6). Clones were generated following the transformation of *E.coli* bacteria with 1 µg of total DNA isolated from CHM (A) Mouse (Chm^Flox+ Cre+ TM+) cells and (B) Human (CHM4 cell line) KO cells 6 weeks following transfection with pCAG-REP1 vector, as described in the text. Undigested plasmid served as a negative control (-), while all bands show identical sizes with the positive control of original pCAG-REP1 plasmid respectively (+), demonstrating the episomal status pCAG-REP1 vector in CHM KO cells. Results are representative of four independent experiments. +TM= Treatment with tamoxifen (TM), L: 1 kb Ladder (Invitrogen).
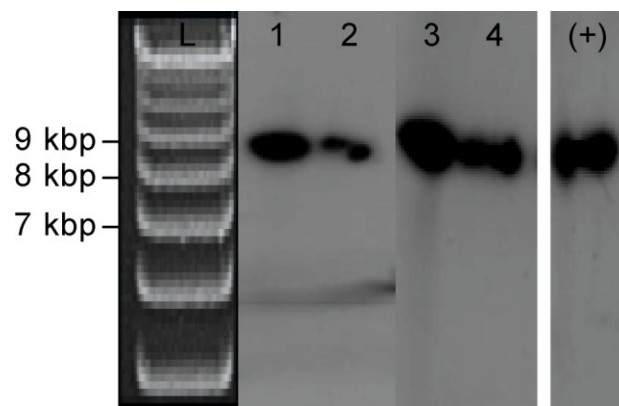
Figure 67: Southern blot analysis of the episomal status of pCAG-REP1 vector isolated from CHM KO cells

Southern blots of total DNA isolated from two clones of CHM Mouse (Chm^Flox+ Cre+ TM+) and Human (CHM4 cell line) KO cells transfected with pCAG-REP1 vector at 6 weeks following transfection, cultured in normal medium. DNA (10 µg) was separated on 0.8% agarose gels and hybridized with ^{32}P-labelled *Alw*NI probe. Lanes 1-2, *Stu*I digested total DNA, from Human KO cells, while lanes 3-4, *Stu*I digested total DNA, from Mouse KO cells. All clones produced a clear distinct band after *Stu*I digestion, identical to the band arising after digestion of 8 ng of corresponding positive control original pDNA pCAG-REP1; (+). Results are representative of three independent experiments. L: 1 Kb ladder (Invitrogen).

3.2.11.5 Correction and in vitro prenylation analysis of stable human and mouse cell lines

Previously it has been reported that the lack of REP1 function in (cells isolated from) CHM patients caused defects in Rab prenylation in isolated cells from these patients; namely Rab27a prenylation defects (Seabra, Ho et al. 1995). Hence we were eager to analyse if by transfecting pCAG-REP1 vector into the CHM KO cells – both human and mouse KO cells described earlier - we were able to provide correction for the prenylation defect seen in these cells. In order to analyse the maximum amount of prenylation correction, CHM KO stable cells expressing the highest amounts of *REP1* transgene levels at 6 weeks post transfection were used, as described in the previous section 3.2.11.3 and Figure 63 (Human and Mouse KO cells transfected with P32 and Q32 AMAXA programmes).

To this end, CHM stable KO human and mouse cells at 6 weeks post transfection with pCAG-REP1 vector were analysed for the prenylation status of Rab27a in these cells by subcellular fractionation and subsequent Western blot analysis as previously described (Seabra, Ho et al. 1995; Anand, Barral et al. 2003; Tolmachova, Anders et al. 2006). Briefly, CHM KO cells were transfected with pCAG-REP1 vector and total protein lysates from transfected cells at 6 weeks post transfection were subjected to subcellular fractionation. This allowed the separation of soluble (S) and pellet (P) fractions from the cells were analysed by Western blot probing with an anti-Rab27a antibody 4B12. In wild-type cells one would expect normally prenylated Rab27a protein to be found in the pellet fraction of cells. In contrast CHM cells which have a defect in Rab27a prenylation should have approximately 50% of the protein in the cytosolic fraction. This is because without prenyl groups, Rabs cannot associate with membranes and so remain cytosolic and dysfunctional. Upon transfection of CHM KO cells with pCAG-REP1, one would expect to observe a similar pattern to that of wild-type cells if the CHM KO cells have been rescued by the transfection of pCAG-REP1 plasmid.

Figure 68 shows the corresponding Western blot carried out on long-term expressing CHM KO cells transfected with pCAG-REP1 vector. The blot shows higher levels of Rab27a protein in the pellet fraction compare to cytosolic fraction of untransfected Flox, Cre+ cells prior to TM treatment (lanes 1 and 2 respectively in Figure 68B). Hence these cells closely resemble

wild-type cells. In contrast, when the untransfected Flox, Cre+ cells are treated with TM (10 μM), a shift in the expression levels of Rab27a is seen, where approximately 50% of the protein is now in the pellet fraction as well as the cytosolic fraction (lanes 3 and 4 respectively in Figure 68B). This confirms the knock-down of REP1 in the cells by TM treatment, where cells now show the expected defect in prenylation of Rab27a observed in CHM cells. Similarly untransfected human KO cells also show an equal amount of Rab27a protein in both cytosolic and pellet fractions analysed reminiscent of the CHM KO phenotype (lanes 1 and 2 respectively in Figure 68A). Excitingly, when one compares the pellet and cytosolic fractions of transfected human KO cells, a clear reduction of Rab27a protein levels is observed in the cytosolic fraction (lanes 3 and 4 respectively in Figure 68A). Similarly reduced levels of Rab27a protein are also observed when comparing the pellet and cytosolic fractions of transfected mouse Flox, Cre+ (+TM dosed) KO cells (lanes 5 and 6 respectively in Figure 68B).

Both these shifts in the cytosolic fraction of Rab27a protein expression shows that Rab27a is able to be correctly prenylated in these cells following the transfection of pCAG-REP1 plasmid. Hence within these cells, Rab27a protein is able to be correctly targeted to intracellular membranes and in turn the phenotypic (functional) rescue of this protein is observed.
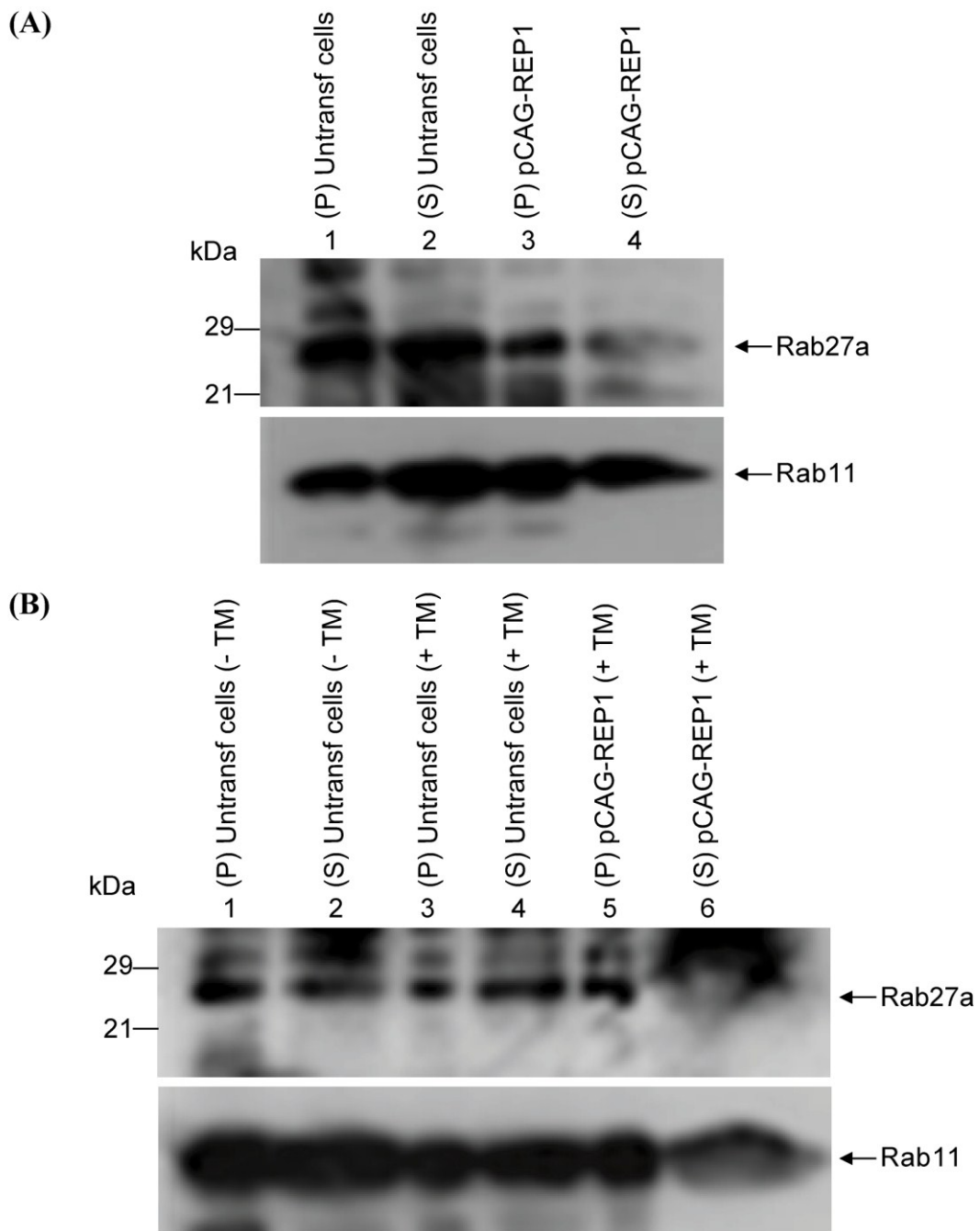
Figure 68: Western analysis showing the phenotypic rescue of Rab27a protein function in CHM KO cells transfected with pCAG-REP1 vector

Total protein lysates were isolated from (A) Human (CHM4 cell line) and (B) Mouse (Chm^Flox+ Cre+ TM+) cells 6 weeks following AMAXA transfection with pCAG-REP1 vector (corresponding to transfection with programmes P32 and Q32 for human and mouse cells respectively). Lysates (25 μg) were subjected to subcellular fractionation, where soluble (S) and pellet (P) fractions were analysed by Western analysis and probed with anti-Rab27a antibody 4B12. Untransfected human cells (lanes 1 and 2) as well as untransfected mouse cells (- TM and +TM lanes 1-2 and 3-4 respectively) were used as a control for the subcellular fractionation. Rab11 was used as a loading control. +TM= Treatment with tamoxifen (TM). Results are representative of one experiment.

In conclusion after the 6 weeks of cultivation and long-term analysis of pCAG-REP1 vector in CHM KO cells, it is clear that pCAG-REP1 was not only able to maintained active transcription of the REP1 gene in wild-type cells, but also in human and mouse CHM KO cells. Indeed REP1 protein and mRNA levels as well as pCAG-REP1 pDNA levels remained stable during this period as analysed by Western blot, PCR and rt-PCR analysis. Furthermore pCAG-REP1 vector was also able to maintain itself as an active episome, as shown by plasmid rescue experiments. Despite both mouse and human KO cells only expressing moderate levels of REP1 protein (~ 20% transfection efficiency at 6 weeks post transfection), we were able to show the correction of the CHM phenotype. Specifically we observed considerable correction of the Rab27a prenylation defect in these cells following the transfection of pCAG-REP1 plasmid.

3.3 Optimisation of EGFP and Luc plasmid delivery in vivo

During the period of vector cloning and optimisation we were also able to obtain an S/MAR plasmid vector containing the *Luciferase* gene driven by either the Ubiquitin-C, cytomegalovirus (CMV) or cytomegalovirus (CMV) early enhancer/chicken beta actin (CAG) promoter from Professor Hans Lipps, University of Witten, Germany, pUbiqC-Luc, pEPI-Luc and pCAG-Luc plasmids respectively. All plasmids were based on the pEPI-EGFP plasmid, hence there was either an Ubiquitin-C or CAG promoter inserted in place of the CMV promoter upstream of the S/MAR region followed by a *luciferase* transgene instead of the *EGFP* transgene.

While the two plasmids pCAG-Luc and pCAG-EGFP are comparable, both plasmids were used for *in vivo* experiments to infer results that complemented one another. Hence for monitoring of long-term transgene expression within the same mouse it was deemed that the luciferase expressing plasmid pCAG-Luc would be most appropriate. This was because bioluminescent imaging of the same mouse could be done non-invasively as described previously for many organs within the mouse including the eye (Chalberg, Genise et al. 2005). Similarly the *EGFP* expressing plasmid pCAG-EGFP would be most appropriate where histological analysis of *EGFP* transgene expression within the retina could be done. This was because standardised protocols have been established within our laboratory for *EGFP* expressing viral vectors (Tolmachova, Wavre-Shapton et al. 2010). Furthermore one could also draw upon experimental outcomes of the pCAG-EGFP and pEFS-EGFP plasmids as they both possessed similar plasmid backbones to the pCAG-REP1 plasmid. Hence any limitations or successes of either plasmid *in vivo* in WT mice could be corroborated and one could assume a similar fate for the pCAG-REP1 plasmid *in vivo* in WT and CHM mice.

The pUbiqC-Luc plasmid also offered us the opportunity to test an additional plasmid harbouring a ubiquitously expressing mammalian/eukaryotic promoter *in vivo.* This allows us to draw upon the possibility of differences in transgene expression levels between commonly used ubiquitous eukaryotic/mammalian promoters. Such promoters included the elongation factor-1 short (EFS) and UbiqC – as well as promoters of a viral origin – including immediate early cytomegalovirus (CMV) and CAG.

Previously, Argyros *et al.* in 2008 found that the long-term luciferase transgene expression of an S/MAR plasmid *in vivo* was due to the synergy between a tissue specific promoter (alpha-1 antitrypsin - AAT) and the S/MAR element (Argyros, Wong et al. 2008). We were interested to see if this synergistic effect was exclusive to tissue specific promoters or indeed non-tissue specific promoters could also yield such long-term expression levels *in vivo.*

3.3.1 Injection strategy for gene delivery to the eye – Subretinal injections

Within the eye one of the most appropriate delivery routes to the RPE and photoreceptor cells is arguably through subretinal injections; whereby vector suspensions are placed in the (potential) space/plasma membrane between the photoreceptors and RPE cells. While this technique has been successfully employed for delivery in numerous animal models of ocular diseases (Liu,Tuo et al. 2011), the actual procedure within the literature remains varied. Numerous approaches have been described including injections via a transcorneal/ transvitreal route (Timmers, Zhang et al. 2001; Johnson, Berglin et al. 2008), transscleral route (Price, Turner et al. 1987) as well as transscleral-transchoroidal-Bruch's membrane route (Gekeler, Kobuch et al. 2004; Gerding 2007).

During our initial experimental set up for our *in vivo* subretinal injections (in WT/MF1 mice), we developed an optimised and improved method. We found this method the most consistent; whereby we standardized the method of Timmers *et al* as well as Johnson *et al* (Timmers, Zhang et al. 2001; Johnson, Berglin et al. 2008). Figure 69 shows images of the single as well as double subretinal injection technique. A video of the single surgical procedure is also submitted with this study (found on the back cover of this thesis). Throughout the results injections in the C57BL/6 mouse strain were initially performed by Dr Tanya Tolmachova; however some injections were also performed by Dr Mariya Moosajee. While all MF1 and CHM mouse injections were performed by Dr Mariya Moosajee.
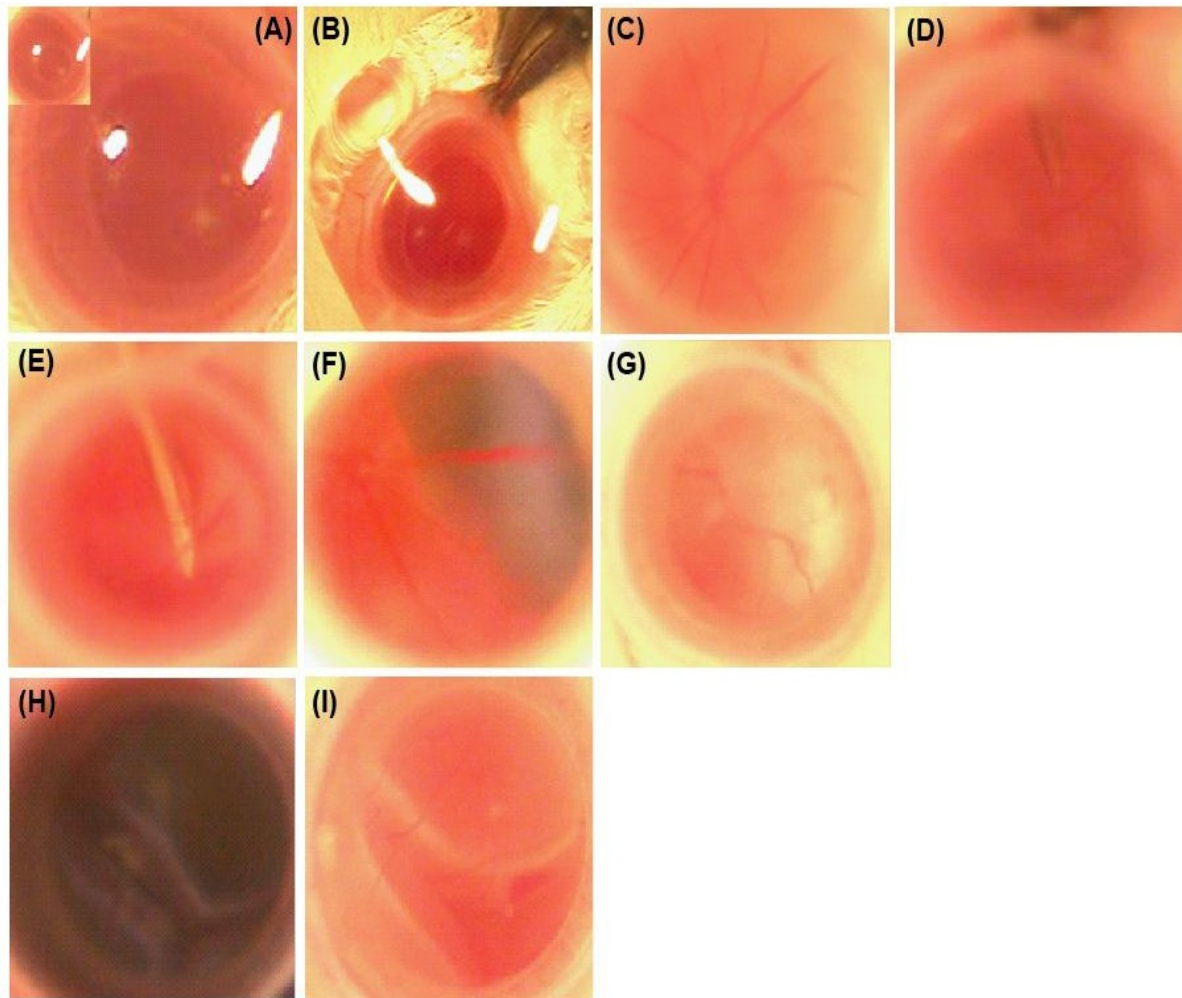
Figure 69: Illustrations of the subretinal injection procedure/technique

Illustrated above are representative pictures (as well as accompanying videos) of the single and double subretinal injections carried out in MF1 mice. Mice were anesthetized and the subretinal injections were performed using a dissecting microscope. (A) The pupil was dilated with tropicamide. Inset shows the pupil prior to dilation. (B) A drop of VidisicR carbomer eye gel was place on the eye and (C) a microscope coverslip was placed onto the gel such that the fundus including its blood vessels were readily seen and examined. (D) The limbus of the eye was grasped gently with forceps and a 33 gauge bevelled needle was used to cut through the cornea near the limbus. This panel shows the positioning of the 33 gauge needle in the centre of the anterior chamber. (E) The needle tip was then advanced to the retina opposite the puncture site where it penetrates the neural retina into the subretinal space. (F) The needle was removed after the injection procedure and the fundus was examined immediately following the subretinal injection. For illustrative purposes a blue dye was used to subretinally inject into the retina and the fundus image clearly show the presence of a single bleb or (G) using the same technique a picture of a single bleb following injection of formulated pDNA is also shown. The mouse was also injected again at the opposite site of the first injection; representative fundus images illustrating the presence of two blebs following the double subretinal injection of (H) blue dye and (I) pDNA are also shown. The imaged mouse eyes are approximately 3 mm in diameter. Blood vessels and fundus images are seen clearer on digital images.

3.3.1.1 Signs of a successful procedure

One of the easiest and quickest methods employed to monitor a successful subretinal injection procedure was the careful fundus examination directly through a dissecting microscope. This was done prior to the start of the injection procedure, to monitor any abnormalities within the retina but more importantly the fundus of all the mice was also evaluated immediately following the injection. The presence of a clear single or double bleb underlying the neural retina was often the best indication of a successful single or double subretinal injection. The presence of a clear bleb showed that the injected formulated pDNA had successfully inflated the subretinal space as well as showing that the pDNA was confined within this region of the eye. Mice which did not observed a clear bleb where not included in any experimental groups, and were often observed to have a damaged retina either prior to the injection procedure due to a genetic abnormality or through a complication during the actual procedure. All blebs raised by injection into the subretinal space regressed with 24-48 hours following injection. As a result of the method of anaesthesias employed during the injection procedure (injectable anaesthesia as opposed to inhalation anaesthesia), mice were observed to be more prone to bleeding (personal observations when comparing procedure outcomes using the different anaesthesias above). Hence where the bleeding in the retina was confined to the small site of needle insertion, these mice were still classed as a successful and included within experiments. However when the bleeding was more comprehensive - spanning into the vitreous body - or if the lens was nicked during the injection procedure, these mice were not included in experimental groups.

3.3.1.2 Potential problems during the procedure

While the video (accompanying this thesis) and illustrations in Figure 69 highlight the successes and correct technique used for the subretinal injection procedure, a number of potential problems were also encountered during the optimisation process. The common problems we met are highlighted within Table 3 where potential solutions and approaches we employed to combat these problems are also shown.

Table 3: Potential problems associated with the subretinal injection procedure.
The table below summarises the main problems encountered during the optimisation process and techniques developed for the subretinal injection of the adult mouse eye.

Problem	Potential causes	Potential solutions
Difficulty with injection procedure	-Technically demanding procedure to achieve alone – positioning needle accurately & stably in retina while pressing down on the syringe to release the delivery solution into the subretinal space, without moving the needle out of position	-Needle mounted onto tubing to allow surgeon to advance it into place & assistant to inject the correct amount of material from the syringe when surgeon ready – minimised movement & damage -Purchase of a foot-pedal operated microinjector pump
Haemorrhage or significant blood in the eye	- Blunt needle used during the procedure - retina nicked causing a hole in the retina - In house sharp needles were made. While tips were sharp, they were also fragile & prone to bending after a few injections	- Needles were monitored before injection & discarded if sharpness was compromised - Sharp custom ordered needles were purchased from Hamilton insuring tips were equally sharp & had standardised bevels
Limited blood in the eye	- Needle penetrated through the retina into the choroid - Ciliary body nicked	- Advance the needle less into the retina - Inject closer to the lens
No clear bleb observed	- Needle did not penetrate correctly -injected material leaked into the vitreous - Retina was torn during the insertion of the needle	- Advance the needle tip further into the retina before injecting the material - Penetrate in a single motion without moving once in place
Bleb poorly inflated or becomes deflated	- Fluid in the subretinal space leaked into the vitreous - Volume injected too high causing leakage into vitreous - Fluid in subretinal space leaked out through the first injection site	- Hold needle in place for 5 sec after injection so pressure equilibrium reached in retina - Inject a maximum of 2 µl per eye, <2 µl if mouse is small - Ensure the two injection sites are far enough apart
Air bubbles	- Injection tubing or solutions not efficiently degassed	- Spin prior to loading syringe - Prime tubing & syringe with water before loading material
Lens cloudy	- Lens nicked	- Avoid the lens
Cornea cloudy	- Cornea was not kept moist during the procedure	- Apply lubrication to eye between anaesthesia as well as before & after injection

3.3.2 Optimisation of luciferase expression in the eye using the bioluminescent technique

The cationic polymer polyethylenimine (PEI) has been successfully used for the complexation of pDNA and has been shown to efficiently condense pDNA (Dunlap, Maggiet al. 1997). Specifically it has been used as a gene transfer agent (GTA) in cell culture as well as *in vivo* using *in vivo*-jetPEI in a wide variety of tissues including the retina (Liao and Yau 2007; Boussif, Lezoualc'h et al. 1995). Hence once the procedure for subretinal injections was standardised within the mouse retina, the next stage involved the optimisation of complexed pDNA with PEI (PEI/DNA) *in vivo* and the efficient delivery of complexes into the retina.

The amount of *in vivo*-jetPEI one can use to form a stable cationic complex between itself and pDNA is determined by the N/P ratio. This is a measure of the ionic balance of complexes; i.e. the number of nitrogen residues of *in vivo*-jetPEI per phosphate in the nucleic acid/DNA. Previously DNA/PEI polyplexes of varying N/P ratio from 8 and 10 have been successfully used for gene transfer *in vivo.* This includes delivery via systemic gene transfer in neonatal mice and subsequent transfection in the spleen, liver, lung, heart, brain and kidney (Wong, Argyros et al. 2011) as well as transfection of ganglion cells within the eye following intravitreal injections in adult mice (Liao and Yau et al 2007). Furthermore DNA/PEI polyplexes were also used to aid transfection *in vitro* in human corneal epithelial cells (HCE) (Hornof, Fuente et al. 2008). Despite these studies, to date and to the best of our knowledge, subretinal injection of PEI/DNA (or PEI/S/MAR pDNA) to the adult mouse retina has not been previously reported using non-viral vectors. Hence to comprehensively optimise the expression of pDNA within the retina using *in vivo*-jetPEI, various N/P ratios of PEI/DNA were examined.

The luciferase expressing plasmid pCAG-Luc was complexed (30 μg) with *in vivo*-jetPEI at N/P ratios varying from 5-9 (based on the manufacturers recommendations for *in vivo* experiments ranging between N/P ratios 6-8), in a 30 μl volume of sterile 5% isotonic glucose solution. The PEI/DNA polyplexes were then separately injected (2 μl) into the retina of MF1 mice following a single subretinal injection (1 μg of PEI:pCAG-Luc delivered to the retina). Luciferase activity in retinal samples was determined 48 hours post injection using a

luminometer. Untreated retinas were included as a negative control to determine the background levels of luciferase expression in the retina. Results from this experiment are shown in Figure 70.

Luciferase expression from all N/P ratios analysed showed substantially higher levels of luciferase expression when compared to control uninjected retinas. This indicates the successful transduction of the retina (at 48 hours) following subretinal injections in MF1 mice. Indeed the success rate of luciferase transduction - irrespective of the N/P ratio used - and in turn success rate of the subretinal injection technique was approximately 70% across all the groups analysed. Optimal levels of luciferase expression were observed for N/P 8 injected retinas (3299 ± 37.69 µg/protein). Levels of luciferase expression were approximately 73% and 65% lower in N/P 5 (887 ± 82.29 µg/protein) and 6 (1160 ± 196.11 µg/protein) injected retinas respectively, when compared to N/P 8 retinas ($p<0.0001$ and $p<0.001$ respectively). In comparison levels of luciferase expression in N/P 7 and 9 injected retinas were more similar to one another (2048 ± 140.13 µg/protein and 2141 ± 82.77 µg/protein respectively); however expression was still approximately 38% and 35% lower respectively when compared to N/P 8 retinas ($p<0.05$).
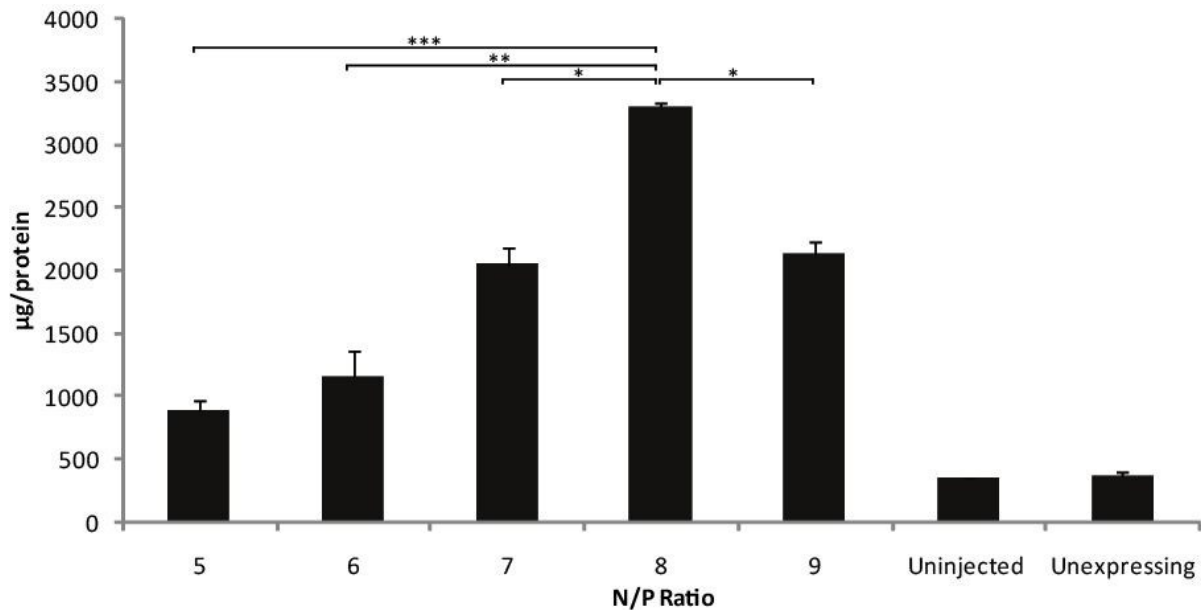
Figure 70: Evaluation of the optimal luciferase expression within the retina 48 hours following single subretinal injections of PEI/pDNA polyplexes of varying N/P ratios

Plasmid DNA pCAG-Luc (30 µg) was complexed with polyethylenimine (PEI) (PEI:pCAG-Luc) at varying N/P ratios of polyplexes (N/P 5-9), and 2 µl (1 µg) of each formulation was subretinally injected into the retina of MF1 mice. Retinal homogenates were subsequently lysed and analysed using a luminometer 48 hours following injection. The bar chart illustrates the quantification of luciferase expression represented as µg/protein. Optimal expression was observed in the following order of highest expression: N/P 8, 9, 7, 6 and finally 5 (3299 ± 37.69, 2141 ± 82.77, 2048 ± 140.13, 1160 ± 196.11 and 887 ± 82.29 µg/protein respectively). Uninjected retinas as well as retinas from mice not expressing luciferase were used as negative controls. *, ** and *** represent statistical significance compared to N/P 8 injected retinas with $P<0.05$, $P<0.001$ or $P<0.0001$ respectively, Student's t test. Results are mean values from four to eight independent experiments. Error bars represent the standard error of the means (s.e.m.).

We were also eager to investigate the optimal S/MAR pDNA vector that expressed the highest levels of *Luciferase* transgene within the retina following subretinal injections of formulated PEI:DNA/ S/MAR polyplexes. Hence we were interested in analysing and comparing the luciferase expression from pCAG-Luc pDNA with the expression from other S/MAR pDNA vectors containing the *Luciferase* gene driven by either the Ubiquitin-C or CMV promoter. To investigate this, *in vivo*-jetPEI was formulated with 30 µg of each plasmid pCAG-Luc, pUbiqC-Luc and pCMV-Luc, respectively, at an N/P 8 ratio, in a 30 µl volume as described earlier, and separately injected into MF1 mice by a single subretinal injection (1

µg of each pDNA was delivered to the retina). Luciferase activity in retinal samples was determined 48 hours post injection as performed previously using a luminometer, where untreated retinas were included as a negative control. Luciferase expression results are shown in Figure 71.
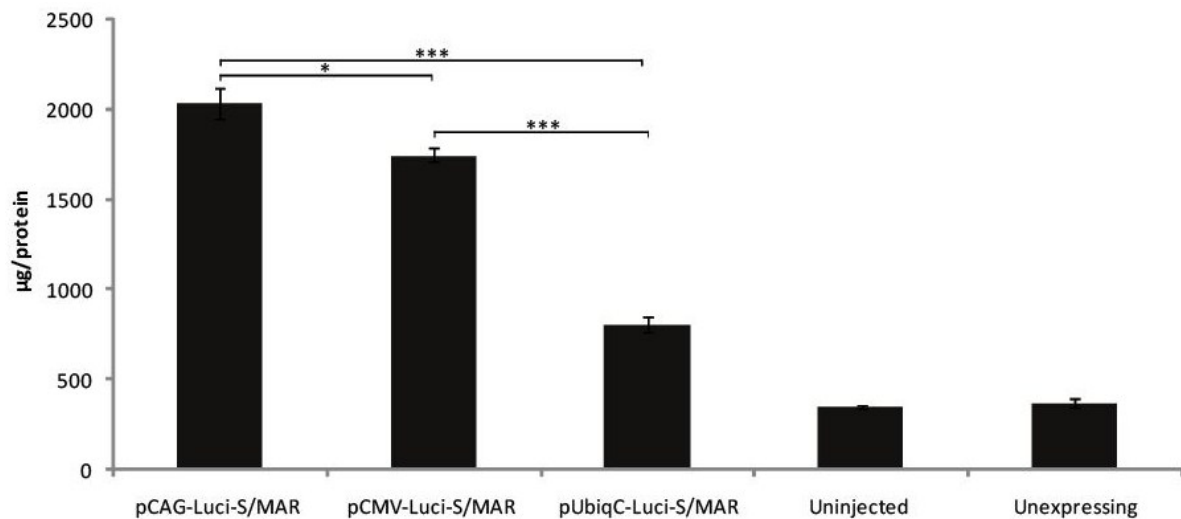
Figure 71: Evaluation of luciferase expression within the retina 48 hours following the single subretinal injection of pDNAs with various promoters - UbiqC, CMV and CAG – formulated with PEI

Plasmid DNA pCAG-Luci, pCMV-Luci or pUbiqC-Luci (30 µg) was complexed with PEI (N/P 8) and delivered to the retina of MF1 mice following a single subretinal injection (2 µl / 1 µg per eye). Retinal homogenates were subsequently lysed and analysed using a luminometer 48 hours following injection. The bar chart illustrates the quantification of luciferase expression represented as µg/protein. The highest levels of luciferase expression were observed in pCAG-Luc, then pCMV-Luc and finally pUbiqC-Luc injected retinas (2033 ± 88.6, 1746 ± 36.43 and 803 ± 42.61 µg/protein respectively). Uninjected retinas as well as retinas from mice not expressing luciferase were used as negative controls. The expression of luciferase within the retina is significantly different between pCAG-Luc and pCMV-Luc (* $p<0.05$, Student's *t* test) as well as being highly significantly different between pCAG-Luc and pUbiqC-Luc or pCMV-Luc and pUbiqC-Luc (*** $p<0.0001$, Student's *t* test). Results are mean values from four to five independent experiments. Error bars represent the s.e.m.

We observed that the levels of luciferase expression with all three pDNAs (pCAG-Luc, pCMV-Luc and pUbiqC-Luc) were clearly higher than the levels of uninjected control samples. Where mice were injected but not observed to be expressing luciferase, levels of expression were comparable to uninjected control samples. Furthermore the levels of luciferase expression between pCAG-Luc and pCMV-Luc injected retinas (2033 ± 88.6 and 1746 ± 36.43

µg/protein respectively) were the most similar where levels were approximately 14% lower in the pCMV-Luc injected retinas (803 ± 42.61 µg/protein) compared to pCAG-Luc injected retinas (p<0.05). In contrast, the luciferase expression from both pDNA (pCAG-Luc and pCMV-Luc) injected retinas was considerable higher than the pUbiqC-Luc injected retinas. Furthermore approximately 60% lower luciferase expression level was observed in pUbiqC-Luc injected retinas when compared to pCAG-Luc injected retinas (p<0.0001). Similarly 54% lower luciferase expression was observed when pUbiqC-Luc injected retinas were compared to pCMV-Luc injected retinas (p<0.0001). Hence the highest levels of luciferase expression were observed for formulated pDNAs in the following order: pCAG-Luc > pCMV-Luc > pUniqC-Luc.

3.3.3 Standardising the bioluminescent imaging technique for obtaining luciferase expression in the eye

To monitor the long-term expression of luciferase within the mouse eye, the *in vivo* bioluminescent imaging (BLI) technique was utilised. BLI is a highly sensitive technique which offers an invaluable approach to visualise, measure and monitor over a time course transgene expression *in vivo* of the same animal non-invasively. The mechanism of bioluminescence used for *in vivo* studies is based on the reaction which occurs when a luciferase substrate, such as luciferin, is oxidised by the enzyme luciferase, in the presence of oxygen, ATP and magnesium ions, to produce an oxidised substrate, such as oxyluciferin, and energy in the form of light as shown in Figure 72. This process is very different from fluorescence, where an external light is absorbed and then remitted at another wavelength. In contrast with BLI, there is no external light source to excite the chemical reaction; hence it has very low levels of background as well as the ability to detect weak signals with high sensitivity.
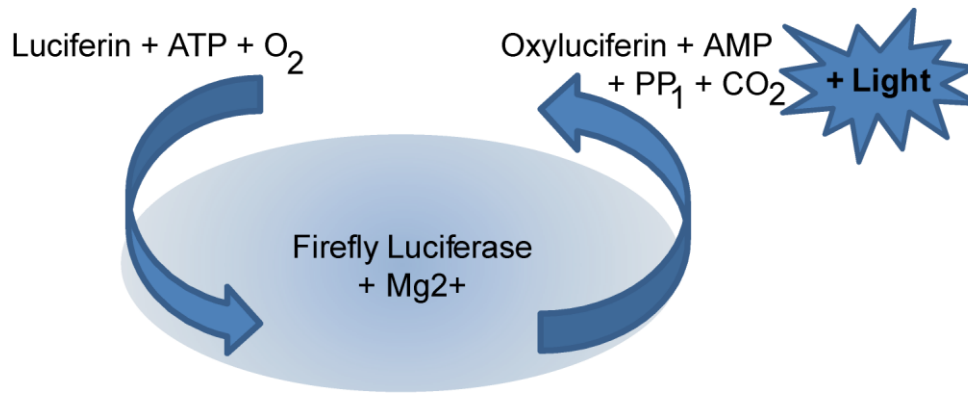
Figure 72: The mechanism of bioluminescence

The luciferin substrate is provided externally and is oxidised in the presence of oxygen and ATP by the luciferase protein produced from the plasmid DNA. This process results in the emission of light photons that are detected by a cooled charged coupled device (CCD) camera, as described in the text.

For *in vivo* studies in mice, in order to observe luciferase expression, the luciferase substrate D-luciferin is delivered intraperitoneally (i.p.) into mice and anesthetized animals are subsequently imaged for bioluminescence in a light-tight chamber by a cooled, charge-coupled device (CCD) camera.

In our studies, luciferase expression was monitored using Xenogen *Living Image* software that allows detection and quantification of expression level as photons/sec/cm^2/seradian (sr). This software is used broadly due to its simplicity in quantifying photons of light emitted and displaying the intensity of luciferase expression from high to low as red to purple (seen in Figure 73).

To obtain reproducible BLI data, we were initially required to standardise the imaging protocol we used in our mice following subretinal injections, including the delay between injections and imaging as well as the position of the mice during imaging. To optimise luciferase expression, we subretinally injected a standard luciferase expressing plasmid (pCAG-Luc) into the retina of an adult MF1 mouse. At 24 hours following injection, a dose of 300 µl D-luciferin (150 mg/ml) substrate was administered and mice were placed immediately onto the warm stage and monitored for expression every two minutes for up to 45 minutes after the delivery of luciferin. The results are shown in the Figure 73.
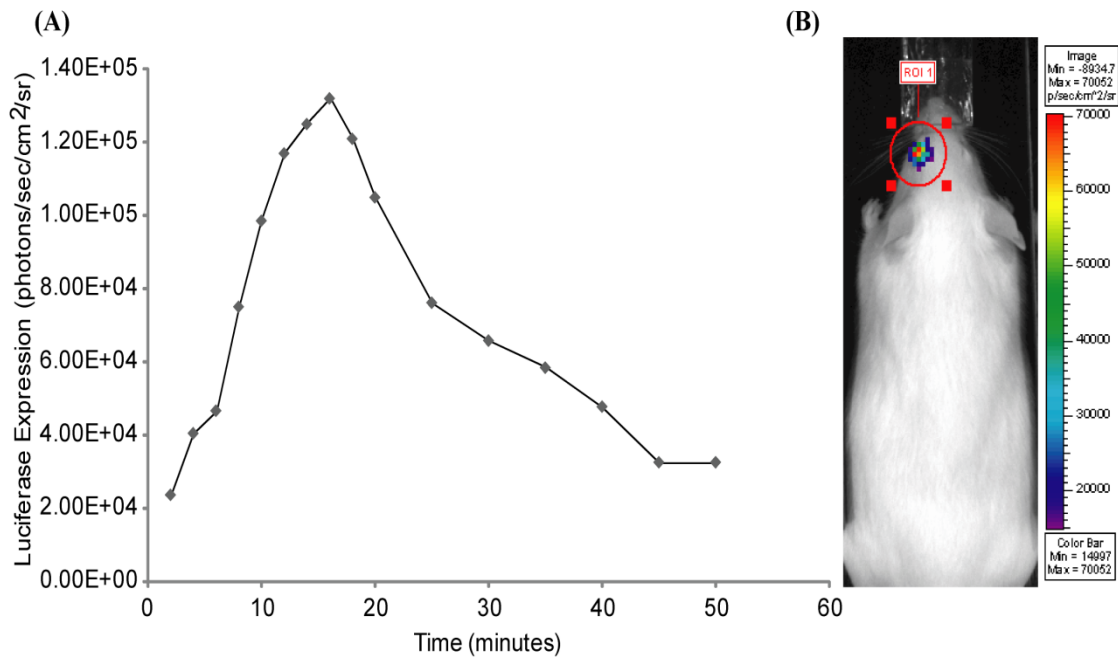
Figure 73: Investigating the maximal luciferase expression within the eye following subretinal injections

To determine the maximum luciferase activity in the eye, luciferin was administered i.p. to an MF1 mouse at 24 hours following the subretinal injection of formulated pCAG-Luc plasmid with PEI (30 µg DNA complexed with PEI (N/P 8)). Bioluminescence was measured every 2 minutes as described in the text and quantified using the Xenogen *Living Image* software (given as photons/sec/cm^2/sr). (A) The chart shows the luciferase activity against time after D-luciferin delivery. Maximum luciferase expression was observed between 14-18 minutes after i.p. delivery of Luciferin (n=1). (B) The picture shows the MF1 mouse expressing luciferase 24 hours after subretinal injection of formulated pCAG-Luc, with the red circle representing the region of interest and the area of measurement (seradian). The intensity of luciferase expression is shown from high to low (red to purple) as seen on the scale.

We observed maximum luciferase expression at approximately 14-18 minutes after D-luciferin administration. Furthermore the maximum expression was observed when mice where either laid on their front or the respected side that the eye had been injected on. Laying the mice on their backs sometimes caused the position of the retina to become obscured. Based on this study, we kept measurements under consistent conditions by monitoring luciferase expression at a constant between 14-18 minutes following injection of 300 µl D-luciferin (150 mg/ml) throughout the project to prevent any irregularities. Furthermore during the imaging process, mice were laid on the uninjected side, so that injected eyes were above the body, in order to maximise luciferase expression.

3.3.4   S/MARs provide long-term luciferase expression *in vivo* in the eye – BL6 mice

While injections and optimisation of the subretinal injection technique were performed in the MF1 mouse strain, we were also interested in performing a longitudinal study to measure the expression of luciferase from S/MAR containing pDNAs within the retina of the C57BL/6 mouse strain. This was the ultimate strain of interest as all CHM mouse strains were also on the C57BL/6 mouse background. Hence longitudinal expression of S/MAR pDNAs in the C57BL/6 mouse strain, following subretinal injections, could also imply that similar longitudinal *REP1* transgene expression were possible in the CHM mouse strains using pCAG-REP1 and/or pEFS-REP1 pDNAs.

As an initial experiment, we were interested in assessing the longitudinal expression of S/MAR pDNAs within the retina; hence we chose to use a luciferase expressing pDNA as the expression can be easily and non-invasively monitored long term. The pUbiqC-Luc pDNA as well as its control pUbiqC-Luc-Control pDNA without an S/MAR element was formulated with *in vivo*-jetPEI (N/P 8) as described earlier, and subretinally injected into the eyes of C57BL/6 mice. The longitudinal expression was then monitored at 48 hours and for a total of six months at regular intervals using the Xenogen *in vivo* bioluminometer. Longitudinal results from these mice are illustrated for both pUbiqC-Luc and as well pUbiqC-Luc-Control pDNA vectors. As a control, mice were also subretinally injected with pEPI-Luc and pEPI-Luc-Control (Figure 74A and B).
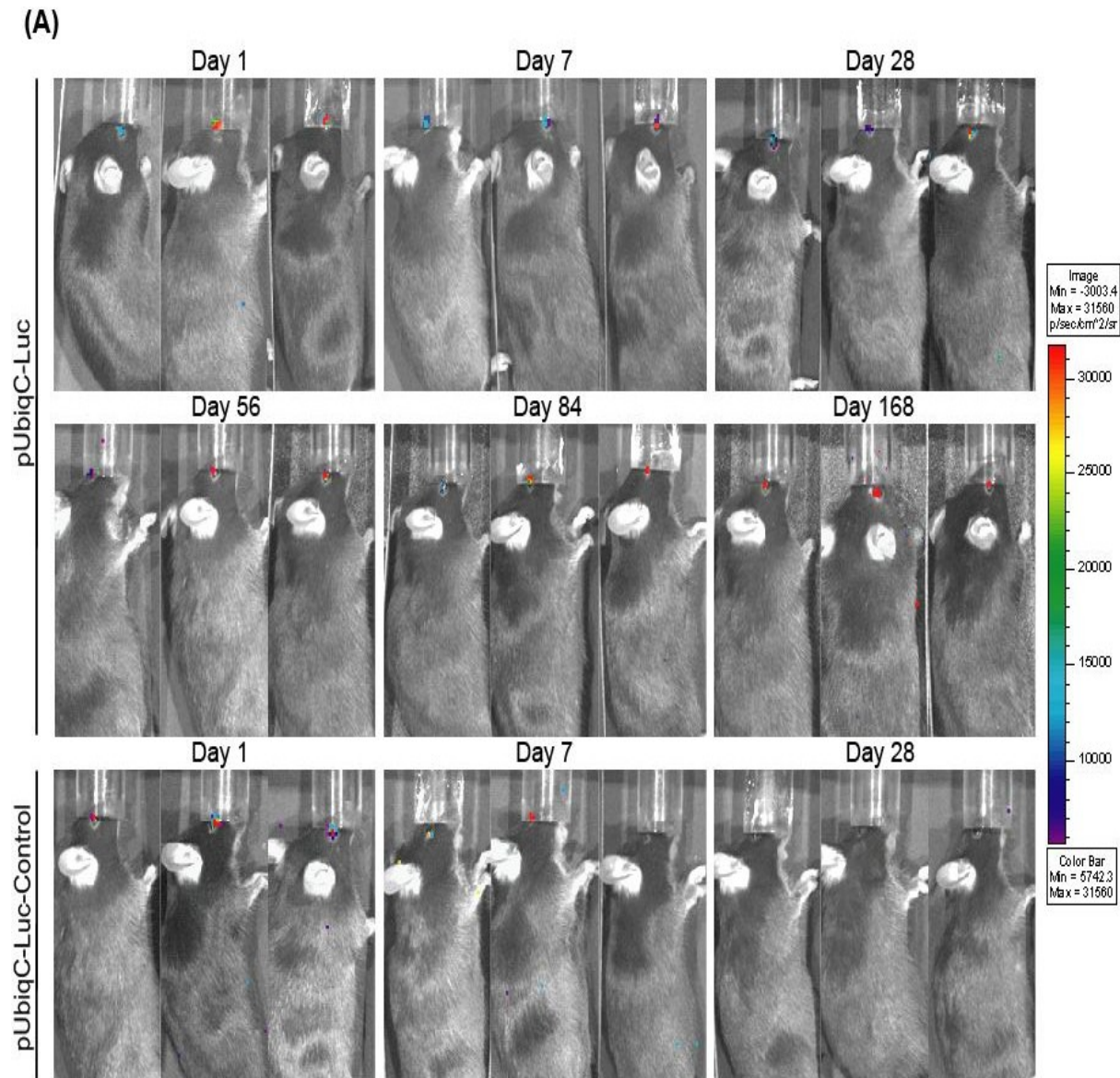
Figure 74: Illustration of luciferase (distribution and) expression in the eye following single subretinal injections in C57BL/6 mice over time

(A) Plasmid DNA pUbiqC-Luci, pUbiqC-Luci-Control, pEPI-Luc and pEPI-Luc-Control (30 μg) was complexed with PEI (N/P 8) and delivered to the retina of C57BL/6 mice following a single subretinal injection (1-2 μl / 0.5-1 μg per eye). All four groups of mice were visualised at regular intervals (from 48 hours post subretinal injection) using a Xenogen bioimager after intraperitoneal (i.p.) injection of D-Luciferin (15 mg/ml). High to low intensity of luciferase expression is graphically shown exclusively within the eye area by red to violet colouring. The colour bar indicates relative signal intensity (as photons/sec/cm^2/sr). The expression of luciferase from pUbiqC-Luc injected mice show prolonged expression of luciferase within the retina, while pUbiqC-Luc-Control injected mice also show loss of luciferase expression within a month of injection. Luciferase expression seen clearer on digital images.
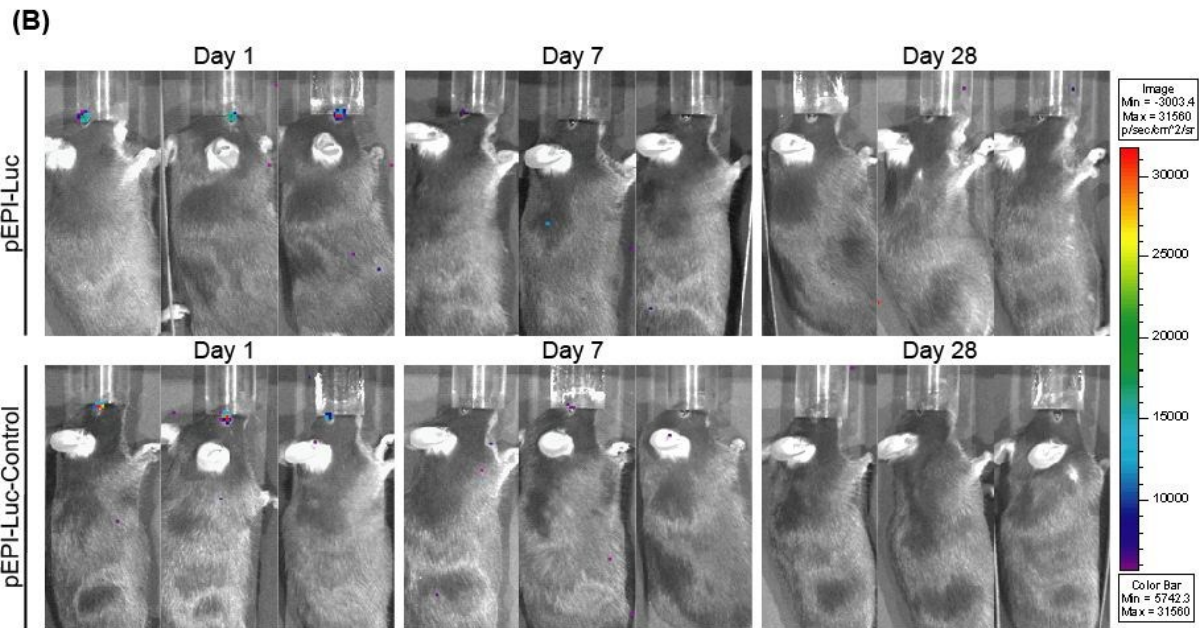
(B)

Figure 74: Illustration of luciferase (distribution and) expression in the eye following single subretinal injections in C57BL/6 mice over time

(B) The expression promoted by pEPI-Luc and pEPI-Luc-Control is initially considerably higher within the retina compared to all other groups of injected mice at one day post injection. However, importantly this level of expression drops precipitously over time whilst that driven by pUbiqC-Luc is maintained long-term. Thus the S/MAR element within this plasmid does not sustain pEPI-Luc expression in the retina.

All pDNA constructs were able to mediate high levels of *luciferase* transgene expression within the retina at 24 hours following subretinal injection. Importantly, no luciferase expression was detected outside of the retina. The highest levels of expression at this early time point were observed from the pEPI-Luc and pEPI-Luc-Control injected mice. Interestingly, thereafter, a rapid decline in transgene expression within the first week of injection brings the levels of luciferase from pEPI-Luc and its control to almost background levels (uninjected retinas). This rapid decline in expression is not surprising and has been observed previously within the retina when the CMV promoter is used. This is primarily due to this viral promoter often being subjected to substantial methylation and hence becomes switched off *in* vivo.

In contrast, while the expression from the pEPI-Luc plasmid was rapidly lost within the first week, the remaining non-S/MAR plasmid, pUbiqC-Luc-Control, did not show such an abrupt decline in expression immediately after injection. Instead a gradual decline was seen and by

1 month following subretinal injections, expression levels in this group had also dropped to background levels (uninjected retinas). Finally, pUbiqC-Luc injected mice were the only group to be able to mediate stable and persistent levels of transgene expression up to 6 months following a single subretinal injection. This shows that the absence of the S/MAR moiety causes a dramatic difference in expression levels between pUbiqC-Luc and pUbiqC-Luc-Control plasmids.

Importantly, this long term expression in C57BL/6 mice after a single subretinal injection of an S/MAR plasmid that contains a ubiquitously expressing promoter - pUbiqC-Luc - *in vivo* has never been shown before. This result arguable brings into question the synergy observed by Argyros et al. between plasmids containing tissue specific promoters and the S/MAR moiety to provide continuous levels of transgene expression *in vivo* (Argyros, Wong et al. 2008).

While luciferase expression was observed in all groups of C57BL/6 mice examined, expression levels were lower than previously published reports showing luciferase expression *in vivo* (Argyros, Wong et al. 2008). Hence we were unable to accurately quantify the luciferase expression (using the Xenogen Living Image software) observed in the mice examined in Figure 74 as levels appeared to be close to the limit for quantification. The combination of low luciferase expression as well as the fact that the C57BL/6 mouse strain is highly pigmented within the retina, may have contributed to the limitations of this mouse strain at this stage within our experimental optimisation.

3.3.4.1 S/MARs provide expression in the RPE cells of injected retina

While the distribution of luciferase within all subretinally injected mice appears to be limited primarily to the eyes - as seen by Figure 74 - we were also eager to analyse the specific tissue distribution of *luciferase* transgene expression within the eye by immunohistochemistry. Eyes were enucleated 1 week following the subretinal injection of pUbiqC-Luc, where mice were shown to be expressing luciferase by imaging on the Xenogen bioimager prior to enucleating. This length of time allowed the bleb within the retina to reabsorb and the neural retina to re-attach to the RPE layer. Both paraffin-imbedded as well as frozen sections were collected and stained for luciferase detection using a rabbit

monoclonal luciferase antibody (Santa Cruz). While all mice prior to histology analysis showed clear luciferase expression when imaged on the Xenogen *in vivo* bioluminometer, no luciferase positive staining was observed in any sections analysed by immunohistochemistry (data not shown).

In a similar approach, C57BL/6 mice were also subretinally injected with pEFS-EGFP plasmid. At 1 week post injection, frozen as well as paraffin-imbedded sections were also analysed by immunohistochemistry detection of EGFP using a rabbit polyclonal EGFP primary antibody (Abcam). Similar to the luciferase immunohistochemistry analysis, no difference in the expression of EGFP was seen between the analysed injected and control sections (data not shown).

One possible explanation for the difficulties in *luciferase* and *EGFP* transgene detection could be due to the highly pigmented retina of the C57BL/6 mice, particularly within the RPE cell layer. Furthermore, as luciferase expression was observed prior to sample histological analysis (on the Xenogen bioimager), it appears the difficulty of luciferase detection may also have been accentuated due to the fact that the expression levels of luciferase from the pUbiqC-Luc plasmid were too low to observe on histological sections. Indeed, in Figure 71 we showed that in the three plasmids analysed within the retina, expression levels of luciferase from the pUbiqC-Luc plasmid - while higher than control uninjected samples - was significantly lower than pCAG-Luc or pCMV-Luc injected retinas. One could speculate that perhaps the same could be true for the pEFS-EGFP plasmid and that low EGFP expression levels from the EFS promoter are not sufficient enough to be observed using immunohistochemistry.

As an alternative more sensitive strategy for the detection of the *EGFP* transgene in the C57BL/6 mice, RPE cells were isolated from the retinas of 10 mice subretinally injected with pEFS-EGFP plasmid as described in the methods. Briefly, eyes were enucleated 1 week following injection of pEFS-EGFP and incubated with Papain solution (1 U) (Sigma), where patches of RPE cells were manually removed with pulses of growth media. As a positive control isolated RPE cells were also analysed from mice 1 month post subretinal injection with Lentivirus pWPT-EGFP (positive samples provided by Dr Tanya Tolmachova), while uninjected RPE cells were used as a negative control. All isolated RPE cells were

subsequently analysed by FACS analysis for EGFP expression. For FACS analysis, cells in each sample were plotted according to side-scatter (SSC-H) - which is a rough measure of cell complexity/granularity - as well as fluorescence in the FL-1 channel – which indicates the level of EGFP fluorescence. We observed low but noticeable levels of EGFP in RPE cells isolated from pEFS-EGFP mice eyes when compared to RPE cells from control uninjected eyes, 6.9% and 1% respectively, as shown in Figure 75A and B. The RPE cells isolated from positive control pWPT-EGFP Lentiviral injected mouse eyes had 10.9% EGFP expression, as show in Figure 75C.

The same RPE cells as well as the neural retina isolated from the pEFS-EGFP injected and control uninjected mice were also lysed and subjected to Western blot analysis for EGFP protein expression. No EGFP protein expression was observed in the RPE cells as well as NR from the pEFS-EGFP injected retinas. These results further emphasise the importance of using a strong and highly expressing promoter in order to successfully monitor robust transgene expression levels *in vivo*.
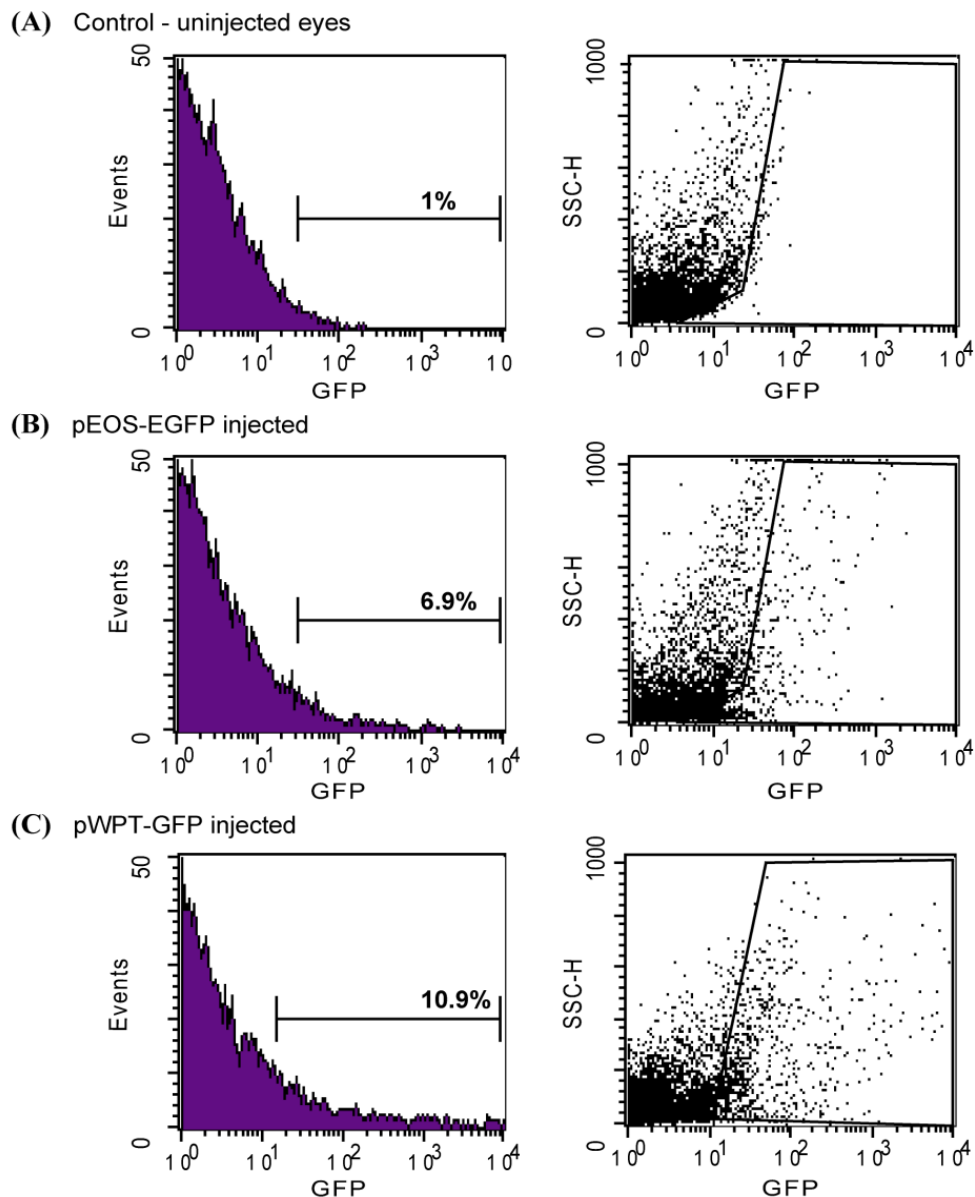
Figure 75: FACS analysis of EGFP expression in RPE cells isolated from pEFS-EGFP injected retinas of C57BL/6 mice 1 week post subretinal injection

The expression of EGFP observed by FACS analysis in RPE cells isolated from (A) Negative control – uninjected eyes, (B) pEFS-EGFP injected eyes (n=10)and (C) Positive control lentivirus pWPT-GFP injected eyes (positive samples provided by Dr Tanya Tolmachova at 1 month post injection). Levels of EGFP expression in isolated RPE cells from both pEFS-EGFP and positive control pWPT-GFP injected eyes both show similar levels of EGFP expression (6.9% and 10.9% respectively). In all cases, histograms (*left panel*) show measured events (*y axis*) against levels of EGFP fluorescence in the FL1-H channel (*x axis*). RPE cells are shown as a purple graph on the left side of all histogram, where gated cells expressing EGFP are expressed as a percentage (%) of the total untransfected population - a threshold of 1% untransfected RPE cells was always set - and appear above the bracketed histogram regions, to ensure that low-level positive events were also included. While all dot plots (*right panel)* show side-scatter (SSC-Height) which is a measure of complexity /granularity (*y axis*) against levels of EGFP fluorescence in the FL1-H channel (*x axis*). Each RPE cell analysed is shown as an individual dot on the plot, where untransfected RPE cells appear as a dense crescent on the left hand side of the plot. In contrast transfected cells from both vectors produce a smear across the plot and appear further to the right of each plot - showing higher levels of EGFP expression in these cells.

3.3.5   S/MARs provide long-term expression in vivo – MF1 mice

Due to the difficulties encountered with analysis of transgene expression in C57BL/6 mice, we decided to progress *in vivo* experiments using another WT mouse strain, MF1 mice. These mice have a normal retina with the exception that the RPE layer which is normally pigmented within the retina of C57BL/6 mice is unpigmented in MF1 mice. We hoped that by using this new mouse strain, we could observe expression within the retina and dissect better the pattern and distribution of expression from our S/MAR constructs.

In a similar experiment to the one carried out in C57BL/6 mice, we also assessed the longitudinal luciferase expression of a number of S/MAR plasmids including: pCAG-Luc, pCAG-Luc-Control, pUbiqC-Luc, pUbiqC-Luc-Control and pEPI-CMV pDNAs. Each of the pDNA expression systems under investigation was formulated with *in vivo*-jetPEI (N/P 8) as described earlier and separately administered to each group of mice by subretinal injection. As a control group, mice were also injected with naked pCAG-Luc (un-complexed). The longitudinal expression was followed up to 6 months (and one year for pCAG-Luc) post injection by *in vivo* bioluminescent imaging (BLI) (Figure 76 and Figure 77).
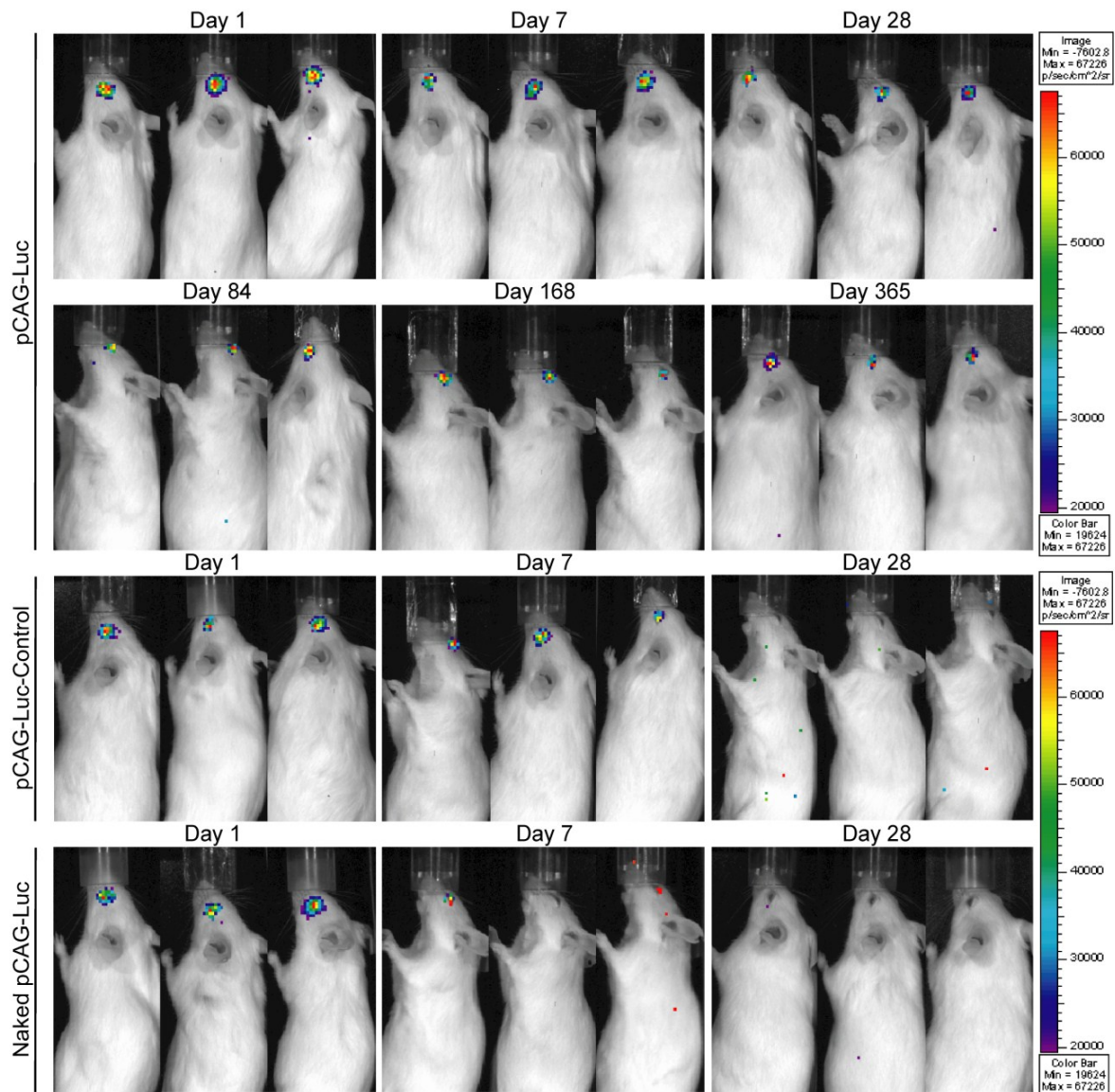
Figure 76: Illustration of luciferase (distribution and) expression in MF1 mice over time following single subretinal injections in the eye of PEI:pCAC-Luc, PEI:pCAG-Luc-Control and naked pCAG-Luc plasmid

Plasmid DNA pCAG-Luci and pCAG-Luci-Control (30 µg) was complexed with PEI (N/P 8) and delivered to the retina of MF1 mice following a single subretinal injection (2 µl / 1 µg per eye). A final group of mice where were also subretinally injected with un-complexed /naked pCAG-Luc pDNA. All mice were visualised at regular intervals (from 24 hours post subretinal injection) using a Xenogen bioimager after intraperitoneal injection of D-Luciferin (15 mg/ml). High to low intensity of luciferase expression is graphically shown exclusively within the eye area by red to violet colouring. The colour bar indicates relative signal intensity (as photons/sec/cm^2/sr). Initially, expression of luciferase is observed in all groups of mice analysed, however levels of expression are only short term in PEI:pCAG-Luc-Control as well as naked pCAG-Luc injected mice, where loss of expression is observed by 1 month and 1 week post injection respectively. In contrast PEI:pCAG-Luc injected mice (as well as PEI:pUbiqC-Luc injected mice – data not shown) have persistent luciferase expression within the retina up to 6 months and 1 year post injection. Luciferase expression seen clearer on digital images.
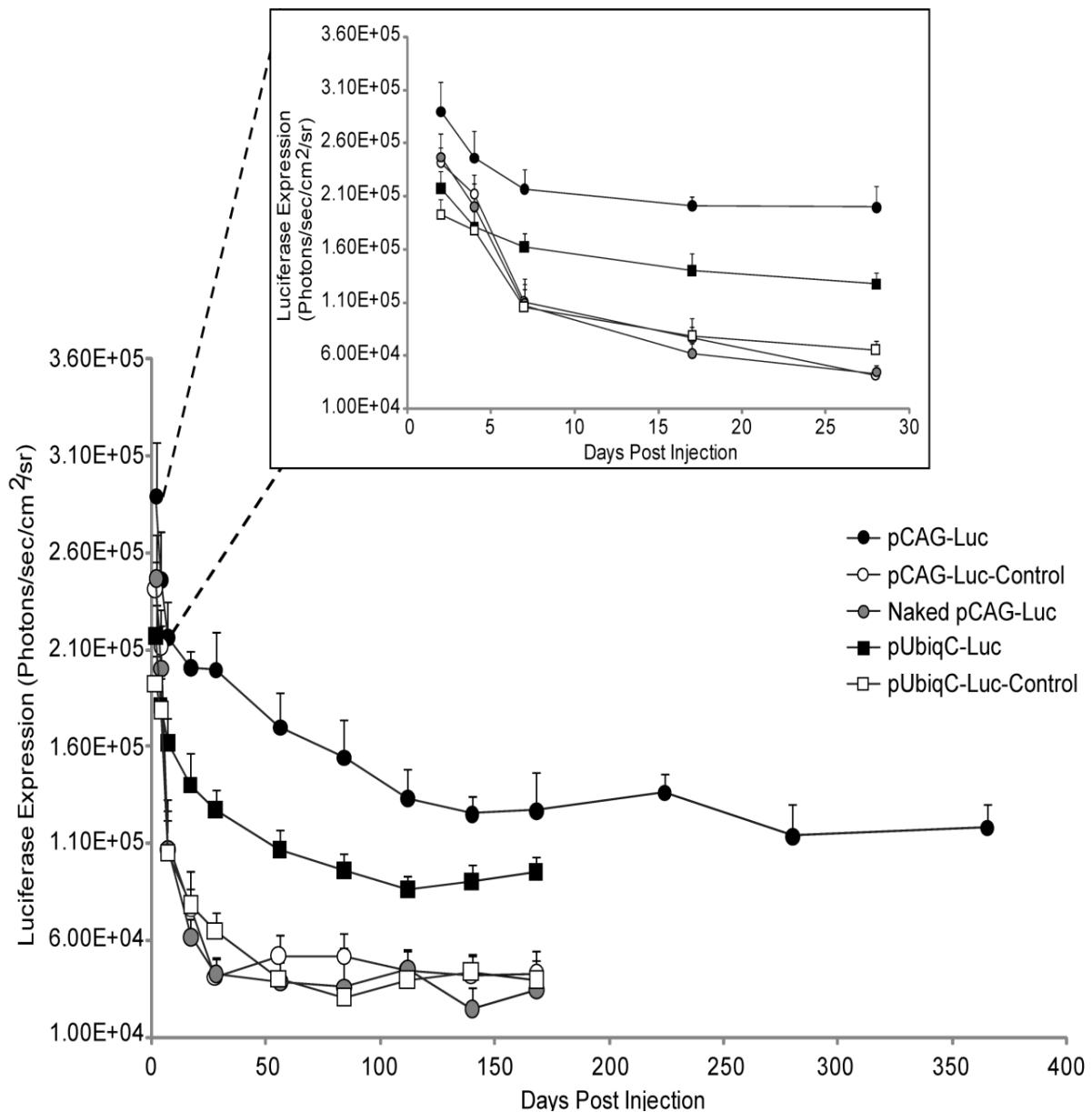
Figure 77: Long-term luciferase expression of formulated pUbiqC-Luc, pCAG-Luc, their control plasmids as well as naked pCAG-Luc

The figure shows the longitudinal luciferase expression up to 6 months and 1 year (for pCAG-Luc) following a single subretinal injection. Luciferase expression was measured using the Xenogen Living Image software and is represented as photons/sec/cm^2/sr. Only the formulated pUbiqC-Luc and pCAG-Luc plasmids are able to persistently express luciferase levels for up 6 months and 1 year respectively. Background levels of light emission from uninjected retinas is 2 x 10^4 photons/sec/cm^2/sr. Results are mean values from six to seven independent experiments (per group). Error bars represent the s.e.m.

One day after the subretinal injection of all five groups of MF1 mice, all plasmid constructs mediated high levels of luciferase expression. However a rapid decline in transgene expression was observed within the first few days following subretinal injections particularly in both control groups, pCAG-Luc-Control, pUbiqC-Luc-Control as well as naked un-complexed pCAG-Luc. While an abrupt decline in transgene expression was observed within a week following injection, expression levels of luciferase transgene were seen to reduce even further over time and we found these levels to decline to above baseline levels within one month post-injection ($p < 0.05$). In contrast, thereafter, we observed high levels of transgene expression mediated by the plasmids pCAG-Luc and pUbiqC-Luc in the retinas of injected mice over the 6 months and 1 year - for pCAG-Luc and pUbiqC-Luc respectively - period of this study ($p < 0.01$ on day 168 for pUbiqC-Luc and $p < 0.01$ on day 365 for pCAG-Luc).

By way of illustration, transgene levels after one month mediated by pCAG-Luc-Control, pUbiqC-Luc-Control as well as naked pCAG-Luc plasmids were all approximately 15-20% of those determined at 24 hours post injection. In contrast, transgene levels after one month mediated by pCAG-Luc and pUbiqC-Luc were still 70% and 60% of the levels determined 24 hours after injection. While a small decline in transgene levels were observed for both plasmids pCAG-Luc and pUbiqC-Luc over the first 100 days, which later stabilised, expression levels are still 5 times higher at 6 months post injection than that of the other plasmids at one week. This vast difference between the expression of pCAG-Luc and pUbiqC-Luc compared to their corresponding control plasmids, shows the importance of the S/MAR moiety in providing a continuous high level of transgene expression *in vivo* within the retina (as seen previously in Figure 74).

In a complimentary experiment, to further measure the kinetics of (short and long term) transgene expression *in vivo,* total DNA was isolated from retinal homogenates of MF1 mice at 1 week and 6 months post subretinal injection of formulated pEFS-EGFP, pCAG-EGFP and the corresponding control plasmids. Total retinal DNA was then analysed for the PCR detection of the appropriate pDNA (Figure 78). PCR analysis revealed the persistent expression of pEFS-EGFP and pCAG-EGFP pDNA within retinal homogenates up to 6 months post injection. Notably however, the expression of both controls, pEFS-EGFP-Control and pCAG-EGFP-Control, was transient and lost within the retina by 6 months post injection.To

further verify these PCR results, total RNA was also extracted from injected retinal homogenates at 1 and 6 months following injection and EGFP RNA levels were analysed in by rt-PCR analysis (Figure 79). Indeed EGFP mRNA transcript levels were undiminished from both groups of S/MAR pDNAs injected retinas, while control samples only showed transient EGFP RNA levels. Considered together, these results from the PCR as well as rt-PCR analyses are in good correspondence with the longitudinal luciferase expression analysis determined by in situ bioluminescent imaging (Figure 74, Figure 76 and Figure 77). As observed previously the long term expression of control non-S/MAR pDNAs were also lost in the retina following subretinal delivery (while in contrast long term expression of the same luciferase pDNAs containing an S/MAR moiety was seen).
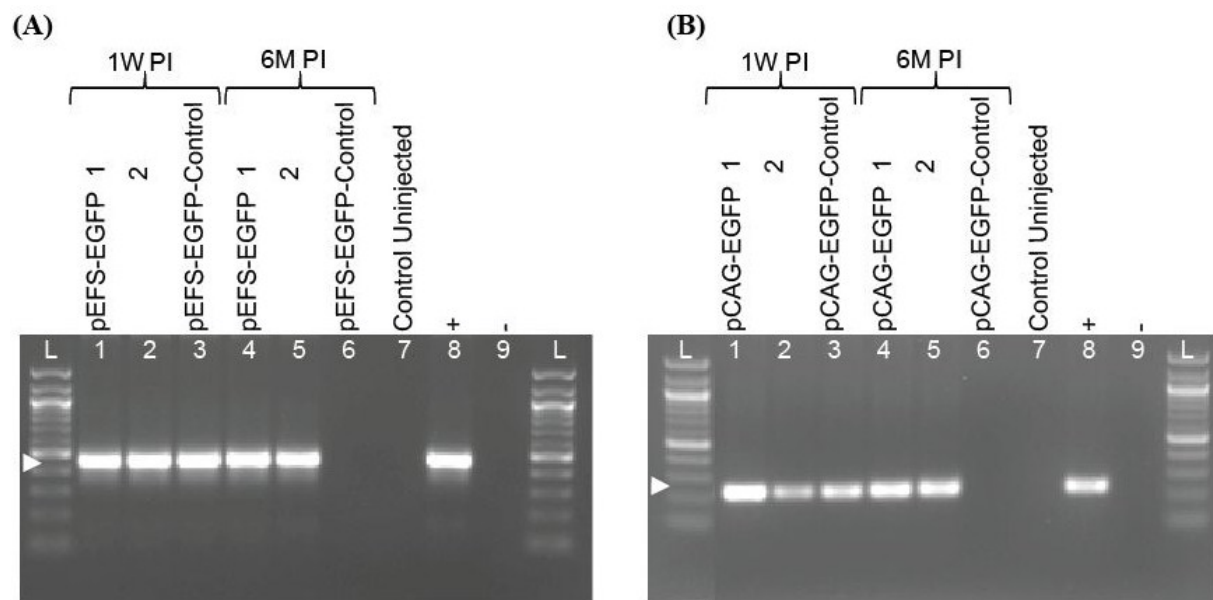
Figure 78: Short and long-term PCR detection of pEFS-EGFP and pCAG-EGFP pDNA vectors in eye homogenates following subretinal injections of WT MF1 mice

PCR analysis of formulated (A) pEFS-EGFP and pEFS-EGFP-Control and (B) pCAG-EGFP and pCAG-EGFP-Control pDNA vectors at 1 week (lanes 1-3) and 6 months (lanes 4-6) post injection (PI). PCR samples were separated by agarose gel electrophoresis and a positive PCR band was observed using EFS-EGFP or CAG-EGFP specific primer sets yielding a product size of 450 bp or 250 bp respectively. The arrowhead indicates the size corresponding to pDNA 450 bp on (A), 250 bp on (B). Uninjected eyes as well as no PCR product/water served as a negative control (lanes 7 and 9 respectively), while pDNA (25ng) pEFS-EGFP (in the case of A) or pCAG-EGFP (in the case of B) served as a positive control (lane 8) for the PCR reaction. Results are representative of three independent experiments. L= 100bp ladder (Invitrogen).
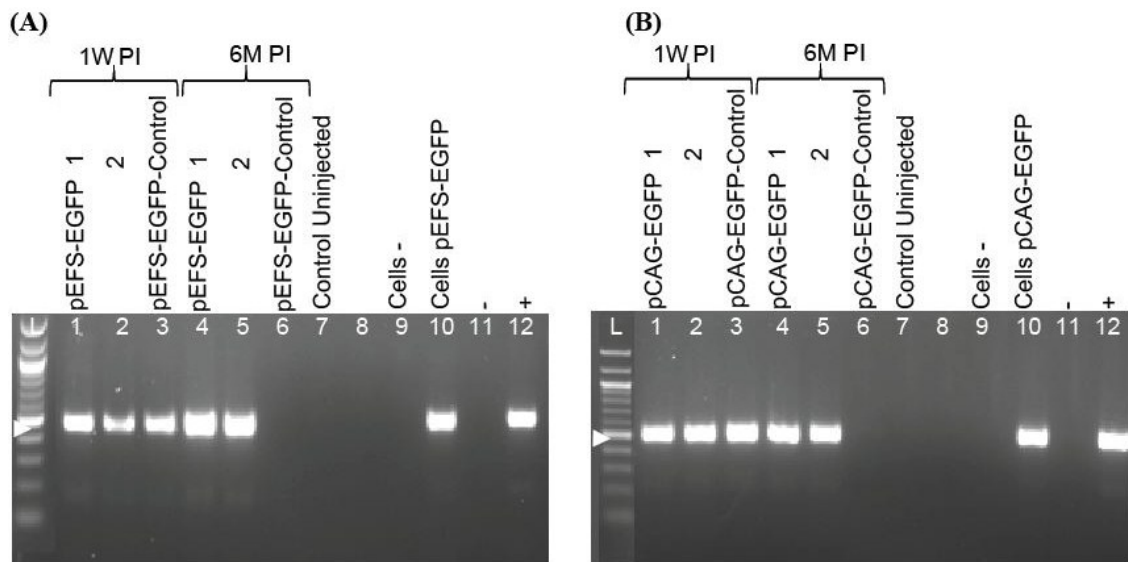
Figure 79: RT-PCR analysis of short and long-term EGFP mRNA from tissue homogenates following subretinal injections of WT MF1 mice with pEFS-EGFP and pCAG-EGFP pDNA vectors

Total RNA was extracted from MF1 mice following single subretinal injections of formulated (A) pEFS-EGFP and pEFS-EGFP-Control and (B) pCAG-EGFP and pCAG-EGFP-Control pDNA vectors at 1 week (lanes 1-3) and 6 months (lanes 4-6) post injection (PI). Total RNA was isolated and used to generate cDNA. PCR was performed with EGFP specific primers to yield a product size of 494 bp, as indicated by the arrowhead on (A) and (B). RNA from uninjected eyes, untransfected AtT20 cells, as well as no RNA product/water served as a negative control (lanes 7, 9 and 11), while AtT20 cells transfected with pEFS-EGFP (in the case of (A)) or pCAG-EGFP (in the case of (B)) served as a positive control (lane 10 and 12). Lane 8 is empty. Results are representative of three independent experiments. L= 100 bp ladder (Invitrogen).

3.3.6 Immunohistochemical detection of luciferase expressing cells in the retina

To analyse the tissue distribution of *luciferase* transgene expression within the eye as well as to localise the luciferase signal to a particular cell type, eyes were enucleated and paraffin-embedded sections were made and analysed by immunohistochemistry. At 1 week post injection, a significant amount of positive luciferase staining was observed in the RPE cell layer following transduction of pUbiqC-Luc pDNA (Figure 80). The presence of luciferase expression (within this retinal sample) is in agreement with the luciferase expression determined by *in situ* BLI analysis - prior to the sample being harvested (Figure 80A). In contrast, no staining was detected in the retinas of control uninjected samples which were incubated with primary and secondary antibody to determine the levels of background luciferase expression in retinal tissues (data not shown). Furthermore additional negative controls included pUbiqC-Luc injected retinal sections incubated without primary antibody and only secondary antibody to further analyse the level of background luciferase staining from the luciferase antibody (Figure 80D). The presence of luciferase expression within the RPE cells correlates with the positive EGFP staining of RPE cells isolated from pEFS-EGFP injected retinal samples (see Figure 75).
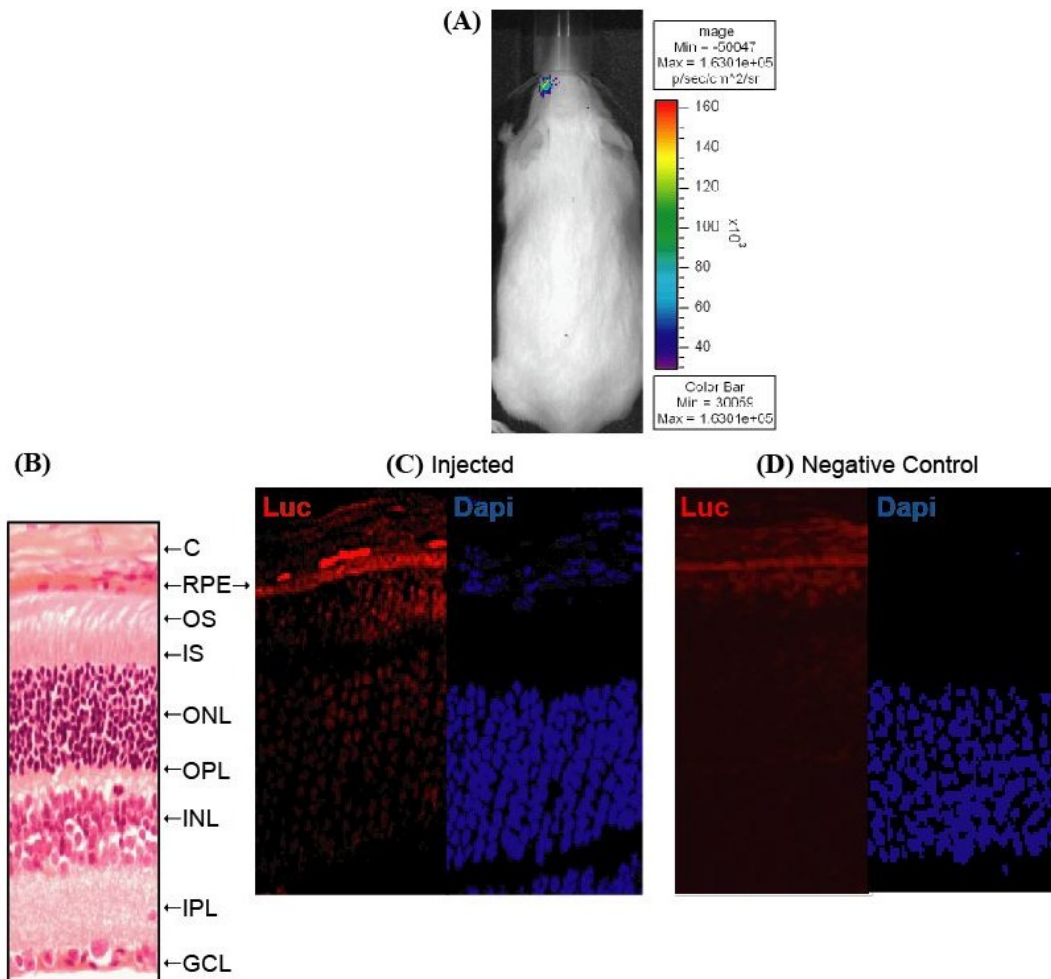
Figure 80: Immunohistochemistry analysis showing the (tissue) distribution of luciferase expression within retinal sections of a pUbiqC-Luc injected mouse retina following subretinal injection at 1 week post injection (single injection)

Luciferase expression from formulated pUbiqC-Luc (30 μg of pDNA, N/P 8) subretinally injected mouse as analysed by (A) *in situ* bioluminescent imaging (BLI). Mice were visualised at 1 week post injection (PI) using a Xenogen bioimager. The retina from the injected pUbiqC-Luc mouse was subsequently harvested and also analysed by immunohistochemistry. (B) H&E analysis reveals normal morphology of the injected eye. (C) Paraffin-embedded retinal sections were stained for luciferase expression (n=1); sections were probed with a rabbit monoclonal luciferase antibody (Santa Cruz), and a secondary Alexa 568. Nuclei were also stained blue using 4', 6-diamidino-2-phenylindole (DAPI). Luciferase expression (red) was observed within the RPE layer of injected eyes, (D) while no expression is observed in the negative control. Fluorescent (*left panel*) and Dapi images (*right*), at 40x magnification are shown. Negative controls included uninjected retinal sections with both primary and secondary antibody (data not shown) as well as positively expressing retinal section incubated with secondary antibody only.

C, choroid; RPE, retinal pigment epithelium; OS, photoreceptor outer segments; IS, photoreceptor inner segments; ONL, outer nuclear layer; OPL, outer plexiform layer; INL, inner nuclear layer; IPL, inner plexiform layer; GCL, ganglion cell layer.

3.3.7 Single vs Double Subretinal injections (-Tissue distribution)

The results presented thus far have shown promisingly that single subretinal injections provide sustainable levels of *EGFP* and *Luciferase* transgenes *in vivo* within the retina. While these results are novel and encouraging, one must also bear in mind that by delivering more pDNA into the subretinal space, one could also in theory provide higher levels of transgene expression within the retina. Indeed many gene therapy trials in mice to-date have involved the double subretinal injection of therapeutic genes into the subretinal space (where viral injections have shown considerable retinal transduction). Such double injections result in half the retina being transduced from the first injection, the mouse is then injected again at another site within the retina – usually opposite the original site, hoping to transduce the remaining half of the retina and maximising transduction. Hence single and double injections allow the required injected material to be placed between the photoreceptors and RPE cells, this causes a retinal bleb between the two layers leading to potentially around half or the entire area of the retina to be reached and in turn transduced. Importantly, further repeat injections, can have incremental risks within the mouse retina, and will undoubtedly not be well tolerated by the mouse eye, where the eye would no longer be able to regress back on itself and hence cause irreparable damage. We were interested in analysing if a similar difference in transduction of the mouse retina could also be observed following the single and double subretinal injections of formulated non-viral S/MAR pDNA.

Mice were injected either by single or double subretinal injection of formulated pCAG-Luc (30 μg of pDNA, N/P 8, 1 μg/2 μl in total per eye) as described earlier. The luciferase expression in retinal samples was determined 48 hours post injection using a luminometer. The comparison of luciferase expression from this experiment is shown in Figure 81.

While the levels observed for the double injected retinas were not double the amount from the single injected retinas, the difference is still significantly higher; levels were approximately 62% lower in single injected retinas compared to double retinas (2033 ± 88.6 and 3299 ± 37.69 μg/protein respectively) ($p < 0.0001$).
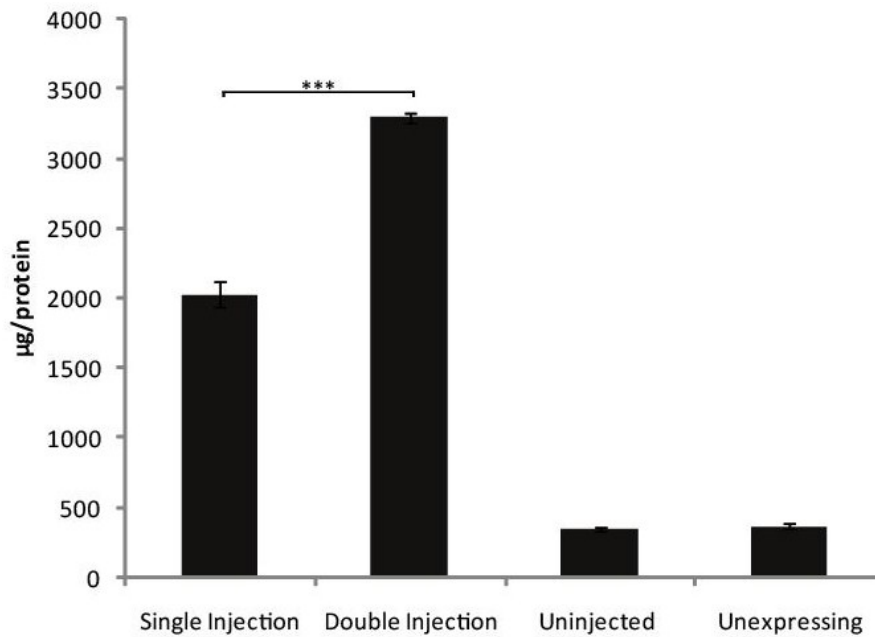
Figure 81: A comparison of luciferase expression at 48 hours within the retina following single and double subretinal injections

Plasmid DNA pCAG-Luc (30 µg) was complexed with PEI (N/P 8) and delivered to the retina of MF1 mice following a single or double subretinal injection (2 µl / 1 µg per eye). Retinal homogenates were subsequently lysed and analysed using a luminometer 48 hours following injection. The bar chart illustrates the quantification of luciferase expression represented as µg/protein. Levels of expression were approximately 1.6 fold higher in double subretinal injected retinas compared to single injected retinas (2033 ± 88.6 µg/protein compared to 3299 ± 37.69 µg/protein respectively). Uninjected retinas as well as retinas from mice not expressing luciferase were used as negative controls. The difference in expression of luciferase between single and double subretinally injected retinal samples is highly significant (*** $p < 0.0001$, Student's *t* test). Results are mean values from four to five independent experiments. Error bars represent the s.e.m.

In a complimentary experiment, mice were also injected either by single or double subretinal injection of formulated pCAG-EGFP (30 μg of pDNA, N/P 8, 1 μg/2 μl in total per eye). The amount of EGFP expression was observed 1 week post injection in retinal whole mounts as described in the methods. Briefly, enucleated eyes were fixed in 4% PFA, cut into flat mounts using iridectomy scissors. Immunohistochemistry was then performed on flat mounts for the expression of EGFP (following both injections/groups of mice), where samples were incubated with an anti-GFP rabbit polyclonal primary antibody (Abcam) and an Alexa-488 conjugated secondary antibody. Controls were made by analysing injected retinas omitting the primary antibody (results not shown) or by carrying out immunohistochemistry on uninjected as well as sham/vehicle alone injected (PBS) whole mount eyes. These controls allowed us to assess the background EGFP expression from the secondary antibody as well as the background EGFP expression in uninjected and sham injected whole eyes respectively. Representative retinal whole mounts are shown in Figure 82.
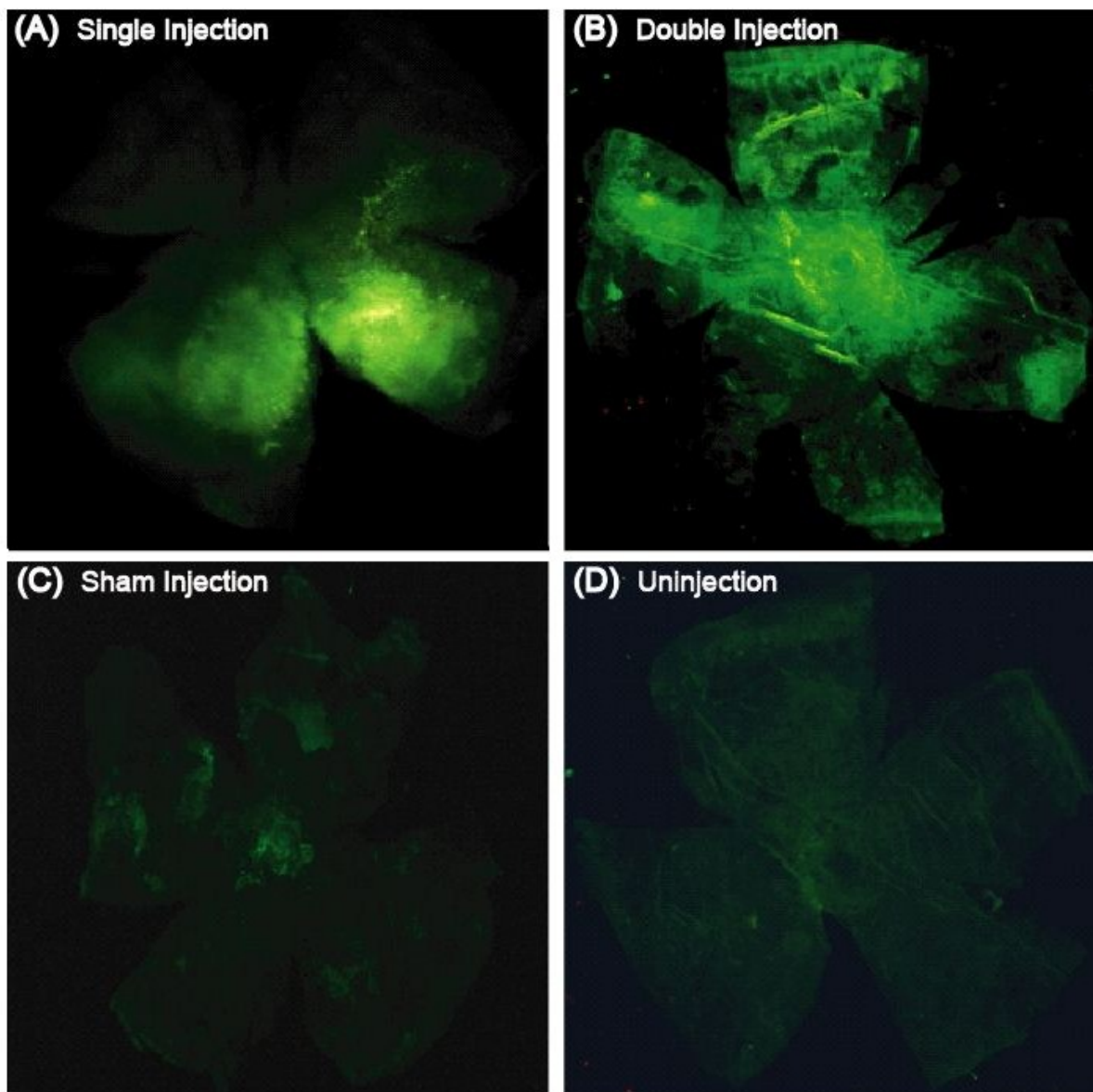
Figure 82: Expression of *EGFP* transgene in the RPE cells (of mouse retinas) from whole mounts of pCAG-EGFP injected retinas following single and double subretinal injections

The expression of EGFP from formulated pCAG-EGFP (30 µg pDNA N/P 8) subretinally injected into the mouse retina and analysed by retina whole mounts 1 week following injection. Shown is the whole mount of the eye following the (A) single or (B) double subretinal injection of pDNA. Control whole mount samples include (C) sham/vehicle (PBS) or (D) uninjected retinas. To detect EGFP expression, all retinal whole mounts were incubated with anti-rabbit polyclonal EGFP primary antibody and Alexa 488 secondary antibody. Fluorescent images at 2.5x (for A and B) and 1.25 x (for C and D) magnification are shown. Images are representative of four-five independent experiments. EGFP expression seen clearer on digital images.

Whole mount analysis from both single and double subretinal injections showed a focus of expression within less than half of the retina or a more dispersed expression throughout the whole retina respectively.

From both analyses performed with pCAG-Luc as well as pCAG-EGFP (Figure 81 and Figure 82) it appears clear that double injections provide higher levels of *Luciferase* and *EGFP* transgenes *in vivo*. One could explain the reason for not observing double the amount of luciferase and EGFP expression within the retina due a number of reasons. One potential problem/limitation of the double injection procedure is the possibility of the vector leaking through both injection sites after removal of the injection needle in the retina. Furthermore leakage through the first injection site during the second injection procedure could also occur. Difficulty in injecting the retina efficiently once it has been pierced after the initial subretinal injection, causing it to no longer be rigid and easy to manipulate into the correct position with a needle is also a potential problem that could be encountered during the double injection procedure.

Despite these problems, the maximum amount of expression observed within the retina using a non-viral vector appears to be following the double subretinal injection of PEI formulated S/MAR pDNAs within the retina. Hence in all subsequent *in vivo* experiments in MF1 mice we used double subretinal injections.

3.3.8 Immunohistochemical detection of EGFP expressing cells in the retina

As well as analysis of whole mount retinas to show the presence of EGFP expression within the RPE cells following subretinal injections of pCAG-EGFP into the retinas, EGFP expression was also investigated by Western analysis. RPE and neural retinal cells were isolated from the retinas of 10 C57BL/6 mice (3-4 months old) 48 hours following the double subretinal injection of pCAG-EGFP and pCAG-Luc-Control plasmids. Samples were lysed and 50 µg of total protein lysates were resolved by 12% SDS-polyacrylamide gel electrophoresis and transferred to a PVDF membrane. The membrane was then probed with an anti-GFP mouse polyclonal antibody (Roche). A representative blot is shown in Figure 83. The Western blot analysis revealed strong expression of EGFP within the RPE cell layer of injected mouse

retinas from both pDNA groups (pCAG-EGFP and pCAG-Luc-Control), while expression was absent in the neural retina of these mice.
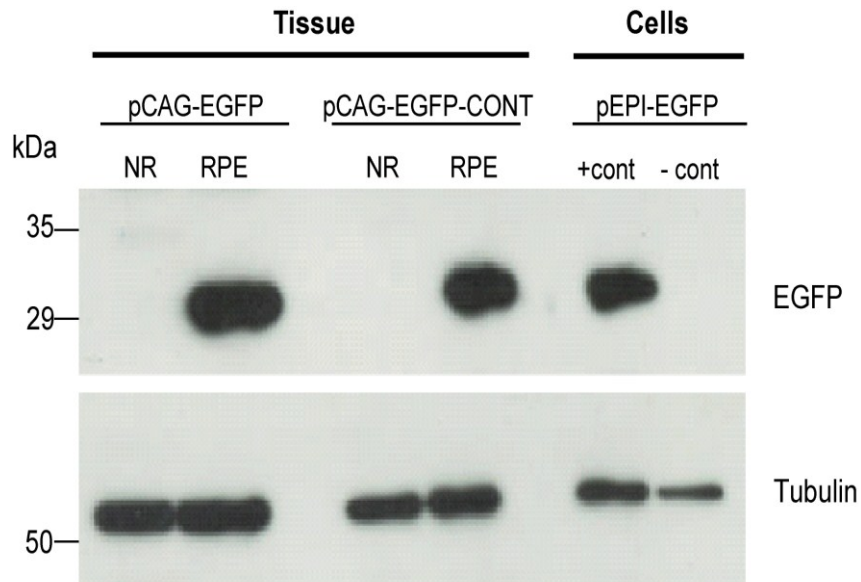
Figure 83: Western blot analysis of RPE and neural retinal cells isolated following the subretinally injected pCAG-EGFP and pCAG-EGFP-Control pDNA vectors

The figure shows the Western blot analysis of EGFP protein levels upon partitioning of the RPE and neural retina (NR) cells (50 μg) from C57BL/6 mice (n=10) 48 hours following the double subretinal injection of plasmids pCAG-EGFP and pCAG-EGFP-Control. Untransfected cells as well as cells transfected with pEPI-EGFP served as a positive and negative control respectively, while α-tubulin was used as a loading control. EGFP expression is exclusively observed in the isolated RPE cells of both injected plasmid groups.

To further complement the EGFP expression observed within the RPE cells by whole mount immunohistochemistry (Figure 82) and Western blot analysis (Figure 83), we also analysed the long term tissue expression of EGFP by immunohistochemistry analysis of retinal sections (Figure 84). At 1 and 6 months post injection, eyes were enucleated and frozen sections were obtained and analysed by confocal microscopy. By examining the whole eye at 1 and 6 months post injection, the blebs that had arisen by the injection procedure appear to have regressed and limited retinal detachment is observed throughout the sections. Furthermore, *EGFP* transgene expression levels appear to be persistent, however expression is limited to the sites of injection (Figure 84A). As such two clear regions of EGFP expression are evident both sides of the retina at 1 and 6 months post injection. Limited regions of the neural retina also show some EGPF expression, however this is probably caused by residual plasmid within the retina from the injection procedure (specifically the insertion and removal of the needle into the retina). Importantly, in the regions were EGFP expression is observed, the outer nuclear layer, inner nuclear layer and ganglion cell layers all exhibit relatively normal thickness. Closer examination of the retina at 1 and 6 months shows the most detectable EGFP expression was localized to the RPE cell layer, where considerable co-localisation with an RPE cell marker protein - Rpe65 - was observed (Figure 84B). No EGFP staining was seen in control uninjected retinas. Notable was the lack of DAPI staining on the nuclei of RPE cells, in injected and control uninjected retinas. This may have been due to the fact that the RPE cells are a single cell layer within the retina, as such are a sparse cell layer which could result in inconsistent DAPI staining within these cells.
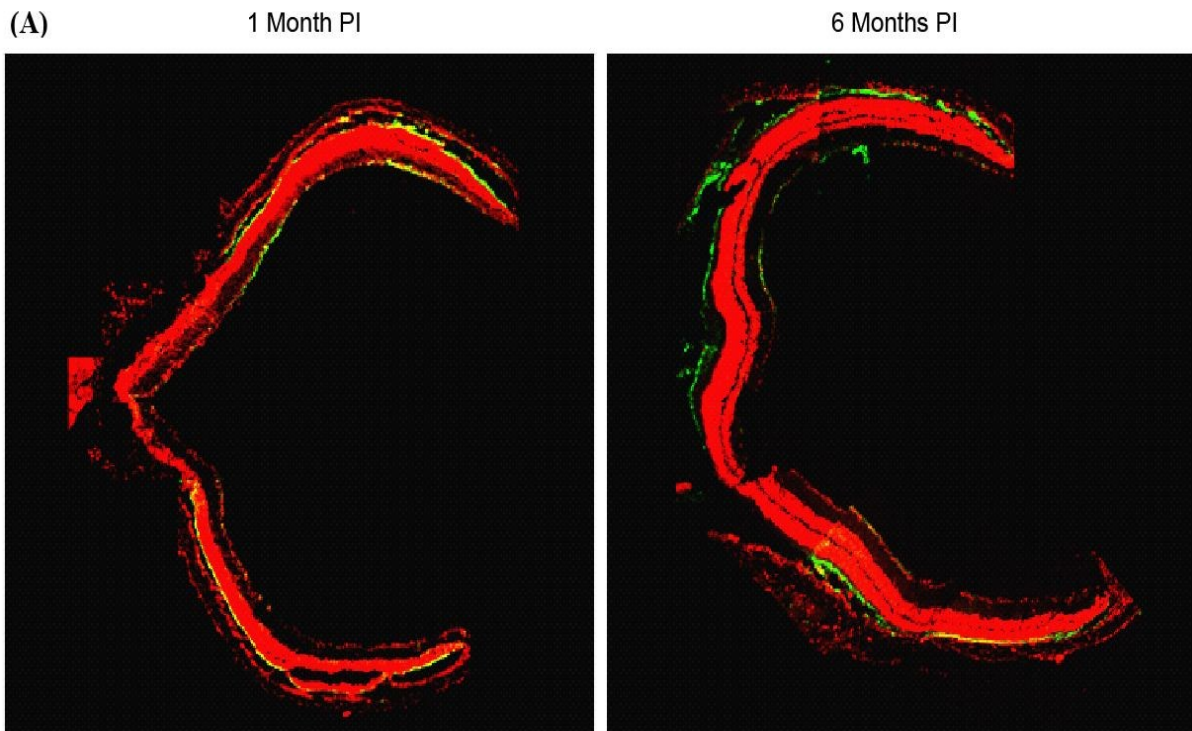
(A) 1 Month PI   6 Months PI

Figure 84: Immunofluorescence detection of EGFP expression in the mouse retina at 1 and 6 months following the double subretinal injection of pCAG-EGFP

(A) The figure shows a collage/composite of the whole retina, where numerous images were taken with 40x objective. Immunofluorescence labelling using an anti-GFP rabbit antibody was performed on frozen sections. Shown are representative images of EGFP immunolabeling on whole retinas from MF1 mice following the double subretinal injection of pCAG-EGFP at (A) 1 month and (B) 6 months post injection. Levels of *EGFP* transgene are persistent at both 1 and 6 months post injection, however expression is limited to the sites of injection. Nuclei were also stained using Propidium Iodide (red). Images are representative of three-four independent experiments. EGFP expression seen clearer on digital images.
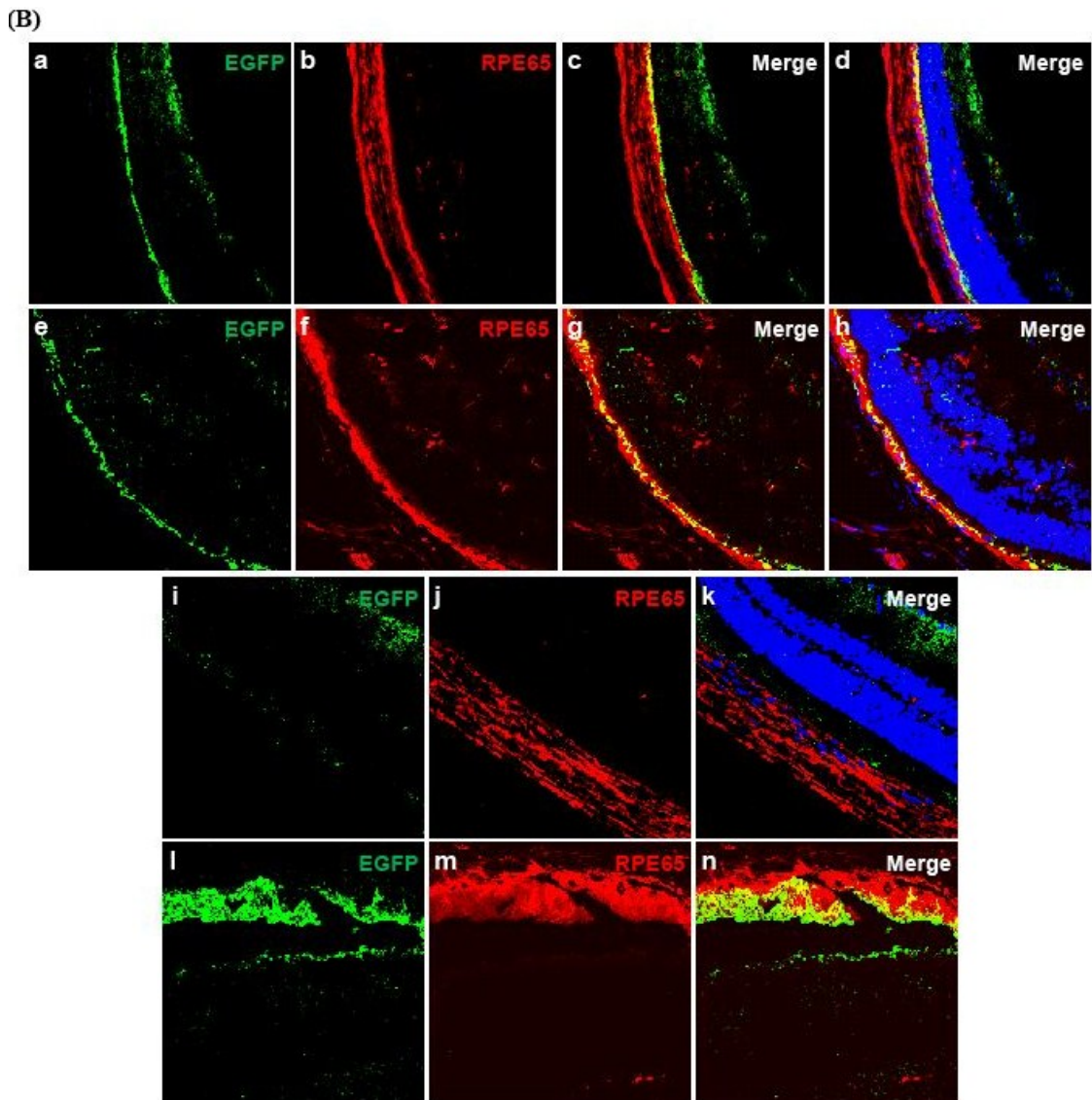
Figure 84: Immunofluorescence detection of EGFP expression in the mouse retina at 1 and 6 months following the double subretinal injection of pCAG-EGFP

(B) The figure shows a collage/composite of the whole retina, where numerous images were taken with 40x objective. Immunofluorescence labelling using an anti-GFP rabbit antibody was performed on frozen sections. Shown are representative images of EGFP immunolabeling on whole retinas from MF1 mice following the double subretinal injection of pCAG-EGFP at (A) 1 month and (B) 6 months post injection. Levels of *EGFP* transgene are persistent at both 1 and 6 months post injection, however expression is limited to the sites of injection. Nuclei were also stained using Propidium Iodide (red). The figure shows representative close-up regions of the retina at 1 month (panels *a-d, i-n*) and 6 months (panels *e-h*) post injection. The retina was examined for the expression of *EGFP* transgene (green) (*a, e, i, l*) and the localization of Rpe65 protein (red) (*b, f, j, m*) within the RPE cells of injected WT MF1 mice. Control samples included injected sample without primary antibody (*i-k*) and showed no EGFP staining. Considerable co-localisation (yellow) of Rpe65 and EGFP is observed within the RPE cell layer of injected retinas at 1 and 6 months post injection. Nuclei were also stained with DAPI (blue) (*d, h, k*). Fluorescent images (*a-d*) (*e-k*) and (*l-n*) are shown at 20x, 40x and 63x magnification respectively.

In a complimentary experiment, EGFP expression was also examined *in situ* (within the retina) following fundus as well as SLO examinations of the retina 1 week following the single subretinal injection of formulated pEFS-EGFP (Figure 85). Control retina images were obtained for fundus examinations however this was not the case for the SLO examinations. While it is unlikely that the fluorescence observed was background fluorescence caused solely due to the injection procedure, this cannot be ruled out as a source or contributor for the fluorescence seen in the SLO images. Thus although the expression appears promising in Figure 85B one must be cautious in the interpretation of the images.
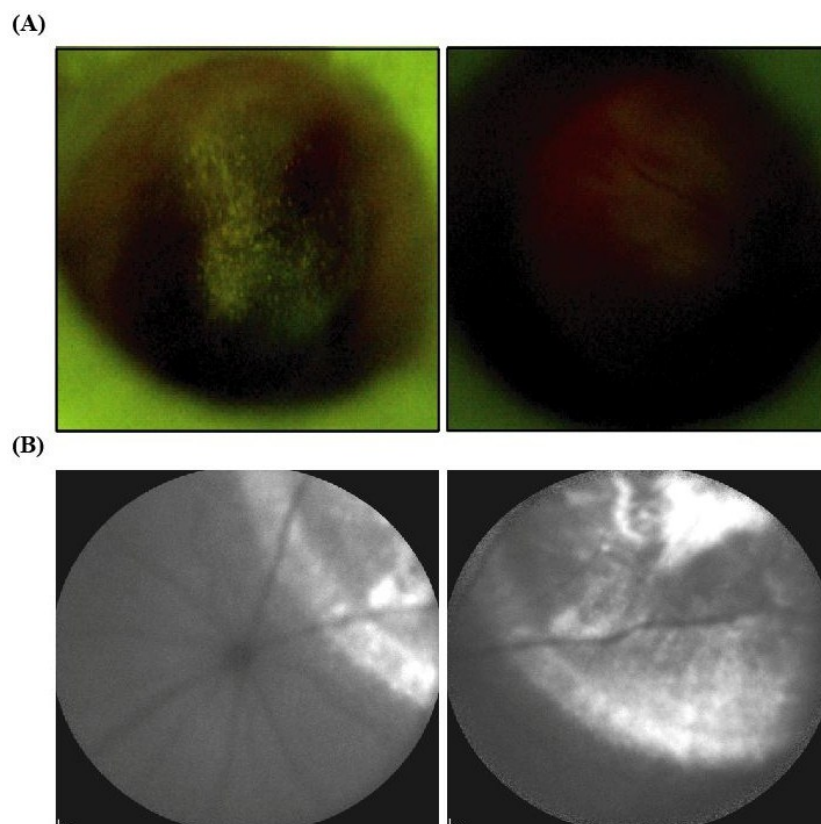
Figure 85: Fundus examination following injection of EGFP/S/MAR plasmids shows the presence of EGFP fluorescence within the retina

Mice were imaged at 1 week following the subretinal injection of formulated pEFS-EGFP pDNA. The fundus was examined *in situ* by either (A) fundus examination using a fluorescent microscope or (B) SLO examination. Shown is the representative EGFP fluorescence observed within the retina of an injected mouse (*left* panel), while no expression is seen in the control uninjected eye of the same mouse (*right* panel). Representative SLO examination of an injected mouse also shows intense fluorescence signal represented by the areas of white (signal). Shown are SLO images with the central view of the retina - where the centre is on the optic nerve (*left* panel), as well as the peripheral image of the same retina (*right* panel). (All SLO examinations were carried out at Oxford University by Professor Robert MacLaren and Dr Peter Issa). Digital images may be clearer.

3.3.9 Histological examinations following subretinal injections

While it is important that we assess and observe the long term *EGFP* and *Luciferase* transgene expression within the retina, specifically in the RPE cell layer of the retina, it is equally important that the area of the injection site as well as surrounding tissue of the retina should also remain normal. Hence detailed histological analysis of retinal sections following subretinal injections of WT MF1 mice was also carried out.

3.3.9.1 Ophthalmoscopic analysis of fundi

To assess potential inflammation or abnormalities within the retina following the subretinal delivery of S/MAR plasmids, we performed fundus examinations (*in situ*) of various groups of MF1 mice that had been double subretinally injected with complexed pCAG-Luc at 1 week and 1 month post injected (PI). We analysed the various groups of MF1 mice by indirect opthalmoscopy. We also assessed the fundi from the following control retinas: naked (uncomplexed) pCAG-Luc pDNA, sterile Glucose alone, PEI-Glucose alone and uninjected WT. Fundus analysis of naked pCAG-Luc injected retinas would reveal if the mice were reacting to the actual pDNA, while Glucose and PEI-Glucose injected retinas would show if the mice were reacting to the injection procedure or the gene delivery agent/vehicle PEI respectively. This length of time was chosen as it allowed the bleb within the retina to be reabsorbed and the neural retina to return contact with the RPE layer.

Representative fundi of all groups of mice analysed are shown in Figure 86. The fundus examinations reveal that all retinas appear normal in all 4 quadrants of the eye (superior, inferior, temporal and nasal) at 1 week and 1 month (for pCAG-Luc) post injection. The retinas appear to show limited inflammation as evident by the healthy colour and clear organised blood vesicles in the eye. Furthermore, all subretinal blebs have regressed and minimal signs of the injections procedure are evident.
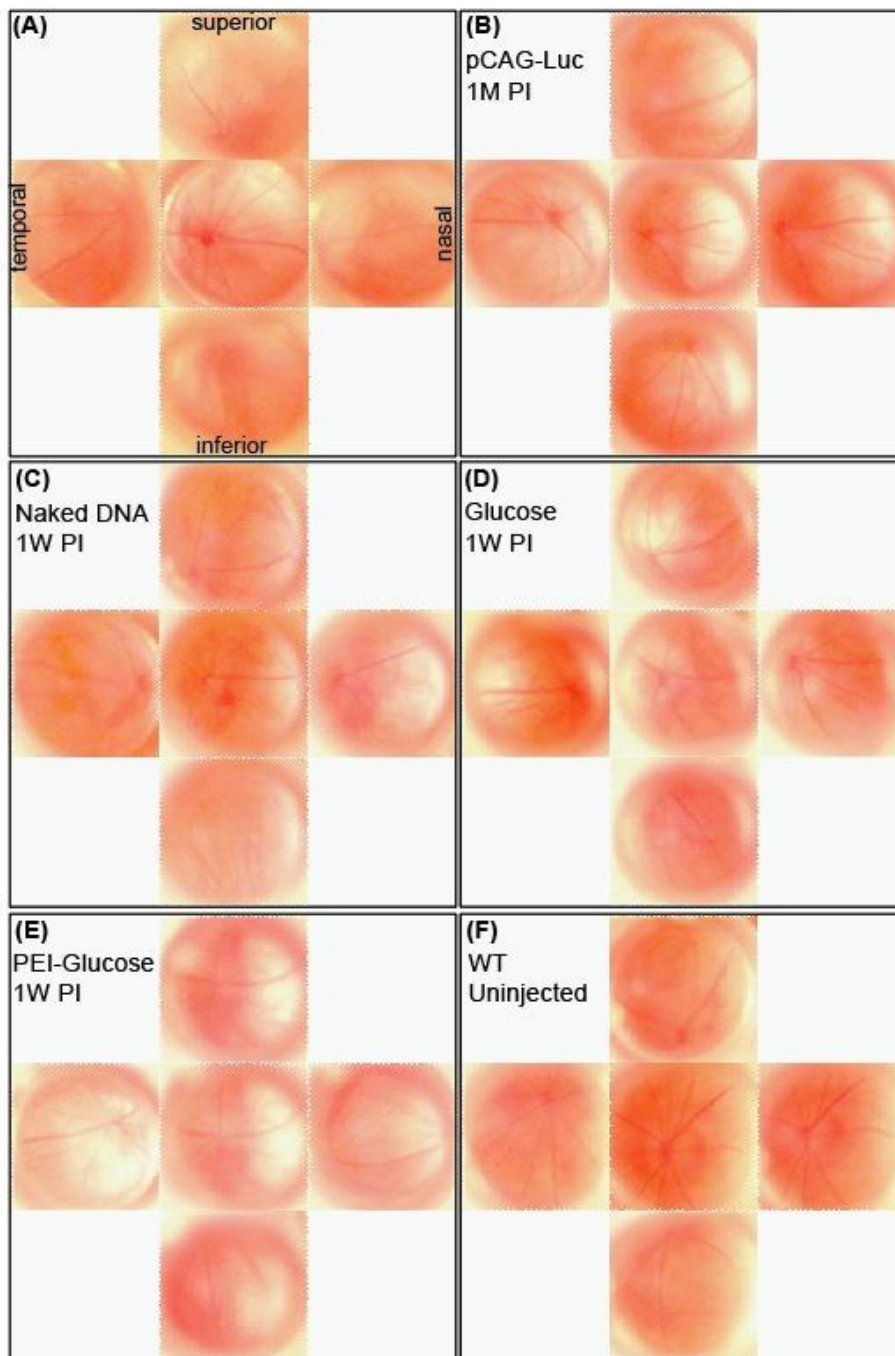
Figure 86: Ophthalmic examinations of fundi following the double subretinal injection of formulated pCAG-Luc mice at 1week and 1 month post injection

MF1 WT mice were double subretinally injected with formulated pCAG-Luc (30 μg pDNA N/P 8) and analysed by fundus examination (*in situ)* at (A) 1 week and (B) 1 month post injection (PI). As negative control the fundus examination was also included of mice double subretinally injected with (C) un-complexed pDNA (Naked DNA), (D) Glucose alone, (E) PEI-Glucose as well as (F) WT uninjected mice. Injected retinas were analysed in the superior, inferior, temporal and nasal regions. All retinas appear health, with clear blood vessels and no evidence of inflammation or abnormality. Images are representative of four-five independent experiments. Digital images may be clearer.

3.3.9.2 Analysis of retinal sections – H&E and TUNEL

To assess whether there was a local inflammatory response within the retinas to S/MAR plasmids, we also examined paraffin-embedded retinal sections of eyes that had been single and double subretinally injected with complexed pCAG-Luc. Furthermore the sections of the same control samples used in the fundus examination were also analysed: naked pCAG-Luc pDNA, sterile Glucose and PEI alone.

We performed haematoxylin and eosin (H&E) staining and examined retinal sections for infiltration and activation of inflammatory cells such as polymorphonuclear leukocytes (PMN), which would indicate an adverse and toxic response present in the retina (Giese, Sumner et al. 1998; Ramadan, Ramirez et al. 2006). Such an inflammation would be mainly localised near or at the site of injection, hence identifying the precise injection site in retinal sections is vastly advantageous and informative. Indeed subretinal injections cause a localised detachment at the site of injection; however retinal detachment can also occur during histology processing. As the site of retinal detachment cannot be the ultimate mark for the site of injection, in our subsequent analyses of retinal sections, we choose to analyse numerous sections taken throughout the entire eye either side of the optic nerve, with the idea to include sections near and far from the site of injection.

Figure 87 shows representative H&E stained whole retinas as well as higher magnification of areas throughout the entire retina. Encouragingly, we did not observed evidence of a cellular inflammatory reaction as judged by an absence of PMN or round cell infiltration with H&E staining of eye sections (Figure 87A).
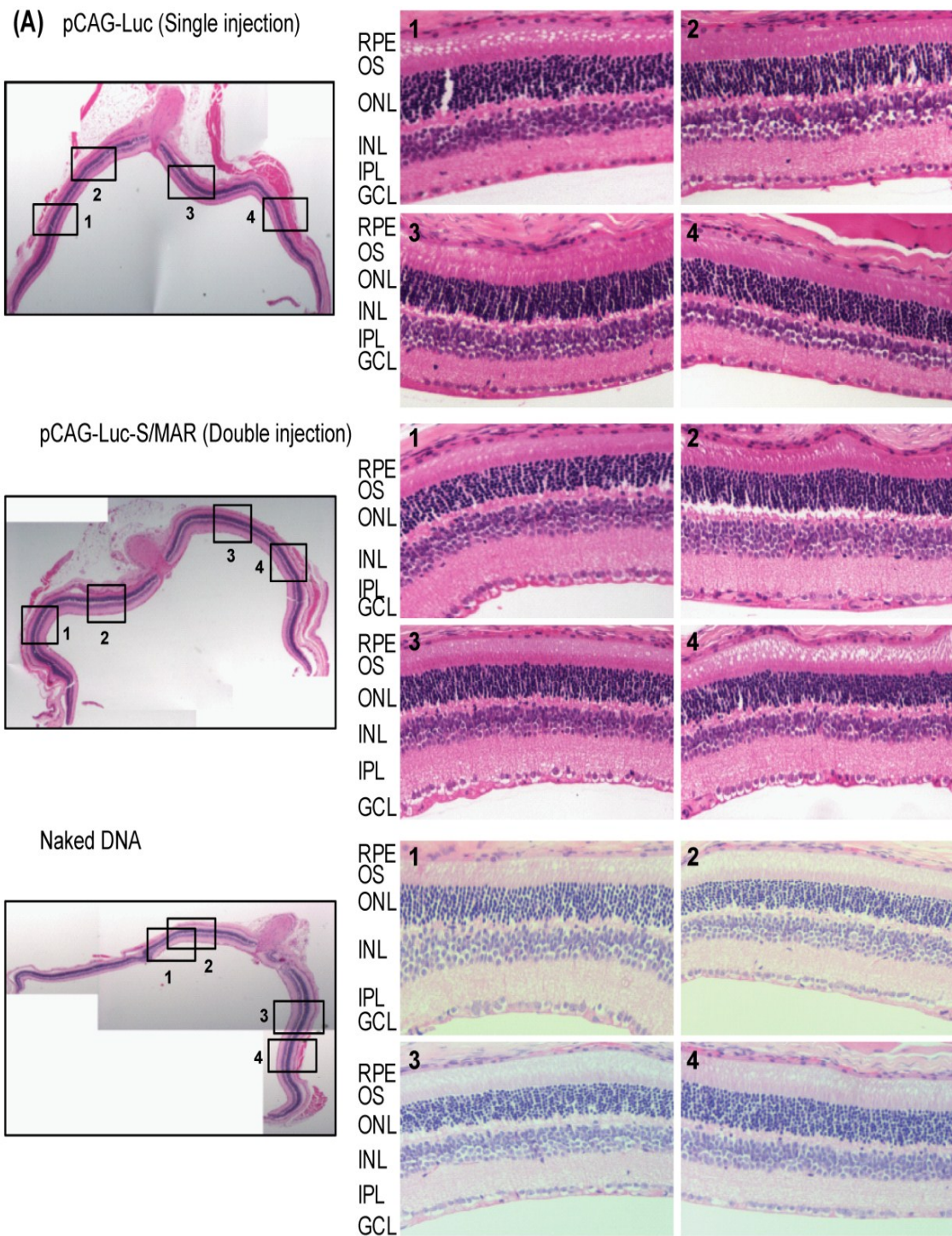
Figure 87: Histological (H&E) examination of inflammatory cell infiltrations in MF1 mouse retinas following the single and double subretinal injections of formulated pCAG-Luc at 1 month post injection

(A) Shown are representative haematoxylin and eosin (H&E) stained retinal sections of MF1 mice subretinally injected with formulated pCAG-Luc at 1 month post injection. As a negative control, retina sections from injected naked (un-complexed) pCAG-Luc (Naked DNA) mice were also analysed. No evidence of a cellular inflammatory reaction is observed within the H&E stained sections. All cell layers exhibit relatively normal thickness and morphology.
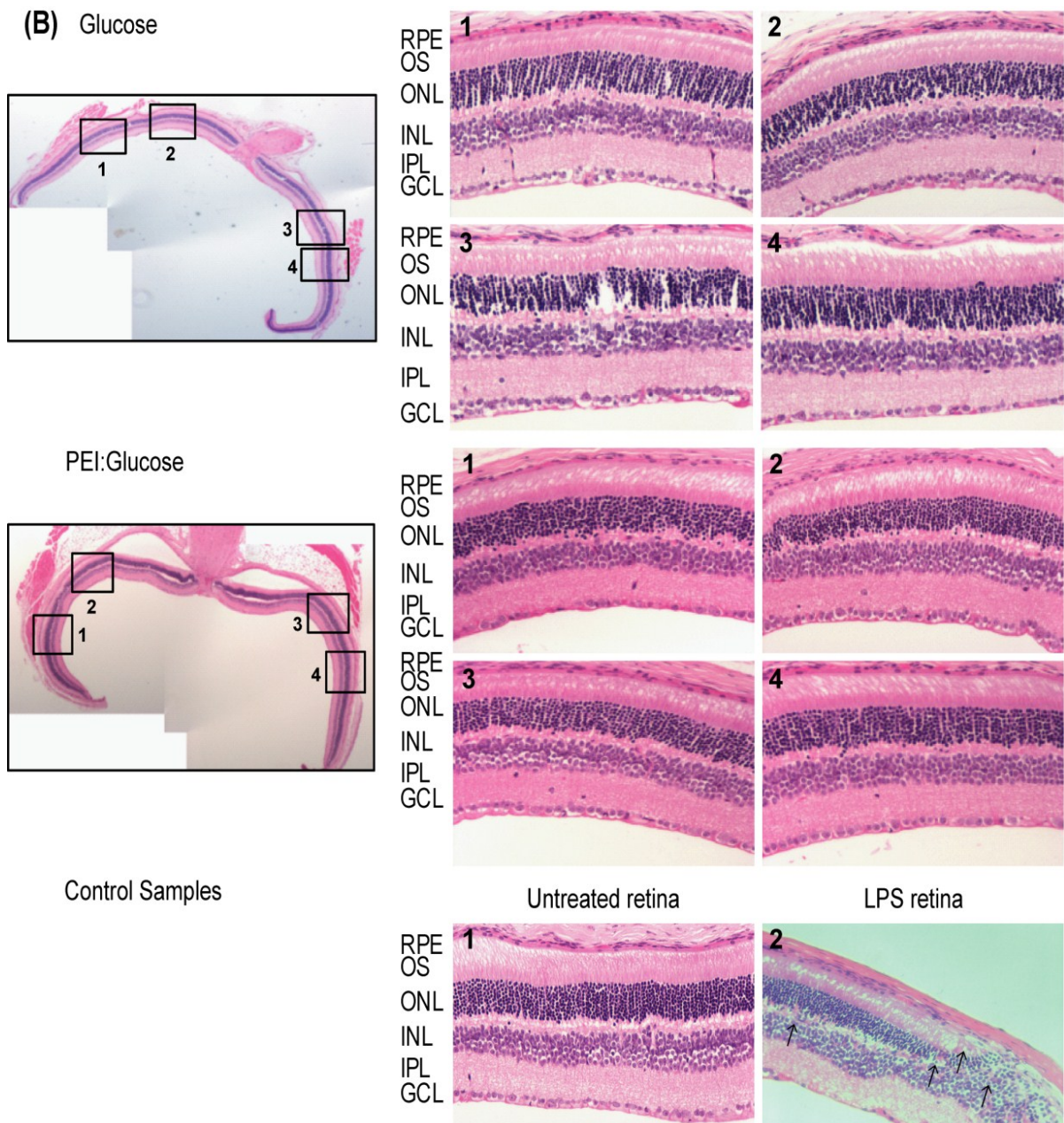
Figure 87: Histological (H&E) examination of inflammatory cell infiltrations in MF1 mouse retinas following the single and double subretinal injections of formulated pCAG-Luc at 1 month post injection

(B) Shown are representative H&E stained retinal sections of negative control MF1 mice subretinally injected with: Glucose, PEI-Glucose alone and uninjected. As a positive control, mice were also injected with *E. coli* Lipopolysaccharides (LPS), where substantial infiltrations of polymorphonuclear leukocytes (PMN), and damage at the site of injection is observed (indicated by the black arrows in the LPS retina - far *bottom right panel*). H&E staining of the whole retina (*left panels*) and highlighted sections as indicated by the black boxes (*right panels*) are shown at 4x and 20x magnification respectively. Images are representative of four-five independent experiments.

RPE, retinal pigment epithelium; OS, photoreceptor outer segments; ONL, outer nuclear layer; INL, inner nuclear layer; IPL, inner plexiform layer; GCL, ganglion cell layer.

Within the cell, numerous barriers can prevent the efficient and persistent transport of pDNA into the nucleus. We have previously shown that through the formulation of S/MAR pDNA and subsequent subretinal injections, persistent expression within the RPE cells is observed; showing that this technique circumvents a number of these barriers. However, as a last resort to the delivery of drugs or pDNA, some cells have been shown to undergo apoptosis (Yew, Zhao et al. 2000). Hence tissue death under these optimised conditions was also examined in the same retinal sections as above using terminal deoxynucleotidyl transferase dUTP nick end labeling (TUNEL) analysis.

Figure 88 shows representative TUNEL staining of whole retinas as well as higher magnification of the same areas analysed by H&E analysis (Figure 87) throughout the entire retina. Analyse of tissue cell death in retinal sections showed no apoptotic events within the retina of any of the groups of mice analysed (Figure 88A).

As a positive control mice were also subretinally injected with *Escherichia. Coli* (*E. coli*) Lipopolysaccharides (LPS) and eyes were collected between 5-15 min post subretinal injection.We observed thinning of the nuclear layers of the retina, cellular infiltrations of PMN, retinal detachment and damage at the site of injection in most sections examined as well as cell death induced apoptosis of cells in the retina (Figure 87B and Figure 88B). As a negative control uninjected retinas were also analysed and showed no inflammation or infiltration of cells as well as no apoptotic cells in the retina (Figure 87B and Figure 88B).
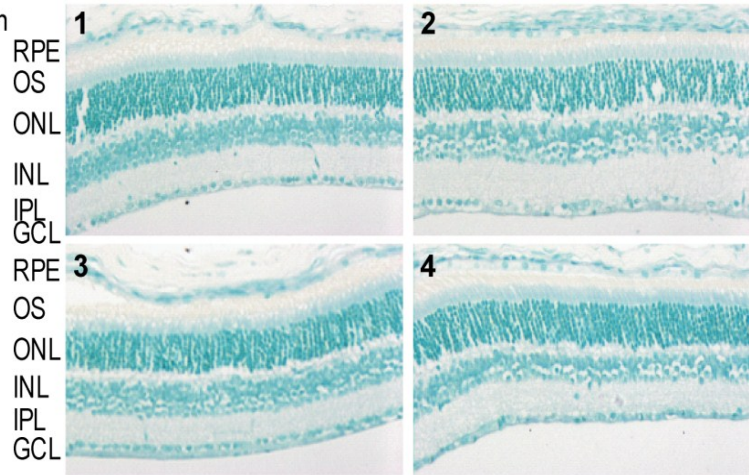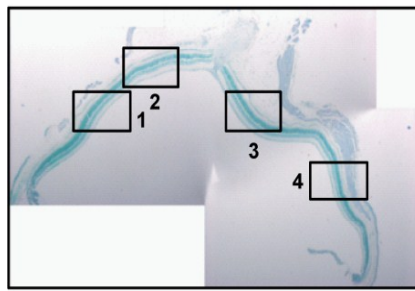
Figure 88: Cell death (TUNEL) examination in MF1 mouse retinas following the single and double subretinal injections of formulated pCAG-Luc at 1 month post injection

(A) Shown are representative TUNEL stained retinal sections of MF1 mice subretinally injected with formulated pCAG-Luc at 1 month post injection. As a negative control, retina sections from injected naked (un-complexed) pCAG-Luc (Naked DNA) mice were also analysed. No evidence of apoptotic cell death was observed within the TUNEL stained sections.
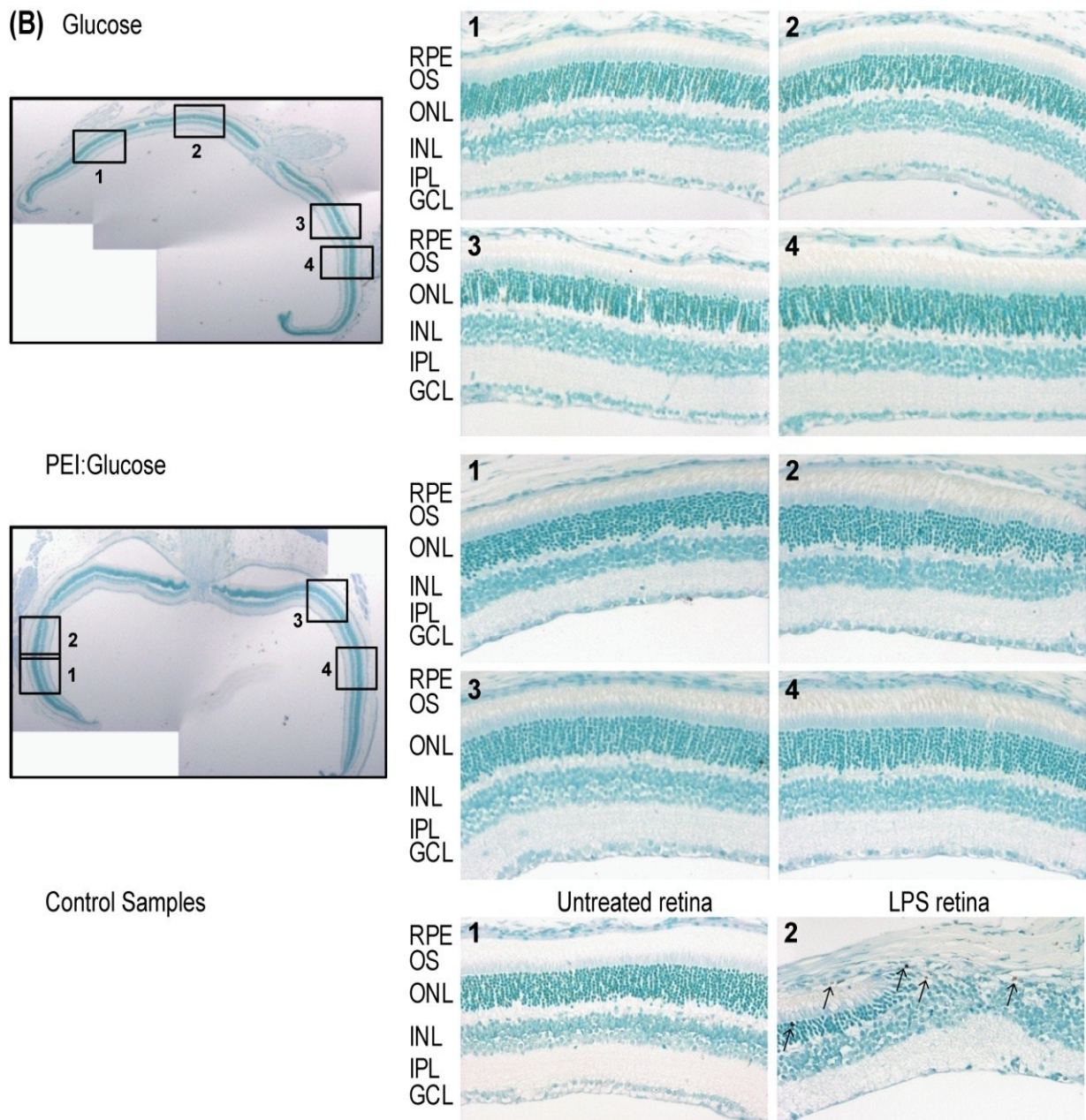
Figure 88: Cell death (TUNEL) examination in MF1 mouse retinas following the single and double subretinal injections of formulated pCAG-Luc at 1 month post injection

(B) Shown are representative TUNEL stained retinal sections of negative control MF1 mice subretinally injected with: Glucose, PEI-Glucose alone and uninjected. As a positive control, mice were also injected with *E. Coli* Lipopolysaccharides (LPS), where substantial apoptotic cell death as shown by black cell staining is observed (indicated by the black arrows in the LPS retina - far *bottom right panel*). TUNEL staining on the whole retina (*left panels*) and highlighted sections as indicated by the black boxes (*right panels*) are shown at 4x and 20x magnification respectively. Images are representative of four-five independent experiments.

RPE, retinal pigment epithelium; OS, photoreceptor outer segments; ONL, outer nuclear layer; INL, inner nuclear layer; IPL, inner plexiform layer; GCL, ganglion cell layer.

3.3.9.3 Analysis of inflammatory Chemokines - ELISA

The retina is often considered an immune privileged organ, however it can present immune activity when put under environmental stress (Wakefield and Lloyd 1992; Jo, Wu et al. 2003; Yeh, Song et al. 2003; Powers, Davies et al. 2005; Chintakuntlawar, Astley et al. 2007) and so is prone to environmental alterations. Specifically, there is evidence for immune-based inflammation in the eye caused by increases in inflammatory cytokines: tumor necrosis factor-α (TNF-α) (Wakefield and Lloyd 1992; Limb, Chignell et al. 1996; Limb, Hollifield et al. 2001; Nakazawa, Matsubara et al. 2006; Nakazawa, Kayama et al. 2011), monocyte chemotactic protein-1 (MCP-1) (Jo, Wu et al. 2003; Yoshida, Yoshida et al. 2003; Nakazawa, Matsubara et al. 2006), interferon-γ (IFN-γ) (Wakefield and Lloyd 1992; Chen, Chauhan et al. 2011; Hooks, Chan et al. 1988; Cathcart, Zheng et al. 2011), as well as potential proapoptotic factors (Brignole, De Saint-Jean et al. 1998; Gao, Schwalb et al. 1998; Brignole, Pisella et al. 2000; Brignole, Pisella et al. 2001; Yang, Elner et al. 2011), TNF and IFN induced apoptosis (Zhang, Covar et al. 2011). Hence we examined the levels of these cytokines by Enzyme-linked immunosorbent assay (ELISA) of retinal homogenates that had been subretinally injected with complexed S/MAR pDNA (pCAG-EGFP), Glucose and PEI alone at 1 and 7 days post injection (Figure 89A). At day one post injection, limited inflammation was observed in retinas injected with pCAG-EGFP by analysis of MCP-1 and IFN-γ protein expression (77 ± 1.54 and 64 ± 2.4 pg/ml respectively) (Figure 89B and C), while a transient increase of TNF-α protein was observed (78 ± 5.24 pg/ml, $p<0.05$)(Figure 89A). Levels of TNF-α protein were also elevated in glucose and PEI-Glucose injected retinas ($p<0.05$ and $p<0.001$ respectively) at the same time point (65 ± 0.69 and 88 ± 7.26 pg/ml respectively). Importantly, despite this by day 7 post injection protein expression levels of all cytokines had returned to control uninjected levels. In contrast, LPS positive control tissues showed significantly elevated levels of all cytokines. Due to the presence of a tight blood-retinal barrier within the eye, one would not expect to find elevated levels of cytokines within the serum of injected mice. However, as bleeding was occasionally observed following subretinal injections, as a control, serum levels of injected mice were analysed for the expression of all three cytokines at the same time points (Figure 90). As expected, no elevated levels of cytokines were observed. In contrast, LPS positive control mice showed significantly high levels of all cytokines.
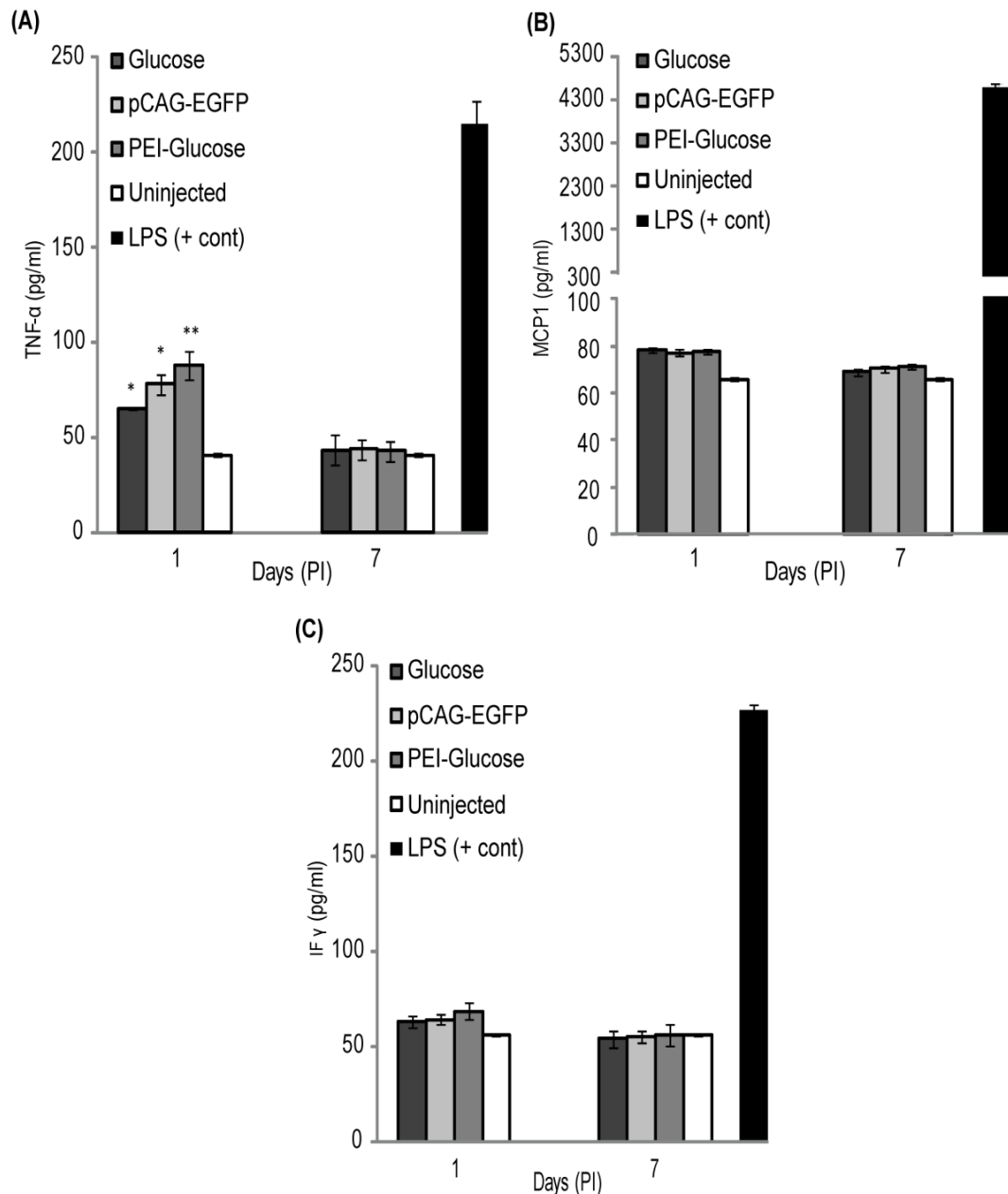
Figure 89: Examination of inflammatory cytokines TNF-α, MCP-1 and IFN-γ expression in mouse retinal homogenates following the subretinal injections of formulated pCAG-EGFP at 1 and 7 days post injection

ELISA was performed to determine the levels of (A) TNF-α, (B) MCP-1 and (C) IFN-γ in the retinas of eyes following the double subretinal injection of pCAG-EGFP at 1 and 7 days post injection (PI). As a negative control Glucose, PEI-Glucose and uninjected retinas were used. As a positive control, *E. coli* LPS was subretinally injected into the retina and significantly high levels of all three cytokines where observed compared to uninjected control levels at day 7 PI. Levels of TNF-α protein were significantly elevated in pCAG-EGFP, Glucose and PEI-Glucose injected retinas (78 ± 5.24, 65 ± 0.69, 88 ± 7.26 pg/ml respectively) (* $p < 0.05$, *$p < 0.05$ and **$p < 0.01$ respectively, Student's *t* test) at day 1 PI with respect to control uninjected retinas, however levels returned to control uninjected levels by day 7 PI. Percentages are mean values from four-five independent experiments. Error bars represent the s.e.m.
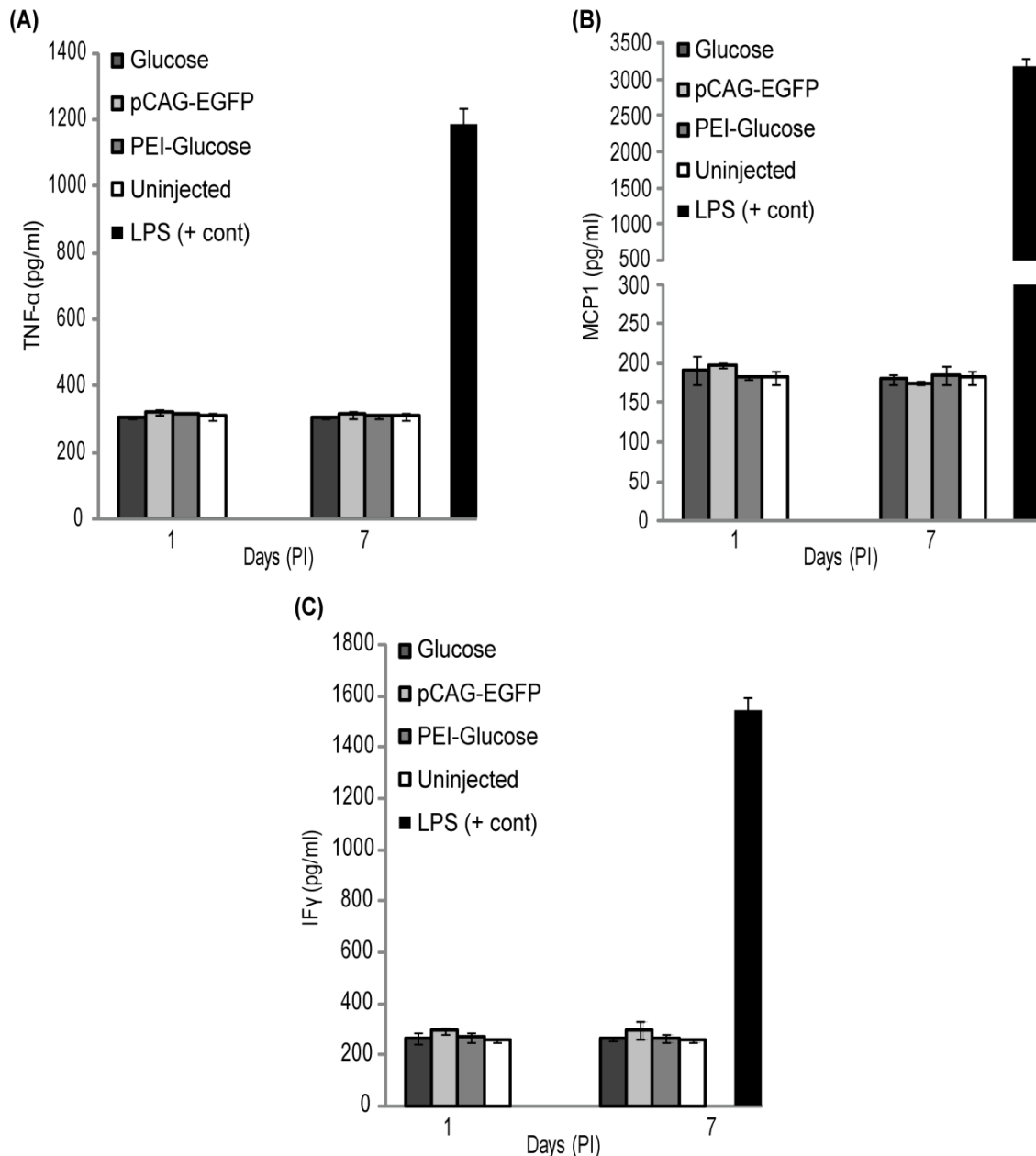
Figure 90: Examination of inflammatory cytokines TNF-α, MCP-1 and IFN-γ expression in the blood serum of mice following the subretinal injections of formulated pCAG-EGFP at 1 and 7 days post injection

ELISA was performed to determine the blood serum levels of (A) TNF-α, (B) MCP-1 and (C) IFN-γ in mice following double subretinal injection of pCAG-EGFP at 1 and 7 days post injection (PI). As a negative control Glucose, PEI-Glucose and uninjected retinas were used. As a positive control, *E. coli* LPS was injected via intraperitoneal (i.p.) injection and significantly high levels of all three cytokines where observed compared to all other groups analysed. No elevated levels of any cytokines were observed at day 1 and 7 PI in all groups analysed. Percentages are mean values from three independent experiments (Student's *t* test). Error bars represent the s.e.m.

3.3.10 Episomal status of EGFP and Luciferase S/MAR plasmids in vivo

In the final analysis of S/MAR pDNA safety *in vivo,* we were also eager to show that S/MAR plasmids were not only persistently expressed within the RPE cells, but also maintained as a passive episome within the RPE cells as well as the entire retina as a whole.

The episomal maintenance *in vivo* was examined by plasmid rescue of pEFS-EGFP and pCAG-EGFP isolated from kanamycin resistant *E.coli* after transformation with total DNA from retinal homogenates of MF1 mice 6 months post subretinal injection. The restriction pattern of the pEFS-EGFP plasmid was analysed using *Xho*I and *Bam*HI*;* giving the fragments 5104 bp and 1080 bp when digested with *Xho*I and linearised plasmid of 6184 bp when digested with *Bam*HI. While *Hind*III and *Afl*III were used for pCAG-EGFP plasmid analysis; giving the fragments 3142 bp and 4549 bp when digested with *Hind*III and fragments 2015 bp, 2752 bp and 2924 bp when digested with AflIII. The restriction patterns of these plasmids were compared to positive controls which were the corresponding original pDNAs and were consistent with unmodified non-integrating plasmid constructs (Figure 91).

Further evidence for episomal maintenance was provided by Southern blot analysis. DNA was isolated from mouse retinas injected with of pEFS-EGFP, pCAG-EGFP, pCAG-Luc and pUbiqC-Luc, as well as all corresponding control non-SMAR plasmids. DNA was digested with *Stu*I restriction enzyme, which has a single restriction site in all 8 pDNAs (pEFS-EGFP, pCAG-EGFP, pCAG-Luc, pUbiqC-Luc and controls), and then subjected to Southern blot analysis. Representative blots showing the analysis of the EGFP and luciferase plasmids can be seen in Figure 92 and Figure 93 respectively. All blots show the band of the expected size in all pDNAs analysed, confirming the presence of an intact episomal pEFS-EGFP, pCAG-EGFP, pCAG-Luc, pUbiqC-Luc plasmid in the mouse retina. Encouragingly, despite the lack of long-term EGFP expression (Figure 78 and Figure 79) as well as the lack of long-term luciferase expression, were levels of luciferase had declined to near-background levels in all control plasmids (Figure 74, Figure 76 and Figure 77) at 6 months post injection, all control plasmids were still maintained as an episome within the retina.
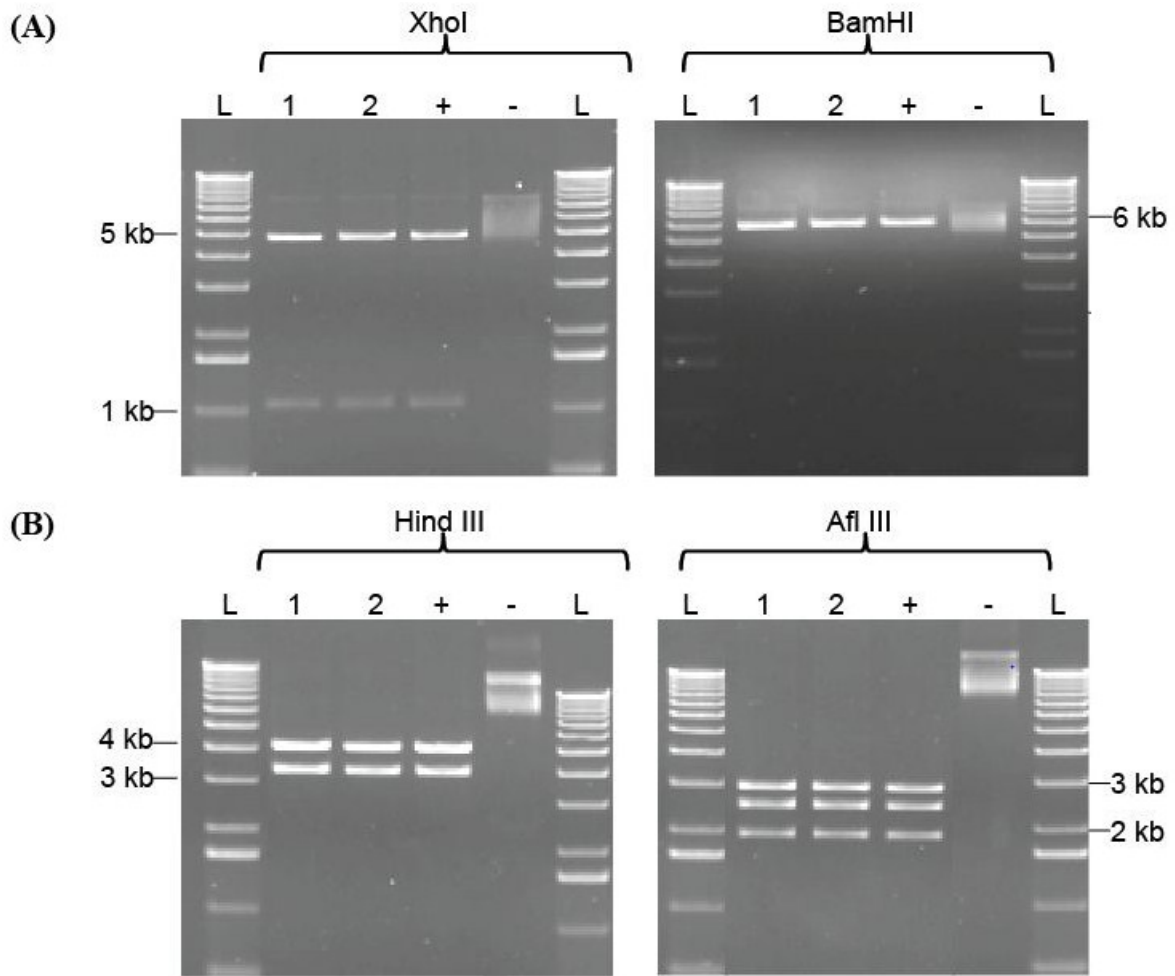
Figure 91: Plasmid rescue analysis of pEFS-EGFP and pCAG-EGFP vectors isolated at 6 months post subretinal injections in MF1/WT mice.

Plasmid rescue analysis of pDNA isolated from 2 randomly chosen clones (lanes 1-2), after transformation of *E.coli* bacteria with 1 μg of total DNA isolated from eye homogenates of MF1 mice 6 months post subretinal injection of (A) pEFS-EGFP and (B) pCAG-EGFP pDNA vectors, performed as described in methods. Undigested plasmid served as a negative control (lane 4 (-)), while all bands show identical sizes with the positive control of original pEFS-EGFP on (A) or pCAG-EGFP on (B) (lane 3 (+)), demonstrating that pEFS-EGFP and pCAG-EGFP vectors are retained episomally in the retinas of injected MF1 mice. Results are representative of two independent experiments. L: 1 kb Ladder (Invitrogen).
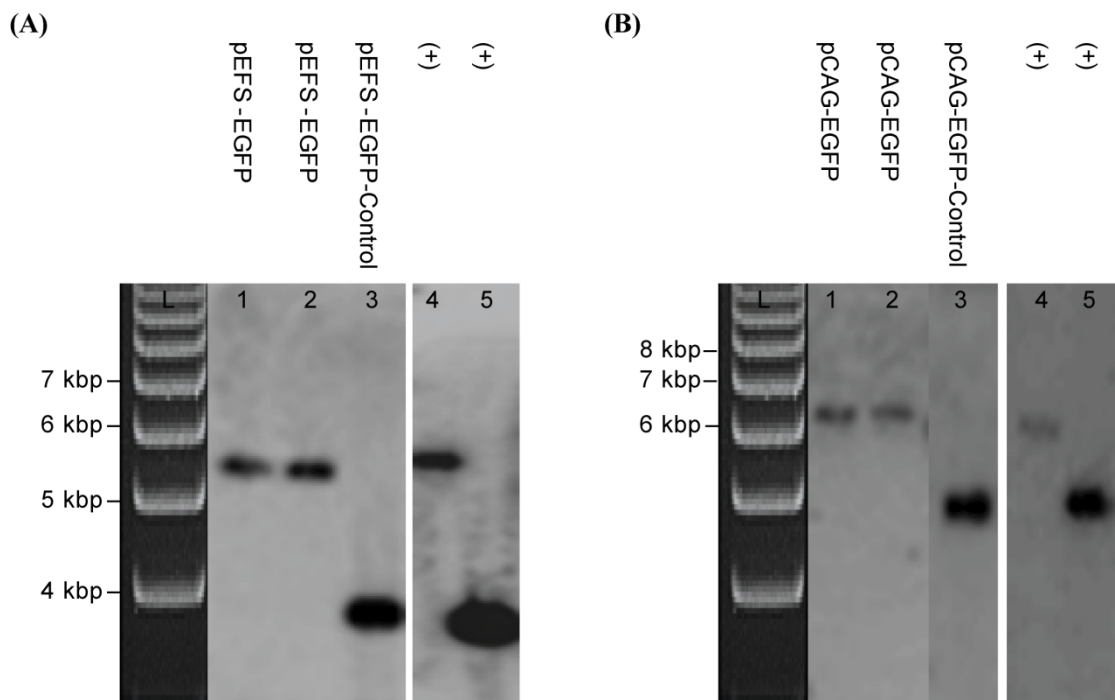
Figure 92: Representative Southern blot of isolated EGFP plasmids isolated at 6 months post subretinal injections in MF1/WT mice

Southern blots of total pDNA isolated from eye homogenates of MF1 mice 6 months post subretinal injection of (A) pEFS-EGFP and pEFS-EGFP-Control and (B) pCAG-EGFP and pCAG-EGFP-Control pDNA vectors, performed as described in methods. DNA (30 µg) was separated on 0.8% agarose gels and hybridized with ^{32}P-labelled *Alw*NI probe. Lanes 1-2, pEFS-EGFP or pCAG-EGFP isolated from eye homogenates (4-5 eyes per lane) by sacrifice 6 months post injection. Lane 3, pEFS-EGFP-Control or pCAG-EGFP-Control isolated from eye homogenates (4-5 eyes per lane) by sacrifice 6 months post injection. All clones produced a clear distinct band after *Stu*I digestion, identical to the band arising after digestion of 8 ng of corresponding positive control original pDNAs. This shows that at 6 months post injections, S/MAR plasmids as well as the corresponding control non-S/MAR plasmids are maintained as an episome within the retina (pEFS-EGFP and pEFS-EGFP-Control on (A) or pCAG-EGFP and pCAG-EGFP-Control on (B); lanes 4 and 5 respectively (+)). Results are representative of two-three independent experiments. L: 1 Kb ladder (Invitrogen).
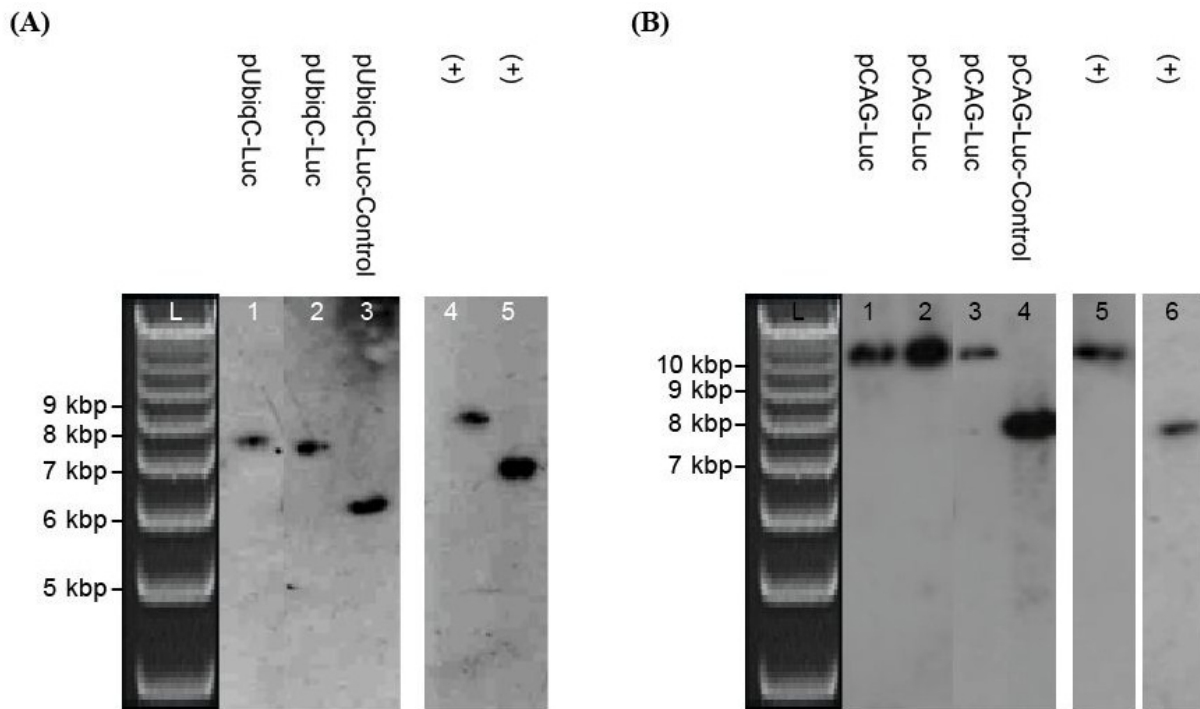
Figure 93: Representative Southern blot of isolated luciferase plasmids isolated at 3 or 6 months post subretinal injections in MF1/WT mice

Southern blots of total pDNA isolated from eye homogenates of MF1 mice 6 months post subretinal injection of (A) pUbiqC-Luc and pUbiqC-Luc-Control and (B) pCAG-Luc and pCAG-Luc-Control pDNA vectors, performed as described in methods. DNA (30 μg) was separated on 0.8% agarose gels and hybridized with ^{32}P-labelled *Alw*NI probe. In (A) lanes 1-2, pUbiqC-Luc isolated from eye homogenates (4-5 eyes per lane expressing luciferase) by sacrifice 6 months post injection. Lane 3, pUbiqC-Luc-Control isolated from eye homogenates (4-5 eyes per lane not expressing luciferase) by sacrifice 6 months post injection. In (B) lanes 1-2, pCAG-Luc isolated from eye homogenates (4-5 eyes per lane expressing luciferase) by sacrifice 3 months post injection. Lane 3, pCAG-Luc isolated from eye homogenates (4-5 eyes per lane expressing luciferase) by sacrifice 6 months post injection, Lane 4 pCAG-Luc-Control isolated from eye homogenates (4-5 eyes per lane not expressing luciferase) by sacrifice 6 months post injection. All clones produced a clear distinct band after *Stu*I digestion, identical to the band arising after digestion of 8 ng of corresponding positive control original pDNAs. This shows that at 6 months post injections, S/MAR plasmids as well as the corresponding control non-S/MAR plasmids are maintained as an episome within the retina (pUbiqC-Luc and pUbiqC-Luc-Control on (A); lanes 4 and 5 respectively (+) or pCAG-Luc and pCAG-Luc-Control on (B); lanes 5 and 6 on (B) respectively (+)). Results are representative of two-three independent experiments. L: 1 Kb ladder (Invitrogen).

In summary, as well as providing long-term expression, SMAR plasmids are able to be maintained episomally within the retina, showing no signs of vector integration seen with other viral vectors as well as further validating the safety of our plasmids in vitro as well as in vivo.

3.3.11 Limitations of PEI as a gene transfer agent

While we have shown no adverse effects within the retinas of injected mice following the subretinal injections of formulated S/MAR pDNA, on the rare occasion, white precipitate was observed following the fundus examination of injected retinas. Representative images are shown in Figure 94. Noteworthy is the fact that mice showing such precipitates were not used for subsequent analyses – particularly transgene analysis of frozen sections.

One could explain this occurrence because of the limited stability of PEI/pDNA complexes in solution. Indeed complexes at concentration exceeding 0.5 µg/µl have been associated with considerable precipitation and in-turn loss of biological efficacy (Davies, McLachlan et al. 2008). During all our subretinal injections, the preparation of complexes was done using freshly prepared, recently quantified pDNA stocks that had been delivered at 0.5 µg/µl - in order to deliver the highest concentrations of formulations to the retina without compromising on stability. Despite this one cannot exclude the possibility that on limited occasions following the subretinal injection of complexes, concentration levels exceeded 0.5 µg/µl.

Regardless of these obvious limitations of PEI as a gene delivery agent within the retina, we can confidently state that when S/MAR vectors are compacted with PEI – at the maximum threshold of 0.5 µg/µl - and injected into the correct or appropriate region of the eye long-term episomal expression as well as limited toxicity is observed.
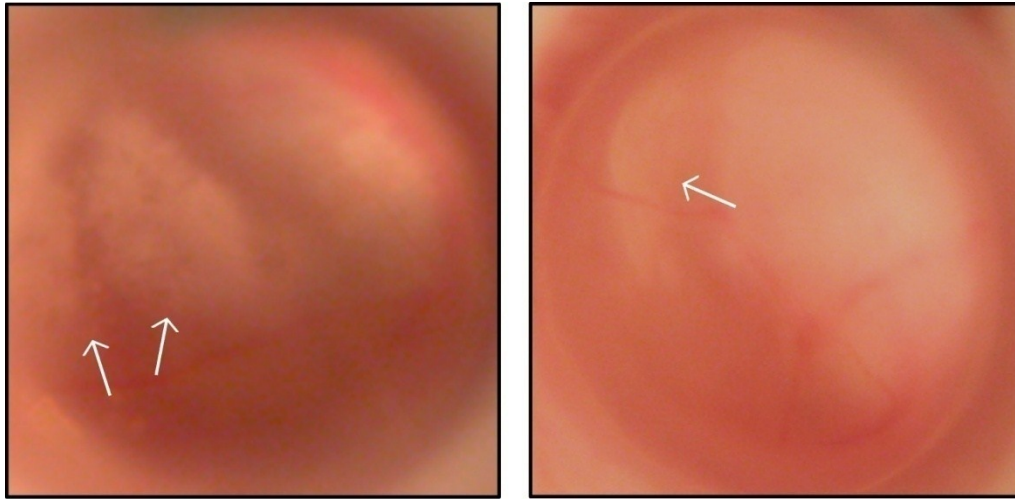
Figure 94: Representative ophthalmic examinations of fundi revealing the presence of precipitate following the subretinal injection of formulated PEI/pDNA

Shown are the fundus examination (*in situ)* of two MF1 WT mice following the subretinally injection of formulated pDNA. On rare occasions, precipitate was observed within the retina as evident by white plaques encompassing the site of the subretinal injection (as indicated by the arrows). Pronounced precipitate is seen in the image on the left while less precipitate as well as a retinal detachment is seen in the image on the right. Such mice were not included in any subsequent analyses. Digital images may be clearer.

3.3.12 Alternative administration routes in the eye - topical instillations and intravitreal injections

Subretinal injections can be arguable considered as the ultimate delivery route to be considered for administration in the eye, specifically to the retina and RPE cells. Indeed we have shown in previous sections that the subretinal delivery of formulated pDNA is able to reach our target RPE cells efficiently. However, we were also eager to analyse alternative administration and delivery routes for gene delivery in the eye. Topical instillations have until recently been considered to have limited efficiencies. Despite this, previous reports show expression in various ocular tissues including corneal epithelium and RPE cells after topical administration of polymer micelles (PM)-formulated pDNA via EDTA enhancer treatment followed by eye drop delivery of pDNA (Liaw, Chang et al. 2001).

Hence utilising a similar principle, briefly as described in the methods, the outbred MF1 mouse strain was used, where eyes were pretreated with 5 mM EDTA (10 µL per mouse eye) which was applied as topical eye-drops to the cornea. Ten minutes following pretreatment,

mice were then delivered with 0.5 µg/µl of formulated pCAG-Luc pDNA with PEI (10 µl per mouse eye, three times per day). As a control the other eye either received plasmid alone or PEI formulated pCAG-Luc pDNA without enhancer pretreatment. At 24 and 48 hours following the first topical administration, the mice were assessed for gene transfer and imaged for luciferase expression using a Xenogen *in vivo* bioluminometer.

Despite this we were unable to achieve any expression in the retina when topical instillations of EDTA enhancer and formulated PEI: pCAG-Luc pDNA, formulated pDNA without enhancer or plasmid alone was applied to the animals (data not shown).

Another alternative method of vector delivery in the retina is through intravitreal injections. Intravitreal injections would deliver injected vectors into the vitreous of the eye, however to be of interest to us, the vectors would need to reach the target RPE cells; hence they would need to diffuse through the vitreous as well as the neural retina before reaching the RPE (Maurice and Mishima 1984; Bishop 2000). We were interested in analysing whether through intravitreal injections – we could observe gene expression within the retina, ideally in the RPE cells and also whether any other cells within the retina could also be transfected too.

Hence in an approach identical to the initial stages of the subretinal injection technique described in section 3.3.1 and Figure 69A-D, MF1 mice were anesthetized and injected with a 32 gauge needle inserted through the sclera into the vitreous chamber of the eye. Mice were injected with 0.5 µg/µl of formulated/complexed pCAG-Luc pDNA with PEI (1-2 µl per mouse eye) as described in the methods. As a control the other contralateral eye remained uninjected, was injected with PBS alone or was injected with naked plasmid alone (uncomplexed). 24 and 48 hours following injection, mice were imaged for bioluminescent expression of luciferase as described earlier. Similar to the outcome seen for the topical instillations, no expression was observed in any of the groups of mice analysed following intravitreal injections of compelxed pCAG-Luc pDNA or naked pCAG-Luc pDNA with the retina (data not shown).

3.4 *In vivo* performance of REP1 plasmids (in WT and CHM mice)

3.4.1 Tissue expression of REP1 in MF1/WT mice

In an approach comparable to the RPE cell analysis of EGFP expression *in vivo*, the expression of REP1 protein was investigated. This was done by Western blot analysis of isolated RPE and neural cells from 10 C57BL/6 mice (3-4 months old) 48 hours following the double subretinal injection of formulated pCAG-REP1 and pCAG-REP1-Control plasmids. Samples were lysed and protein lysates (50 μg) were resolved on a 7% SDS-polyacrylamide gel. After this they were transferred to a PVDF membrane and probed with an anti-mouse REP1 antibody 2F1 which specifically recognises human Rep1 protein. A representative blot is shown in Figure 95. As expected, the Western analysis shows no expression within the neural retina while strong REP1 expression is seen within the isolated RPE cell layer from mouse retinas injected with both pCAG-REP1 and pCAG-REP1-Control pDNAs.

Noteworthy, is the fact that the similar Western blot experiment involving the subretinal injection of formulated pEFS-REP1 plasmid was unsuccessful; showing no expression within either of the two isolated cell layers.
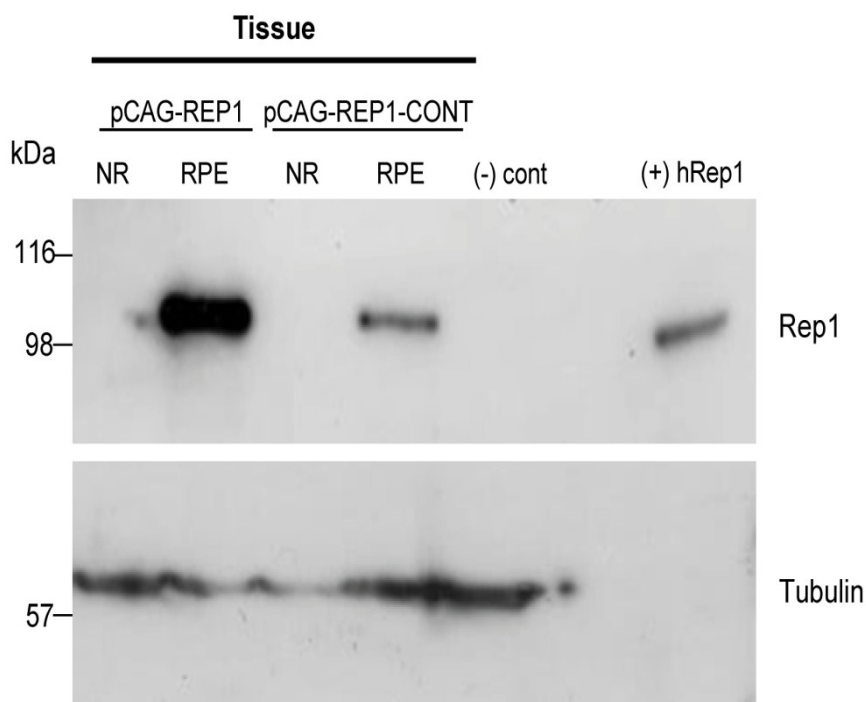
Figure 95: Western analysis of RPE and neural retinal cells isolated following the subretinal injection of pCAG-REP1 and pCAG-REP1-Control pDNA vectors

The figure shows the expression of REP1 protein levels by Western analysis after separation of the RPE and neural retina (NR) cells (50 µg) from C57BL/6 mice (n=10) 48 hours following the double subretinal injection of plasmids pCAG-REP1 and pCAG-REP1-Control. The expression of REP1 was observed using anti-mouse REP1 antibody 2F1 which specifically recognises human Rep1 protein. Strong REP1 protein levels are observed exclusively in the isolated RPE cells of both injected plasmid groups. Untransfected RPE cells served as a negative control. Human Rep1 protein (hREP1) served as a positive control (40 ng), while α-tubulin was used as a loading control.

While the expression of REP1 was confirmed in the RPE cells of injected C57BL/6 mice, we also wanted to show this localised expression by immunohistochemistry analysis of retinal sections. As we encountered considerable problems with the immunohistochemistry detection of EGFP S/MAR plasmids in C57BL/6 mice (described in the previous section 3.3.4.1), we performed immunohistochemical analysis of *REP1* transgene levels in MF1 mice. Mice were subretinally injected with pCAG-REP1 plasmid and at 1 week post injection eyes were enucleated and frozen sections were obtained. Sections were then analysed by immunohistochemistry for the detection of REP1 transgene levels using the 2F1 anti-mouse monoclonal REP1 antibody which recognises only human Rep1 protein. Unfortunately, no difference in the expression of REP1 was seen between the analysed injected and control

sections; where considerable background staining was observed in both sections (data not shown).

A possible explanation for the difficulties in detecting *REP1* transgene levels in these sections could be due to the lack of specificity of the 2F1 antibody, potentially due to the fact that this antibody is a mouse antibody which is being used on mouse tissue. While the 2F1 antibody is a mouse monoclonal antibody raised against recombinant human REP1 (Santa Cruz), the immunohistochemical analysis of mouse retinal samples, shows that as a monoclonal antibody, the 2F1 antibody, is not specific for a single epitope of the human REP1 protein, but rather when used on mouse tissue it also recognising the mouse REP1 epitope. Similar problems were also reported by others within our group when analysing retinal sections for REP1 expression levels using the 2F1 anti-mouse antibody.

3.4.2 Long-term expression of REP1 plasmids *in vivo* in WT/ MF1 mice

To analyse the long term transgene expression of REP1 *in vivo* in WT MF1 mice, total DNA was isolated from retinal homogenates at 1 week and 6 months following the subretinal injection of pEFS-REP1, pCAG-REP1 and control plasmids and analysed by PCR (Figure 96). PCR analysis of pEFS-REP1 and pCAG-REP1 pDNA revealed the long-term persistence of both plasmids within retinal homogenates. In contrast both control plasmids were absent at 6 months post injection. These long term pDNA results are in agreement with previous analyses of EGFP and luciferase S/MAR plasmids *in vivo*.

Total RNA was also extracted and REP1 RNA levels were analysed in retinal homogenates at 1 and 6 months post injection by rt-PCR analysis (Figure 97). Similar to the pDNA PCR results above, REP1 mRNA analysis shows the long-term mRNA levels of REP1 from both pEFS-REP1 and pCAG-REP1 injected retinas. The control injected samples in comparison loose REP1 mRNA levels by 6 months following injection.
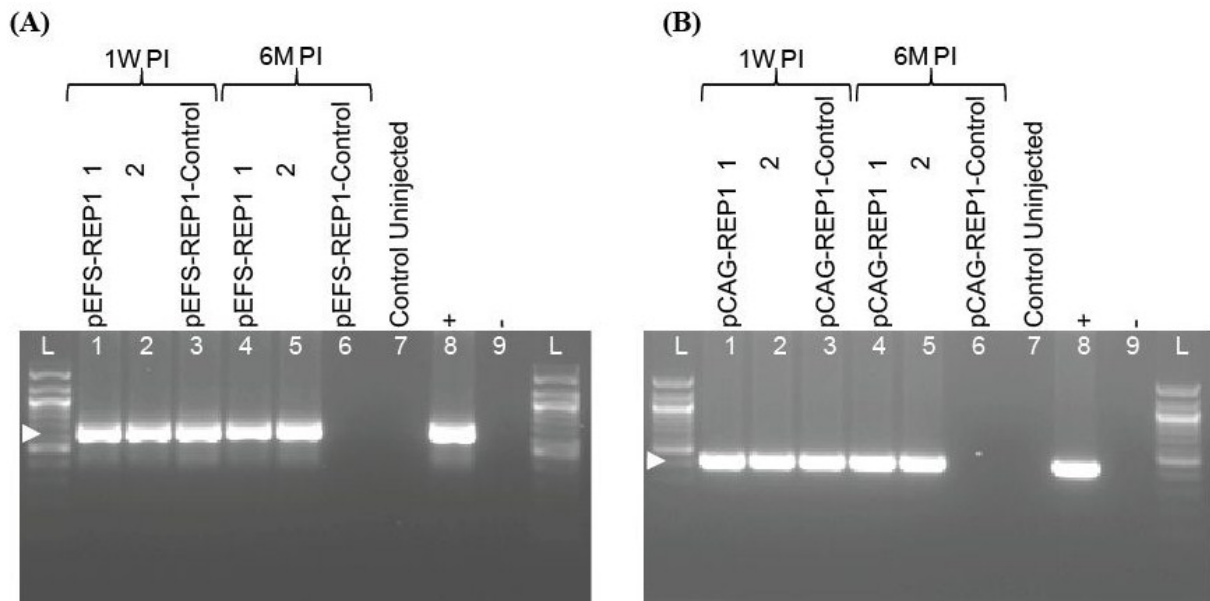
Figure 96: Short and long-term PCR detection of pEFS-REP1 and pCAG-REP1 pDNA vectors from eye homogenates following subretinal injections of MF1/ WT mice

PCR analysis of (A) pEFS-REP1 and pEFS-REP1-Control and (B) pCAG-REP1 and pCAG-REP1-Control pDNA vectors at 1 week (lanes 1-3) and 6 months (lanes 4-6) post injection (PI). PCR samples were separated by agarose gel electrophoresis and a positive PCR band was observed using EFS-REP1 or CAG-REP1 specific primer sets yielding a product size of 650 bp or 430 bp respectively. The arrowhead indicates the size corresponding to pDNA 650 bp on (A), 430 bp on (B). Uninjected eyes as well as no PCR product/water served as a negative control (lanes 7 and 9 respectively), while pDNA (25ng) pEFS-REP1 (in the case of A) or pCAG-REP1 (in the case of B) served as a positive control (lane 8) for the PCR reaction. Results are representative of three independent experiments. L= 100bp ladder (Invitrogen).
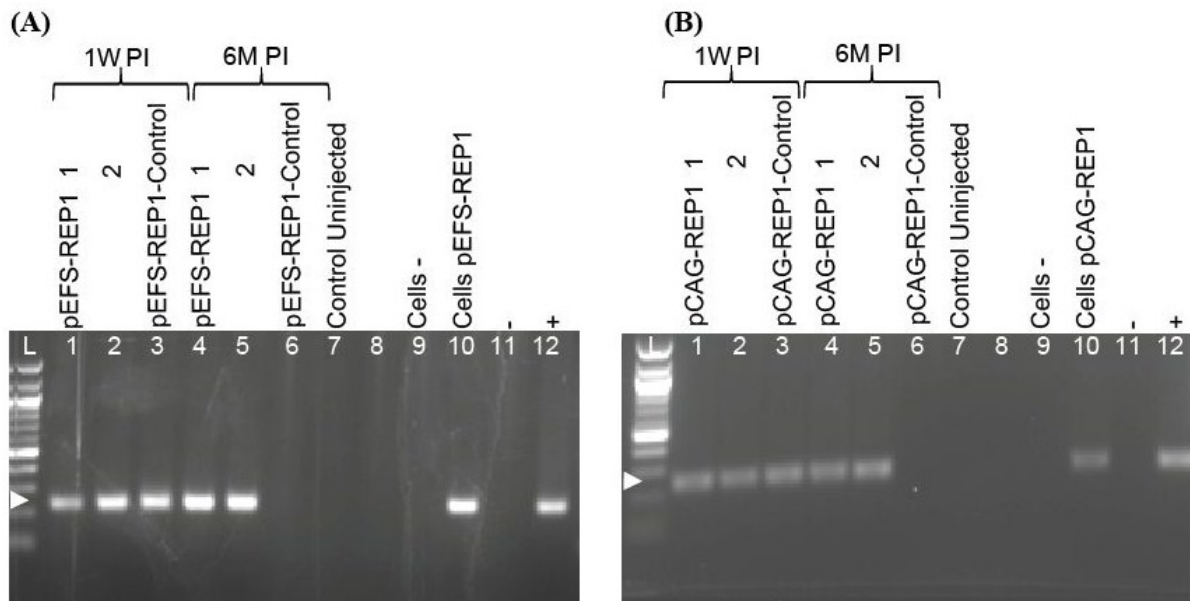
Figure 97: RT-PCR analysis of short and long-term REP1 mRNA from tissue homogenates following subretinal injections of MF1/ WT mice with pEFS-REP1 and pCAG-REP1 pDNA vectors

Total RNA was extracted from MF1/WT mice following single subretinal injections of (A) pEFS-REP1 and pEFS-REP1-Control and (B) pCAG-REP1 and pCAG-REP1-Control pDNA vectors at 1 week (lanes 1-3) and 6 months (lanes 4-6) post injection (PI). Total RNA was isolated and used to generate cDNA. PCR was performed with human REP1 specific primers to yield a product size of 240 bp as indicated by the arrowhead on (A) and (B). RNA from untransfected AtT20 cells as well as no RNA product/water served as a negative control (lanes 9 and 11), while AtT20 cells transfected with pEFS-REP1 (in the case of (A)) or pCAG-REP1 (in the case of (B)) served as a positive control (lane 10 and 12). Lane 8 is empty/blank. Results are representative of three independent experiments. L= 100 bp ladder (Invitrogen).

3.4.3 Episomal status of REP1 S/MAR plasmids in vivo

To confirm the episomal state of both REP1 constructs in the RPE cells of the retina, total DNA was isolated from retinal homogenates at 6 months post injection. Following this plasmid rescue analysis was performed on the pEFS-REP1 and pCAG-REP1 isolated from *E.coli* bacterial cells after transformation with 1 µg of total DNA. The restriction pattern of the pEFS-REP1 plasmid was analysed using *Eco*RI and *Xho*I; giving the fragments 3400 bp, 2301 bp and 1651 bp with *Eco*RI and fragments 1150 bp, 1300 bp and 4902 bp with *Xho*I. In contrast, the digestion pattern of pCAG-REP1 plasmid was analysed using *Eco*RI and *Eco*RV; giving the fragments 4830 bp, 2300 bp and 1700 bp with *Eco*RI and 2110 bp and 6720 bp with *Eco*RV. In all cases the restriction pattern was identical to those observed with the positive control of the digested original pDNA - pEFS-REP1 and pCAG-REP1 (Figure 98).

The episomal state was further confirmed by Southern analysis. Total retinal DNA was also isolated from non-S/MAR control plasmids of both REP1 constructs. Isolated DNA (30 µg) was digested with *Stu*I restriction enzyme and analysed by Southern hybridization with a ^{32}P-labeled *Alw*NI fragment - common to all S/MAR plasmids - that was used as a probe for the Southern blot. The hybridisation pattern clearly shows the episomal state of both pEFS-REP1 and pCAG-REP1 plasmids with distinct bands identical to the size of the original plasmids (Figure 99). Importantly, both control plasmids are still maintained episomally within the retina, although expression is observed to be only transient (Figure 96 and Figure 97).
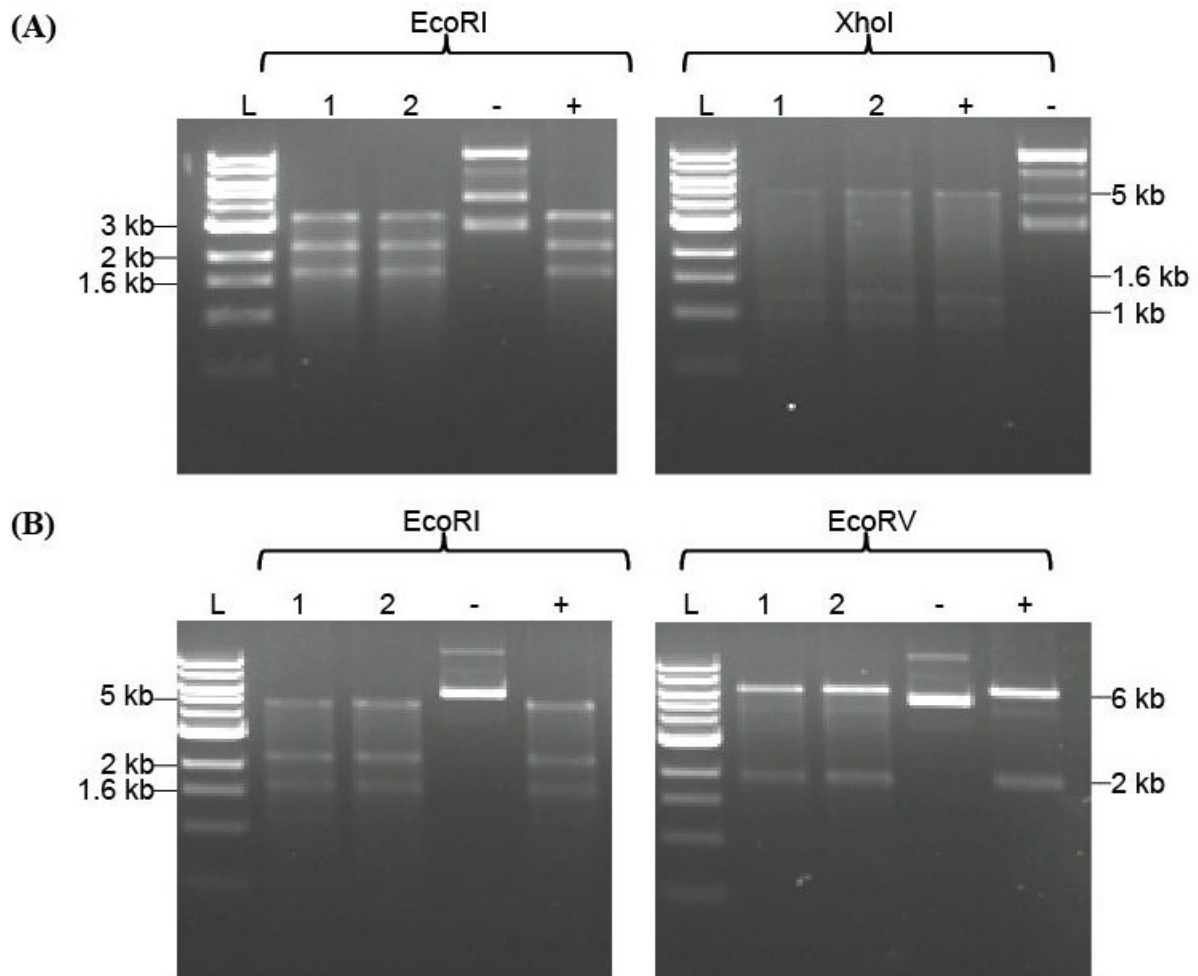
Figure 98: Plasmid rescue analysis of the episomal status of REP1 plasmids isolated at 6 months post subretinal injections in MF1/WT mice

Plasmid rescue analysis of pDNA isolated from 2 randomly chosen clones (lanes 1-2), after transformation of *E.coli* bacteria with 1 μg of total DNA isolated from eye homogenates of MF1 mice 6 months post subretinal injection of (A) pEFS-REP1 and (B) pCAG-REP1 pDNA vectors, performed as described in methods. Undigested plasmid served as a negative control (-), while all bands show identical sizes with the positive control of original pEFS-REP1 on (A) or pCAG-REP1 on (B) (+), demonstrating that pEFS-REP1 and pCAG-REP1 vectors are retained episomally in the retinas of injected MF1 mice. Results are representative of two independent experiments. Some fragments may be faint but seen clearer on the digital image. L: 1 kb Ladder (Invitrogen).
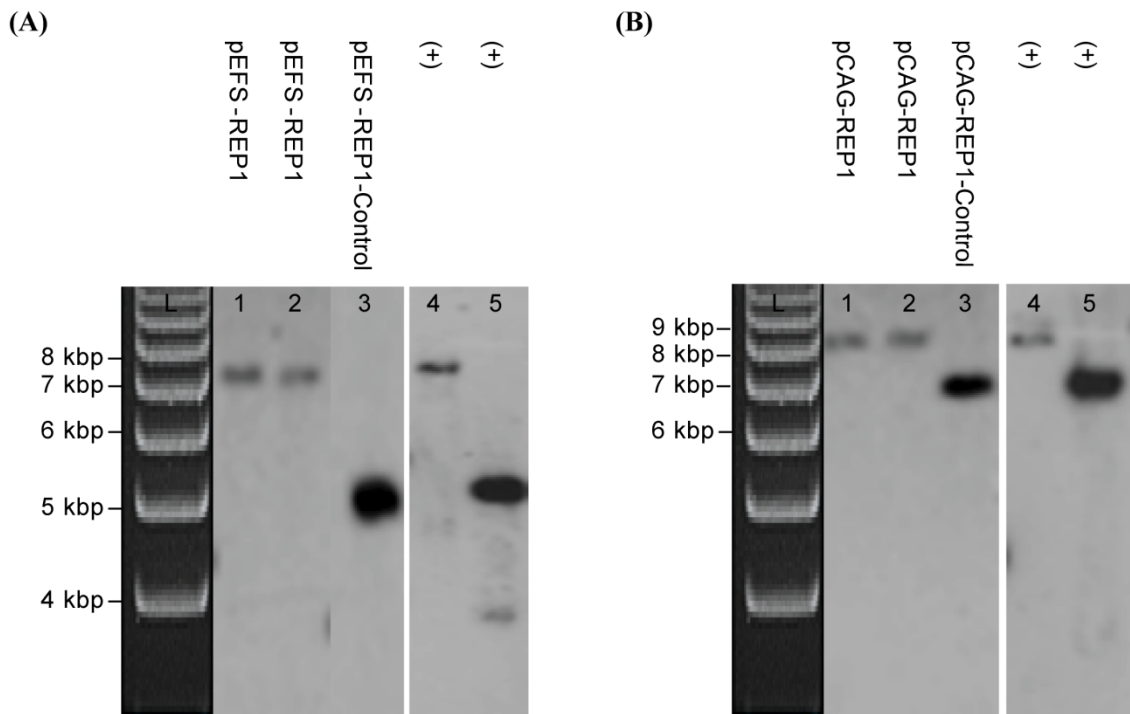
Figure 99: Southern blot analysis of the episomal status of REP1 plasmids isolated at 6 months post subretinal injections in MF1/WT mice.

Southern blots of total pDNA isolated from eye homogenates of MF1 mice 6 months post subretinal injection of (A) pEFS-REP1 and pEFS-REP1-Control and (B) pCAG-REP1 and pCAG-REP1-Control pDNA vectors, performed as described in methods. DNA (30 μg) was separated on 0.8% agarose gels and hybridized with ^{32}P-labelled *Alw*NI probe. Lanes 1-2, pEFS-REP1 or pCAG-REP1 isolated from eye homogenates (4-5 eyes per lane) by sacrifice 6 months post injection. Lane 3, pEFS-REP1-Control or pCAG-REP1-Control isolated from eye homogenates (4-5 eyes per lane) by sacrifice 6 months post injection. All clones produced a clear distinct band after *Stu*I digestion, identical to the band arising after digestion of 8 ng of corresponding positive control original pDNAs (pEFS-REP1 and pEFS-REP1-Control on (A) or pCAG-REP1 and pCAG-REP1-Control on (B); lanes 4 and 5 respectively (+)). Results are representative of two independent experiments. L: 1 Kb ladder (Invitrogen).

3.4.4 Tissue expression of REP1 in CHM mice

The ultimate aim of this study is to develop a non-viral S/MAR plasmid harbouring the *REP1* transgene, to be used as a potential novel therapeutic option for treating CHM mice *in vivo.* As shown in Section 3.3.4.1, S/MAR plasmids harbouring the EFS promoter show considerably lower plasmid expression *in vivo.* Hence despite both plasmids (pEFS-REP1 and pCAG-REP1) showing persistent expression in WT MF1 mice, only the pCAG-REP1 plasmid and its control were used for injections in CHM mice. We were eager to analyse the ability of pCAG-REP1 to mediate long-term REP1 transgene levels in CHM mice, as well as to assess the episomal status and any potential phenotypic or genotypic functional rescue within the retina following injections.

The CHM mouse models chosen for analysis where: CHM^{Flox}, Tyr-Cre^{+} mice and $Chm^{null/WT}$. In male and female mice, the CHM null alleles cause embryonic lethality; hence various CHM mouse models have been created to overcome these problems (Tolmachova, Anders et al. 2006). As CHM is X-linked, one such mouse model chosen is the CHM$^{null/WT}$ mice where heterozygous-null females are chimeras; approximately 50% of cells are expected to be knockout (KO) cells, showing no REP1 function, while the remaining cells are normal with normal REP1 function. As CHM$^{null/WT}$ mice show progressive degeneration of the retina by 4-8 months – as evident by patchy degeneration seen in both RPE and photoreceptor cells – these mice are the 'true' CHM mouse model to use for long term analyses. Hence 1 month old mice would be injected with formulated pCAG-REP1 prior to the onset of disease, and would be assess at 6 months post injection for the phenotypic rescue of degeneration within the retina - via detailed ophthalmic examination (using a scanning laser ophthalmoscope-SLO for detailed fundus examination), electroretinographic analysis (using an electroretinogram-ERG for detailed analysis of retinal function particularly in various cell types within the retina including the photoreceptors and ganglion cells) as well as histological analysis of injected retina sections.

In contrast, the CHM^{Flox}, Tyr-Cre^{+} mice are a tissue specific KO mouse model, showing complete KO within the RPE and other pigmented cells only, while the photoreceptors and remaining neural retina are normal. These mice were used for all short term experiments for genotypic rescue, where the assessment of *REP1* transgene levels as well as the rescue

of the prenylation defect, particularly rescue of Rab27a prenylation which is known to be defective in *CHM* mice would be assessed.

3.4.4.1 Long term expression in CHM mice

To assess the persistence of *REP1* transgene expression following the subretinal injection of formulated pCAG-REP1 and pCAG-REP1-Control in CHM injected mice, total DNA and RNA was isolated from retinal homogenates injected with both plasmids. For short-term expression, CHM^{Flox}, Tyr-Cre$^+$mouse homogenates were analysed 1 month post injection (PI), while CHM$^{null/WT}$ mouse homogenates were assessed for long-term expression at 6 months PI. Representative PCR analysis shows expression of both plasmids (pCAG-REP1 and pCAG-REP1-Control) at 1 month PI in CHM^{Flox}, Tyr-Cre$^+$analysed retinas. By 6 months PI only expression of pCAG-REP1 was observed in the CHM$^{null/WT}$ analysed retina, while expression of pCAG-REP1-Control was lost (Figure 100A).

Similarly rt-PCR shows high levels of REP1 mRNA from pCAG-REP1 plasmid at 1 and 6 months PI corresponding to the CHM^{Flox}, Tyr-Cre$^+$and CHM$^{null/WT}$ retinas respectively, while REP1 mRNA levels were lost by 6 months PI from the retina of a CHM$^{null/WT}$ mouse injected with pCAG-REP1-Control plasmid (Figure 100B).
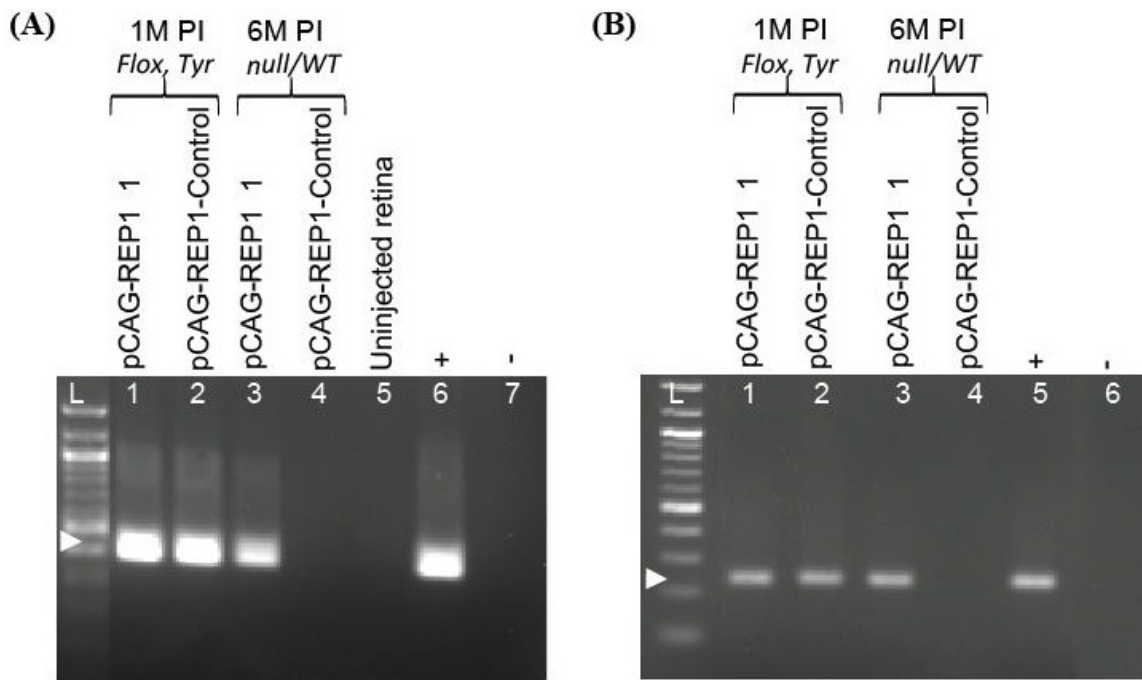
Figure 100: Analysis of short and long-term pCAG-REP1 pDNA and REP1 mRNA from tissue homogenates following subretinal injections of CHM mice with pCAG-REP1 pDNA vector

CHM^{Flox}, Tyr-Cre$^+$ (*Flox, Tyr*) and CHM$^{null/WT}$ (*null/wt*) mice were subretinally injected with pCAG-REP1 and pCAG-REP1-Control pDNA vectors, performed as described in methods. (A) Isolated DNA was extracted from injected retinas at 1 month (lanes 1-2) and 6 months (lanes 3-4) post injection (1M and 6M PI respectively). PCR samples were separated by agarose gel electrophoresis and a positive PCR band was observed using CAG-REP1 specific primer sets yielding a product size of 430 bp as indicated by the arrowhead. Uninjected retinas from *CHM^{Flox}*, Tyr-Cre$^+$ mice, as well as no PCR product/water were included as a negative control (lanes 5 and 7), while pDNA (25ng) pCAG-REP1 served as a positive control (lane 6) for the PCR reaction.
(B) Total RNA was isolated and used to generate cDNA. PCR was performed with human REP1 specific primers to yield a product size of 240 bp as indicated by the arrowhead. As a negative control no RNA product/water was used (lane 6), while RNA from human CHM4 KO cells transfected with pCAG-REP1 served as a positive control (lane 5). Each lane represents one retina analysed. L= 100 bp ladder (Invitrogen).

3.4.5 Episomal status in CHM mice

In order to investigate the status of the pCAG-REP1 plasmid in the retina at 1 and 6 months PI, total DNA from the corresponding *CHM^Flox,* Tyr-Cre^+ and CHM^null/WT mice were obtained and analysed by plasmid rescue for episomal maintenance. *E.coli* cells were transformed with 1 µg of total DNA and kanamycin-resistant colonies were obtained the next day at a rate of between 3-5 colonies per plate. This low number signifies that the pCAG-REP1 plasmid is maintained at a low plasmid copy number within the retina, as shown previously for pCAG-REP1 and pEFS-REP1 in WT mice. Plasmids isolated from two colonies for the pCAG-REP1 plasmid (using a MiniPrep kit) were digested with *Eco*RI and *Eco*RV restriction enzymes*.* The fragments 4830 bp, 2300 bp and 1700 bp were observed with *Eco*RI and 2110 bp and 6720 bp with *Eco*RV. The restriction patterns of this plasmid are consistent with an unmodified non-integrating plasmid construct (Figure 101).
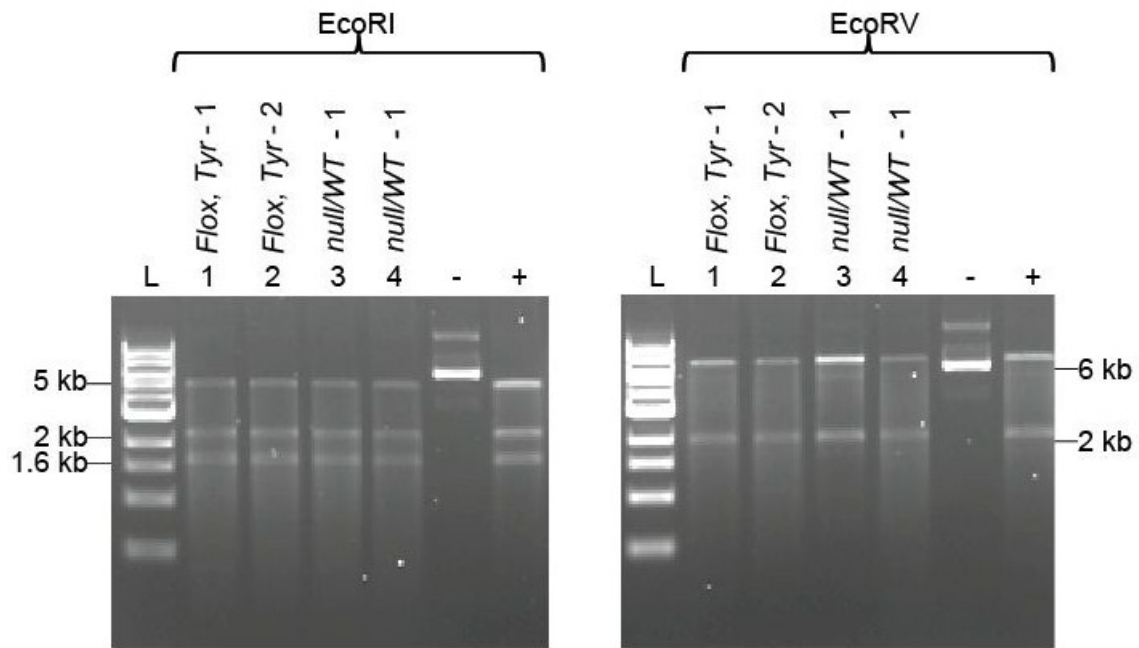
Figure 101: Plasmid rescue analysis of the episomal status of pCAG-REP1 vector isolated at 1 month and 6 months post subretinal injections in CHM mice

Plasmid rescue analysis of total DNA isolated from eye homogenates of *CHM^Flox,* Tyr-Cre^+ (*Flox, Tyr*) and CHM^null/WT (*null/wt*) mice at 1 and 6 months post injection (PI) of pCAG-REP1 plasmid. The left panel shows the *EcoRI* restriction pattern of pDNA isolated from 2 randomly chosen clones after transformation of *E.coli* bacteria with 1 µg of total DNA isolated from eye homogenates of *CHM^Flox,* Tyr-Cre^+ mice at 1 month PI (lanes 1-2) and CHM^null/WT mice at 6 months PI (lanes 3-4). The right panel shows the *Eco*RV analysis of the same 2 clones at 1 and 6 PI. Undigested plasmid served as a negative control (lane 5; -), while all bands show an identical size to the positive control pCAG-REP1 (lane 6; +), verifying the episomal status of pCAG-REP1 vector in the retinas of injected CHM mice. L: 1 kb Ladder (Invitrogen).

3.4.6 Functional long-term rescue in CHM mice

To determine if the long-term expression of REP1 protein within the retinas of injected CHM mice was able to provide functional rescue of the CHM phenotype, we analysed the prenylation status of Rab27a protein within the RPE cells of injected CHM$^{null/WT}$ mice at 6 months post injection (PI). We have shown previously that following subretinal injections of S/MAR pDNAs into the retina, RPE cells are transduced. Hence, RPE cells were isolated from 4 injected retinas as described previously. RPE cells were isolated and used for subsequent analysis rather than intact retinal homogenates, as we wanted to increase the chances of seeing a functional phenotypic effect. Thus this was most likely to be within the cells we know we have been able to transfect in the past. Isolated RPE cells were also collected from uninjected retinas of the same mouse. Briefly, we isolated the RPE cells from these mice and analysed the Rab27a prenylation status by subjecting cells to subcellular fractionation and subsequent immunoblot analysis probing with an anti-Rab27a antibody 4B12.

Figure 102 shows the Western blot performed on the RPE cells isolated from the long-term expressing CHM$^{null/WT}$ mice at 6 months post injection (PI) with pCAG-REP1 plasmid. The blot shows the presence of Rab27a protein in both the cytosolic and pellet fractions in the RPE cells isolated from uninjected CHM$^{null/WT}$ mice. This expression pattern shows that the Rab27a protein within these cells is not correctly prenylated and so remains in the cytosol and in turn is dysfunctional. Excitingly, when this expression pattern is compare to that of isolated RPE cells from injected CHM$^{null/WT}$ mice at 6 months PI, a clear shift and subsequent reduction in the expression of Rab27a protein levels in the cytosolic fraction is observed. This shows that after 6 months following the subretinal injection of pCAG-REP1 pDNA vector in CHM$^{null/WT}$ mice, we were able to observe the functional phenotypic rescue of Rab27a protein expression within the RPE cells isolated from injected retinas.

Despite the clear Rab27a rescue observed, many reports have also indicated that a number of other as yet unidentified Rab proteins may also be defective in CHM cells (Tolmachova, Anders et al. 2006, Seabra 1996; Seabra, Ho et al. 1995). Hence while these results are extremely exciting, one cannot rule out that other Rab proteins (which have not been analysed in these samples) may not have been functionally rescued and indeed the defect of prenylation in these other Rab proteins may not be observed.
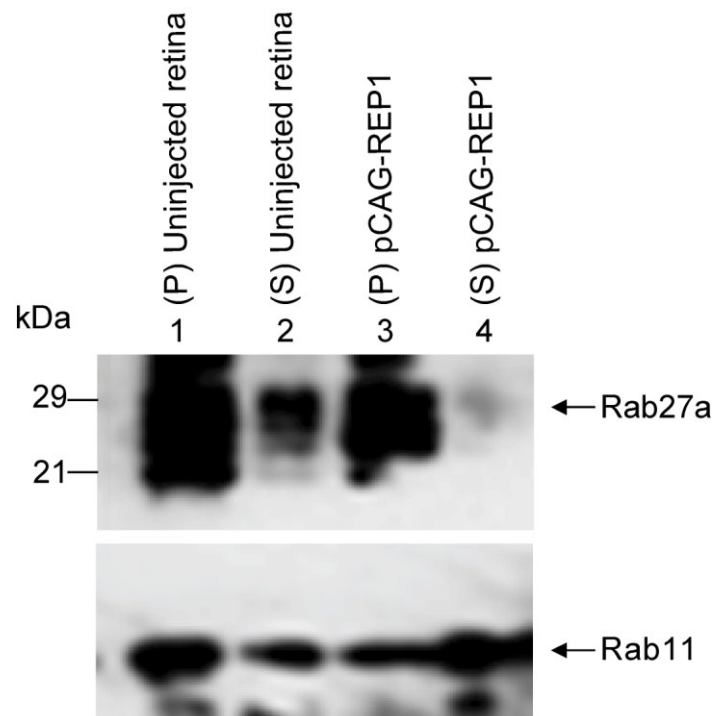
Figure 102: Western analysis showing the phenotypic rescue of Rab27a protein function in CHM^{null/WT} mice at 6 months post subretinal injection of pCAG-REP1 vector

RPE cells were isolated from CHM^{null/WT} mice at 6 months following the subretinal injection of pCAG-REP1 pDNA vector. Cells were lysed (25 μg) and subjected to subcellular fractionation where soluble (S) and pellet (P) fractions were analysed by Western analysis and probed with anti-Rab27a antibody 4B12. RPE cells from injected CHM^{null/WT} mice at 6 months PI show a clear shift and reduction of Rab27a protein expression in the soluble fraction compared to the pellet fraction, indicating that these isolated RPE cells have less unprenylated Rab27a protein in the cytosol, and so a functional rescue of Rab27a protein is observed. Rab11 was used as a loading control. Results are representative of one experiment.

Out of 9 CHM^{null/WT} mice injected in total, by 6 months following injection, 6 mice had developed dense iatrogenic cataracts; i.e. these cataracts were induced inadvertently following the subretinal injection procedure. This was most probably due to the lens being touched during the injection procedure. At the stage of injection, all 9 CHM mice were extremely small as they were only 1 month old, thus these mice were probably more vulnerable to iatrogenic cataracts, due to the small size of all retinas. Unfortunately all iatrogenic cataracts were too dense to allow subsequent fundus examinations. Furthermore the remaining 3 CHM mice, while all had milder iatrogenic cataracts, only partial fundus examinations were possible. Despite this, we decided to analyse these three mice for

additional functional rescue, where the mice were transferred to a collaborator Prof Robert MacLaren at Oxford University for further analysis (SLO and ERG analysis). Due to time restraints, these experiments were still ongoing at the end of this study and so were not included in this project.

4   DISCUSSION
_____

4.1   The ideal gene therapy vector – Summary of project

Viral vectors have long been the preferred system in the majority of experimental and clinical studies for ocular gene therapy. However, several safety issues have been highlighted in recent times (Provost, Le Meur et al. 2005; Stieger, Colle et al. 2008), paving the way for alternative delivery routes. Despite this, alternative non-viral vectors have often been plagued by low transfection efficiencies and transient transgene expression in vivo. These problems have rendered them unacceptable as gene delivery options for the clinic. The exception to the rule has possibly been the development of nanoparticles and their successful long-term expression *in vivo* (Farjo, Skaggs et al. 2006; Cai, Nash et al. 2009). We hoped to utilise vectors harbouring scaffold/matrix attachment regions (S/MARs) as an alternative non-viral delivery tool. To this end, the aim of this study was to develop a novel, non-viral, episomal gene therapy vector for stable, long-term gene expression *in vitro* with ocular applications. Specifically, we aimed towards the development of a non-viral gene therapy strategy for Choroideremia (CHM).

The ideal non-viral vector for human gene therapy must be able to mediate long-term levels of therapeutic transgene expression as well as having no detrimental effect on the host at the cellular or somatic level. The recently described pEPI vector possesses key features of replication and episomal retention. This appears to be solely through the use of an S/MAR which functions as a *cis*-acting element for episomal retention (Jackson, Juranek et al. 2006). Of particular interest are the mammalian S/MAR elements, the human β-interferon gene cluster. This class of S/MAR elements has been shown *in vitro* to prevent S/MAR-containing pDNA vectors from integration (Piechaczek, Fetzer et al. 1999), epigenetic transgene silencing while also promoting extra-chromosomal and mitotic stability (Jenke, Stehle et al. 2004). Noteworthy is the fact that these key characteristics are provided without the need for viral encoded proteins (Piechaczek, Fetzer et al. 1999; Papapetrou, Ziros et al. 2006). The ability to provide mitotic stability is thought to be due to the direct interaction of the S/MAR element with the components of the nuclear matrix (Jenke, Fetzer et al. 2002; de Jong

2006). In particular, the S/MAR element from the pEPI plasmid was found to preferentially associate with the scaffold attachment factor A (SAF-A) protein which is a principle component of chromatin and chromosomes (Kipp, Gohring et al. 2000). This interaction most likely brings pEPI into contact with the host replication machinery, which is located on the nuclear matrix, hence facilitating pEPI replication once per cell cycle.

Furthermore, S/MAR pDNAs have also recently been shown to provide persistent transgene expression *in vivo* following hydrodynamic delivery to the murine liver (Argyros, Wong et al. 2008). However the precise mechanism by which S/MAR elements provide this key sustainability *in vivo* has not been investigated.

The CMV promoter of the pEPI plasmid has been shown to provide high transgene levels *in vitro.* However, *in vivo* expression is transient. This is primarily due to viral promoters such as CMV, becoming transcriptionally silenced due to methylation of the promoter (Jenke, Stehle et al. 2004; Brooks, Harkins et al. 2004; Kachi, Esumi et al. 2006; Kachi, Oshima et al. 2005). Hence to minimise the potential loss of transgene expression we developed other plasmids harbouring different promoters.

Previous studies for targeted delivery to specific cell types within the retina have utilised tissue specific promoters. The promoters of interphotoreceptor retinoid binding protein (IRBP) (Semple-Rowland, Eccles et al. 2007) as well as rhodopsin (RHO) genes (Bemelmans, Bonnel et al. 2005) have been effectively used for delivery to the photoreceptor cells. In contrast, the vitelliform macular dystrophy (VMD2) and tyrosinase related protein-1 (Tyrp1) or tyrosinase (Murisier, Guichard et al. 2006) promoters have been shown to selectively express in RPE cells (Kachi, Oshima et al. 2005; Kachi, Esumi et al. 2006). However as CHM is a disease primarily of both these cell layers, we chose to create plasmids with ubiquitously expressed promoters based on the elongation factor-1 (EF1-α and its intronless version EFS) and (CMV) early enhancer/chicken beta actin (CAG) promoters. Both promoters have been shown in the past to maintain efficient expression in the RPE and photoreceptor cells (Kostic, Chiodini et al. 2003; Cashman, McCullough et al. 2007). We show that the inclusion of an S/MAR element into an EFS and CAG promoter-driven plasmid is able to provide persistent transgene expression *in vitro.* However, perhaps more importantly, following the

subretinal delivery into the mouse retina, we show the unparalleled long-term transgene expression from both these S/MAR vectors in ocular tissue. To our knowledge this is the first attempt with pDNA to correct for CHM, where we showed a partial correction of the phenotype *in vitro* as well as *in vivo.*

While this is extremely exciting*,* the results provided in this study have some limitations. Furthermore improvements can be made to our current episomal plasmids to enhance and stabilise gene expression.

4.2   Experimental Limitations

A substantial limitation to the experiments described throughout this thesis has been the lack of appropriate 'negative rt' controls in all rt-PCR experiments. During RNA preparations, it is virtually impossible to completely eliminate genomic DNA. Therefore it is important to include a minus-reverse transcriptase control in all rt-PCR experiments; typically this would include a mock reverse transcription containing all rt-PCR reagents, except the reverse transcriptase. If a product is observed with the negative rt control, this would indicate that contaminating DNA is present in the sample. As this important control is missing from all rt-PCR experiments, and thus genomic DNA contamination cannot be ruled out, one must be cautious with the interpretation of these results.

An additional limitation due to time restraints was the fact that all prenylations experiments were only performed once. While long term Western analysis showing phenotypic rescue of Rab27a protein function *in vitro* as well as *in vivo* with the pCAG-REP1 vector was demonstrated clearly, further repeat experiments would add confidence to these experiments.

4.3 Long-term expression *in vitro*

4.3.1 Immortalised cell lines

Following the generation of stable pEGFP-S/MAR and pREP1-S/MAR vectors in AtT20 cells, we were able to show that both plasmid vectors were able to mediate persistent transgene expression *in vitro.* This is in agreement with previously published reports for pEPI plasmid in cell lines including the Chinese hamster ovary (CHO-K1) cells (Piechaczek, Fetzer et al. 1999; Papapetrou, Zoumbos et al. 2005), human cervical cancer (HeLa) cells (Schaarschmidt, Baltin et al. 2004) and mouse embryonic fibroblast (NIH 3T3) (Broll, Oumard et al. 2010). Furthermore efficient replication and episomal maintenance was observed in these cells. We show that all plasmids were maintained at a low-copy number (vector molecules/cell) *in vitro.* Similar finding were seen in previous studies where less than 10 copies/cell have been reported for the pEPI plasmid (Piechaczek, Fetzer et al. 1999; Baiker, Maercker et al. 2000).

Interestingly we show that *in vitro* the promoter is not the principle requirement for long-term transgene expression. Indeed the active transcription of the promoter upstream of the S/MAR and then continuation past the promoter and extending part of the way into the S/MAR is believed to be crucial for long-term expression *in vitro* (Stehle, Scinteie et al. 2003).

While long-term expression was observed, an initial selection pressure in the form of antibiotic (G418) was required. This was because without this selection pressure, expression was readily lost *in vitro* (personal observations). Suggestions have been made that following G418 selection, pEPI is able to be maintained in nuclear compartments called 'replication factories'. These factories aid in the ability of pEPI to persistently express transgenes (Cook, Gattone et al. 1983; Zaidi, Young et al.2005). This hypothesis suggests that several molecules of DNA polymerase are located and only active within the nucleus at these replication factories. Therefore one can propose that following the transcription of the neo/kan gene within these plasmids, as well as the treatment with the G418 antibiotic, these cells were able to be maintained within these replication factories. If the maintenance of plasmids in these factories is a rare event, the necessity for this initial selection pressure becomes clear. Furthermore our plasmids are maintained extra-chromosomally possibly due

to the binding the S/MAR elements within our plasmids to the SAF-1 protein. This theory could also explain the reason why we were able to observe episomal maintenance of all S/MAR and non-S/MAR plasmids *in vitro*, despite the lack of persistent transgene expression from the non-S/MAR plasmids.

4.3.2 Primary fibroblasts

We were also able to perform the novel proof-of-principle experiments were we showed long-term expression of pCAG-REP1 in CHM KO human (CHM4 fibroblasts) and mouse (Flox, MerCreMer[+], tamoxifen-induced) cells. Both primary KO cell lines expressed moderate levels of the human REP1 protein up to 6 weeks *in vitro*. The lack of REP1 function in CHM is thought to be caused by Rab prenylation defects, in particular Rab27a (Seabra, Ho et al. 1995). Therefore in order to assess the ability to rescue the function of these cells *in vitro,* we assessed the prenylation status of Rab27a within our long-term expressing cells. We were able to observe a shift in the pattern of Rab27a protein, from the cytosolic to the pellet fraction. This suggested that following transfection with the pCAG-REP1 plasmid, these KO cells are able to correctly prenylate Rab27a and subsequently correctly target Rab27a to intracellular membranes. These novel experiments highlighted the utility of S/MAR vectors for CHM therapy.

4.4 Long-term expression *in vivo*

4.4.1 Effective Subretinal injections and formulations

We have also shown unparalleled long-term transgene expression and efficient delivery of our S/MAR vectors within the retinas of injected mice for up to 1 year following a single subretinal injection. Furthermore, we also showed the episomal maintenance within the RPE cells of the retina for up to 6 months following injections of pDNA. Noteworthy is the observation that there was minimal adverse effect from the subretinal injection of S/MAR pDNA into the mouse eye. This was analysed by H&E analysis, TUNEL staining, fundus imaging as well as ELISA analysis showing normal morphology as well as limited levels of inflammatory cytokines in the retina.

Interestingly, we observed for that upon comparison of complexed vector DNA from both S/MAR and control (non-S/MAR) plasmids, transgene expression levels were diminished in all control plasmids as early as one month post injection. This was seen regardless of whether the pDNA expressed luciferase or EGFP. Indeed this pattern of transient expression is in agreement with previously published studies where non-S/MAR plasmids showed a sharp decline in transgene levels within one week of injection in the liver (Argyros, Wong et al. 2008; Wong, Argyros et al. 2011). The authors suggested this was due to extensive methylation of the promoter sequence in these non-S/MAR plasmids (Argyros, Wong et al. 2008). However, there are also numerous other reasons for transcriptional silencing within the eye following injections of vectors including histone deacetylation (Fedor and Daniell 1980) as well as cytokine-induced suppression (Fiorentini and Maffei 1976). One can elucidate that the latter is unlikely to be attributed to transcription silencing in our study, as no elevated levels of cytokines were detected in subretinally injected retinas. However additional work is needed to clearly establish the mechanism of the transcriptional silencing of control plasmids in the retina.

Regardless of this, we have shown that pDNA vectors harbouring an S/MAR moiety with a ubiquitously expressing promoter are indeed protected from silencing in the eye. Interestingly, this is contrary to previous reports that show synergy between S/MAR elements and tissue specific promoters (Argyros, Wong et al. 2008). One can speculate that the within the retina as the cells are non-dividing, ultimately, if one is able to direct pDNA efficiently with an S/MAR plasmid containing a strong promoter - regardless of whether this is a tissue specific promoter or not - one can obtain long-term expression. Therefore the need for tissue specific promoters may only apply to rapidly dividing tissues such as the liver. Within the retina, we are able to effectively complex our pDNAs with the cationic polymer polyethylenimine (PEI) and subsequently, this together with the efficient delivery to the retina via a subretinal injection is able to mediate long-term transgene level *in vivo*.

In our study, we observed that the luciferase expression following administration of naked/un-complexed pDNA (pCAG-Luci-S/MAR) was initially similar to the expression of complexed pDNA (PEI: pCAG-Luci-S/MAR). In first light this appears puzzling, however this may be explained by the low nuclease activity in the eye (Napirei, Ricken et al. 2004; Kurreck 2009). Hence after a brief period of expression, naked pDNA is either shed away by

nucleases or switched off by a number of ways indicated previously, due to the lack of a PEI protective barrier surrounding the pDNA upon subretinal injection in the eye.

4.4.2   Lack of expression following alternative routes

During this study, we were also eager to analyse whether by utilising different delivery routes in the eye we could potentially target transgene expression to different regions of the eye. Previously, polymer micelles (PM) have been formulated with pDNA and delivered efficiently to the eye via topical instillations (Liaw, Chang et al. 2001). Interestingly, this report showed successful delivery to the cornea as well as other cells of the eye (at a lower level) using an enhancer treatment of EDTA prior to pDNA delivery. Utilising a similar approach, we found no expression in the cornea or retina after EDTA enhancer and formulated PEI:S/MAR pDNA was applied to the corneas of mice. While the mechanism of EDTA transport is largely unclear in the cornea, it has been proposed that internalisation is influenced by endocytosis and the opening of the tight junctions at the corneal epithelium (Liaw, Chang et al. 2001; Tong, Chang et al 2007). It is important however to note that, the transport mechanism of complexed PEI is known to be through the proton-sponge mechanism (Boussif, Lezoualc'h et al. 1995; Behr 1997) and indeed the escape from the endocytic pathway. Hence as the transport mechanism of PEI is not through endocytosis, it perhaps is not surprising that no expression was observed in corneal tissues or other areas of the retina following eye drop delivery of S/MAR formulated pDNA. Importantly the fact that naked/un-complexed DNA also showed no expression in the eye perhaps highlights the limitations of this approach in reaching not only corneal cells but also cells of the inner retina.

As an alternative method, we also attempted to deliver pDNA formulations to the retina via intravitreal injections; however this also resulted in no expression within the retina. This may be explained by studies which have looked into the complex network within the vitreous, namely the negatively charged glycosaminoglycans (GAGs). Within the vitreous, GAGs bind to positively charged complexes such as cationic lipids if delivered to the vitreous without shielding their surface with polyethylenegylcol (PEG; named 'pegylation') (Peeters, Sanders et al. 2005; Pitkanen, Ruponen et al. 2003). Hence one can explain the lack of

expression following the intravitreal injections of formulated pDNA with PEI due to the lack of pegylation of these pDNAs prior to injection. Indeed as GAGs are negatively charged, they have a high affinity for positively charged lipids whereby they bind and form aggregates within the retina if delivered unpegylated (Peeters, Sanders et al. 2005; Peeters, Sanders et al. 2007). Furthermore, the neural retina - in particular the inner limiting membrane (ILM) - is also poorly permeable to unpegylated complexes including PEI polyplexes we used within our study, as shown previously (Pitkanen, Ruponen et al. 2004).

While we observed no expression following intravitreal injection of PEI/DNA polyplexes at a nitrogen/phosphate ratio of 8:1 (N/P 8), we did not optimise the transfection efficiencies using this approach. Indeed others have found that following the intravitreal injection of PEI/DNA polyplexes at N/P 10, transgene expression was evident in the ganglion cell layer of the retina (Liao and Yau 2007). Our current formulations are efficient at delivering transgenes to the subretinal space, specifically well suited to targeting the RPE cell layer. However future optimisation of formulations coupled with intravitreal injections could allow the expression of transgenes to other cell types such as ganglion cells. This is seen in recent studies which have shown the restoration of photosensitivity in mice that have degenerated rod and cone cells. In these studies following intravitreal injections, virus-mediated expression of channel rhodopsin, which is a photosensitive ion channel, was observed in ganglion cells (Bi, Cui et al. 2006). Thus future developments of this approach could have considerable implications for targeting other cell types in the retina.

4.4.3 Improvements in the gene delivery vehicle

PEI has been shown to efficiently condense pDNA *in vitro* as well as *in vivo* (Boussif, Lezoualc'h et al. 1995). Furthermore the significant expression observed in the retinas of injected mice also shows that PEI has considerable utility for ocular gene therapy. Unfortunately however, the ultimate development of clinically viable formulation of PEI, appear to be limited. This is mainly due to the limited stability as well as the low concentration of PEI/pDNA complexes (0.5 µg/ µl) in solution prior to the loss of stability – normally in the form of precipitate.

Indeed in some rare situations we saw the presence of precipitates within the retinas of injected mice. However noteworthy is the fact that, despite the observation of precipitate, luciferase expression was still seen within the eye. One could argue that the occurrence of precipitates within the retina may not have been solely due to the instability of PEI/DNA complexes in solution. It may be likely that the vector which was injected into the retina may not have completely entered the subretinal space, while small amounts of vector could also have entered the vitreous. As mentioned previously, GAGs found in the vitreous have been shown to cause severe aggregation of lipoplexes within the vitreous (Peeters, Sanders et al. 2005; Pitkanen, Ruponen et al. 2003). Interestingly the aggregation of nanoparticles in the vitreous is overcome by shielding their surface through pegylation (Peeters, Sanders et al. 2005; Peeters, Sanders et al. 2007). Hence in the future perhaps pegylation of S/MAR pDNA vectors could be examined as a route to avoid aggregation of the vectors in the vitreous.

The problem of low concentrations of PEI/DNA complexes is heightened by the limited size of the retina. This is particularly evident in the mouse retina, as following stable complex formulations a maximum volume of 1-2 μl can be injected into the retina before which irreparable damage is observed. Davies *et al*. recently introduced a method of concentrating pDNA/PEI complexes using ultracentrifugation, whereby concentration levels of pDNA/PEI formulations were dramatically increased from 0.2 to >8 mg/ml pDNA (Davies, McLachlan et al.2008). For future experiments one could take these results forward and potentially enhance the concentration of pDNA/PEI complexes delivered to the retina using ultracentrifugation.

4.5 A therapeutic option for Choroideremia

The ultimate aim of this project was the development of non-viral vectors for CHM gene therapy. Hence we hoped to apply the success of our preliminary proof-of-principle experiments in CHM KO cells to show that our plasmids were able to also provide phenotypic correction *in vitro.* To this end, we initially showed the transient and long-term expression of pCAG-REP1 in the RPE cells of two CHM models: Tyr-Cre[+] and CHM[null/WT] mice.

Furthermore we also showed that pDNA in the retinas of injected mice was maintained as an episome. However our ultimate intereste was to analyse whether long-term REP1 protein within injected retinas of CHM mice could provide functional rescue of the CHM phenotype in the CHM$^{null/WT}$ mice. Tolmachova *et al.* have previously shown this mouse model to have prenylation defects, namely defects of Rab27a (Tolmachova, Anders et al. 2006). We were able to observe a shift in the cytosolic fraction of Rab27a protein which showed that Rab27a was able to be correctly prenylated in the RPE cells of these mice following the subretinal injection of pCAR-REP1 plasmid. Hence a partial phenotypic rescue in the RPE cells of the CHM$^{null/WT}$ mice was observed. While these results *in vitro* as well as *in vivo* are extremely promising, many reports have indicated that a subset of Rabs underlay the CHM phenotype or at least are responsible for its appearance (Tolmachova, Anders et al. 2006, Seabra 1996; Seabra, Ho et al. 1995). Interestingly, Rab27a deficiency mice (*ashen* mice) do not show signs of retinal degeneration (Gibbs, Azarian et al. 2004); hence one cannot rule out other Rab proteins that may be defective within these cells that have not been analysed.

Despite this, as virtually no functional REP1 is produced in CHM, the presence of a low level of functional REP1 protein localised within the eye, could potentially prenylate enough critical Rab proteins within the eye, resulting in the normal function and in turn potentially also preventing or arresting disease development and progression.

4.5.1 Future work for CHM gene therapy

4.5.1.1 Further development of the current construct

The current pREP1-S/MAR vectors created during this project can be modified by a number of ways. The REP1 expressing S/MAR plasmids could be modified to containing reporter gene such as *EGFP* or *Luciferase* which would be advantageous and allow easier detection of *REP1* transgene levels *in vivo*. This could be done using a bicistronic cassette (with an internal ribosome entry site (IRES)) would allow translation of two proteins under the control of a single promoter. Hence this would enable the simple monitoring of our protein

of interest (REP1) through the observation of an easily detectable reporter gene either *EGFP* or *Luciferase*.

It may also be interesting to explore the idea of subretinally injecting two pREP1-S/MAR vectors with two different tissue specific promoters for the treatment of CHM. As CHM is a disease primarily of photoreceptor and RPE cells, the use of tissue specific promoters for both these cell types could be an interesting alternative approach for CHM therapy. A combination of RHO or IRBP promoter alongside a VMD2 or Tyrp1 promoter would allow the targeting of both photoreceptor and RPE cells as shown previously (Semple-Rowland, Eccles et al. 2007; Bemelmans, Bonnel et al. 2005; Kachi, Oshima et al. 2005; Kachi, Esumi et al. 2006). Using this approach one would make formulations of both vectors and subretinally inject equal amounts of each vector into the subretinal space of CHM mice. This approach could efficiently allow transfection of both tissues in the retina. Furthermore, one would hypothesis that if CHM mice are treated early enough before the onset of deterioration, phenotypic correction may also be observed in both tissues. This could lead to the prevention of progressive retinal degeneration as well as the potential for the restoration of sight. Indeed these experiments could unravel many new and exciting therapeutic options that if successful in CHM mice, could also be clinically applicable to CHM patients.

4.5.1.2 Improvements in transcriptional levels

We have shown long-term transgene expression levels *in vivo* for all our S/MAR pDNA vectors. However upon immunohistological analysis, the spread of transgene expression within the retina appears to be limited primarily to the site of injection. One could utilise alternative approaches to improve the transcriptional levels of REP1 within the retina, thereby increasing the chances of profound visual rescue in these mice.

As plasmids used for *in vivo* experiments are produced in *E. coli,* their cytidine-phosphate-guanosine (CpG) sequences are often unmethylated, which in turn cause immune responses through the host defense mechanism. However, the reduction of CpG sequences on plasmid vectors has been shown to reduce the inflammatory responses from these vectors. Furthermore plasmid vectors have been shown to have significantly increase levels of expression *in vivo* while also increasing the persistence of expression (Ehrhardt, Peng et al.

2003; Le Hir, Gatfield et al. 2001). Therefore one could hypothesis that reducing or preferably removing all CpG sequences from the bacterial backbone of our pCAG-REP1 plasmid could provide even higher *REP1* transgene expression levels in the retina.

One such approach appears to be the creation of minicircles which consist of a minimal DNA vector that has had all the bacterial control regions from the pDNA vector removed from it including the origin of replication as well as the antibiotic resistance marker. In an interesting study by Riu *et al.* minicircle plasmids with transgene under the control of the α 1-anti trypsin (AAT), EF1-α and UbC promoters were shown in all cases to have considerably higher levels of expression compared to the original plasmids with bacterial sequences (Riu, Chen et al. 2007). In another study minimally sized S/MAR minicircles were also shown to provide higher and more substantial transgene expression *in vitro* as well as *in vivo* (Wong, Argyros et al. 2011). These promising results demonstrate the possibility of creating an ideal REP1 minicircle for CHM disease. Ultimately, such a novel S/MAR minicircle may represent the ideal gene therapy vector for CHM therapy, as the S/MAR moiety would lack a bacterial backbone and one would hypothesise would provide higher and persistent atoxic *REP1* gene expression.

4.5.1.3 Further analyses in CHM mice

Unfortunately due to time constraints the $CHM^{null/WT}$ mice which were injected with pCAG-REP1 while they showed partial prenylation correction, ultimately this does not mean that the retinal degeneration or indeed that the sight of these mice was corrected. Numerous behavioural tests on these mice could help elucidate these remain unanswered questions. These can include the use of relatively crude tests of visual system function by measuring the optokinetic reflex from mice by manually scoring the reflexive head turning which is elicited when an animal is placed in the center of a slow turning drum (Douglas, Alam et al. 2005; Thaung, Arnold et al. 2002). Furthermore detailed scanning laser ophthalmic (SLO) and electroretinographic (ERG) examinations could also reveal invaluable insights into the retinas of these injected mice as performed previously (Tolmachova, Anders et al. 2006).

Hence one can compare the progression of retinopathy within the control eye to that of the injected eye. While our formulations have shown been shown to successfully transfect and potentially rescue the RPE cells of these mice, it would also be interesting to analyse if by treating one cell type this would be sufficient to stop degeneration of the another cell type, namely the photoreceptor cells. Hence the analysis of the outer retina, including the separate contributions of rod and cone systems, as quantified by ERG could potentially prove to be an extremely interesting analysis.

Furthermore, histological analysis of injected retinas could also provide valuable insight into the potential rescue of the retinal outer nuclei layer (ONL) which has been shown to deteriorate considerably in old $CHM^{null/WT}$ mice (Tolmachova, Anders et al. 2006).

4.6 Concluding remarks

In this current study we have presented extremely encouraging results that show how naturally occurring S/MAR elements can be exploited for the efficient non-viral gene therapy of ocular tissue. The ability to effectively compact S/MAR vectors as well as the combination of utilising an effective delivery route has proven crucial to this success. We have shown unparalleled phenotypic correction of CHM by the pCAG-REP1 pDNA vector *in vitro* as well as *in vivo*. However, our results also highlight some limitations of this vector system. Indeed the ability to overcome these limitations could potentially pave the way to a successful non-viral therapeutic approach for CHM. Importantly future experiments need not be limited to CHM alone. Our current experiments support the use and application of non-viral S/MAR-mediated therapy for the treatment of numerous inherited retinal diseases. These including diseases affecting the RPE, as well as other areas of the eye by either using tissue specific promoters directed towards specific cell types such as photoreceptors, or by delivering S/MAR vectors to different regions of the eye such as ganglion cells via intravitreal injections or corneal cells via intracameral injections.

Cumulatively at this stage in biological research, realistic improvements to S/MAR-based vectors will undoubtedly place these vector systems along the path of future ocular gene therapy.

REFERENCES

_____

Acland, G. M., G. D. Aguirre, et al. (2005). "Long-Term Restoration of Rod and Cone Vision by Single Dose rAAV-Mediated Gene Transfer to the Retina in a Canine Model of Childhood Blindness." Mol Ther **12** (6): 1072-1082.

Acland, G. M., G. D. Aguirre, et al. (2001). "Gene therapy restores vision in a canine model of childhood blindness." Nat Genet **28** (1): 92-95.

Aguirre, G. D., V. Baldwin, et al. (1998). "Congenital stationary night blindness in the dog: common mutation in the RPE65 gene indicates founder effect." Mol Vis **4** (23).

Ahmed, E. and J. Loewenstein (2008). "Leber Congenital Amaurosis: Disease, Genetics and Therapy." Semin Ophthalmol **23** (1): 39-43.

Aiuti, A., S. Slavin, et al. (2002). "Correction of ADA-SCID by stem cell gene therapy combined with nonmyeloablative conditioning." Science **296**: 2410–2413.

Ala-Laurila P., K. A. Crouch, et al. (2006). "Visual cycle: Dependence of retinol production and removal on photoproduct decay and cell morphology." J Gen Physiol **128** (2): 153-169.

Alexandrov, K., H. Horiuchi, et al. (1994). "Rab escort protein-1 is a multifunctional protein that accompanies newly prenylated rab proteins to their target membranes." EMBO J **13** (22): 5262-5273.

Ali, S. H., J. S. Kasper, et al. (2004)."Cul7/p185/p193 binding to simian virus 40 large T antigen has a role in cellular transformation." J Virol **78** (6): 2749-57.

Allocca, M., A. Tessitore, et al. (2006). "AAV-mediated gene transfer for retinal diseases." Expert Opin Biol Ther **6** (12): 1279-1294.

Alory, C. and W. E. Balch (2000). "Molecular Basis for Rab Prenylation." J Cell Biol **150** (1): 89-104.

Anand, V., D. C. Barral, et al. (2003). "Gene therapy for choroideremia: in vitro rescue mediated by recombinant adenovirus." Vision Res **43** (8): 919-926.

Anant, J. S., L. Desnoyers, et al. (1998). "Mechanism of Rab Geranylgeranylation: Formation of the Catalytic Ternary Complex." Biochemistry **37** (36): 12559-12568.

Andres, D. A., M. C. Seabra, et al. (1993). "cDNA cloning of component A of Rab geranylgeranyl transferase and demonstration of its role as a Rab escort protein." Cell **73** (6): 1091-1099.

André, F. and L. M. Mir (2004). "DNA electrotransfer: its principles and an updated review of its therapeutic applications." Gene Ther **11**, Suppl 1: S33-42.

Antoniou, M., L. Harland, et al. (2003). "Transgenes encompassing dual-promoter CpG islands from the human TBP and HNRPA2B1 loci are resistant to heterochromatin-mediated silencing." Genomics **82** (3): 269-79.

Argyros, O., S. P. Wong, et al. (2008). "Persistent episomal transgene expression in liver following delivery of a scaffold/matrix attachment region containing non-viral vector." Gene Ther **15** (24): 1593-605.

Arnell, H., M. Mäntyjärvi, et al. (1998). "Stargardt disease: linkage to the ABCR gene region on 1p21-p22 in Scandinavian families." Acta Ophthalmol Scand **76** (6): 649-652.

Attal, J., M. Cajero-Juarez, et al. (1995). "The effect of matrix attached regions (MAR) and specialized chromatin structure (SCS) on the expression of gene constructs in cultured cells and in transgenic mice." Mol Biol Rep **22** (1): 37-46.

Auriche, C., D. Carpani, et al. (2002). "Functional human CFTR produced by a stable minichromosome." EMBO Rep 3 (9): 862-8.

Baiker, A., C. Maercker, et al. (2000). "Mitotic stability of an episomal vector containing a human scaffold/matrix-attached region is provided by association with nuclear matrix." Nat Cell Biol **2** (3): 182-4.

Bainbridge, J. W. (2008). "Effect of gene therapy on visual function in leber's congenital amaurosis." N Engl J Med **358**: 2231.

Bainbridge, J. W. and R. R. Ali (2008). "Success in sight: The eyes have it! Ocular gene therapy trials for LCA look promising." Gene Ther **15** (17): 1191-1192.

Bainbridge, J. W., A. J. Smith, et al. (2008). "Effect of Gene Therapy on Visual Function in Leber's Congenital Amaurosis." N Engl J Med **358**(21): 2231-2239.

Bainbridge, J. W., M. H. Tan, et al. (2006). "Gene therapy progress and prospects: the eye." Gene Ther **13** (16): 1191-1197.

Barral, D. C. and M. C. Seabra (2004). "The Melanosome as a Model to Study Organelle Motility in Mammals." Pigment Cell Res **17** (2): 111-118.

Basu, J. and H. F. Willard (2005). "Artificial and engineered chromosomes: non-integrating vectors for gene therapy." Trends Mol Med **11** (5): 251-8.

Baum, C., O. Kustikova, et al. (2006). "Mutagenesis and Oncogenesis by Chromosomal Insertion of Gene Transfer Vectors." Hum Gene Ther **17** (3): 253-263.

Behr, J. P. (1997). "The proton sponge: A trick to enter cells the viruses did not exploit." Chimia **51**: 34.

Bemelmans, A. P., S. Bonnel, et al. (2005). "Retinal cell type expression specificity of HIV-1-derived gene transfer vectors upon subretinal injection in the adult rat: influence of pseudotyping and promoter." J Gene Med **7** (10): 1367-74.

Benham, C., T. Kohwi-Shigematsu, et al. (1997). "Stress-induced duplex DNA destabilization in scaffold/matrix attachment regions." J Mol Biol **274** (2): 181-96.

Blaese, R. M., K. W. Culver , et al. (1995). "T lymphocyte-directed gene therapy for ADA- SCID: initial trial results after 4 years." Science **270** (5235): 475-80.

Bloomfield, V. A. (1997). "DNA condensation by multivalent cations." <u>Biopolymers</u> **44** (3): 269-82.

Bode, J., C. Benham, et al. (2000). "Transcriptional augmentation: modulation of gene expression by scaffold/matrix-attached regions (S/MAR elements)." <u>Crit Rev Eukaryot Gene Expr</u> **10** (1): 73-90.

Bode, J., Y. Kohwi, et al. (1992)."Biological significance of unwinding capability of nuclear matrix-associating DNAs." <u>Science</u> **255** (5041): 195-7.

Bode, J., S. Winkelmann, et al. (2006). "Correlations between scaffold/matrix attachment region (S/MAR) binding activity and DNA duplex destabilization energy." <u>J Mol Biol</u> **358** (2): 597-613.

Bondi, M. L., A. Azzolina, et al. (2007)."Novel cationic solid–lipid nanoparticles as non-viral vectors for genedelivery." <u>J Drug Target</u> **15** (4): 295–301.

Bonifer, C., M. Vidal, et al. (1990). "Tissue specific and position independent expression of the complete gene domain for chicken lysozyme in transgenic mice." <u>EMBO J</u> **9** (9): 2843-8.

Bonnet, M. E., P. Erbacher, et al. (2008). "Systemic delivery of DNA or siRNA mediated by linear polyethylenimine (L-PEI) does not induce an inflammatory response." <u>Pharm Res</u> **25** (12): 2972-82.

Boshart, M., F. Weber, et al. (1985). "A very strong enhancer is located upstream of an immediate early gene of human cytomegalovirus." <u>Cell</u> **41** (2): 521-30.

Boussif, O., F. Lezoualc'h, et al. (1995). "A versatile vector for gene and oligonucleotide transfer into cells in culture and in vivo: polyethylenimine." <u>Proc Natl Acad Sci USA</u> **92** (16): 7297-7301.

Bovolenta, P., A. Mallamaci, et al. (1998). "Expression pattern of cSix3, a member of the Six/sine oculis family of transcription factors." <u>Mech Dev</u> **70** (1-2): 201-203.

Brigham, K. L., B. Meyrick, et al. (1989). "In vivo transfection of murine lungs with a functioning prokaryotic gene using a liposome vehicle." <u>Am J Med Sci</u> **298** (4): 278-81.

Brignole, F., M. De Saint-Jean, et al. (1998). "Expression of Fas-Fas Ligand Antigens and Apoptotic Marker APO2.7 by the Human Conjunctival Epithelium. Positive Correlation with Class II HLA DR Expression in Inflammatory Ocular Surface Disorders." <u>Exp Eye Res</u> **67** (6): 687-697.

Brignole, F., P.-J. Pisella, et al. (2000). "Flow Cytometric Analysis of Inflammatory Markers in Conjunctival Epithelial Cells of Patients with Dry Eyes." <u>Invest Ophthalmol Vis Sci</u> **41** (6): 1356-1363.

Brignole, F., P. -J. Pisella, et al. (2001). "Flow cytometric analysis of inflammatory markers in KCS: 6-month treatment with topical cyclosporin A." <u>Invest Ophthalmol Vis Sci</u> **42** (1): 90-95.

Broll, S., A. Oumard, et al. (2010). "Minicircle Performance Depending on S/MAR–Nuclear Matrix Interactions." <u>J Mol Biol</u> **395** (5): 950-965.

Brooks, A. R., R. N. Harkins, et al. (2004). "Transcriptional silencing is associated with extensive methylation of the CMV promoter following adenoviral gene delivery to muscle." <u>J Gene Med</u> **6** (4): 395-404.

Budker, V., G. Zhang, et al. (1996). "Naked DNA delivered intraportally expresses efficiently in hepatocytes." <u>Gene Ther</u> **3** (7): 593-598.

Bunt-Milam, A. H. and J. C. Saari (1983). "Immunocytochemical localization of two retinoid-binding proteins in vertebrate retina." J Cell Biol **97** (3): 703-712.

Cai, X., Z. Nash, et al. (2009). "A Partial Structural and Functional Rescue of a Retinitis Pigmentosa Model with Compacted DNA Nanoparticles." PLoS ONE **4** (4): e5290.

Calero, M., C. Chen, et al. (2003). "Dual prenylation is required for Rab protein localization and function." Mol Biol Cell **14** (5): 1852-1867.

Campochiaro, P. A., Q. D. Nguyen, et al. (2006). "Adenoviral Vector-Delivered Pigment Epithelium-Derived Factor for Neovascular Age-Related Macular Degeneration: Results of a Phase I Clinical Trial." Hum Gene Ther **17** (2): 167-176.

Carter-Dawson, L. and M. Burroughs (1992). "Interphotoreceptor retinoid-binding protein in the cone matrix sheath. Electron microscopic immunocytochemical localization." Invest Ophthalmol &Vis Sci **33** (5): 1584-1588.

Casey, P. J. and M. C. Seabra (1996). "Protein prenyltransferases." J Biol Chem **271** (10): 5289-5292.

Cashman, S. M., L. McCullough, et al. (2007). "Improved Retinal Transduction In Vivo and Photoreceptor-specific Transgene Expression Using Adenovirus Vectors With Modified Penton Base." Mol Ther **15** (9): 1640-1646.

Cathcart, H. M., M. Zheng, et al. (2011). "Interferon-gamma, Macrophages, and Virus Spread after HSV-1 Injection." Invest Ophthalmol & Vis Sci **52** (7): 3984-3993.

Cavazzana-Calvo, M., S. Hacein-Bey, et al. (2000). "Gene therapy of human severe combined immunodeficiency (SCID)-X1 disease." Science **288** (5466): 669-72.

Chalberg, T. W., H. L. Genise, et al. (2005). "φC31 Integrase Confers Genomic Integration and Long-Term Transgene Expression in Rat Retina." Invest Ophthalmol & Vis Sci **46** (6): 2140-2146.

Chan, A. W. S., K. Y. Chong, et al. (2001). "Transgenic Monkeys Produced by Retroviral Gene Transfer into Mature Oocytes." Science **291** (5502): 309-312.

Chen, Y., S. K. Chauhan, et al. (2011). "Interferon-γ-secreting NK cells promote induction of dry eye disease." J Leukoc Biol **89** (6): 965-972.

Chen, Y., G. Moiseyev, et al. (2006). "RPE65 Gene Delivery Restores Isomerohydrolase Activity and Prevents Early Cone Loss in Rpe65−/− Mice." Invest Ophthalmol & Vis Sci **47** (3): 1177-1184.

Chintakuntlawar, A., R. Astley, et al. (2007). "Adenovirus type 37 keratitis in the C57BL/6J mouse." Invest Ophthalmol & Vis Sci **48** (2): 781-788.

Choate, K. A. and P. A. Khavari (1997). "Direct Cutaneous Gene Delivery in a Human Genetic Skin Disease." Hum Gene Ther **8** (14): 1659-1665.

Choi, Y. H., F. Liu, et al. (1998). "Polyethylene glycol-grafted poly-L-lysine as polymeric gene carrier." J Control Release **54** (1): 39-48.

Cideciyan, A., T. Aleman, et al. (2008). "Human gene therapy for RPE65 isomerase deficiency activates the retinoid cycle of vision but with slow rod kinetics." Proc Natl Acad Sci USA **105** (39): 15112-15117.

Clever, J., M. Yamada, et al. (1991). "Import of simian virus 40 virions through nuclear pore complexes." Proc Natl Acad Sci USA **88** (16): 7333-7.

Cockerill and Garrard (1986). "Chromosomal loop anchorage sites appear to be evolutionarily conserved." FEBS Lett **204** (1): 5-7.

Colella, P., G. Cotugno, et al. (2009). "Ocular gene therapy: current progress and future prospects." Trends Mol Med **15** (1): 23-31.

Conese, M., C. Auriche, et al. (2004). "Gene Therapy Progress and Prospects: Episomally maintained self-replicating systems." Gene Ther **11** (24): 1735-1741.

Cook, G. A., V. H. Gattone, et al. (1983). "Structural changes of isolated hepatocytes during treatment with digitonin." Biochim Biophys Acta **763** (4): 356-67.

Cremers, F. P., S. A. Armstrong, et al. (1994). "REP-2, a Rab escort protein encoded by the choroideremia-like gene." J Biol Chem **269** (3): 2111-2117.

Cremers, F. P., C. M. Molloy, et al. (1992). "An autosomal homologue of the choroideremia gene colocalizes with the Usher syndrome type II locus on the distal part of chromosome 1q." Hum Mol Genet **1** (2): 71-75.

Cremers, F. P. M., D. J. R. van de Pol, et al. (1990). "Cloning of a gene that is rearranged in patients with choroideraemia." Nature **347** (6294): 674-677.

Cremers, F. P. M., J. A. J. M. van den Hurk, et al. (2002). "Molecular genetics of Leber congenital amaurosis." Hum Mol Genet **11** (10): 1169-1176.

Das, S. R., N. Bhardwaj, et al. (1992). "Muller cells of chicken retina synthesize 11-cis-retinol." Biochem J **1** (285): 907-913.

Davies, L. A., G. McLachlan, et al. (2008). "Enhanced lung gene expression after aerosol delivery of concentrated pDNA/PEI complexes." Mol Ther **16** (7): 1283-90.

Dejneka, N. S., E. M. Surace, et al. (2004). "In Utero Gene Therapy Rescues Vision in a Murine Model of Congenital Blindness." Mol Ther **9** (2): 182-188.

de Jong, P. T.(2006). "Age-Related Macular Degeneration." N Engl J Med **355** (14): 1474-1485.

Delmas, V., S. Martinozzi, et al. (2003). "Cre-mediated recombination in the skin melanocyte lineage." Genesis **36** (2): 73-80.

Del Priore, L. (2005). "Effect of sham surgery on retinal function after subretinal transplantation of the artificial silicone retina." Arch Ophthalmol **123** (8): 1156-1157.

Desnoyers, L., J. S. Anant, et al. (1996). "Geranylgeranylation of Rab proteins." Biochem Soc Trans **24** (3): 699-703.

Dezawa, M., M. Takano, et al. (2002). "Gene transfer into retinal ganglion cells by in vivo electroporation: a new approach." Micron **33** (1): 1-6.

Dickinson L. A., T. Joh, et al. (1992). "A tissue-specific MAR/SAR DNA-binding protein with unusual binding site recognition." Cell **70** (4): 631-45.

Dif, F., C. Djediat, et al. (2006). "Transfection of multiple pulmonary cell types following intravenous injection of PEI-DNA in normal and CFTR mutant mice." J Gene Med **8** (1): 82-89.

DiLoreto, D. A., M. R. Martzen, et al. (1995). "Müller cell changes precede photoreceptor cell degeneration in the age-related retinal degeneration of the Fischer 344 rat." Brain Res **698** (1-2): 1-14.

Douglas, R. M., N. M., Alam, et al. (2005). "Independent visual threshold measurements in the two eyes of freely moving rats and mice using a virtual-reality optokinetic system." Vis Neurosci **22** (5): 677-84.

Dowty, M. E., P. Williams, et al. (1995). "Plasmid DNA entry into postmitotic nuclei of primary rat myotubes." Proc Natl Acad Sci USA **92** (10): 4572-4576.

Dunlap, D. D., A. Maggi, et al. (1997). "Nanoscopic structure of DNA condensed for gene delivery." Nucleic Acids Res **25** (15): 3095-101.

Duvvuri, S., S. Majumdar, et al. (2003). "Drug delivery to the retina: challenges and opportunities." Expert Opin Biol Ther **3** (1): 45-56.

Ebersole, T. A., A. Ross, et al. (2000). "Mammalian artificial chromosome formation from circular alphoid input DNA does not require telomere repeats." Hum Mol Genet **9** (11): 1623-31.

Edwards, A. O., L. A. Donoso, et al. (2001). "A Novel Gene for Autosomal Dominant Stargardt-like Macular Dystrophy with Homology to the SUR4 Protein Family." Invest Ophthalmol Vis Sci **42** (11): 2652-2663.

Edwards, A. O., R. Ritter, et al. (2005). "Complement Factor H Polymorphism and Age-Related Macular Degeneration." Science **308** (5720): 421-424.

Ehrhardt, A., P. D. Peng, et al. (2003). "Optimization of cis-acting elements for gene expression from nonviral vectors in vivo." Hum Gene Ther **14** (3): 215-25.

Eudy, J. D., M. D. Weston, et al. (1998). "Mutation of a gene encoding a protein with extracellular matrix motifs in Usher syndrome type IIa." Science **280** (5370): 1753-1757.

Farjo, R., J. Skaggs, et al. (2006). "Efficient Non-Viral Ocular Gene Transfer with Compacted DNA Nanoparticles." PLoS ONE **1** (1): e38.

Farnsworth, C. C., M. C. Seabra, et al. (1994). "Rab geranylgeranyl transferase catalyzes the geranylgeranylation of adjacent cysteines in the small GTPases Rab1A, Rab3A, and Rab5A." Proc Natl Acad Sci USA **91** (25): 11963-11967.

Farr, C. J., M. Stevanovic, et al. (1992). "Telomere-associated chromosome fragmentation: applications in genome manipulation and analysis." Nat Genet **2** (4): 275-82.

Faure, V., C. Hecquet, et al. (1999). "Role of Interferon Regulatory Factor-1 and Mitogen-activated Protein Kinase Pathways in the Induction of Nitric Oxide Synthase-2 in Retinal Pigmented Epithelial Cells." J Biol Chem **274** (8): 4794-4800.

Fechheimer, M., J. F. Boylan, et al. (1987). "Transfection of mammalian cells with plasmid DNA by scrape loading and sonication loading." Proc Natl Acad Sci USA **84** (23): 8463-8467.

Fedor, M. J. and E. Daniell (1980). "Acetylation of histone-like proteins of adenovirus type 5." J Virol **35** (3): 637-643.

Felgner, P. L., T. R. Gadek, et al. (1987). "Lipofection: a highly efficient, lipid-mediated DNA-transfection procedure." Proc Natl Acad Sci USA **84** (21): 7413-7.

Ferrari, S., E. Moro, et al. (1997). "ExGen 500 is an efficient vector for gene delivery to lung epithelial cells in vitro and in vivo." Gene Ther **4** (10): 1100-1106.

Fink, T. L., P. J. Klepcyk, et al. (2006). "Plasmid size up to 20 kbp does not limit effective in vivo lung gene transfer using compacted DNA nanoparticles." Gene Ther **13** (13): 1048-1051.

Fiorentini, A. and L. Maffei (1976). "Spatial contrast sensitivity of myopic subjects." Vision Res **16** (4): 437-438.

Fitzsimons, H. L., J. M. Mckenzie, et al. (2001). "Insulators coupled to a minimal bidirectional tet cassette for tight regulation of rAAV-mediated gene transfer in the mammalian brain." Gene Ther **8** (22): 1675-81.

Flannery, J. G., A. C. Bird, et al. (1990). "A histopathologic study of a choroideremia carrier." Invest Ophthalmol Vis Sci **31** (2): 229-236.

Frisch, M., K. Frech, et al. (2002) "In silico prediction of scaffold/matrix attachment regions in large genomic sequences." Genome Res **12** (2): 349-54.

Fu, Y. and K. -W. Yau (2007). "Phototransduction in mouse rods and cones." Pflügers Arch **454** (5): 805-819.

Fujiki, K., Y. Hotta, et al. (1999). "REP-1 gene mutations in Japanese patients with choroideremia." Graefes Arch Clin Exp Ophthalmol **237** (9): 735-740.

Furuta, Y., O. Lagutin, et al. (2000). "Retina- and ventral forebrain-specific Cre recombinase activity in transgenic mice." Genesis **26** (2): 130-132.

Galande, S., P. K. Purbey, et al. (2007). "The third dimension of gene regulation: organization of dynamic chromatin loopscape by SATB1." Curr Opin Genet Dev **17** (5): 408-14.

Gao, J., T. A. Schwalb, et al. (1998). "The Role of Apoptosis in the Pathogenesis of Canine Keratoconjunctivitis Sicca: The Effect of Topical Cyclosporin A Therapy." Cornea **17** (6): 654.

Gao, X., K. -S. Kim, et al. (2007). "Nonviral gene delivery: What we know and what is next." AAPS J **9** (1): E92-E104.

Garca-Hoyos, M., R. Sanz, et al. (2005). "New approach for the refinement of the location of the X-chromosome breakpoint in a previously described female patient with choroideremia carrying a X;4 translocation." Am J Med Genet A **138** (4): 365-368.

Garcia-Hoyos, M., I. Lorda-Sanchez, et al. (2008). "New Type of Mutations in Three Spanish Families with Choroideremia." Invest Ophthalmol Vis Sci **49** (4): 1315-1321.

Gehlbach, P., A. M. Demetriades, et al. (2003). "Periocular injection of an adenoviral vector encoding pigment epithelium-derived factor inhibits choroidal neovascularization." Gene Ther **10** (8): 637-646.

Gekeler, F., K. Kobuch, et al. (2004). "Subretinal electrical stimulation of the rabbit retina with acutely implanted electrode arrays." Graefes Arch Clin Exp Ophthalmol **242** (7): 587-596.

Gerding, H. (2007). "A new approach towards a minimal invasive retina implant." J Neural Eng **4** (1): S30-S37.

Gene Therapy Clinical Trials Worldwide: Vectors used in Gene Therapy Clinical Trials 2011 (Available from: www.wiley.co.uk/genmed/clinical).

Gibbs, D., S. M., Azarian, et al. (2004). "Role of myosin VIIa and Rab27a in the motility and localization of RPE melanosomes." J Cell Sci **117** (Pt 26): 6473-83.

Giese, M. J., H. L. Sumner, et al. (1998). "Cytokine expression in a rat model of Staphylococcus aureus endophthalmitis." Invest Ophthalmol Vis Sci **39** (13): 2785-2790.

Gill, D. R., S. E. Smyth, et al. (2001). "Increased persistence of lung gene expression using plasmids containing the ubiquitin C or elongation factor 1alpha promoter." Gene Ther **8** (20): 1539-1546.

Girod, P. A., D. Q. Nguyen, et al. (2007). "Genome-wide prediction of matrix attachment regions that increase gene expression in mammalian cells." Nat Methods **4** (9): 747-53.

Goetze, S., A. Gluch, et al. (2003). "Computational and in vitro analysis of destabilized DNA regions in the interferon gene cluster: potential of predicting functional gene domains." Biochemistry **42** (1): 154-66.

Goldman, L. A., E. C. Cutrone, et al. (1996). "Modifications of Vectors pEF-BOS, pcDNA1,and pcDNA3 Result in Improved Convenience and Expression." Biotechniques **21** : 1013-1015.

Gomes, A., B. Ali, et al. (2003). "Membrane targeting of Rab GTPases is influenced by the prenylation motif." Mol Biol Cell **14** (5): 1882-1899.

Gonzalez-Fernandez, F., C. A. Baer, et al. (2003). "Interphotoreceptor retinoid-binding protein—an old gene for new eyes." Vision Res **43** (28): 3021-3036.

Goula, D., J. S. Remy, et al. (1998). "Size, diffusibility and transfection performance of linear PEI/DNA complexes in the mouse central nervous system." Gene Ther **5** (5): 712-717.

Gragoudas, E. S., A. P. Adamis, et al. (2004). "Pegaptanib for Neovascular Age-Related Macular Degeneration." N Engl J Med **351** (27): 2805-2816.

Grayson, C. and R. S. Molday (2005). "Dominant Negative Mechanism Underlies Autosomal Dominant Stargardt-like Macular Dystrophy Linked to Mutations in ELOVL4." J Biol Chem **280** (37): 32521-32530.

Grosshans, B., D. Ortiz, et al. (2006). "Rabs and their effectors: achieving specificity in membrane traffic." Proc Natl Acad Sci USA **103** (32): 11821-11827.

Hacein-Bey-Abina, S., C. von Kalle, et al. (2003a). "A serious adverse event after successful gene therapy for X-linked severe combined immunodeficiency." N Engl J Med **348** (3): 255-256.

Hacein-Bey-Abina, S., C. Von Kalle, et al. (2003b). "LMO2-associated clonal T cell proliferation in two patients after gene therapy for SCID-X1." Science **302** (5644): 415-419.

Halbert, C., A. D. Miller, et al. (2006). "Prevalence of neutralizing antibodies against adeno-associated virus (AAV) types 2, 5, and 6 in cystic fibrosis and normal populations: Implications for gene therapy using AAV vectors." Hum Gene Ther **17** (4): 440-447.

Halford, S., M. S. Freedman, et al. (2001). "Characterization of a novel human opsin gene with wide tissue expression and identification of embedded and flanking genes on chromosome 1q43." Genomics **72** (2): 203-208.

Halweg, C., W. F. Thompson, et al. (2005). "The rb7 matrix attachment region increases the likelihood and magnitude of transgene expression in tobacco cells: a flow cytometric study." Plant Cell **17** (2): 418-29.

Harrington, J. J., G. Van Bokkelen, et al. (1997). "Formation of de novo centromeres and construction of first-generation human artificial microchromosomes." Nat Genet **15** (4): 345-55.

Hassani, Z., J. -C. Franois, et al. (2007). "A hybrid CMV-H1 construct improves efficiency of PEI-delivered shRNA in the mouse brain." Nucleic Acids Res **35** (9): e65-e65.

Hauswirth, W., T. Aleman, et al. (2008). "Treatment of leber congenital amaurosis due to RPE65 mutations by ocular subretinal injection of adeno-associated virus gene vector: short-term results of a phase I trial." Hum Gene Ther **19** (10): 979-990.

Hemmi, H., O., Takeuchi, et al. (2000). "A Toll-like receptor recognizes bacterial DNA." Nature 408 (6813): 740-5.

Heng, H. H. Q., S. Goetze, et al. (2004). "Chromatin loops are selectively anchored using scaffold/matrix-attachment regions." J Cell Sci **117** (7): 999-1008.

Henkind , P., R. I. Hansen, et al. (1979). "Physiology of the human eye and visual system" Ocular circulation In: Records RE, editor. New York: Harper & Row: 98-155.

Hickman, M. A., R. W. Malone, et al. (1994). "Gene Expression Following Direct Injection of DNA into Liver." Hum Gene Ther **5** (12): 1477-1483.

Hooks, J. J., C. C. Chan, et al. (1988). "Identification of the lymphokines, interferon-gamma and interleukin-2, in inflammatory eye diseases." Invest Ophthalmol Vis Sci **29** (9): 1444-1451.

Hornof, M., M. Fuente, et al. (2008). "Low molecular weight hyaluronan shielding of DNA/PEI polyplexes facilitates CD44 receptor mediated uptake in human corneal epithelial cells."J Gene Med **10** (1): 70-80.

Hsieh, Y. W., X. M. Zhang, et al. (2002). "The homeobox gene Six3 is a potential regulator of anterior segment formation in the chick eye." Dev Biol **248** (2): 265-280.

Humme, S., G. Reisbach, et al. (2003). "The EBV nuclear antigen 1 (EBNA1) enhances B cell immortalization several thousandfold." Proc Natl Acad Sci USA **100** (19): 10989-94.

Ideno, J., H. Mizukami, et al. (2007). "Prevention of diabetic retinopathy by intraocular soluble flt-1 gene transfer in a spontaneously diabetic rat model." Int J Mol Med **19** (1): 75-79.

Ito, Y., S. Kawakami S, et al. (2009). "Evaluation of proinflammatorycytokine production and liver injury induced by plasmid DNA/cationic liposome complexes with various mixing ratios in mice." Eur J Pharm Biopharm **71** (2): 303-9.

Jackson, D. A., S. Juranek, et al. (2006). "Designing Nonviral Vectors for Efficient Gene Transfer and Long-Term Gene Expression." Mol Ther **14** (5): 613-626.

Jacobson, S., A. Cideciyan, et al. (2006). "Remodeling of the human retina in choroideremia: rab escort protein 1 (REP-1) mutations." Invest Ophthalmol Vis Sci **47** (9): 4113-4120.

Jaissle, G. B. (2004). "In vivo and in vitro assessment of degenerative processes of retine, RPE, and vascular systems following the loss of photoreceptor cells in the rhodopsin knockout mouse." I Invest Ophthalmol Vis Sci **45** (E-Abstract 5079).

Jans, D. A., C. Y. Xiao, et al. (2000). "Nuclear targeting signal recognition: a key control point in nuclear transport?." Bioessays **22** (6): 532-44.

Jenke, B. H., C. P. Fetzer, et al. (2002). "An episomally replicating vector binds to the nuclear matrix protein SAF-A in vivo." EMBO Rep **3** (4): 349-354.

Jenke, A. C., M. F. Scinteie, et al. (2004). "Expression of a transgene encoded on a non-viral episomal vector is not subject to epigenetic silencing by cytosine methylation." Mol Biol Rep **31** (2): 85-90.

Jenke, A. C. W., I. M. Stehle, et al. (2004). "Nuclear scaffold/matrix attached region modules linked to a transcription unit are sufficient for replication and maintenance of a mammalian episome." Proc Natl Acad Sci USA **101** (31): 11322-11327.

Jenuwein, T., W. C. Forrester, et al. (1997). "Extension of chromatin accessibility by nuclear matrix attachment regions." Nature **385** (6613): 269-72.

Jo, N., G. -S. Wu, et al. (2003). "Upregulation of chemokine expression in the retinal vasculature in ischemia-reperfusion injury." Invest Ophthalmol Vis Sci **44** (9): 4054-4060.

Johansen, J., J. Tornøe, et al. (2003). "Increased in vitro and in vivo transgene expression levels mediated through cis-acting elements." J Gene Med **5** (12): 1080-9.

Johnson, C., L. Berglin, et al. (2008). "Technical brief: subretinal injection and electroporation into adult mouse eyes." Molecular vision **14**: 2211-2226.

Jones, G. J., R. K. Crouch, et al. (1989). "Retinoid requirements for recovery of sensitivity after visual-pigment bleaching in isolated photoreceptors." Proc Natl Acad Sci USA **86** (23): 9606-9610.

Jordens, I., M. Marsman, et al. (2005). "Rab proteins, connecting transport and vesicle fusion." Traffic **6** (12): 1070-1077.

Jung, Y. -D., J. -W. Huh, et al. (2011). "Quantitative analysis of transcript variants of CHM gene containing LTR12C element in humans." Gene **489** (1): 1-5.

Kachi, S., N. Esumi, et al. (2006). "Sustained expression after nonviral ocular gene transfer using mammalian promoters." Gene Ther **13** (9): 798-804.

Kachi, S., Y. Oshima, et al. (2005). "Nonviral ocular gene transfer." Gene Ther **12** (10): 843-851.

Kaemmerer, W. F., R. G. Reddy, et al. (2000). "In vivo transduction of cerebellar Purkinje cells using adeno-associated virus vectors." Mol Ther **2** (5): 446-57.

Kalos, M., R. E. Fournier, et al. (1995). "Position-independent transgene expression mediated by boundary elements from the apolipoprotein B chromatin domain." Mol Cell Biol **15** (1): 198-207.

Kellum, R. and P. Schedl (1992). "A group of scs elements function as domain boundaries in an enhancer-blocking assay."Mol Cell Biol **12** (5): 2424-31.

Kim, D. W., T. Uetsuki, et al. (1990). "Use of the human elongation factor 1 alpha promoter as a versatile and efficient expression system." Gene **91** (2): 217-223.

Kipp, M., F. Gohring, et al. (2000). "SAF-Box, a conserved protein domain that specifically recognizes scaffold attachment region DNA." Mol Cell Biol **20** (20): 7480-7489.

Kircheis, R., L. Wightman, et al. (2001). "Polyethylenimine/DNA complexes shielded by transferrin target gene expression to tumors after systemic application." Gene Ther **8** (1): 28-40.

Klein, R. J., C. Zeiss, et al. (2005). "Complement Factor H Polymorphism in Age-Related Macular Degeneration." Science **308** (5720): 385-389.

Koenekoop, R. K. (2004). "An overview of leber congenital amaurosis: a model to understand human retinal development." Surv Ophthalmol **49** (4): 379-398.

Koenekoop, R. K. (2008). "Successful RPE65 Gene Replacement and Improved Visual Function in Humans." Ophthalmic Genet **29** (3): 89-91.

Kohn, D. B., M. Sadelain et al. (2003) "Occurrence of leukaemia following gene therapy of X-linked SCID."Nat Rev Cancer **3** (7): 477-488.

Kolb, H. (2003). "How the Retina Works." Am Sci **91** (1): 28.

Konstan, M. W., P. B. Davis, et al. (2004). "Compacted DNA Nanoparticles Administered to the Nasal Mucosa of Cystic Fibrosis Subjects Are Safe and Demonstrate Partial to Complete Cystic Fibrosis Transmembrane Regulator Reconstitution." Hum Gene Ther **15** (12): 1255-1269.

Kostic, C., F. Chiodini, et al. (2003). "Activity analysis of housekeeping promoters using self-inactivating lentiviral vector delivery into the mouse retina." Gene Ther **10** (9): 818-821.

Krock, B. L., J. Bilotta, et al. (2007). "Noncell-autonomous photoreceptor degeneration in a zebrafish model of choroideremia." Proc Natl Acad Sci USA **104** (11): 4600-4605.

Krzystolik, M. G., M. A. Afshari, et al.(2002). "Prevention of experimental choroidal neovascularization with intravitreal anti-vascular endothelial growth factor antibody fragment." Arch Ophthalmol **120** (3): 338-346.

Kurreck, J. (2009). "RNA interference: from basic research to therapeutic applications." Angewandte Chemie (International ed. in English) **48** (8): 1378-1398.

Kwak, N., N. Okamoto, et al. (2000). "VEGF Is Major Stimulator in Model of Choroidal Neovascularization." Invest Ophthalmol Vis Sci **41** (10): 3158-3164.

Kwoh, D. Y., C. C. Coffin, et al. (1999). "Stabilization of poly-L-lysine/DNA polyplexes for in vivo gene delivery to the liver." Biochim Biophys Acta **1444** (2): 171-90.

Lai, C. -C., W. -C. Wu, et al. (2001). "Suppression of Choroidal Neovascularization by Adeno-associated Virus Vector Expressing Angiostatin." Invest Ophthalmol Vis Sci **42** (10): 2401-2407.

Lam, A. M. I. and P. R. Cullis (2000). "Calcium enhances the transfection potency of plasmid DNA–cationic liposome complexes." Biochim Biophys Acta - Biomembranes (2): 279-290.

Lamb, T. D. and E. N. Pugh (2006). "Phototransduction, Dark Adaptation, and Rhodopsin Regeneration The Proctor Lecture." Invest Ophthalmol Vis Sci **47** (12): 5138-5152.

Larijani, B., A. N. Hume, et al. (2003). "Multiple Factors Contribute to Inefficient Prenylation of Rab27a in Rab Prenylation Diseases." J Biol Chem **278** (47): 46798-46804.

Lavigne, M. D. and D. C. Górecki (2006). "Emerging vectors and targeting methods for nonviral gene therapy."Expert Opin Emerg Drugs **11** (3): 541-57.

Lawrie, A., A. F. Brisken, et al. (2000). "Microbubble-enhanced ultrasound for vascular gene delivery." Gene Ther **7** (23): 2023-2027.

Lechardeur, D., A. S. Verkman, et al. (2005). "Intracellular routing of plasmid DNA during non-viral gene transfer." Adv Drug Deliv Rev **57** (5): 755-767.

Le Hir, H., D. Gatfield, et al. (2001). "The exon-exon junction complex provides a binding platform for factors involved in mRNA export and nonsense-mediated mRNA decay." EMBO J **20** (17): 4987-97.

Leung, K., R. Baron, et al. (2007). "Rab GTPases containing a CAAX motif are processed post-geranylgeranylation by proteolysis and methylation." J Biol Chem **282** (2): 1487-1497.

Li, M., P. Atmaca-Sonmez, et al. (2006). "CFH haplotypes without the Y402H coding variant show strong association with susceptibility to age-related macular degeneration." Nat Genet **38** (9): 1049-1054.

Li, D., R. Zhao, et al. (2003). "Structure of the replicative helicase of the oncoprotein SV40 large tumour antigen." Nature **423** (6939): 512-8.

Liaw, J., S. F. Chang, et al. (2001). "In vivo gene delivery into ocular tissues by eye drops of poly(ethylene oxide)-poly(propylene oxide)-poly(ethylene oxide) (PEO-PPO-PEO) polymeric micelles." Gene Ther **8** (13): 999-1004.

Limb, G. A., A. H. Chignell, et al. (1996). "Distribution of TNF alpha and its reactive vascular adhesion molecules in fibrovascular membranes of proliferative diabetic retinopathy." Br JOphthalmol **80** (2): 168-173.

Limb, G. A., R. D. Hollifield, et al. (2001). "Soluble TNF receptors in vitreoretinal proliferative disease." Invest Ophthalmol Vis Sci **42** (7): 1586-1591.

Lipps, H. J., A. C. W. Jenke, et al. (2003). "Chromosome-based vectors for gene therapy." Gene **304**: 23-33.

Liu, J., T. N. Lewis, et al. (1998). "Non-invasive assessment and control of ultrasound-mediated membrane permeabilization." Pharm Res **15** (6): 918-24.

Liu, G., D. Li, et al. (2003). "Nanoparticles of Compacted DNA Transfect Postmitotic Cells." J Biol Chem **278** (35): 32578-32586.

Liu, J., Y. Itagaki, et al. (2000). "The Biosynthesis of A2E, a Fluorophore of Aging Retina, Involves the Formation of the Precursor, A2-PE, in the Photoreceptor Outer Segment Membrane." J Biol Chem **275** (38): 29354-29360.

Liu, M. M., J. Tuo, et al. (2011). "Gene therapy for ocular diseases." Br J Ophthalmol **95**: 604-612

Liu, J., Q. Zhang, et al. (2001). "Nanostructured materials designed for cell binding and transduction." Biomacromolecules **2** (2): 362-8.

Lopes, V., J. Ramalho, et al. (2007). "The ternary Rab27a-Myrip-Myosin VIIa complex regulates melanosome motility in the retinal pigment epithelium." Traffic **8** (5): 486-499.

Lorda-Sanchez, I. J., A. J. Ibañez, et al. (2000). "Choroideremia, sensorineural deafness, and primary ovarian failure in a woman with a balanced X-4 translocation." Ophthalmic Genet **21** (3): 185-189.

Lufino, M. M., R. Manservigi, et al. (2007). "An S/MAR-based infectious episomal genomic DNA expression vector provides long-term regulated functional complementation of LDLR deficiency." Nucleic Acids Res **35** (15): e98.

Luzio, J. P., B. M. Mullock, et al. (2001). "Relationship between endosomes and lysosomes." Biochem Soc Trans **29** (Pt 4): 476-80.

Lyman, S. K., T. Guan, et al. (2002). "Influence of cargo size on Ran and energy requirements for nuclear protein import." J Cell Biol **159** (1): 55-67.

MacDonald, I. M., D. Y. Mah, et al. (1998). "A practical diagnostic test for choroideremia." Ophthalmology **105** (9): 1637-1640.

Madara, J. L., D. Barenberg, et al. (1986). "Effects of cytochalasinD on occluding junctions of intestinal absorptive cells: Further evidence thatthe cytoskeleton may influence paracellular permeability and junctionalcharge selectivity." J Cell Biol **102**: 2125-2136.

Maguire, A. M., F. Simonelli, et al. (2008). "Safety and Efficacy of Gene Transfer for Leber's Congenital Amaurosis." N Engl J Med **358** (21): 2240-2248.

Mahato, R. I., Y. Takakura, et al. (1997). "Nonviral vectors for in vivo gene delivery: physicochemical and pharmacokinetic considerations. " Crit Rev Ther Drug Carrier Syst **14** (2): 133-72.

Makarova, O., G. Gorneva, et al. (1996). "Incorporation of nuclear matrix attachment regions into the herpes simplex virus type 1 genome does not induce long-term expression of a foreign gene during latency." Gene Ther **3** (9): 829-33.

Maller, J. B., J. A. Fagerness, et al. (2007). "Variation in complement factor 3 is associated with risk of age-related macular degeneration." Nat Genet **39** (10): 1200-1201.

Maller, J., S. George, et al. (2006). "Common variation in three genes, including a noncoding variant in CFH, strongly influences risk of age-related macular degeneration." Nat Genet **38** (9): 1055-1059.

Manzini, S., A. Vargiolu, et al. (2006). "Genetically modified pigs produced with a nonviral episomal vector." Proc Natl Acad Sci USA **103** (47): 17672-7.

Marlhens, F., C. Bareil, et al. (1997). "Mutations in RPE65 cause Leber's congenital amaurosis." Nat Genet **17** (2): 139-141.

Maurice, D. M. (2002). "Drug Delivery to the Posterior Segment from Drops." Surv Ophthalmol **47** Supplement 1(0): S41-S52.

Maurice, D. M. and S. Mishima. (1984). "Ocular pharmacokinetics." Handbook of Experimental Pharmacology. Pharmacology of the eye In: Sears MC. Berlin: Springer-Verlag. **69**: 19–116.

Mazda, O., E. Satoh, et al. (1997). "Extremely efficient gene transfection into lympho-hematopoietic cell lines by Epstein-Barr virus-based vectors." J Immunol Methods **204** (2): 143-151.

McBee, J. K., K. Palczewski, et al. (2001). "Confronting Complexity: the Interlink of Phototransduction and Retinoid Metabolism in the Vertebrate Retina." Prog Retin Eye Res **20** (4): 469-529.

McCulloch, C. (1969). "Choroideremia: a clinical and pathologic review." Trans Am Ophthalmol Soc (annual meeting) **67**: 142-195.

McTaggart, K., M. Tran, et al. (2002). "Mutational analysis of patients with the diagnosis of choroideremia." Hum Mutat **20** (3): 189-196.

Mearini, G., P. E. Nielsen, et al. (2004). "Localization and dynamics of small circular DNA in live mammalian nuclei." Nucleic Acids Res **32** (8): 2642-51.

Mesiwala, A. H. and P. D. Mourad. (2002). "Monitoring of biologic effects of focused ultrasound beams on the brain." Radiology **224** (1): 294-6.

Meyer, K. B., M. M. Thompson, et al. (1995). "Intratracheal gene delivery to the mouse airway: characterization of plasmid DNA expression and pharmacokinetics." Gene Ther **2** (7): 450-460.

Miao, C. H., X. Ye, et al. (2003). "High-level factor VIII gene expression in vivo achieved by nonviral liver-specific gene therapy vectors." Hum Gene Ther **14** (14): 1297-305.

Mielke, C., Y. Kohwi, et al. (1990). "Hierarchical binding of DNA fragments derived from scaffold-attached regions: correlation of properties in vitro and function in vivo." Biochemistry **29** (32): 7475-7485.

Miller, A. D. (1998). "Cationic liposome systems in gene therapy." IDrugs **1** (5): 574-83.

Mintzer, M. A. and E. E. Simanek. (2009). "Nonviral vectors for gene delivery." Chem Rev **109** (2): 259-302.

Mirkovitch, J. and M. E. Mirault. (1984). "Organization of the higher-order chromatin loop: specific DNA attachment sites on nuclear scaffold." Cell 39 (1): 223-32.

Mishra, S., P. Webster, et al. (2004). "PEGylation significantly affects cellular uptake and intracellular trafficking of non-viral gene delivery particles." Eur J Cell Biol **83** (3): 97-111.

Mitragotri, S. (2005). "Healing sound: the use of ultrasound in drug delivery and other therapeutic applications." Nat Rev Drug Discov **4** (3): 255-260.

Miyazono, S., Y. Shimauchi-Matsukawa, et al. (2008)."Highly efficient retinal metabolism in cones." Proc Natl Acad Sci USA **105** (41): 16051-6.

Mo, X., A. Yokoyama, et al. (2002). "Rescue of axotomized retinal ganglion cells by BDNF gene electroporation in adult rats." Invest Ophthalmol Vis Sci **43** (7): 2401-5.

Moiseyev, G., Y. Chen, et al. (2005). "RPE65 is the isomerohydrolase in the retinoid visual cycle." Proc Natl Acad Sci USA **102** (35): 12413-12418.

Molday, L. L., A. R. Rabin, et al. (2000). "ABCR expression in foveal cone photoreceptors and its role in Stargardt macular dystrophy." Nat Genet **25** (3): 257-258.

Mönkkönen, J. and A. Urtti. (1998). "Lipid fusion in oligonucleotide and gene delivery with cationic lipids." Adv Drug Deliv Rev **34** (1): 37-49.

Moosajee, M., M. Tulloch, et al. (2009). "Single choroideremia Gene in Nonmammalian Vertebrates Explains Early Embryonic Lethality of the Zebrafish Model of Choroideremia." Invest Ophthalmol Vis Sci **50** (6): 3009-3016.

Mura, M., C. Sereda, et al. (2007). "Clinical and functional findings in choroideremia due to complete deletion of the CHM gene." Arch Ophthalmol **125** (8): 1107-1113.

Murata, T. (2001). "Response of experimental retinal neovascularization to thiazolidinediones." Arch Ophthalmol **119** (5): 709.

Murisier, F., S. Guichard, et al. (2006). "A conserved transcriptional enhancer that specifies Tyrp1 expression to melanocytes." Dev Biol **298** (2): 644-55.

Nabirochkin, S., M. Ossokina, et al. (1998). "A nuclear matrix/scaffold attachment region co-localizes with the gypsy retrotransposon insulator sequence." J Biol Chem **273** (4): 2473-9.

Nakai, H., E. Montini, et al. (2003). "AAV serotype 2 vectors preferentially integrate into active genes in mice." Nat Genet **34** (3): 297-302.

Nakazawa, T., M. Kayama, et al. (2011). "Tumor Necrosis Factor-α Mediates Photoreceptor Death in a Rodent Model of Retinal Detachment." Invest Ophthalmol Vis Sci **52** (3): 1384-1391.

Nakazawa, T., A. Matsubara, et al. (2006). "Characterization of cytokine responses to retinal detachment in rats." Mol Vis **12**: 867-878.

Napirei, M., A. Ricken, et al. (2004). "Expression pattern of the deoxyribonuclease 1 gene: lessons from the Dnase1 knockout mouse." Biochemical J **380** (3): 929-937.

Narfström, K., M. L. Katz, et al. (2003). "In Vivo Gene Therapy in Young and Adult RPE65−/− Dogs Produces Long-Term Visual Improvement." J Hered **94** (1): 31-37.

Nayler, O., W. Strätling, et al. (1998). "SAF-B protein couples transcription and pre-mRNA splicing to SAR/MAR elements." Nucleic Acids Res **26** (15): 3542-9.

Niidome, T. and L. Huang (2002). "Gene therapy progress and prospects: nonviral vectors." Gene Ther **9** (24): 1647-52.

O'Brien, J. and S. C. R. Lummis (2002). "An improved method of preparing microcarriers for biolistic transfection." Brain Res Brain Res Protoc **10** (1): 12-15.

O'Connor, T. P. and R. G. Crystal (2006). "Genetic medicines: treatment strategies for hereditary disorders." Nat Rev Genet **7** (4): 261-76.

Ohana P., O. Gofrit, et al. (2004). "Regulatory sequences of the H19 gene in DNA-based therapy of bladder cancer." Gene Ther Mol Biol **8**: 181-192.

Ohana, P., P. Schachter, et al. (2005). "Regulatory sequences of H19 and IGF2 genes in DNA-based therapy of colorectal rat liver metastases." J Gene Med **7** (3): 366-374.

Oshima, Y., T. Sakamoto, et al. (2002). "Targeted gene transfer to corneal stroma in vivo by electric pulses." Exp Eye Res **74** (2): 191-8.

Oshima, Y., T. Sakamoto, et al. (1998). "Targeted gene transfer to corneal endothelium in vivo by electric pulse." Gene Ther **5** (10): 1347-54.

Ottaviani, D., E. Lever, et al. (2008). "Anchoring the genome." Genome Biol **9** (1): 201.

Pack, D. W., A. S. Hoffman, et al. (2005). "Design and development of polymers for gene delivery." Nat Rev Drug Discov **4** (7): 581-93.

Pang, J. -j., B. Chang, et al. (2006). "Gene Therapy Restores Vision-Dependent Behavior as Well as Retinal Structure and Function in a Mouse Model of RPE65 Leber Congenital Amaurosis." Mol Ther **13** (3): 565-572.

Papapetrou, E. P., P. G. Ziros, et al. (2006). "Gene transfer into human hematopoietic progenitor cells with an episomal vector carrying an S/MAR element." Gene Ther **13** (1): 40-51.

Papapetrou, E. P., N. C. Zoumbos, et al. (2005). "Genetic modification of hematopoietic stem cells with nonviral systems: past progress and future prospects." Gene Ther **12** (S1): S118-S130.

Parker, A. L., C. Newman, et al. (2003). "Nonviral genedelivery: techniques and implications for molecular medicine." Expert Rev Mol Med **5** (22): 1-15.

Pecha, R. and B. Gompf (2000). "Microimplosions: Cavitation Collapse and Shock Wave Emission on a Nanosecond Time Scale." Physical Review Letters **84** (6): 1328-1330.

Peeters, L., N. N. Sanders, et al. (2005). "Vitreous: A Barrier to Nonviral Ocular Gene Therapy." Invest Ophthalmol Vis Sci **46** (10): 3553-3561.

Peeters, L., N. N. Sanders, et al. (2007). "Challenges in non-viral ocular gene transfer." Biochem Soc Trans **35** (Pt 1): 47-9.

Perales, J. C., T. Ferkol, et al. (1994). "An evaluation of receptor-mediated gene transfer using synthetic DNA-ligand complexes." Eur J Biochem **226** (2): 255-66.

Perales, J. C., G. A. Grossmann, et al. (1997). "Biochemical and functional characterization of DNA complexes capable of targeting genes to hepatocytes via the asialoglycoprotein receptor." J Biol Chem **272** (11): 7398-407.

Pereira-Leal, J. B., A. N. Hume, et al. (2001). "Prenylation of Rab GTPases: molecular mechanisms and involvement in genetic disease." FEBS Letters **498** (2-3): 197-200.

Perrault, I., J. -M. Rozet, et al. (1999). "Leber Congenital Amaurosis." Mol Genet Metab **68** (2): 200-208.

Pfeffer, S. (2005). "Structural clues to Rab GTPase functional diversity." J Biol Chem **280** (16): 15485-15488.

Pfeffer, S. R. (2001). "Rab GTPases: specifying and deciphering organelle identity and function." Trends Cell Biol **11** (12): 487-491.

Piechaczek, C., C. Fetzer, et al. (1999). "A vector based on the SV40 origin of replication and chromosomal S/MARs replicates episomally in CHO cells." Nucleic Acids Res **27** (2): 426-428.

Pike-Overzet, K., M. van der Burg, et al. (2007). "New insights and unresolved issues regarding insertional mutagenesis in X-linked SCID gene therapy." Mol Ther **15** (11): 1910-6.

Pitkänen L., M. Ruponen, et al. (2004). "Neural retina limits the nonviral gene transfer to retinal pigment epithelium in an in vitro bovine eye model." AAPS J **6** (3): e25.

Pitkänen, L., M. Ruponen, et al. (2003). "Vitreous Is a Barrier in Nonviral Gene Transfer by Cationic Lipids and Polymers." Pharm Res **20** (4): 576-583.

Ponjavic, V., M. Abrahamson, et al. (1995). "Phenotype variations within a choroideremia family lacking the entire CHM gene." Ophthalmic Genet **16** (4): 143-150.

Powers, M., M. Davies, et al. (2005). "Increased expression of chemokine KC, an interleukin-8 homologue, in a model of oxygen-induced retinopathy." Curr Eye Res **30** (4): 299-307.

Preising, M. and C. Ayuso (2004). "Rab escort protein 1 (REP1) in intracellular traffic: a functional and pathophysiological overview." Ophthalmic Genet **25** (2): 101-110.

Price, J., D. Turner, et al. (1987). "Lineage analysis in the vertebrate nervous system by retrovirus-mediated gene transfer." Proc Natl Acad Sci USA **84** (1): 156-160.

Provost, N., G. Le Meur, et al. (2005). "Biodistribution of rAAV Vectors Following Intraocular Administration: Evidence for the Presence and Persistence of Vector DNA in the Optic Nerve and in the Brain." Mol Ther **11** (2): 275-283.

Rädler, J. O., I. Koltover, et al. (1997). "Structure of DNA-cationic liposome complexes: DNA intercalation in multilamellar membranes in distinct interhelical packing regimes." Science **275** (5301): 810-4.

Rak, A., O. Pylypenko, et al. (2004). "Structure of the Rab7:REP-1 Complex: Insights into the Mechanism of Rab Prenylation and Choroideremia Disease." Cell **117** (6): 749-760.

Ramadan, R., R. Ramirez, et al. (2006). "Acute inflammation and loss of retinal architecture and function during experimental Bacillus endophthalmitis." Current Eye Res **31** (11): 955-965.

Raper, S. E., N. Chirmule, et al. (2003). "Fatal systemic inflammatory response syndrome in a ornithine transcarbamylase deficient patient following adenoviral gene transfer." Mol Genet Metab **80** (1-2): 148-58.

Rattner, A. and J. Nathans (2005). "The genomic response to retinal disease and injury: evidence for endothelin signaling from photoreceptors to glia." J Neurosci **25** (18): 4540-4549.

Rattner, A. and J. Nathans (2006). "Macular degeneration: recent advances and therapeutic opportunities." Nat Rev Neurosci **7** (11): 860-872.

Redmond, T. M., E. Poliakov, et al. (2005). "Mutation of key residues of RPE65 abolishes its enzymatic role as isomerohydrolase in the visual cycle." Proc Natl Acad Sci USA **102** (38): 13658-13663.

Redmond, T. M., S. Yu, et al. (1998). "Rpe65 is necessary for production of 11-cis-vitamin A in the retinal visual cycle." Nat Genet **20** (4): 344-351.

Riu, E., Z. Y. Chen, et al. (2007). "Histone modifications are associated with the persistence or silencing of vector-mediated transgene expression in vivo." Mol Ther **15** (7): 1348-55.

Rivera, A., S. A. Fisher, et al. (2005). "Hypothetical LOC387715 is a second major susceptibility gene for age-related macular degeneration, contributing independently of complement factor H to disease risk." Hum Mol Genet **14** (21): 3227-36.

Rosenblatt, M. I., and D. T. Azar (2004). "Gene Therapy of the Corneal Epithelium." Int Ophthalmol Clin **44** (3): 81-90.

Ruponen, M., S. Ylä-Herttuala, et al. (1999). "Interactions of polymeric and liposomal gene delivery systems with extracellular glycosaminoglycans: physicochemical and transfection studies." Biochim Biophys Acta - Biomembranes **1415** (2): 331-341.

Saari, J. C. and D. L. Bredberg (1989). "Lecithin:retinol acyltransferase in retinal pigment epithelial microsomes." J Biol Chem **264** (15): 8636-8640.

Sakai, M., M. Nishikawa, et al. (2005). "Hepatocyte-targeted gene transfer by combination of vascularly delivered plasmid DNA and in vivo electroporation." Gene Ther **12** (7): 607-16.

Schaarschmidt, D., J. Baltin, et al. (2004). "An episomal mammalian replicon: sequence-independent binding of the origin recognition complex." EMBO J **23** (1): 191-201.

Schmidt, S., M. A. Hauser, et al. (2006). "Cigarette smoking strongly modifies the association of LOC387715 and age-related macular degeneration." Am J Hum Genet **78** (5): 852-64.

Schorpp, M., R. Jäger, et al. (1996). "The Human Ubiquitin C Promoter Directs High Ubiquitous Expression of Transgenes in Mice." Nucleic Acids Res **24** (9): 1787-1788.

Seabra, M. C. (1996). "New insights into the pathogenesis of choroideremia: a tale of two REPs." Ophthalmic Genet **17** (2): 43-46.

Seabra, M. C., M. S. Brown, et al. (1992). "Purification of component A of Rab geranylgeranyl transferase: possible identity with the choroideremia gene product." Cell **70** (6): 1049-1057.

Seabra, M. C., M. S. Brown, et al. (1993). "Retinal degeneration in choroideremia: deficiency of rab geranylgeranyl transferase." Science **259** (5093): 377-381.

Seabra, M. C., J. L. Goldstein, et al. (1992). "Rab geranylgeranyl transferase. A multisubunit enzyme that prenylates GTP-binding proteins terminating in Cys-X-Cys or Cys-Cys." J Biol Chem **267** (20): 14497-14503.

Seabra, M. C., E. H. Mules, et al. (2002). "Rab GTPases, intracellular traffic and disease." Trends Mol Med **8** (1): 23-30.

Seabra, M. and C. Wasmeier (2004). "Controlling the location and activation of Rab GTPases." Curr Opin Cell Biol **16** (4): 451-457.

Seabra, M. C., Y. K. Ho, et al. (1995). "Deficient geranylgeranylation of Ram/Rab27 in choroideremia." J Biol Chem **270** (41): 24420-24427.

Semple-Rowland, S. L., K. S. Eccles, et al. (2007). "Targeted expression of two proteins in neural retina using self-inactivating, insulated lentiviral vectors carrying two internal independent promoters." Mol Vis **13**: 2001-11.

Sergeev, Y. V., N. Smaoui, et al. (2009). "The functional effect of pathogenic mutations in Rab escort protein 1." Mutat Res **665** (1-2): 44-50.

Shahar, J. (2006). "Electrophysiologic and retinal penetration studies following intravitreal injection of bevacizumab (Avastin)." Retina **26** (3): 262.

Shen, F. and M. C. Seabra (1996). "Mechanism of digeranylgeranylation of Rab proteins. Formation of a complex between monogeranylgeranyl-Rab and Rab escort protein." J Biol Chem **271** (7): 3692-3698.

Shi, W., J. A. J. M. van den Hurk, et al. (2004). "Choroideremia gene product affects trophoblast development and vascularization in mouse extra-embryonic tissues." Dev Biol **272** (1): 53-65.

Shichida, Y. and H. Imai. (1998). "Visual pigment: G-protein-coupled receptor for light signals." Cell Mol Life Sci **54** (12): 1299-1315.

Simon, A., U. Hellman, et al. (1995). "The Retinal Pigment Epithelial-specific 11-cis Retinol Dehydrogenase Belongs to the Family of Short Chain Alcohol Dehydrogenases." J Biol Chem **270** (3): 1107-1112.

Sinclair, J. H., J. Baillie, et al. (1992). "Repression of human cytomegalovirus major immediate early gene expression in a monocytic cell line." J Gen Virol **73** (Pt 2): 433-5.

Smyth Templeton, N. (2001). "Liposomal delivery of nucleic acids in vivo." DNA Cell Biol **21** (12): 857-67.

Sotirova, V. N., M. A. Calciano, et al. (2006). "Inclusion of a matrix-attached region in a 7SK pol III vector increases the efficiency of shRNA-mediated gene silencing in embryonic carcinoma cells." Plasmid **55** (3): 216-26.

Starr, C. J., J. A. Kappler, et al. (2004). "Mutation of the zebrafish choroideremia gene encoding Rab escort protein 1 devastates hair cells." Proc Natl Acad Sci USA **101** (8): 2572-2577.

Stehle, I. M., M. F. Scinteie, et al. (2003). "Exploiting a minimal system to study the epigenetic control of DNA replication: the interplay between transcription and replication." Chromosome Res **11** (5): 413-421.

Steinwaerder, D. S. and A. Lieber (2000). "Insulation from viral transcriptional regulatory elements improves inducible transgene expression from adenovirus vectors in vitro and in vivo." Gene Ther **7** (7): 556-67.

Stenmark, H. and V. Olkkonen (2001). "The Rab GTPase family." Genome Biol **2** (5).

Stieger, K., M. -A. Colle, et al. (2008). "Subretinal delivery of recombinant AAV serotype 8 vector in dogs results in gene transfer to neurons in the brain." Mol Ther **16** (5): 916-923.

Strauss, O. (2005). "The Retinal Pigment Epithelium in Visual Function." Physiological Reviews **85** (3): 845-881.

Syed, N., J. E. Smith, et al. (2001). "Evaluation of retinal photoreceptors and pigment epithelium in a female carrier of choroideremia." Ophthalmology **108** (4): 711-720.

Takahashi, M., H. Miyoshi, et al. (1999). "Rescue from Photoreceptor Degeneration in the rd Mouse by Human Immunodeficiency Virus Vector-Mediated Gene Transfer." J Virol **73** (9): 7812-7816.

Takai, Y., T. Sasaki, et al. (2001). "Small GTP-binding proteins." Physiol Rev **81** (1): 153-208.

Taniyama, Y., K. Tachibana, et al. (2002a). "Development of safe and efficient novel nonviral gene transfer using ultrasound: enhancement of transfection efficiency of naked plasmid DNA in skeletal muscle." Gene Ther **9** (6): 372-80.

Taniyama, Y., K. Tachibana, et al. (2002b). "Local delivery of plasmid DNA into rat carotid artery using ultrasound." Circulation **105** (10): 1233-9.

Taylor, G. S., T. A. Haigh, et al. (2004). "Dual stimulation of Epstein-Barr Virus (EBV)-specific CD4+- and CD8+-T-cell responses by a chimeric antigen construct: potential therapeutic vaccine for EBV-positive nasopharyngeal carcinoma." J Virol **78** (2): 768-78.

Terakita, A. (2005). "The opsins." Genome Biol **6** (3): 213.

Thaung, C., K. Arnold, et al. (2002). "Presence of visual head tracking differentiates normal sighted from retinal degenerate mice." Neurosci Lett **325** (1): 21-4.

Thomas, C., A. Ehrhardt, et al. (2003). "Progress and problems with the use of viral vectors for gene therapy." Nat Rev Genet **4** (5): 346-358.

Thoma, N. H., A. Iakovenko, et al. (2001). "Allosteric regulation of substrate binding and product release in geranylgeranyltransferase type II." Biochemistry **40** (1): 268-274.

Thomas, M. and A. M. Klibanov (2003). "Non-viral gene therapy: polycation-mediated DNA delivery." Appl Microbiol Biotechnol **62** (1): 27-34.

Timmers, A. M., H. Zhang, et al. (2001). "Subretinal injections in rodent eyes: effects on electrophysiology and histology of rat retina." Mol Vis **22** (7): 131-137.

Tolmachov, O. (2009). "Designing plasmid vectors." Methods Mol Biol **542**: 117-129.

Tolmachova, T., R. Anders, et al. (2006). "Independent degeneration of photoreceptors and retinal pigment epithelium in conditional knockout mouse models of choroideremia." J Clin Invest **116** (2): 386-394.

Tolmachova, T., S. T. Wavre-Shapton, et al. (2010). "Retinal Pigment Epithelium Defects Accelerate Photoreceptor Degeneration in Cell Type–Specific Knockout Mouse Models of Choroideremia." Invest Ophthalmol Vis Sci **51** (10): 4913-4920.

Tong, Y. C., S. F. Chang, et al. (2007). "Eye drop delivery of nano-polymeric micelle formulated genes with cornea-specific promoters." J Gene Med **9** (11): 956-66.

Tonjum, A. (1974). "Permeability of horseradish peroxidase in the rabbit corneal epithelium." Acta Ophthalmol **52**: 650-658.

Tonjum, A. (1977). "Movement of horseradish peroxidase in the cornea, sclera and the anterior uvea." Acta Ophthalmol (Copenh) **55**: 771-780.

Trezise, A. E. (2002). "In vivo DNA electrotransfer." DNA Cell Biol **21** (12): 869-77.

Turner, B. M. (2002). "Cellular memory and the histone code." Cell **111** (3): 285-91.

van Bokhoven, H., J. A. van den Hurk, et al. (1994). "Cloning and characterization of the human choroideremia gene." Hum Mol Genet **3** (7): 1041-1046.

van den Hurk, J. A., W. Hendriks, et al. (1997). "Mouse choroideremia gene mutation causes photoreceptor cell degeneration and is not transmitted through the female germline." Hum Mol Genet **6** (6): 851-858.

van den Hurk, J. A., M. Schwartz, et al. (1997). "Molecular basis of choroideremia (CHM): mutations involving the Rab escort protein-1 (REP-1) gene." Hum Mutat **9** (2): 110-117.

van den Hurk, J. A., D. J. van de Pol, et al. (2003). "Novel types of mutation in the choroideremia (CHM) gene: a full-length L1 insertion and an intronic mutation activating a cryptic exon." Hum Genet **113** (3): 268-275.

von Kries, J. P., H. Buhrmester, et al. (1991). "A matrix/scaffold attachment region binding protein: identification, purification, and mode of binding." Cell **64** (1): 123-35.

Vooijs, M., H. te Riele, et al. (2002). "Tumor formation in mice with somatic inactivation of the retinoblastoma gene in interphotoreceptor retinol binding protein-expressing cells." Oncogene **21** (30): 4635-4645.

Wade-Martins, R., R. E. White, et al. (2000). "Stable correction of a genetic deficiency in human cells by an episome carrying a 115 kb genomic transgene." Nat Biotechnol **18** (12): 1311-4.

Wakabayashi-Ito, N. and S. Nagata (1994). "Characterization of the regulatory elements in the promoter of the human elongation factor-1 alpha gene." J Biol Chem **269** (47): 29831-29837.

Wakefield, D. and A. Lloyd (1992). "The role of cytokines in the pathogenesis of inflammatory eye disease." Cytokine **4** (1): 1-5.

Ward, C. M., M. L. Read, et al. (2002). "Systemic circulation of poly(L-lysine)/DNA vectors is influenced by polycation molecular weight and type of DNA: differential circulation in mice and rats and the implications for human gene therapy." Blood **97** (8): 2221-9.

Wasan, E. K., D. L. Reimer, et al. (1996). "Plasmid DNA is protected against ultrasonic cavitation-induced damage when complexed to cationic liposomes." J Pharm Sci **85** (4): 427-33.

Wasmeier, C., A. N. Hume, et al. (2008). "Melanosomes at a glance." J Cell Sci **121** (24): 3995-3999.

Weinreb, R. N. (2001). "Enhancement of scleral macromolecular permeability with prostaglandins." Trans Am OphthalmolSoc (annual meeting) **99**: 319-343.

Wells, D. J. (2004). "Gene therapy progress and prospects: electroporation and other physical methods." Gene Ther **11** (18): 1363-9.

Wen, R., Y. Song, et al. (1995). "Injury-induced upregulation of bFGF and CNTF mRNAS in the rat retina." J Neurosci **15** (11): 7377-7385.

White, R. E., R. Wade-Martins, et al. (2001). "Sequences adjacent to oriP improve the persistence of Epstein-Barr virus-based episomes in B cells." J Virol **75** (22): 11249-52.

Wiersma, E. J., D. Ronai, et al. (1999). "Role of the intronic elements in the endogenous immunoglobulin heavy chain locus. Either the matrix attachment regions or the core enhancer is sufficient to maintain expression." J Biol Chem **274** (8): 4858-62.

Wightman, L., R. Kircheis, et al. (2001). "Different behavior of branched and linear polyethylenimine for gene delivery in vitro and in vivo." J Gene Med **3** (4): 362-72.

Wilson, R. W. and V. A. Bloomfield(1979). "Counterion-induced condesation of deoxyribonucleic acid. a light-scattering study." Biochemistry **18** (11): 2192-2196.

Wiseman, J. W., C. A. Goddard, et al. (2003). "A comparison of linear and branched polyethylenimine (PEI) with DCChol/DOPE liposomes for gene delivery to epithelial cells in vitro and in vivo." Gene Ther **10** (19): 1654-1662.

Wolff J. A., R. W. Malone, (1990). "Direct gene transfer into mouse muscle in vivo." Science **23** (247): 1465-1468.

Wolff, J. A., P. Williams, et al. (1991). "Conditions affecting direct gene transfer into rodent muscle in vivo." Biotechniques **11** (4): 474-485.

Wong, S. P., O. Argyros, et al. (2011). "Non-viral S/MAR vectors replicate episomally in vivo when provided with a selective advantage." Gene Ther **18** (1): 82-87.

Wu, Q., L. R. Blakeley, et al. (2007). "Interphotoreceptor Retinoid-Binding Protein Is the Physiologically Relevant Carrier That Removes Retinol from Rod Photoreceptor Outer Segments." Biochemistry **46** (29): 8669-8679.

Wu, H., D. F. Ceccarelli, et al. (2000). "The DNA segregation mechanism of Epstein-Barr virus nuclear antigen 1." EMBO Rep **1** (2): 140-4.

Wu, C. H., J. M. Wilson, et al. (1989). "Targeting genes: delivery and persistent expression of a foreign gene driven by mammalianregulatoryelements in vivo." J Biol Chem **264** (29): 16985-7.

Yang, D., S. G. Elner, et al. (2011). "MCP-1-activated monocytes induce apoptosis in human retinal pigment epithelium." Invest Ophthalmol Vis Sci **52** (8): 6026-34.

Yates, J. R. W., T. Sepp, et al. (2007). "Complement C3 Variant and the Risk of Age-Related Macular Degeneration." N Engl J Med **357** (6): 553-561.

Yeh, S., X. Song, et al. (2003). "Apoptosis of ocular surface cells in experimentally induced dry eye." Invest Ophthalmol Vis Sci **44** (1): 124-129.

Yew, N. S., H. Zhao, et al. (2000). "Reduced inflammatory response to plasmid DNA vectors by elimination and inhibition of immunostimulatory CpG motifs." Mol Ther **1**: 255–262.

Yoshida, S., A. Yoshida, et al. (2003). "Role of MCP-1 and MIP-1alpha in retinal neovascularization during postischemic inflammation in a mouse model of retinal neovascularization." J Leukoc Biol **73** (1): 137-144.

Yurek, D. M., A. M. Flectcher, et al. (2009). "Compacted DNA nanoparticle gene transfer of GDNF to the rat striatum enhances the survival of grafted fetal dopamine neurons." Cell Transplant **18** (10): 1183-1196.

Yusufzai, T. M., G. Felsenfeld, et al. (2004). "The 5'-HS4 chicken beta-globin insulator is a CTCF-dependent nuclear matrix-associated element." Proc Natl Acad Sci USA **101** (23): 8620-4.

Zaidi, S. K., D. W. Young, et al. "The dynamic organization of gene-regulatory machinery in nuclear microenvironments." EMBO Rep **6** (2): 128-33.

Zarbin, M. A. (2004). "Current concepts in the pathogenesis of age-related macular degeneration." Arch Ophthalmol **122** (4): 598-614.

Zderic, V., J. I. Clark et al. (2004). "Ultrasound-enhanced transcorneal drug delivery." Cornea **23** (8): 804-11.

Zderic, V., S. Vaezy, et al. (2002). "Ocular drug delivery using 20-kHz ultrasound." Ultrasound Med Biol **28** (6): 823-9.

Zelenin, A. V., V. A. Kolesnikov, et al. (1997). "Bacterial β-galactosidase and human dystrophin genes are expressed in mouse skeletal muscle fibers after ballistic transfection." FEBS Letters **414** (2): 319-322.

Zelphati, O., L. S. Uyechi, et al. (1998). "Effect of serum components on the physico-chemical properties of cationic lipid/oligonucleotide complexes and on their interactions with cells." Biochim Biophys Acta **1390** (2): 119-33.

Zerial, M. and H. McBride (2001). "Rab proteins as membrane organizers." Nat Rev Mol Cell Biol **2** (2): 107-117.

Zhang, M., J. Covar, et al. (2011). "Lack of TNF-α Promotes Caspase-3–Independent Apoptosis during Murine Cytomegalovirus Retinitis." Invest Ophthalmol Vis Sci **52** (3): 1800-1808.

Zhang, X. Y., Y. S. Ni, et al. (1995). "Increasingbinding of a transcription factor immediately downstream of the cap site of a cytomegalovirus gene represses expression." Nucleic Acids Res **23** (15): 3026-33.

Zhong, W., M. Gulotta, et al. (1990). "DNA solution conformation via infrared circular dichroism: experimental and theoretical results for B-family polymers." Biochemistry **29**: 7485-7491.

Ziady, A. G., C. R. Gedeon, et al. (2003). "Transfection of airway epithelium by stable PEGylated poly-L-lysine DNA nanoparticles in vivo." Mol Ther **8** (6): 936-947.

Znoiko, S. L., R. K. Crouch, et al. (2002). "Identification of the RPE65 Protein in Mammalian Cone Photoreceptors." Invest Ophthalmol Vis Sci **43** (5): 1604-1609.